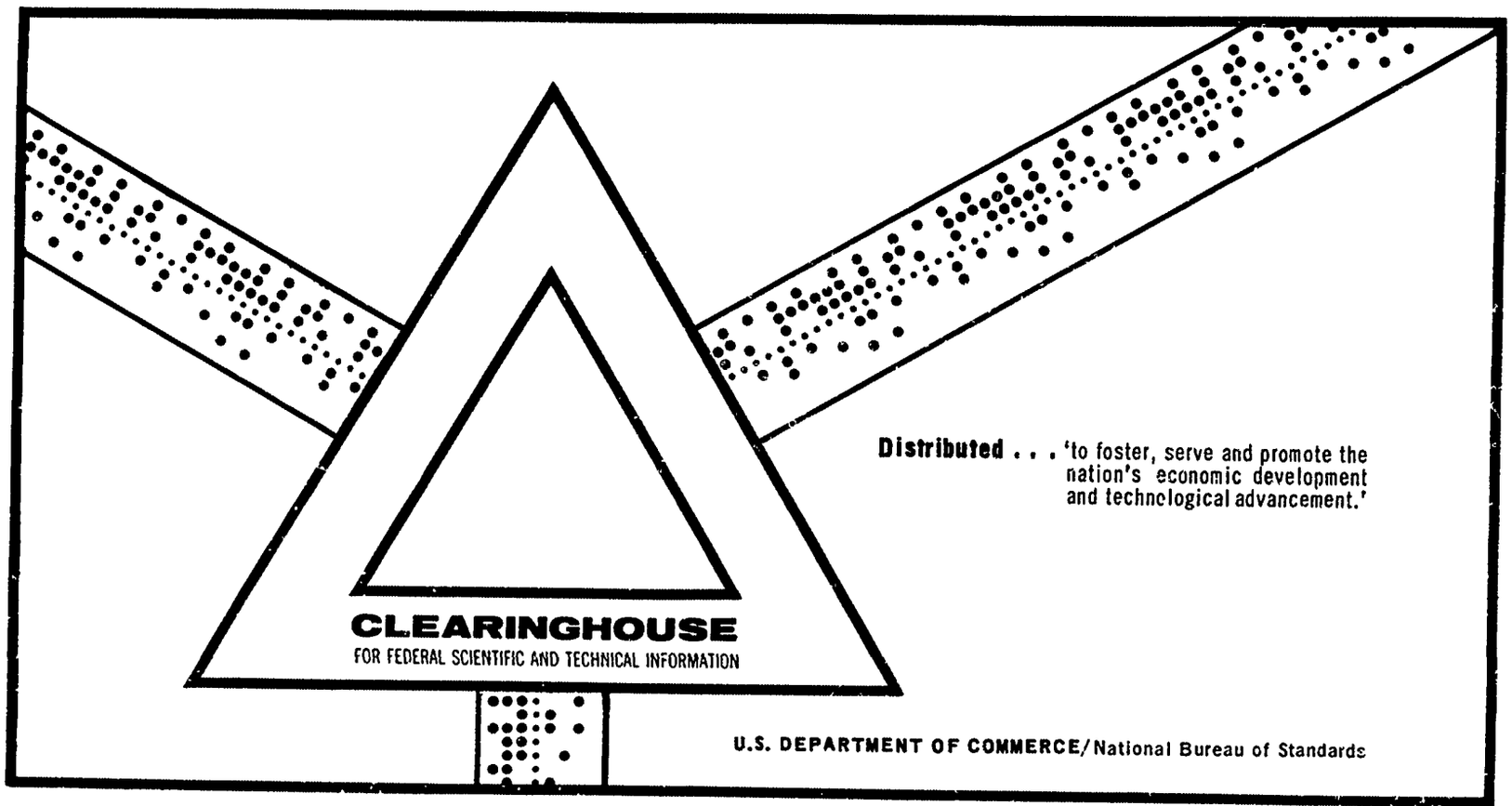
AD 697 956

AEROSPACE-AFML CONFERENCE ON NDT OF PLASTIC/COMPOSITE STRUCTURES, DAYTON, OHIO, MARCH 18-20, 1969

Air Force Materials Laboratory
Wright-Patterson Air Force Base, Ohio

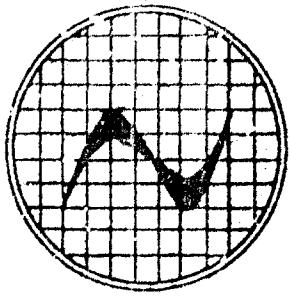
20 March 1969



This document has been approved for public release and sale.

697956

AEROSPACE-AFML CONFERENCE ON



NDT OF PLASTIC/COMPOSITE STRUCTURES

DDC
RECEIVED
DEC 15 1969
B

MARCH 18-20, 1969

DAYTON, OHIO

This document has been approved for public release and sale; its distribution is unlimited

Best Available Copy

CONFERENCE CO-CHAIRMEN

Richard R. Rowand
George Epstein

PROGRAM COORDINATOR

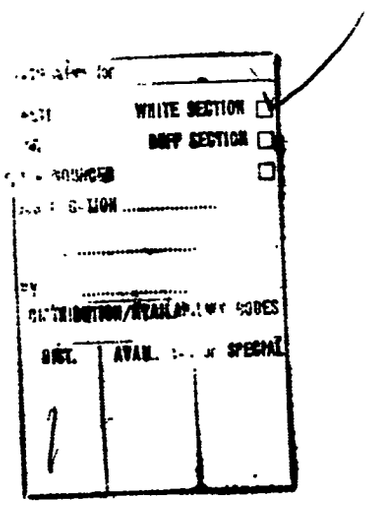
1/Lt. Lee R. Gulley

CONFERENCE COORDINATOR

James M. Miller

CONFERENCE SECRETARY

Mrs. Audrey G. Sachs



Unclassified

Classification

DOCUMENT CONTROL DATA - R & D

(Security classification of title, body of abstract and indexing annotation must be entered when the overall report is classified)

ORIGINATING ACTIVITY (Corporate author) AFML(MANX) WPAFB, OHIO 45433	2a. REPORT SECURITY CLASSIFICATION Unclassified 2b. GROUP N/A

3. REPORT TITLE

Aerospace-AFML Conference on NDT of Plastic/Composite Structures

4. DESCRIPTIVE NOTES (Type of report and inclusive dates)

Conference Proceeding-Papers

5. AUTHOR(S) (First name, middle initial, last name)

N/A

6. REPORT DATE	7a. TOTAL NO. OF PAGES	7b. NO. OF REFS
18-20 March 1969	Approx. 300	53

8a. CONTRACT OR GRANT NO.	9a. ORIGINATOR'S REPORT NUMBER(S)
N/A b. PROJECT NO. 735109001	N/A
c. d.	9b. OTHER REPORT NO(S) (Any other numbers that may be assigned this report) N/A

10. DISTRIBUTION STATEMENT

This document has been approved for public release and sale, its distribution is unlimited.

11. SUPPLEMENTARY NOTES	12. SPONSORING MILITARY ACTIVITY
Proceedings were paid for by registration fees of industrial attendees. Not a government document.	N/A (See Block 1)

13. ABSTRACT

The document contains a collection of twenty papers presented by nondestructive testing engineers and scientists at the Aerospace-AFML conference on NDT of Plastic/Composite Structures held in March, 1969. Topics covered included a state of the art review, acoustic optical imaging, x-ray mapping of flaws by computer graphics, ultrasonics, microwave and thermal techniques.

DD FORM 1 NOV 65 1473

Unclassified

Security Classification

KEY WORDS	LINK A		LINK B		LINK C	
	ROLE	WT	ROLE	WT	ROLE	WT
Nondestructive Testing						
Composites						
Plastics						
Non metallics						
Adhesively Bonded Structures						
Quality Assurance						

CONFERENCE ON NDT OF PLASTIC/COMPOSITE STRUCTURES / 1969

18 - 19 - 20 March

Technical Papers



Sponsored By:

Air Force Materials Laboratory (MAMN)
The Aerospace Corporation
University of Dayton
Place: Sheraton-Dayton Hotel, Dayton, Ohio

FOREWORD

The papers are included in each author's original form and have not been edited in order to expedite their distribution. This post print has been published in limited numbers for the convenience of the conferees and to provide maximum usefulness of the information presented at the conference.

TABLE OF CONTENTS

Materials/NDT Panel Members.....i
Response to Questionaires.....ii

SYSTEMS APPLICATIONS FOR NDT
W. Riley
Director of the Materials Sciences Laboratory
Aerospace Corporation.....1

STATE-OF-THE-ART REVIEW: NONDESTRUCTIVE TESTING TECHNIQUES FOR COMPOSITES
G. Martin
Program Manager, Materials and Producibility
North American Rockwell Corporation.....2

Chairman: T.D. Cooper
Air Force Materials Laboratory

TRW ACOUSTO OPTICAL IMAGING NON-DESTRUCTIVE TESTING TECHNIQUE
R. Aprahamian, P. G. Bhuth
TRW, Inc.....3

MICROWAVES IN NONDESTRUCTIVE TESTING
R. W. Cribbs
Electro-Physics Co.....4

APPLICATION OF SONIC AND MICROWAVE INSPECTIONS TO COMPOSITE NONMETALLIC STRUCTURES
A. D. Lucian and M. W. Standart
Aerojet-General Corporation.....5

Chairman: G. Epstein
Aerospace Corporation

X-RAY MAPPING OF FLAWS BY COMPUTER GRAPHICS
F. Hartmann
North American Rockwell Corporation.....6

A STUDY OF SYSTEM CONCEPT TO DERIVE THE HIGHEST DEGREE OF DATA PRESENTATION WITH A MINIMUM EFFORT
C. S. Phelan
Shurtronics Corporation.....7

PHYSICAL PROPERTY EVALUATION OF COMPOSITE MATERIALS USING FRESNEL OPTICAL PRINCIPLES IN THE MICROWAVE REGION
J. C. Plunkett
Martin Marietta Corporation.....8

NDT OF AN ADVANCED GEOMETRY COMPOSITE BLADE
R. D. Whealy
Boeing-Vertol.....9

QUALITY CONTROL METHODS APPLIED TO AN ADVANCED COMPOSITE F-111 HORIZONTAL TAIL
J. A. Tiegert and G. D. Darnell
General Dynamica/Fort Worth.....10

Chairman: 1/Lt. Lee R. Gulley
Air Force Materials Laboratory

STUDIES OF COMPOSITE MATERIALS AND FAYING SURFACES UTILIZING THE SCANNING ELECTRON MICROSCOPE
C. V. Cagle and H. Lee
The Epoxylite Corportion.....11

ULTRASONIC INSPECTION TECHNIQUES FOR ADHESIVE BONDED COMPOSITES
W. Mattson
Boeing-Renton.....12

NONDESTRUCTIVE EVALUATION BY SCHLIEREN METHOD OF ADHESIVELY BONDED STRUCTURES
A. E. Holt and A. S. Greer
Bell Helicopter.....13

NDT DEVELOPMENT FOR MEASURING ADHESIVE BOND STRENGTH IN HONEYCOMB COMPOSITES
J. Moore
North American Rockwell Corporation.....14

APPLICATION FO NONDESTRUCTIVE TESTING OF ADHESIVE BONDED STRUCTURES FOR NORTHROP NORAIR'S F-5 AND T-38 AIRCRAFT
R. E. Clemens
Northrop Norair.....15

THERMAL INSPECTION OF ADHESIVE BONDED STRUCTURES
E. J. Barton
Automation Industries.....16

Chairman: L. Hjelm
Air F orce Materials Laboratory

PRELIMINARY NONDESTRUCTIVE EVALUATION OF RESIN MATRIX COMPOSITES SUBJECTED TO IMPULSIVE LOADING
J. L. Cook, J. S. Evangelides, D. F. Moon, and J. E. Zimmer
McDonnell Douglas Astronautics Company.....17

VARIANT PROPERTIES OF COMPOSITE MATERIALS
J. R. Zurbrick
Avco.....18

APPLICATION OF NONDESTRUCTIVE TESTING FOR ADVANCED COMPOSITES
R. T. Anderson and T. J. DeLacy
General Dynamics/Convair.....19

MATERIALS/NDT PANEL MEMBERS

Chairman: Goerge Epstein (Aerospace Corp.)

Materials Representatives:

Mr. L. Kelly	Advanced Composites Division AFML
Mr. H. Schwartz	Non-Metallic Materials Division AFML
Mr. J. D. Ray	Non-Metallic Materials Division AFML
Mr. E. R. Bartholomew	Federal Aviation Administration Wash., D. C.

NDT Representatives:

Dr. G. Martin	North American Rockwell Corp.
Mr. C. Hastings	AVCO Corp.

RESPONSE TO QUESTIONNAIRE

The following is an abridged collection of comments made by attendees of the conference. Only 25 percent of the attendees responded by completing the written questionnaires and thus the opinions expressed were not necessarily those of the majority. Be that as it may, some of the more interesting comments, both pro and con, are included here as follows:

Materials people did too much listening, not enough talking.

Some people did not care for the display of equipment by individuals of several companies. They felt it was commercial and should not have been permitted. Others felt that these displays were constructive and served some useful purpose in a non-commercial vein.

One person felt that one paper on the Fokker Bond Tester was enough, instead of the four that were presented. It should be noted, however, that each paper was quite different in content though dealing gererally with an identical subject technique.

It was suggested that there be a session entitled "A/Other Discipline(s) Look(s) at NDT".

An attempt should be made to interrelate with ASTM Committee D-5.

The methodical adherence to schedule was appreciated and novel to other conferences attended.

Show movies when available.

Emphasize more NDT in terms of performance properties. Less emphasis on flaws and defects unless defined in terms of performance.

Perhaps a few papers by designers with respect to NDT.

Fewer talks about off-the-shelf instruments.

More panel discussion, please, especially for the speakers. Many of them don't see the woods for the trees in front of them.

We needed some comments on what makes a strong or a weak adhesive bond.

Speakers should state both the advantage and limitations of the techniques they discuss. Other factors to be discussed should include:

1. Suitability for production
2. Suitability for complex as well as simple shapes
3. Cost of equipment and time rrquired to train operators to handle it properly
4. General availability of equipment

Suggestion for a paper: "Laboratory vs. Service and Relation of NDT Evaluation" (Technical Paper)

There is often a lot of duplication of effort in research. It should be coordinated to eliminate this problem.

SYSTEMS APPLICATIONS FOR NDT

by Wm. C. Riley

Director, Materials Sciences Laboratory

Aerospace Corporation

Is there a need for NDT of plastic and composite structures? From the systems point of view, the need is not for NDT, but rather for nondestructive evaluation (NDE). The distinction between NDT and NDE is of extreme importance. Evaluation implies that a correlation has been made between those parameters that can be determined by NDT and the performance of the component in the environment of the system. Further, it is the lack of convincing correlations that deters the use of NDT in some systems.

By way of illustration, consider some of the problems encountered in utilizing NDT in launch vehicle, satellite, and reentry systems. In each example, the effect of the lack of such correlations will be obvious. Also, suggestions will be made for promoting more effective utilization of NDT in future systems. Security classification and proprietary rights preclude reference to specific systems.

In recent years, systems engineers have often been critized by the R&D community for not taking advantage of the more sophisticated NDT techniques that are available. I believe that the major barrier to utilizing these techniques is the fact that the systems engineer is not convinced that the correlation between the results from advanced NDT techniques and the component performance in the system environment, is an adequate basis for acceptance or rejection of components. In short, he doesn't believe that NDE has been established. He is perfectly willing to buy improved reliability, but he simply isn't sure he's getting it from NDT.

Part of the problem is that the usefulness of NDT frequently must be established during the course of system design or while the feasibility of the system is being established. Each system has some conditions unique unto itself, to which the structures and materials will be subjected. Frequently these conditions are not clearly delineated until the system is well into the development phase. This is particularly true of mechanical stress and temperature conditions that can vary widely depending on the particular missions to be flown. As a consequence, timing and planning are extremely critical and limiting factors in establishing appropriate NDT methods and the necessary correlation with performance.

Another major constraint is the system design. If, for example, weight is critical, then structural members may be designed with very limited safety margins. Thus, nondestructive evaluation must be geared to both the particular conditions that the component must withstand in service and constraints imposed by the design.

Other factors deterring utilization of NDT may be financial or psychological in nature. To obtain a good correlation between NDT results and performance of a component in a simulated environment, it may be necessary to test hardware with a broad range of defects. Convincing a systems engineer or program manager that a large number of components are to be constructed and tested to failure may be a major task in itself. Nonetheless, more often than not, there is no other way to adequately establish NDE.

In this regard, there is an ever increasing emphasis on "cost effectiveness without sacrifice of reliability," particularly in advanced aerospace systems. When interpreted relative to NDT, this means that it is not feasible to eliminate 1000 expensive components of a given type when only one of these might fail in the system environment. Ultimately, the cost of rejecting components that would perform satisfactorily, and in some cases the time lost in replacing them, must be balanced against the cost of optimizing the correlation between NDT observations and performance in the simulated service environment.

An extreme example of the problems in applying NDT is in the ballistic reentry systems, where plastic composites are required for thermal protection. Probably more plastic composite materials have been used in these systems than in any other class of systems. For some ballistic trajectories, the conditions encountered in flight cannot be reproduced in ground testing. Both the enthalpy and the heating rate can be achieved in different facilities, but the synergistic effects cannot be found in any ground test presently available. Thus, expensive flight tests would be required to obtain an exact correlation between the defects measurable by NDT and the performance of the system or component. NDT has been used to discover cracks, gross delaminations, and voids in reentry system components. However, use of this information seems to be largely a matter of judgement. For example, in a given component, the detection of delaminations in one production unit may not in itself indicate an incipient failure; but it does mean that the processing conditions for this particular unit were out of control and not as specified. In the delaminated component, important properties not measured by NDT may be adversely affected. For this reason, the component may be rejected.

The impact of NDT or lack thereof on materials selection for launch vehicle systems can be illustrated by a problem in a payload protection fairing. Originally, weight considerations indicated the use of a reinforced-plastic adhesive-bonded honeycomb sandwich structure. However, numerous structural problems were encountered leading to a review of the quality control procedures; this revealed that the soundness of the adhesive bond was determined by nothing more than "coin tapping" and an educated ear. Ultimately, program management decided to make a change and the plastic fairing was replaced by an aluminum alloy construction. The major reason for this change-over was the inadequacy of the NDT technique. The cost of this change was high, not only in dollars, but through time delays in subsequent launches. The change-over probably could have been averted had the need for more sophisticated NDT of the plastic composite been foreseen at the time the original design was initiated. This illustrates an important

point relative to the use of reinforced plastics and composites in aerospace systems. To date, design and systems engineers are inclined to have a great deal more confidence in metals. In fact, at the time of the substitution of aluminum for the fairing, one of the cognizant systems people stated: "We have had nothing but trouble with plastics and composites;" and piously, added: "The Good Lord gave us metals to use in structures." I believe that before we see general usage of plastic composite materials in advanced systems, we will have to show design and systems engineers that NDT techniques are available and can be readily adapted to the particular nondestructive evaluation needs of their system.

A more hopeful note ... A milestone in the use of plastic composites in satellite systems was attained recently when a defense satellite was launched with an adhesive-bonded reinforced-plastic honeycomb sandwich construction as a primary load-carrying structure. This structure also served to mount the solar cells necessary for powering electronic equipment when in orbit. In particular, the aft solar panel structure was required to support the full launch loadings for the entire satellite. Failure of this structure would cause loss of the entire satellite and the mission. This was the first satellite system of the USAF Space and Missile Systems Organization to use reinforced plastics as major structural members.

There was deep concern about this concept. In the interest of weight savings, the structure had to be designed with a minimum of redundancy and quite limited safety margins. But even more serious -- the only NDT inspection was visual examination and limited "coin tapping." Here is another instance in which, because of short planning and scheduling time, there had been no adaptation of the more sophisticated NDT techniques to the particular needs of this system. Nonetheless, the launch was successful and the particular contractor involved plans to use a similar type of structural member on other satellite systems that are now in the systems design and planning stage. To his great credit, he is continuing studies to adapt more sophisticated NDT to the evaluation of structural reinforced plastics.

How can we more effectively utilize NDT in future systems? First, I think it goes without saying that additional funds are needed for research and development on NDT methods. Indeed, from what I have seen, this appears to be coming about. There remains the basic question, of course, whether or not the funding is commensurate with the future requirements for NDT. For some time now, the Materials Advisory Board has had a committee consisting of some of the outstanding scientific and engineering personnel in the field making an in-depth study of this very vital question. Their recommendations, which will be published soon, probably will have a strong effect on future funding levels. Secondly, as the new advanced systems come to the proposal stage, the potential contractors should be required to present in their proposals, criteria for hardware acceptance with emphasis on NDT. In fact, the response to this question might well be one of the evaluation criteria upon which contractor selection is based. Requirements for nondestructive evaluation, specified in the RFP, should be particularly effective in stimulating appropriate contractor activities. Thirdly, as indicated above, funds must be appropriated within the system contracts for adaptation of available NDT techniques to hardware evaluation, taking into account conditions unique to that system and the particular component design. In this regard, NDT must be coupled with the design, and should influence but not compromise it.

Finally, as outstanding work in the adaptation of NDT to systems' problems is accomplished, it is important that this information be brought to the attertion of system designers and systems engineers. Failures are always publicized; successes seldom are. Symposia and conferences on NDT can be a vital part of this educational process. I only hope that design personnel and systems decision-makers will be present at such meetings and thus become directly aware of the impact this technology can make on the capability and reliability of future systems.

NONDESTRUCTIVE TESTING TECHNIQUES

FOR COMPOSITES

by

George Martin
Research and Engineering
North American Rockwell Corporation

Prepared for Presentation at the
Conference on Nondestructive Testing
Dayton, Ohio
March 18-20, 1969

ABSTRACT

This paper is a short survey of the state-of-the-art of the nondestructive testing of filamentary reinforced composite materials, with special reference to plastic matrices. The area is surveyed from the point of view of property/imperfection/NDT method interactions for the materials involved in these composites. Interpretation of such interactions are limited by our understanding of the mechanics of composite materials, the property variations of the composite constituents and the variations introduced into composites during manufacture. Such limitations seem to be at present more of a challenge than the actual developments of NDT methods, with better defect detecting ability. Existing methods seem to have reached a state where their resolution is better than our ability to interpret signals in terms of effects on properties. It appears that the most promising direction for future developments of NDT methods is towards the development of methods directly related to composite properties.

The ancient Britons put straw into the mud walls of their wattle huts to keep out the wolves. We keep the wolves out of plastics by reinforcing the plastic with filaments. The rapid rise of output of these materials is quite staggering. In 1967[1] it was predicted that by 1975 a production of 860 million pounds would be reached. Recently [2] the SPI reported the shipments for 1968 as 760 million pounds and forecasts almost a billion pounds for 1969. The aerospace industry uses about 8% of all reinforced plastic, the major share, accounting for about 25% of the total is used by the marine industry.

In addition to plastic composites reinforced with filaments, a whole host of other composites is available. Best known is probably the rubber filament composite used to drive automobiles on. Reliability here is achieved by manufacturing practice improvements following field tests and the common nondestructive test applied by the user seems to be a kick with the boot. However, the inspection of aircraft tires has received considerably more attention. Metal matrix composites are well into the prototype stage, both as material for structural members and for engine parts. Finally, ceramic matrix composites have entered the experimental stage. In all cases of composites, reinforcement can be effected by parallel filaments, two or three dimensionally woven filaments and short fibers or whiskers and flakes.

It is the aerospace usage of this deluge of plastic matrix composites which concerns us here. Aerospace parts are characterized by the fact that they generally have to act as load carrying members - in addition to any other functions - and that they have to carry those loads with a much higher reliability than is required by other industries. Now, there are two approaches by which we can use NDT methods to give us the required reliability assurance. Either we can use NDT methods to determine local defects or imperfections deviating from a standard known to have acceptable properties and then correlate those deviations with changes in properties, or we can measure deviations from desired properties directly. In the case of homogeneous materials, the effects of local defects or imperfections are, relatively speaking, reasonably well understood. There the inspector hounding his holes or cracks has a well established niche. However, in the case of composites, the hounder of holes is on much less sure ground. The reason is that the effect of holes, of voids, of debonds and cracks, is so much less understood in the complex micromechanics of a composite material than in homogeneous materials. A further reason is the fact that plastics are relatively unstable materials. A composite structure may be perfect when it leaves the shop, but will it be perfect after 5 years service? More important, will it then have the same properties which the designer expected and the inspector checked? The need for NDT methods relating to properties rather than defects or imperfections is therefore much more acute in the case of composites than in the case of homogeneous materials. It is most gratifying that this need appears to have been recognized by a much wider range of speakers here than is usually the case in NDT symposia.

To give a state-of-the-art review just prior to such a conference is just asking for trouble. Because, generally, what we read is an account published six months ago of results obtained 1-1/2 years ago by carrying out experiments conceived four years ago. And this is an optimistic view. This conference will describe the state-of-the-art! What I shall try is to identify the different NDT approaches in their relation to the material with the intention of helping assess their relative usefulness and, hopefully, stimulate further and new developments.

Let us first consider some properties of the raw materials of our plastic composites. The plastic is the result of a polymerization reaction, which is not necessarily finished with the process cure. The reaction is affected by environmental factors, such as moisture and temperature, and can therefore produce a variety of mechanical and physical properties. However, a certain property value is not always uniquely connected to a certain stage of the reaction. Let me give you some examples of these reaction/effect interactions. Figure 1 is the change of electric resistivity of an epoxy with time at different temperatures [3] and figure 2 shows the changes in the dissipation factor over a longer time range.[4] Both graphs indicate that if we wish to utilize electric conductivity or dissipation factor measurements as a nondestructive measure of the cure state, both the exact material and the cure time and temperature will have to be standardized. Polymerization is affected by radiation, although, as figure 3 shows, radiation exposures of about $10^6 - 10^8$ roentgens are required for sizeable effect.[5] Now, for instance, a 1 curie source of cobalt 60 produces a radiation exposure of $.136 \times 10^5$ roentgens at a distance of one centimeter, Cobalt 60 of course produces hard radiation in the MeV range, whereas the soft radiation from smaller industrial X-ray units is absorbed much more rapidly in air. However, the example indicates the need for considering the actual intensity at the specimen in the case of radiography.

Radiography has been applied widely to the inspection of composites. In the case of boron filaments, single filaments even in multilayer composites can generally be observed under routine conditions. Even higher resolution can be obtained using microradiographic or neutron readiographic techniques. The reason is the high opacity of the tungsten core of boron to X-rays or of the boron itself to neutrons, as compared to the opacity of the matrix. Now, in the case of plastic/glass filament or plastic/carbon filament the differences in opacity, i.e. the differences in the attenuation coefficients, of the constituents is very much less. Nevertheless, the numerous radiographs made of such materials indicate relatively gross imperfections in filament alignment, as well as other imperfections such as voids. Investigators generally report that the lower the radiation energy, the better the result. Naturally, we wish to optimize radiography parameters in order to obtain the maximum resolutions of either filament or of voids. The ratio of the incident intensity I_o to the transmitted

intensity I_d is given by

$$I_d/I_o = \exp\left(-\frac{\mu}{\rho}\rho d\right)$$

where μ is the mass attenuation coefficient, ρ the density and d the thickness penetrated. For a three component system, the total mass attenuation coefficient $\left[\mu/\rho\right]_s$ is given by

$$\left[\frac{\mu}{\rho}\right]_s = \frac{1}{d_m + d_f + d_a}\left\{\left[\frac{\mu}{\rho}\rho d\right]_m + \left[\frac{\mu}{\rho}\rho d\right]_f + \left[\frac{\mu}{\rho}\rho d\right]_a\right\}$$

where the subscripts m, f and a refer to the matrix material, the filament material and to the gas filling the voids.

As a first approximation, we can equate the thicknesses with the volume fractions of the three components. Now, if we knew the mass attenuation coefficients, which are a function of the radiation energy, optimum parameters can be selected. Figure 4 shows mass attenuation coefficients for air and carbon,[6] together with mass attenuation coefficients for some plastic polymers calculated from their stochiometric composition. The value marked X has been obtained by calculation from more general data given by Zurbrick [7] for a 65% glass filament plastic composite. The values calculated for epoxy and polyimides are so close as to fall in a single curve. Contrast depends on the difference in mass attenuation coefficients and these differences for various composite combinations have been plotted in figure 5. Bearing in mind the logarithmic relationship between the mass attenuation coefficient and the incident and transmitted intensity, a difference in the mass attenuation coefficient of 0.1 indicates an absorption of about 10% for unit density and thickness. Figure 5 shows, that up to about 40 keV reasonable contrasts can be obtained between silica filaments or air bubbles and plastics. However, the position is going to be more critical when the newly developed carbon filaments will come into use. Here much lower X-ray energies will have to be employed if reasonable contrast is the goal of radiography. Admittedly, the above two figures make two assumptions: that thickness effects of the various phases is equal to their volume fraction and that mass attenuation coefficients are additive for low energies. The validity of these assumptions will have to be determined experimentally. An interesting approach has been proposed by Hagemaier,[8] who suggested the addition of opacifiers to the plastic matrix, such as antimony trioxide, which do not seem to affect the mechanical properties.

In the case of filaments, examination of batches have shown a wide scatter of properties such as the fracture strength, prior to fabrication. In plastic composites, relatively little process or service effects have been observed on the filament strength, but we are all familiar with the matrix/filament interaction problems in metal matrix composites. If we combine this strength variation with the observed variations in filament packing volume over small distances and local changes in the matrix behavior, we arrive at the everpresent resolution problem. What is the smallest unit of structure area or volume which our NDT method has to resolve? The obvious answer, that this unit should be the smallest area or volume, which, if imperfect, would jeopardize the ability of the entire structure to fulfil its mission. Simple as that answer is, in practice it is very rarely obtained. The reasons seem to be principally our basic lack of knowledge of material behavior around imperfections, particularly in composites and the fact that the effect of imperfections is not only a function of the material, but also of its application, including its macro and micro stress state within the structure. Of the two approaches available to provide an answer, the empirical approach may yield a result for a single type of structure, material and application, which can rarely be extrapolated. The other approach, a systematic analysis is in the case of composites, usually very complex.

By way of example, let us consider the problem of broken filaments. Hedgepeth,9 assuming a composite model where parallel filaments, arranged in a single layer, carry all the tensile load and the matrix serves only to transmit shear, has calculated both the static stress concentration factor and the dynamic response factor when 1, 2, 3..... adjacent filaments break. His analytical results are shown in figure 6. The dynamic response factor which is the ratio between the maximum stress after sudden fracture to static stress of a given number of filaments, has a limit value of 1.27. However, the static stress increases locally more rapidly as increasing numbers of filaments break. In the Hedgepeth composite a single broken filament would increase the stress on its neighbor by 33%, leaving that filament in effect with a load carrying capacity of only 75% its original strength. If the overall loads on the composite never exceed that 75% limit, no further damage is done. However, if that 75% load is exceeded, the next filament snaps, which not only increases the stress concentration on the third filament statically, but also dynamically. That third filament under these conditions can carry only $1/(1.6 \times 1.15) = .54$ or 54% its original load. The crack is thus progressive.

In real composites, several factors reduce this effect. The first is the limited shear strength of the matrix and the second the fact that filaments are not arrayed in a single layer, but are closely packed. The increased stress due to a single filament failing is thus taken up by, ideally six neighbors and is in any case limited by the shear strength of the plastic. Furthermore, plastic composite structures generally use

preimpregnated bundles of filaments in their fabrication. No analysis involving these factors appears to have been carried out. However, such an analysis would give us some idea of the number of neighboring filament breaks which are critical for any given composite. That some process of the type given by Hedgepeth occurs in practice seems indicated by the general experience that composites with about 50% filaments with a nominal strength of 400,000 psi or better fail at about 190,000 psi.

Even less is known about the effects of delaminations on properties. Here, too, the effects are as much a function of the location of the delamination within the stress pattern of the structure as of its size. Present QC requirements for "a structure substantially free from delaminations" may cause overinspection in some cases and yet miss important stress concentrating delaminations in others, because the minimum limit of detectable delamination is somewhere around 1/4 inch, though smaller delaminations can be detected with dye penetrants, if these delaminations intersect the surface.

Some idea of the importance of delaminations can be obtained from a simple elastic analysis of a basic structure such as a beam, as shown in figure 7. Consider the beam made up of elements of reinforced plastic, as shown, with a delamination at level x. At the vertical cross section through the beam at the affected zone we have in fact two beams, one with depth 'x' and another with depth '(d-x)'. The section modulus of the beam without the delamination is $db^2/6$. The section modulus of the beam with the delamination is

$$bd^2/6 - bx(d - x)/3$$

The modulus of the damaged section is symmetrical about the center plane and a maximum if the delamination is at this plane. That maximum modulus at $x = d/2$ is $bd^2/12$ or one half the undamaged modulus. If the delamination occurs near the upper or lower surface, its effect is much less. The total effect on the load carrying ability of the beam will depend on the position of the delamination along the length of the beam i.e. its position respective to the bending moments. In the cantilever beam shown a delamination at the point of support in the center of the beam would halve the load carrying ability of the structure. A delamination at the free end, of course, is immaterial.

Those two examples indicate the complexity of defect characterization in terms of properties. So let's measure properties directly. There are two types of properties which we shall consider here. One is the actual strength of a composite, the other a service modulus, which may or may not be the elastic modulus. In the case of metals, there is no relation between these two types of properties. However, in the case of plastics the degree of cross linkage and chain lengths appears to affect both

modulus and strength. An example of this relationship will be given later during this conference by Mr. Moore. However, in a composite the properties of the plastic matrix affect the properties of the composite to an approximate proportionate extent only, so that, generally, modulus measurements in a composite are not generally indicative of strength.

Two approaches have been found successful for the measurement of elastic moduli. The first is the measurement of ultrasonic velocity, which has to be corrected for density variations, at least in plastic matrix composites. As figure 8 shows, the relationship for metal matrix composites appears to be more direct. [10] In the case of plastic composites, Zurbrick[7] has shown good correlation of modulus with an acoustic velocity/density ratio. The other approach is by means of vibrational methods of much lower frequency and measurement of peaks and shifts of peaks indicative of resonant frequencies. This frequency is a function of both the elastic moduli and also of the geometry, so that for the varying geometry of various filament densities, for instance, a correcting factor must be introduced. That factor could, quite conveniently, be the density. The measurement of resonant frequency in variety of modes for the measurement of defects and dimensional geometry has been worked out by Draper[11] and has been applied to the inspection of complete plastic composite engine shrouds.

Vibrational methods depend on the availability of a wide spectrum exciter and vibration measurement device. The latter is less of a problem than the first. Capacitance microphones, optical systems and pressure sensitive transducers as well as more sophisticated methods such as the use of the Moessbauer effect or holography give a wide range of amplitudes and frequencies which can be scanned. Directly coupled drives such as tapping with the half dollar are also available for a wide range of frequencies but generally complicate accurate measurements. Noncoupling drivers are preferred. For system incorporating a metal, eddy current drives are suitable, and a supersonic nozzle and siren arrangement has been checked out for nonmetals, but further development is required.

The development of direct methods for the determination of strength is desirable not only from the point of view of an initial inspection, but also because of the intrinsically unstable properties of plastics, particularly under the influence of high stresses and elevated temperatures. Long term effects may be quite pronounced. Figure 9 shows the effects of exposure on tensile and interlaminate shear strength and indicates also the problem of extrapolating from one property measurement (here the tensile strength) to another apparently similar property (here the interlaminate shear strength).

Three roads to strength measurement appear, to me, to be open. One is the determination of filament density and void content, which for a given composite, does theoretically correlate with strength. A number of methods and combination of methods have been shown to be feasible for these measurements, such as radiography, microwaves, or ultrasonic velocity measurement. However, comprehensive correlations seem to be lacking. Several possible explanations for this lack of data appear feasible. For one assumption, that of "a given composite", in practice involves variables rather than a constant. Another explanation is that the destructive determination of composite strength is not without problems, even for simple shapes, and considerable spread of results has been obtained for allegedly similar composite specimens. Then there is the already mentioned resolution problem: was the nondestructively inspected area actually the same as the destructively inspected area?

The other road to strength determination is the measurement of damping. Now, the damping factor is the ratio of the energy absorbed per cycle of deformation to the total energy input per cycle. Attempts to correlate the strength of plastic composites with the damping or attenuation of ultrasound were reported as early as 1961 by Hastings, LoPilato and Lynworth [12]. They claim a correlation to within about 500 psi, equivalent to about 15%, but mention one of the major problems in using ultrasonic attenuation measurements: that of coupling between transducer and test part. Generally, that coupling has to be of a far higher standard than can be attained under industrial conditions to obtain repeatable and reliable results. Damping measurements at lower frequencies of vibration seem to be more promising. Again, if we knew more about the micromechanics of composites we could select optimum frequencies. The damping coefficient is given by the relationship

$$\delta = \frac{\omega\left[\tau_\epsilon \quad \tau_\sigma\right]}{1 + \omega^2 \tau_\epsilon \tau_\sigma}$$

where ω is the frequency and τ_ϵ and τ_σ are the relaxation times for stress at constant strain and for strain at constant stress respectively. The equation peaks at $\omega^2 \tau_\epsilon \tau_\sigma = 1$ and a frequency versus loss factor graph indicates a number of characteristic peaks, which can be associated with specific phenomena. Some of those peaks have been empirically determined and correlation with adhesive strength will be shown later. We are presently attempting to find strength related frequency peaks for m metal matrix composites.

In order to obtain reliable and repeatable results from vibrational methods, a number of factors must be borne in mind very clearly. First, resonant frequencies of structures are geometry dependent, which includes any clamping or constraints on the structure. Only rarely can such clamping be assumed to be rigid. Furthermore, changes in section, faying surfaces etc. will produce changes in resonant frequencies also in adjacent parts and this distance effect must be evaluated. Second, the fact that damping can be stress dependent must be considered. If such stress dependency exists over the test stress, then the variation in stress over the cross section under test loading must be considered. For instance in bending this stress varies from a maximum tensile stress to zero to a maximum compressive stress. Correction integrals are available from most vibration handbooks. Third, the nature of relaxation time must be understood. Relaxation time can be related to an activation energy and the temperature by an exponential relationship. The activation energy will determine the relative effects of temperature variations on relaxation time and hence on damping. This energy appears to vary both for the type of plastic and also its cure state.

Finally, a measurement of the plastic related part of the composite strength may be obtained by measurement of chemical bond related factors of the plastic. Methods studied include nuclear magnetic resonance.[13] Both studies of the polymerization process and studies on tracers embedded in the plastic have been carried out. Instrumentation limitations and lack of sensitivity in tracers seem to limit these methods at present to the laboratory.

The real advantage of property related NDT methods over defect related NDT methods lies in the fact that such property related methods could be utilized for a much broader field than the inspection of products. Such methods could become part of the actual production cycle and be used to control processing parameters to fabricate products known to conform to a desired standard. Vibration methods, for instance, could be used <u>during</u> the cure cycle and control through suitable feedback loops to actual cure processing, amplifying or even, eventually, replacing parametric control.

We have been dealing here with the interaction of two areas, both of which are in a state of rapid flux and growth: composites and NDT. It is therefore not surprising that the above comments are studded with "feasible", and "promising" and "somebody should". The first two are characteristic of our optimism, that there is a better way. The latter is a measure of our personal involvement with the problems and the hope that we ourselves might be part of that search for a better way.

REFERENCES

1. Anon., Reinforced Plastic and Composites World, V. 6, No. 5, 1967, p. 14

2. Anon., Release by the Reinforced Plastics/Composites Division of the Society of Plastics Industries, Inc.

3. Aukward et al. "Change in Electrical Resistivity of some High Polymers during Isotherm Polymerization", J. Polymer Sc., Jan 1958

4. Delmonte "Electrical Properties of Epoxy Resins during Polymerization" Epoxy Resin Symposium of SPE, Minneapolis, October 1958

5. Lee and Neville "Handbook of Epoxy Resins", Publ. McGraw and Hill, NY 1967

6. Grodstein "X-ray Attenuation Coefficients from 10 keV to 100 keV" National Bureau of Standards Circular 583, 1957

7. Zurbrick, "Development of NDT Methods for the Quantitative Evaluation of Glass Reinforced Plastics", AFML-TR-66-269, March 1967

8. Hagemaier "NDT of Silica - Phenolic Materials for Small Ablative Thrust Chambers "Symposium on Testing Techniques for Filament Reinforced Plastics, Sept. 1966

9. Hedgepeth "Stress Concentrations in Filamentary Structures" NASA-TN-D-882, May 1961

10. Martin and Moore "The Nondestructive Testing of Metal Matrix Composites" to be published by ASTM

11. Draper "Application of Stiffness Method of Solution to a Flat Plate to find Frequencies and Nodal Patterns using Square Elements", Rolls Royce Report ASR 2668, 1963

12. Hastings, LoPilato and Lynnworth "Ultrasonic Inspection of Reinforced Plastics and Resin-Ceramic Composites", American Society for Metals, Western Metals Congress, Los Angeles, March 1961.

13. Mazelski "Nondestructive Inspection of Reinforced Elastic Structures by Nuclear Quadrupole Resonance Method, Part II, ARA Report 91A, Naval Air Systems Command, Contract N 00019-67-C-0415, 1967

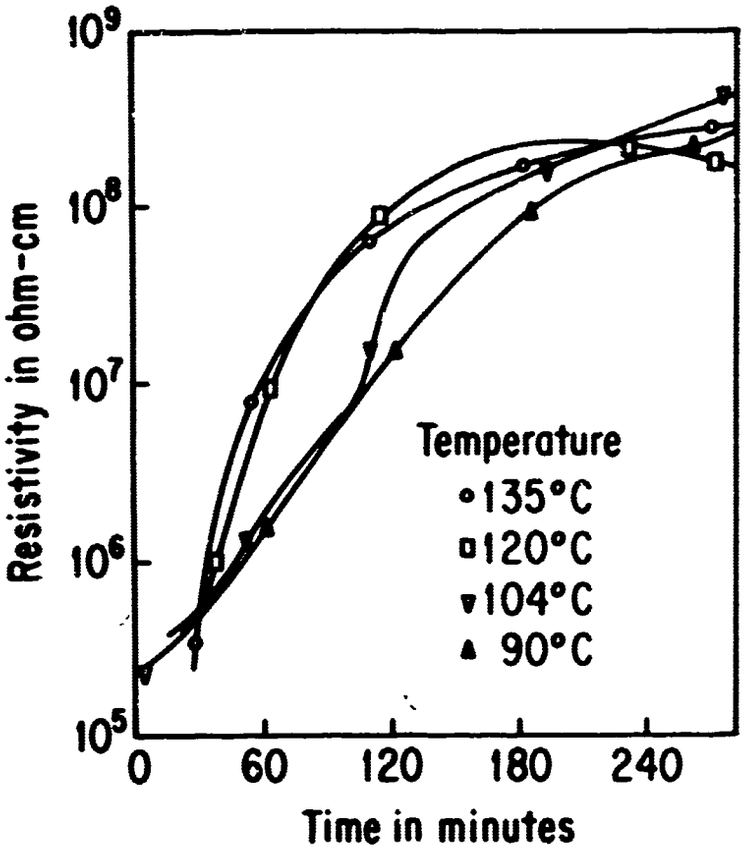


Figure 1. Volume Resistivity During Isothermal Polymerization of Epoxy

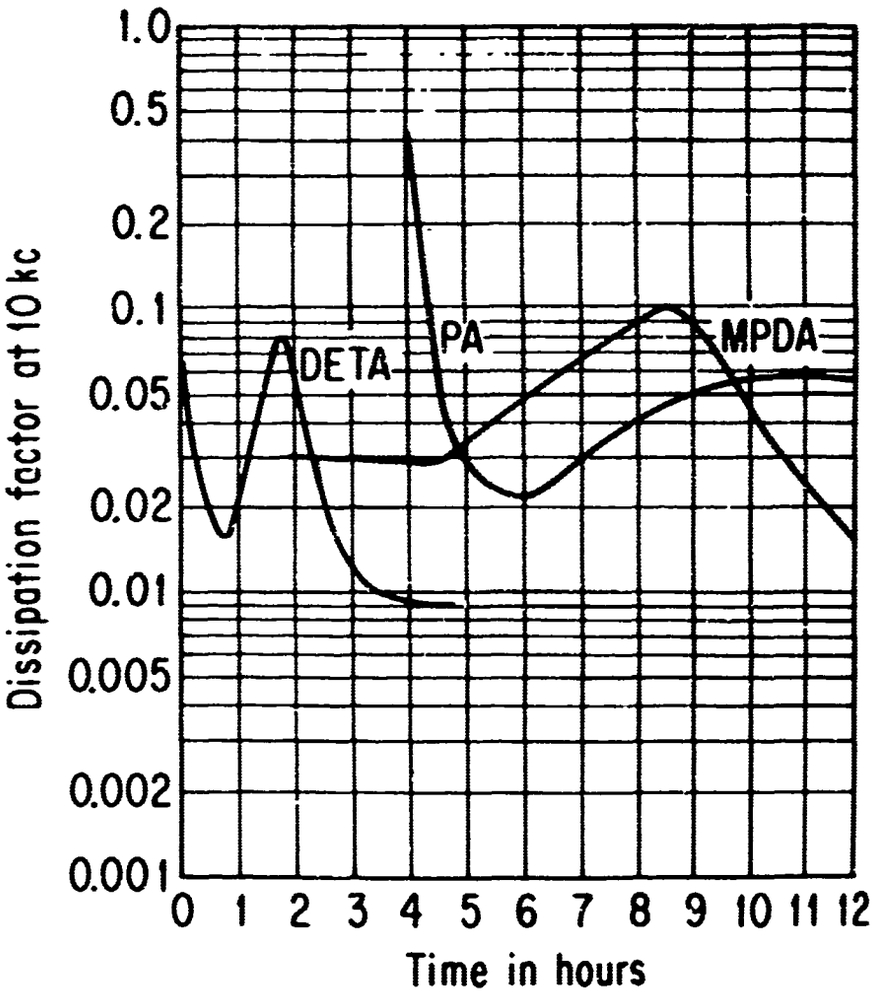


Figure 2. Dissipation Factor of Epoxy During Polymerization with Various Curing Agents

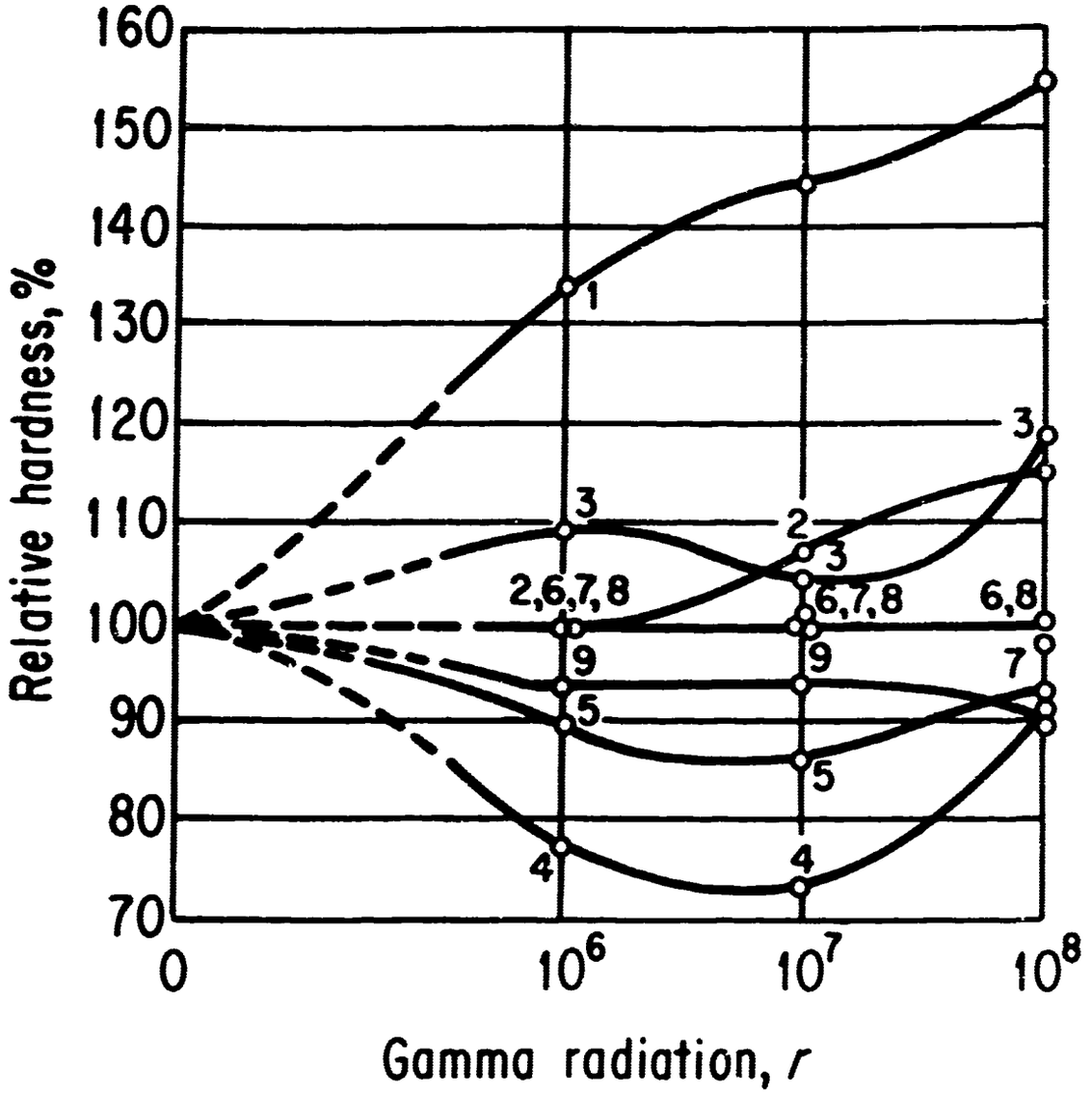


Figure 3. Effects of Gamma Radiation on Hardness of Epoxy Systems

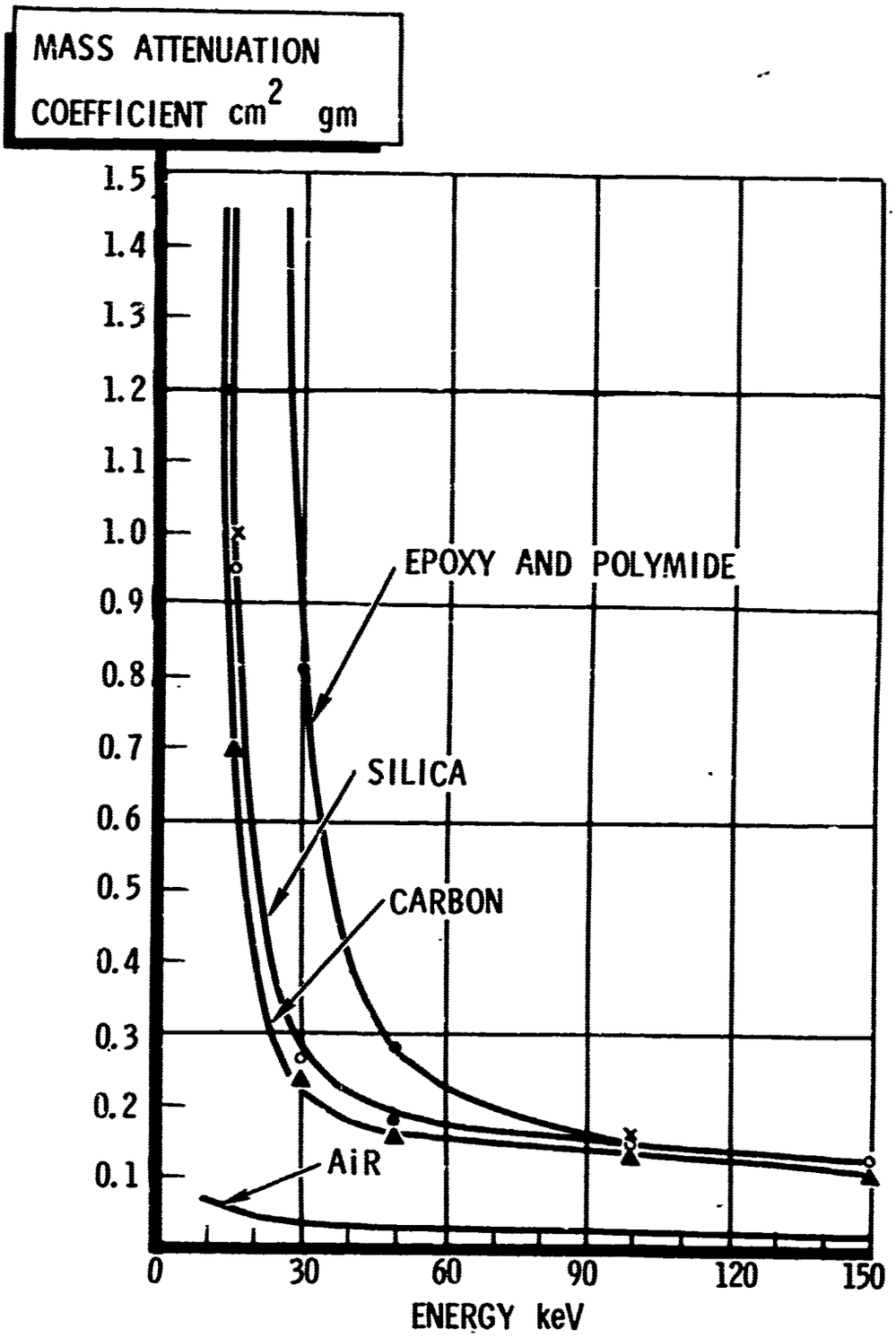


Figure 4. Mass Attenuation Coefficients

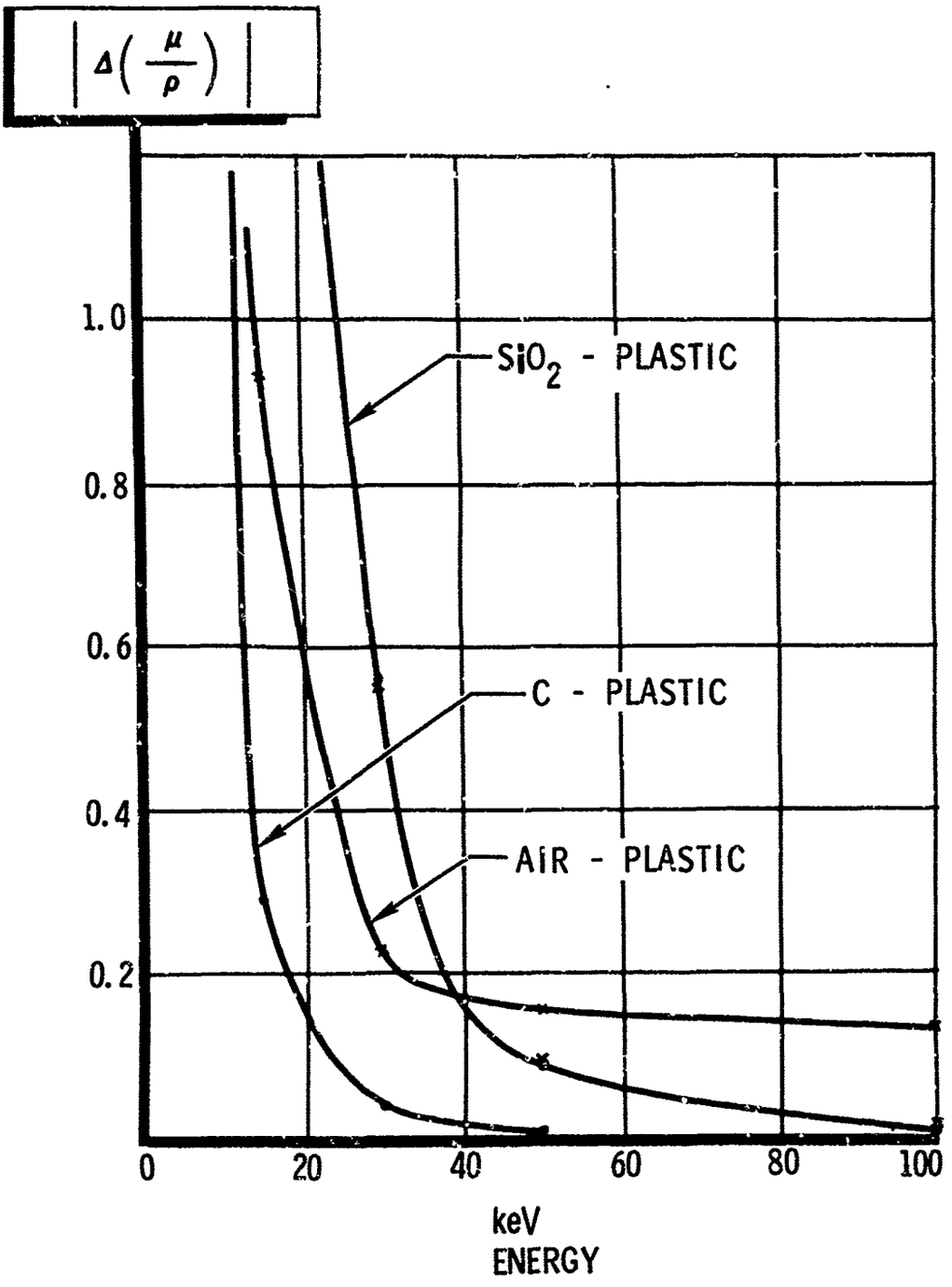


Figure 5. Relative Difference in Xray Mass Attenuation Coefficients

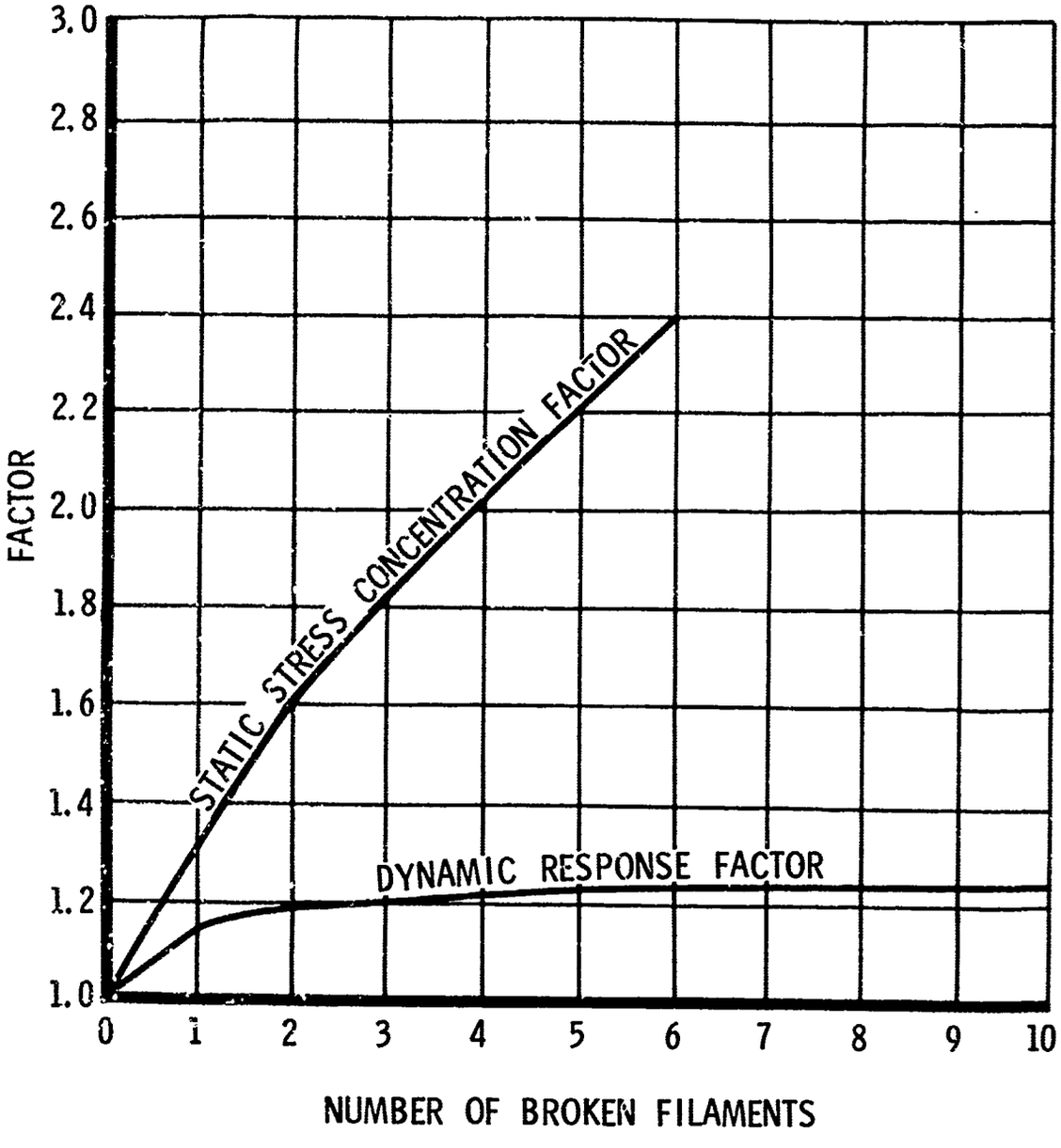
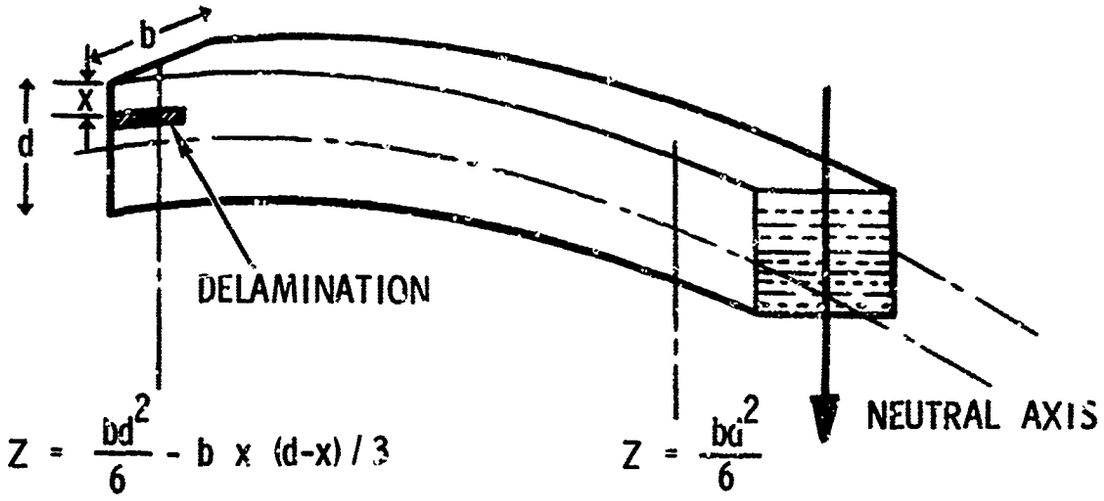


Figure 6. Stress Concentration and Dynamic Response Factors Due to Failure of Individual Filaments



$$\text{MAX. ELEMENT STRESS} = \frac{Z}{\text{BENDING MOMENT}}$$

Figure 7. Effects of Delaminations on Composite Beam Strength

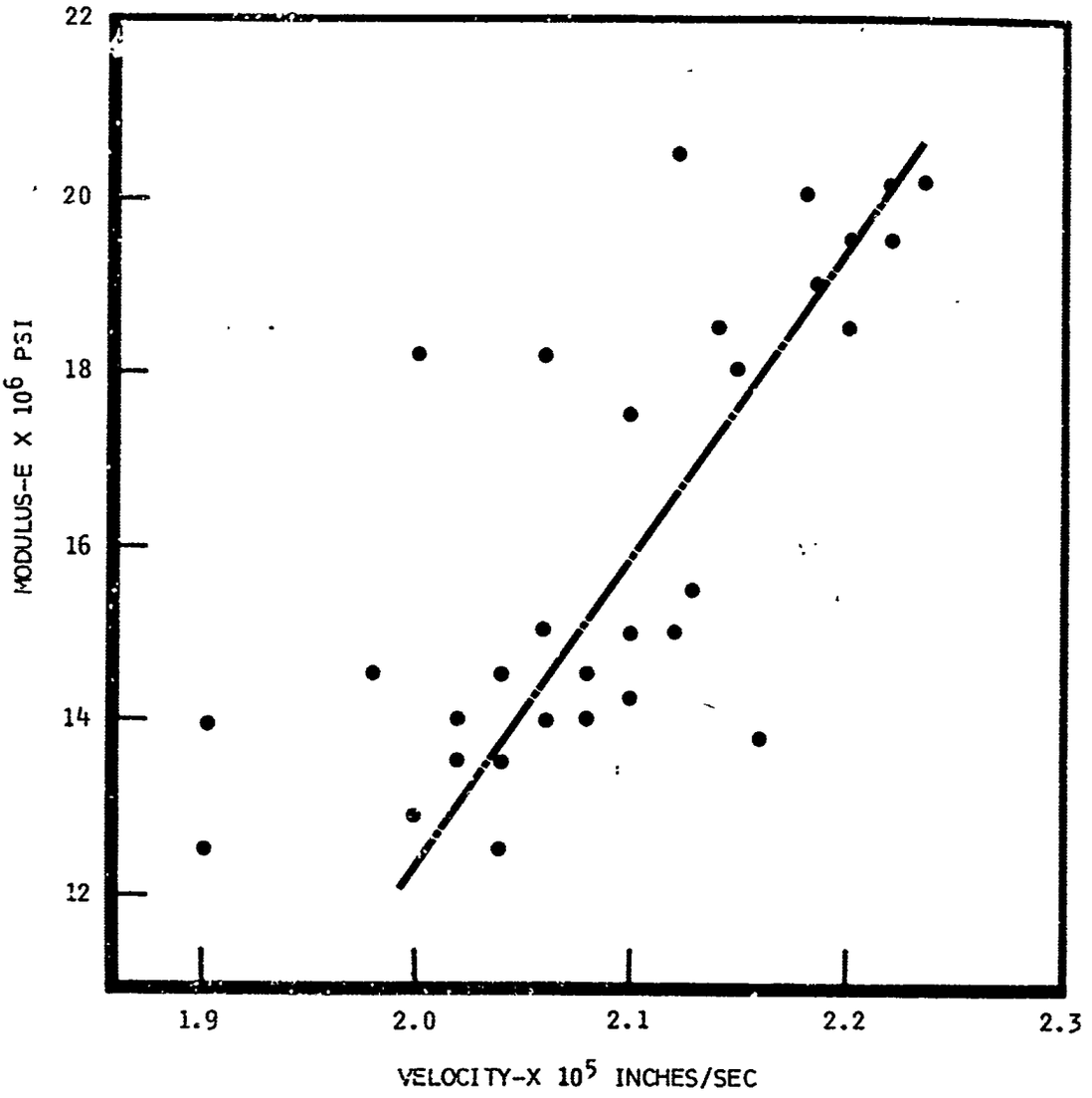


Figure 8, Relationship Between Acoustic Velocity and Elastic Modulus of B-Al

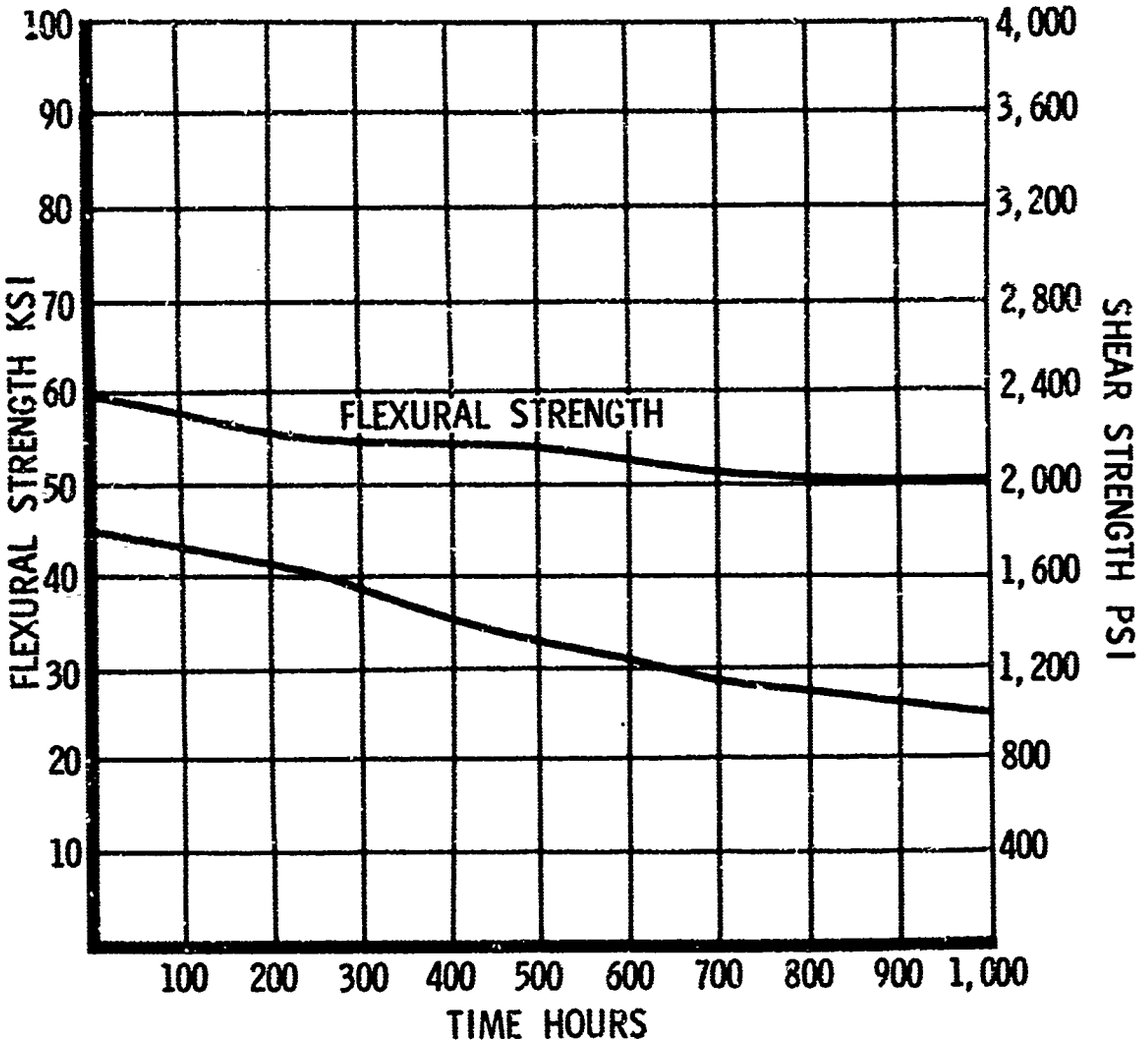


Figure 9. Flexural and Interlaminate Room Temperature Shear Strength of Polymide After Elevated Temperature Exposure For Given Time

TRW ACOUSTO OPTICAL IMAGING NON-DESTRUCTIVE TESTING TECHNIQUE

by

Robert Aprahamian
Pravin G. Bhuta
Applied Mechanics Laboratory
TRW Systems Group
Redondo Beach, California

For Presentation at the
Symposium on Nondestructive Testing
Dayton, Ohio
March 18, 1969

ABSTRACT

The subject of this paper is to describe the technique of TRW Acousto-Optical Imaging and its application to non-destructive testing. During the last few years interest in the area of non-destructive testing has greatly increased. This has been due to the fact that it is no longer sufficient to know whether or not a flaw exists in a material but also one now needs to know the location of the flaw and its dimensions in the test specimen. Current techniques, while being able to serve in the former capacity, are lacking in the latter.

A new technique, termed Acousto-Optical Imaging, is described whereby the information contained in the distorted acoustic wavefronts which have traveled through a body can be made into a visual image by its interaction with light (Bragg Reflection). The theory of Acousto-Optical Imaging is presented describing the Bragg Reflection phenomenon and the analytical equations which govern the characteristics of the system derived.

Also included in this report are the results of several tests performed on metal and metal-plastic composite samples which conclusively establish the capability of TRW Acousto-Optical Imaging to determine the existence of a flaw as well as its size. This technique has an advantage over other techniques in that it provides a real time visual image of flaws contained in the interior of a body either optically transparent or optically opaque. Since a visual image can be made to project onto a viewing screen one may record this image in various ways--most notably on conventional photographic film. This then allows one to monitor the image in either real time or at his leisure.

Since this technique uses only acoustic waves and light waves there is no danger to human personnel as with x-ray techniques.

INTRODUCTION AND SUMMARY

The detection and identification of flaws, such as cracks and inclusions in structural members can sometimes present insurmountable problems to manufacturers and quality assurance personnel. For some products, such as helicopter blades, jet engine turbine blades and critical welds in submarines, the detection and identification of these flaws may well be a matter of life and death. There are many non-destructive testing techniques presently employed throughout industry to detect defective products. Well known among these are x-ray techniques and ultrasonic methods. As is the case with other NDT techniques, these two methods have limited use. In the case of x-rays, the information recorded is essentially a measure of the amount of x-ray energy absorbed or scattered by the material as the x-rays passed through its thickness. Hence, for a very narrow crack, very little x-ray energy may be absorbed, thus allowing the crack to go undetected. While it may sometimes be possible to deduce information regarding the width of an internal flaw by x-rays, no information related to its depth is obtained. In conventional echo ultrasonics one relies on the acoustic reflective properties of flaws to obtain information; generally, depth information may be obtained but not size. For both techniques, of course, well trained observers are required and still the results of a testing program are quite subjective.

In this paper, the results of applying a technique which may be used to provide a three-dimensional image of the interior of an optically opaque but at least partially acoustically transparent body is presented. This technique, is termed Acousto-Optical Imaging.

To use this technique, in a conventional sense, one transmits ultrasonic waves through the material to be tested. Due to the inhomogeneities in the material, these waves, as they propagate through the medium, undergo absorption and scattering resulting in an alteration of their wave fronts. The sound waves which do emerge from the body are then made to interact with a beam of monochromatic light in a coupling medium (usually water). This interaction causes the light wave to undergo a frequency modulation resulting in a series of optical sidebands. By optically processing any one of these sidebands, a visual two-dimensional image of the interior of the object is produced on a viewing screen. The advantages of this technique over other non-destructive methods lie in its ability to afford visual images of flaws in real time. Thus size as well as depth information may readily be obtained.

THEORY OF ACOUSTO-OPTICAL IMAGING

Background

The interaction of light and sound was postulated in 1922 by Brillouin.[1] He reasoned that since a train of acoustic waves represented cyclic regions of relative compression and relief a situation very similar to a common optical diffraction grating would exist. Perhaps due to the lack of proper instrumentation, experimental verification did not occur until 1932 when Sears and Debye[2] succeeded in demonstrating the phenomenon. The immediate applications of Brillouin scattering, as the phenomenon has become known, lie in the area of determining the elastic properties of liquid materials. Many research papers (e.g. Ref. 3) were written relating critical parameters such as acoustic power density, the amplitude and wave length of light, and of more concern to us here, the angle at which the light wave interacts with the acoustic waves and the distance over which the light and sound waves interact. We will see that these two parameters have a pronounced effect on Acousto-Optical Imaging.

Interaction of Light and Sound

In order to fully describe the interaction of light with sound, one must understand the mechanical properties of sound. Simply stated, a train of sound waves is comprised of cyclic regions of relative compression and relief. Over the distance of one acoustic wave length, Λ, the material supporting the acoustic wave experiences a change of pressure, P, density, ρ, and index of refraction, n, ranging from a maximum to a minimum and back again to a maximum as depicted in Figure 1 for a plane acoustic wave.

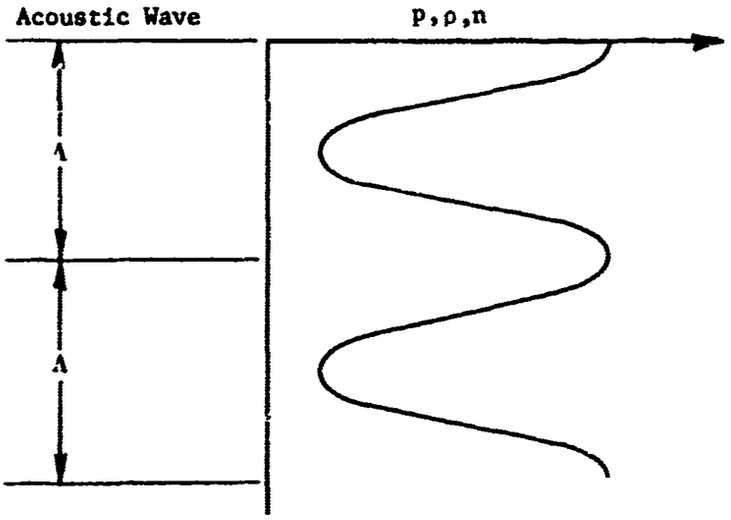


Figure 1. Pressure, density and index of refraction distribution as a function of position for a plane acoustic wave train of wave length Λ.

1. Sears-Debye Condition

Consider now a set of plane monochromatic light waves impacting a acoustic column of width, d. Since the velocity of light, c, depends on the index of refraction of the medium in which it is propagating according to

$$c = \frac{c_o}{n} \qquad (1)$$

where c_o is the speed of light in vacuo, and n the index of refraction, the light will experience a time delay and a phase shift as it propagates through the acoustic wave column. As a consequence of the refraction being a function of position in the acoustic wave train and the fact that the acoustic wave is moving, each point in the material experiences a cyclic time variation of its index of refraction. As a result, the incident light becomes modulated in phase and also in frequency. It can be shown that if the acoustic column is sufficiently narrow, a carrier wave having the frequency of the incident light and a set of sidebands will emerge from the acoustic column as depicted in Figure 2.

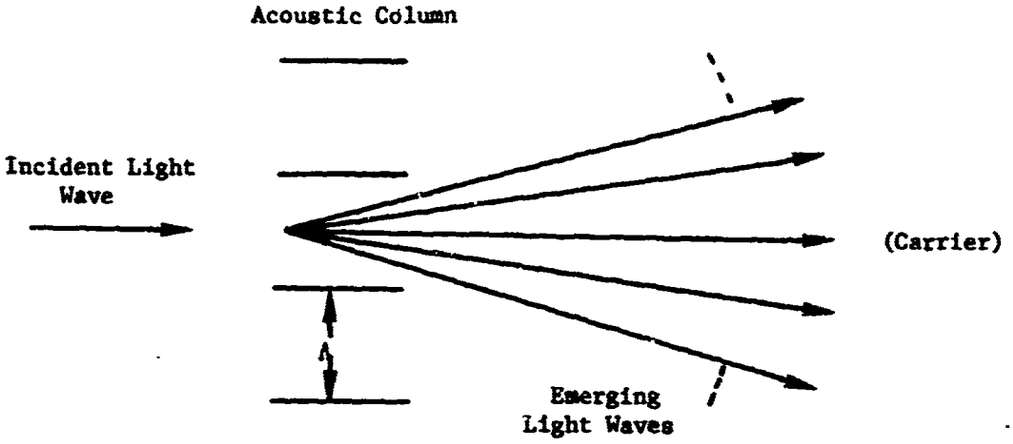


Figure 2. The Creation of Sidebands Caused by Frequency Modulation on Incident Plane Light Wave by a Plane Acoustic Wave Train.

The phrase "sufficiently narrow" was used above to describe the width of the acoustic column. The reason for this lies in the fact that the incident light breaks up into its sidebands immediately upon entering the acoustic column and begins to diverge angularly from the carrier. It may then travel through parts of the wave front having different indices of refraction. As a result, destructive interference may occur and the intensity of these bands will be greatly reduced. It is possible to use the interference phenomenon to our advantage by simply impacting the acoustic column with light waves at a properly chosen angle so constructive interference will occur.

2. Bragg Reflection

To describe constructive interference we need to consider Bragg reflection. Bragg's law expresses the condition under which a crystal or any diffraction grating will reflect an incident wave with maximum intensity. Mathematically, the condition is expressed as

$$\sin \theta_B = \frac{N\lambda}{2D} \qquad (2)$$

where

θ_B = Bragg angle
N = integer
D = grating spacing
λ = wave length of incident wave

Physically, this condition insures that parts of the wavefront which reflect from different strata of the grating are in phase when they recombine. Figure 3 shows schematically the Bragg reflection process when Λ is the grating spacing.

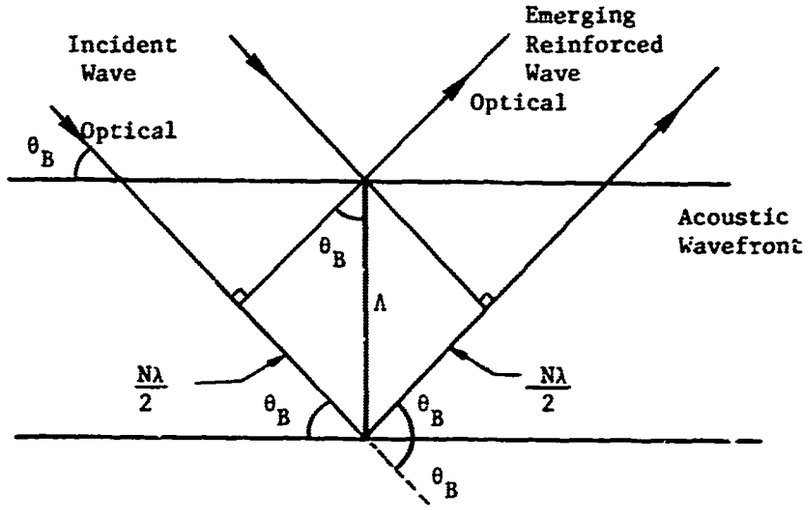


Figure 3. Bragg Condition for Constructive Interference

As seen in the Figure, the path length difference of the wave which reflects from the top stratum, and the second stratum is $N\lambda$. This insures constructive interference when these waves recombine. Bragg reflection, as described here, is the basis for acousto-optical imaging.

ACOUSTO-OPTICAL IMAGING

Consider a point source of sound, S, from which single frequency acoustic waves are emanating and also a point source of light, 0, from which monochromatic light waves are emanating. In the region where the spherical wave fronts of light and sound satisfy the Bragg equation, $\sin \theta_B = \lambda/(2\Lambda)$, maximum reinforcement will occur. If one then traces back these diffracted rays, one finds that they intersect at a single point. Mathematically, this condition is identical to there being a new spherical wave emanating from a point 0'. This point at 0' is then considered to be the virtual image of the sound source, S. Figure 4 depicts this situation for N = 1. Three propagation vectors (→) are shown leaving the light source, 0, which interact with three propagation vectors (⇢) which emanate from the sound source, S, at the Bragg angle θ_B. At these points, diffracted light rays (⇢) are created which when traced back (- - -) intersect at a common point, 0'.

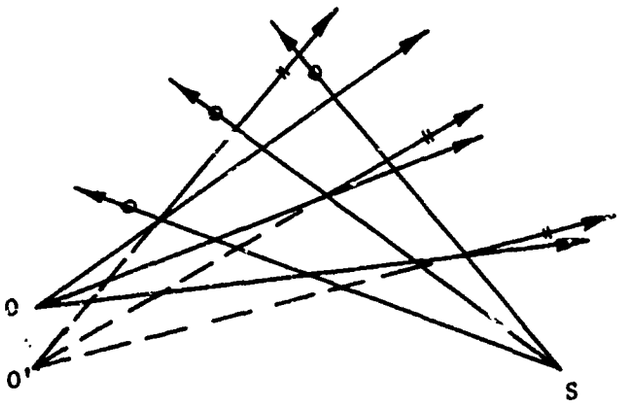


Figure 4. Acousto-Optical Imaging of a Sound Source, S, by a Light Source 0, to Produce a Virtual Image 0'

Of course if there were more than one sound source, say S^1, S^2, S^3,..., then multiple images, O_1', O_2', O_3',... will be created. Reference 4 shows that a magnification, M, given by

$$M = \frac{\lambda}{\Lambda} \qquad (3)$$

will result. For example, if sound sound sources S^1 and S^2 were separated by a distance S^1S^2, then their images will be separated by a distance $\lambda/\Lambda\ S^1S^2$. This concept may be generalized to a body merely by considering the body to be made up of many "point" sources, each giving rise to an image. The sum of these images will represent a three-dimensional image of the object.

Figure 5 shows a typical laboratory setup used for TRW Acousto-Optical Imaging. An object is placed in a tank containing a good acoustic wave transmitter, usually water. This we will refer to as a wave coupler or Bragg Cell. Attached to the bottom of the tank is a transducer which generates acoustic waves when excited by a generator. These waves pass through the object and in so doing "excite" every point of the object. These points then in turn also act as sound sources. As a result, sound waves which are a superposition of all the point sound sources within the object are emitted from the object.

Using a proper monochromatic light source, e.g., a laser, one may induce Bragg reflection from each of these waves thereby obtaining an image of <u>every</u> point of the object.

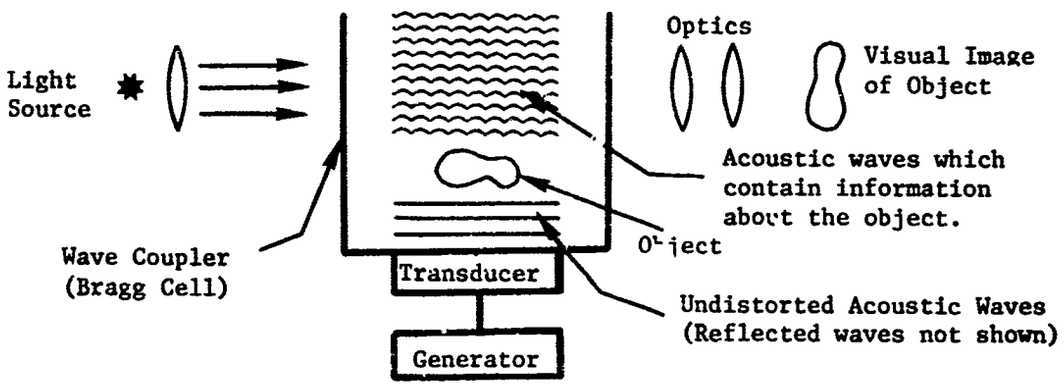


Figure 5. Acousto-Optical Imaging of a Solid Body Which is at Least Partially Transparent to Sound

As is shown in Figure 5, a three-dimensional image of the object is visually displayed. The object's image undergoes magnification according to $M = \lambda/\Lambda$. By using proper optics, one may view the object by focusing on various planes of the image and also induce desired magnification or demagnifications.

The resolution of the acousto-optical images is on the order of the wavelength of the sound source in the media, wherein the light and sound interact. Since

$$\Lambda = \frac{V}{f} \qquad (4)$$

where

V = velocity of sound in the coupling media
f = frequency of sound (cps)

it is advantageous to use ultrasonic waves for high resolution.

EXPERIMENTAL RESULTS

The results of two non-destructive testing experiments using the apparatus as shown in Figure will be discussed in this section. The first experiment was performed on a 6" x 1" x 1/4" prismatic beam having a surface crack extending across its width. The second experiment involves a laminated aluminum-plastic structure containing debonded areas.

Rectangular Beam - Crack Detection

The specimen was cut from a 1/4" thick sheet of 6061-T6 aluminum stock. A jewelers' saw was used to saw a 1/4" cut into the two edges. Next, a weight was attached to one end of the beam and placed on a shaker so as to vibrate the beam in its fundamental mode. As a result, a surface fatigue crack was formed across the width of the beam connecting the two saw cuts. The saw cuts were then cut from the specimen. Figure 6 is a photograph taken of the specimen containing the saw cuts and the crack.

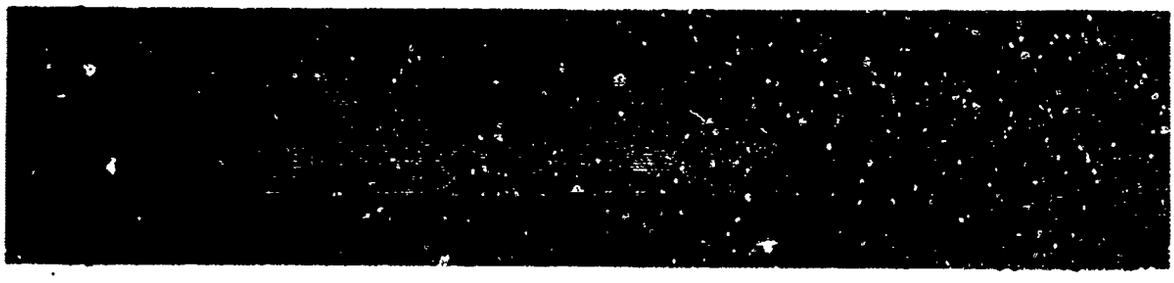


Figure 6. Beam Specimen Containing a Surface Crack Across Its Width

Figure 7 shows a series of three photographs. The first one was taken of the viewing screen with the apparatus turned on but no object placed in the Bragg cell. Essentially it represents an image of the transducer. The second photograph was taken of the viewing screen when a portion of rectangular beam which did not contain the crack was placed between the acoustic transducer and the converging cone of light. In the last photograph, the beam was placed such that the crack did perturb the sound waves before they interacted with the light cone. By comparing the second two photographs, one may readily identify the crack.

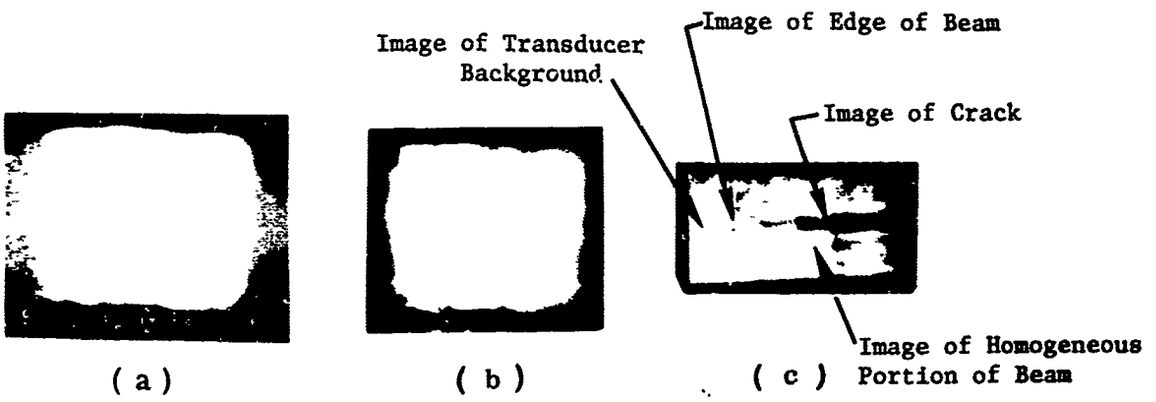


Figure 7. (a) Acousto-Optical Image of the Transducer
(b) Acousto-Optical Image of a Portion of the Beam Containing no Cracks
(c) Acousto-Optical Image of a Portion of the Beam Containing a Crack

Composite Specimens

The TRW Acousto-Optical Imaging technique was used to identify debonded areas in a specially prepared composite specimen. The specimen was made by bonding a 1/8th inch thick plate of plastic (Plexiglas) to a 1/8th inch thick plate of aluminum in such a way that two areas remained unbonded (Figure 8). Eastman 910 was used as the bonding agent.

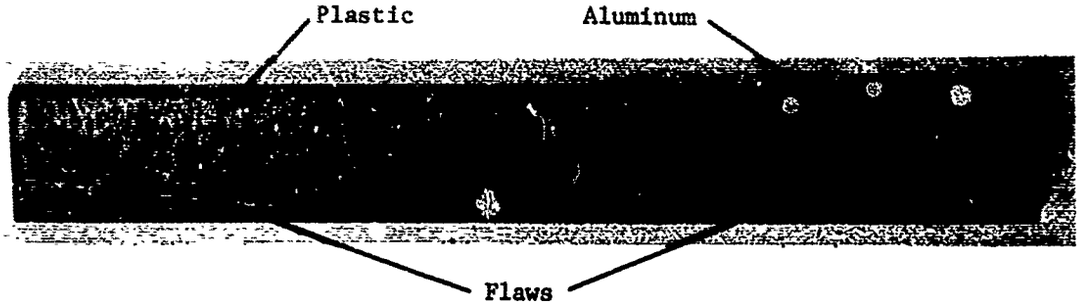


Figure 8. Laminated Beam Structure Used to Demonstrate the Ability of TRW Acousto-Optical Imaging to Detect Debonded Areas

When the specimen was subjected to the TRW Acousto-Optical Imaging non-destructive testing technique, both flaws were identified as shown in Figure 9.

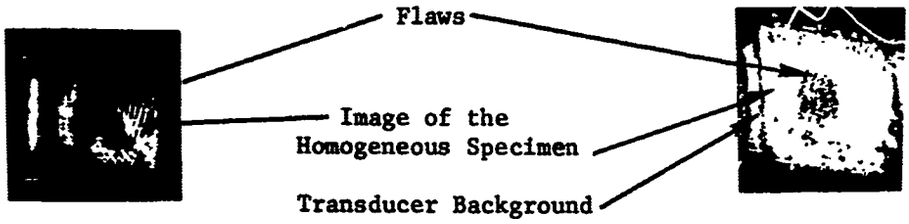


Figure 9. Images of the Debonded Areas Between the Interfaces of a Composite Structure

As a final experiment a layer of 1/8th inch thick aluminum plate bonded to the composite specimen shown in Figure 8. This specimen, Figure 10, was then subjected to the Acousto-Optical Imaging technique.

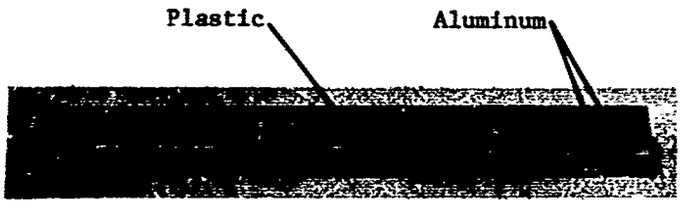


Figure 10. Sandwich Specimen Used to Demonstrate the Ability of TRW Acousto-Optical Imaging to Identify Debonded Areas

Again the debonded areas between the plastic and first layer of aluminum were visually displayed, Figure 11.

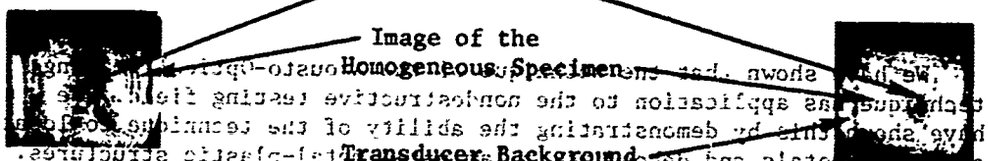


Figure 11. Acousto-Optical Image of Two Areas of Debonding in a Composite Structure

By comparing Figures 9 and 11 it is evident that the same areas of debonding were identified.

CONCLUSIONS

We have shown that the technique of the Acousto-Optical Imaging technique has application to the nondestructive testing field. We have shown this by demonstrating the ability of the technique to locate cracks in metals and debonding in laminated metal-plastic structures. It is felt that this technique as with other ultrasonic techniques has use at least on plain geometrical surfaces. However, additional elements will need to be included into the system if one wishes to image through more complicated geometries, e.g. cylindrical or spherical. Conventional methods used in ultrasonic testing techniques which are used to couple acoustic energy into bodies of complicated geometries should also be applicable for use in this system.

REFERENCES

1. Brillouin, L., Ann. Phys. (France) Vol. 17, pg 88 (1922).

2. Debye, P. and Sears, F. W., Proc. Nat. Acad. Sci. (USA), Vol. 18, pg 409 (1932).

3. Willard, G. W., J. Acoust. Soc. Am., Vol. 21, pg. 101 (1949).

4. Aprahamian, R. and Bhuta, P. G., "TRW Acousto-Optical Imaging Tunnel Detection System," TRW Report 99900-6677-RO-00, July 1968.

MICROWAVES IN NONDESTRUCTIVE TESTING

by

Robert W. Cribbs
General Manager
Electro-Physics Co.
Folsom, California 95630

For Presentation at the
Conference on NDT of Advanced Plastic/Composite Structures
Dayton, Ohio
18-20 March 1969

MICROWAVES IN NONDESTRUCTIVE TESTING

Introduction and Summary

Until recently most applications of microwaves to nondestructive testing utilized continuous-wave, single-frequency signals. This paper describes a microwave technique with depth resolution; that is an ultra-high resolution radar.

The Frequency Domain Interferometer (FDI) combines the characteristics of the interferometer and radar. It has the ability to measure distance to a small fraction of a wavelength, and can produce a simple display which may be interpreted in the same way as with the more familiar radar and pulse-echo ultrasonic instruments. The primary display of the FDI is an oscilloscope trace with the horizontal scale representing distance to the reflecting targets, and the height of the peaks representing the strength of the reflections from them. The device is thus usable for detecting flaws in dielectric solids and also for measuring distance. The latter gives rise to a very convenient method for determining refractive index directly.

The increasing use of nonmetallic materials in Aerospace industries has caused severe problems in nondestructive testing. Since many of the nonmetallic structures are composites, a new class of defects has risen to prominence. It has been found that the conventional nondestructive test techniques are seldom satisfactory for such materials.

Since the new nonmetallic composites are usually transparent to microwaves, the use of microwave testing is obviously promising. Consideration of the basic interactions of microwaves and solid dielectrics shows that most of the defects expected in nonmetallic structures will have some effect upon a microwave beam. In fact, the situation is similar to that encountered in ultrasonic testing except that microwaves can traverse empty space and, of course, do not penetrate significantly in electrical conductors. The principal disadvantage of microwaves had always been one of equipment and technique. Much of the success of ultrasonic testing has been a result of the relative ease with which pulse-echo measurements can be made. The speed of electromagnetic waves, however, is so great that it is difficult, if not impossible, to generate the short pulses required. Thus, while fairly good definition of beam cross section is possible, it had always been a problem to obtain adequate depth resolution.

With the Frequency Domain Interferometer it is possible to produce an oscilloscope display quite similar to that of a pulse-echo ultrasonic test unit, and to interpret it in exactly the same manner. Depth resolution can be obtained down to a small fraction of a wave length, and under favorable conditions this can mean as little as $\pm$ .1 mm.

Microwaves readily penetrate most commercial plastics and glass reinforced structures. Penetrations of 5 feet (10 feet path length) into solid rocket motor propellant have been achieved. Delaminations down to 2 mils have been detected and located.

Microwave Technique

Two microwave techniques will be described: continuous-wave and frequency modulated. A continuous-wave reflectometry technique was used to detect delaminations and separations. This technique has the advantage of simplicity and illustrates the defect sensitivity that can be obtained. However, the range or depth of the defect cannot be determined. The CW technique is applicable to thin laminar structures where there is a priori knowledge of the depth of the defect, if any, or a defect at any depth is cause for rejection.

Defect Sensitivity - C.W. Technique

To determine defect sensitivity a specimen with built-in defects was constructed. The specimen consisted of a 3-foot length of the cylindrical section of a solid rocket chamber cast with propellant. The case is a quarter-inch thick glass filament-epoxy composite lined with a quarter-inch thick rubber insulation. This specimen has as 8" web and cylindrical-core grain. The specimen has a case-insulation separation, a bonded insulation patch, an unbonded patch and insulation-propellant separations. The insulation-propellant separations were made by waxing steel shims to the case wall and withdrawing them after cure. Shims of .025", .020", .015", .008", and .002" thickness were used.

After curing, the specimen was placed on a turntable and scanned as shown in Figure 1. The turntable rotates and also moves vertically.

The detection of delaminations and separations depends upon the change in reflection coefficient which results from the sharp discontinuity in dielectric constant between air and glass, insulation, or propellant. The directional coupler allows only the reflected signal to reach the crystal detector. This signal consists of a large reflection from the outer surface of the case, and smaller ones from the glass-insulation and insulation-propellant interface. If any unbond occurs, the reflection is increased. Of course, the spacing of the

interfaces is critical, and the frequency must be chosen so that the reflections from two discontinuities will not be 1/4 wavelength apart and be cancelled out by destructive interference.

Figure 2 shows scans of a region free from defects, or at least free from insulation-propellant separations. There is some evidence of more subtle defects which are not well resolved. Figure 3 shows an adjacent area which contained a separation produced by withdrawing a 25 mil shim 6" wide which had been waxed and stuck against the case during cast and cure. As can be seen, this defect is clearly mapped out.

Figures 4 and 5 show scans of the other separations. Figure 4 is especially interesting. Note that the indications for .025", .020", and .015" separations are almost identical. Theoretically, as long as there is an air film present, the thickness of it should have little effect so long as it does not become significant compared to a quarter-wavelength. Examination of the scans of the .008" and .002" separations, as well as Figure 5 which shows the .008" separation at a different point and higher gain offers some explanation for the poor resolution of the thin separations. As the separations become thinner, there is evidence of a tendency to close up at the center. In all probability it is reduced area of actual separation rather than the thinning of the separations which accounts for the weak indications for the .008" and .002" separations.*

Figure 6 shows an insulation-case separation. This defect was produced by slitting the insulator, and wedging a screwdriver between case and insulation to form a pocket. The adhesive was removed with trichloroethylene, the pocket dusted with talcum to prevent re-bonding and the slit sealed with neoprene cement. While it has not been possible to X-ray the specimen as yet, it is believed that the shape of this defect is roughly as follows after cure. The entrapped bubble of air, somewhat compressed, should be at the top of the defect. At the bottom there is a lump of glass-epoxy scrapings and talcum. The result should be two cavities joined by a separation of varying thickness. The irregular indications shown in Figure 6 are in good agreement with the probable structure of this defect.

*Later experiments with the f.m. technique at a higher frequency (Ka-band; 26.5 to 40 GHz) more clearly resolved the edges of the 2 mil separation. These measurements verified that the defect closedup in the center.

These experiments, as well as others, illustrate that laminar separations as small as 2 mils thick can be detected. They also illustrate the basic difficulty of the C.W. technique. There is no way to determine which interface is separated. The indications could be due in this case to delaminations in the case, case-to-insulation separations, delaminations in the insulation, or insulation-to-propellant separations.

The F.M. Principle

It is natural for NDT practitioners whose attention is drawn to microwaves to consider the possibility of ranging defects with a pulse-echo device. What is needed, it would appear, is an ultra-high resolution radar. The radar beam would be directed into the dielectric being inspected. Any discontinuities would reflect back a portion of the pulse, and the time of arrival of the reflected pulse could be used to locate the defect. To get high resolution, it would be necessary to produce a pulse as short in duration as possible.

There are both practical and theoretical difficulties in building such a system. A more general analysis of the problem shows that a large microwave bandwidth is all that is required for high resolution. A convenient way to get this is to linearly sweep the microwave transmitter frequency as shown in Figure 7. The microwave signal travels down the waveguide and reflects off discontinuities in front of the horn. The crystal detector then sees two signals, the transmitted signal and the reflected signal.

The detector output contains the sum and difference frequencies. Since the sweep is linear, the difference frequency is a constant as shown in Figure 8. A mathematical analysis shows the detected signal for a single reflector to be:

$$S_d(t) = A \cos (w_o - w't)\tau \qquad o \leq t \leq T \qquad (1)$$

$$S_d(t) = o \qquad T < t \leq T_r$$

A = the amplitude

$w_o = 2\pi f_o$ = the starting microwave angular frequency

$w' = \frac{w_o - w_1}{T}$ = the microwave sweep rate

τ = the time of travel of the microwave signal from the detector to reflector and back to the detector

t = time

T = sweep duration

T_r = sweep repetition period

As can be seen the frequency ($w'\tau$) is proportional to τ, hence distance. Furthermore, the phase ($w_o\tau$) is proportional to distance.

It would appear that several reflectors in the beam could be resolved by frequency analyzing the signal. A natural device for doing this is a spectrum analyzer. The power spectrum of the signal from one reflector is:

$$P_s(m) = \frac{1}{2T_r^2} \frac{\sin^2\left(\frac{\pi m}{T_r} - \frac{w'\tau}{2}\right)T}{\left(\frac{\pi m}{T_r} - \frac{w'\tau}{2}\right)^2} \qquad (2)$$

where $P_s(m)$ = power at frequency $\frac{2\pi m}{T_r}$

m = an integer

Note that the phase information in the received signal is lost, i.e., there is no $w_o\tau$ term. Furthermore, the spectrum is a line spectrum. For example, if T_r were 0.001 sec, there would be power only at harmonics of one Kilohertz. Finally note that the power spectrum is always positive.

The FM Microwave Interferometer does not take the power spectrum. A cross-correlation detector is used. Its output is:

$$C(w) = \frac{\sin\left[(w - w'\tau)\,T + w_o\tau\right) - \sin w_o\tau}{w - w'\tau}$$

where $C(w)$ = cross-correlation detector output

$w = 2\pi f$ = angular frequency

Note that the phase information ($w_o\tau$) is retained. The signal may be either positive or negative. Further note that the frequency term occurs as $w_o\tau$ in this transform, not $\frac{w_o\tau}{2}$ as in the power spectrum. Hence, the transform method yields twice the resolution.

The significance of these observations is shown in Figure 9. Suppose the microwave transmitter is operating in K-band, i.e., sweeping from 26.5 GHz to 18 GHz. Suppose that the duty cycle is 50%, i.e., $T = 0.5T_r$. Suppose further that a reflector is placed in the beam at such a point that it produces a beat frequency ($w'\tau$) which is an exact multiple of the repetition frequency ($w'\tau = \frac{2\pi m}{T_r} = 2\pi m f_r$ where m is an integer).

Then the display of this signal on a high resolution spectrum analyzer is shown in Figure 9a. For convenience the horizontal axis is shown in distance rather than frequency or delay time. The spectral envelope is dotted in and goes to zero at 18 mm.

A display of the correlation detector output for the same signal is shown in 9b. In this case the phase is zero ($w_o\tau$ is a multiple of 2π). Note this display is a smooth curve and goes to zero in 9 mm.

Now suppose the reflector moves a distance that causes the phase to shift $\frac{\pi}{2}$ radians.

$$w_o \delta\tau = 2\pi f_o \frac{2\delta D}{C} = \frac{\pi}{2}$$

This corresponds to a distance of

$$\delta D = \frac{C}{8f_o} = \frac{3 \times 10^{10}}{8(26.5 \times 10^9)} = 0.14 \text{ cm} = 1.4 \text{ mm}$$

where $\delta\tau$= the change in delay time

δD = the distance moved

C = velocity of light

$f_o = \frac{w_o}{2\pi}$ = microwave starting frequency

The display of the spectrum analyzer and correlation detector are shown in Figures 9c and 9d respectively. Note that the position of the lines in the spectra do not move - only the position of the envelope. The only indication of the change in position of the reflector is the slightly unsymmetrical sideband structure.

In sharp contrast the change in the correlation detector output is most conspicuous. Initially the curve had a shape like:

$$y = \frac{\sin x}{x}$$

The new curve has a

$$y = \frac{\cos x - 1}{x}$$

shape. This curve crosses zero at the 1.4 mm mark. A further 1.4 mm movement of the reflector has a relatively minor effect on the spectrum analyzer output but changes the correlation detector output to a curve like:

$y = \frac{-\sin x}{x}$, shown in Figures 9e and 9f.

The negative peak on this curve occurs at 2.8 mm. Further increments of 1.4 mm changes the correlation detector output to a curve like:

$$y = - \frac{\cos x - 1}{x}$$

then back to

$$y = \frac{\sin x}{x}$$

This distance (5.6 mm) corresponds to 2π radians.

Some experimental results in Ku-band (12.4 to 18 GHz) are shown in Figure 10. Figure 10a shows the front (at 2.7 cm) and back (7.0 cm) reflection from a 2-in.-thick block of plexiglas. Note that the front reflector is in phase and the back approximately 180° out of phase. Figure 10b shows a single stationary reflector with the phase control rotated by 90° increments. Figure 10c shows the reflection from a reflector moved in 2.7 mm increments. Note the final position is displaced 0.5 cm on the display. This represents a distance of 1.08 cm displacement.

In practice an inexperienced operator can easily see a 30° shift corresponding to a 0.46 mm distance in air. In a dielectric the resolution is better because the velocity of microwaves is c/n where n is the index of refraction. For most dielectrics n is about 1.3 to 1.7.

If the microwave horn were scanning a laminar structure for delaminations, the position of the delamination could be determined to better than 0.5 mm in K-band. Higher microwave frequencies would result in still higher resolution.

In using the FDI to measure dielectric constant it is necessary to measure the microwave path length to a metal reflector. An operator with some experience can make these measurements to $\pm$.03 mm in K-band. The metal reflector can be located more accurately than separations because the metal reflector provides 100% reflection. This reflection is stronger than other reflectors in the beam. Furthermore, the other reflectors are located well away from the metallic reflector.

Figure 11 shows a typical indication of a defect. The large indication at the left is the reflection produced by the microwave beam entering the part. This double exposure shows the trace over a normal region and over a defect.

Instrumentation

There are 3 outputs of the FDI: the correlation detector output, the correlation output shifted 90°, and an output corresponding to the spectral envelope (the dotted lines in figure 9).

The spectral envelope has less resolution than the correlation detector output. Furthermore, it contains no phase information. This output is useful for looking for voids and inclusions in relatively thick dielectrics. The usual electronic tricks of zero suppression and variable gain-vs-depth can be applied to this signal. This display mode is also useful in scanning operations where the distance from the horn to the various interfaces cannot be held constant.

The spectral envelope display is very similar to the "A" scan in pulse-echo ultrasonics. The only difference in interpretation is that the reflectors are at positions corresponding to the peak of the "blip" rather than the leading edge of the blip. This is a desirable difference since the peak is always more easily discernible than the leading edge. No error is introduced if the zero or base line is suppressed.

The correlation output contains much more information: both frequency and phase. Furthermore, the display for multiple reflections is strictly the sum of the indications from each. These two properties allow very high resolution of defects in thin, laminar structures.

Suppose that a quarter-inch thick composite consisting of two materials, for example filament wound glass and rubber liner, required inspection for delaminations and separations. Suppose further that there are different acceptance limits for area of glass delaminations, glass-to-liner separations, and liner delaminations. Thus when separations are detected, it is necessary to determine exactly which interface is involved.

Since so many interfaces are so close together the overlapping reflections on the primary display would be difficult to interpret. However, a simple way exists for determining both the interface that is separated as well as the gap size. The signal analyzer is manually set for the approximate center of the composite. The two correlation detector outputs are then put on the x and y axis of an x-y plotter. With a flawless sample in front of the horn the x-y plotter pen is set to the center. Then as the horn scans the composite a deflection from the center indicates a defect. The angle of the deflection indicates the depth of the defect, and the radius indicates gap size. This angle is the $w_o\tau$ term in equation (2).

Penetration of Air Gaps

Unlike ultrasonics, microwaves are not totally reflected at interfaces between solids and air. This property gives microwaves the ability to detect separations under other separations or air gaps. The reflection coefficient for an interface between two materials is

$$R = \frac{(n' - n'')^2}{(n' + n'')^2}$$

where n' and n" are the refractive indices. For example at an interface between air and a material with a dielectric constant of 1.5, 4% of the beam is reflected.

The ability to penetrate gaps is illustrated by figure 12. The two traces are made with and without an air gap. In the trace with the air gap the back surface reflection is merely reduced in amplitude. The small indication at 3.2 cm is from the mouth of the horn.

The reflection from air gaps can be directly measured with the FDI. A plot of reflection verses gap width for plexiglas in Ku-band (12.4 to 18 GHz) is shown in figure 13. It is interesting that the reflected amplitude does not extrapolate to zero for zero gap size. An exact mathematical analysis shows that for gaps less than 5 mils in Ku-band there is considerable variation in reflection with frequency. This results in "blurring" of the reflection and nonlinear behavior. At 40 mils the curve starts to flatten and at still larger gap sizes the display shows two reflections: one where the microwave beam enters the gap, and one where it leaves.

Measurement of Refractive Index

The conventional procedure for determining the refractive index of solids at microwave frequencies can be very precise, but is far from convenient. It involves filling a length of waveguide with the material to be measured, and determining the complex impedance of the filled section by standing wave measurements. From the impedance, the electrical properties, including dielectric constant can be computed. The refractive index is, of course, determined by the dielectric constant. This method is not as simple as the description might imply. Data reduction is exceedingly involved and tedious, and sample preparation can be a problem since the waveguide must be perfectly filled. Another obvious problem is that a large slab can only be tested by cutting samples from it.

With the FDI one need only have a specimen with flat, parallel faces. The antenna, generally a horn, is placed on one side of the specimen, a plane metal reflector on the other side. The reflector is mounted on a micrometer screw so that it can be moved a measured distance along the horn's axis. See figure 14.

The distance from horn to reflector is then determined from the FDI display. This indicated range is, of course different from the actual distance. The FDI measures distance in wave lengths, and the wave length is shorter in the dielectric sample. After the indicated range has been noted, the sample is removed, and this causes the indicated range of the reflector to revert to its true value. The reflector is then moved away from the horn until its indicated range is the same as it had been with the sample present. The reflector travel required to do this is noted. The refractive index is then calculated as follows:

$$n = \frac{t + d}{t}$$

where t is specimen thickness, d is the reflector travel, and n is the refractive index. The FDI avoids the impossibly difficult problem of generating ultra-short pulses by using a full-band frequency sweep for determining target range. Thus, taking Ku-band as an example we have a frequency band of 12.4 - 18 GHz used. Fortunately the dielectric properties of most materials change very slowly with frequency over a waveguide band. The FDI measurement of refractive index is, of course a band average, adequate for most purposes. The measurement of distance is good to about $\pm$0.01 cm. For dielectrics such as plexiglas or polystyrene, for example, the refractive index is about 1.6 and thus with a 1 cm thick slab the reflector travel will be about 0.6 cm. Assuming adequate precision in measuring t, the uncertainty in n is then $\pm$0.6% for Ku-band. For higher frequencies and thicker specimens accuracy is, of course, better. Specimens of high attenuation are measured somewhat less accurately, as are curved specimens, or liquid specimens in tanks (the latter because of multiple reflections from the tank walls). It should be noted, however, that curved specimens, or specimens with irregular surfaces can be measured for a rough check if a loss of accuracy is acceptable, and curved specimens can be compared if they are identically positioned, and are of uniform dimensions.

As regards size, the 1 cm thick specimen used in the example is very convenient. Specimens 6" thick have been measured, and thin ones can be used, but with the obvious loss in precision. The cross section of the specimens may be as small as $2\frac{1}{2}$" X $2\frac{1}{2}$" for Ku-band (center frequency 15 GHz) for other bands the size increases with decreasing frequency and vice-versa. For Ka-band (center frequency 22 GHz) about 1-3/4" square specimens suffice. This assumes the use of standard gain horns of approximately 20 db gain. With lens correction smaller specimens can be used, although diffraction effects prevent collimation of a microwave beam into a fine line: parallel beams and focal spots cannot be narrowed down below a wavelength. The limit is aperture diffraction, and may be estimated from the optical formulas. For a circular aperture a, the angular half-width of the main lobe (Airy's disc) is given by

$$\sin \phi = \frac{1.22 \lambda}{a}$$

thus an aperture of 2λ will have a spread of about 38° for the main lobe, about what one would get from a good horn of similar aperture. In fact this is the sort of horn generally used. Thus it can be seen that it is futile to attempt to constrict the beam to a diameter much below two wavelengths, since it will spread beyond the aperture. The limit previously cited for specimens in Ku-band is about 3λ for the center frequency.

It should be noted that for many dielectrics the refractive index does not change very much between 1 and 40 GHz so that a linear extrapolation is quite adequate in many cases, and measurements can be made in Ka-band with a center wavelength of 9 mm allowing specimens as small as 1" X 1" with no loss of accuracy.

FDI units can now be made for any band between L (1-2 GHz) and Ka (26 - 40 GHz). Antenna size becomes inconveniently large at lower frequencies, and full-band sweepers and ferrite isolators, an absolute necessity, are hard to come by above Ka-band. Extension to higher frequencies is quite feasible whenever these items of equipment become commercially available.

Applications

The impetus for starting research in the F.M. microwave technique was the need for inspecting the solid propellant in the 260" diameter rocket motor. During the feasibility demonstration program a back surface reflection was obtained off a 52" thick solid propellant specimen using the 1-to-2 GHz microwave band. NASA is now sponsoring a program for more extensive testing with improved equipment and larger propellant samples.

The FDI is being used for the production inspection of ablative nozzle skirts used in the Titan family of rocket motors. The frequency band used is 26.5 to 40 GHz (Ka-band). A paper is being presented on this application later in this conference.

The most recent application has been on randoms used in re-entry bodies. In this application it is used to measure both variations of dielectric constant across the windows and variations from window to window.

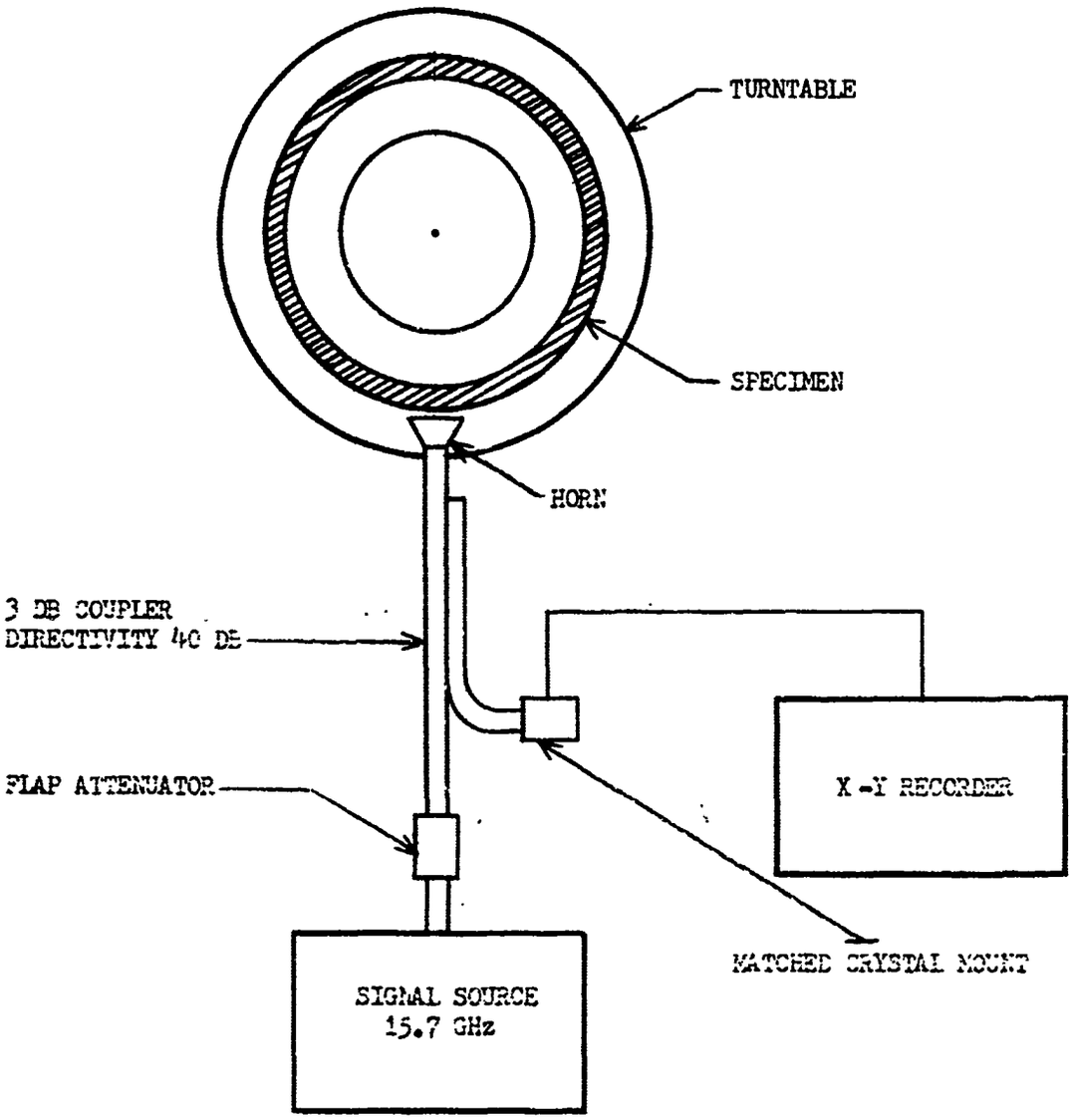
Conclusions

The Frequency Domain Interferometer can be used to inspect nonmetallics for flaws and dielectric constant. Samples from a fraction of an inch thick to over 4 feet thick have been inspected. Defects down to 2 mils thick can be detected and located to 10 mils accuracy.

It is now possible to measure the dielectric constant of production parts with high accuracy. The FDI eliminates the need to machine samples from the part for insertion into a waveguide. It also permits several readings to be taken across the face of the part to determine homogeneity.

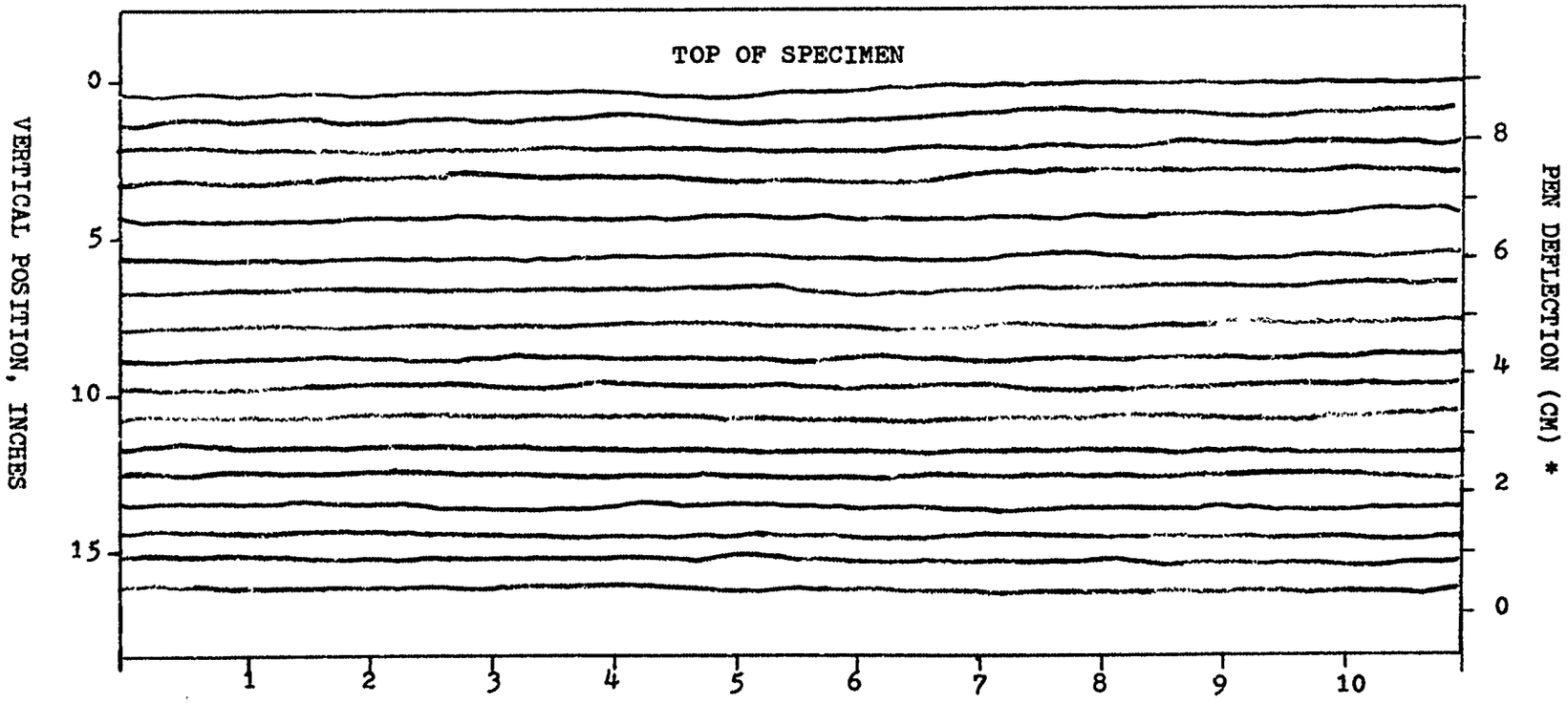
Acknowledgements

The development of the F.M. microwave system was sponsored by the Office of Advanced Research and Technology, National Aeronautics and Space Administration, Washington, D.C. The assistance of Gil Lewis, technical manager of the program, is greatly appreciated. Mr. Lewis is with the Jet Propulsion Laboratory. Much of the development work was done at the Aerojet-General Corporation. The work there was under the administrative direction of Tom Harrington, Mel Standart, and Tony Lucian. Billy Lamb and Ed Mills supplied invaluable technical assistance.



REFLECTOMETER USED FOR MOTOR EXPERIMENTS

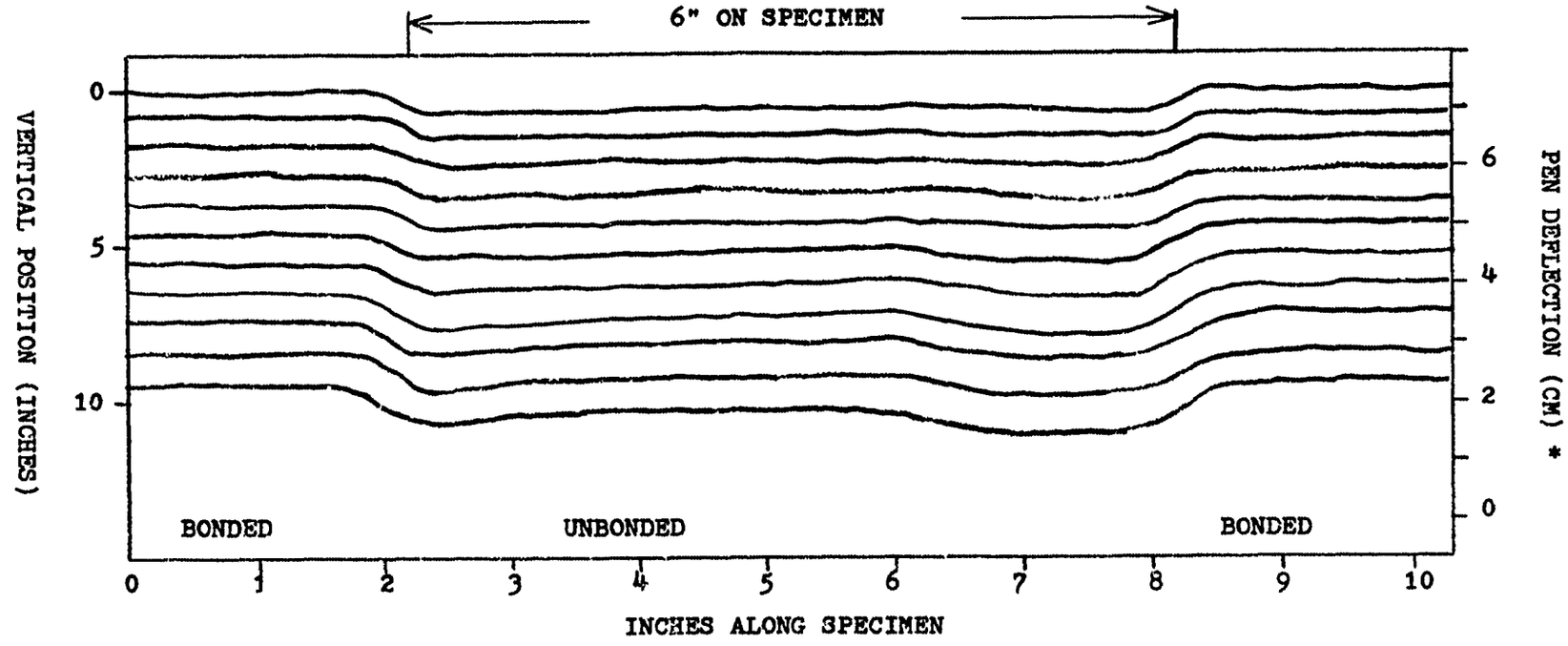
FIGURE 1



ROTATIONAL SCAN OF WELL BONDED REGION

* PEN DEFLECTION OF 1 CM DOWNWARD IN A TRACE INDICATES 0.1V INCREASE IN CRYSTAL DETECTOR OUTPUT.

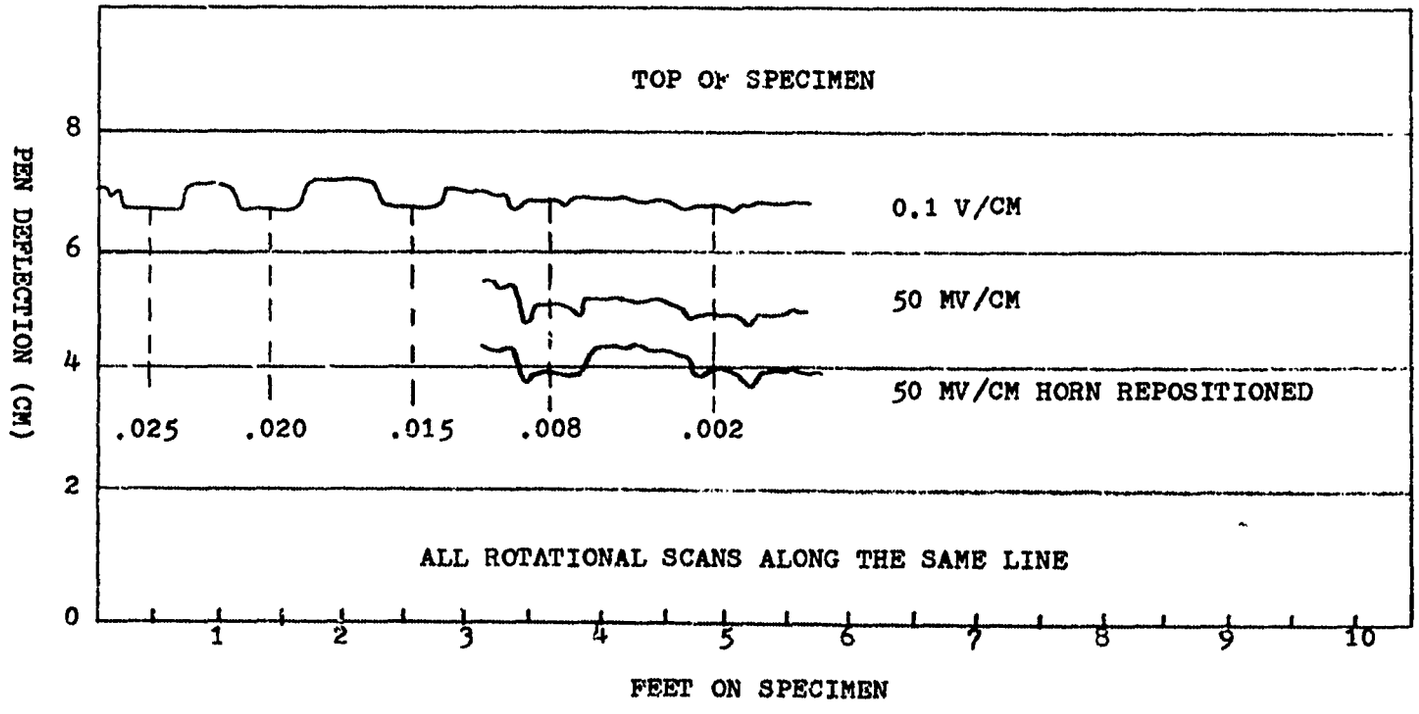
FIGURE 2



ROTATIONAL SCAN OF SEPARATED PROPELLANT-INSULATION INTERFACE

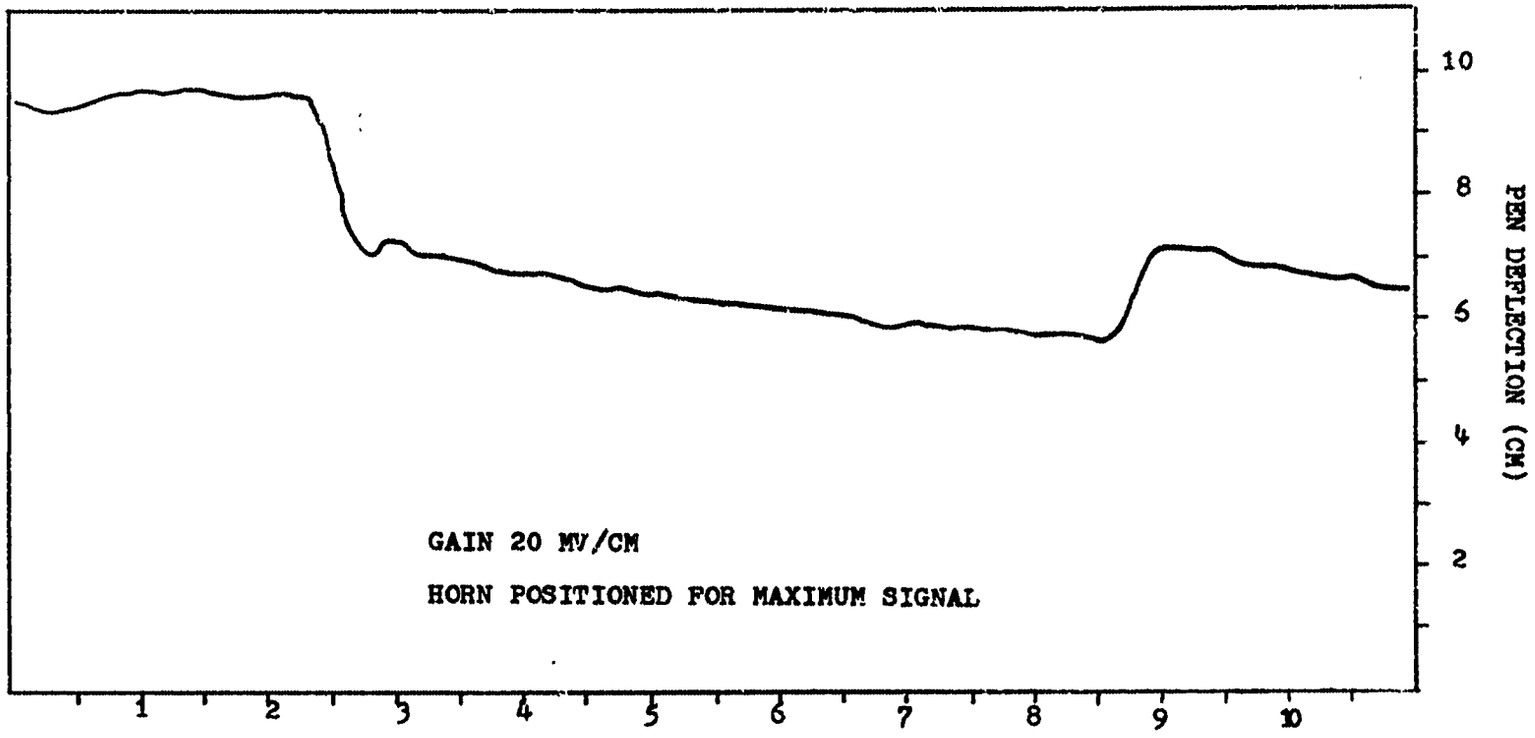
* A PEN DEFLECTION OF 1CM IN A SINGLE TRACE (DOWNWARD) INDICATES A 0.1V INCREASE IN CRYSTAL DETECTOR OUTPUT.

FIGURE 3



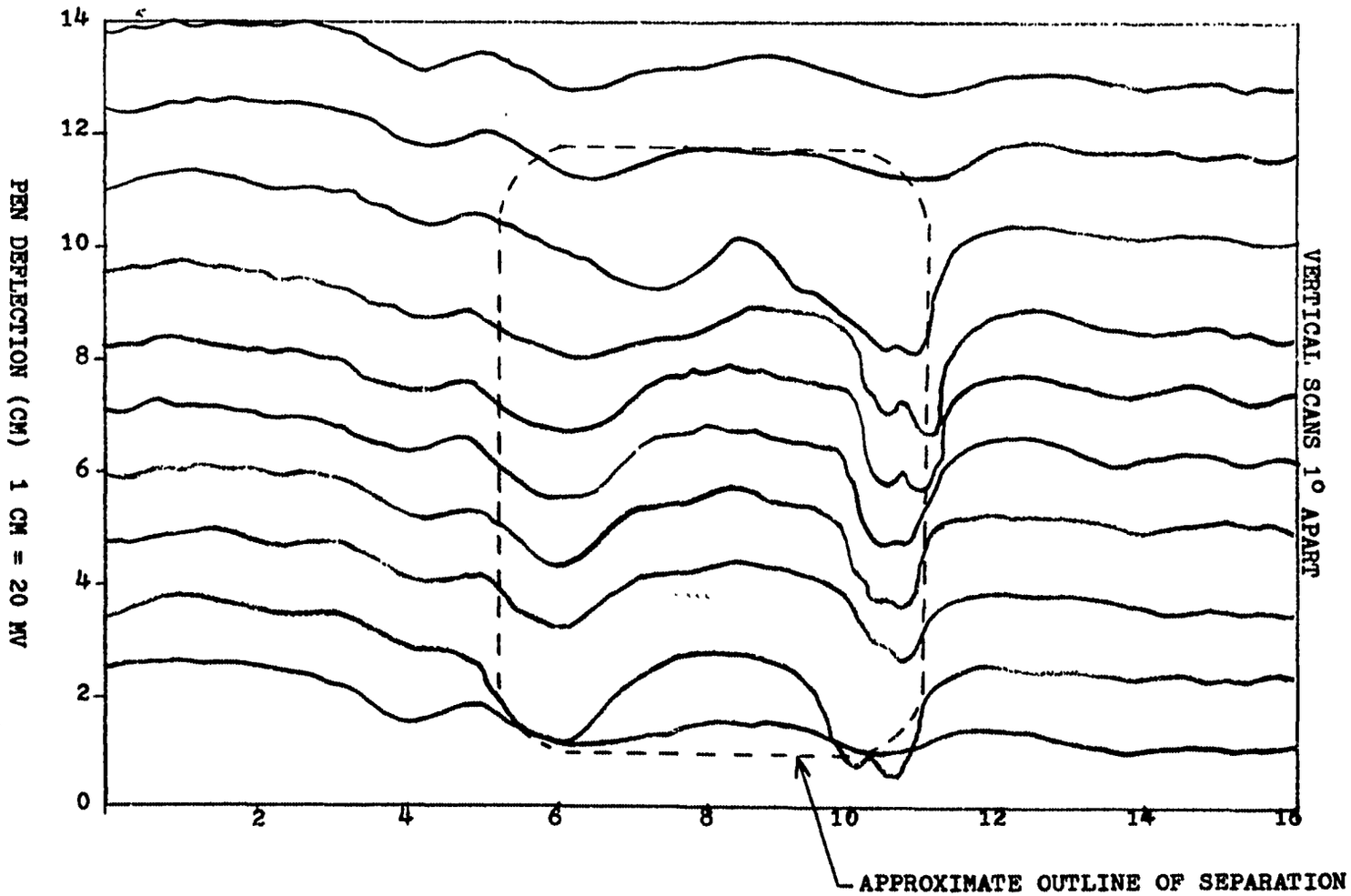
SCANS OF ALL PROPELLANT-INSULATION SEPARATIONS

FIGURE 4



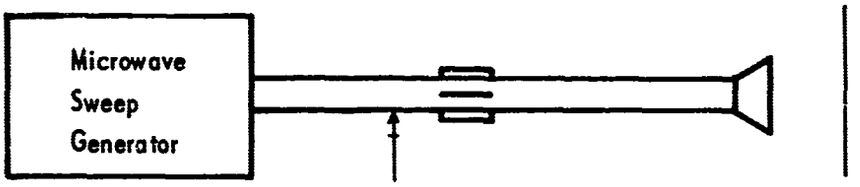
ROTATIONAL SCAN OF .008 INCH SEPARATION

FIGURE 5

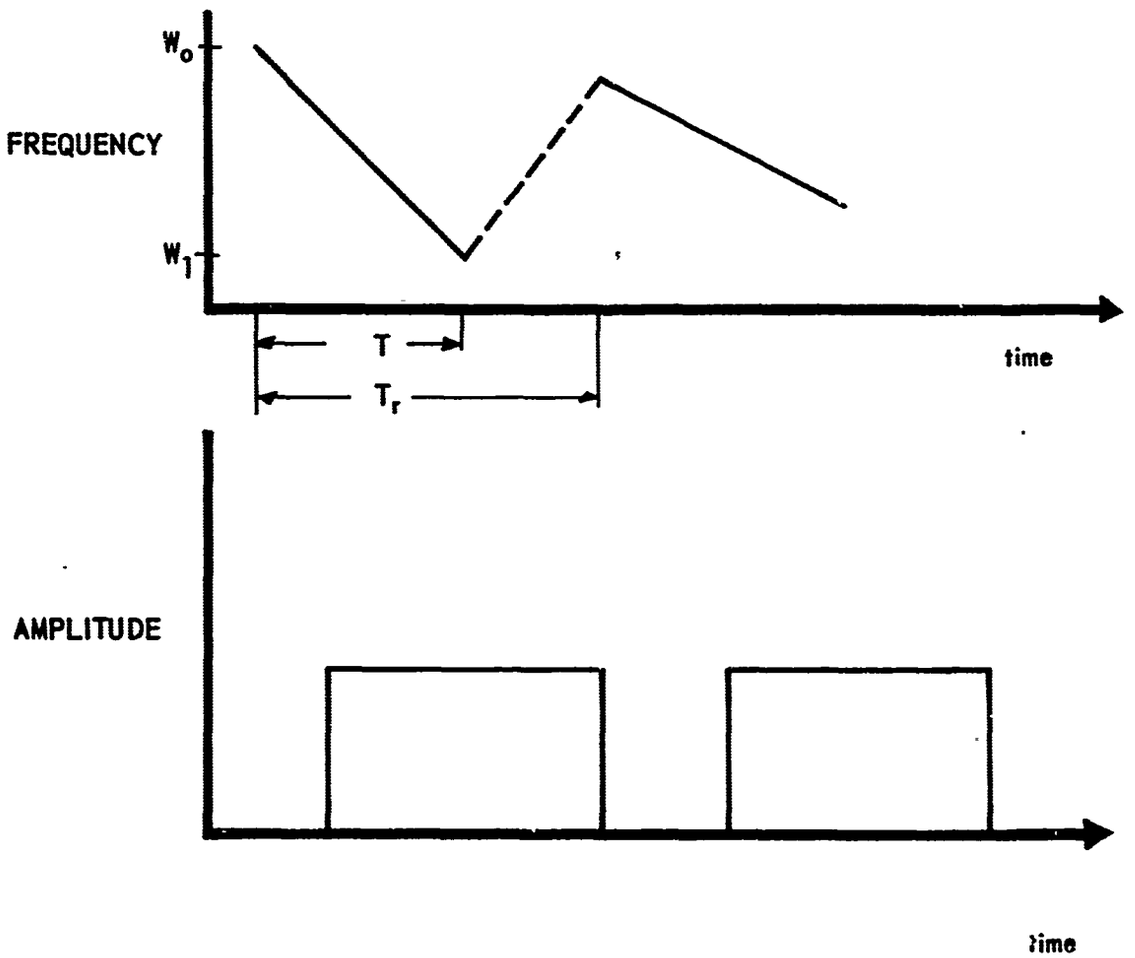


SCANS OF CASE-INSULATION SEPARATION

FIGURE 6

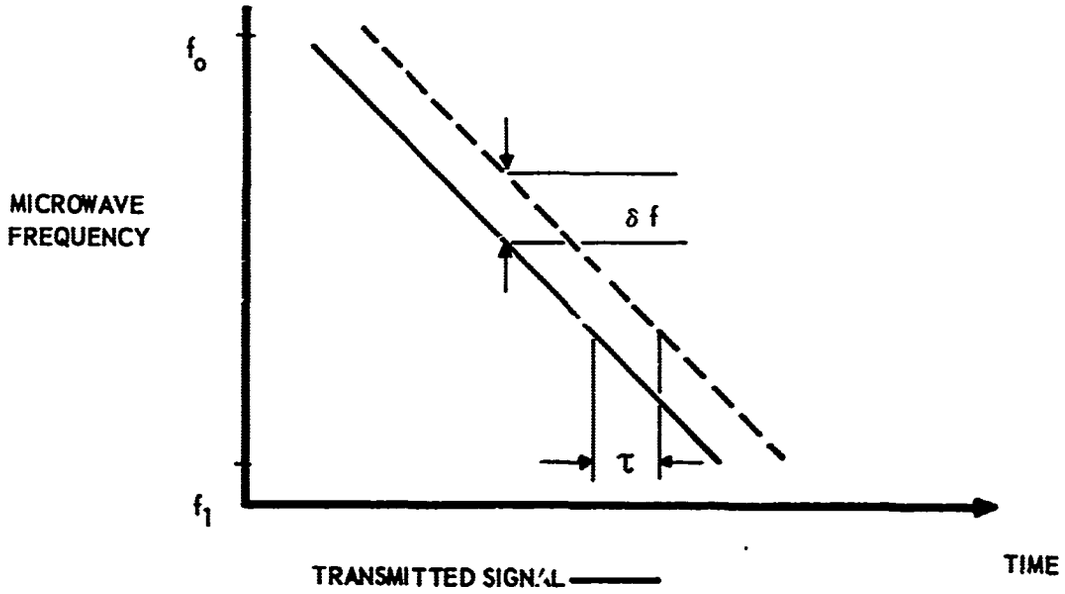


TRANSMITTED SIGNAL:



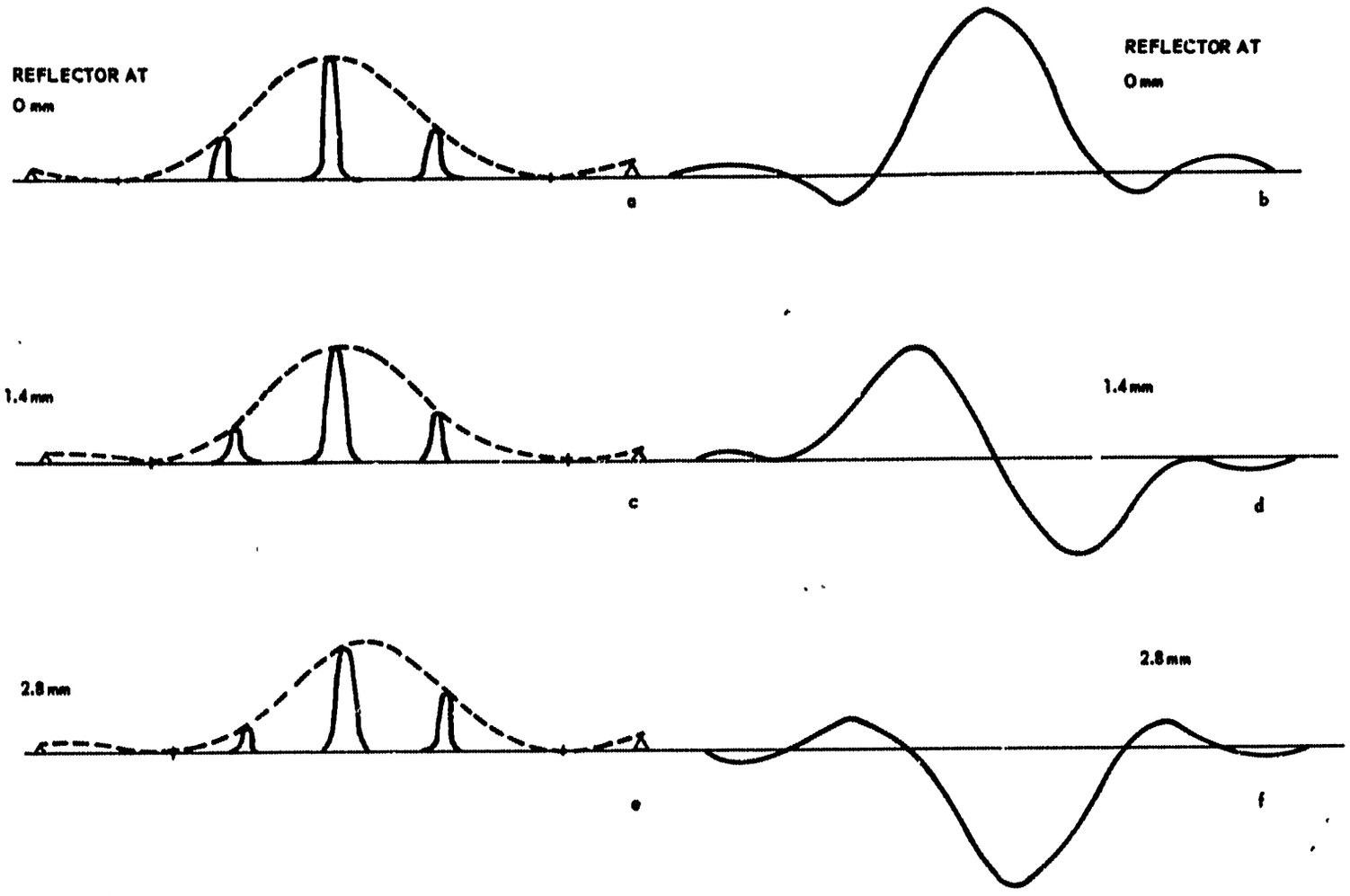
BASIC FM TECHNIQUE

FIGURE 7



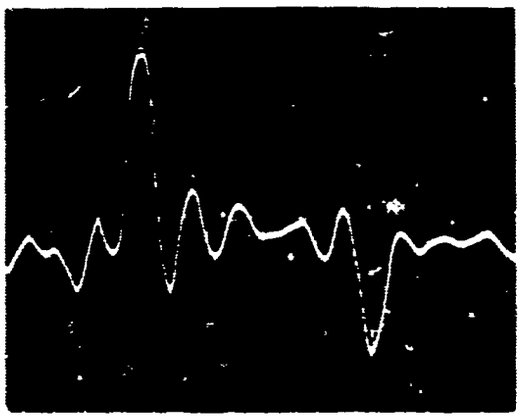
METHOD OF CONVERTING DELAY TIME TO FREQUENCY

FIGURE 8

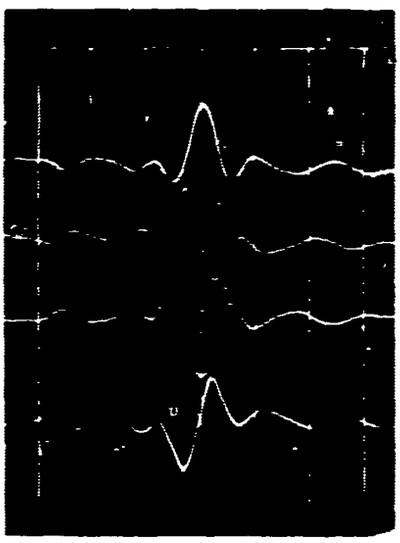


SPECTRUM ANALYZER

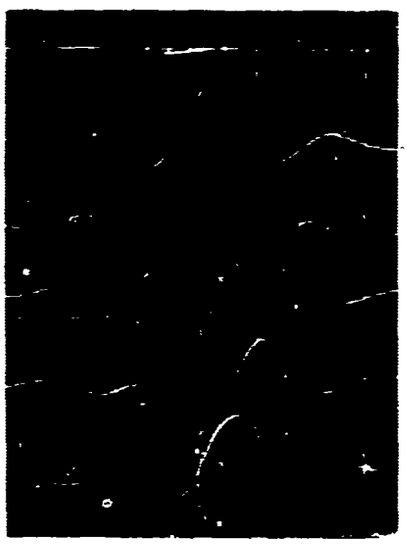
FIGURE 9



a. FRONT AND BACK REFLECTION OF 2 IN. AT PLEXIGLAS IN Ku BAND



b. DISPLAY WITH PHASE CONTROL ROTATED IN 90° INCREMENTS

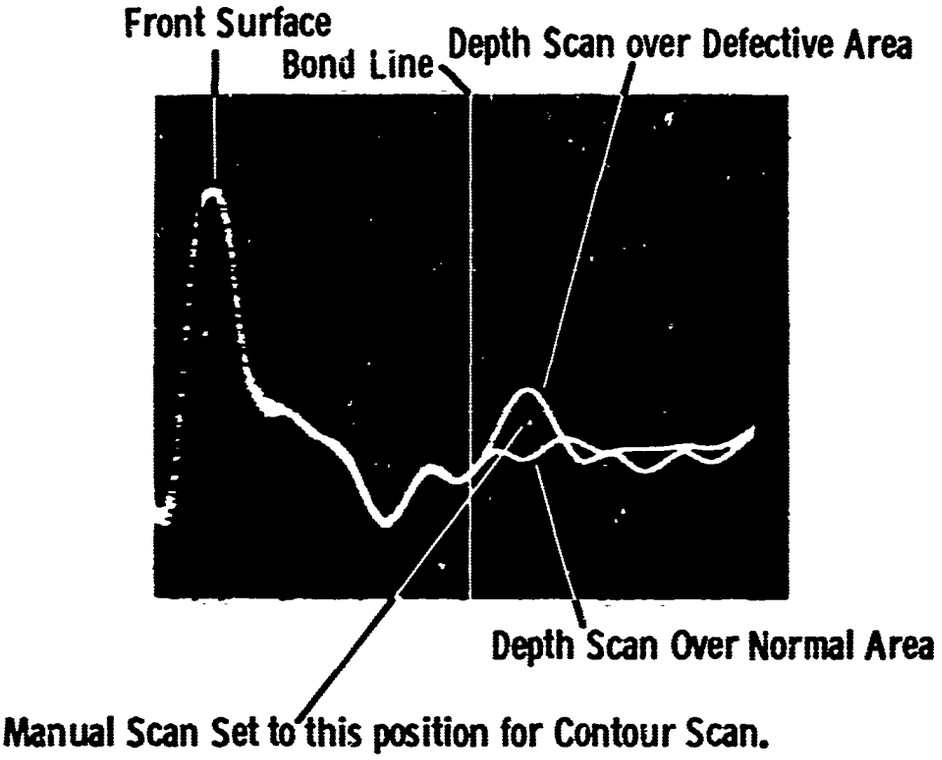


c. DISPLAY WITH REFLECTOR MOVED IN 2.7 mm INCREMENTS

TYPICAL DISPLAYS

FIGURE 10

PRIMARY DISPLAY PATTERNS USED IN ESTABLISHING A FIXED-DEPTH C-SCAN



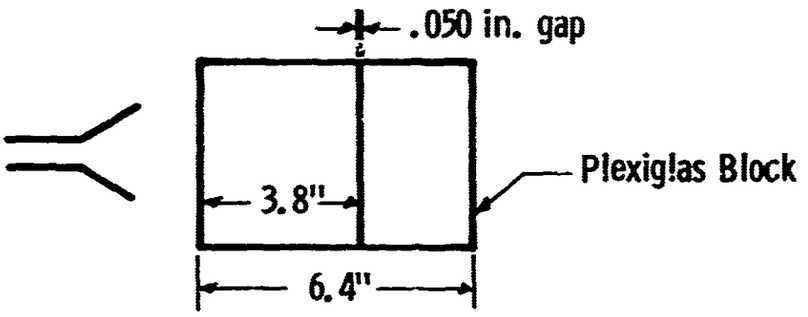
The Defect map is made by scanning across specimen with the signal analyzer set as shown above the DC level (vertical position of Spot) is recorded

FIGURE 11

DEPTH SCANS







ALL TRACES HAVE THE SAME GENERAL FORM REGARDLESS OF HORIZONTAL POSITION.

FIGURE 12

INDICATION VS SEPARATION THICKNESS DATA

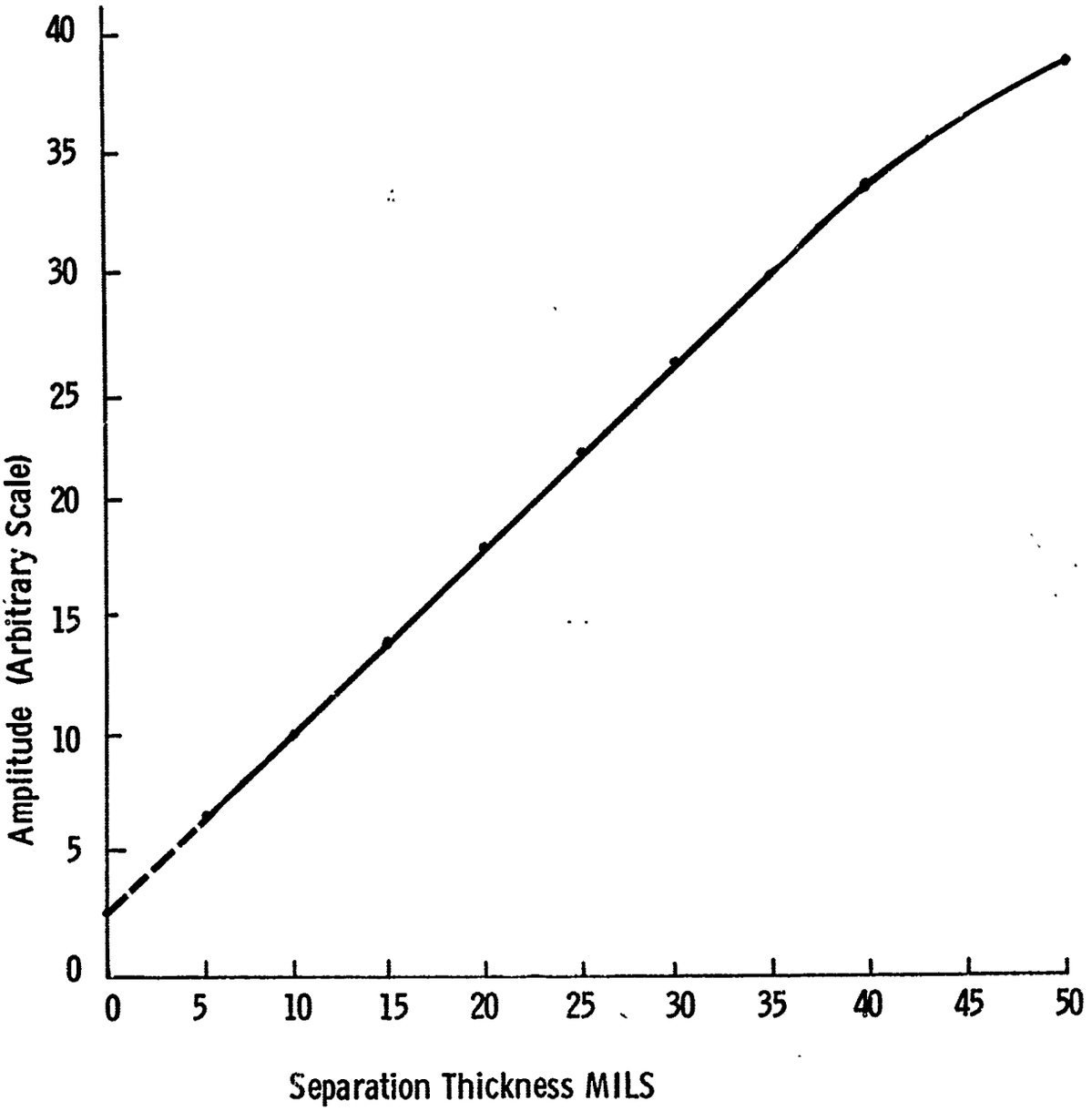
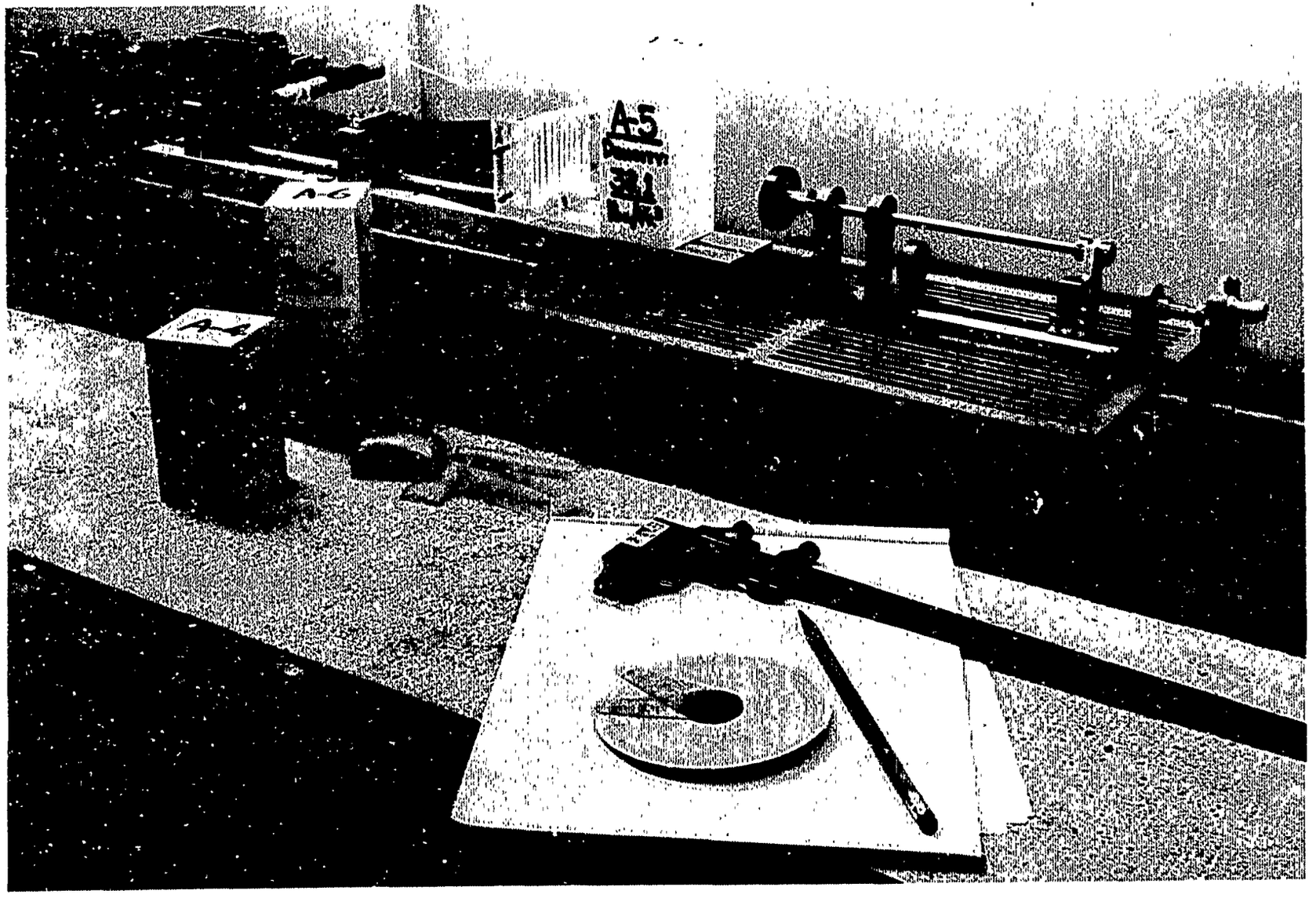


FIGURE 13



APPARATUS FOR DIELECTRIC CONSTANT MEASURMENT
FIGURE 14

THE APPLICATION OF SONIC AND MICROWAVE INSPECTIONS TO COMPOSITE NONMETALLIC STRUCTURES

by

A. D. Lucian
Consulting Physicist
Propulsion Division
Aerojet-General Corporation
Sacramento, California

M. W. Standart
Technical Assistant
Propulsion Division
Aerojet-General Corporation
Sacramento, California

For Presentation at the
Symposium on Nondestructive Testing of Plastic/Composite Structures
Dayton, Ohio

March 18-20, 1969

ABSTRACT

The structural characteristics of nozzle-exit components for large liquid-rocket engines are discussed and a description of honeycomb glass-laminate processing and NDT history is presented.

A microwave short-range radar signal processing unit has been developed for the inspection of large solid-rocket grains under the sponsorship of NASA. This high-resolution signal processor combined with microwave swept-frequency generators in the range of one- to 40 GHz has been applied to the inspection of nonmetallics.

Initial experiments on sub- and full-scale sections demonstrated the feasibility of microwave inspections and techniques for automating a sonic inspection. Inspection objectives were established and a sonic/microwave production inspection system was developed. The resulting system, its operation since July 1968, and inspection data are described.

INTRODUCTION

In the thrust chamber of a liquid rocket engine, thermal energy of the combustion products is converted into the kinetic energy of exhaust gases to produce thrust. In the course of this conversion, nozzle walls encounter temperatures considerably in excess of their melting points and therefore means must be provided for cooling. Three basic means are available for providing this cooling process: (1) regenerative cooling wherein the liquid propellants are circulated around the chamber exterior prior to entry into the injector, (2) film cooling wherein a small amount of propellant is sprayed on the interior of the thrust chamber wall and (3) ablative cooling wherein a nonmetallic surface is deliverately allowed to erode and char at a controlled rate. Nonmetallic ablative materials are used chiefly in the combustion chambers for space engines where propellant flow is insufficient to provide adequate cooling and in nozzle extensions or "skirts" whose physical size interferes with the achievement of acceptable propellant flow characteristics.

The environment seen by ablative nozzle skirts is especially severe. The rapidly increasing gas velocity in the skirt area provides good conditions for heat transfer to the walls. In addition, the vibration and gravity forces encountered during missile firings impose additional threats to ablative skirt structural integrity. The importance of this structural integrity cannot be overemphasized since it relates directly to missile performance. It may be shown mathematically that optimum thrust is achieved when the pressure of the exhaust gases at the skirt exit area is equal to the atmospheric pressure. This condition is achieved

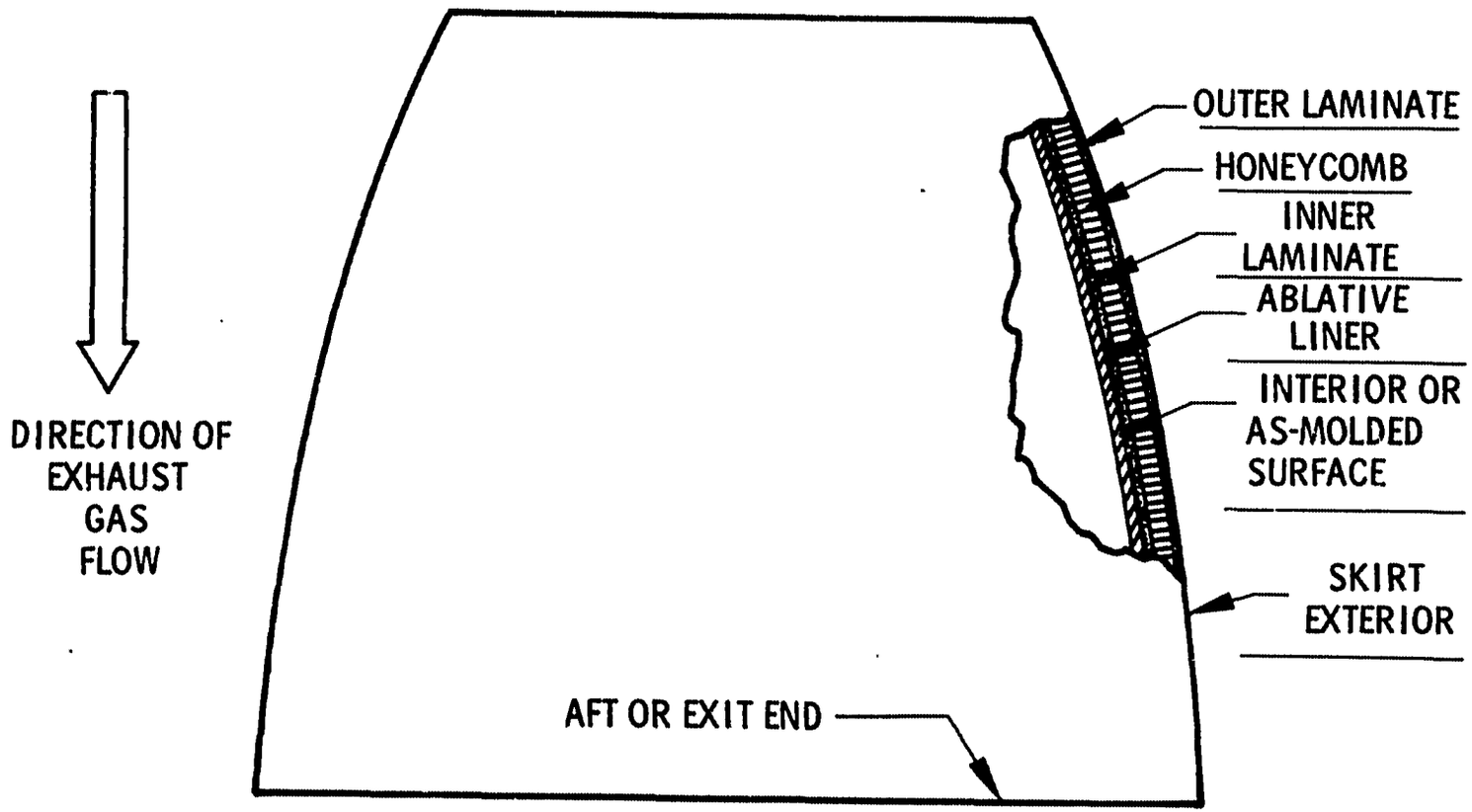
or at least reasonably approximated by designing ablative skirts such that the ratio of throat to exist area will allow sufficient exhaust gas volume increase and concurrent pressure drop to approach atmospheric pressure at the exit area. Obviously, this requires some compromise since a missile encounters continually changing atmospheric pressure during its ascent. Despite this compromise, however, the significant point remains that optimum missile performance depends upon the design and proper performance of the ablative skirt function. If the ablative skirt is consumed by the heat of the exhaust gases or disintegrates from acceleration forces, less than optimum thrust will be generated; if a section of the skirt is lost, undesirable side thrusts will be created for which the missile guidance system may or may not be able to compensate. In either event, the successful accomplishment of the mission objectives will be seriously jeopardized. Therefore, the structural integrity of ablative skirts is not only of definite concern but developing objective evidence of that integrity provided nondestructive testing with a formidable challenge.

ABLATIVE SKIRT STRUCTURE

The formidability of this challenge is most easily visualized from a discussion of the structure and fabrication of a typical ablative skirt used on the Titan III vehicle. Figure 1 portrays a typical skirt in cross-section with the thicknesses of the various layers of material exaggerated for illustrative purposes.

TITAN III NDT DEVELOPMENT PROGRAM

TYPICAL ABLATIVE SKIRT - NO SCALE



AEROJET GENERAL®

PROPULSION DIVISION

Figure 1

AGCS-0100-52 (REV. 1/68)

The liner or inner-most part of an ablative skirt is in direct contact with the hot exhaust gases. It is fabricated of an asbestos tape pre-impregnated with phenolic resin. The tape is wound on a mandrel, cured, and the outer surface machined to size. The inner or as-molded surface wrapped on the mandrel requires no machining. Following liner machining, several layers of glass cloth are bonded to the machined surface of the liner and also cured. These layers form the inner laminate. After inner laminate cure, the phenolic honeycomb is bonded in place with a film adhesive and its outer surface contoured to print. Finally, several more layers of glass cloth are bonded to the exterior of the honeycomb and this exterior layer becomes the outer laminate.

ABLATIVE SKIRT TESTING HISTORY

Originally, nondestructive testing of this structure was limited (excluding visual and dimensional checks) to a dye penetrant inspection of the liner as-molded surface for surface cracks and delaminations. (For purposes of this discussion, delaminations are defined as separations parallel to and between the plies or layers of tape, whereas cracks are defined as separations occurring across the plies.) The presence of cracks or delaminations is particularly critical since they could permit hot gases to enter the inner laminate area which is not designed to withstand such a condition. If delaminations are present in the liner structure which are not open to the as-molded surface, dye penetrant inspection will not detect this condition. Such delaminations, however, may become

open to the as-molded surface as that surface erodes and chars during an engine firing. As a result, dye penetrant alone is not sufficient to adequately characterize the condition of the liner with respect to cracks and delaminations. Moreover, dye penetrant will not detect the presence of inclusions between the plies which can also contribute to structural weaknesses in the liner.

Since no NDT methods were available to satisfactorily inspect the remainder of the skirt structure, reliance was placed upon in-process control to ensure skirt reliability. Raw materials were subjected to laboratory analysis to ensure conformance to the applicable material specifications, and in-process conditions such as cure temperatures were closely monitored. However, the state-of-the-art in nonmetallics manufacture often produces a measurable degree of lot-to-lot variability for the pre-impregnated materials used in liners and laminates. This condition tends to diminish confidence in the nearly exclusive use of raw material and in-process controls. As a result, the Air Force asked Aerojet to recommend the development and/or adoption of applicable NDT techniques for inspecting the entire skirt structure. The possible defects which the NDT techniques should be able to detect were:

Part or Interface	Possible Defects
Liner	Cracks, Delaminations, Inclusions
Liner to Inner Laminate	Unbond
Inner Laminate	Delaminations
Inner Laminate to Honeycomb	Unbond

Part or Interface	Possible Defects
Honeycomb	Crushing of either face
Honeycomb to Outer Laminate	Unbond
Outer Laminate	Delaminations

Experience had indicated that X-ray was unable to resolve any of these defects in the relatively small size range believed important. It was also known that ultrasound was limited by its inherent inability to penetrate beyond the first discontinuity; and the limitations of penetrant inspection discussed earlier were equally well-known.

With these NDT methods essentially eliminated from further consideration, attention was turned to possible application of a sonic tap test. Experience had indicated that coin tapping of ablative skirts produced audible variations corresponding to differences in honeycomb and outer laminate quality. Application of this technique was regarded as promising provided that the subjective interpretation of human hearing could be replaced with electronic signal processing and permanent data recording.

Simultaneously, it appeared probable that swept-frequency microwave techniques under exploratory development at Aerojet[1] for inspection of solid propellant could be applicable to other composite materials such as those which comprised the ablative skirt liner and inner laminate. In addition, both the sonic and microwave techniques possessed theoretical limits of detection compatible with the sizes of defects that the tentative inspection criteria considered desirable for detection.

---

[1] Cribbs, Robert W., Microwaves in Nondestructive Testing; Conference on NDT of Plastic/Composite Structures, March 1969, Dayton, Ohio

On the basis of these theoretical considerations, a feasibility study was undertaken using samples with known defects. For these studies, a 2 x 2 ft panel duplicating the skirt configuration was fabricated in the laboratory. A saw cut was used to simulate a liner crack; metal shims were inserted at various interfaces in the laminates and bond lines and removed after cure to simulate unbond and delamination conditions; a wheel-like device was assembled to crush honeycomb in a manner which was representative of skirt handling-tooling misalignment.

For purposes of the sonic feasibility study, a mechanical impactor or "tapper" was built. This tapper consisted of an AC motor driving a cam-actuated arm to "tap" the skirt specimen at precise intervals with constant strength. A microphone picked up this sound, filtered the signal, and displayed it on a recorder. This phase of the feasibility study was extended to a full scale skirt which had suffered handling damage to its honeycomb layer. It was shown conclusively that crushed honeycomb and/or delaminated outer laminate areas of a skirt resonated differently when tapped than did acceptable areas, and that the frequency differences were sufficient for meaningful data recording.

Simultaneously, the microwave study was progressing to demonstrate its feasibility. It was learned that satisfactory defect resolution required operation in higher frequencies than had been previously investigated but that the signal processing equipment was capable of responding to this requirement since it handles only the difference frequencies between transmitted and reflected signals. The defect specimen was

subjected to a microwave inspection using a hand-held probe or horn and the laboratory electronics bread-boarded for previous microwave development studies. The results of these efforts are depicted in Figure 2 wherein the response of this laboratory microwave equipment clearly indicates the presence of the known defects.

PROTOTYPE EQUIPMENT DEVELOPMENT

Based upon the encouraging results of the feasibility studies, plans were formulated to design, fabricate, install and checkout an actual inspection system for Titan III skirts. The following criteria were established for performance of the system:

1. The system and associated skirt handling tooling must be sufficiently flexible to accommodate the three different sizes of ablative skirts being manufactured.

2. The system must be able to detect flaws as small as 1/4 x 1/4-in. during microwave inspections and 1/2 x 1/2-in. during sonic inspections.

3. The read-out must be able to provide flaw size information.

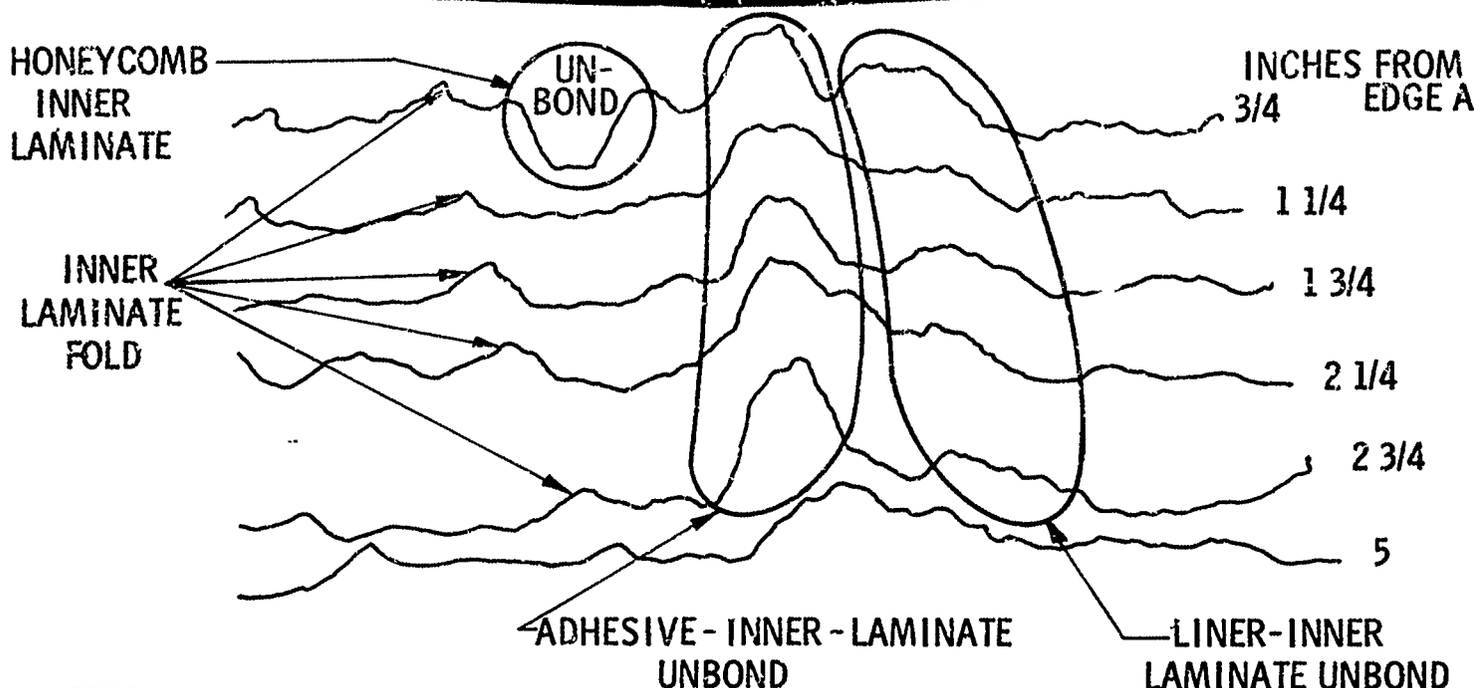
4. The read-out must be able to relate defect indications to their respective locations on the skirt being inspected.

5. The system should be operable by bargaining unit inspectors (as opposed to the engineers who performed the feasibility studies) and, therefore, should be as nearly automatic as possible.

The design of the system was begun in February of 1968 and contracts for its manufacture were let in April of that year. By the middle of June,

TITAN III NDT DEVELOPMENT PROGRAM





AEROJET GENERAL ®

PROPULSION DIVISION

Figure 2

installation of all system components was complete and checkout was begun using both available ablative skirts and subscale defect specimens similar to the one described earlier.

EQUIPMENT COMPONENTS

Figures 3 through 7 show the completed system as it currently exists and is being used to inspect ablative skirts. By reference to these figures it is also possible to see how all the performance criteria were achieved.

Inspection Unit

Figure 3 illustrates the basic inspection unit. In the approximate center of the unit is the turntable upon which the skirts rest during inspection. The top of the unit or "bridge" is removable for positioning a skirt on the turntable prior to inspection or removing it afterward. Only two cannon plugs are disconnected to permit bridge removal or reconnected when the bridge is replaced on the unit. Suspended from this bridge is the microwave carriage and its associated drive mechanisms which fit inside the skirt. To the right of the skirt is the sonic tapper and its drive mechanisms. The main drive motor is located at the lower left of the unit where it is connected directly to both the turntable and a selsyn transmitter. Two independent selsyn receivers drive the microwave carriage and/or sonic tapper vertically by means of the leadscrews shown. In this manner, the relationship of turntable rotational and microwave or sonic vertical travel speeds is kept constant permitting 1 in. of vertical travel per turntable revolution, regardless of turntable speed.

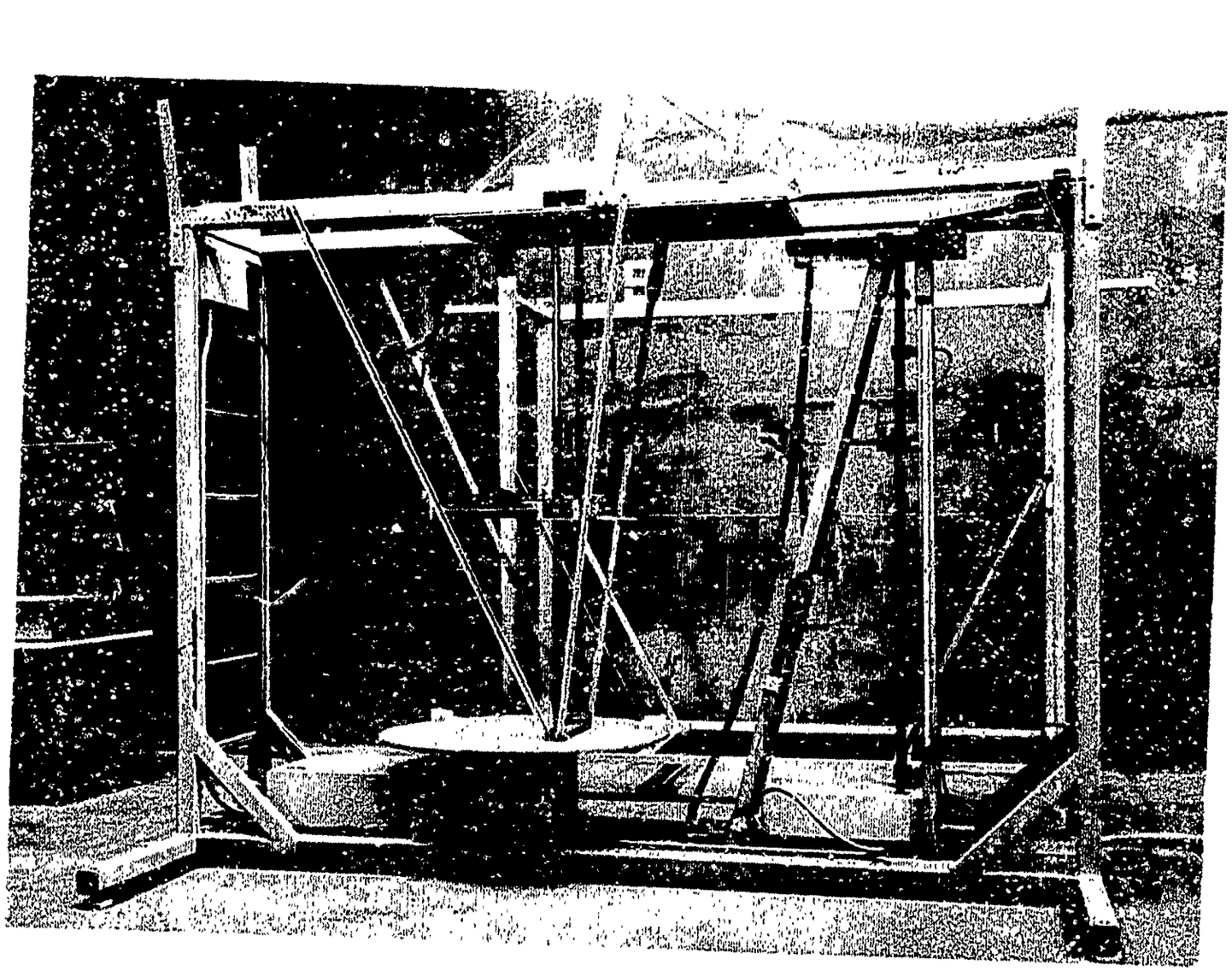


FIGURE 3 BASIC INSPECTION UNIT

Figure 4 is a close-up view of the microwave carriage showing not only its leadscrew drive but also the oscillator, antenna or horn, and interconnecting wave guide. The negator springs hold the horn against the interior of the skirt with constant pressure despite the constantly changing skirt radius.

Figure 5 is a comparable close-up of the sonic tapper. The wheel allows the tapper to ride along the skirt exterior at a relatively fixed position so that each tap will strike the skirt with equal force. Negator springs are used here also to maintain a constant wheel pressure against the skirt. The microphone picks up the sound of the tapper as it strikes the skirt and transmits this sound to the control console shown in Figure 6.

Control Console

The righthand side of the control console contains the oscilloscope, turntable and vertical drive controls, and the microwave sweep generator. The oscilloscope portrays the entire depth trace of the microwave signal. For recording purposes, as many as three discrete depths along this trace may be selected. These depths are selected by positioning electronic gates along the depth trace as portrayed on the oscilloscope. Each depth selected produces output on one of the three recorder channels.

The drive controls permit selection of sonic, microwave and/or turntable drives, adjustment of the speed from 0.5 to 6.0 rpm, and choice of either up or down directions for the vertical drive as well as clockwise or counterclockwise turntable rotation.

The sweep generator provides an input to the oscillator causing it to sweep the microwave frequencies in the Ka Band (26.5 to 40 GHz) at a repetition rate of 1,000 times per second.

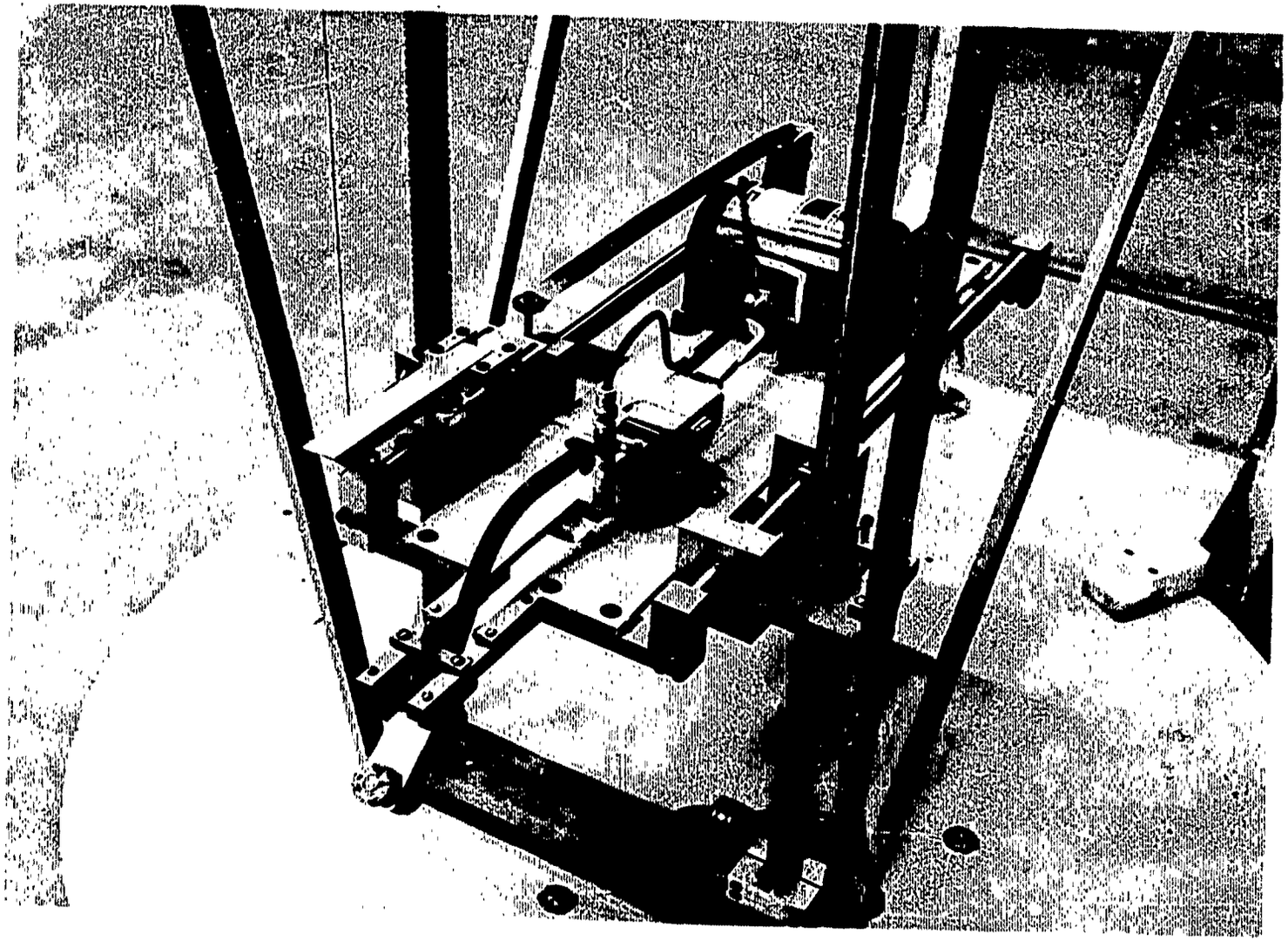


FIGURE 4 MICROWAVE CARRIAGE

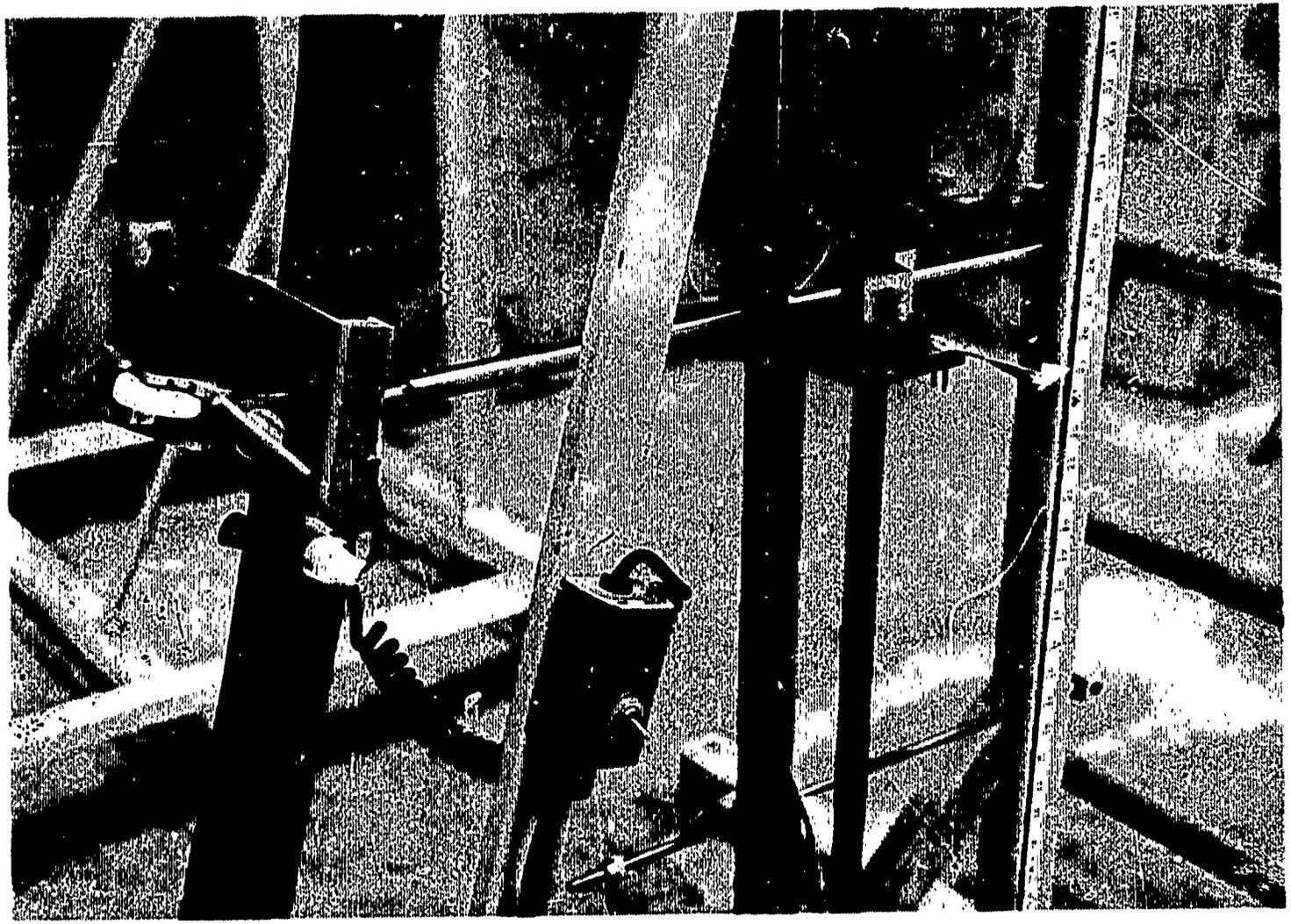


FIGURE 5 SONIC TAPPER

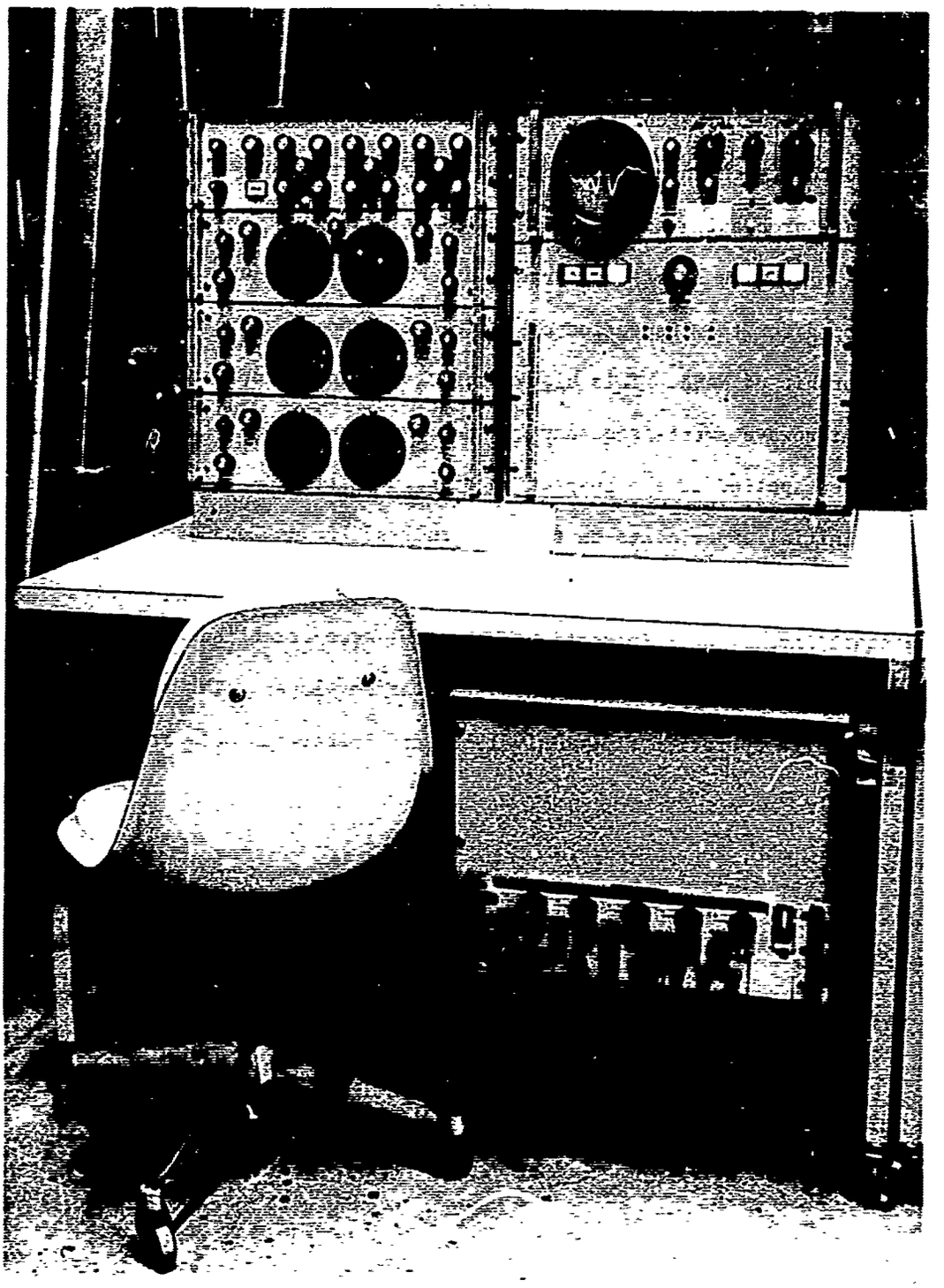


FIGURE 6 CONTROL CONSOLE

The microwave controls for depth selection, phasing, gain, and the like are located at the top left of the console. Three identical sets of controls are available for independent settings of each of the three available recording channels. Below these microwave controls are the three channels of sonic inspection controls. The large dials adjust the low and high pass filters which determine which band of sonic frequencies will be recorded on each channel. Zero-suppression, limiting gain, and time-constant controls are also available for each channel increasing the flexibility of data presentation.

Recorder

Figure 7 shows the three channel drum recorder on which either sonic or microwave data may be displayed. The pens are of the heated stylus type which eliminated the ink clogging problems often encountered on long runs with ink-pen recorders. The most significant feature of this recorder is its synchronization with both the rotational and vertical drives of the inspection unit. The drums revolve once for each turntable rotation and the pens move left or right 1/2 in. for every vertical inch of microwave carriage or sonic tapper travel. Moreover the drum circumference is exactly 18-in. so that each inch of this circumference corresponds to 20° of arc on the skirt being inspected, regardless of its size or configuration.

SYSTEM OPERATION

After the skirt is positioned on the turntable, the microwave carriage is driven to the top and the horn slid into contact with the as-molded surface in line with an arbitrarily established skirt zero.

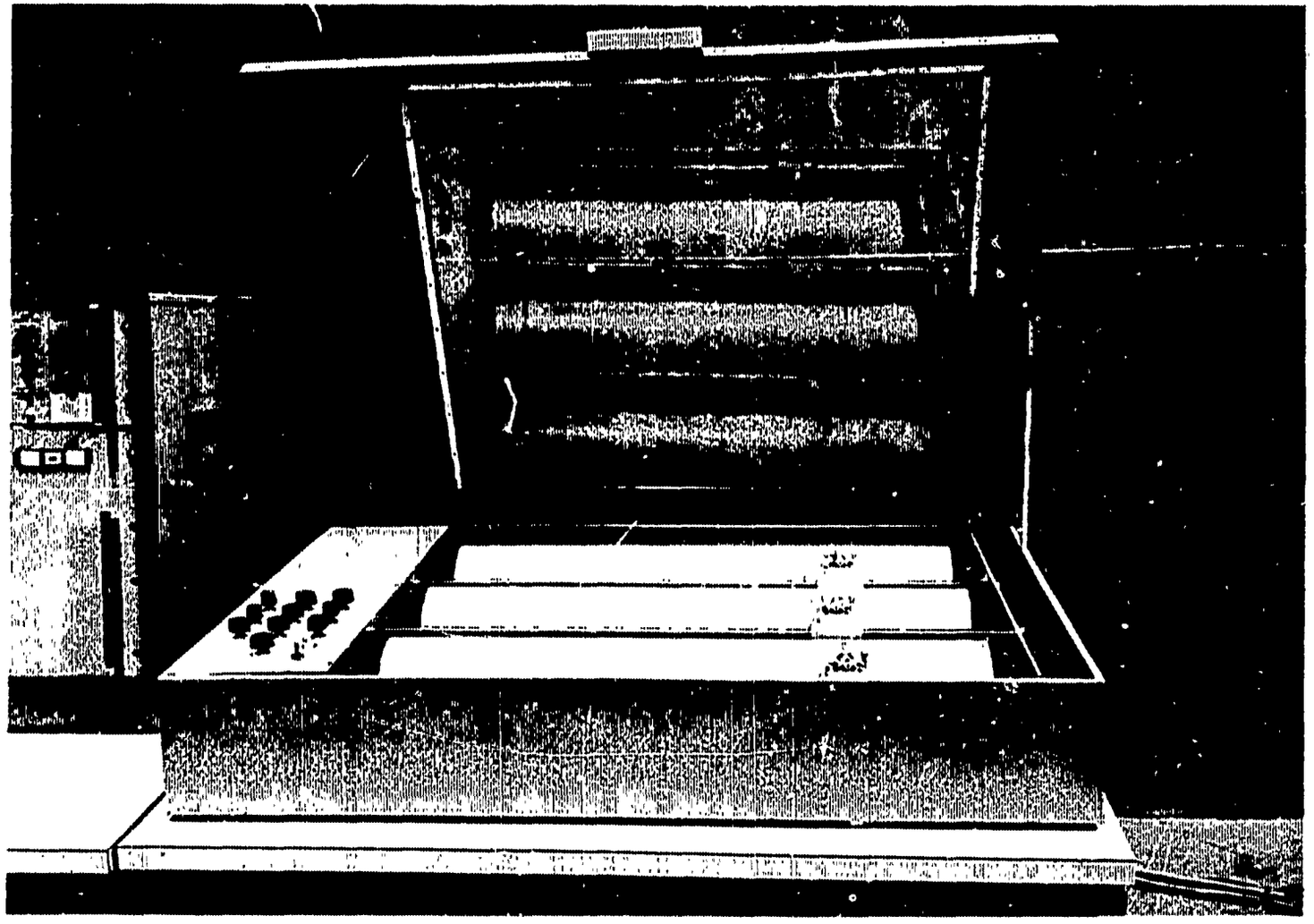


FIGURE 7 THREE-CHANNEL DRUM RECORDER

The oscilloscope trace is used to establish the desired inspection depths and the speed control is set for approximately 2 rpm. As the turntable rotates and the leadscrew drives the microwave carriage down, a spiral inspection pattern is inscribed over the entire as-molded surface. The data is processed electronically and displayed on the drum recorder.

Figure 8 is a photograph of the data from one channel during an in-process inspection of a skirt liner with inner laminate applied. The layers of glass cloth which comprise the inner laminate are applied in twelve double overlapping sections and these overlaps are clearly indicated on the recorder trace. No defects were found in this particular skirt.

At the conclusion of a run in which a suspect area has been noted, the carriage is returned to an area an inch or so above the suspect area and "mapping" scans are made. For these scans, the skirt is inspected during one rotational turn, the carriage moved downward 1/4-in. and a second rotational scan is accomplished. This alternate vertical and rotational process is continued until a complete map of the suspect area is on the recorder. An example of this type of mapping is shown on Figure 9. Three series of scans were made on this occasion in an effort to determine optimum conditions for mapping, but one such series is normally sufficient. Determination of defect height and width during such mapping scans requires consideration of the overlapping effect of the microwave horn with respect to the actual defect dimensions. This situation and its solution are illustrated in Figure 10 using a liner delamination as an example.

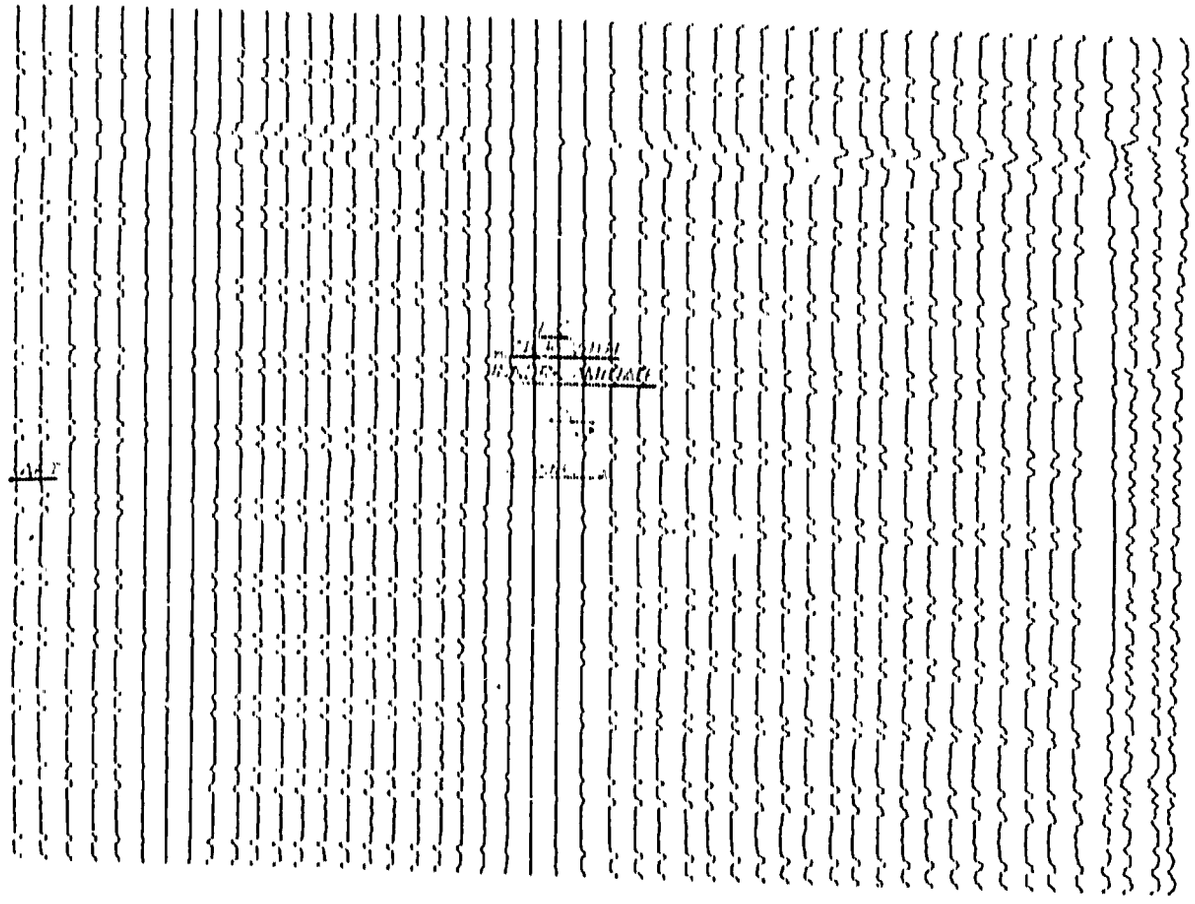


FIGURE 8

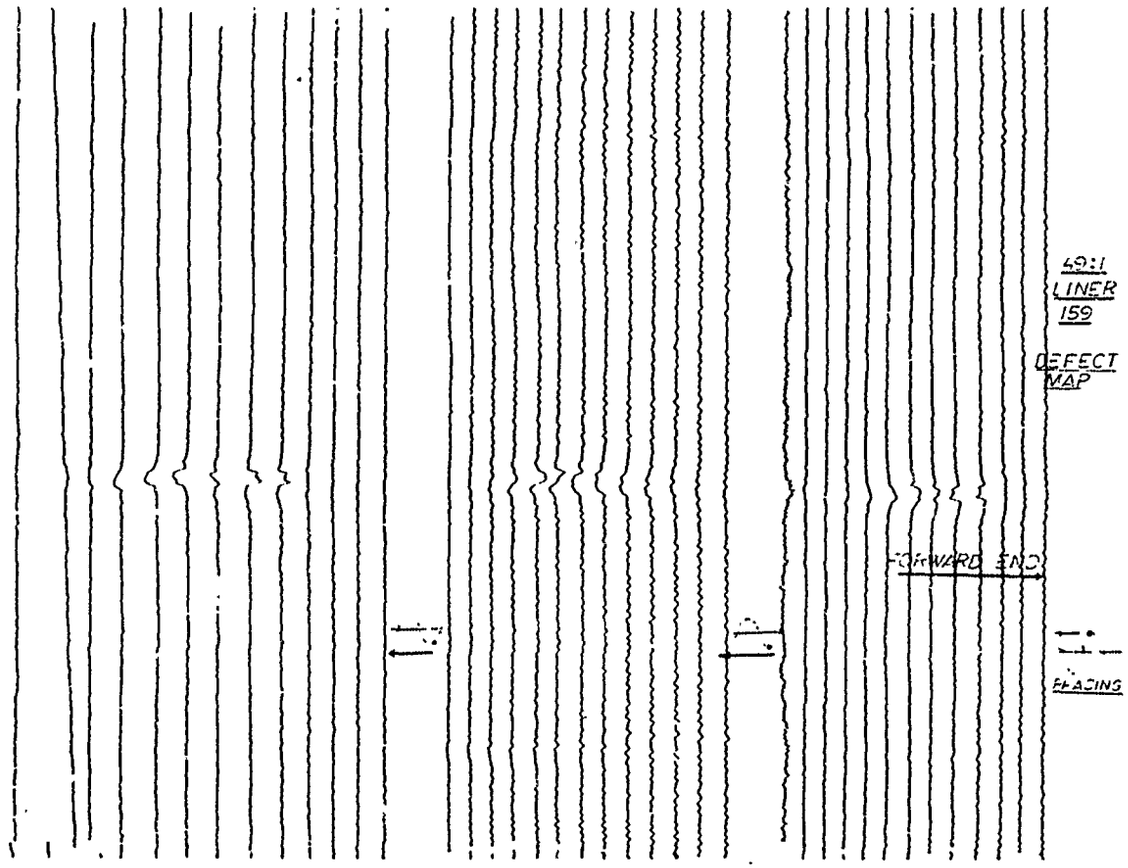
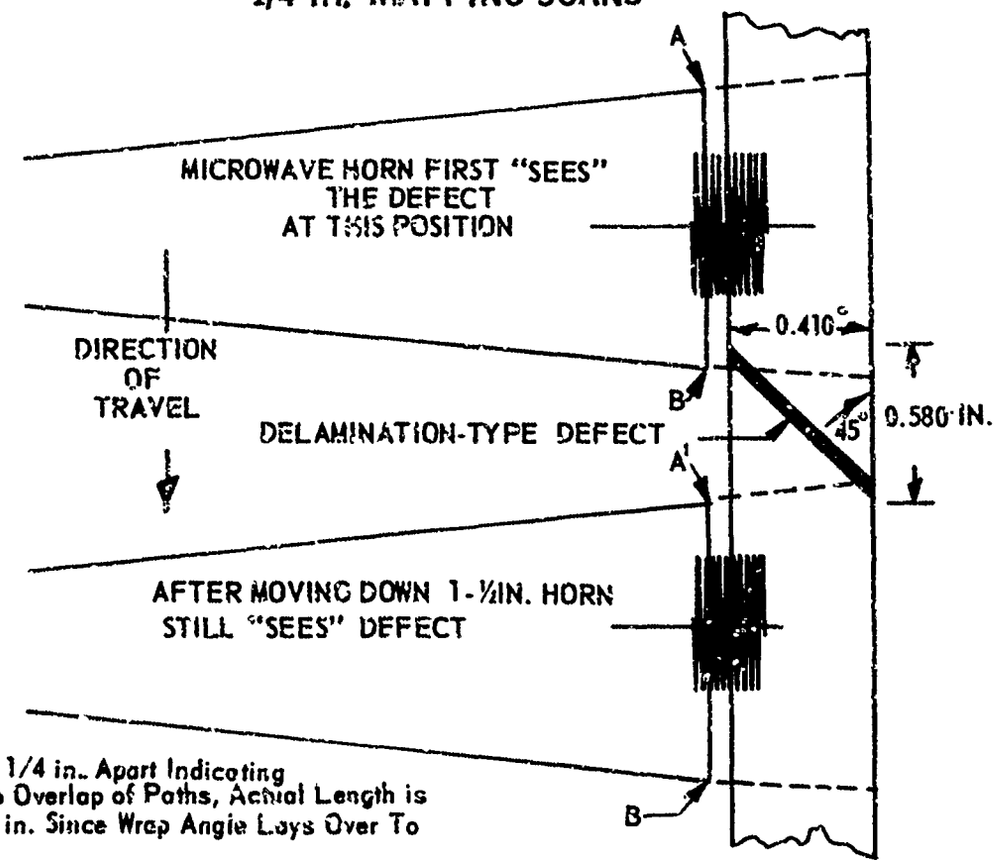


FIGURE 9

TITAN III NDT DEVELOPMENT PROGRAM

1/4 IN. MAPPING SCANS



Defect Appears on 6 Traces, 1/4 in. Apart Indicating 1-½ in. Defect Length. Due to Overlap of Paths, Actual Length is About 1/3rd or Closer to 0.5 in. Since Wrap Angle Lays Over To Less Than 45°

AEROJET GENERAL®

PROPULSION DIVISION

FIGURE 10

AGCS-0100-52 (REV. 1/68)

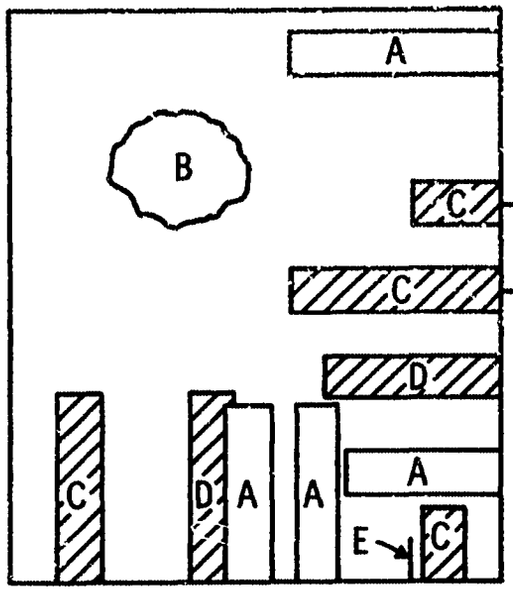
Depth of a suspect area within a part is determined partly by knowledge of the original depth settings and the channel or channels on which the defect indication appeared. This information is usually supplemented by comparing the entire depth trace on the oscilloscope with equivalent presentations obtained from the defect specimens mentioned previously. Figure 11 illustrates this principle by using double exposure scope photographs wherein the "A" trace represents the signal from the indicated type of defect. On these scope photos, the first major peak from the left represents the specimen's front surface reflection and depth into the part increases toward the right. On Figure 11, the upper photograph displays a built-in defect slightly deeper into the specimen than does the lower photograph and the major change in the trace occurs somewhat further to the right for this slightly deeper defect.

The sonic system processes signals obtained by tapping ablative skirts in essentially the manner shown on Figure 12. After the characteristic frequency spectra had been determined experimentally for each skirt configuration, it is a relatively simple process to set the frequency controls to pass only the desired signals. Only two channels are shown being used in Figure 12, but the third is normally set to duplicate the lower trace as backup information since a suspect area is somewhat more apparent on this type of trace. The sonic tapper inscribes a spiral pattern on the exterior of the skirt comparable to that of the microwave horn on the interior. As a result, the location of suspect areas can be determined from the recorder read-out in substantially the same manner.

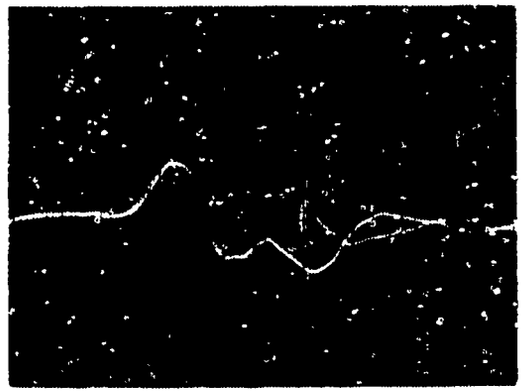
TITAN III NDT DEVELOPMENT PROGRAM

DEFECT SPECIMENS

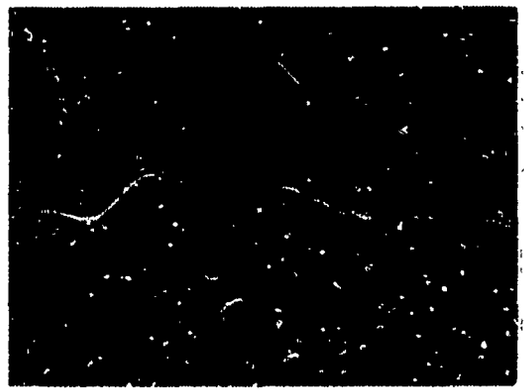
Defect Specimen #3



"A" Designates Good Trace



Honeycomb To Film Adhesive Unbond



Inner Laminate To Film Adhesive Unbond

A. Outer Laminate Delamination
B. Crushed Honeycomb
C. Honeycomb/Inner Laminate Unbond
D. Liner/Inner Laminate Unbond
E. Cracked Liner

☐ Defect for Sonic Test
▨ Defect for Microwave Test

AEROJET GENERAL

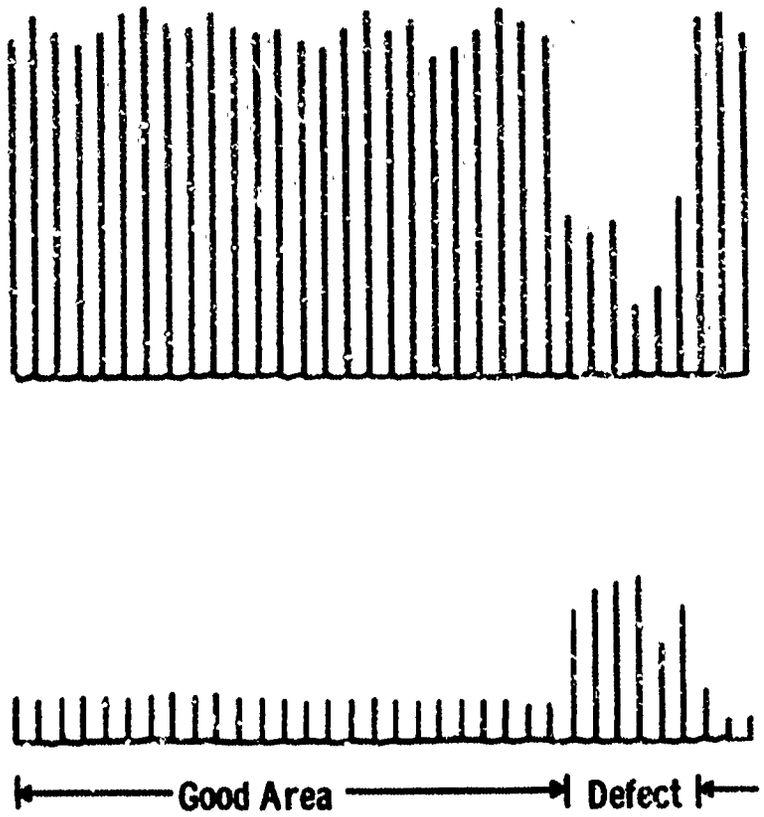
PROPULSION DIVISION

FIGURE 11

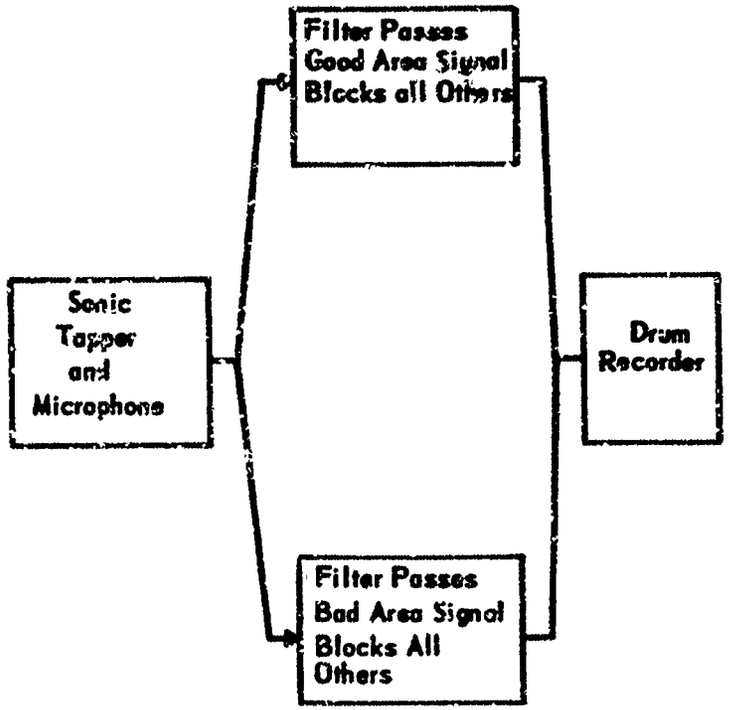
TITAN III NDT DEVELOPMENT PROGRAM

REPRESENTATION OF SONIC DATA

Recorder Display



SYSTEM OPERATION



AEROJET GENERAL

PROPULSION DIVISION

FIGURE 12

The sonic system will not depth-differentiate between outer laminate and honeycomb defects; but this information proved unnecessary since a repair of either layer is normally accomplished by replacement of both the honeycomb and outer laminate layers in the defective area.

CONCLUSION

The sonic/microwave system for inspection of ablative skirts has been in virtually continual operation since July of 1968. Skirts receive microwave inspections following fabrication of the liner and again after addition of the inner laminate to the liner. Following application of the honeycomb and outer laminates, skirts receive both sonic and microwave inspections after which the article is essentially ready for delivery as a completed, acceptable unit.

The program to develop these NDT methods for Titan III Ablative Skirts may be characterized as a complete success. All inspection goals were achieved and, in less than 12 months, both sonic and microwave techniques progressed through feasibility study, completed prototype development, and have become routine nondestructive testing methods for all ablative skirts.

SD 68-986

X-RAY MAPPING OF FLAWS BY COMPUTER GRAPHICS

November 1968

By

Frederick Hartmann

SPACE DIVISION
NORTH AMERICAN ROCKWELL CORPORATION

FOREWORD

This paper describes a new method of three-dimensional analysis of weld defects developed at the Space Division of North American Rockwell Corporation. The author would like to express his thanks to several persons: to B. J. Huffman, who not only designed and directed the construction of the shape reconstruction computer but also contributed to other phases of the problem; to Miss J. A. Brown and J. H. Bosler, who performed most of the X-ray work; to R. C. Setzer, who did a great deal of programming and other mathematical calculations; and to S. Young, Jr., and R. G. Poe, who carried out microdensitometric and other work.

ABSTRACT

A new process that gives a three-dimensional picture of the shape and location of invisible discontinuities (gas holes, cracks, etc.) in metallic or nonmetallic materials has been reduced to practice.

Two X-ray films of the defective structure are taken from different angles, with a provision for accurate registration between them. A standard wedge of the same composition is X-rayed simultaneously. Density readings—obtained from microdensitometer scans at given intervals—are converted into thickness values, with a correction for scattering if necessary. The resulting data are digitized and put on tape. This is fed into a specially built "shape reconstruction computer," which, by means of a novel superposition algorithm, computes for each scan the cross section of the defect and displays it on its cathode ray tube. Tape feed, computation, and photography of the CRT display take only a few seconds. A series of cross sections yields a three-dimensional picture.

Samples of sheet aluminum and welds containing defects were analyzed in this manner. Very good agreement was obtained when computer-derived pictures of shape and location of the defects were compared with photographic enlargements of the sectioned samples.

CONTENTS

	Page
INTRODUCTION	1
SINGLE-FILM RADIOGRAPHY	3
THREE-DIMENSIONAL X-RAY MAPPING	7
Superposition of Two Films	7
Shape Algorithm	9
Inclusions and Composite Materials	11
Oblique Angles	12
Nonconvex and Multiple Shapes	12
Inconsistency	14
SHAPE RECONSTRUCTION COMPUTER	17
SAMPLE CASES	23
Materials and Procedures	23
Results	29
Weld Samples	33
SUMMARY	37
REFERENCES	39

ILLUSTRATIONS

Figure		Page
1	X-Rays and Photographic Density	4
2	Transformation of Optical Density Into Sample Thickness	5
3	Three-Dimensional Location of a Discontinuity	8
4	Thickness Problem	9
5	Algorithm Rules	10
6	An 11 by 11 Problem and Its Digital Solution	11
7	Oblique Illumination	13
8	Inconsistency of Data Due to Digitization	14
9	Shape Reconstruction Computer	18
10	Data Processor Control Panel	20
11	Three Regions (Flesh, Bone, and Marrow) in Finger Cross Section	21
12	Dimensions of Sample	24
13	Radiographic Density of Defect Region (0°)	26
14	Radiographic Density of Calibration Wedge (0°)	26
15	Densitogram of Defect Region (45°R)	27
16	Densitogram of Right Edge of Sample (45°R)	27
17	Three Views of Cross-Section A	30
18	Actual and Computed Shape and Location of Flaw	32
19	Weld Sample No. 26: Metallographic Section at Plane D (10X)	34
20	Left Upper Part of Figure 19 (25X)	34
21	Computed Shape and Location of Flaws of Sample 26, Plane D (About 25X)	34
22	Densitogram of Defect Region, 0°, of Weld Sample 26, Plane D	35
23	Densitogram of Defect Region, 0°, of Sample 27, Plane C	35

INTRODUCTION

Faultless welding, under the best of circumstances, is no simple task. For a large structure, and particularly one used in manned space flight, its problems lie at the boundary of present technology. Integrity of welded junctures is of such concern that large amounts of effort and money are spent just for inspection, repair, and re-inspection.

For most defects—porosity voids, incomplete penetration, incomplete fusion, longitudinal oxide folds, etc. —acceptance or rejection of the weld depends on the type, size, and location of the faulty areas. Since a single X-ray film shows only the projection of a defect onto the x-y plane, it gives only limited information on these three characteristic features. Inspection of the film tells little about the depth of the defect and nothing about whether it is closer to the outer or inner surface of the structure. Occasionally two pictures are taken to locate, by triangulation, the z distance of some ill-defined part of the defect. Almost nothing, however, is known about its three-dimensional shape.

Many advantages could be expected from a precise three-dimensional picture of defects obtained through non-destructive testing. First, there would be a saving in repair costs from the knowledge of where to start the repair work and how far to go. Next, there would be the benefit of differentiating between a defect in a non-stress region (where the weld may be acceptable) and a stress region (where it has to be rejected). There also would be the possibility of finding a crack underneath a harmless gas hole. There are probably other shape-specific features that would permit a redefinition of the accept-reject criteria in sharply defined terms. Adoption of the new criteria, together with routine three-dimensional measurements, would lead to a better assessment of the integrity of a welded section. The resulting combination of higher reliability and lower repair cost would be a notable advance in welding technology

This report describes a novel method which yields the desired three-dimensional description of the shape and location of voids, inclusions, and other defects. Accurate densitometric records of two X-ray pictures of the defect taken at known angles are obtained for selected planes (profiles) of the defect. From these records precise location limits of the defect can be read off almost immediately. Density data are converted into metal thickness values along two directions; a novel superposition algorithm combines the thickness values into a picture of the cross section of the defect. A special-purpose "shape reconstruction computer"—built to use the

superposition algorithm—is fed a tape of the digitized data. Within a few seconds it computes and displays on its cathode ray tube the desired cross section of the defect for each profile pair. Several cross sections yield a three-dimensional description. As test cases, several defective aluminum samples and welds containing flaws were X rayed and analyzed.

The method can be used easily with other materials and in other techniques. Instead of filmed X-ray records one could employ, for example, a system in which a beam of collimated gamma rays scanning the sample sequentially is measured by scintillation counters and either recorded on magnetic tape or fed directly into the shape computer. Other forms of directed energy (e.g., neutrons, ultrasonics) could be used to map properties of an unknown sample by the correlation of two or more signals obtained after absorption, reflection, refraction, or scattering. While the present investigation deals with metal voids and inclusions, other structural features in metals and non-metals can be determined. The application to medical radiology (bone density and bone shape) is obvious and was actually the starting point of this investigation. The extension of the method to other techniques and materials will be handled in later reports.

SINGLE-FILM RADIOGRAPHY

The method of obtaining quantitative data from a single X-ray film combines the technique of ordinary industrial or medical radiography (see Reference 1) for x-y information with that of film densitometry (Reference 2) for z data. Figure 1 shows the essential features of the method.

Figure 1A depicts schematically the X raying of an aluminum block (with a hole) and a calibration wedge of the same material. It is convenient to use a coordinate system with the origin at the left lower corner of the block; the x direction is thus from left to right of the figure, z represents the thickness, and "profile" refers to a given y value. This coordinate system remains firmly anchored in the block even though the latter may be moved.

The developed film is shown in Figure 1B. Using an X-ray tube with a small focal spot and a film with a fine-grained emulsion and a steep characteristic curve (blackening versus logarithm of relative exposure), one obtains a picture of good definition and sharp contrast. Scattering effects must also be low (this is true for aluminum of not more than moderate thickness).

Figure 1C shows in schematic form the recording made by a densitometer at the profile (y plane) B_1B_2. Curve C_0 to C_8 shows the film density obtained in the recording. Block and wedge reduce the intensity of the X-ray beams, largely through absorption. Under ideal conditions and for monochromatic X rays, the fractional reduction is proportional to the narrow beam attenuation coefficient, μ, and to the layer thickness, dz, :

$$-\frac{dI}{I} = \mu\, dz$$

Ordinary X rays, however, emit a whole spectrum of wave lengths which, together with secondary effects (geometry and buildup factor), prevent the determination of the thickness z through integration of the equation (Reference 3). In lieu of theory, an experimental internal standard (e. g., a wedge of known thickness) is used and the unknown is compared with this standard in the hope that differences in geometry do not seriously influence the results. In Figure 1C the calibration wedge produces a gradual nonlinear density reduction between C_4 and C_7. The wedge also corrects for density changes due to film development and other factors.

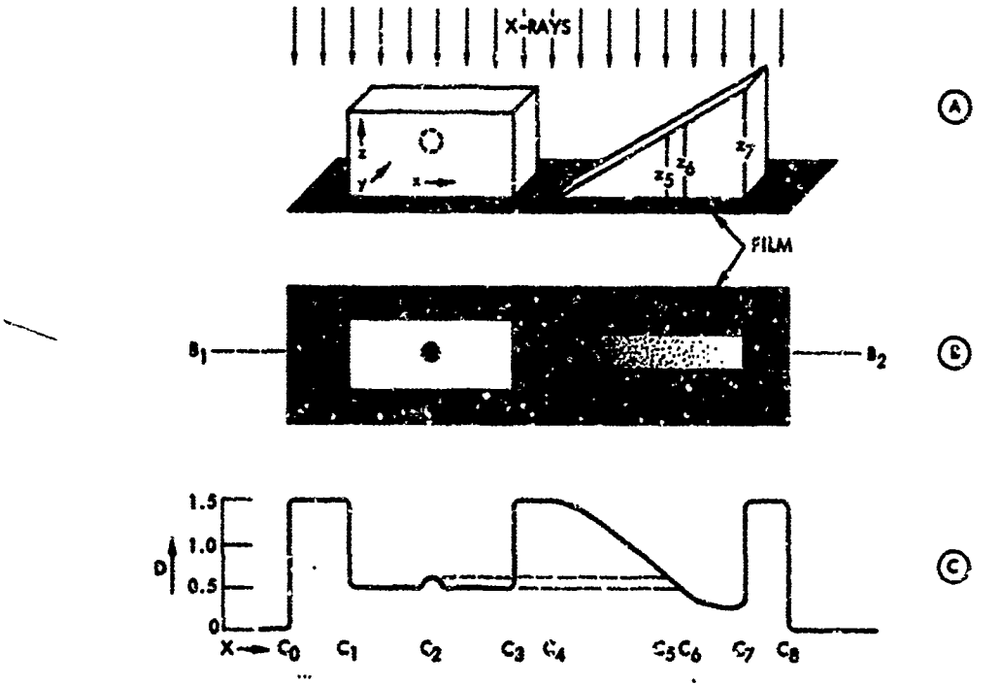


Figure 1. X Rays and Photographic Density

Comparing lines of equal D value, one finds that the block has a thickness z_6 outside the hole and z_5 at the center of the hole. Maximum hole depth thus equals $z_6 - z_5$. Figure 2 shows, on a larger scale, the graphical construction (inverse function formation, which is easily computerized) by which all hole (or thickness) dimensions in the neighborhood of point C_2 of Figure 1C can be found. In Figure 2A, the density record of the calibration wedge C_4 to C_7 of Figure 1C has been changed from a D-x to a D-z plot. The density of the sample near the hole is shown in Figure 2B as the D-x densiometer recording. Figure 2C gives as the result of a simple construction (dashed lines) the curve $T'_z(x)$, the sample thickness in the z direction as a function of x. Assuming that the sample has a uniform external thickness, T'_z max, the shaded area indicates hole thickness.

This shaded area is the total information on the hole cross-section at the plane B_1 B_2 that may be obtained from single-film densitometry. It points out the fundamental limitations of the method. In the first place, it says nothing about the location of the hole along the z axis (i.e., whether it is near the upper or lower face of the block). Secondly, an infinity of shapes is consistent with the shading. The shape may be an elliptical void, or a void hiding a crack, as shown in Figure 2D. Finally, two or more separate voids whose combined thickness (for each x) equals that of the shaded area, are consistent with the results shown in Figures 1B, 1C, and 2C. To describe the holes in terms of location and shape, a different approach is needed.

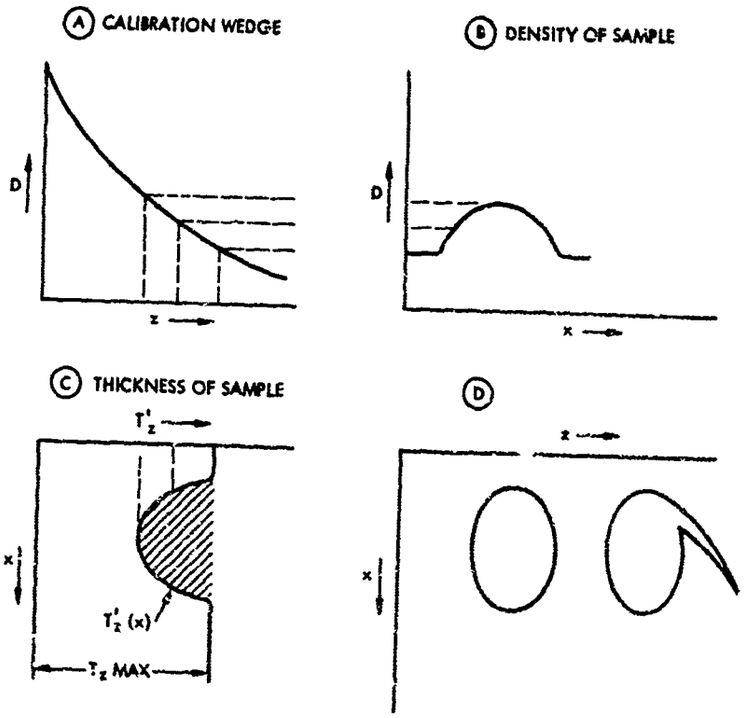


Figure 2. Transformation of Optical Density Into Sample Thickness

THREE-DIMENSIONAL X-RAY MAPPING

SUPERPOSITION OF TWO FILMS

Three-dimensional mapping by X rays, described for the first time in this report, is based on the correlation of densitometric information from two or more X-ray films taken at an angle to each other.

The process is the equivalent of photogrammetry, a method of terrain mapping with the aid of two or more photographs. A single photograph, representing the mapping of space through a central projection onto a plane, yields only limited dimensional information. In photogrammetry, two or more such central projections—usually photographs taken from an airplane—are combined into a map that contains separate terrain (x, y) features, contour lines (z), etc. The combination process, essentially a linear transformation (Reference 4), is performed by special drafting machines first developed in Germany in the 1920's. More than 80 percent of all maps in the U. S. are now prepared in this manner.

The image-formation process for X rays is, unfortunately, totally different from that for optical rays. In lieu of sharp shadows of objects, one obtains only density gradations which follow complicated absorption and photographic interaction laws; the comparatively simple linear transformation is not valid at all.

To illustrate the new X-ray mapping process, the same example as in Figure 1 (the block with hole plus standard wedge) will be used. The first X-ray film is taken as before. For the second X-ray the block (but not the wedge) is turned on its left side (i.e., on the y-z plane so that the X-rays are now parallel with the x axis). The density of the developed film is recorded for the same y profile (the plane determined by B_1B_2) and yields a graph C'_0 to C'_8 (not shown) similar to C_0 to C_8 of Figure 1C. From this graph the thickness of the block in the x direction, $T'_x(z)$, can be determined as before for all values of z. A convenient arrangement of the two thickness functions together with the object that they describe is given in Figure 3.

Figure 3A shows schematically a cross-section of the block taken at profile $y=y_0$, with an invisible elliptical hole near the lower right corner. Figure 3B, repeating Figure 2C in a downward manner, gives the thickness of the block in the z direction, $T'_z(x)$, while Figure 3C shows in a similar manner the thickness in the x direction, $T'_x(z)$. The length unit is the same in all parts of the figure.

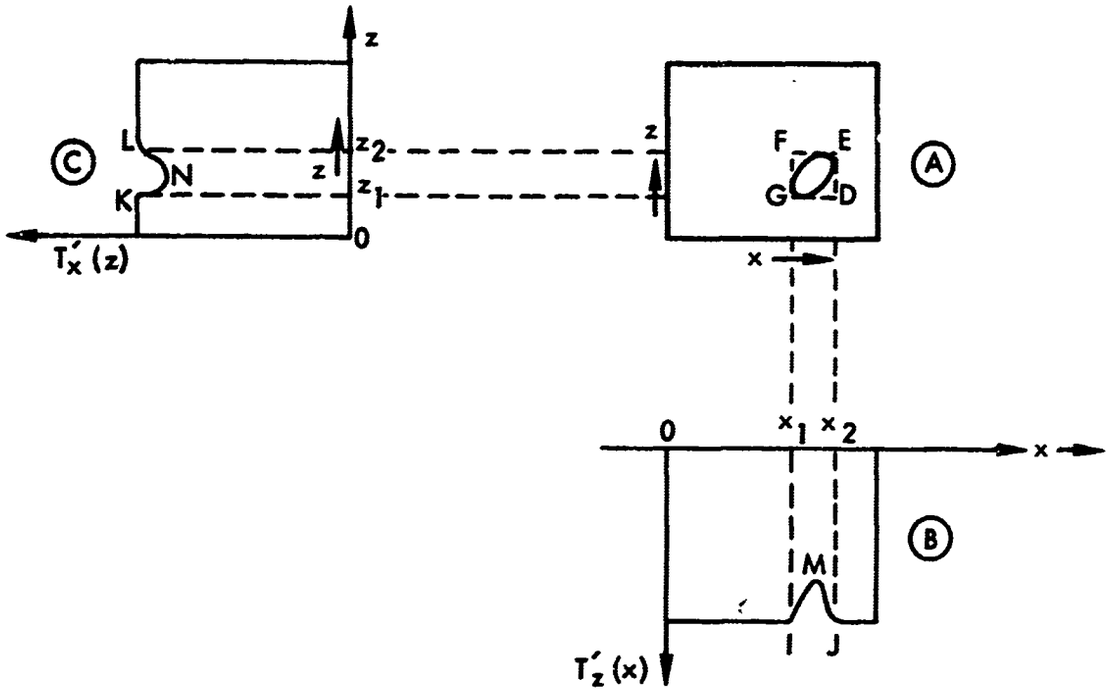


Figure 3. Three-Dimensional Location of a Discontinuity

The spatial location of the hole—or rather its cross-sectional limits at the plane $y=y_o$—can now be read off immediately. The sudden change of thickness, $T'_z(x)$ at points I and J locates the left and right limits at x_1 and x_2 (dashed lines); similarly K and L determine z_1 and z_2. A characteristic rectangle, DEFG (dashed lines), is thus defined, the sides of which are tangents to the hole in the x and z directions.

Although the location limits of the hole are very easily determined. its shape is a more formidable problem. Hole thickness, T, in each dimension is given by the difference between maximum and actual thickness, $T_z(x) = T_z^{max} - T'_z(x)$ and $T_x(z) = T_x^{max} - T'_x(z)$, and is thus shown as the inversion of the curves IMJ and KNL, respectively. The situation is illustrated on an enlarged scale in Figure 4, which is restricted to the dimensions of the hole. The problem, now one of pure geometry, can be stated as follows: "Given the thickness values of a closed curve in two perpendicular directions, determine the perimeter of the curve."

The difficulty of the problem lies in the fact that although at any level (e. g., at z_o) the curve thickness is given by the length $T_x(z_o)$, the location

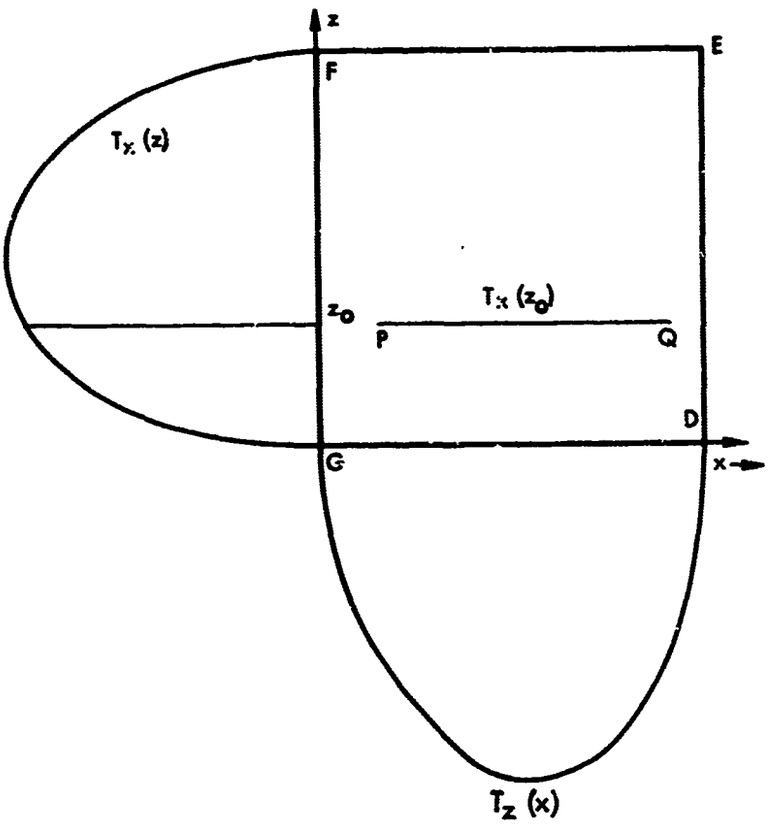


Figure 4. Thickness Problem

of the end points P and Q is unknown. No generally valid answer to the problem seems to exist (References 5, 6) although approaches using power or Fourier series coefficients look not unpromising. At this time, the author's algorithm, developed in early July 1966, remains the only practical approach.

SHAPE ALGORITHM

The algorithm starts with an area which is proved to lie totally inside the desired boundary and one or several areas outside of it. In a series of converging steps the perimeters of inside and outside areas approach each other until they finally merge. The solution may be obtained in a continuous or discrete (digital) manner. The digitization process assumes a ruled grid of sufficient fineness, in which the squares inside the curve are designated as 1's and those outside as 0's. The input data, $T_z(x)$ and $T_x(z)$, are now simply a series of numbers. It is furthermore assumed that the closed curve has not more than two intersection points with any straight line in the x or z direction (x-z convexity). To find the starting areas for the 1's and 0's, two rules are used which are illustrated in Figure 5.

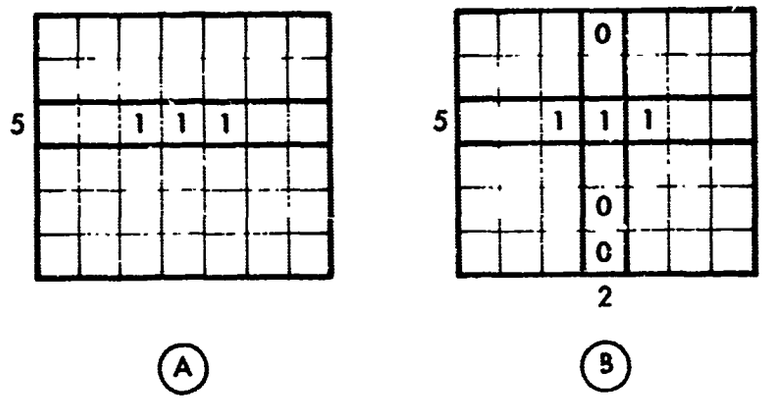


Figure 5. Algorithm Rules

The basic rectangle of Figure 5 has the dimensions 7 x 6. In Figure 5A, the input length for the third row is given as 5 units. Counting from the left and from the right side, one has an overlap of three units. The central three squares must be "occupied" while at this stage nothing else is known about this row. This rule of overlap, applied to all rows and columns in which more than half of the length is occupied, leads to the formation of the initial inner core.

Figure 5B shows that Column 4 calls for a total of two length units, one of which has already been found in the step of Figure 5A. Since the other must be immediately above or below, the three remaining squares in the column must be 0's. Applied to all rows and columns in which previously proven 1's were found, the initial outer (zero) areas are defined. Alternating row and column search for 1's and 0's will gradually increase both areas until all squares are occupied. The zigzag boundary between 1's and 0's forms the digitized version of the desired perimeter. Figure 6 shows inputs and solution of the problem illustrated in Figure 4 on a grid size 11 by 11.

For cases where no start or no end of the algorithm can be found, one arbitrarily assumes a 1 (or a 0) in a square and carries on until either a contradiction or a solution is found. Although sometimes more than one solution is possible, it is believed that the use of a finer grid will usually lead to a preference of one over the other result. If serious doubts remain, an X ray taken from a third direction will remove the ambiguity.

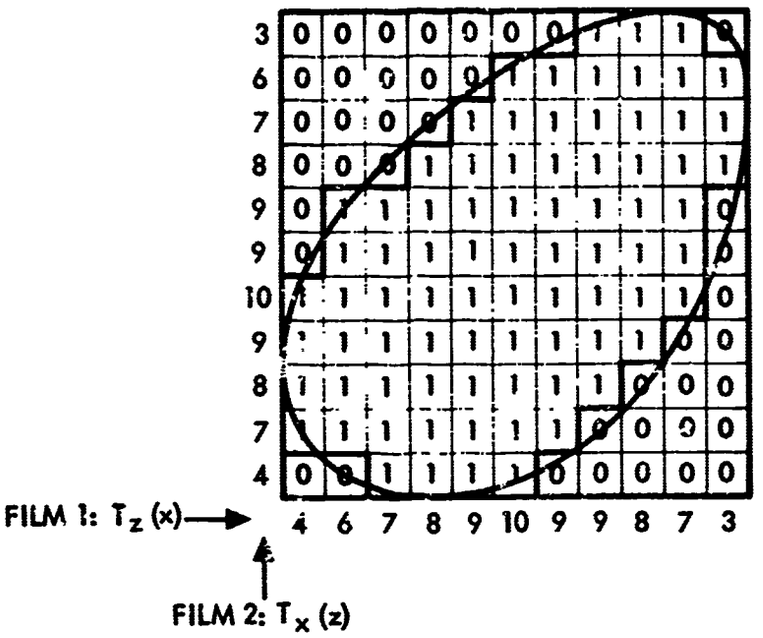


Figure 6. An 11 by 11 Problem and Its Digital Solution

Using the above two rules plus others, the algorithm was programmed for computers and several sample problems were solved in a few seconds' computer time (Reference 7).

The solution given so far holds for a rather restricted problem. It depends on a set of consistent thickness data obtained from two 90-degree X-ray pictures of a homogeneous material with a single convex void. In the following paragraphs, these restrictions will be removed, partial or complete solutions of the extended problems will be described, and, where no solution exists, the direction of future research indicated.

INCLUSIONS AND COMPOSITE MATERIALS

If the defect consists of an inclusion (e.g., an oxide or precipitated material whose composition differs from the parent metal), the superposition algorithm can be applied in a slightly modified form provided the external dimensions of the piece are known. One prepares two standard wedges, one of inclusion material (wedge angle α) and one of parent material (angle β), with a base of equal size. The wedges are put on top of each other in such a manner that the thickness of one material (inclusion) changes only in the x-direction, that of the other (parent) changes only in the y-direction.

Standard and sample are X-rayed simultaneously. Plotting lines of equal density and of equal total thickness of the standard wedge on one chart makes it easy to calculate the unknown thicknesses of the inclusion and parent body and thus reduce the problem to the case treated before. Details are given in Reference 8.

OBLIQUE ANGLES

In metallurgical and medical applications it is often impossible to take X-ray pictures at a 90-degree angle to each other, either because the material thickness becomes too great or because of an interfering structure. It is very fortunate, therefore, that method and algorithm can easily be extended to any angle. In taking two pictures with an oblique angle to each other, one may either keep each film perpendicular to the direction of the beam or have at least one film deviate from perpendicularity. The latter technique is, for example, advisable for a large cylindrical structure to which one likes the film to adhere closely no matter what direction the X rays came from.

Attention has therefore to be paid to the angle that the films make with the direction of the X-ray beam. Calling the angle between the perpendicular to a film and the X-ray direction θ, Figure 7 illustrates a case in which θ is 0 degree for Film 1, and 45 degrees for Film 2. The sketch shows the same near-elliptical hole that was used in Figure 6.

While the area unit in the 90-degree case is a square, it is a rhombus of angle 90- θ in the general case. (This rhombus, although its sides are 1 unit long, has an area of only $\cos\theta$, which is the reason that the sum of the thickness values in Figure 7 is much larger than that of Figure 6 (115 cos 45° = 81). The greater number of readings, $T_0(x)$, on Film 1 of Figure 7 is due to the type of graph paper used: distance between vertical lines is $\cos\theta = 0.707$, instead of 1.) On Film 2, on which the distance between readings is 1 unit, each value of $T_{45}(z)$ refers to the number of unit rhombi of area $\cos\theta$. The number of readings in each direction (m x n) yields a "basic parallelogram," ABCD, the sides of which are tangents to the unknown shape. The algorithm—applied to the rhombi—proceeds as before.

NONCONVEX AND MULTIPLE SHAPES

Work is presently being done to deal with problems of nonconvex and multiple shapes because of their frequent occurrence in the two main fields of application (cracks, generalized porosity, kidneys, vertebrae, etc). In the case of a kidney-shaped hole, for example, it is usually possible to split the thickness data curves into an "outer" and "inner" part and solve for each part separately. A similar solution applies to double holes which are only

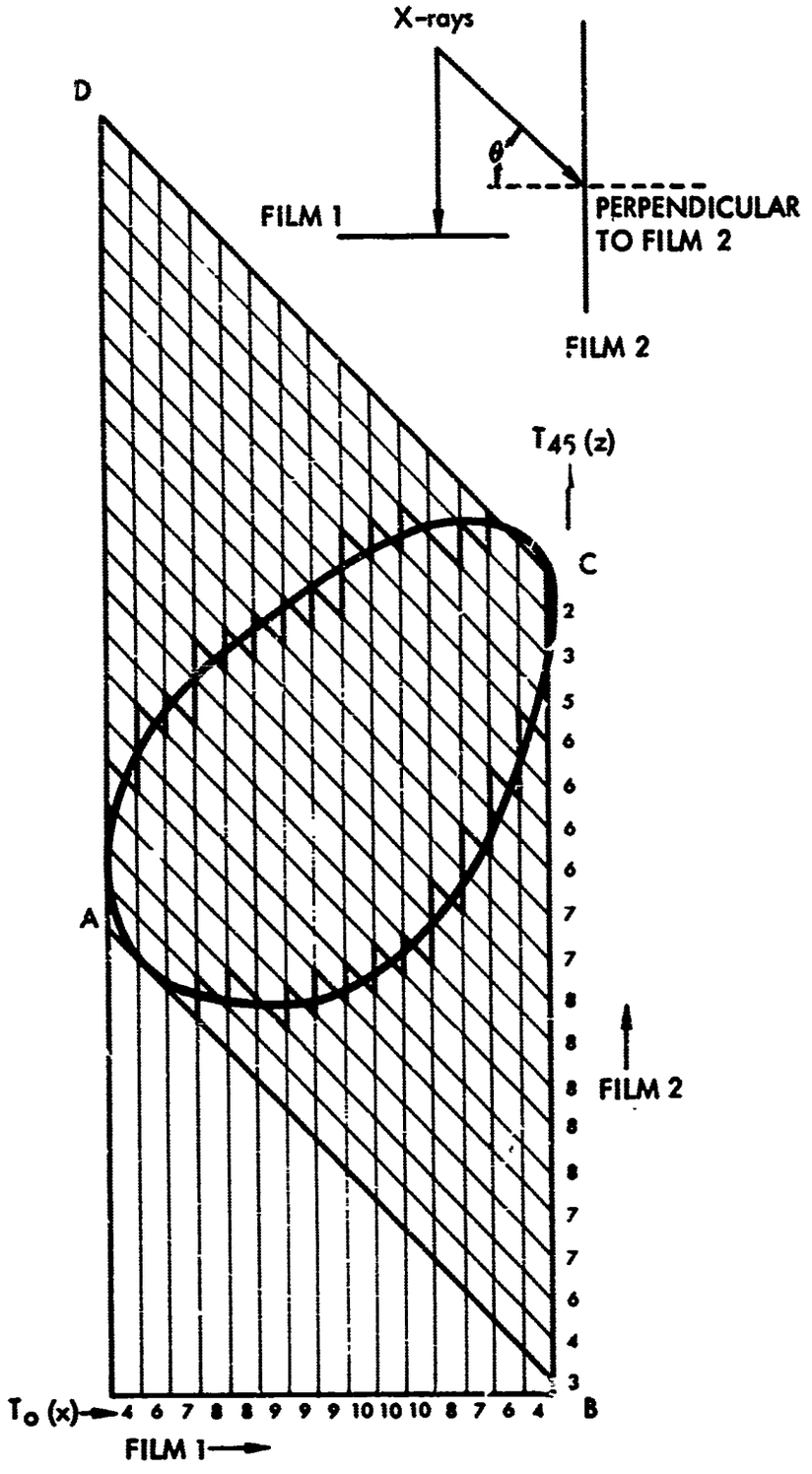


Figure 7. Oblique Illumination

partly separated. The methods are greatly simplified and possible ambiguities removed if a third X ray is added and made part of the calculation.

Further investigation is obviously needed for cases of general porosity, a frequent occurrence in metallurgical and biological specimens. Since the average density of a porous region is lower, one may, as a first approximation, consider all holes as a single uniform region and reduce the problem to the two-region, low-density inclusion case.

INCONSISTENCY

Inconsistency is a pervasive difficulty in the analysis of three-dimensional structures. It may occur as the result of at least three conditions: (1) deviations from the single convex shape that the original algorithm dealt with; (2) the digitization process (round-off error); and (3) experimental errors. Very often, two or three of these conditions occur simultaneously.

An example for Condition 1 was given previously, the nonconvexity of a kidney-shaped figure. Condition 2 is illustrated in Figure 8. For a grid size of 3 x 3, experimentally derived thickness values (for internal midpoints) are shown in Figure 8A. If one rounds them off in the usual manner. Figure 8B shows a double inconsistency. Figures 8C to 8F show four ways to change the inputs to obtain consistency under the assumption that the original data were 1, 2.5^-, or 2.5^+. The changes necessary to obtain consistency (i.e., to obtain a closed figure) should be made within the limits of experimental error. If there are several inconsistent input data, the least total change, perhaps in the form of a $\Sigma\ (\Delta^2)$ function, to obtain consistency is desired.

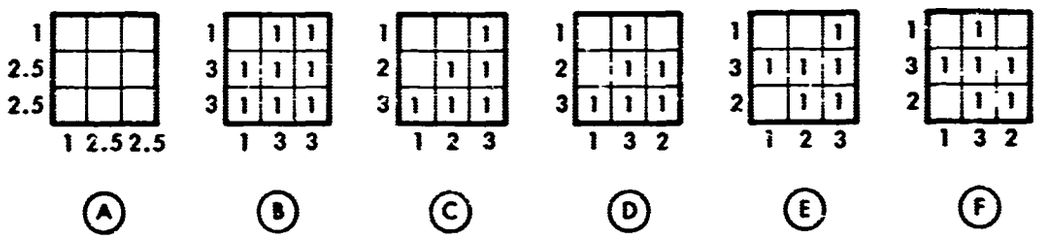


Figure 8. Inconsistency of Data Due to Digitization

No systematic way is presently known by which inconsistent input data can be made consistent through a minimum total change—at least not in cases of multiple inconsistencies. A trial and error method carried out by an experience operator with good judgment, however, will give near-optimum results. Since multiple inconsistencies occur in almost all practical problems, a fast reacting man-machine system must be designed to obtain reconcilation of input data. It is largely for this reason that a special-purpose computer with a direct display was built. It permits rapid changes of input data, with a completely new result in a second or so.

SHAPE RECONSTRUCTION COMPUTER

The shape reconstruction computer was designed and developed by B. J. Huffman. It was fabricated in the Communications and Control Laboratory of the Space Division's Laboratories and Test section of North American Rockwell Corporation.

The requirements for the computer were:

1. Implement basic algorithm by high-speed computation.
2. Display input data and results on a cathode ray tube (CRT).
3. Permit computation to proceed either continuously or, for better understanding, in steps of various size.
4. Show inconsistency (if present) by interrupting computation process and flagging location.
5. Provide for easy change of input data.
6. Permit growth capability to include optimum resolution of inconsistency, two- and three-region computation and display, and automatic transformation from density to thickness.

The shape reconstruction computer (Figure 9) processes digitized thickness data to determine unknown cross-sectional shapes and display them as areas of intensified dots. It consists of a special-purpose digital data processor, a 4096-word, 24-bit core memory (24 core planes), a cathode ray oscilloscope, a punched tape reader, and power supplies.

A detailed view of the data processor control panel is shown in Figure 10. Toggle switches for setting the matrix size (up to 128 by 128) and entering input or preset data occupy the bottom row. Controls for core plane information display, proven 1 or 0 entry, column, row, and program preset and program advance are provided for in the second row.

The data processor consists of the control panel, eight plug-in circuit cards, and input-output connectors, all mounted together on an aluminum chassis. Each circuit card has room for 90 14-lead integrated circuit

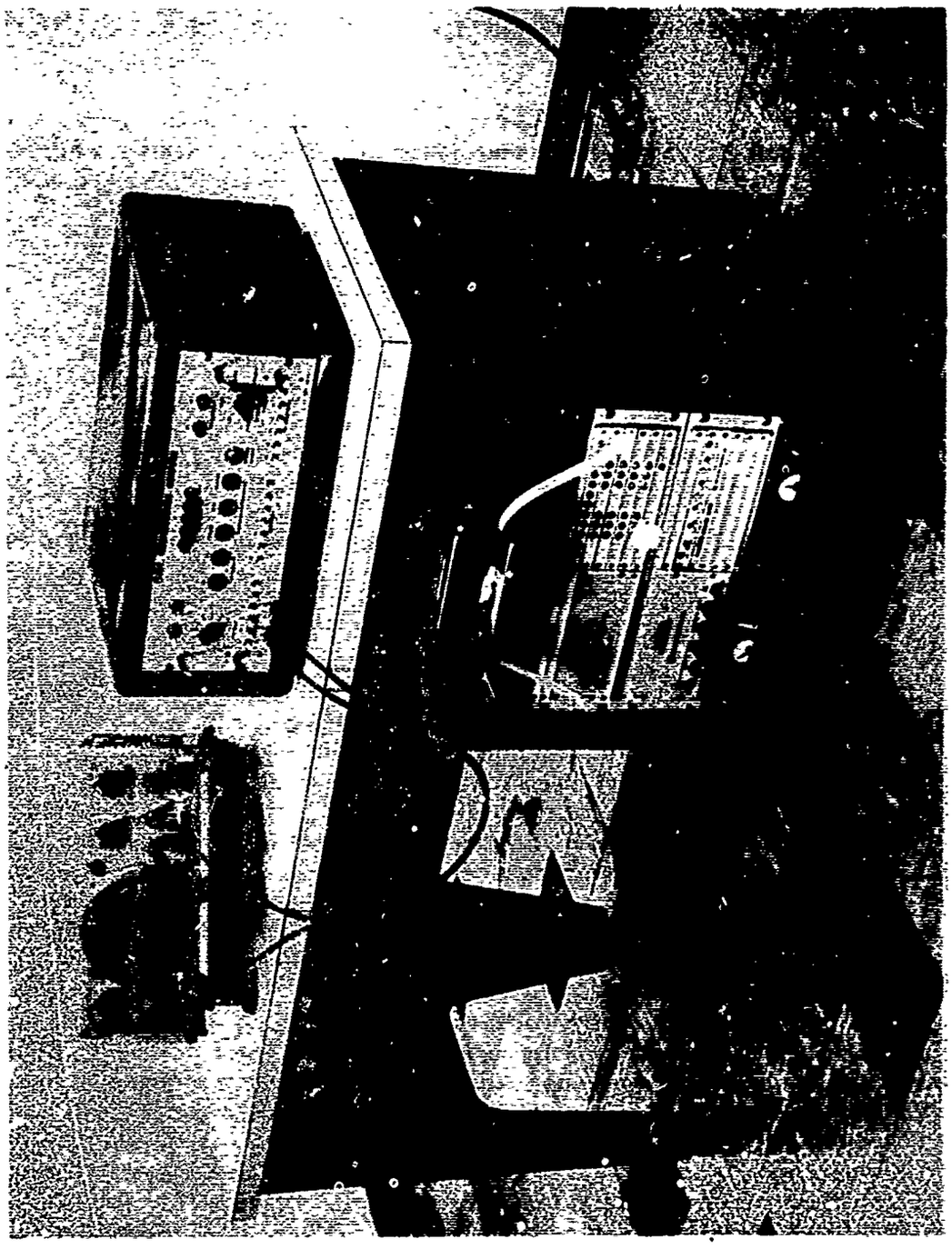


Figure 9. Shape Reconstruction Computer

packages. The integrated circuits are flip-flops and gates. Banks of flip-flops are interconnected with gates to form counters, decoders, and control logic circuitry for the memory, cathode ray tube, and control panel.

All data processing steps are controlled by the program counter. The program counter state is displayed in the top center of the processor panel (see Figure 10).

The computation proceeds in two stages. In the first, the input data are stored and the first region of proven 1's (obtained through overlap) is obtained. This stage is not repeated. In the second stage, the first outer (0) zone and the next inner (1) zone are described and the information is stored. The steps of the second stage are repeated over and over until the process ends. As long as a cycle produces new proven 1's or 0's, a flip-flop activates a new cycle. Cycling ends when no new 1's or 0's are produced. The computation process will stop for three possible reasons, clearly distinguishable on the display tube:

1. A unique solution has been found (no bianks left; all elements are either 1's or 0's).

2. Some blanks remain.

3. Input data are inconsistent, either by themselves or as a deviation from basic rules (e.g., in cases of nonconvexity), which is indicated by an intensified display spot.

If the display shows some remaining blanks, a 1 or 0 is tentatively entered at one of the blanks and cycling is continued. In actual problems, the occurrence of genuine multiple solutions seems to be rare; however, most actual problems show a moderate number of small inconsistencies.

An inconsistency, due to the occurrence of a proven 1 and a proven 0 in the same location, results in the stopping of the cycling process. Simultaneously, the spot where it occurs is intensified, and the state of the program counter (displayed in the front panel) indicates whether the inconsistency is due to an excess or a deficiency and whether it occurs in a row or column. Correction of an inconsistency is performed by changing the input data of the line involved. After correction, the cycling process may be resumed.

Display of two or three regions is accomplished by solving the regions separately, storing the first result (largest region) in one core plane, the second largest region in another core plane, and displaying these regions with the smallest region, which is stored in a third core plane. To display

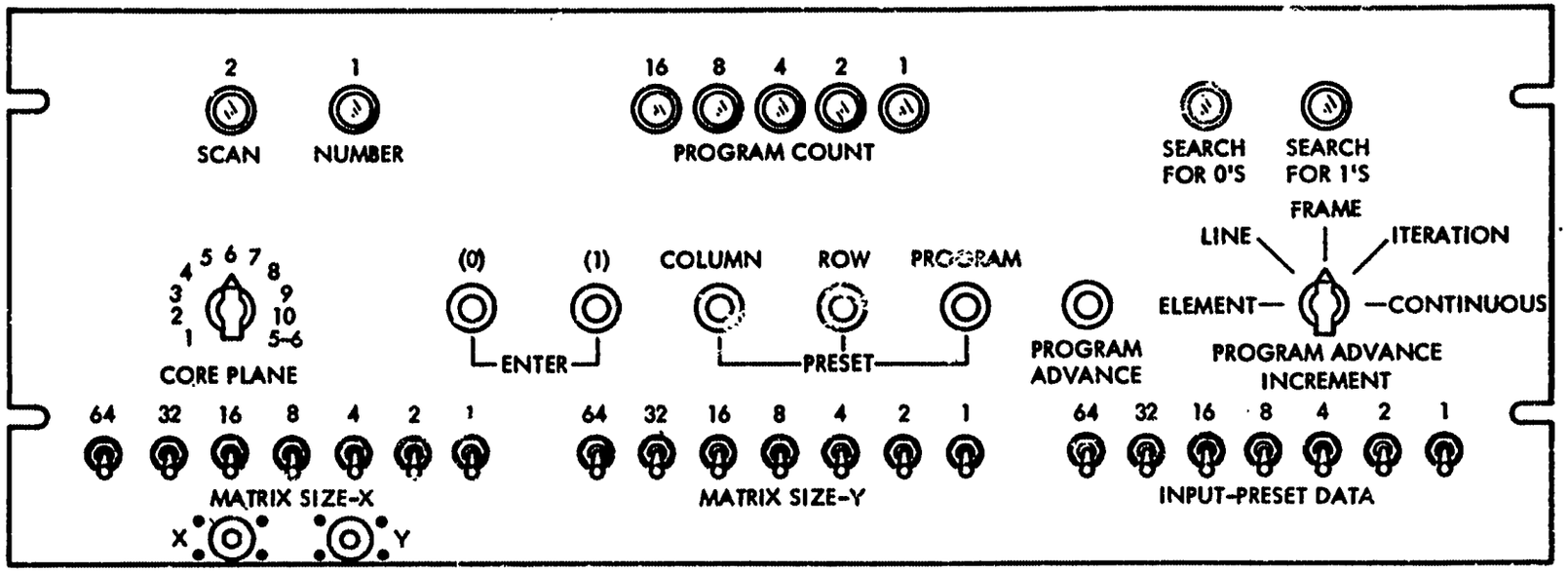


Figure 10. Data Processor Control Panel

several regions, one alternates bright and dim areas. Figure 11 (based on actual X-rays), shows the cross-section of a finger perpendicular to its axis, with areas displaying flesh, bone, and marrow.

To obtain thickness data from views other than 90 degrees apart, a skewed display is required; examples are given in Figure 18.

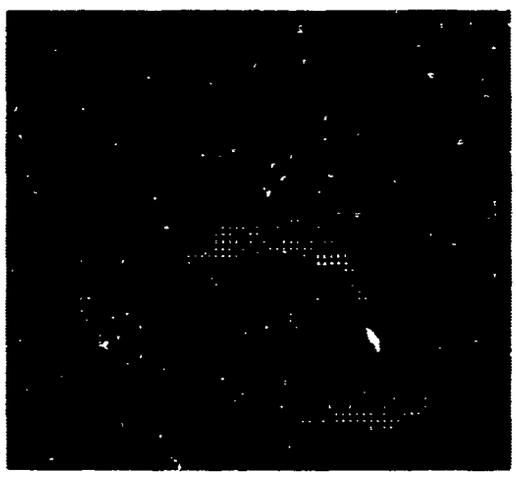


Figure 11. Three Regions (Flesh, Bone, and Marrow) in Finger Cross-Section

SAMPLE CASES

MATERIALS AND PROCEDURES

To test the validity of the method several simulated metal flaws were machined out of aluminum 2014 sheets; standard wedges of the same material also were prepared. In other cases 2014 welds made with the 2319 filler and containing gas holes were used. X rays of samples and standards were taken at 0, 45 degrees right (R), and sometimes 45 degrees left (L). For each sample, a microdensitometric record of a specific y plane (e.g., plane A, Figure 12) was obtained, with great care being taken that the same plane be scanned on each film. As a rule, several y planes were measured. Using the density record of the filmed standard wedge, calibration curves of optical density versus thickness were calculated. From the calibration curves the final input data—thickness dimension of the flaw in each direction—were obtained, digitized, and tape fed into the shape reconstruction computer. After reconciling the data the CRT display of the computer-derived cross-sections was photographed on Polaroid film. The samples were then cut at the registration plane, photographed, and measured. Finally, for better comparison, the Polaroids were either superimposed on the photographic pictures of the actual cross-section of the flaw at 15-fold enlargment and the error between measured and computed shape and location determined, or a visual comparison at 25-fold magnification was made.

Out of the samples prepared, X rayed, and scanned for density, one is described below in detail as an example of the procedure. Dimensions of the sample are given in Figure 12. The flaw was prepared by drilling a hole of approximately 3/32-inch diameter at a 45-degree angle into a 3/16-inch sample. Any plane for which y = constant (for example, plane A) thus yields a flaw with an elliptical cross-section. The X rays were taken at 90 kilovolts and 4 mA with an exposure time of 90 seconds. The tube was a Dunlee beryllium window type with a nominal focal diameter of 0.4 millimeter. Sample and standard were kept flat on a lead vinyl covered table, with a distance of 36 inches between focal spot and film. Eastman Kodak's M film was developed by hand at 68°F for 6 minutes. A lead strip at the edge of the sample was used as a registration mark to define the distance of planes A, B, and C for all views.

The films were scanned in GAF's automatic recording microdensitometer, Model 4. A strip chart recorder continuously plots radiographic density values as the film is scanned. To simulate conditions of a very small

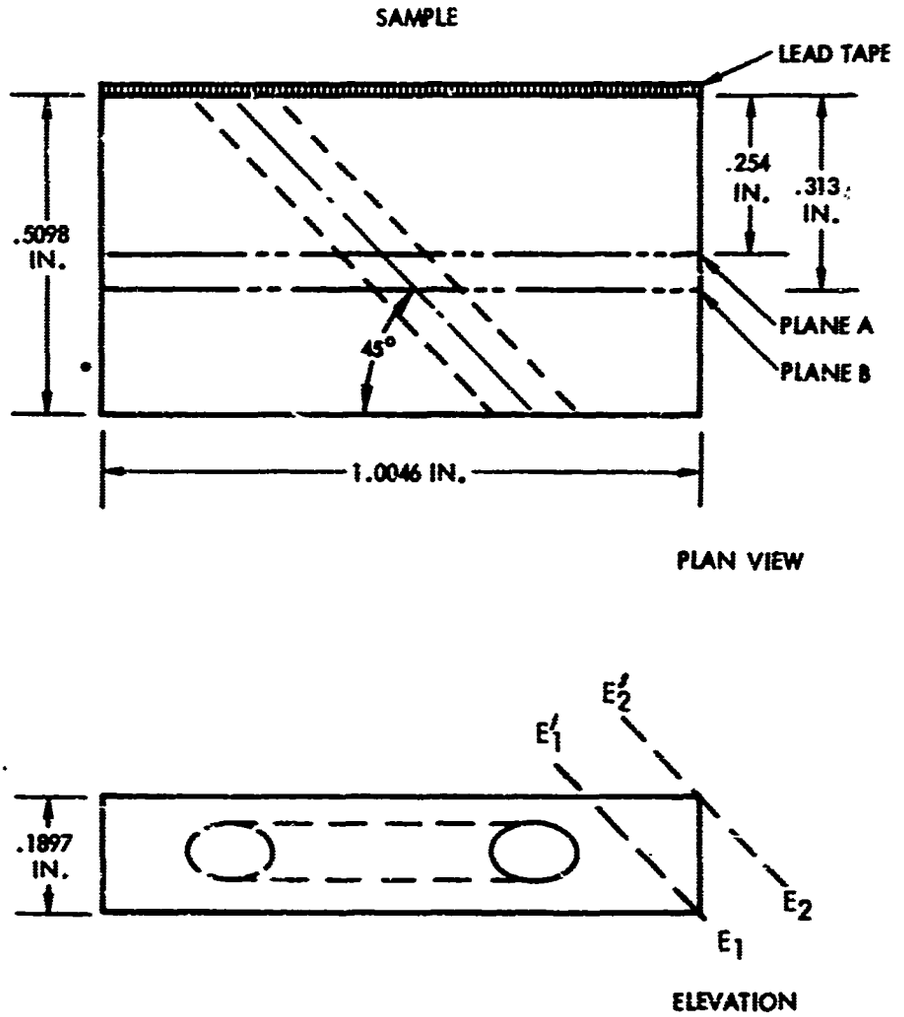


Figure 12. Dimensions of Sample

flaw, a microscope magnification of 254 was used. The aperture was made quite small; the effective scanning spot on the film consisted of a circular area of 10-micron diameter. Travel and chart speed were such that a linear x- magnification of 33.8 was obtained. This factor was carefully checked and found to be quite constant.

Figure 13 shows a graph of the density of the flaw and its neighborhood in plane B at 0 degrees X-ray angle. The amount of noise is not excessive for the very small aperture and includes a small amount of scattering. This scattering is part of the general degradation due to unsharpness that any photographic film shows. It is usually dealt with in terms of spatial frequency response or modulation transfer function (References 8, 9, 10, 11). Density is 0.41 in the background and 0.93 at the center of the hole. These and other density values are obtained by drawing a smooth "best" line through the data. The flaw as measured between the two vertical lines in the x direction is 0.140-inch long.

To evaluate the depth of the hole one uses the wedge calibration curve, the relevant part of which is shown in Figure 14. With the wedge dimensions changing in a linear fashion along the x-axis, thickness dimensions T° (x) can now be assigned to each part of the flaw of Figure 13 with the aid of the calibration curve.

A different calibration method was used in the two 45-degree films. Figure 15 shows the pertinent part of the flaw densitogram for 45 degrees R and Figure 16 the density of the right edge of the sample. As indicated by the dashed lines $E_1'E_1$ and $E_2'E_2$ of Figure 12, the layer penetrated by the X-ray beam at 45 degrees changes its thickness linearly from $\sqrt{2}$ x 0.1897 inches to zero. One thus has a built-in calibration, and no separate wedge is necessary. The method was applied to 45R and 45L densitograms and the corresponding $T(x)^{45R}$ and $T(x)^{45L}$ values obtained for all parts of the flaw. Length of the flaw between AA' and BB' is 0.1715 inches in both 45-degree directions.

The three thickness curves (T°, T^{45R}, and T^{45L} versus x) must be digitized before a combination of any two of them can be used for shape calculations. Assuming a unit length, u, of 0.00318 inch, one obtains a 54 by 44 unit parallelogram with sides of 0.00318 inch and 0.0045 inch for the 0 and 45-degree case, and 38 by 38 unit squares (standing on a corner) of 0.00318-inch length for the 45R and 45L case. To digitize the data, for example, for the 45R, 45L case, one divides the total length of 0.1715 inch into 38 equal parts, reads (at the center of each part) the corresponding T value (on a scale of unit length u = 0.00318 inch) and rounds off all data to the nearest integer, [T]. Table 1 shows the raw readings, T(x) and the integral round-off values [T] for the case of plane A. (The data for plane B

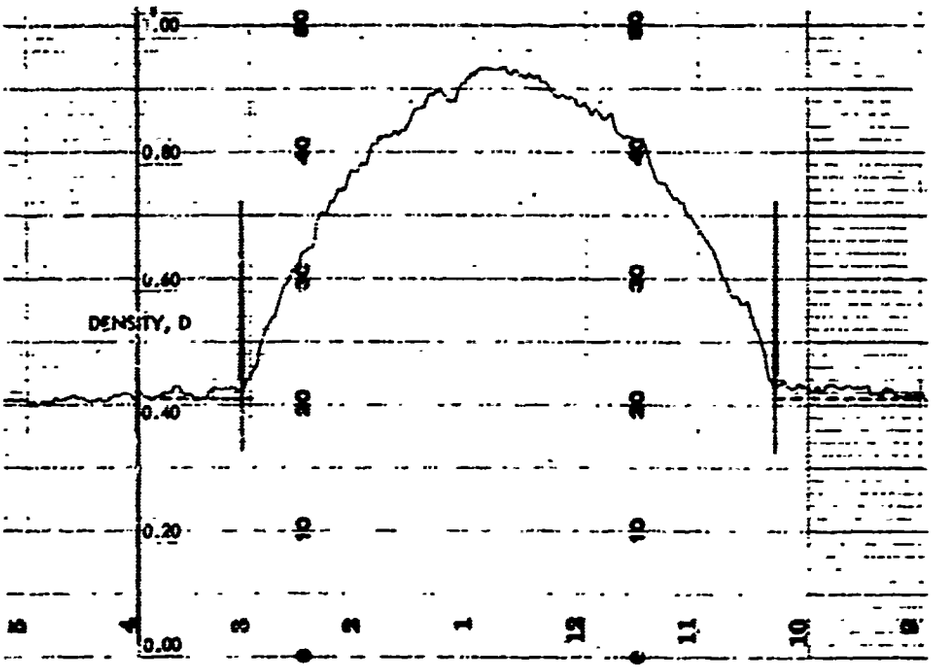


Figure 13. Radiographic Density of Defect Region (0°)

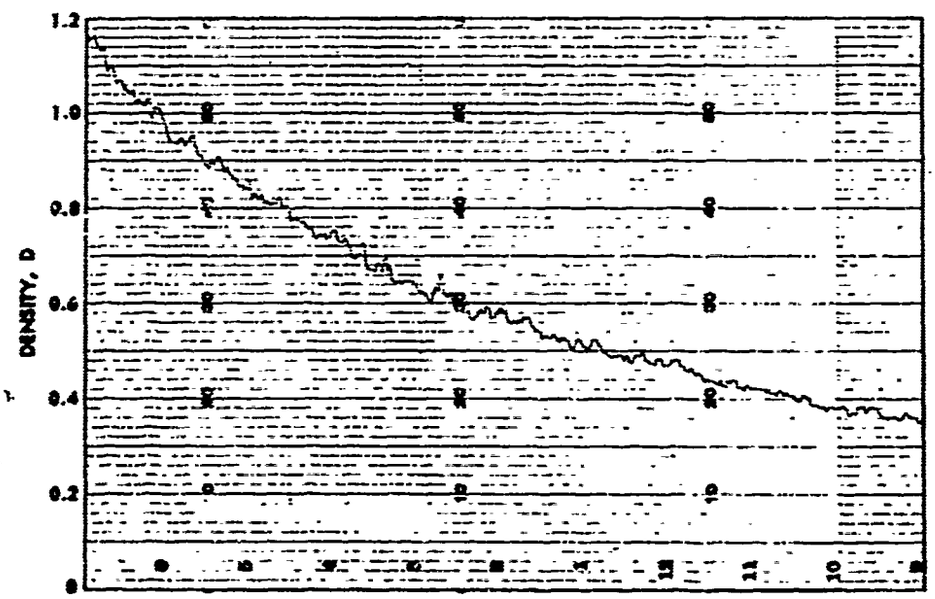


Figure 14. Radiographic Density of Calibration Wedge (0°)

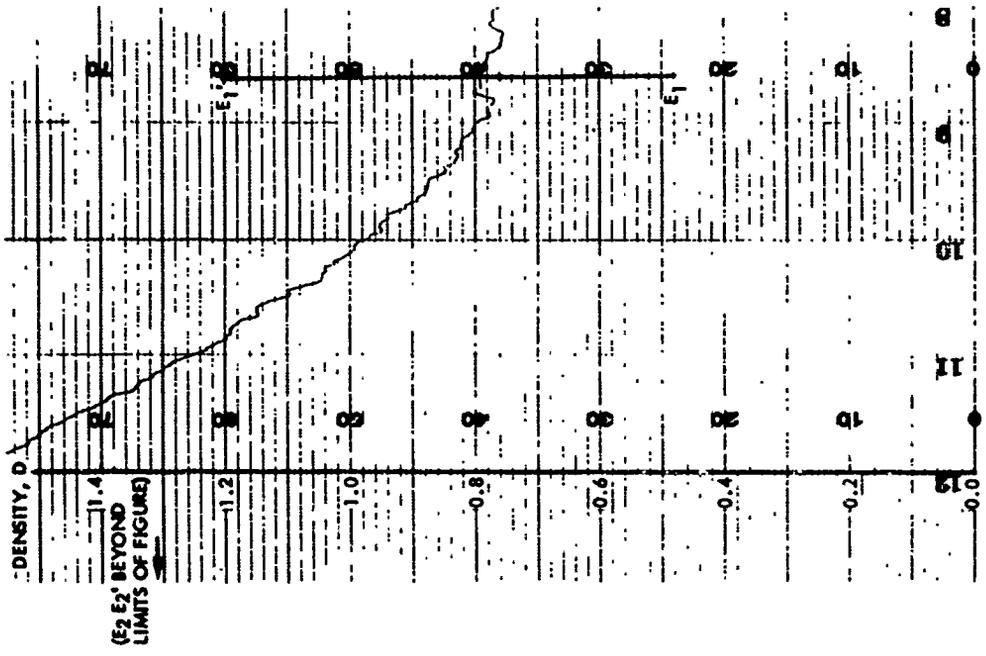


Figure 16. Densitogram of Right Edge of Sample (45°R)

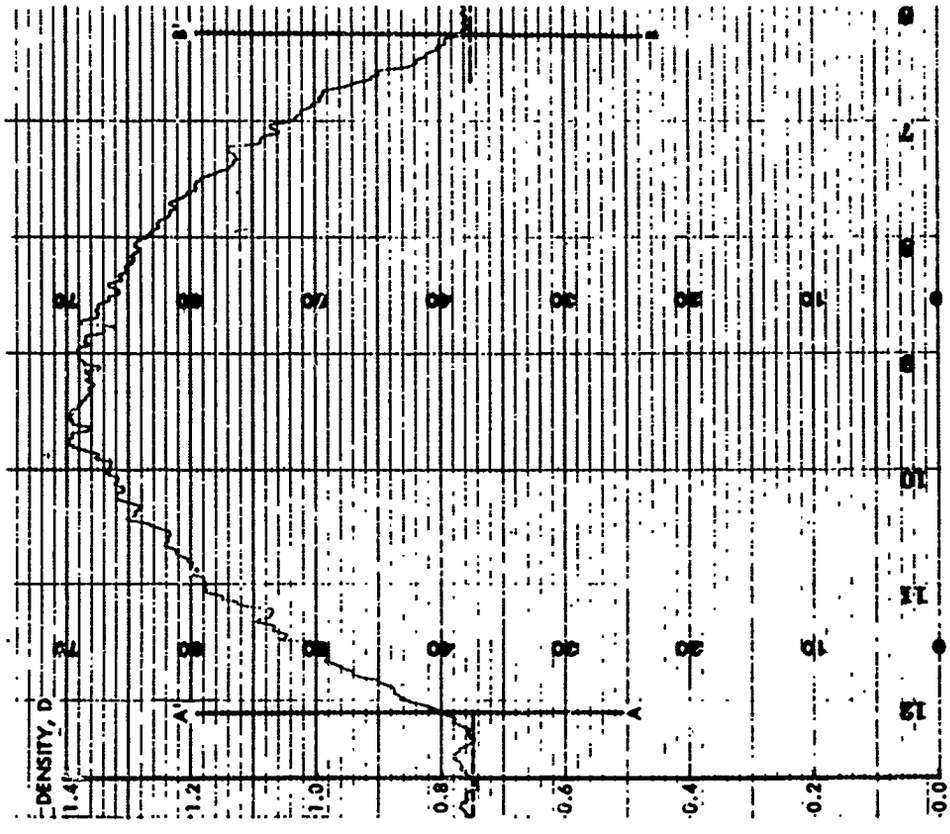


Figure 15. Densitogram of Defect Region (45°R)

Table 1. Thickness of Flaw, Plane A, at 45°L and 45°R, in Terms of Unit Length u = 0.00318 inch

X (Unit #)	T^{45L}	T^{45R}	$[T^{45L}]$	Reconciliation	$[T^{45R}]$	Reconciliation
1	10.7	9.9	11		10	
2	16.1	14.6	16		15	(-1)
3	19.2	18.0	19		18	
4	20.5	21.1	21	(-1)	21	
5	23.4	23.2	23		23	
6	25.3	25.3	25		25	
7	26.9	26.8	27		27	
8	28.3	28.3	28		28	
9	29.7	29.6	30		30	
10	30.9	30.6	31		31	
11	31.6	31.4	32		31	
12	32.4	32.3	32	(+1)	32	
13	33.0	33.1	33		33	
14	33.7	33.7	34		34	
15	34.3	34.3	34		34	
16	34.7	34.9	35		35	
17	35.0	35.1	35		35	
18	35.2	35.4	35		35	(+1)
19	35.3	35.6	35	(+1)	36	
20	35.2	35.6	35		36	
21	35.1	35.5	35		35	(+1)
22	34.9	35.2	35		35	
23	34.6	34.8	35		35	
24	34.1	34.2	34		34	
25	33.6	33.7	34		34	
26	33.0	32.9	33		33	
27	23.2	32.1	32		32	
28	31.5	31.4	32	(-1)	31	
29	30.6	30.4	31	(-1)	30	
30	29.4	29.3	29		29	
31	27.8	27.8	28		28	
32	25.8	26.0	26		26	
33	24.2	24.6	24		25	
34	22.2	23.0	22		23	
35	20.0	20.8	20		21	(-1)
36	17.0	18.1	17		18	(-1)
37	13.5	13.8	14		14	
38	7.4	7.3	7		7	
Total	1058.4	1059.7	1059	(-1)	1059	(-1)

are almost identical.) The rounding-off procedure includes an equalization to 1059 units of the slightly different sums of the T values.

RESULTS

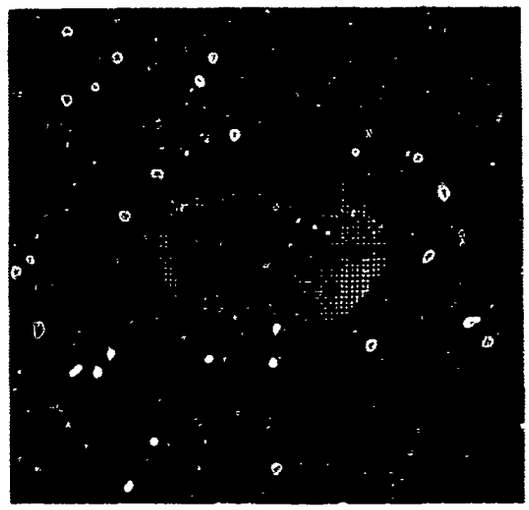
To obtain the unknown shape of the flaw, the three combinations of any two sets of [T] data were punched on tape and fed into the computer. In all cases, inconsistencies prevented an immediate solution; using the partial solution and the location and type of the inconsistency indicated by the program counter state of the computer at the moment of interruption, the operator would change the input data and continue to the next interruption. By a gradual process of reconciliation, a consistent shape eventually would be found which showed only minor discrepancies with the original input data.

Table 1 shows the changes needed to obtain consistency in the 45R, 45L example. With 10 changes of 1 unit each (indicated by the figures in parenthesis), the sum of all adjustments is less than 1 percent of the total area. In the two other combinations (0 and 45-degree views), the number of changes (each of 1 unit) to obtain a consistent shape was about 1.5 percent of the total.

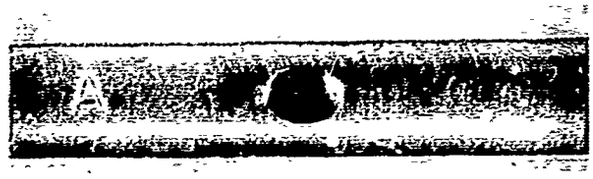
These low values are possibly due to the fact that the defect was quite large and the existence of a smooth cross-sectional shape could be assumed. The 10 to 15 changes per pair can be effected in many different ways, indicating many tiny variations of the periphery of an essentially well-defined shape. The number of multiple solutions could, however, be reduced if all three views could be simultaneously checked for inconsistency. In any case, the problem requires more investigation.

It was quite easy to determine the location of the flaw within the bar. As Figures 13 and 15 show, the beginning and end of the flaw are well defined, even at 34-fold magnification. Using the densitogram to show the distance of the two marginal rays of the defect from a brass marker, a simple parallel line construction permits the placement of the characteristic parallelogram (See Figure 3) within the bar. The original densitograms are too long (about a yard) for reproduction. The location data were also digitized, put on tape, and the computed hole and bar photographed as a two-region display.

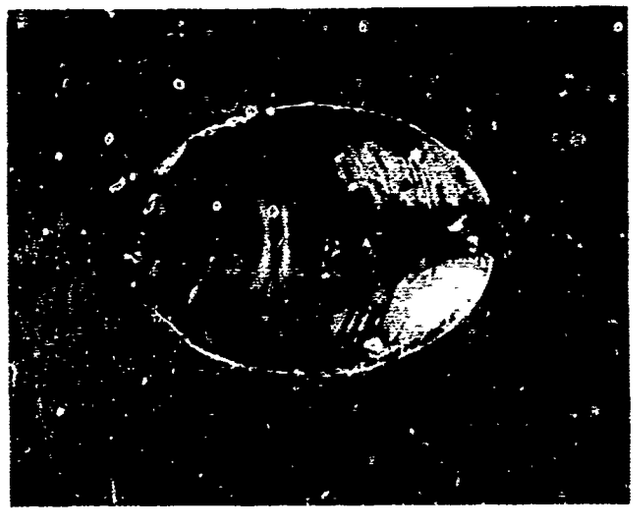
As an example of the complete location and shape of the flaw, cross-section A was analyzed from all three views. The computer-derived pictures of the defect were photographed directly from the CRT on Polaroid film. An example is shown in Figure 17A, a computed view of the defect from 0 and 45-degree data. To compare the computer results with reality, the sample was sectioned at plane A and a photograph of the section taken (See Figure 17B). Part of Figure 17B was further enlarged to about 15 times original



A. Computer Picture of Defect From 0° and 45°R Data



B. Sample Sectioned at Vertical Plane A (3X)



C. Sample Center With Defect (15X) (Burr at Left Edge Due to Sectioning)

Figure 17. Three Views of Cross-Section A

size. This part is shown in Figure 17C, where the upper and lower limits of the picture indicate the corresponding limits of the sample. For better comparison the computer-derived Polaroid pictures (e.g., Figure 17A) were photographically enlarged and superimposed upon the picture of the sectioned plane A of Figure 17C. The long axis of the ellipse gave an almost perfect match; counting the dots along this axis at 0.00318 inch each, any difference between actual and computed length was found to be less than one dot. As to the depth of the flaw, Figure 18A, 18B, and 18C show actual and computed shape while Figure 18D gives a comparison of both shape and location within the sample. (The dots in this picture represent solid aluminum while in the other three comparisons they represent the hole. The fact that no dots appear in the left upper and right lower part of Figure 18D is due to the small size of the computer memory.) As the pictures indicate, a high degree of accuracy has been obtained for both shape and location.

The difference between actual and computer flaw may be expressed as the percentage of dots misplaced (i.e., as the sum of the absolute values of deficiencies, D, and excesses, E, expressed as a fraction of the actual area):



This is a rigorous test: even a perfectly computed flaw shape, if displaced in any direction, would cause a considerable error. Conversely, small error values, particularly if distributed over wide parts of the total contour, indicate only minor deviations in both shape and location.

There is no noticeable error in the location of the defect within the sample. The shape errors (expressed as percentage of misplaced dots) for the three views are:

	0° and 45°R	0° and 45°L	45°R and 45°L
Error (percent)	1.5	2.8	1.1

The high accuracy of the results is partly due to the fact that the cross-sections of the flaw was known to have a smooth perimeter (making

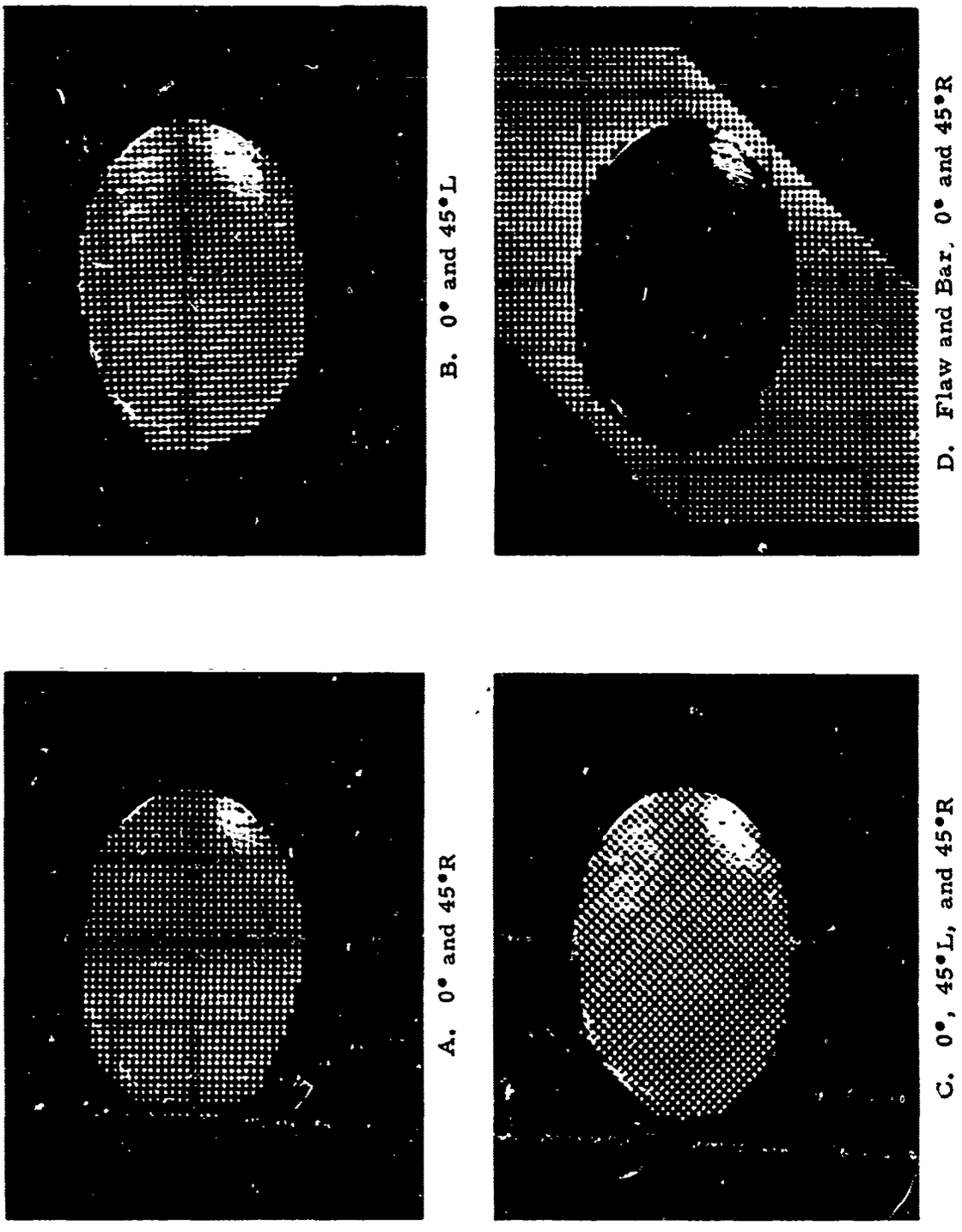


Figure 18. Actual and Computed Shape and Location of Flaw

interpolation easy) and partly that a large hole inside a thin piece of aluminum gives a high signal-to-noise ratio.

WELD SAMPLES

Several pieces of welded aluminum containing gas holes have been subjected to the same analysis and verification procedure. One example, Sample No. 26, an approximately quarter-inch weld section of parent material Al 2014 and filler, 2319, is shown in Figures 19 and 20. All pictures refer to cross section D, going essentially through the center of the flaws. Figure 19 shows the metallographic section in a 10-fold enlargement; Figure 20 the left upper part of this section in a 25-fold magnification. Figure 21 is a computer-derived view of the same cross section obtained from 0° and 45° R X-ray films. Each dot corresponds to 0.0015 inch. There is again almost no error in the location of the five flaws; fidelity, however, is not quite as high as in the previous example because of the irregular character and the overlap of several holes. For example, the two small gas holes to the right were not resolved, due to the noise inherent in regular X-ray film and shown in the densitogram of Figure 22.

Later experiments with Kodak's high-resolution plate show higher accuracy (through less grain noise), obtainable at the expense of larger exposure times. Figure 22 is a densitogram of the defect region of Sample 26 at 0° incidence, used as one of the two computer inputs from which the computer-picture shown in Figure 21 was obtained. The noise in this densitogram is many times greater than that of Figure 23, a densitogram of another sample (No. 27) taken with high-resolution plates.

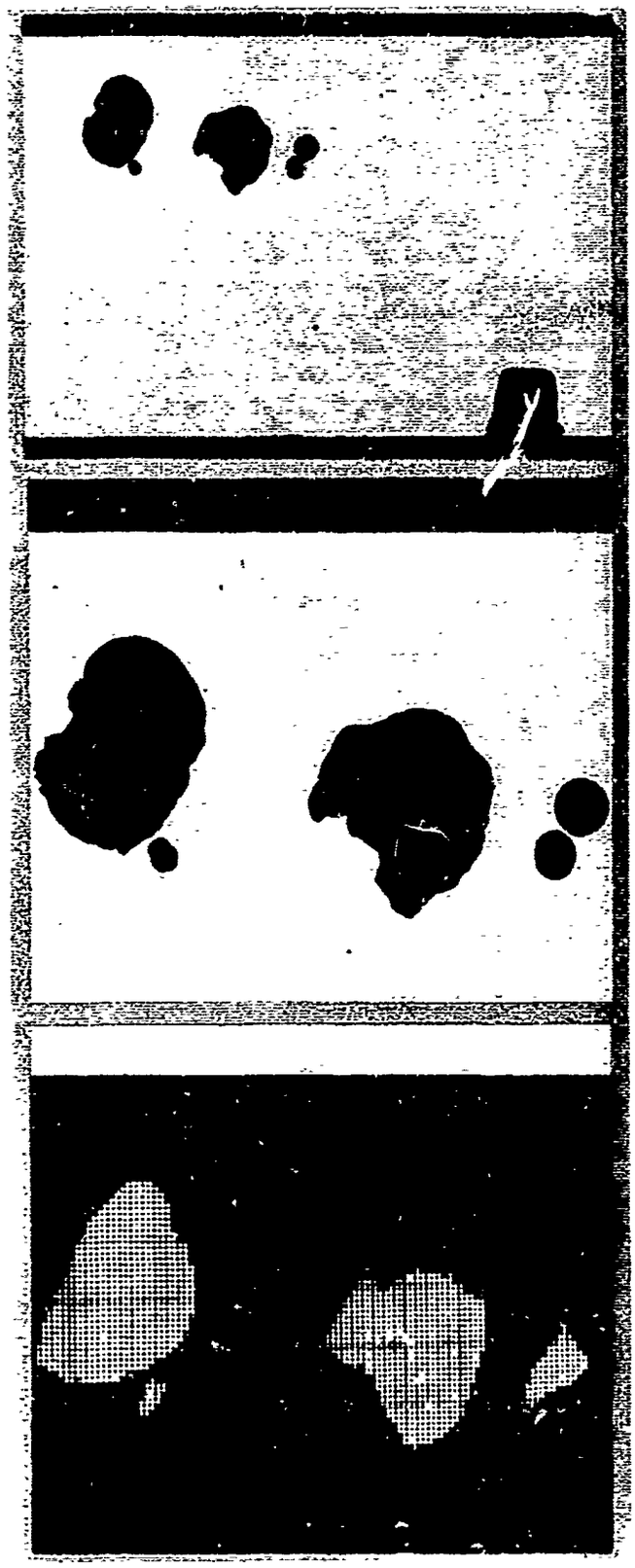


Figure 19. Weld Sample No. 26: Metallographic Section at Plane D (10X)

Figure 20. Upper Left Part of Figure 19 (25X)

Figure 21. Computed Shape and Location of Flaws of Sample 26 (25X)

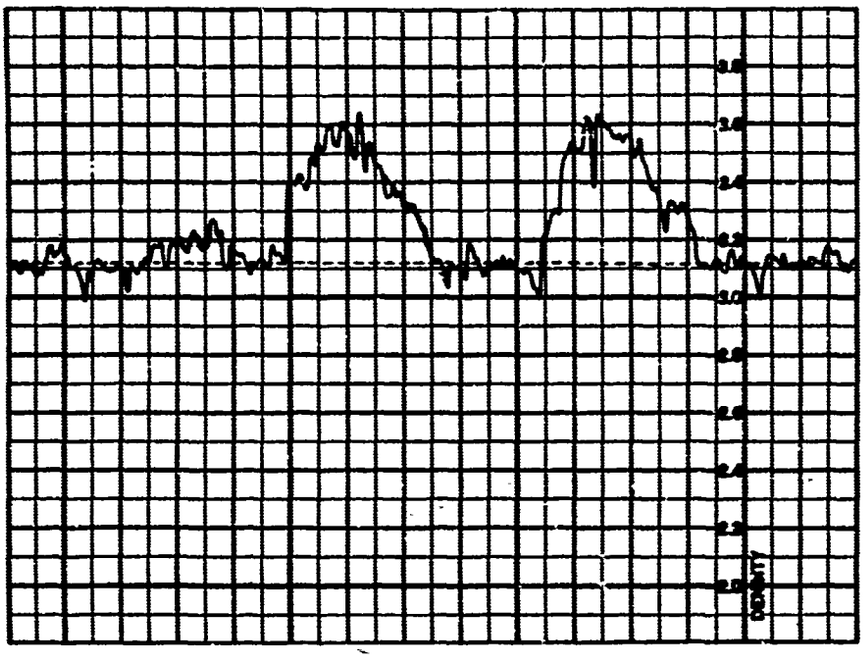


Figure 22. Densitogram of Defect Region, 0°, of Weld Sample 26, Plane D (Based on Kodak R film)

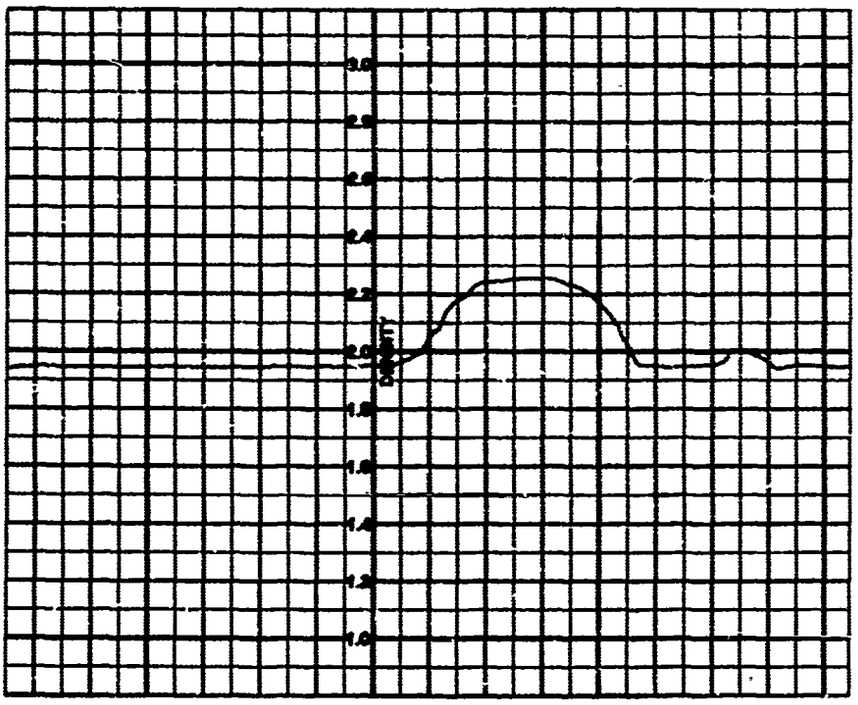


Figure 23. Densitogram of Defect Region, 0°, of Sample 27, Plane C (Based on Kodak High-Resolution Plate)

SUMMARY

Theory and experiment show that, under certain circumstances, it is possible to obtain cross-sectional pictures of the location and shape of invisible flaws in metals from two X-ray films taken at angles to each other. A special purpose shape reconstruction computer has been built and several sample cases tested. Satisfactory agreement between actual and computer-derived photographs of the defects has been obtained.

A great deal of further work has to be done to advance to the computation of unknown small defects in fairly thick welds of irregular cross section. This work is now in progress, especially along the following lines:

1. Automate and digitize the work of noise averaging and calibration.

2. Develop a computer routine to deal with inconsistent input data in an efficient manner.

3. Reduce the effects of scattering and film granularity by analytical correction methods; incorporate later into the computer routine.

4. Develop theory and practice to deal with nonconvex and multiple defects.

5. Develop an algorithm for simultaneous three-angle superposition.

6. Experiment with a number of actual flaws of various shapes, inclinations, and locations in weldments of different thicknesses and materials.

REFERENCES

1. J.A. Crowther, editor, Handbook of Industrial Radiology, 2nd edition, 1949. Edward Arnold & Co., London.

2. Radiography in Modern Industry, 2nd edition, 1957. Eastman Kodak Co., X-Ray Division, Rochester, N.Y.

3. J.H. Hubbel and M.J. Berger, Photon Attenuation and Energy Absorption Coefficients Tabulation and Discussion. Nat. Bureau of Standards Report 8681, U.S. Dept. of Commerce, Sept. 1966.

4. F. Klein, Elementary Mathematics From an Advanced Standpoint—Geometry, translated from 3rd German edition, 1939. Dover Publications, Inc.

5. H. Rumsey, Jr. and E.C. Posner, "Joint Distribution With Prescribed Moments," American Mathematics and Statistics, Vol. 36, No. 1, 1965, p. 286-298.

6. T.A. Brown, Reconstructing Triangles From Thickness Functions, Rand Report RM-5199-PR, Nov. 1966.

7. F.J. Douglas and G. Stone, Digital Program PDD 917, "Curve Reconstruction." NAA/S&ID (Aug. 1966).

8. F. Hartmann, Three-Dimensional Analysis of Weld Defects, North American Rockwell, Space Division, SD 67-980, June 1968.

9. R.H. Morgan, "The Frequency Response Function," American Journal of Roentgenology, Radium Therapy, and Nuclear Medicine, Vol. LXXXVIII, July 1962.

10. C.H. Dyer and E.L. Criscuolo, "Measurement of Spatial Frequency Response of Certain Film Screen Combinations to 10-Mev X Rays," Materials Evaluation, Vol. XXIV, Nov. 1966, p. 631-634.

11. J.B. Minkoff, S.K. Hilal, W.F. Konig, M. Arm, and L.B. Lambert, Optical Filtering to Compensate for Degradation of Radiographic Images Produced by Extended Sources," Applied Optics, Vol. VII, No. 4, April 1968, p. 633-641.

A STUDY OF SYSTEM CONCEPT TO DERIVE THE HIGHEST DEGREE OF DATA PRESENTATION WITH A MINIMUM EFFORT

by
C. S. Phelan
Director of Research and Development

Shurtronics Corporation
Santa Ana, California

For Presentation at the
Conference on NDT of Plastic/Composite Structures
Dayton, Ohio
March, 1969

The basic airframe in the new generation of the aircraft are being guaranteed for 20,000 hours of service life. Little factual data backs up the guarantee on the bonded joints. A small amount of background data has been developed in Europe by several aircraft operators but there is still a vast amount of work to be done in this area. The Fokker Bond Tester with its capability of being able to discern the cohesive strength of the glue line in terms of actual psi provides an ideal means of building this data. The curve of degradation is already available. The only need is to apply a time base. The bond tester system also has the capability of providing a permanent record in several data forms. With this data available, it should be relatively straight-forward to build up basic information on joint strength to be later checked during service with the same instrument. This same instrument can also serve as a screening test for void and delamination. The fundamental nature of bond-line failure is still somewhat hazy, but we have the advantage with this system of being able to correlate bond tester response with actual bond-line strength. Figure 1 and Figure 2 illustrate the type of data backup developed by the various aircraft companies.

These curves have been developed based on actual test specimens with correlating bond tester readings. There is little service experience with respect to the deterioration of a bonded joint during extended environmental fatigue cycles. Certain military specifications establish a number of tests which give some indication but these results are not absolute values.

The bond-line strength is a function of bond-line thickness, porosity, and other factors which vary as a result of manufacturing tolerances. The Fokker System can give the strength in terms of relative values which can be correlated with curves as shown in Figures 1 and 2. The philosophy is a resonant frequency system whose concept is purely mechanical. It, in a sense, applies a vibratory force through a bonded joint and the resulting dampening or attenuation of the vibration medium is read on a meter-display. A number of major aircraft companies in the United States have developed this system to a finite degree where they can anticipate the actual strength level of the joint within a very close degree.

The new modified epoxy adhesive systems in use at the present time are under intense development and this information will be available when the new aircraft reach the user. One must recognize the fact that as in all areas of development, as the technology moves forward, the demand becomes more rigorous. Take for example an automobile tire of the 1920's when thirty to forty miles an hour was about the nominal speed. Compare this with the automobile of today where seventy miles an hour is legal, and eighty to ninety miles an hour on the open road is not unusual. Think of the infinitely greater stress and strain applied to the modern tire as opposed to the tire of the 20's. The ground rules that applied "way back when" are no longer valid considering modern aircraft vs. the aircraft of only a decade ago. Landing speeds then were fifty to eighty knots maximum. Modern jet liners land at one-hundred knots plus and, in addition to this, they carry anywhere from five to ten times as many passengers and cargo. Air speeds are upped three to four times. The control and inspection of the various

components must advance accordingly. Part of this requirement has been anticipated by the Fokker System. Whether in realization or accidental, the facts are there. Since methods were developed that could read the glue-line strength reliably and a system of recording is provided with storage and recall capability, it is possible that the airline operator may, five or ten years from now, use the same instrument that read a joint during manufacture. With a record of how it started out and a means of checking it during service, a picture of its performance will begin to emerge. Some degree of this work has been done in England but only to a limited degree. The data at the present time is being compiled on aircraft such as the 747 and others to give the capability of being able to develop some backup data on joint durability.

We are not talking here about simple unbond and delamination. We are discussing the life of a well bonded joint where the strength gradually is reduced as a result of the rigors of service life. The bond is subject to all manner of deterioration factors such as vibration, radiation, electro-static discharge, moisture, chemical attack and heat. It is known for certain that these conditions contribute to the deterioration of a glue line. The only needed information is, how much and how fast. With information from the aircraft manufacturer on the actual strength of the joint when the airplane left the factory, and coupling this with a means of identification (part number and location) the task should be greatly simplified with the use of the Fokker System. The airline operator then must set up a test program based on some frequency and on some sampling basis that will least interfere with the aircraft operation schedule. Essentially, this program will be broken down into two phases (1) should be a screen test to rapidly determine delamination or unbond as its principal objective (2) should be the more detailed inspection considering the bond-line deterioration. The Fokker System can be utilized for both phases.

In addition to the Fokker System intended primarily for both quantitative and qualitative information, the Shurtronics Corporation offers a second unit called a harmonic bond tester. This device can rapidly scan any given area particularly with respect to honeycomb to give a "go" and "no-go" indication. A unique advantage of this system is that it does not require a couplant nor does it require actual contact with the surface. This device can easily be used in both lap shear and flatwise tensile inspection to provide the screening test. This unit is called a Shurtronics Harmonic Bond Tester. Essentially, this puts out an energy pulse that vibrates the top surface of the joint. The degree to which the joint vibrates is an indication of its attachment. In other words, if it is completely loose as in an unbond, the maximum signal level will be attained. Adjustment levels are provided on the fact of the instrument. Its degree of resolution can be adjusted to detect as little as one cell unbond in 1/4" honeycomb. (See Figure 4 - Harmonic Bond Tester)

In summary, industry as a whole is offered a means of controlling structural bonding. It is evident that certainly no one instrument is going to give the full picture. It is also evident that a great deal of ground work is yet to be done. The next decade of development hopefully will see the solution to many of these problems. In the meantime, many agencies, both private and government, are engaged in intensive engineering development to provide the answers.

###

In this modern scheme of things, many systems are presented for non-destructive testing of adhesive bonds and composite structures. Included is the "coin tap method." In general, all of these systems have worked well in one instance or the other. The success or failure of any system falls, to a degree, within the skill of the operator or the control of the Q. C. system. In all instances, it is relatively costly to inspect anything. Therefore, the attitude of management is very important. One system or the other has worked where the need was great and the requirements ideal. Other systems have worked to a much lesser degree where the atmosphere has been less tolerant or cooperative.

In the early days of structural adhesive bonding, there were few systems available since there was only a small amount of bonding being accomplished. In the last decade there has been a tremendous increase. New and different systems have been advanced as fool-proof schemes to do the necessary inspection. Exorbitant claims have been made by some instrument manufacturers based on success in one small area.

Experience has shown that one single system cannot satisfy all the demands of inspection. The same reasoning applies to a mechanic carrying a box full of tools. No one tool is capable of doing the entire job regardless of its versatility. Early systems developed around through transmission and pulse echo satisfied themselves by simply looking for unbond and void areas. In fact, in some instances, this "go" or "no-go" type of inspection was entirely adequate. With very few exceptions, the American aircraft manufacturers have not been involved in primary structure bonding. Companies that have bonded aircraft to 60% or 70% of the total assembly will readily admit that until recently, they have not considered total structural bonding. The explanation is simple; in every case, there has been a mechanical fastener backup to take over if the bonding failed. The only true primary structural bonding accomplished to date, in the United States, has been the various helicopters and the Fokker F27.

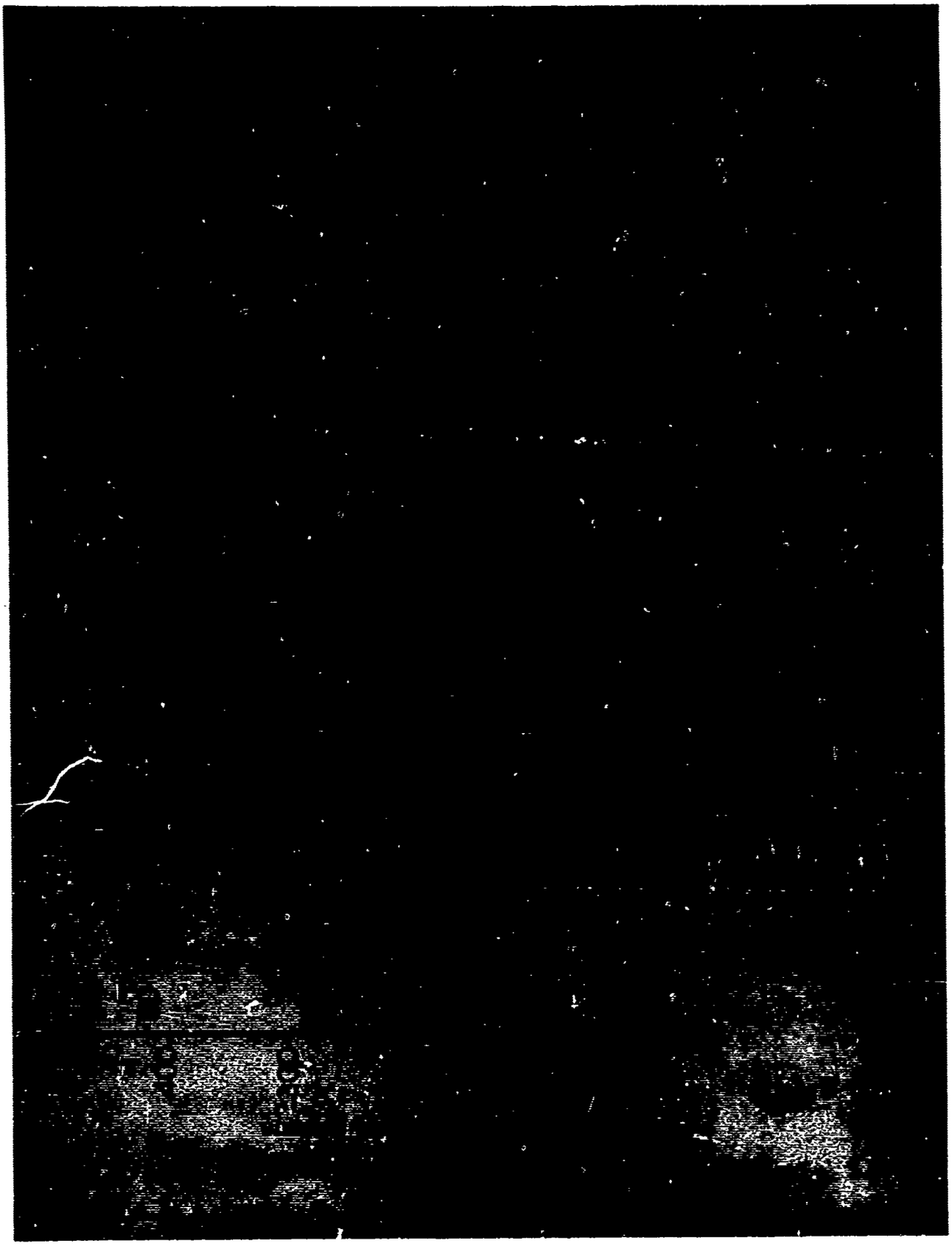
With the concept in mind that future aircraft will undoubtedly have more and more bonding and this bonding will be in the area of basic structure with little or no mechanical backup, something more will be needed in the way of inspection during fabrication as well as in service. No longer will it be sufficient to simply check for voids and unbonds. A means will be required that will predict both quantity and quality of the joint during the building and service life. The widely used "go" and "no-go" inspection method will have to be relegated to the categories of "screening test only."

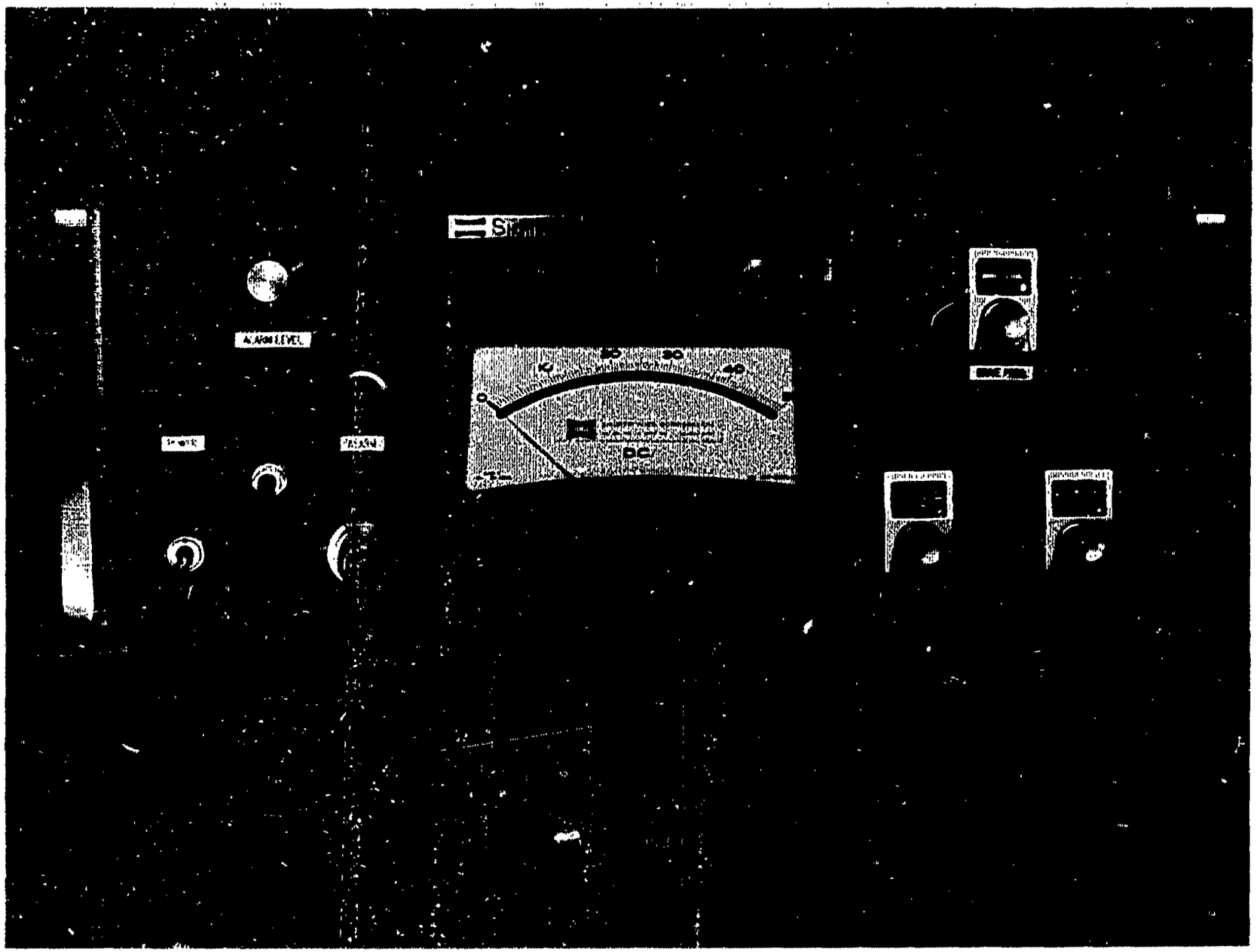
The aircraft operator as well as the military have set some rather stringent long-range durability requirements on these new aircraft. More rigorous standards have been established for the control of the adhesion. Hopefully, development in technology will produce an instrument that will give both quantity as well as a quality reading non-destructively. Within the philosophy of bonding, the adhesion must always be greater than the cohesion. The "T" peel test used by the manufacturer gives this information by sample control. It is considered that this is representative of the actual part. Some experience has indicated that there are problems of long-term adhesion failure that cannot be predicted. Almost in every instance some form of surface corrosion has been present. Intensive studies are under way to overcome this problem. The total solution may just be around the corner.

In the meantime, a means of testing the other factor of bonding control has been developed to a fine art. Cohesion can be tested non-destructively for values of both quantity and quality. This capability is offered by the Fokker Bond Tester System. Many of the major aircraft and missile companies are using this system at the present time. Approximately ten years of development have gone into this to date to furnish a wealth of backup data. The Air Force has established a specification control issued under Federal Standard 175 and Military Specification 860. (See Figure 3 - Fokker Unit)

Beyond the basic requirement for the aircraft manufacturer to exercise control during manufacturing, there is a need to provide a permanent record for every bonded element shipped. The permanent record must give information by part number, location, and actual strength reading. The airline operator has a somewhat different need; he must have a means of follow-up. There is the requirement to check the bonding on a periodic basis to monitor its degradation. The philosophy of predicting failure in basic metal structure parts has been under consideration for a long time. Certain dramatic strides have been made in terms of strain gage application and other sensing devices. Correspondingly, all structural elements have a potential fatigue life. Considering bonded structures, the need is to have a curve of degradation so that the rate of deterioration can be anticipated.

Aircraft of a few years ago simply did not have the need for this type of inspection. Essentially, they belonged to the "Model A" days of aviation. Their flight hours were not extensive, they flew when the weather was good, and relatively long periods of layover was generally the way the industry worked. Five-thousand flight hours on an aircraft structure then might take years to achieve. Today's aircraft with their high degree of sophistication and their relatively high cost must essentially fly all the time. They are, in a sense, a transportation factory. Just as a factory on the ground must produce economically, so must the aircraft produce. With virtually around-the-clock flying in good weather and bad, an aircraft must now stand 20,000 or 30,000 hours for a safe operating life. It is fairly evident that the aircraft of the future will have more and more bonded sections. Their nature will change from secondary to primary structure. With this in mind, some means of monitoring becomes a must.





PHYSICAL PROPERTY EVALUATION OF COMPOSITE MATERIALS USING FRESNEL OPTICAL PRINCIPLES IN THE MICROWAVE REGION

by

Joseph C. Plunkett
Martin Marietta Corporation
Orlando, Florida

For Presentation at the
Conference on Nondestructive Testing
of
Plastic/Composite Structures
Dayton, Ohio
March 18-20, 1969

ABSTRACT

A unique approach to nondestructive evaluation of the physical properties of nonmetallic composite materials is described. An intuitive discussion of the dielectric properties of composite materials is presented to theoretically support the approach used. Fresnel optical characteristics of the power reflection and transmission in the microwave region are utilized as parameters for measuring variations in density or porosity of the material. Measurements were made using a swept frequency microwave system. Shift of the critical points (minimum or maximum) of the response appears to be linearly related to density/porosity variations and thickness variations of the material in the range of interest. Correlation of the nondestructive microwave data was obtained by destructive density measurement and photomicrographic data showing porosity content of the composite.

The technique is applicable to nondestructive evaluation of the composite structures which provide access to one side only, provided that they are bonded to or in contact with a metallic substrate. When both sides are accessible, through-transmission techniques using the same principle are applicable. A novel technique (Martin Marietta "MAGNEMIKE", pat. pending) is used for measurement and correction of thickness variations which could otherwise mask density measurements. A nomographic calculator has been developed for application of the thickness corrections which could otherwise mask density readings. Advantages and limitations of the method are discussed.

INTRODUCTION

In the manufacture of most multiphase structural composite systems such as reinforced glass-resin composites, control of fabrication techniques and process variables is not sufficient to assure that density/porosity variations in the finished product fall within acceptable limits. Nor can random destructive sampling be relied upon to indicate the degree of homogeneity within the structure. To alleviate this problem, Martin Marietta initiated a program to develop a nondestructive technique for the evaluation of density/porosity variations in the finished composite structure using a swept frequency microwave system.

Causes of Porosity

Density/porosity variations are caused by material and process variables such as glass-to-resin ratios, fiber pre-impregnation wettability characteristics, and variations in cure pressure, time, or temperature. In the case of phenolics, silicones, and melamine resins, polymerization involves the evolution of water and requires special procedures for dealing with this problem, e.g., time must be allowed in compression molding to permit the water to outgas during the cure cycle. Incomplete out-gassing of the water during the cure cycle, as well as the other variables mentioned above, can cause a porosity condition to develop in the material.

Effects of Porosity on Mechanical Properties

The presence of pores in a structure will obviously reduce the cross-sectional area exposed to an applied load, and in addition will act as stress concentrators. The results, in turn, reduce the rupture strength and modulus of elasticity of the material or structure. However, because of the complex multiphase composition of most reinforced composite structures, porosity effects must be considered on an empirical basis. Not only is there no satisfactory mathematical model for porosity in these complex structures, but the situation is further complicated by the fact that it is impossible to completely isolate the effects of other important variables.

The effects of porosity are also very pronounced in ceramic composites. Pores are assumed to have zero Young's modulus. The work of Ryskewich[1] indicates that the strength (σ) decreases exponentially with increasing porosity for ceramics and is related in the following manner:

$$\sigma = \sigma_o \exp(-nV)$$

where n is in the range of 4-7 and V is the volume fraction of porosity.

A small volume porosity of 10 percent has been observed to reduce the rupture strength to approximately half that of a non-porous material. The decrease in fractional elastic moduli with an increase in the volume fraction of pores has been shown by Coble, Kingery, Kerner, and McKinney.[2]

The shape of pores is also important. The stress concentration varies considerably, from very high values with elliptical shapes oriented in a direction in which the major axis is at right angles to the stress axis, to relatively low values with fine, rounded pores.[3] Angular pores also serve as microcrack initiators under applied stress.

RELATIONSHIP OF DIELECTRIC PROPERTIES TO PHYSICAL/MECHANICAL PROPERTIES

An intuitive understanding of the molecular processes related to dielectric and mechanical properties of composite materials is a very important factor not only in the establishment of failure modes, but also in the logical selection of techniques for nondestructive measurement of physical characteristics and mechanical properties of these materials. Obviously, the intermolecular arrangements as well as the nature of the molecules in polymers and glasses will necessarily determine many of their physical and electrical properties.

Dielectric Nature of Polymers

As with simple low molecular weight organic compounds, polymers are divided into two groups. First, there are non-polar polymers, structures in which there are no permanent dipole moments. These generally have fairly low dielectric constants practically no dielectric loss and very slight frequency dependence on these qualities. Examples are polyethylene and polytetrafluorethylene (Teflon). Second, the vast majority of polymers have structures containing permanent dipoles and many exhibit dielectric dispersion (frequency-dependent dielectric constant and loss) superimposed on atomic and electronic polarization. Most of the structural plastics of interest to the Aerospace Industry are in this group of polar materials. The breadth of the dispersion regions of polar polymers is generally much greater than observed in simple compounds and much greater distribution of relaxation times must therefore be postulated to account for the observations.

Not only are thorough studies of dielectric dispersion of polymers over a broad-frequency range extremely scarce, but it is a fact that due to impurities or multiple dispersion regions that are generally attributed to multiple phases or modes of dipole rotation, few polymers exhibit dielectric dispersion uncomplicated by conductance. Although studies of this nature are quite incomplete, efforts of many investigators in recent work on mixed systems involving co-polymers and polymers mixed with fillers have given new insight into polymer molecular physics. Although a theoretical treatment of this area is much too detailed to discuss here, a few facts concerning the mechanical and dielectric relaxation will be mentioned to serve as a basis for the application and interpretation of microwave energy to composite materials studies.

The molecular relaxation process in polymers which gives rise to dielectric relaxation also gives rise to mechanical relaxation. This can be characterized by the shear strain response to a sinusoidal shear stress of unit amplitude. This is usually a complex quantity, $J^* = J' + iJ''$. The real part, J' is analogous to ε', and the imaginary part to ε'' of the complex permittivity ($\varepsilon = \varepsilon' + i\varepsilon''$). The mechanical loss tangent J''/J', is analogous to the electrical loss tangent. In view of this phenomena, the mechanical and dielectric relaxation of polymers can be represented conveniently by plots of J', J'', ε', or ε'' as a function of frequency or temperature.[4]

In these graphical relationships, J' and ε' usually appear on sloping nonlinear functions of frequency and temperature, whereas J'' and ε'' (loss tangent) usually have peaks and valleys as a function of frequency and temperature. The frequencies at which these changes occur are dependent upon the molecular structure and also upon the macro-structure (porosity content, etc.). Because of the theoretical relationship between modulus of elasticity and relaxation time of a material, the relationship between porosity content of a material and its modulus of elasticity is theoretically explained as well as empirically verified for many materials.

Dielectric Nature of Glasses

Under the direction of von Hippel at MIT a large number of materials, including many glasses, have been measured for both loss tangent and ε'.(5) Morey has also made extensive studies of the dielectric properties of glass.(6) For quartz and fuzed quartz glass, Morey(6) shows an almost completely linear relationship between ε' and the density of the glass. ε' is a direct measure of the polarizability per unit volume. The denser the material the more electrons and ions there are to polarize. Density, in turn, is calculable directly from composition. Therefore, ε' should vary smoothly with composition changes. However the rigidity of the structure is quite important, since it affects the ionic polarizability, which in turn affects the complex permittivity.

Stevels (7) (8) (9) (10) (11) has made major contributions to our understanding of the dielectric properties of glasses. He divides the relaxation phenomena into three parts: conduction losses, dipole relaxation losses, and deformation losses. Conduction losses are considered negligible above 100 hertz. Dipole relaxation losses are apparent at very low frequencies and then fall to near zero in the kilohertz region.

Deformation loss is a term used to describe even more limited motions of atoms in glass. The maximum deformation loss occurs at about 10^{13} hertz at room temperature. Deformation losses can appear at low temperatures in the kilohertz-megahertz region, but at high temperatures they have moved up in frequency leaving a minimum near 10^6-10^8 hertz. Vibration losses occur at frequencies from 10^{10} and above.(4) This loss results from the fact that all the atoms in glass can vibrate around their equilibrium positions at frequencies that are determined both by their mass and by the restoring force in their potential well. Whenever the applied electric field alternates at a frequency near that of one of the constituent atoms, the atoms are excited to high resonant amplitudes and cause high dielectric losses. This vibrational loss is one of the most important losses which can affect the swept

frequency spectrum in the X-band and K_a-band of the microwave region and is strongly dependent upon the microstructure and macrostructure of the glass.

Since the complex permittivity and the complex shear stress constant are related to both the molecular structure and the macro-structure of composite materials, it is entirely logical to utilize microwave and ultrasonic energy to study the structure of these materials. Moreover, since there is a wide variation of both the real part and the imaginary component of the complex dielectric constant as a function of both frequency and the material structural properties, it is evident that the studies are significantly enhanced by swept frequency capabilities.

THE SWEPT FREQUENCY MICROWAVE PROGRAM
FRESNEL REFLECTION AND THE COMPLEX POWER RELATIONS

Based upon the inter-relationships of dielectric properties, mechanical properties, and physical characteristics of composite materials, Martin Marietta has developed a unique approach to the measurements of density/porosity variations in unidirectional and bidirectional reinforced composite materials using swept frequency microwave techniques. Figure 1 shows a typical system for the reflection mode and Figure 2 shows the same basic system for the through-transmission case.

The basic theory behind the approach is too cumbersome to develop in detail, but a limited explanation of the theoretical basis of the technique for the through-transmission case is presented in the ensuing paragraphs. The reflection case is based upon the same concepts, except it is a little more complicated.

The through transmission system is shown in Figure 2. The signal incident upon the test part is continuously swept from 8.2 to 12.4 GHz or from 26.5 to 40 GHz. The amount of power reflected or transmitted from the first and second interface of the material for any specified frequency (and therefore wavelength) is related to the power reflection or transmission coefficients as shown below for perpendicular polarization where ρ is the reflection and τ is the transmission coefficient.[12]

$$\rho = r \frac{[1 - \exp(-2\Psi Lo - 2j\Psi)]}{1 - r^2 \exp(-2\Psi Lo - 2j\Psi)} \tag{1}$$

$$\tau = \frac{(1 - r^2) \exp(-\Psi Lo - j\Psi)}{1 - r^2 \exp(-2\Psi Lo - 2j\Psi)} \tag{2}$$

$$\text{where } \Psi = \text{electrical thickness} = \frac{2\pi d}{\lambda} \left(\frac{\varepsilon}{\varepsilon_o} - \sin^2\theta\right)^{\frac{1}{2}} \tag{3}$$

$$Lo = \text{attenuation due to loss} = \frac{\left(\frac{\varepsilon}{\varepsilon_o}\right) \tan\delta}{2\left(\frac{\varepsilon}{\varepsilon_o} - \sin^2\theta\right)}$$

$$r = \text{Fresnel (interface) reflection coefficient} = \frac{1 - \sqrt{\varepsilon_e} + jL_1}{1 + \sqrt{\varepsilon_e} - jL_1}$$

$$\varepsilon_e = \text{equivalent dielectric constant} = \frac{\left(\frac{\varepsilon}{\varepsilon_o}\right) - \sin^2 \theta}{\cos^2 \theta}$$

$$L_1 = \text{reactance due to loss} = \frac{\left(\frac{\varepsilon}{\varepsilon_o}\right) \tan \delta}{2 \cos \theta \left[\left(\frac{\varepsilon}{\varepsilon_o}\right) - \sin^2 \theta \right]^{\frac{1}{2}}}$$

θ = incident angle measured from normal

d/λ = thickness of specimen in wavelengths

$\tan \delta$ = loss tangent

$\varepsilon/\varepsilon_o$ = relative dielectric constant of specimen.

The important facts readily discernable from the above relationships are:

1 The power reflection and transmission coefficient, equations (1) and (2), and therefore the amount of power reflected or transmitted at a specified frequency is a function of Fresnel's reflection equations, the electrical thickness of the specimen, and the attenuation due to dielectric loss.

2 The Fresnel reflection as well as attenuation due to loss are, in turn, significantly affected by variations in both the real part (ε') and the loss tangent of the complex permittivity of the material, which is in turn relatable to density (porosity content).

3 The electrical thickness, equation 3, in turn, is dependent upon the physical thickness of the material and the real component of the relative permittivity of the material.

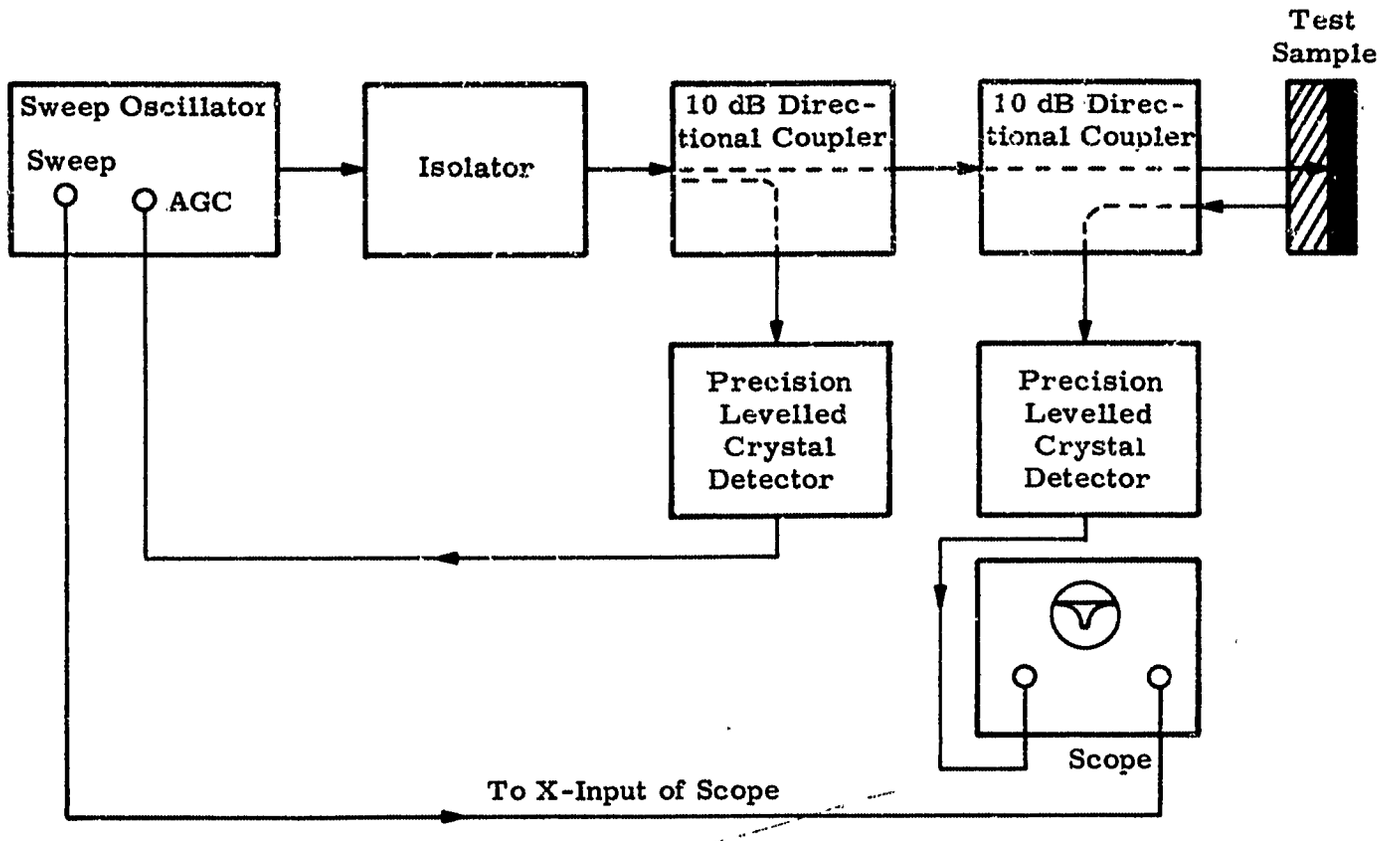


Figure 1. Microwave Swept Frequency Reflectometer System for Measurement of Density/Porosity Variations in Composite Materials

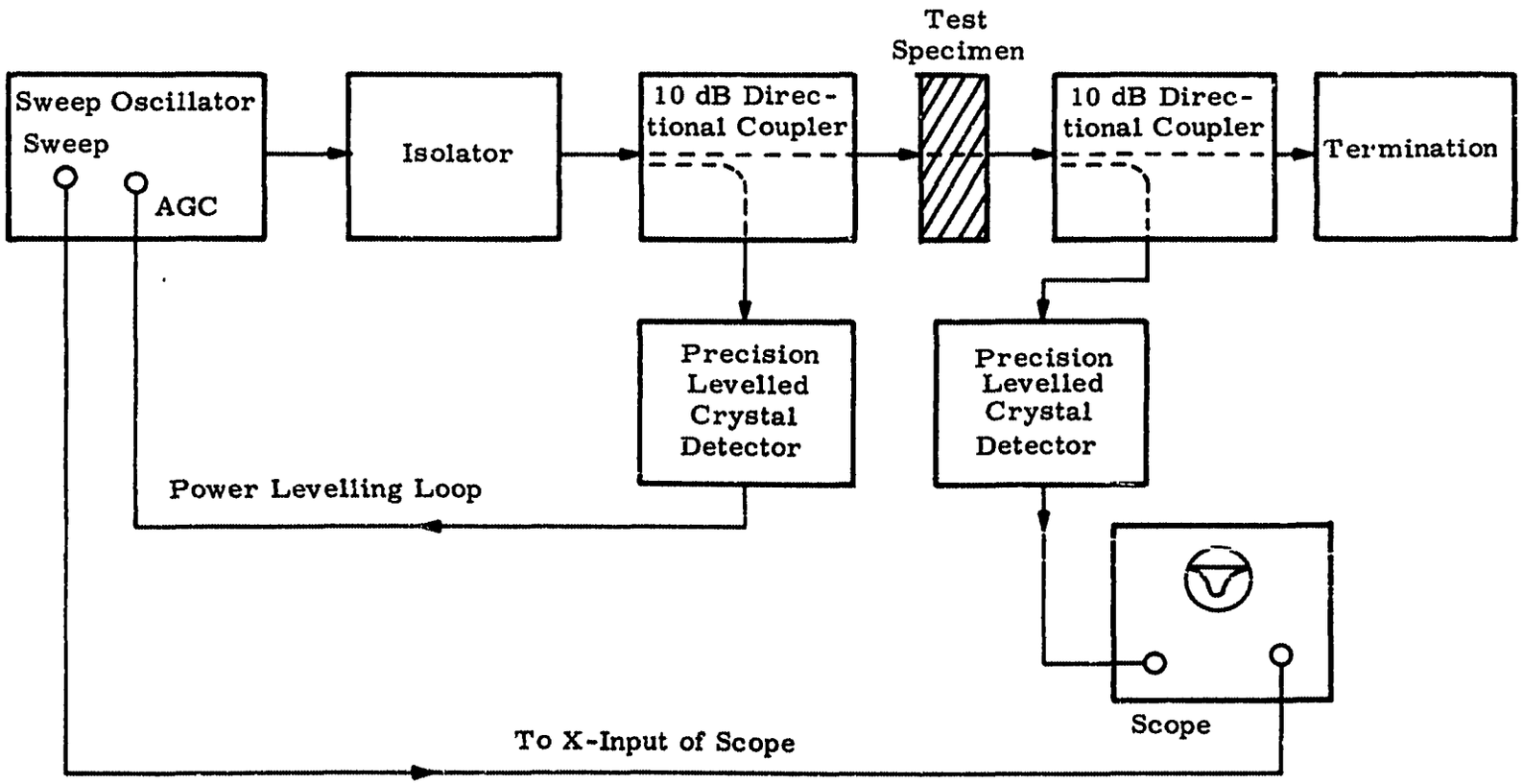


Figure 2. Microwave Swept Frequency Through-Transmission System for Measurement of Density/Porosity Variations in Composite Materials

Data Display

The reflected or transmitted power as a function of frequency is displayed on an oscilloscope as shown in Figure 1. As the frequency spectrum is swept for any given test specimen of a specific thickness and complex permittivity, there will exist some point on the spectrum in which the maximum power will be reflected or transmitted. This point will appear as a minimum (or maximum) depending upon the polarity of the detection system.

Moreover, the power spectrum will gradually taper off on each side of the minimum as the frequencies (and therefore wavelengths) become more and more unsuitable for optimum power reflection. Therefore, the power spectrum gives the appearance of a resonance peak. Sophisticated scopes are not required for the display system. However, it is recommended that a scope with a vernier-type expandable X-scale and a Y-scale expandable to one millivolt per centimeter be used.

An X-Y recorder such as the HP-Moseley 7035A also proved to be sufficient to display the data. The chief limitation of the recorder is that time must be allowed for the recorder to trace the frequency sweep across the page with adequate resolution. By comparison, the scope instantaneously displays the response shifts.

Test Specimens

Bidirectional reinforced Narmco 4085/2 test specimens were fabricated. The material was basically fabricated from high-silica fiberglass tapes preimpregnated with a nitrile-modified novolac phenolic resin. The reinforcement tapes were laid up at a 30 degree angle from normal. Variations in density/porosity were created by functionally varying the cure temperature and pressure. The specimens were then machined to a uniform thickness to isolate the thickness variable from the functional density/microwave relationship. Properly cured specimens of the same material were later used to determine the thickness function.

NDT Measurements

The system was assembled as shown in Figure 1. All measurements were taken with the specimen in contact with the waveguide to minimize angle-of-incidence variations and guide-to-sample distance variations.

Measurements of the shift in frequency of the Fresnel minimum as a function of density/porosity on the 9 samples are shown in Figure 3. Specimens A, B, C, and D shown in the figure were subsequently sectioned and photomicrographed. The porosity gradations are shown in Figure 4. Destructive density measurements were made for correlation purposes.

Results

Results indicate that, within reasonable limits likely to be encountered in a production operation, the shift in the Fresnel minimum is linearly related to density/porosity variations in the test specimens. The shift due

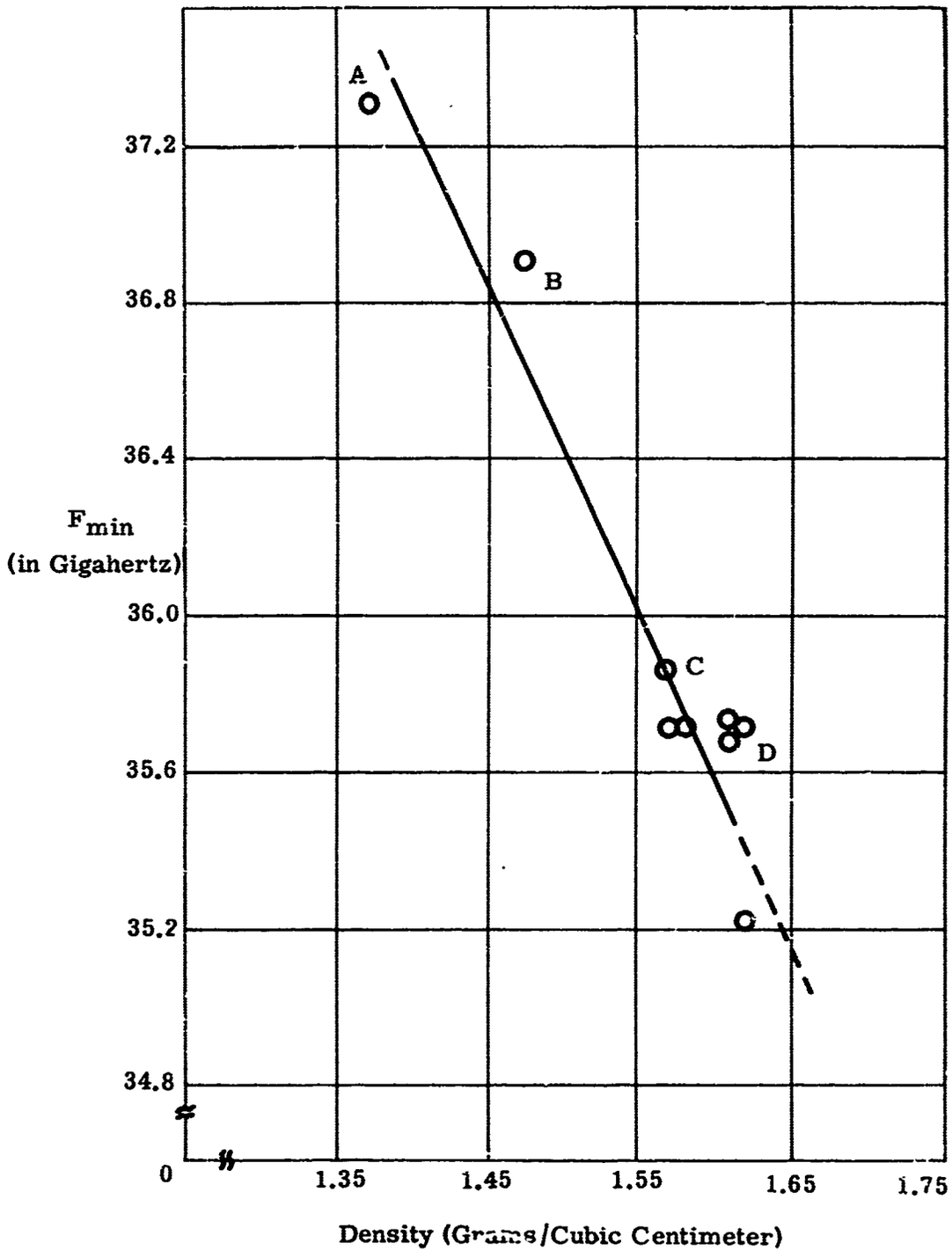


Figure 3. Shift of Fresnel Minimum for K_a-Band Microwave (26.5 to 40 GHz) as a Function of Density/Porosity for Narmco 4085/2 Panels

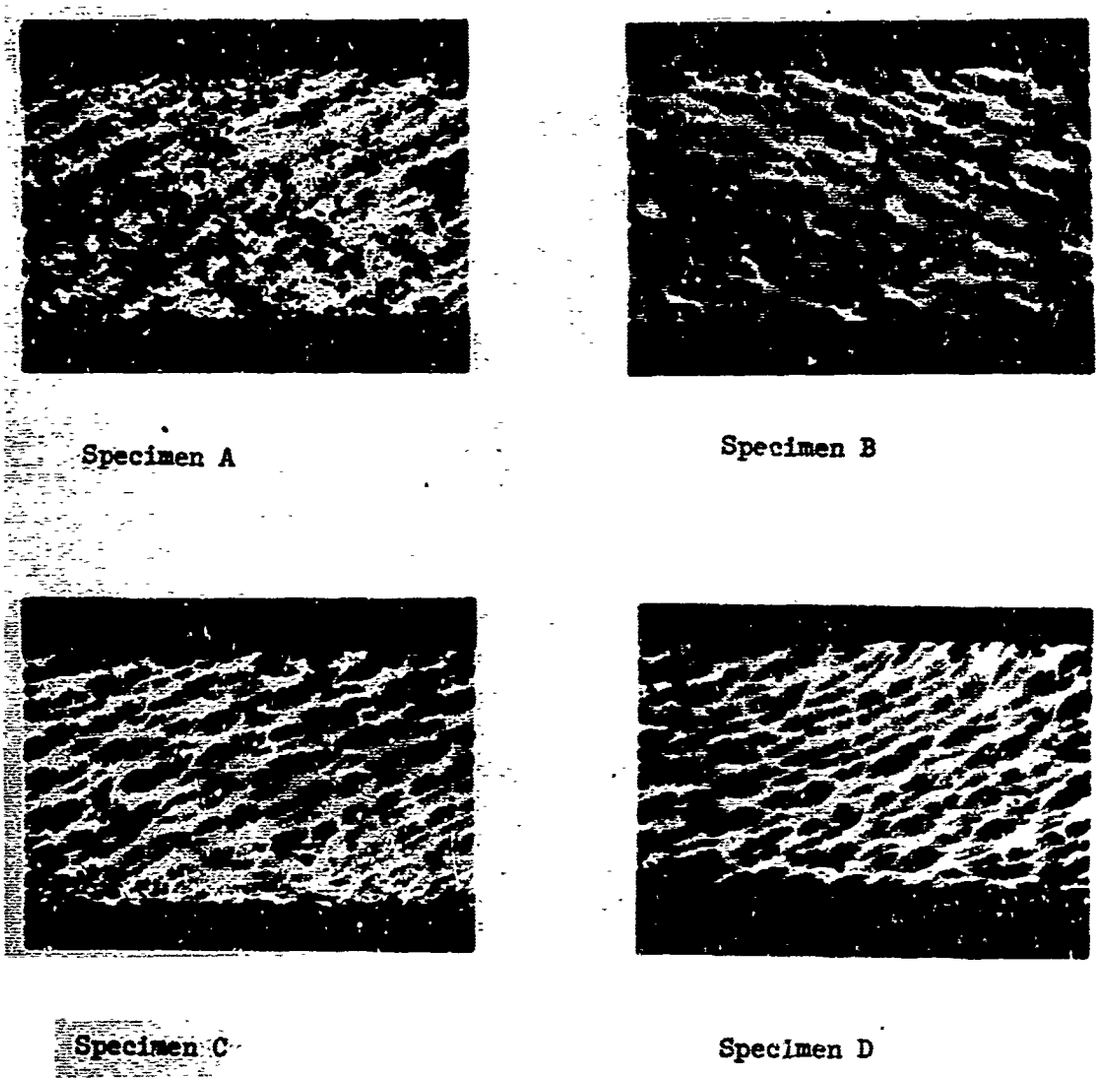


Figure 4. Porosity Variations in Narmco Microwave Test Panels

to density/porosity variations is attributed to the resulting changes of the complex permittivity (dielectric constant and loss tangent), and therefore, the index of refraction of the material.

Further tests also show the shift of the response to be linearly related to thickness changes in the range of interest. Although thickness functions must be generated for each kind of material tested, a typical thickness function to illustrate linearity is shown in Figure 5.

Thickness Variations

Since the shift of the response minimum is related to physical thickness variations, it appears on the surface that slight thickness variations could mask the shift due to density/porosity variations. Martin Marietta has overcome this problem by using a magnetic field thickness gauge, the Magnemike*, (developed and patented by Martin Marietta) which will very easily determine the thickness nondestructively from one side access only. When this technique is used in conjunction with the microwave measurements, the shift in the Fresnel minimum can be readily corrected for thickness variations on the production part.

A typical oscilloscope readout suitable for production purposes is shown in Figure 6. Go-no go limits can be marked on the scope and when the density/porosity falls out of the specified limits, the item would be rejected.

Since the shift of the Fresnel minimum is a linear function of both thickness and density/porosity variation in our range of interest, a handy slide rule has been developed to quickly convert a thickness deviation as read on the Magnemike into an appropriate Fresnel shift correction. The slide rule is illustrated in Figure 7.

CONCLUSIONS

1. Definitive relationships between density/porosity variations and the shift of the Fresnel critical point using swept frequency microwave techniques have been established. These relationships are linear over an appreciably wide range.

2. A functional relationship between thickness variation and Fresnel shift has been established, which is sufficiently linear over the range of interest.

3. Thickness variation can be compensated for by use of the Magnemike and a slide rule nomograph.

*The Magnemike was developed by William R. Randle of Martin Marietta. Further information can be obtained from the Martin Marietta Corporation Contracts Division, Orlando, Florida.

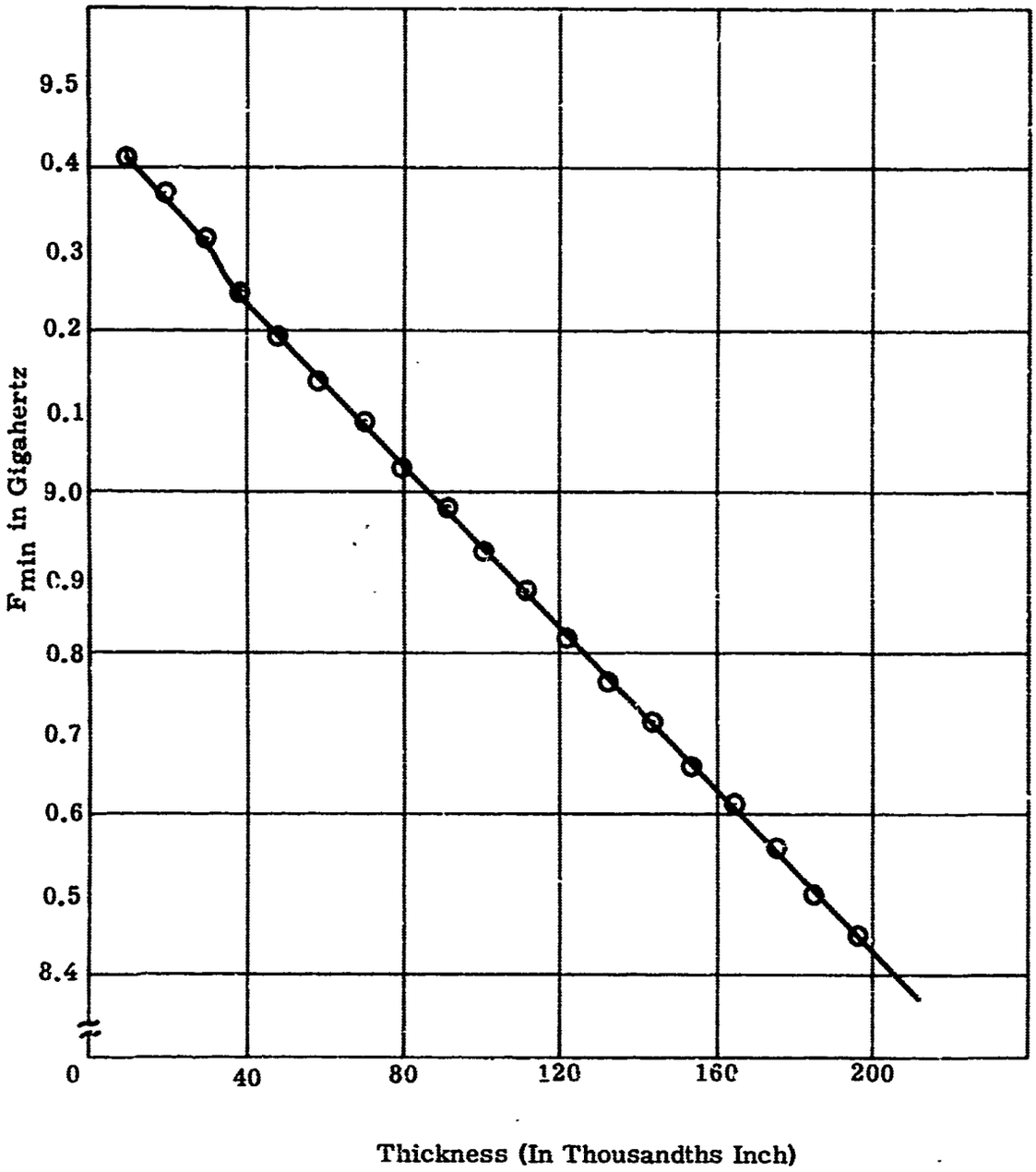


Figure 5. Frequency Shift of Response Minimum for X-Band Microwave as a Function of Thickness for Bicycle Playing Cards Successively Stacked

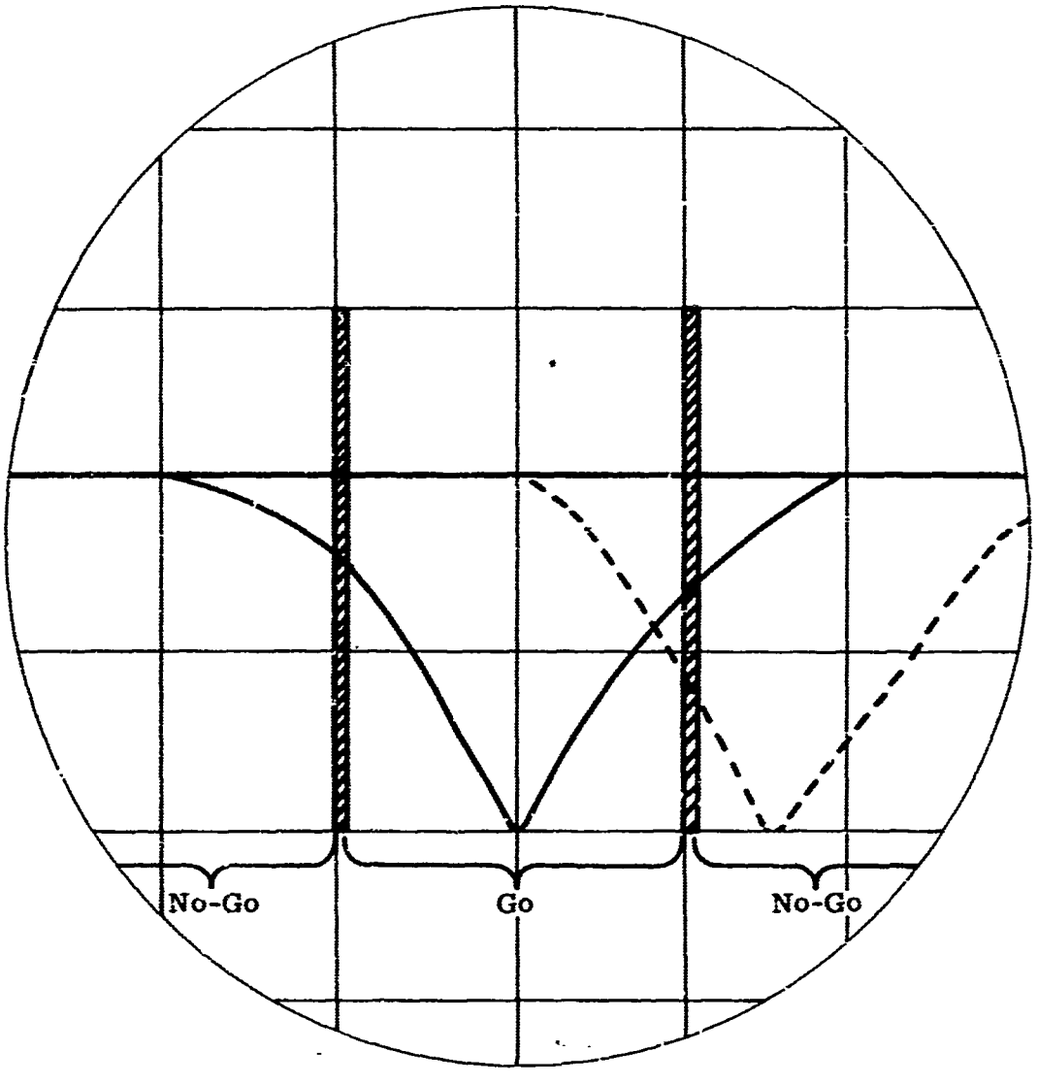


Figure 6. Shift of Fresnel Minimum on Oscilloscope Trace Showing Typical Go-No Go Limits for Production Applications

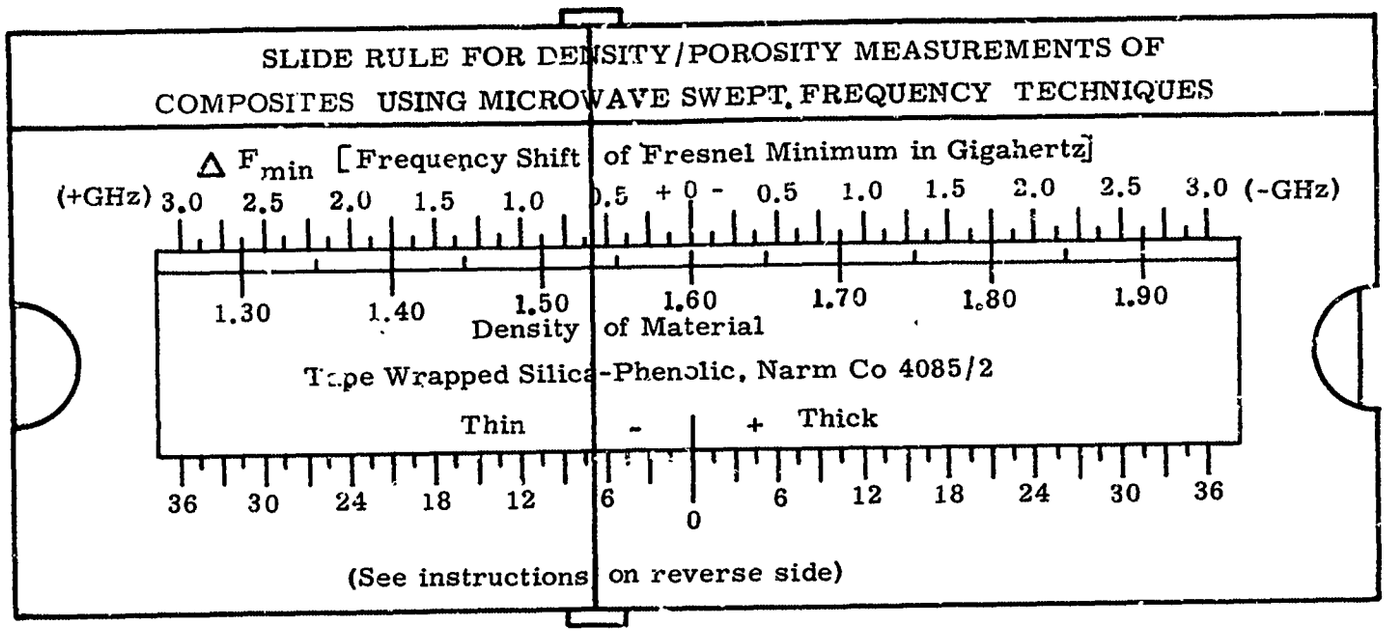


Figure 7. Slide Rule Developed for Thickness Corrections to the Fresnel Shift

4. Depending upon the production requirements, varying degrees of automation such as closed loop thickness corrections, etc. can be implemented into the system.

5. The swept frequency technique offers significant advantages over fixed frequency, microwave bridge, and other techniques because of instantaneous display capability, its wide frequency coverage, its numerical measurement capability, and because it is more readily adaptable to the testing of a finished product.

6. The K_a-band (26.5 to 40 Ghz) provides more definitive results for density/porosity variations than does the X-band (8.2 to 12.4 GHz).

FUTURE WORK

Although the investigation during this program was conducted using one material, it is recognized that the swept frequency technique is equally applicable to a large number of composite dielectric materials having various construction geometries. Future efforts will be directed toward using the technique with a variety of applicable materials. Efforts will also be directed toward refining the geometry of the system and the test set-up to enhance the actual testing of production items with greater ease and efficiency.

The results of this program have firmly established the feasibility of using swept frequency microwave techniques for the nondestructive measurement of physical property variations in composite materials, and it therefore conclusively adds swept frequency microwave to the family of nondestructive testing techniques.

REFERENCES

1. Ryskewitch, J. Am. Ceram. Soc., 36 (1953) 65

2. Coble, R. L. and Kingery, W. D., J. Am. Ceram. Soc., 39 (1956) 379

3. Lloyd, D. E., "Ceramic Systems," Composite Materials, Holliday, Elsevier Publishing Company, New York, 1966

4. Birks, J. B., et al, Progress in Dielectrics, Volume 2, Wiley & Sons, New York, 1960

5. Von Hippel, Dielectric Materials and Applications, M.I.T. Press, 1954

6. Morey, G. W., Properties of Glass, 2nd Edition, Reinhold, New York, 1954

7. Stevels, J. M., Progress in the Theory of Physical Properties of Glass, Elsevier, New York, 1948

8. Stevels, J. M., "The Electrical Properties of Glass," in Encyclopaedia of Physics (Handbuch der Physik), Vol XX, pp 350-391 (Springer, Berlin, 1957)

9. Stevels, J. M., "Silicates Ind.," 22,325 (1957)

10. Stevels, J. M., et al, "Philips Res. Rep.," 8,452 (1953)

11. Stevels, J. M., Philips Res. Rep. 6, 34 (1951)

12. Jasik, Henry, Antenna Engineering Handbook, McGraw-Hill, 1961

VERTOL DIVISION • BOEING CENTER

NONDESTRUCTIVE INSPECTION OF AN ADVANCED GEOMETRY COMPOSITE BLADE

BY

Robert L. Whealy

Manager, Quality Assurance
Research and Development

A. J. Intrieri

Senior Engineer
Quality Assurance
Research and Development

Conference on NDT Plastic/Composite Structures

March, 1969

Dayton, Ohio



ABSTRACT

This paper presents the approach taken by The Boeing Company, Vertol Division, in providing an integrated Quality Assurance Plan for an Advanced Geometry Composite Rotor/Propeller Blade Program. Included is a detailed discussion of the nondestructive test (NDT) plan containing specific applications that will be used to control the quality of the rotor blade throughout the fabrication process. In addition, examples of existing inspection systems utilizing the recommended NDT methods is given to demonstrate their suitability for production application. These include:

Inspection of Rotor Blade Honeycomb Box Assemblies for Voids Utilizing Infrared Techniques.

Inspection of the Internal Quality of Rotor Blades Utilizing a Semiautomatic X-Ray Sensitive Vidicon/Image Intensifier System.

Inspection of the Bond Quality of Rotor Blades Utilizing a Semiautomatic Tape Controlled Ultrasonic System.

Inspection of steel spars utilizing magnetic perturbation techniques, new approach in nondestructive inspection.

INDEX OF FIGURES

FIGURE	DESCRIPTION
1	Typical Rotor Blade Loads
2	Blade Build-Up Cut-Away
3	Typical Composite Blade Construction
4	Boeing Advanced Geometry Rotor Blade
5	Boeing Tilt-Wing Blade Model
6	Rotor Blade 1/7th Scale Demonstration Article-Quality Assurance Research and Development Study Chart
7	Nondestructive Test Plan
8	Rotor Blade Spar Tube Ultrasonic Inspection System
9	CH46/47 Rotor Blade Spar Tube
10	Spar Tube Inspection System Instrumentation and Bridge
11	Shearwave Ultrasonic Scope Presentation
12	Rotor Blade Magnetic Perturbation System
13	Magnetic Perturbation Inspection Principle

FIGURE	DESCRIPTION
14	Magnetic Perturbation Inspection System Probe Carriage
15	Magnetic Perturbation Inspection System Console
16	Magnetic Perturbation Defect Signal
17	Radiograph of Lead Glass Strands in Solid Laminate
18	Ultrasonic Reflector Concept
19	Ultrasonic Recording of Flat Bottom Holes in a Wedge Ranging in Thickness From 1/16" to 3/4"
20	Advanced Geometry Blade C-Spar Ultrasonic Inspection
21	Beta Backscatter and Ultrasonic Longitudinal Wave Velocity Correlation to Resin Content
22	Comparative Recordings of Voids in Boron Sandwich Structure
23	Infrared Techniques
24	CH47B Rotor Blade Box
25	Infrared Inspection System
26	Infrared Presentation Showing Bondline Voids
27	Infrared Bond Inspection System Parts Handling & Heating Sub-System

FIGURE	DESCRIPTION
28	Ultrasonic Recording of Fiberglass Honeycomb Sandwich
29	Boron Stabilized Core in the Automatic Ultrasonic Inspection System
30	Mass Absorption Coefficient Vs. Atomic Number
31	Neutron Radiographs of Honeycomb Sandwich Structure
32	Conceptual Sketch of the Automated Ultrasonic Inspection and Recording System
33	Automatic Ultrasonic Inspection and Recording System
34	Control Console & Tape Reader for the Automatic System
35	Full Length Ultrasonic Recording for CH47B Rotor Blade
36	X-Ray Sensitive Vidicon and Image Intensifier System Concept
37	X-Ray Sensitive Vidicon and Image Intensifier System
38	Control Console and Video Monitor for the X-Ray Sensitive Vidicon System

FIGURE	DESCRIPTION
39	Typical Vidicon Monitor Presentations
40	Comparison of AGB Blade/ VTOL Propeller Geometry
41	Rotor Blade Contour Inspection System Manual and/or Automated System
42	Dimensional Control Laboratory Test Set-Up
43	Separated Y-Z Plane Views of Compared Point-to-Point Data- Sta. 86 thru 92
44	Grid Routine for Rotor Blade Dimensional Inspection
45	Rotor Blade-Root End Demonstration Article - Quality Assurance Research and Development Study Chart
46	Ultrasonic C-Scan Recording of Broken Core Material in a Fatigue Specimen
	Ultrasonic C-Scan Recording of a Defective Bonded Joint in a Fatigue Specimen
47	Ultrasonic Recording of 75% Attenuation Level in Composite Material
	Ultrasonic Recording of 75% Attenuation Level in Composite Material
48	Ultrasonic Records for Monitoring of Questionable Areas During Test

NONDESTRUCTIVE INSPECTION OF AN ADVANCED GEOMETRY COMPOSITE ROTOR/PROPELLER BLADE

INTRODUCTION

Significant performance improvements in rotor/propeller blades can be realized by proper utilization of composite materials. The Boeing Company's Vertol Division is engaged in very ambitious research and development programs to improve the performance of VTOL and STOL aircraft. One of these programs involves the design, construction, and flight evaluation of an advanced geometry fiber reinforced composite rotor blade. The program includes the use of several different fiber reinforced materials.

One of the most important tasks in the utilization of composites is the development of the nondestructive inspection capability to assure that the hardware to be tested is of known quality. Some of the most challenging effort comes not in the selection of what nondestructive technique to use, but in the mechanism necessary for practical application of that technique to the complex structure of a rotor/propeller blade.

This is a discussion of the approach taken at The Boeing Company's Vertol Division in the development of a nondestructive inspection capability and an outline of some of the more interesting nondestructive inspection methods and systems utilized in quality measurement of advanced Boeing Helicopter rotor blades.

BLADE DEVELOPMENT

In the early phases of aircraft development, a variety of materials; such as, wood, metal, and fabric, was used for rotor/propeller blade construction. Since early helicopter designs were limited by the power plants available, it was necessary to design the rotor blade for maximum performance, and the literature covering the period from 1908 to 1945 shows a great variety of geometric rotating airfoil designs.

The materials available to the early designers had many problems. For example, maintenance difficulities and geometric and balance variations, as a result of inadequate weather resistance, proved to be major operational problems; but those materials did allow the designer a wide latitude in selecting the geometry he desired.

In the 1950's, the development and availability of the turbine engine, coupled with available metal alloys and fabrication techniques, drastically changed blade design concepts. Power became available, and mass production of reliable blades having closely matched properties of stiffness, weight, and moisture resistance became the industry goal. This approach, however, had its penalty. Geometric design freedom was lost. Metal working mass production technology forced the designer to create helicopter rotor blades with a constant chord, constant airfoil, and constant twist.

The result has been an almost uniform limit on current helicopter speed and performance. The problems of advancing tip mach number and retreating tip stall, coupled with dynamic instability limits inherent in monolithic metal, constant cross-section, rotating airfoils, resulted in blade lift to drag ratios around 8 to 140 knots.

Wind tunnel tests have shown that significant rotor performance improvements can be realized through the selection of a rotor geometry in which the blade airfoil sections progressively change along the radius to match each zone of its aerodynamic environment.

Fiber reinforced composite materials currently available to industry allow the designer to recapture the geometric freedom of the past and design his blade to perform under high power and load conditions by varying the strength, weight, and stiffness of his materials, thus controlling dynamic response. In addition, he can tailor the blade geometry to satisfy specific aerodynamic requirements, and at the same time improve fatigue life and eliminate the corrosion problems inherent in metal structures. In a flight and materials research program requiring a limited number of blades, the composite blades required can be produced with a much lower investment in tooling.

PAST EXPERIENCE

The use of fibrous reinforced composite materials has been increasing rapidly in the past few years. Significant progress has been made since 1960 in the development of composite materials and their utilization in advanced aerospace and aircraft structures.

The Boeing Company has been closely associated with the use of composite materials in aircraft and aerospace structures. Extensive practical experience has been gained in such vehicles as the B-47, B-52, 707, 727, Minuteman, and CH-46/CH-47 Helicopters. The use of composites has steadily increased from a few pounds on the B-47 to approximately 7½ percent of the airframe weight on the 747 program and with a substantial percentage planned for the Light Intra-Theater Transport (LIT).

A technology base has already been established at Boeing for the application of glass-fiber reinforced composites in the fabrication of helicopter rotor blades and other structures. From 1954 to 1962, intensive research into materials and fabrication techniques, backed up by component and sample fatigue testing, was performed. Three E-glass fiber reinforced epoxy matrix composite rotor blades with a 29.5 - foot radius and 25-inch chord, suitable for the CH-47 Chinook Helicopter, were fabricated and have successfully completed 142 hours of whirl tower testing. Since then, Boeing has continued its efforts to advance the technology of fiber reinforced composites. These efforts have included the design and fabrication of 12 Advanced Geometry S-glass Reinforced Composite (AGB) Rotor Blades. In addition, an Advanced Geometry Rotor Blade Program, utilizing high modulus (boron) filaments, is currently being conducted under contract to the Air Force Materials Laboratory.

The successful use of fiber reinforced composite materials in helicopter rotor blades leads naturally to an improved capability for a successful V/STOL propeller design. The V/STOL propeller is, by nature, a high performance aerodynamic system requiring design features which include spanwise variations in chord thickness, twist and airfoil section. Its aerodynamic requirements over the flight range, from hover to maximum forward speed, represents a level of design sophistication exceeding that for current helicopter rotor blades.

ROTOR BLADE LOADING AND STRUCTURE

In order to fully appreciate the enormity and importance of the nondestructive inspection job to be done, one must be aware of the types of loads rotor blades "see" and the general construction of the blade.

Rotor blades in service are subjected to a variety of static and cyclic loads. These loads include beam, centrifugal, torsional, and flapwise and chordwise bending. Some of these loads are schematically shown as Figure 1.

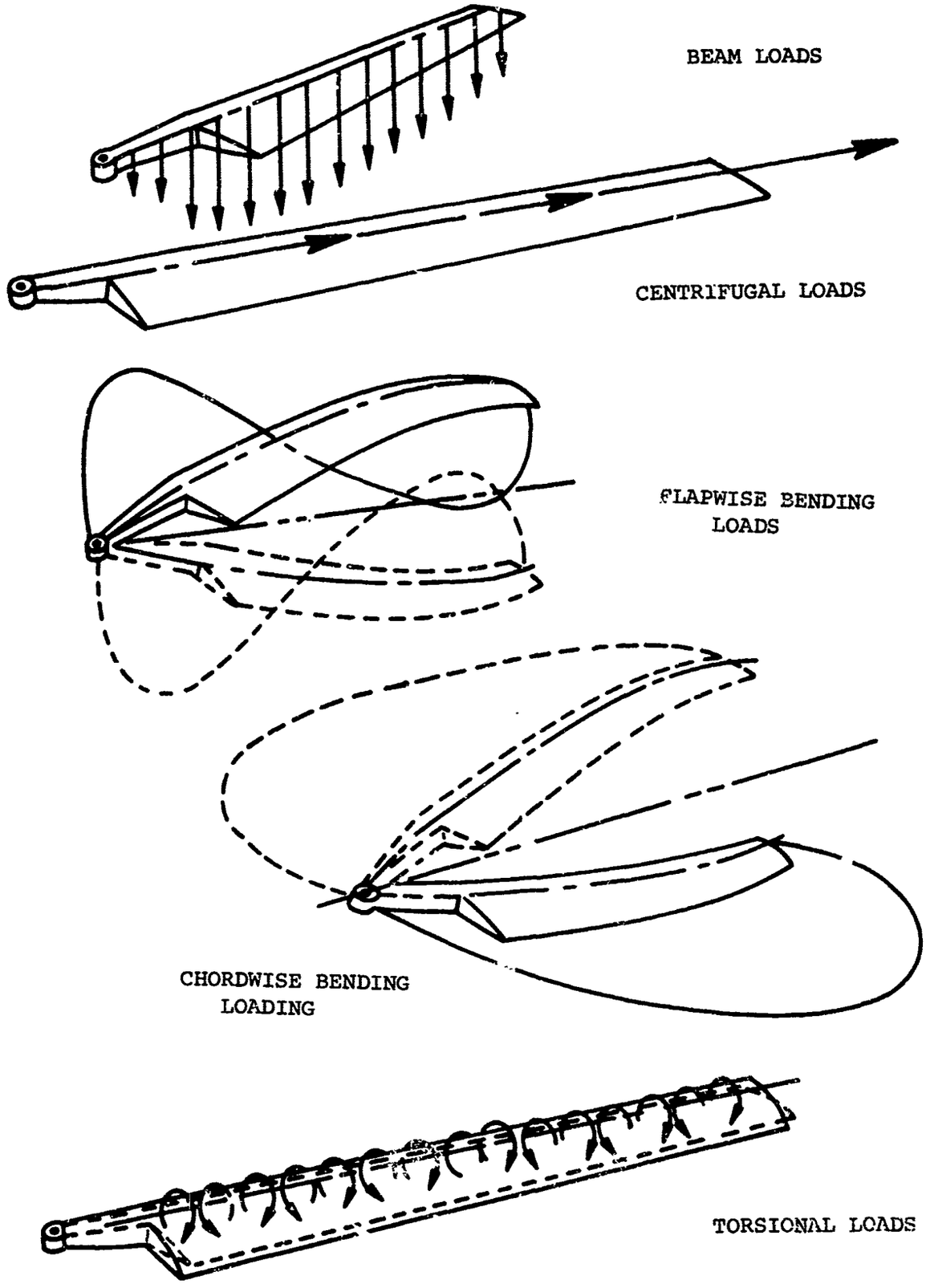


FIGURE 1
TYPICAL ROTOR BLADE LOADS

The Boeing Company's advanced geometry composite rotor blade is shown in a cut-away and sub-assembly sketch as Figure 2.

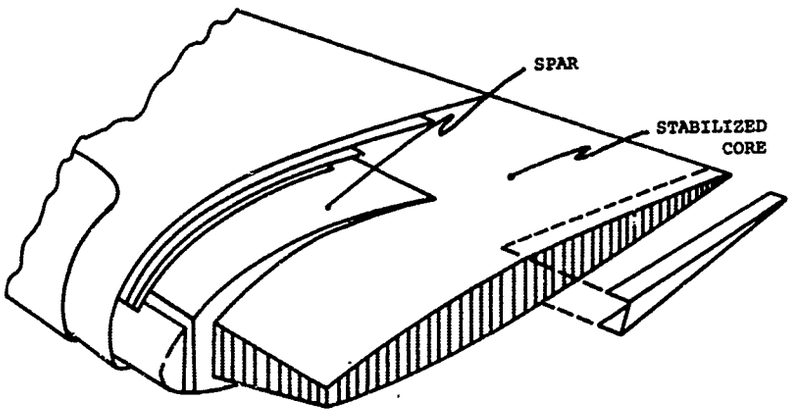


FIGURE 2
BLADE BUILD-UP CUT-AWAY

The main structural member, the spar, is a combination unidirectional and crossply layup. The unidirectional fibers provide the blade spanwise strength, while the corssply or bias layup offers torsional stiffness. The stabilized core is composed of aluminum honeycomb core covered with a single ply of fiberglass as a stiffner. During construction, the stabilized core is inserted in the spar and bonded. This sub-assembly, after addition of the leading edge weight, is then completely wrapped with fiberglass. A titanium or stainless steel nosecap is added to provide erosion protection.

The above discussion has been greatly simplified and does not include all details, but will be satisfactory for the purpose of this paper.

Figure 3 shows cross-sectional construction views of some of the composite rotor/propeller blades that are either in use now or proposed for use in the near future.

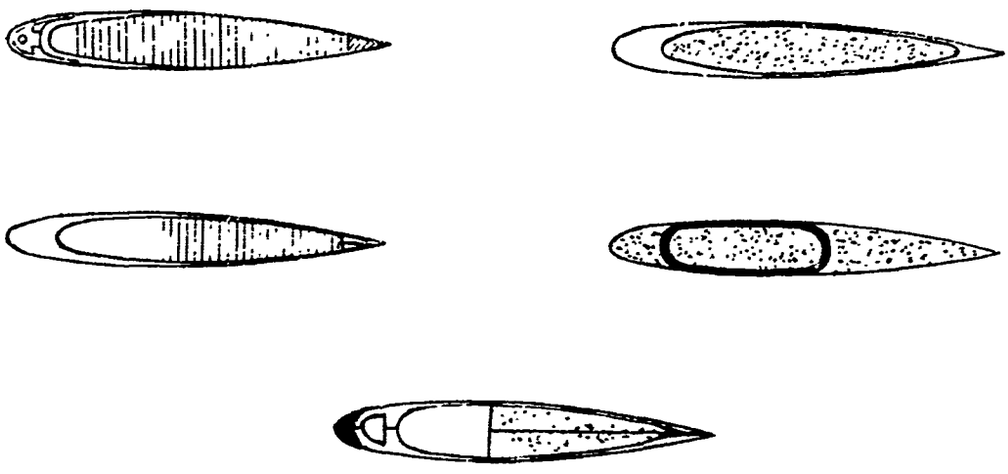


FIGURE 3

TYPICAL COMPOSITE BLADE CONSTRUCTION

Figure 4 shows the plan view of The Boeing Company/Vertol Division advanced geometry composite rotor blade, and Figure 5 shows a full scale model of a tilt wing composite propeller blade under development by the Vertol Division.

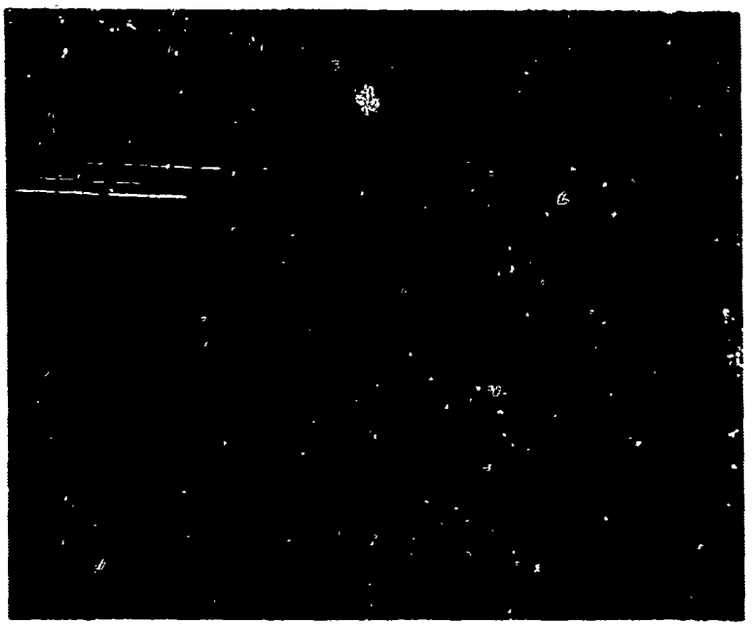


FIGURE 4

BOEING ADVANCED GEOMETRY
ROTOR BLADE

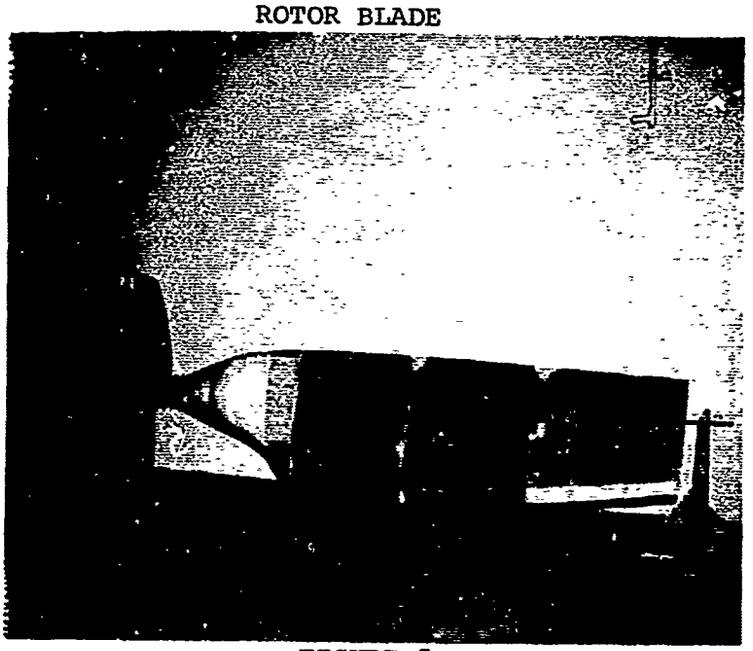


FIGURE 5

BOEING TILT-WING BLADE MODEL

NONDESTRUCTIVE INSPECTION CONSIDERATIONS

Nondestructive inspection technology has not been advanced to the point where it alone is capable of assuring product quality. There are a number of variables in the materials and processes used in composite structures that must be very carefully controlled in view of nondestructive inspection technology limitations. These controls used in conjunction with available nondestructive inspections can go a long way toward assuring product quality. All too often, industry tries to design and build complex composite structures and then, upon completion, attempts to measure quality. Obviously, it cannot be done and the result has led to a series of disappointments which have undoubtedly hampered the advancement of application of composites to critical structures. There is not, for instance, any reliable nondestructive technique to measure bond strength. This can only be assured through good process control and a nondestructive inspection for voids and/or unbonded (disbonded) areas.

Bonded sub-assemblies must be nondestructively inspected prior to incorporation in the end assembly. This situation can sometimes be a real problem from the contamination standpoint. In some cases, this situation can dictate hardware design and in almost all cases, affects both prior and subsequent processing.

QUALITY CONTROL CAPABILITY STUDY AND NDT PLAN

The Quality Control Capability Study, originated at Boeing, is one of the basic techniques used to assure that all characteristics of the design are considered in determining design inspectability. This study is made concurrent with design and, as such, any design and/or process changes required to enable measurement of quality can be easily accomplished.

A typical Capability Study, shown as Figure 6, involves a detailed breakdown of the design and processing to the basic characteristics that must be controlled. The Study shown is one that was performed for a 1:7 scale wind tunnel test blade.

FIG. 6 INTENTIONALLY OMITTED

The Nondestructive Test Plan evolves during the Capability Study. This plan forms a guide for nondestructive technology development as well as a skeleton plan for hardware inspection. Figure 7 shows the Nondestructive Test Plan that was developed for our Advanced Geometry Rotor Blade. The Nondestructive Test Plans being developed for the Boeing composite rotor and propeller blade production programs are much more complete and take advantage of some of the nondestructive test methods, such as magnetic perturbation, microwave, electric injection, neutron radiography, and ultrasonic longitudinal wave velocity which are in development in our laboratories. The plan shown is not completed in detail, but it does illustrate the general flow of processing and the nondestructive inspection methods to be considered for use at each sub-assembly phase.

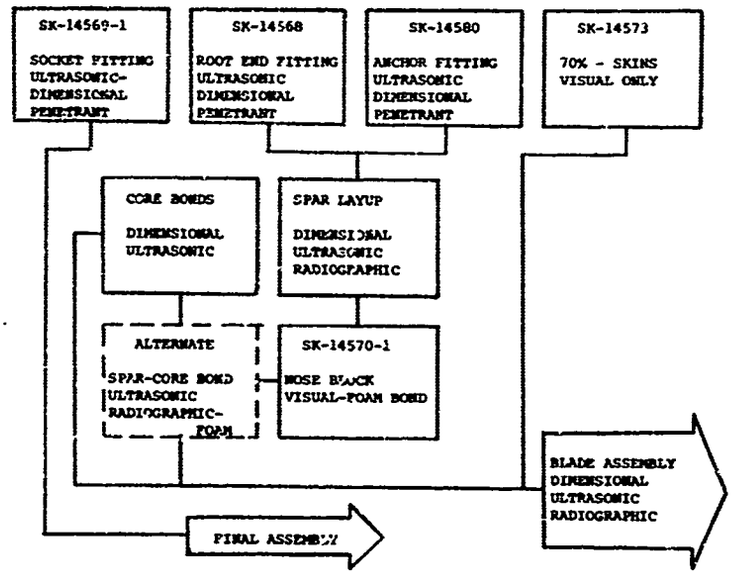


FIGURE 7

NONDESTRUCTIVE TEST PLAN

NONDESTRUCTIVE INSPECTION METHOD DISCUSSION

The following discussion will treat certain of the inspection methods shown on the NDT Plan from both a conceptual and actual standpoint.

Spar Inspection

The main structural member of the blade can be either a metallic or a composite structure. For the purpose of this discussion, we will assume that the metallic spar is tubular and that the composite spar is a solid laminate structure. From the nondestructive inspection standpoint, we must be concerned with notch-type defects and inclusions in the metallic structure and laminar defects and fiber orientation in the composite structure. In addition, material conditions such as hardness and structure in the metallics and resin content and degree of cure in the composites must be considered.

Magnetic particle, liquid penetrant, and ultrasonic techniques have been accepted methods of defect detection in wrought metals for several years. Recent developments by The Southwest Research Institute have resulted in a relatively new inspection method called magnetic perturbation. The technique obviously is applicable to ferro-magnetic materials only. This inspection technique is now being utilized on H-46 helicopter rotor blade spars that were fabricated prior to the time that ultrasonic inspection was incorporated in the H-46 spar production program. Eddy current and ultrasonic techniques are under study for use in establishing material phase condition in titanium alloys. The following offers a brief description of the ultrasonic and magnetic perturbation inspection techniques and equipment in use at Boeing for rotor blade spar inspection:

Ultrasonic Inspection

Detection of very tight surface originating and internal material defects in CH-46 and CH-47 rotor blade spar tubes is accomplished utilizing a four-directional shear wave ultrasonic technique.

The inspection system, shown as Figure 8, consists of a tank 45 feet long equipped with a variable speed bridge, a 4-channel ultrasonic system, and a tube bow following transducer manipulator.



FIGURE 8
ROTOR BLADE SPAR TUBE
ULTRASONIC INSPECTION SYSTEM

The rotor blade spar tube, Figure 9, is rotated at 108 RPM during inspection with a bridge speed set for a 1/8" per tube revolution index. The four transducers are mounted in such a manner that shear waves are introduced into the spar material in opposite peripheral and opposite transverse directions. The bridge arrangement is shown as Figure 10.

FIGURE 9 -CH46/47
ROTOR BLADE SPAR TUBE

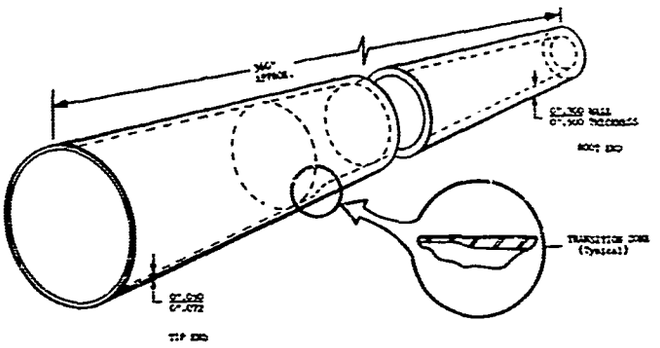


FIGURE 10 - SPAR TUBE
INSPECTION SYSTEM
INSTRUMENTATION AND BRIDGE

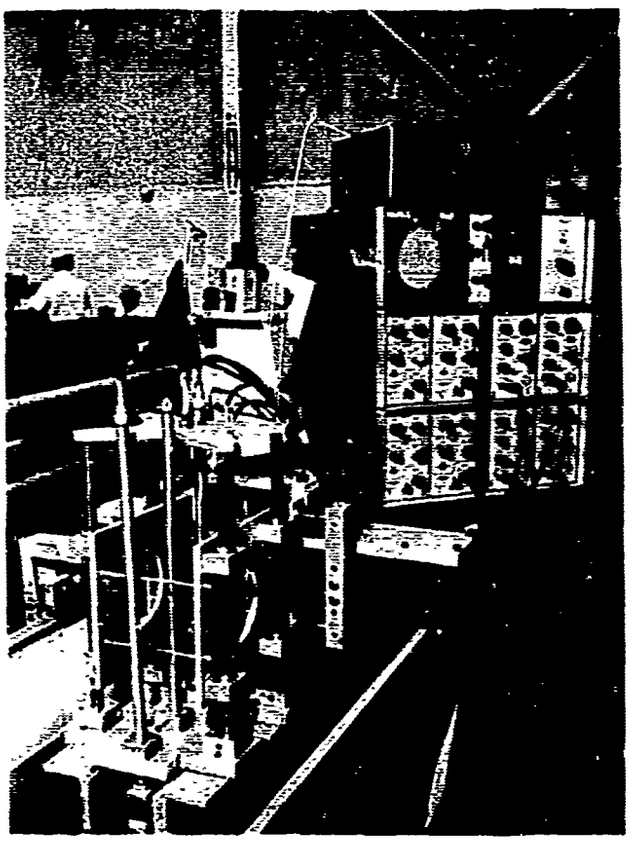
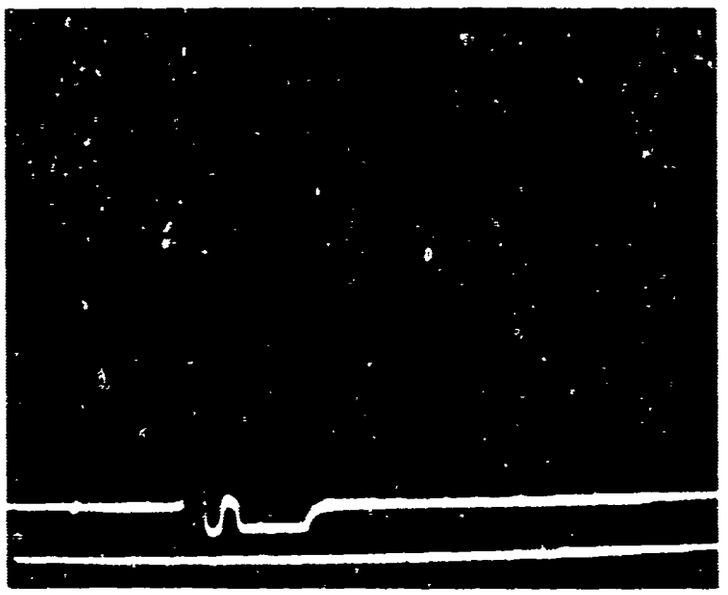
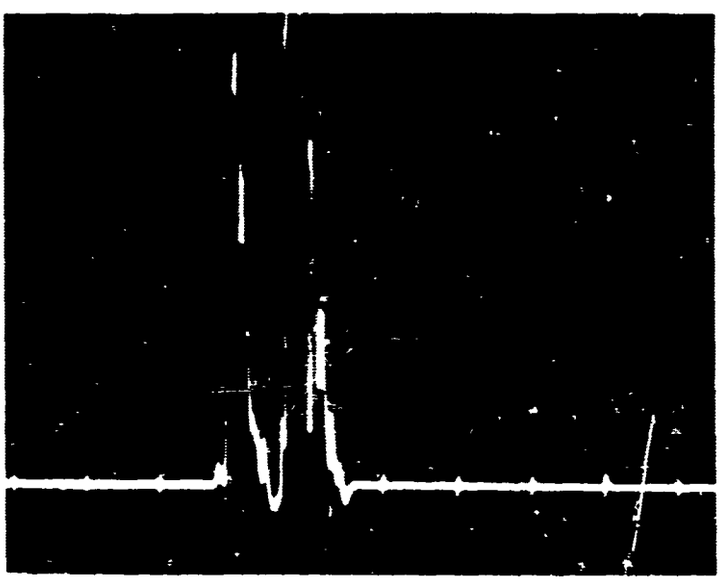


Figure 11 shows the scope trace for an acceptable and a rejectable condition. The rejectable condition shown is for a reference standard slot of .005" deep and .100" long.



ACCEPTABLE



NOT
ACCEPTABLE

FIGURE 11
SHEARWAVE ULTRASONIC
SCOPE PRESENTATION

Magnetic Perturbation Inspection

The fact that small laps, not detectable by standard magnetic particle inspection techniques, could possibly exist in the CH-46 rotor blade spars prompted the development of a nondestructive inspection technique which is proving to be an advancement in the state-of-the-art. The technique, magnetic perturbation, improved and refined by The Southwest Research Institute; in conjunction with The Boeing Company, Vertol Division, is being applied to blades that have been in service. The system is shown as Figure 12.

Basically, the technique works as follows: When an external magnetic field is applied to a ferromagnetic work piece, the induced flux in the metal is dependent on the strength of the field constant, any localized area of decreased permeability, such as a lap, will offer reluctance to the flux, causing it to seek a path of higher permeability around this area. In taking this path, the adjacent flux lines are displaced from their normal paths, hence the name "magnetic perturbation". This displacement affects the flux lines at the surface of the metal and forces them to take a curved path, part of which extends above the surface of the metal.

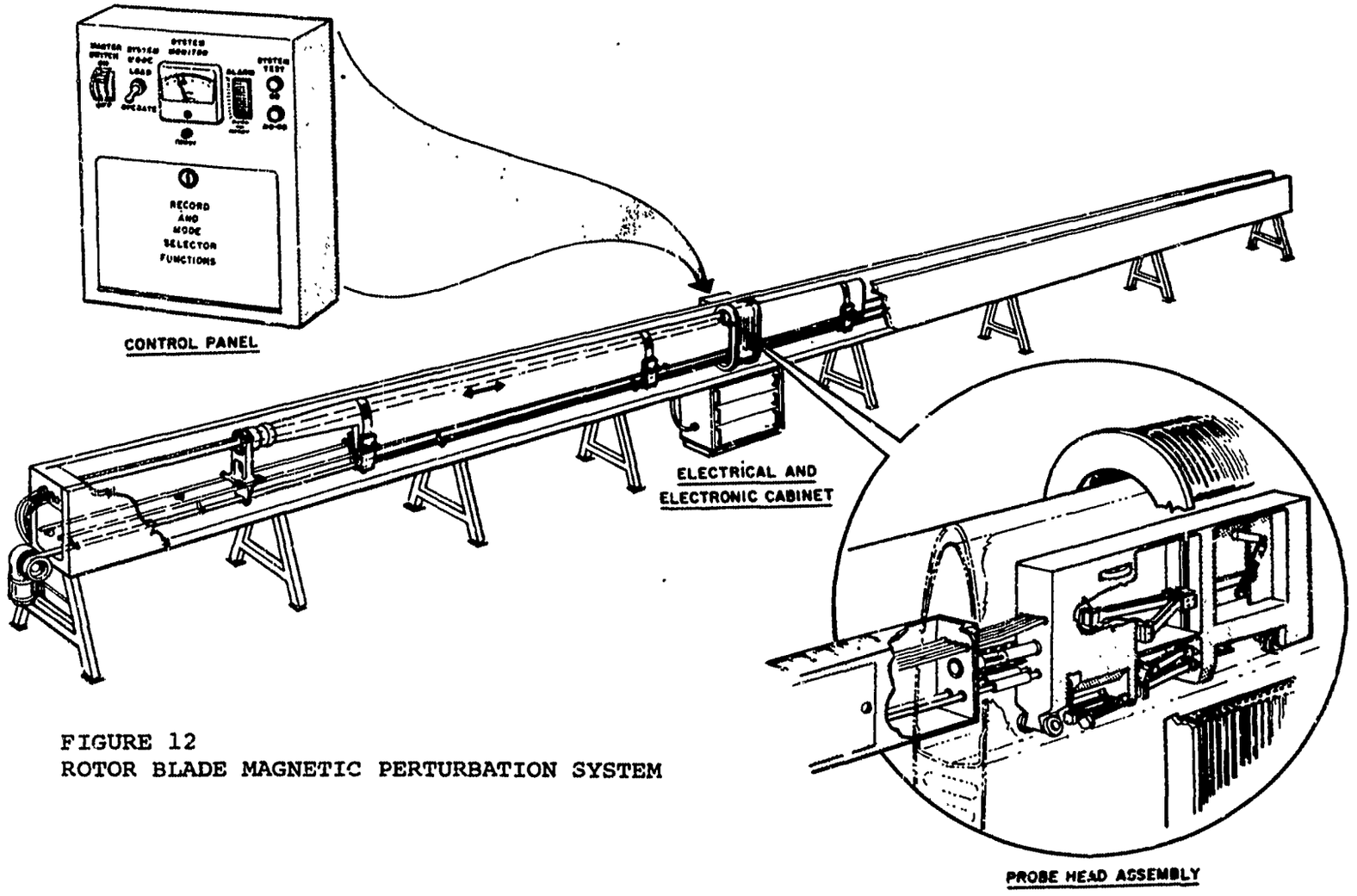


FIGURE 12
ROTOR BLADE MAGNETIC PERTURBATION SYSTEM

This situation is depicted in a sketch shown as Figure 13. When a coil or Hall element probe is moved parallel to the surface of the metal, it will cut these "perturbed" flux lines both at the point of emergence and/or re-entry, causing a voltage to be induced in the probe. Measurement and analysis of the voltage is the heart of the magnetic perturbation technology. This technique has been applied to the CH-46 rotor blade configuration. The system is designed for nearly automatic operation. The envelope is four feet wide by sixty-three feet long. Two moving carriages support the blade which is attached at the tip weight studs and at the root end clamp band. The blade is bridged (root end first) through a magnetizing solenoid coil which is located at the center of the envelope. The drive system oscillates the blade from one end of the base to the other at speeds of 250-450 inches per minute, depending on the area of the spar being inspected.

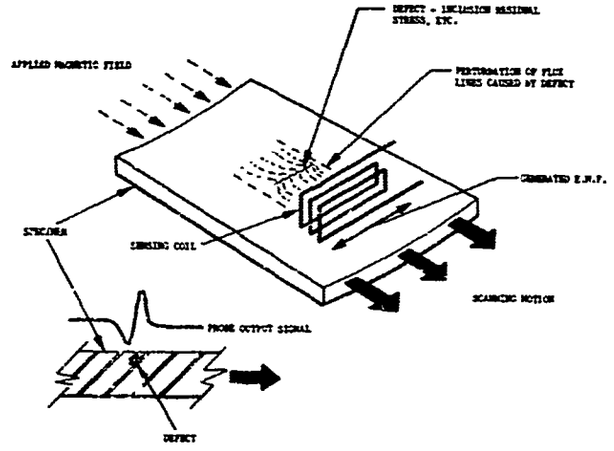


FIGURE 13
MAGNETIC PERTURBATION INSPECTION PRINCIPLE

The probe carriage, shown as Figure 14, is cantilevered on the end of a 27' long support arm such that it is positioned in the center of the solenoid, and enters the I.D. of the spar at the root end, as the blade is initially positioned through the solenoid. Once the carriage is in the spar, it rides on the aft, or heel, surface.

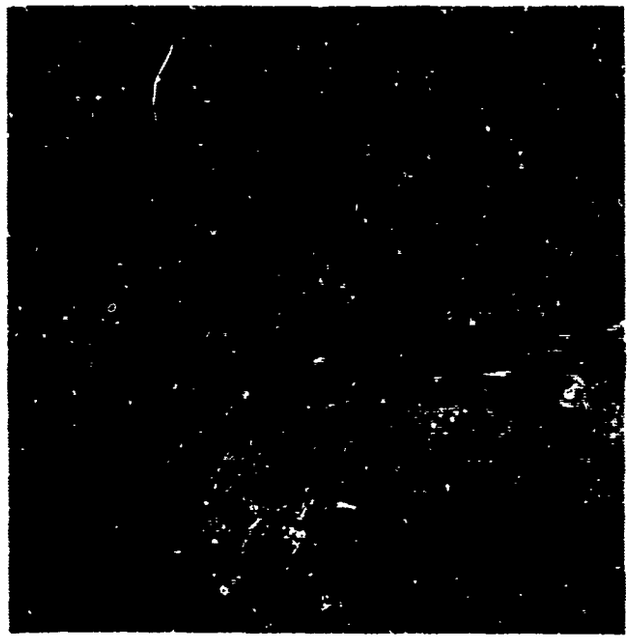


FIGURE 14
MAGNETIC PERTURBATION
INSPECTION SYSTEM
PROBE CARRIAGE

The probe assemblies contain various numbers of coils and are mounted to the carriage with pre-loaded springs. Lift off is accomplished by means of air coupling and averages between one and two mils off the inside surface.

Defects on the outside surface of the spar, sub-surface, and on the inside surface are detected by this scan of the I.D. The paint layer on the I.D. has negligible effect on signal strength except where excessive paint causes increased lift-off from the spar. If this occurs, the malfunction alarm sounds and, after analysis, the paint is removed.

No more than 10 coils are scanning during any one scan cycle. A scan cycle consists of one complete round trip between scan limits and over the same scan track. There are three conditions of read-out analyzed and alarmed by the system--- defect, malfunction, and hi-level. The "defect" alarm is triggered by a signal having a voltage above a preset standard. The "malfunction" alarm is triggered by loss of background such as would occur with excessive lift-off or a broken coil. The "hi-level" alarm will trigger if excessive background should occur which could drown out a defect signal. The latter capability was added as a precaution in the event isolated spars would contain "different" permeability levels. Of 25 spars run at vendor checkout no hi-level condition was experienced. Under all three aforementioned conditions, the machine stops, an alarm bell sounds, and an identifying signal light comes on.

A manual or "record" mode is built into the unit but this capability is not readily available to the operator. The manual controls, which are behind a locked panel, permit qualified personnel to vary operating speeds, magnetism, and to record signal shape for analysis. The control console is shown as Figure 15. Based on previous research data, signal shape defines various characteristics of a defect; such as, size, distance from the surface, type of defect, etc. A typical recording of a .005" deep X .100" long defect is shown as Figure 16.

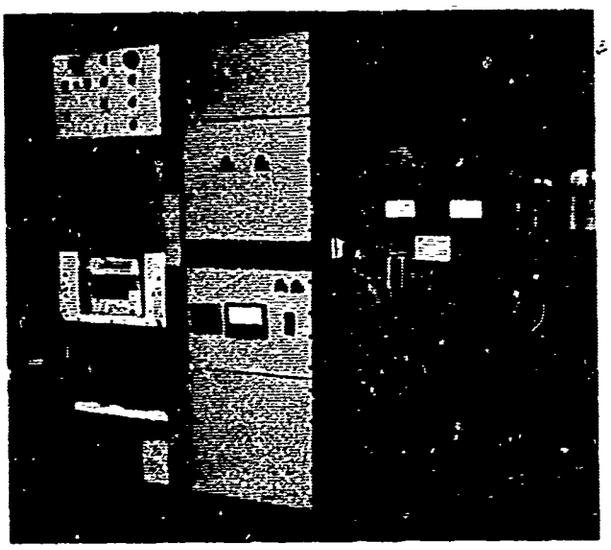


FIGURE 15

MAGNETIC PERTURBATION
INSPECTION SYSTEM
CONSOLE

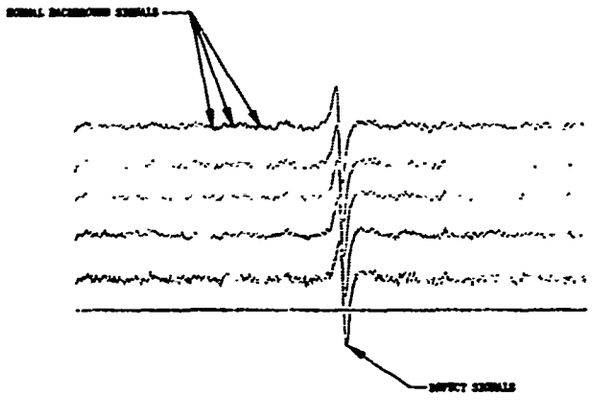


FIGURE 16

MAGNETIC PERTURBATION DEFECT SIGNAL

The magnetic perturbation technique offers a wide range of opportunity for nondestructive testing of paramagnetic materials to a degree of sensitivity beyond current capability. Within applicable limits, resolution and definition are as good as, if not better than, any other method of nondestructive testing.

Radiographic and Ultrasonic Inspection

Penetrating radiation and ultrasonic inspection are the most common nondestructive inspection methods utilized for detection of laminar defects in solid fiber-resin laminates. The incorporation of a dense tracer fiber during lay-up is very helpful in determining uniform laminate structure. The tracer fiber is readily visible on the radiographic film or imaging device during normal x-ray inspection. Figure 17 is a radiograph showing the lead silicate fibers incorporated during the lay-up of The Boeing Company's Advanced Geometry Composite Rotor Blade Spar.

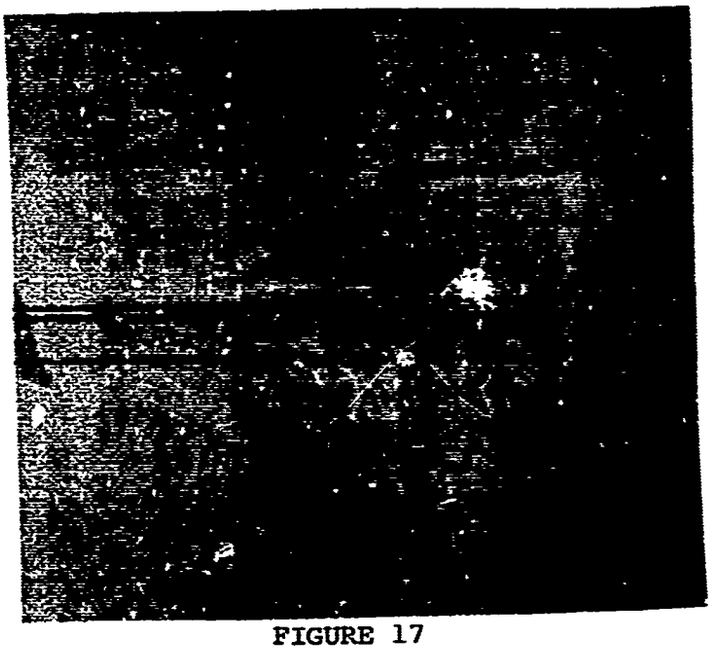


FIGURE 17
RADIOGRAPH OF LEAD GLASS
STRANDS IN SOLID LAMINATE

The detection of laminar defects and voids is of paramount importance in the inspection of the main structural member of the blade. Ultrasonic techniques are the most commonly used for this inspection. We have selected ultrasonic techniques for the detection of voids and laminar defects in the advanced geometry composite rotor blade spar. The basic technique involves the use of a reflector plate placed within the spar, Figure 18.

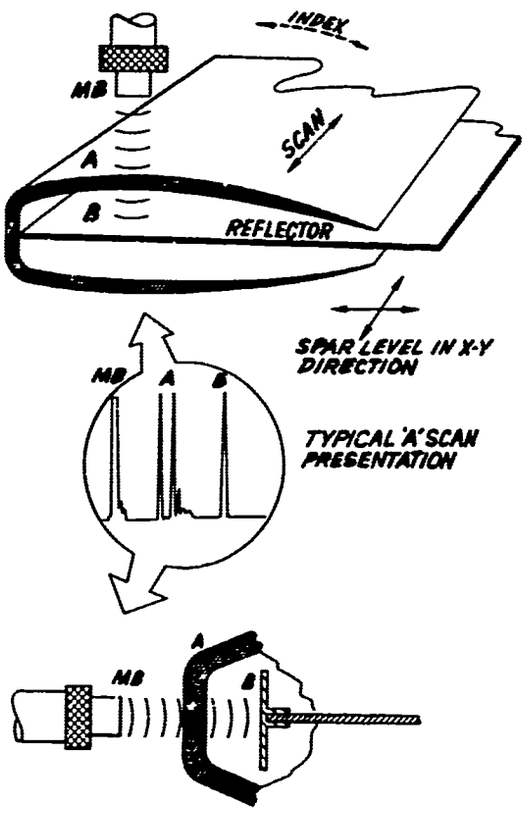


FIGURE 18
ULTRASONIC REFLECTOR CONCEPT

The percentage loss of back signal reflection is utilized for the detection of voids and laminar defects. The part is immersed in water and inspected utilizing a 2.25 mc-1/2" transducer. Figure 19 shows an ultrasonic C-scan recording of a wedge ranging from 1/16" to 1" in thickness, with built-in laminar defects. Figure 20 shows a full length spar being inspected using the reflector plate concept.

Resin Content

Experience has shown that in the fabrication of fiber reinforced structures, not enough is known about controlling process parameters to enable the production of reproducibly uniform parts. Consequently, the normal result is the production of hardware showing considerable variability between and within similar parts.

The strength and fatigue life of fiber reinforced composite structures depend upon many factors. A very important one is the resin/reinforcement ratio. At present, this ratio is determined on process control specimens by burn-out analysis. Investigations are being conducted to develop or define a nondestructive test technique to perform this inspection on actual hardware.

Two NDT techniques are being investigated, the beta backscatter method and ultrasonic longitudinal wave velocity. It has been concluded, on the results obtained to date, that a good correlation exists between the test results from both NDT techniques and resin content.

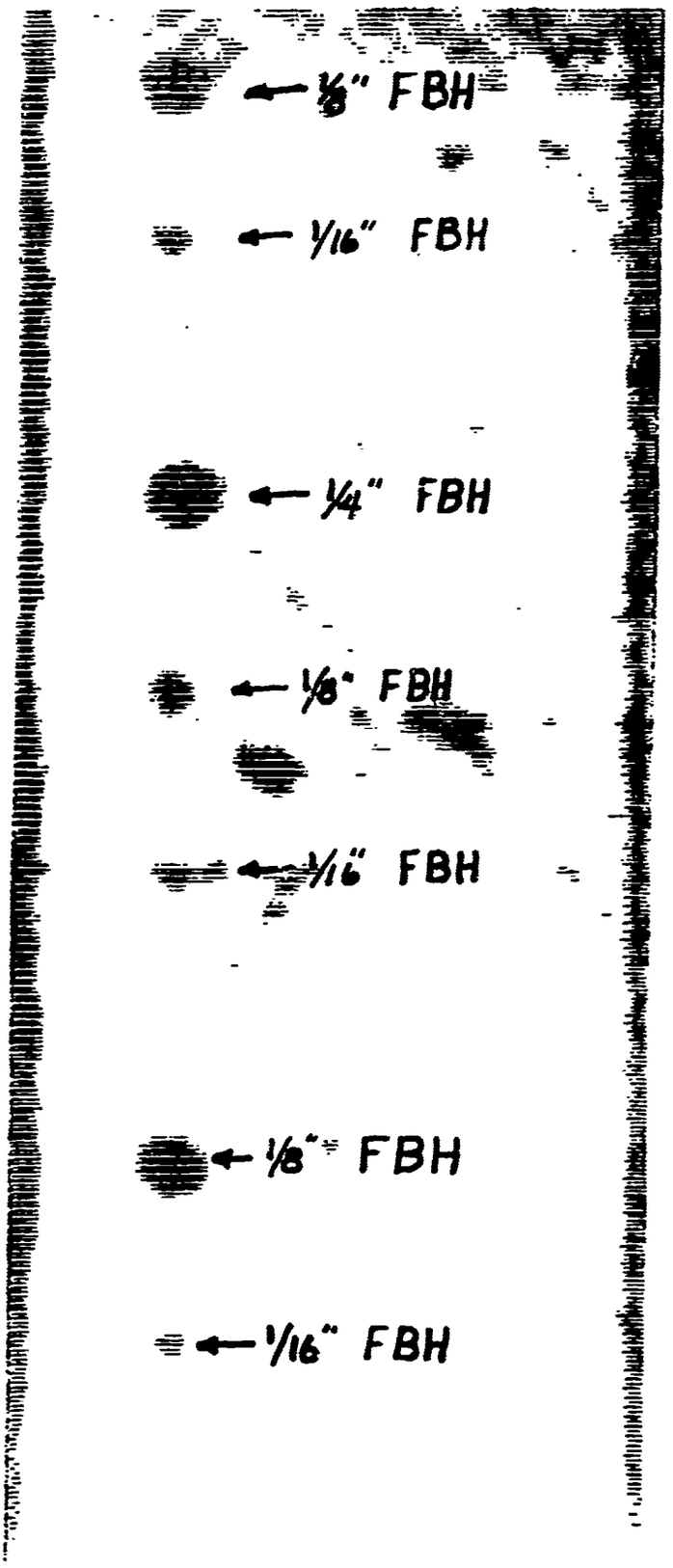


FIGURE 19

ULTRASONIC RECORDING OF FLAT BOTTOM HOLES IN A WEDGE RANGING IN THICKNESS FROM 1/16" to 3/4"

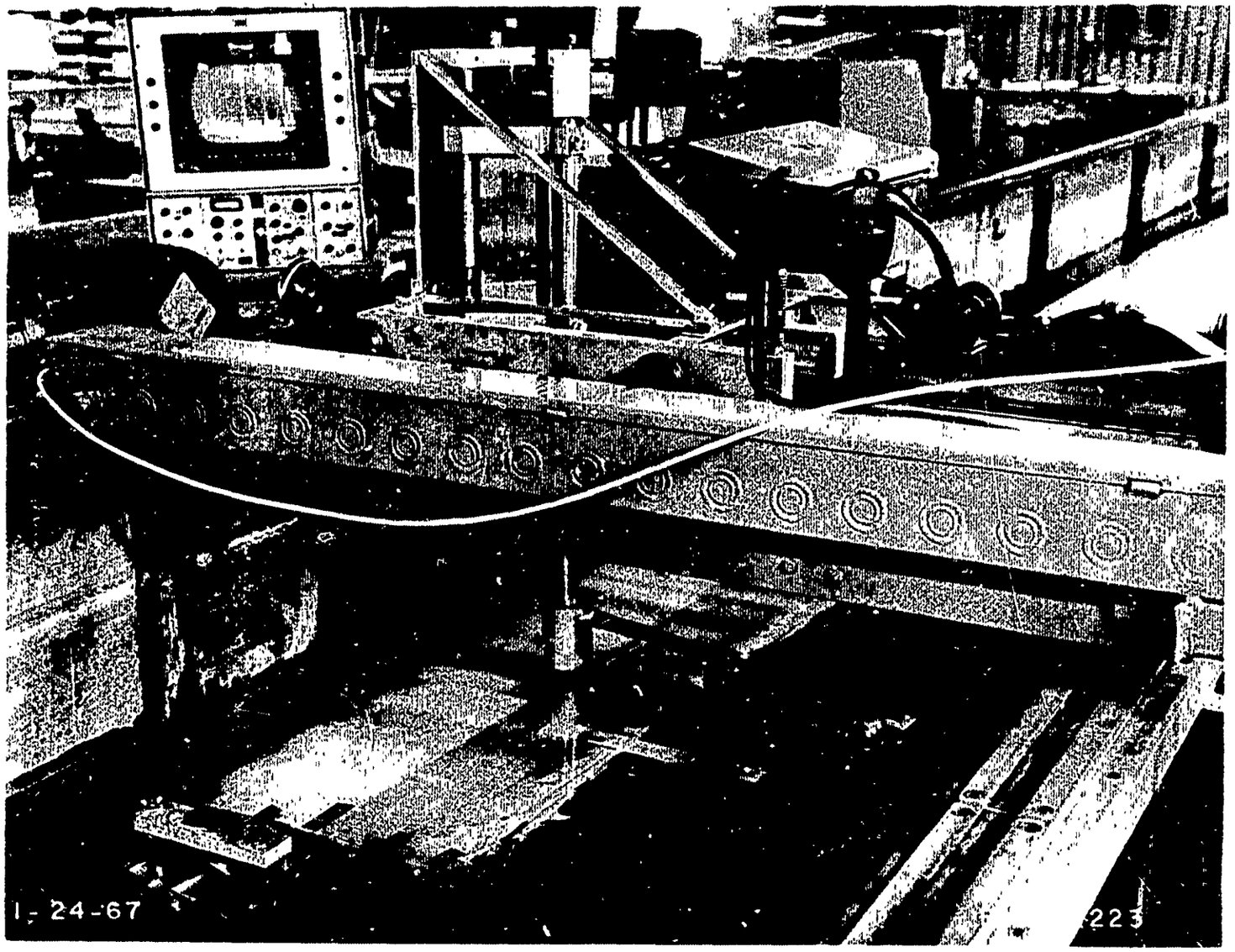


FIGURE 20
ADVANCED GEOMETRY BLADE C-SPAR ULTRASONIC INSPECTION

Figure 21 is a calibration curve that has been generated by plotting the nondestructive test results against resin content as determined by an average of three burn-out readings per specimen. Regression analysis for each set of points indicates that the relationship is a linear one and can be accurately represented by a straight line. The ultrasonic longitudinal wave velocity measurement is the more desirable of the two in that it represents the total thickness of the part rather than just the surface as is the case with beta backscatter.

Microwaves

Microwaves have been used for years in the field of communications, but their application to nondestructive inspection is a relatively new technology. The nature of microwaves is such that they may be suitable for flaw detection, moisture determination, thickness gaging, and many other material characteristics.

We are presently engaged in efforts, utilizing microwaves, to determine resin content and uniformity, measure material thicknesses from one side, detect flaws, and determine "state of cure" of non-metallic structures. Our work in this area is not far enough along to draw good conclusions, but the literature indicates that the use of microwave inspection techniques has good application in certain areas.

Core Inspection

The skin supporting structure for composite blades can take several forms. In the case of the Boelkow BO 105 Helicopter Rotor Blade, the core is foam; in the case of the Boeing Advanced Geometry Rotor Blade, the core is fiberglass skin-stabilized honeycomb; and in the case of the Marco blades in the Boeing V/STOL wind tunnel, the outer skin is supported by integral ribs and webbing.

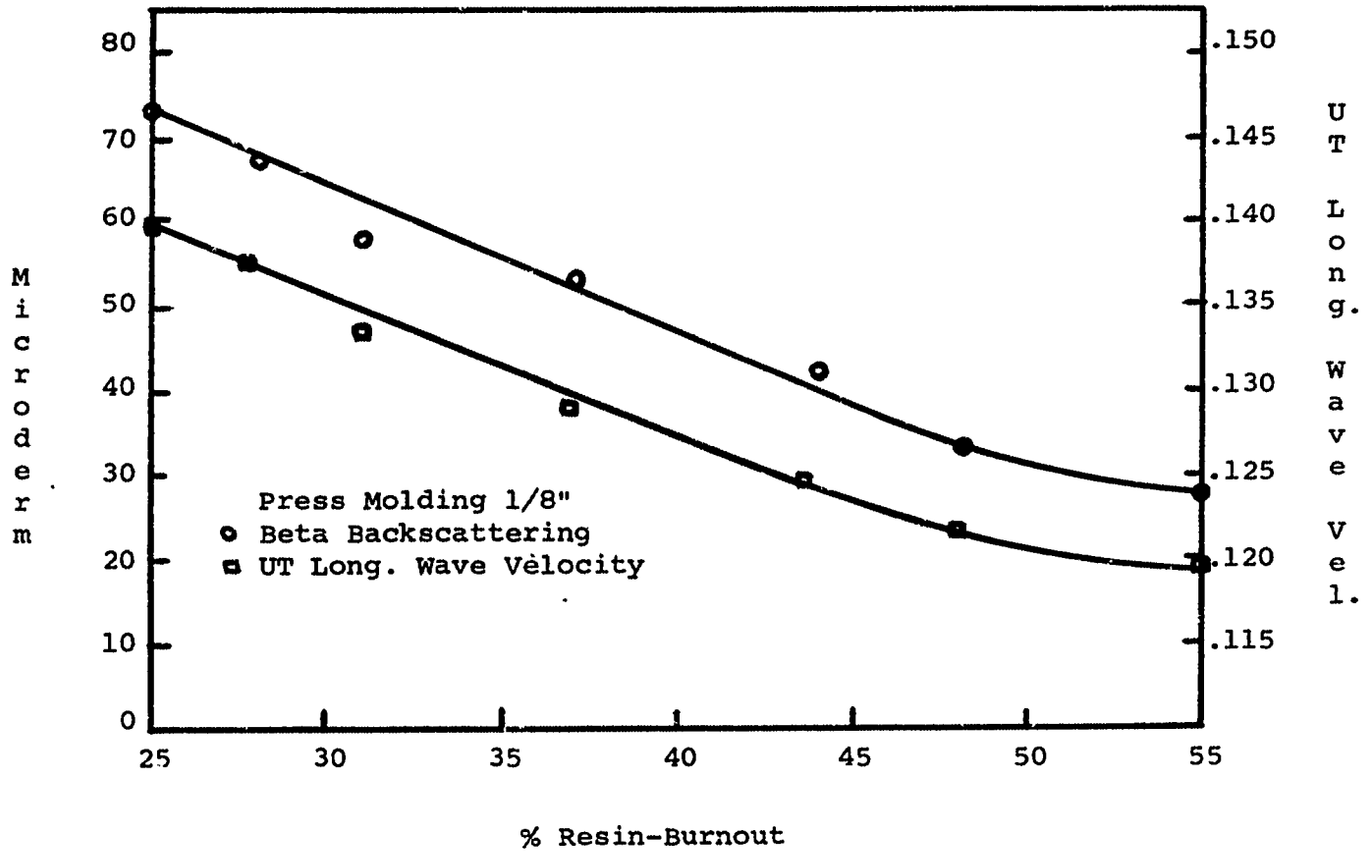


FIGURE 21
BETA BACKSCATTER AND ULTRASONIC LONGITUDINAL WAVE VELOCITY
CORRELATION TO RESIN CONTENT

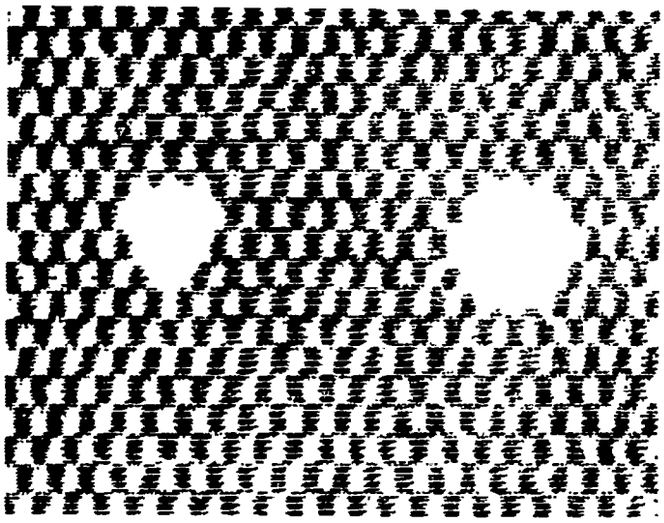
The amount of inspection performed on the foam core, as a detail, is not extensive and may involve as little as just penetrating radiation inspection for voids and completely unfoamed areas. Development effort is underway to utilize gamma absorption and microwave techniques to determine completeness of cure, but material and process controls are still the primary basis for acceptance.

Integral stiffening does not result in skin support details, therefore, inspection is performed on the finished structure as discussed later in the text.

Skin stabilized honeycomb core, which is the outer core support on the Boeing Advanced Geometry Composite Rotor Blade, can provide some interesting nondestructive inspection applications. The primary area of concern is the presence of voids or unbond between the stabilizing skin and the honeycomb. Both infrared and ultrasonic techniques are candidates for this inspection. Figure 22 shows comparative ultrasonic and infrared recordings of a boron skin honeycomb sandwich panel.

Infrared Inspection

Infrared techniques are very good for this inspection in that the stabilized core does not necessarily become contaminated as is the case with ultrasonic methods. Both the transient and thru-transmission methods can be used. These two techniques are schematically shown as Figure 23.





INFRARED

FIGURE 22

COMPARATIVE RECORDINGS OF
VOIDS IN BORON SANDWICH STRUCTURE

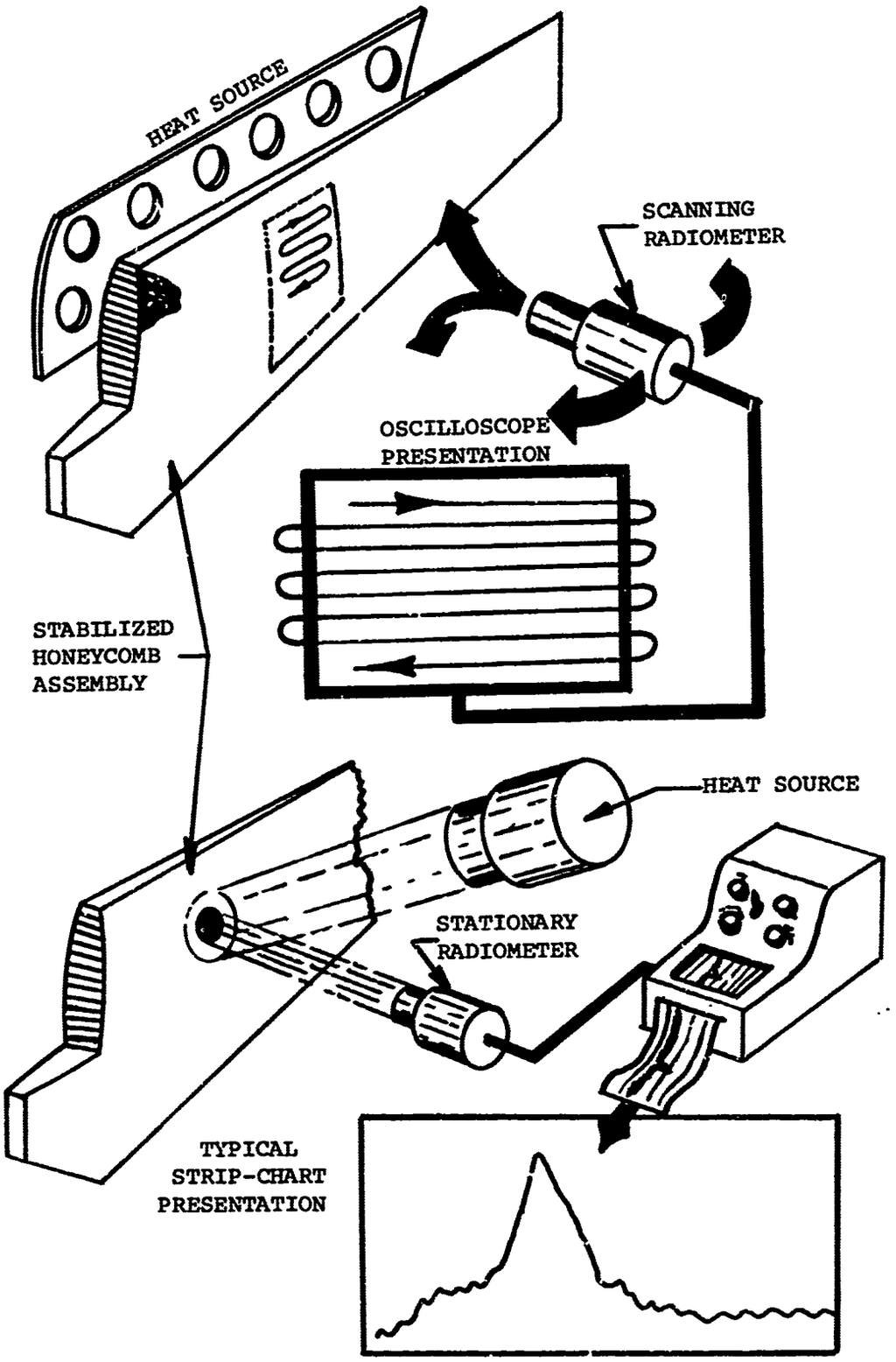


FIGURE 23
INFRARED TECHNIQUES

An example of this application is the Infrared Bond Inspection System used for detection of bondline voids in the CH-47B Rotor Blade Box, Figure 24. The system is a closed circuit video unit capable of generating and displaying a presentation of the normally invisible infrared energy radiating from the material. The radiation pattern from the scanned object appears as a visible image, containing approximately 15,000 picture elements, on a CRT display unit.

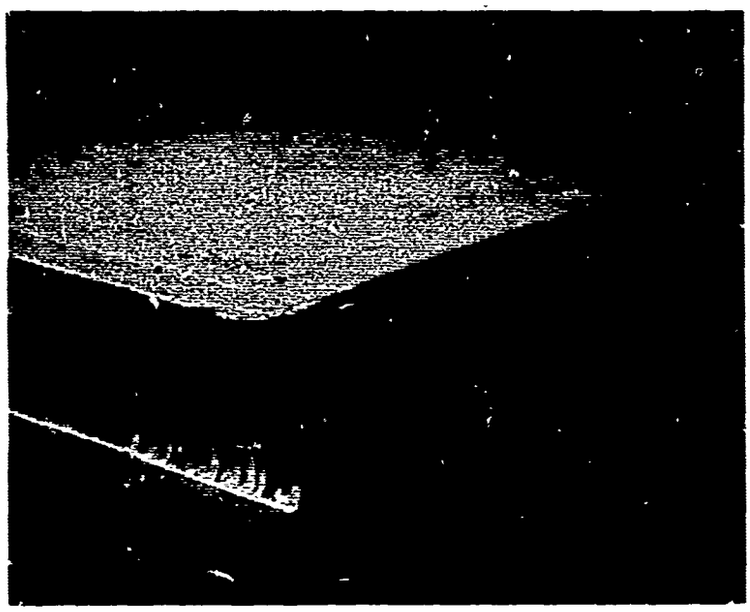


FIGURE 24

CH47B ROTOR BLADE BOX

The System, shown as Figure 25, was designed and built by Sierra Electronic Division of The Philco-Ford Company to specifications supplied by The Boeing Company/Vertol Division.

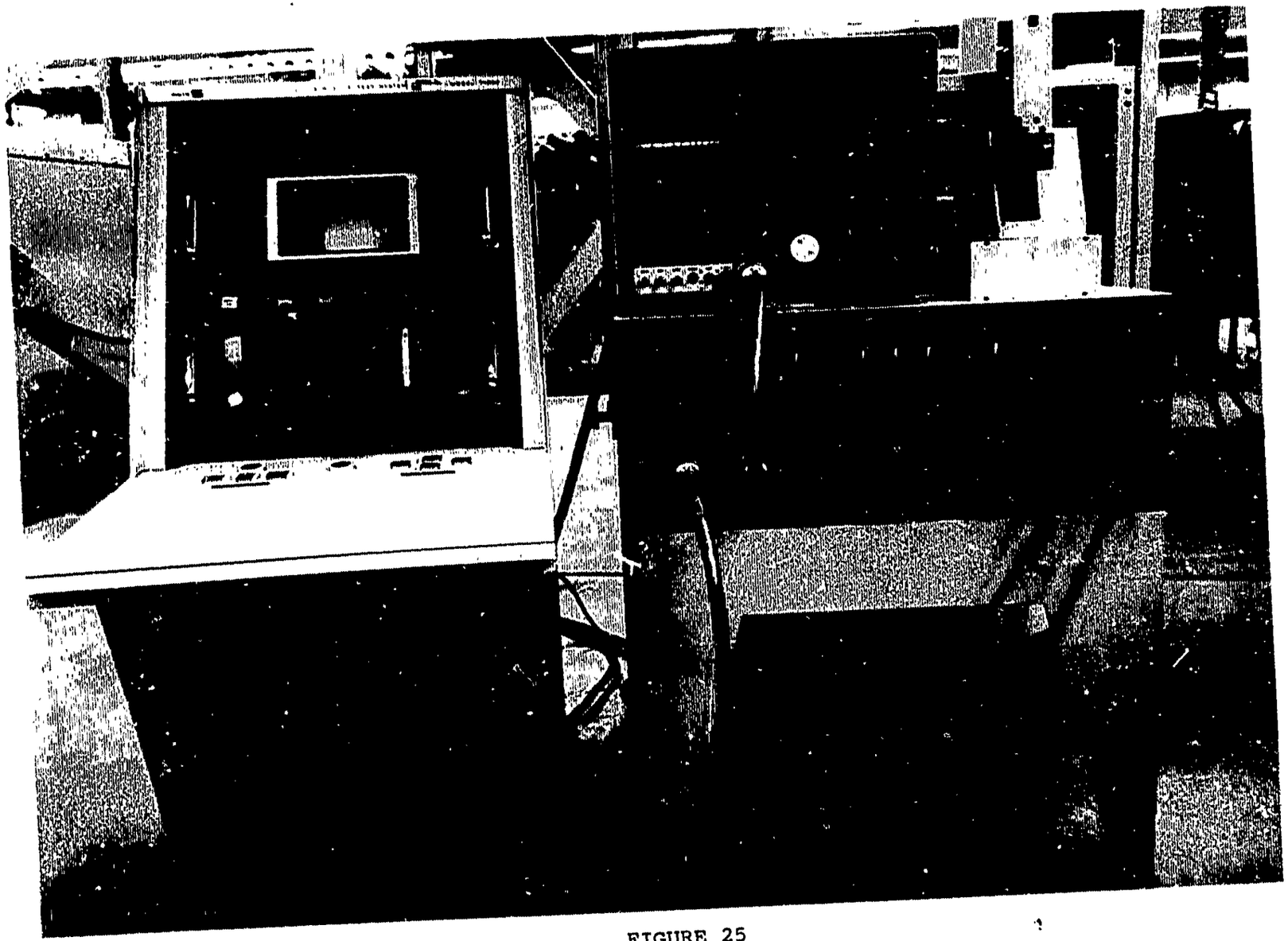


FIGURE 25
INFRARED INSPECTION SYSTEM

A thermal or infrared pattern is generated on the front surface of the structure being inspected by the strategic application of heat to the back and side surfaces of the honeycomb box and the application of forced air cooling to the front surface. The applied heat is readily transmitted to the front surface of the honeycomb box if the bonded joint is acceptable. Cool spots on the front surface of the box, which represent bondline defects, are readily detected and are presented for analysis on the display console. A photograph of the display showing bondline voids is shown as Figure 26. Both "A" and "C" scan presentations are shown.

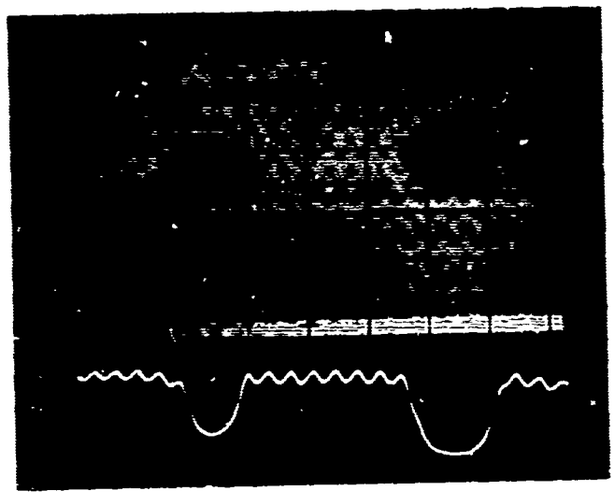


FIGURE 26
INFRARED PRESENTATION SHOWING
BONDLINE VOIDS

The system provides a means for conveniently heating and cooling the appropriate surfaces of the box sections and moving the structure through the infrared field of view. The cooling elements and parts handling subsystem are shown in Figure 27.

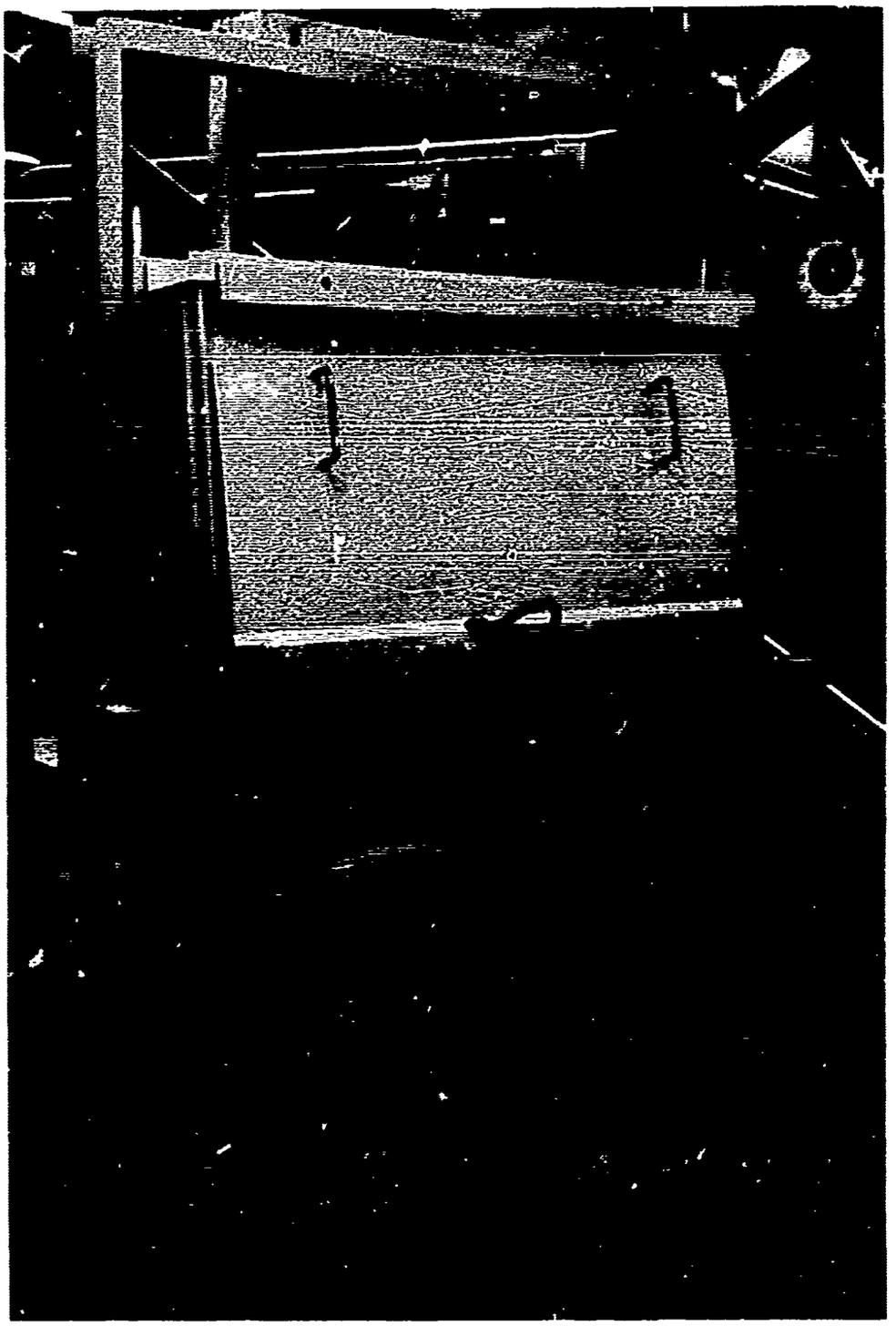


FIGURE 27
INFRARED BOND INSPECTION SYSTEM
PARTS HANDLING & HEATING SUB-SYSTEM

When the operator at the console detects a bondline void, provisions have been made by the use of a remote control spotlight for identifying the location of the flaw so that it can be marked on the structure itself. A separate display with a polaroid back is mounted in the console to permit permanent photographic records of any bondline defects.

Ultrasonic Inspection

Ultrasonic Inspection is very applicable to detection of bondline voids between the stabilizing skin and honeycomb core; provided a peel-ply is integral on the skin, or the structure is cleaned after inspection. Figure 28 is an ultrasonic recording showing skin-core voids in a typical sandwich structure.

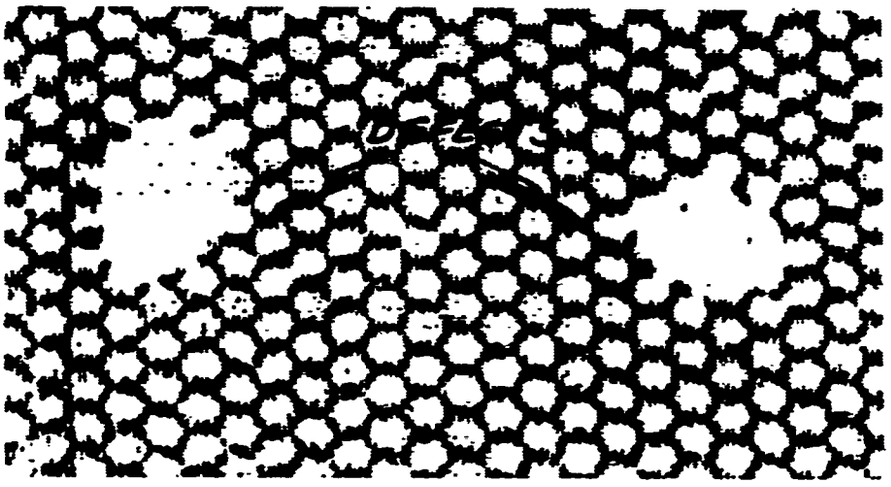


FIG. 28- ULTRASONIC RECORDING OF FIBERGLASS HONEYCOMB SANDWICH

Figure 29 shows the stabilized core of the advanced geometry composite (boron) rotor blade being ultrasonically inspected in the Automated Ultrasonic Inspection System at the Boeing Company/Vertol Division facility. The Automated Ultrasonic Inspection System is discussed in detail later in the text.

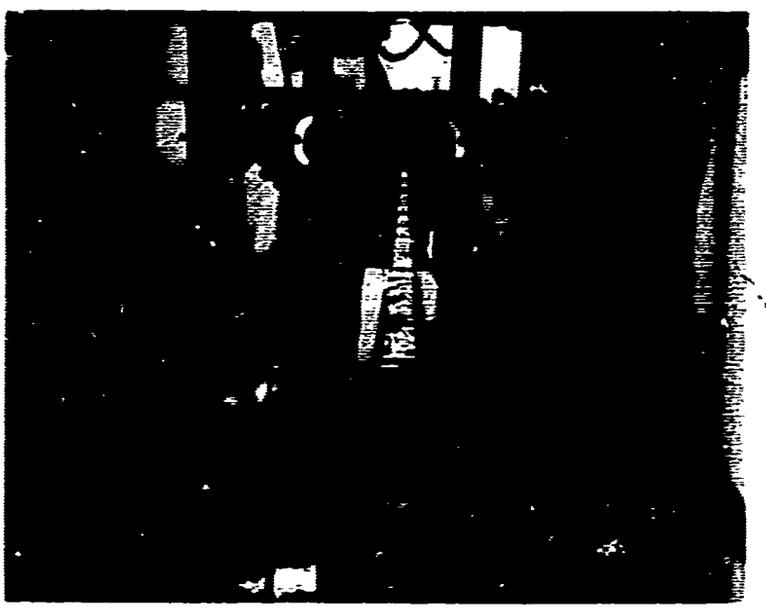


FIGURE 29
BORON STABILIZED CORE
IN THE AUTOMATIC ULTRASONIC INSPECTION SYSTEM

Neutron Radiography

One of the newer technologies in nondestructive inspection of composites is neutron radiography. Neutron radiography, as reported by Edward Perry of our Wichita Division, offers a unique method for the nondestructive examination of composites because the nonmetallic members are usually stronger neutron absorbers than most of the common structural metals. This singular selectivity is in sharp contrast with other forms of penetranting radiation such as gamma, beta, and x-rays. These all require a relatively high energy to penetrate the outer metallic cover, such as aluminum, magnesium, and steel, whereas the low density, low atomic numbered adhesives and filaments are virtually transparent. Gamma, beta, and x-radiography of such composites is difficult and usually impossible to perform.

An examination of the Mass Absorption Coefficient versus Atomic Number Chart, Figure 30, shows that attenuation of x-rays increases with increasing atomic number. The attenuation of thermal neutrons by the elements does not follow any recognizable pattern, and this property of elemental materials is almost completely independent of the atomic number. In general, thick, dense objects appear lighter on radiographic film than do thinner, less dense objects; but there are notable exceptions. Radiography with thermal neutrons is especially selective to hydrogen (which adhesives and resins contain in significant amounts); also with boron (such as in the monofilament, and in the borosilicate fiberglass); and also with cadmium and gadolinium. Note that the structural metals magnesium, aluminum, vanadium, chromium, iron, nickel, copper and zine produce only very slight differences in mass absorption coefficients. Silver, indium, iridium and gold provide slightly higher thermal neutron attenuation than do the structural metals, but again the small range in mass absorption values would make identification of these elements difficult by neutron radiography.

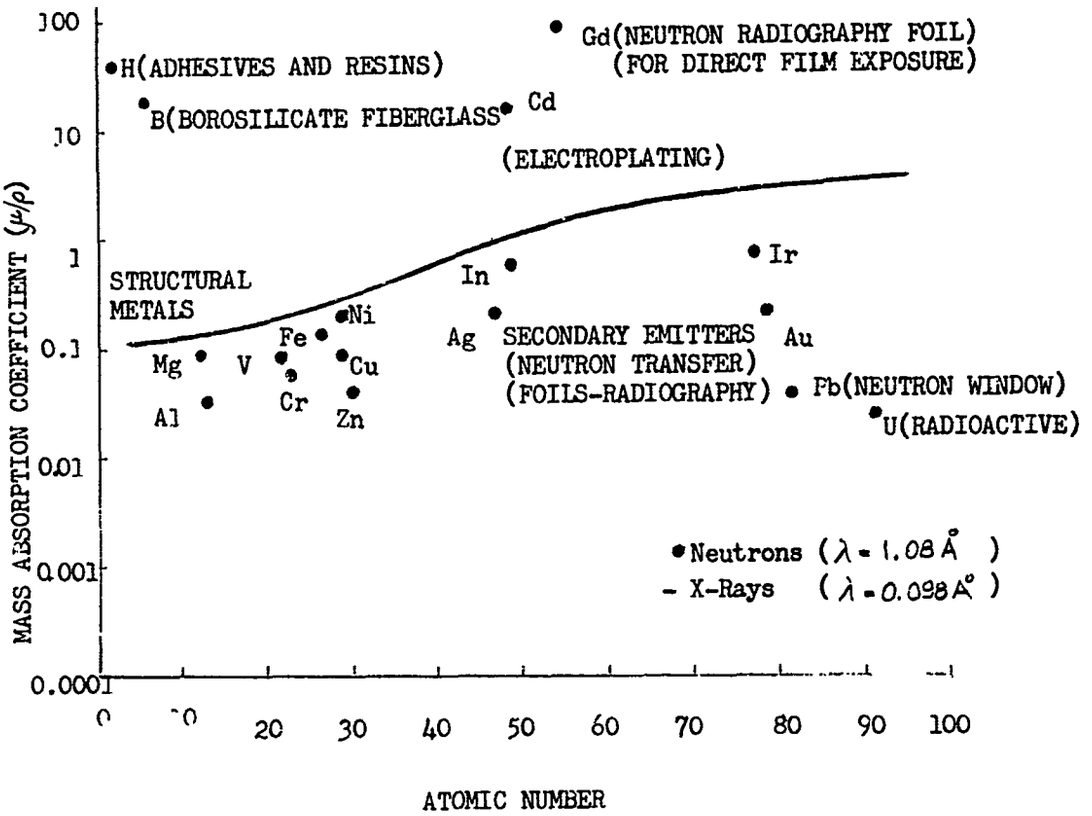


FIGURE 30
MASS ABSORPTION COEFFICIENT VS. ATOMIC NUMBER

Lead is often termed a window for thermal neutrons, and uranium would be also except that fission events occur to release additional energy forms. Translated to radiographic film, fiberglass and boron reinforced polymers and adhesives are easily shown beneath layers of aluminum, steel, magnesium, or titanium structural metal alloys, when thermal neutrons are beamed through the composite.

Images showing a resolution of better than 4 mils per inch of object thickness have become routine, and higher resolutions are obtainable by decreasing the beam aperature and increasing the exposure time. The use of a gadolinium foil behind the film allows a direct film exposure technique, when the beam is free of gamma radiation, and this method produces better resolution than the foil transfer technique. In the foil transfer technique, the dysprosium or indium foil is exposed and then laid on the film during the radioactive decay of the foil.

Figure 31 shows some neutron radiographs of typical composite structures. The significant thing to note is that the honeycomb pattern shown is the adhesive fillet, not the actual aluminum honeycomb.

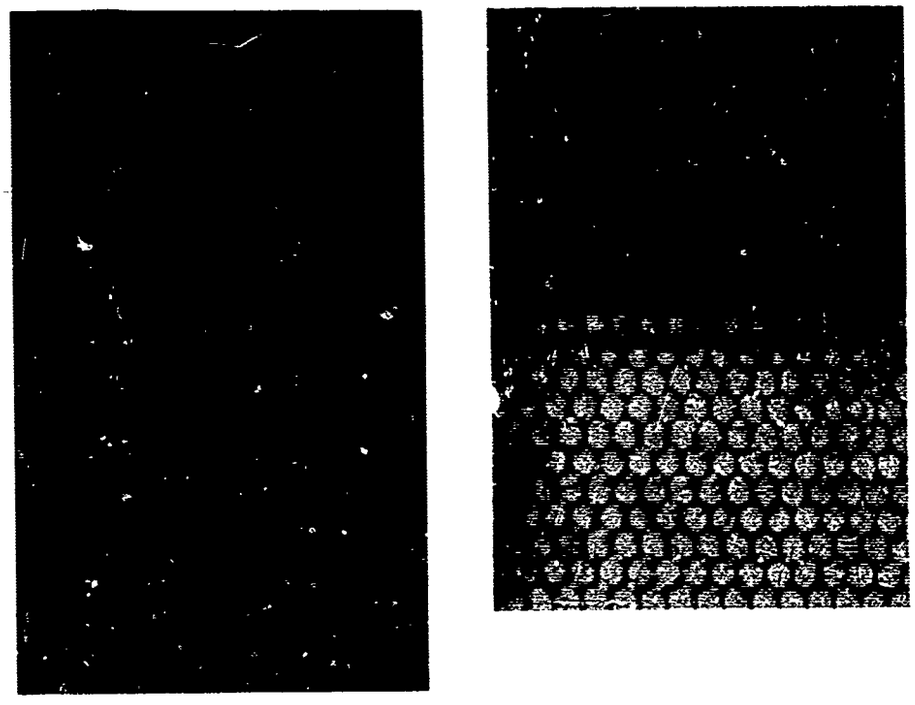


FIGURE 31
NEUTRON RADIOGRAPHS OF HONEYCOMB SANDWICH STRUCTURE

Completed Blade Inspection

The completed blade can be subjected to a variety of inspections too numerous to discuss here, but most certainly ultrasonic, penetrating radiation, and dimensional inspections will be performed. The inspection equipment to be utilized should be automated in order to provide uniformity of inspection and to sustain production schedules.

Ultrasonic Inspection

Figure 32 shows a concept of an automated ultrasonic equipment suitable for inspection of complex controu surface structures such as rotor/propeller blades. The concept provides for spanwise scanning with chordwise indexing. Transducer attitude, which must be nearly normal to the inspection surface, is provided by tape control. Recording platens, utilizing dry recording paper, are mounted on each side of the tank. Provision is made for both thru-transmission and pulse-echo modes of inspection. The inspection equipment, suitable for both immersion or enclosed water column inspection, has two independent ultrasonic systems to allow for pulse-echo inspection on each side of the blade simultaneously.

Equipment utilizing this concept is in use at our facility. The equipment, designed by The Budd Company, Instruments Division to Boeing specifications, is shown as Figures 33 and 34.

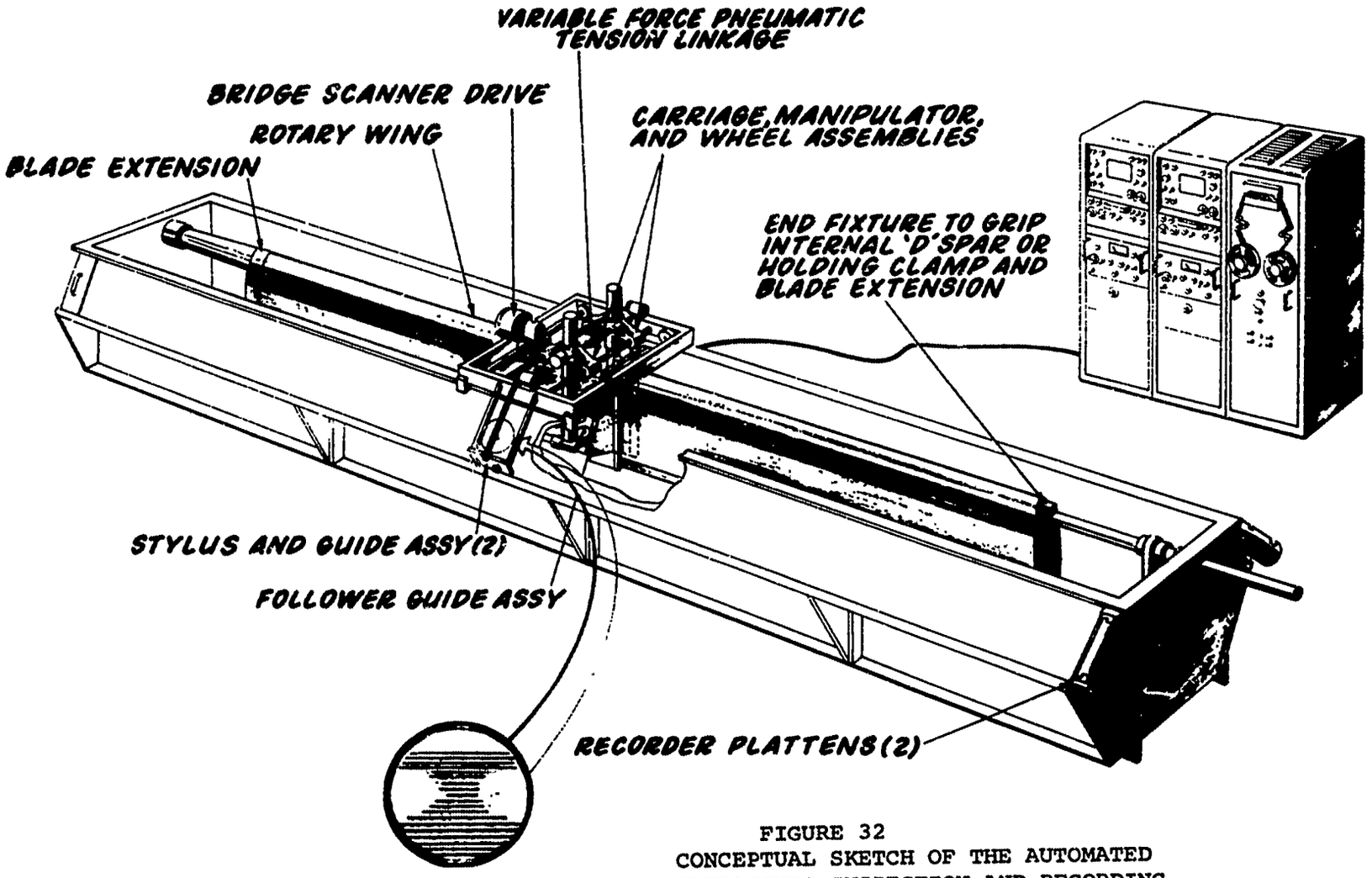


FIGURE 32
CONCEPTUAL SKETCH OF THE AUTOMATED ULTRASONIC INSPECTION AND RECORDING SYSTEM

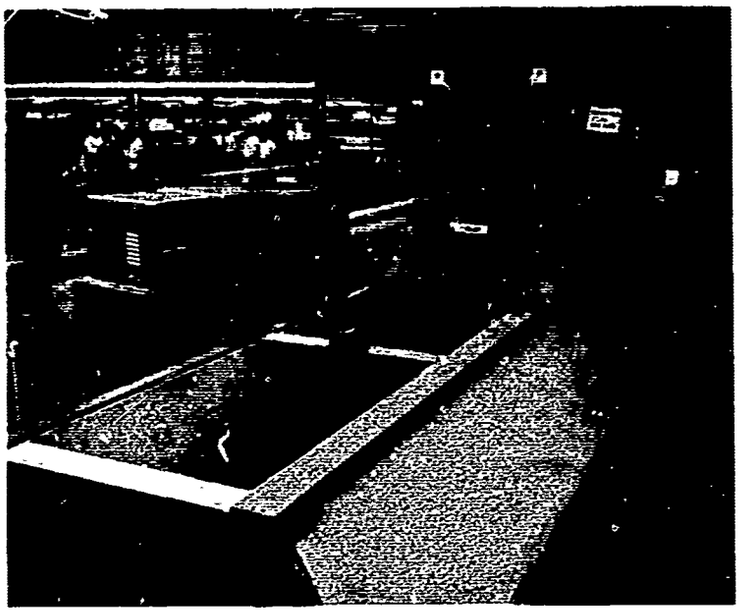


FIGURE 33
AUTOMATIC ULTRASONIC INSPECTION AND RECORDING SYSTEM

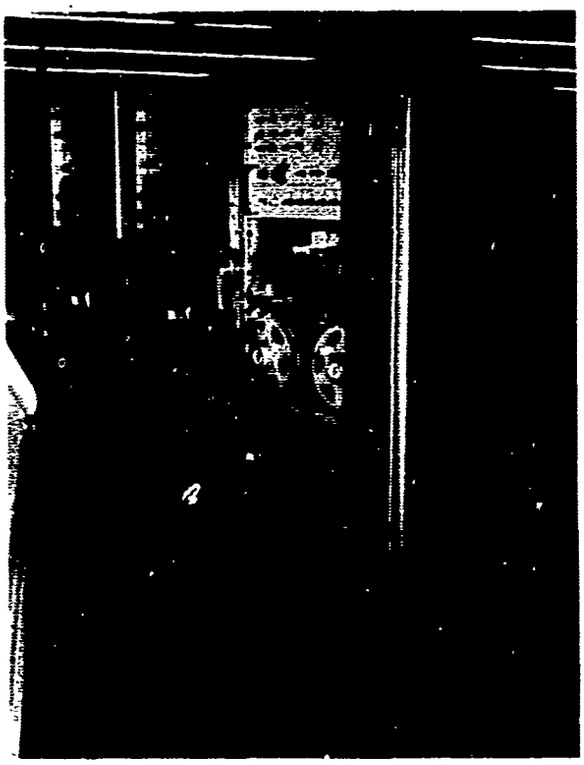


FIGURE 34
CONTROL CONSOLE & TAPE READER FOR THE AUTOMATIC SYSTEM

Figure 35 shows a full scale CH47B rotor blade ultrasonic recording. The equipment can be easily switched back and forth between thru-transmission and pulse-echo modes. Indexing (up to 60 lines per inch) and recording ratio (up to 1:1) can be easily selected to suit the acceptance criteria.

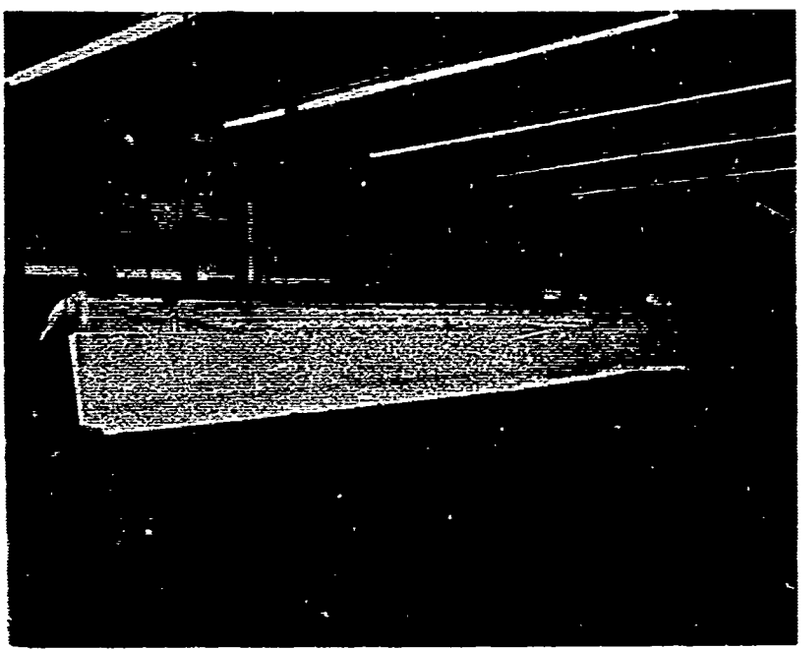


FIGURE 35
FULL LENGTH ULTRASONIC RECORDING
FOR CH47B ROTOR BLADE

Penetrating Radiation Inspection

Figure 36 shows a concept of an automated penetrating radiation inspection equipment. The equipment provides for an x-ray sensitive vidicon and image intensifier presentation. The system is basically a mobile x-ray unit in which the blade is fixed within two tracks and the enclosed generator-pickup system traverses the length of the rotor blade.

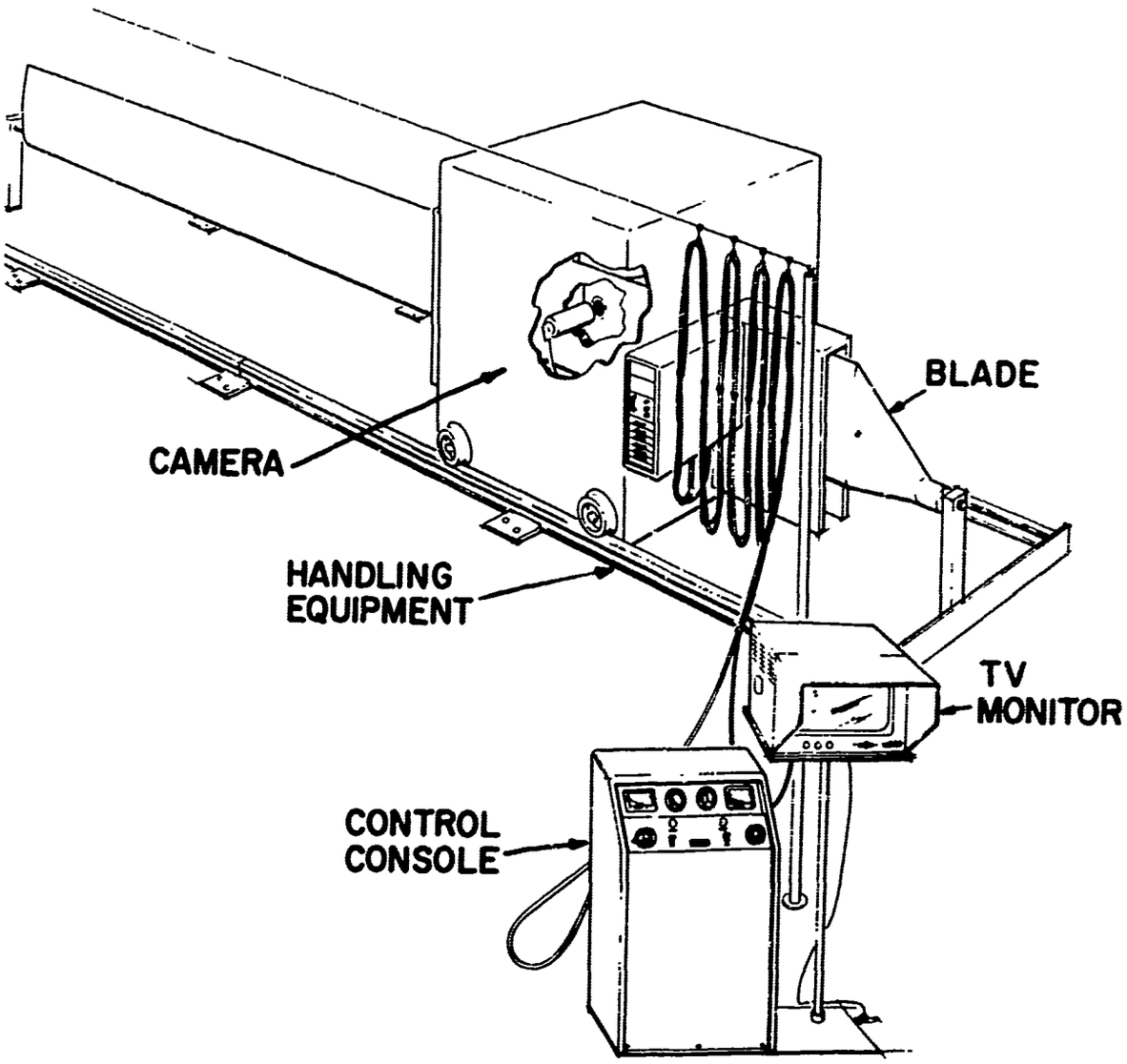


FIGURE 36

X-RAY SENSITIVE VIDICON
AND IMAGE INTENSIFIER SYSTEM
CONCEPT

The x-ray vidicon image is presented on a remote 17" video screen at about 30X. The image amplification system also presents a view on the same screen at 1:1. The viewing area using the vidicon tube is about 1/2" X 1/2" with 1%-2% penetrameter sensitivity, while the viewing area of image amplification is about 8" X 8" with 3%-4% penetrameter sensitivity.

Both the x-ray generator and pickup tubes have free 90° movement to allow for whatever viewing angle proves to be most desirable. Viewing speed is variable, with the maximum speed being limited by interpreter perception. All controls and viewing apparatus are remote.

Equipment utilizing this concept is in use at our facility. The equipment, designed by The Picker X-Ray Corporation to Boeing specifications, is shown as Figures 37 and 38.

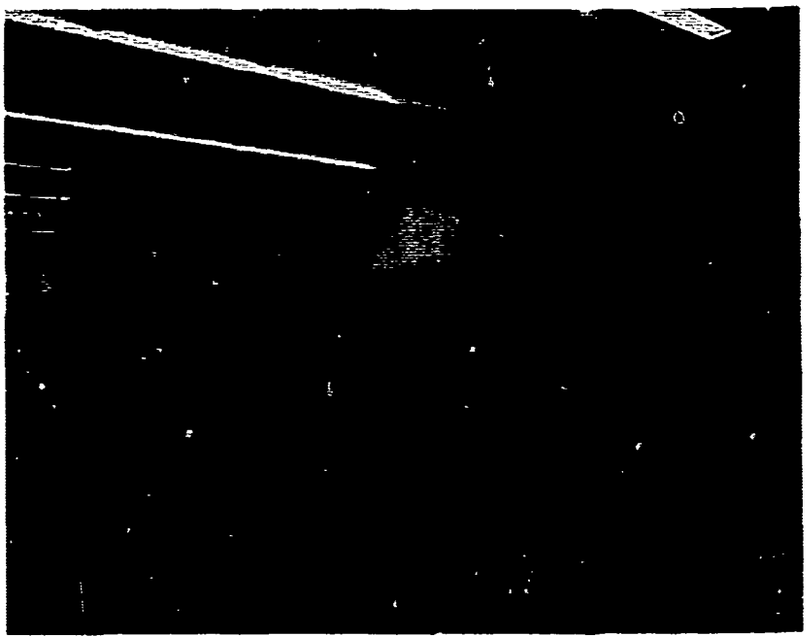


FIGURE 37

X-RAY SENSITIVE VIDICON AND IMAGE INTENSIFIER SYSTEM

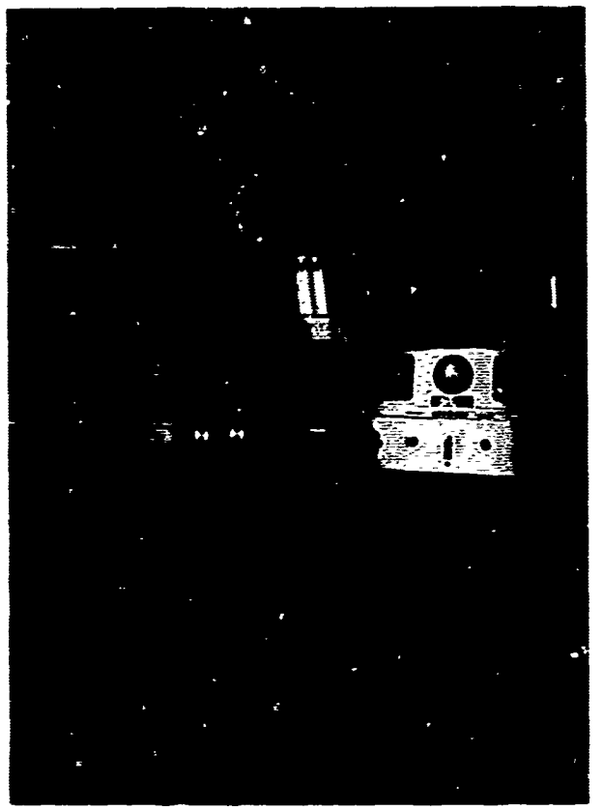
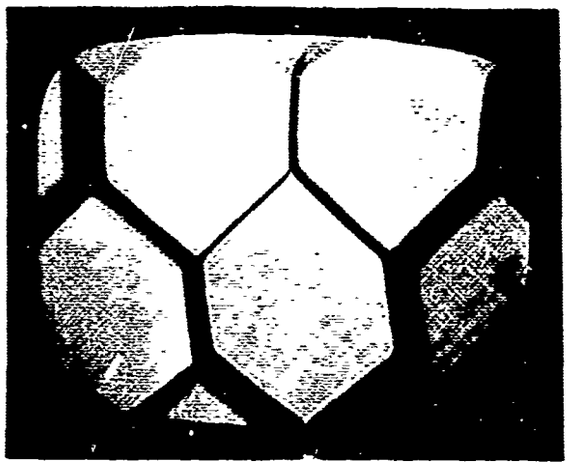


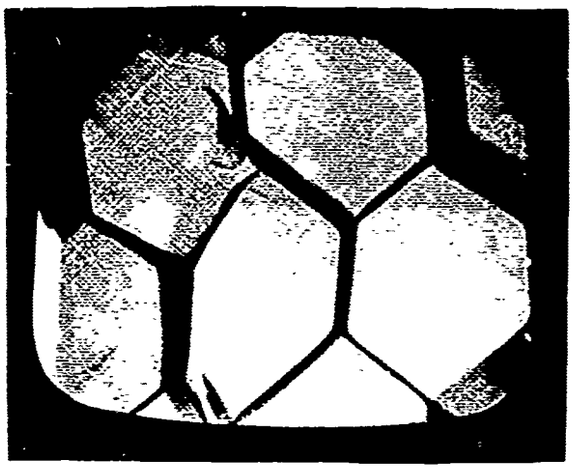
FIGURE 38

CONTROL CONSOLE AND VIDEO MONITOR
FOR THE X-RAY SENSITIVE VIDICON SYSTEM

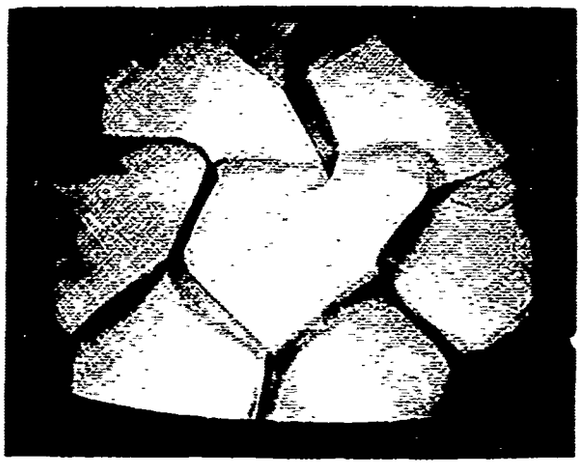
Figure 39 shows some photographs taken of the video screen showing various conditions and discontinuities.



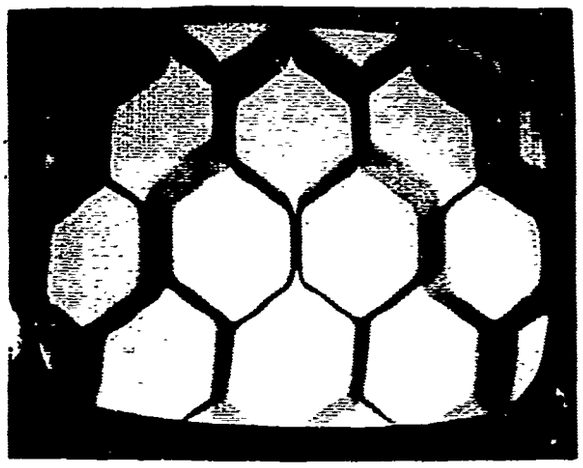
HONEYCOMB WITH BORON
CROSSPLY SKINS



HONEYCOMB CELL WALL
DAMAGE



HONEYCOMB CELL
DISTORTION



HONEYCOMB RIBBON
SEPARATION

FIGURE 39

TYPICAL VIDICON MONITOR PRESENTATIONS

Dimensional Inspection

A comparison of the complex geometry of the advanced geometry rotor blade (AGB) and the V/STOL propeller is shown in Figure 40. The geometry of these structures should indicate the magnitude of the dimensional control problem. For example, our advanced geometry composite rotor blade is 30' long with the chord being 36" at the widest point. The geometry is further complicated by a twist. Obviously, conventional dimensional measurement equipment would be cumbersome and extremely expensive.

Boeing has developed a new concept in dimensional control, called Surface Contour Analysis, for complex curvature hardware, that is relatively inexpensive and very versatile. The Surface Contour Analyzer, shown in concept as Figure 41, utilizes a null detector system which senses the vertical movement or relative position of a projected spot of light as it is scanned about a test surface. The position of the pinpoint of light is defined relative to a given horizontal reference plane, by a position transducer and introduced into a special recorder. The accumulated data, representing the surface contour is then processed by a computer to provide the desired illustrated results--drawings, mathematical equations, and/or comparison data.

Figure 42 shows a 1/5 scale blade mounted in the laboratory Surface Contour Analyzer. Computer drawings of chordwise sections are shown as compared to what the blade should be in Figure 43.

Figure 44 shows a grid of the inboard section of rotor blade. The approach will be to measure each line intersection and integrate. It is estimated that 30,000 measurement points can be processed in 15 minutes.

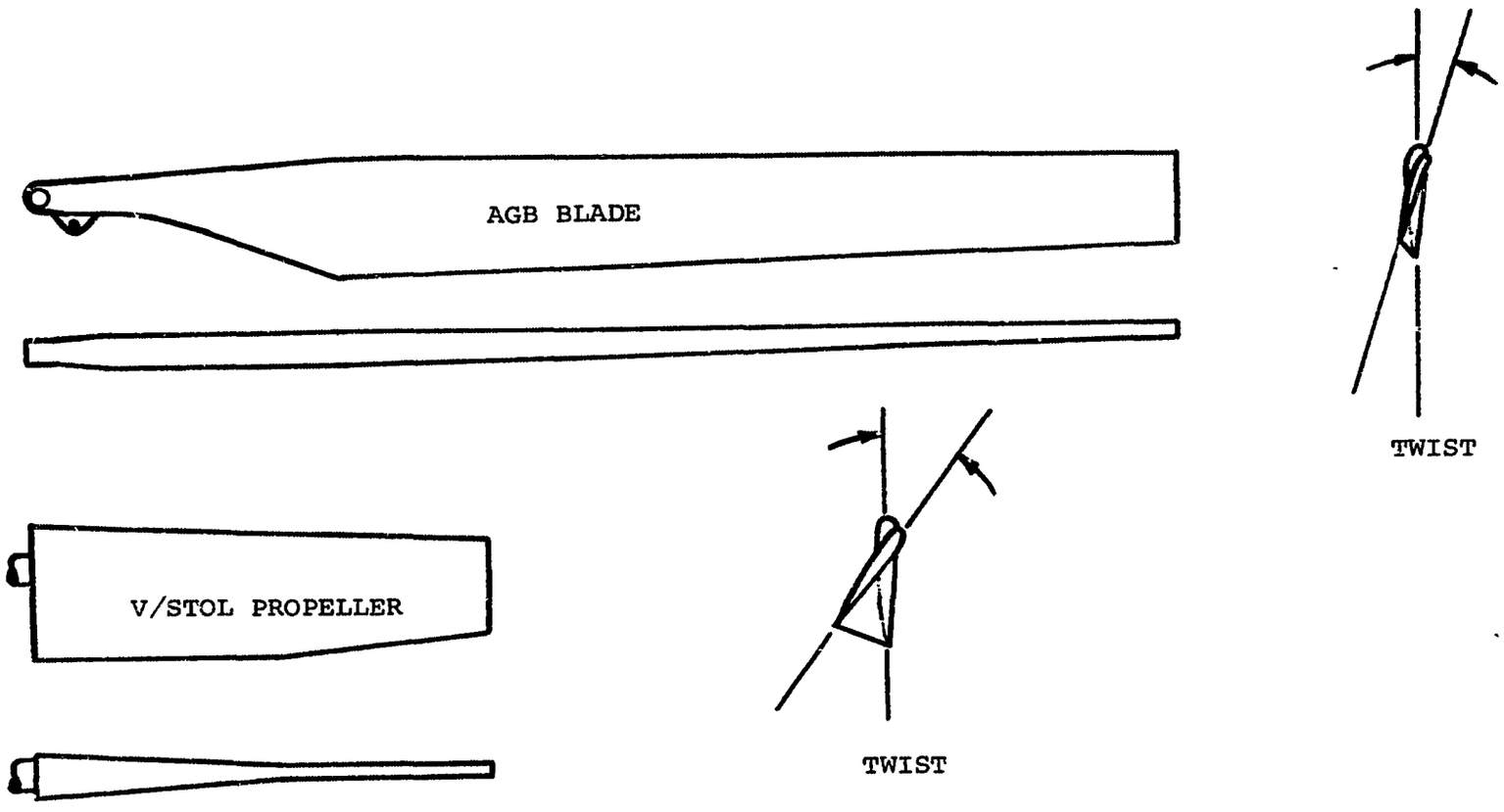


FIGURE 40

COMPARISON OF AGB BLADE/VTOL PROPELLER GEOMETRY

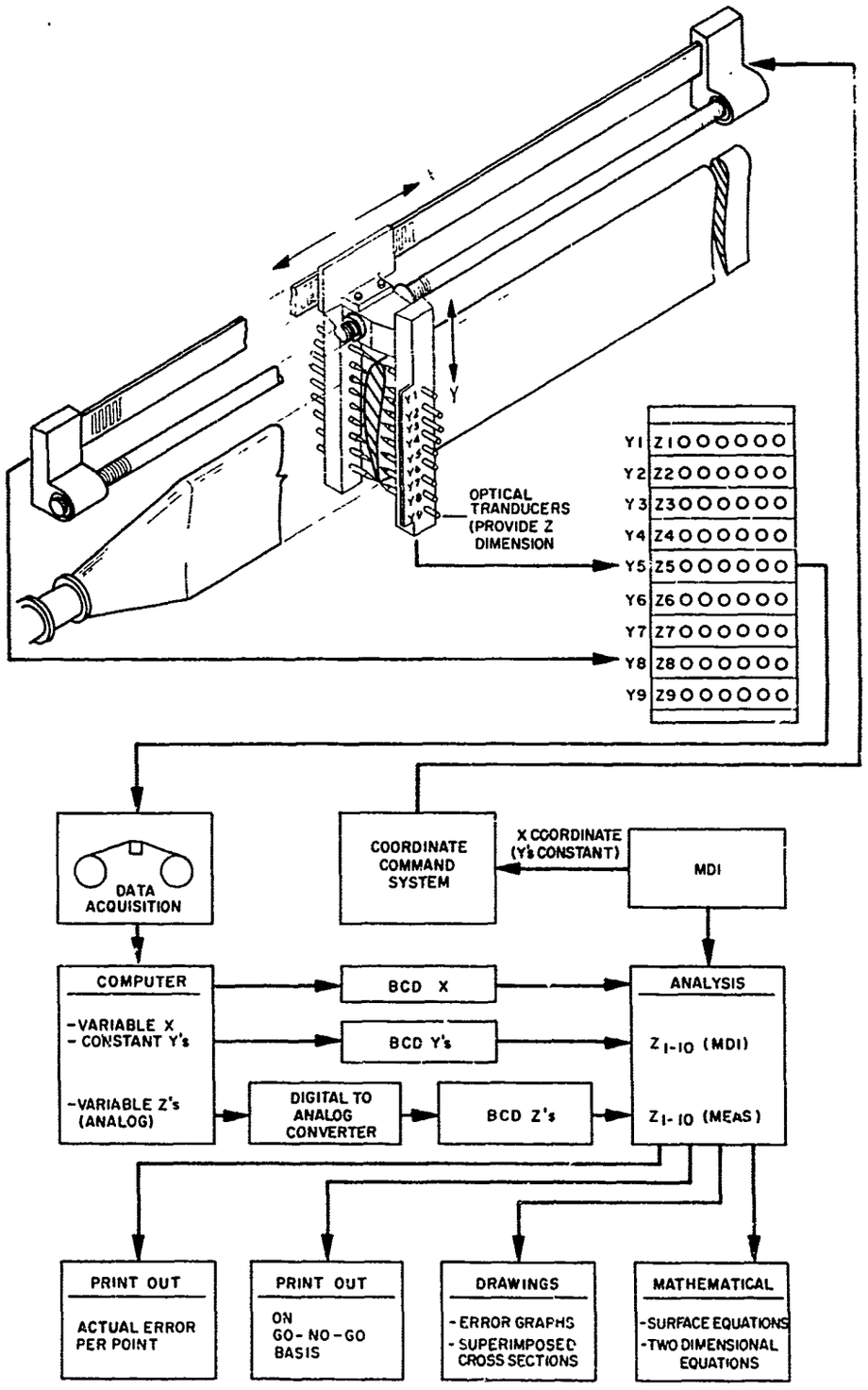


FIGURE 41
ROTOR BLADE CONTOUR INSPECTION SYSTEM
MANUAL AND/OR AUTOMATED SYSTEM

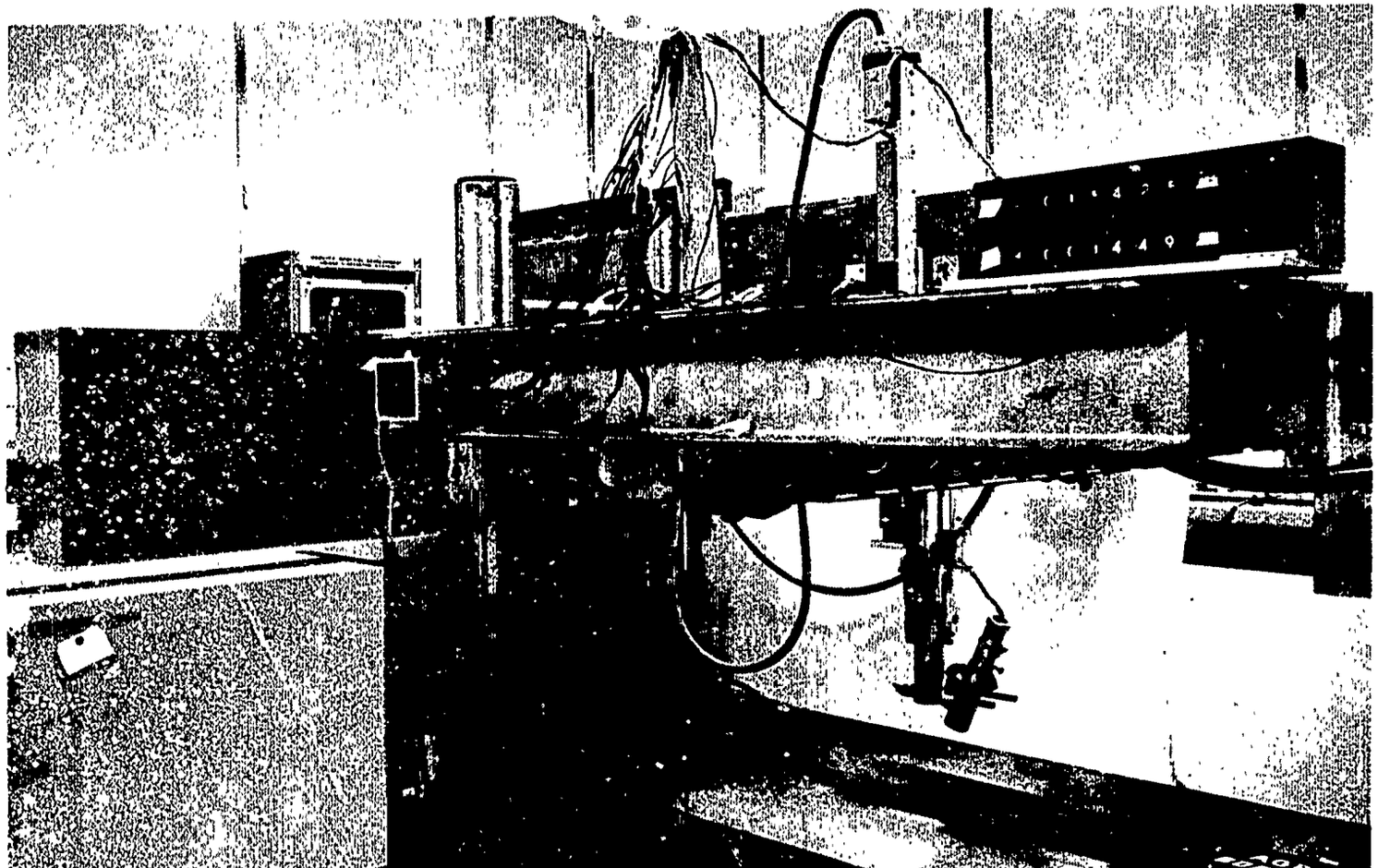


FIGURE 42
DIMENSIONAL CONTROL LABORATORY TEST SET-UP

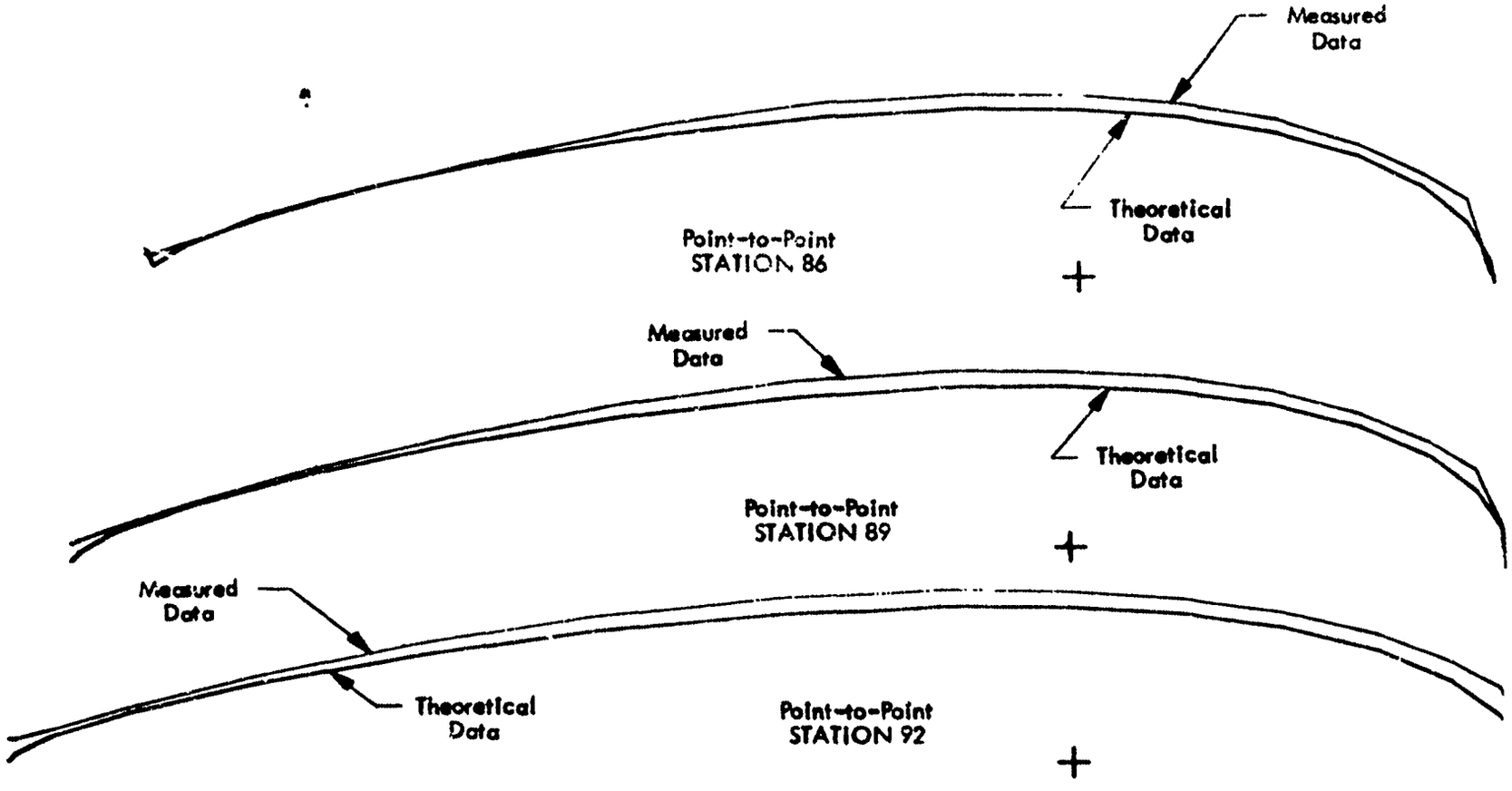


FIGURE 43
SEPARATED Y-Z PLANE VIEWS OF COMPARED
POINT-TO-POINT DATA - STA. 86 THRU 92

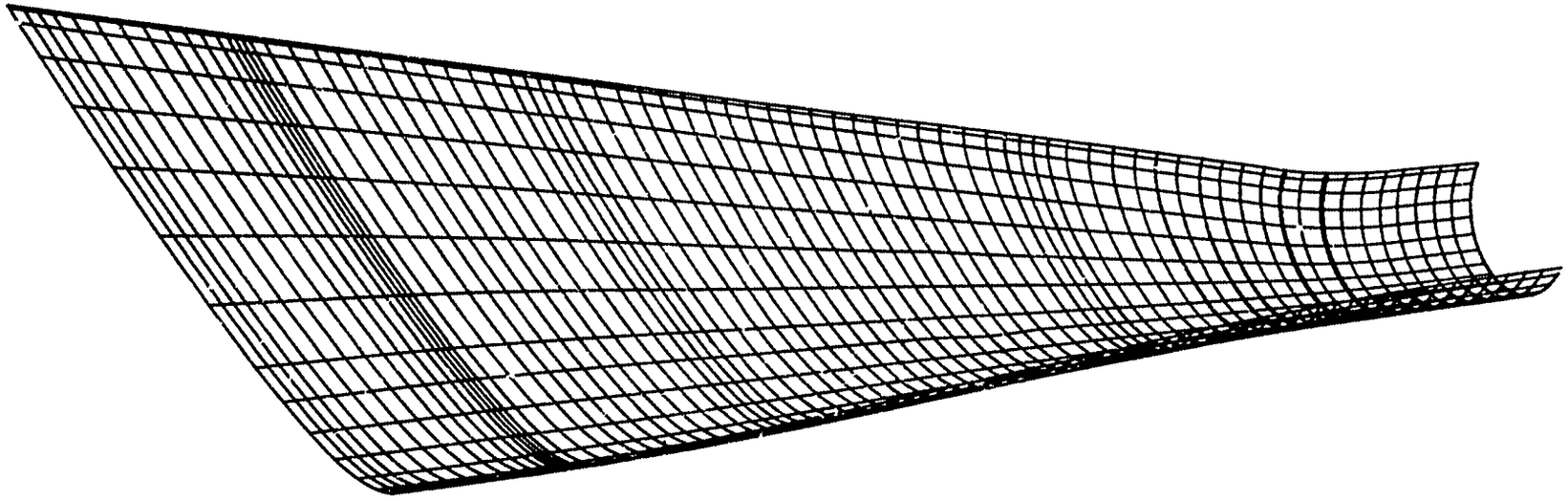


FIG. 44 - GRID ROUTINE FOR ROTOR BLADE DIMENSIONAL INSPECTION

DESIGN/ACCEPTANCE CRITERIA DEVELOPMENT

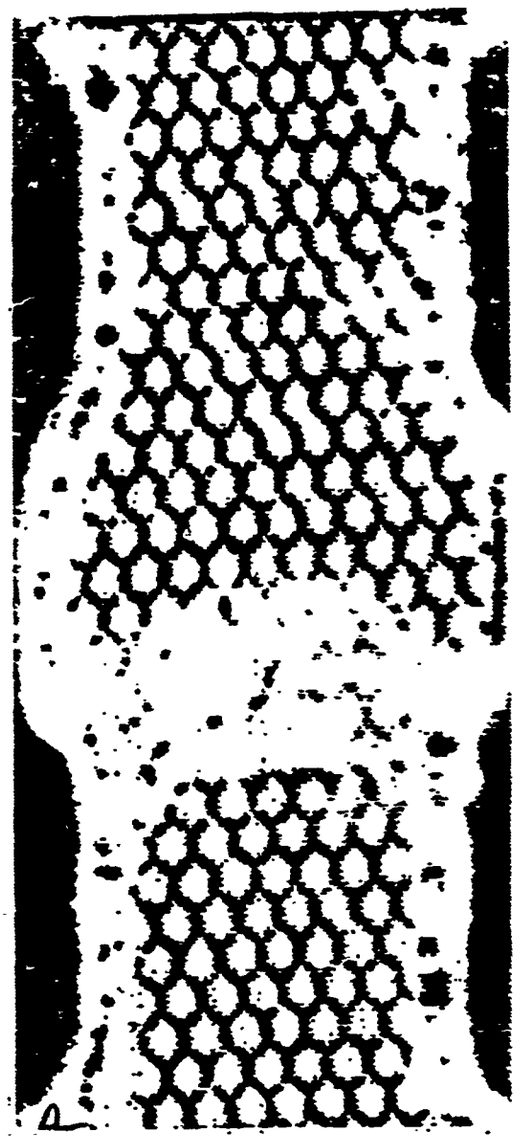
Both of our Advanced Geometry Rotor Blade efforts (glass fiber and boron fiber) have extensive material test programs. There is no question that one big problem that has to be overcome on any composite structure program is the determination of allowables, both from the design standpoint and from the discontinuity acceptance standpoint. Obviously, there is a threshold, but the threshold changes depending on materials, processes, part usage, and the methods used to detect defective areas.

Based on the premise that test data is only as good as the specimen being tested, we perform a Quality Control Capability Study on all complex structural test articles and subject the materials, processes and end item test article to the highest level of inspection that we can. Figure 45 shows the Quality Control Capability Study that was generated for the advanced composite root end test article.

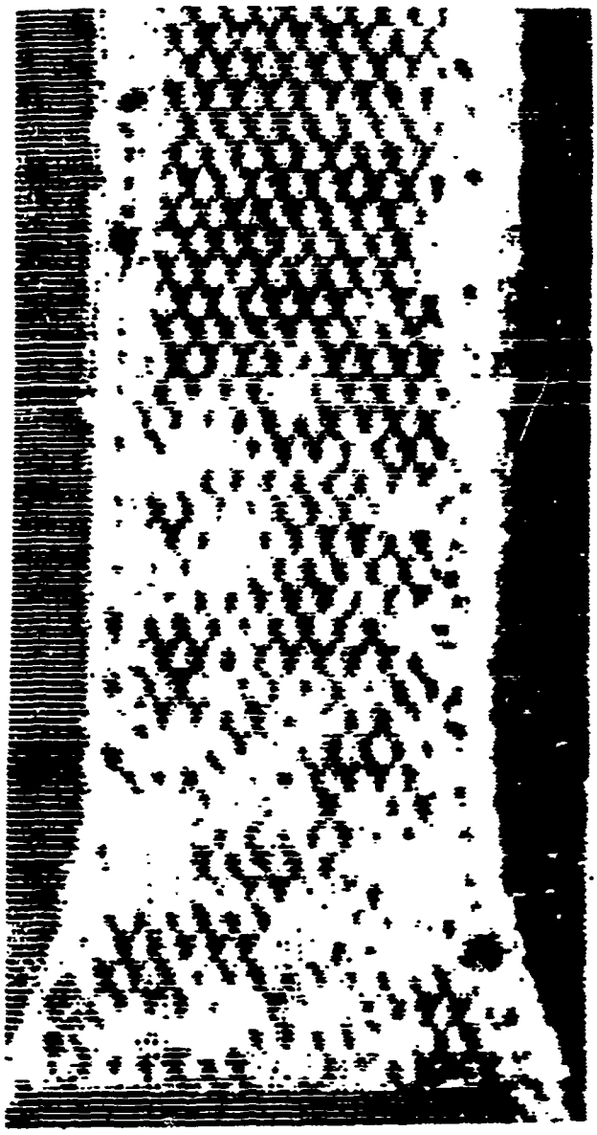
In addition to the structural articles built and tested to verify design, we are continuing the fabrication of a variety of test specimens under very carefully controlled conditions.

These specimens, some with "built-in" defects, are then subjected to a variety of nondestructive tests utilizing pulsed and resonant ultrasound, x-ray, and infrared techniques. After very carefully recording all defects or abnormalities, the specimens are subjected to static and fatigue tests run to ultimate failure. Failure modes and characteristics during static and dynamic testing are observed for correlation with material, processing, and nondestructive test results. Figure 46 is a typical ultrasonic recording showing discontinuities in test specimens.

FIG. 45 INTENTIONALLY OMITTED



ULTRASONIC C-SCAN RECORDING
OF BROKEN CORE MATERIAL IN
A FATIGUE SPECIMEN



ULTRASONIC C-SCAN RECORDING
OF A DEFECTIVE BONDED JOINT
IN A FATIGUE SPECIMEN

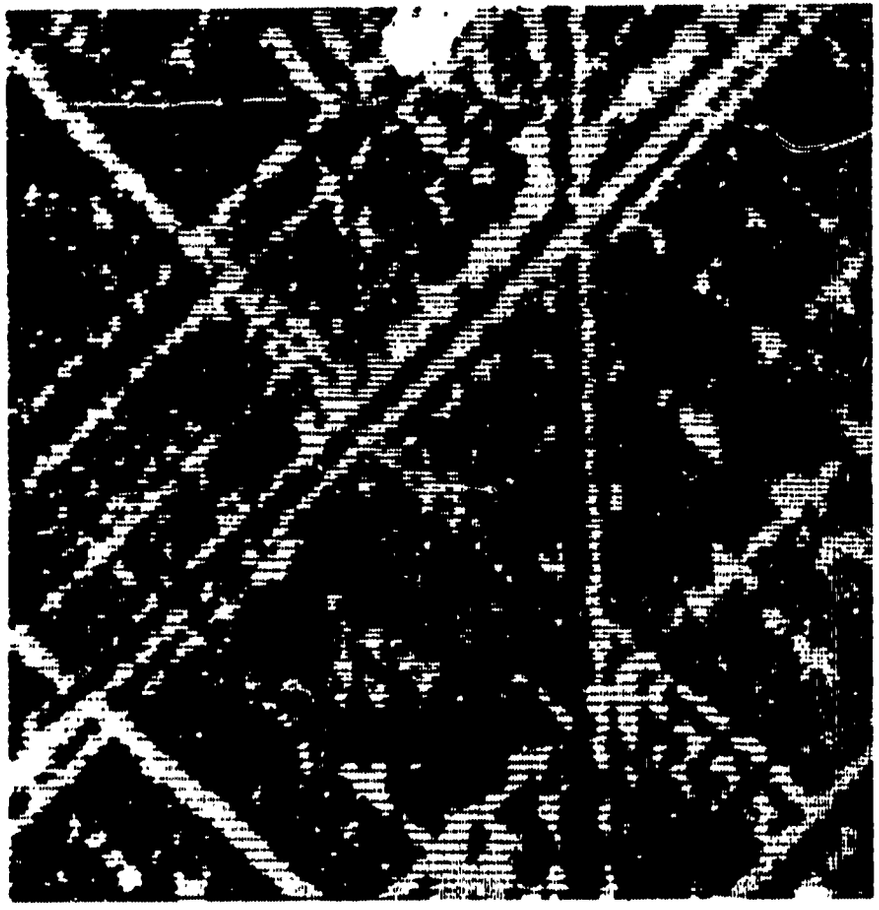
FIGURE 46

Additional work is being done in trying to correlate total material sound attenuation with fatigue test data. Typical ultrasonic recordings showing 75% attenuation and 50% attenuation levels in a boron laminate are shown as Figure 47. In this manner, we are increasing design, materials, and fabrication confidence in composite applications, as well as confidence in our nondestructive testing. Only flight test and service performance can determine the validity of our acceptance criteria.

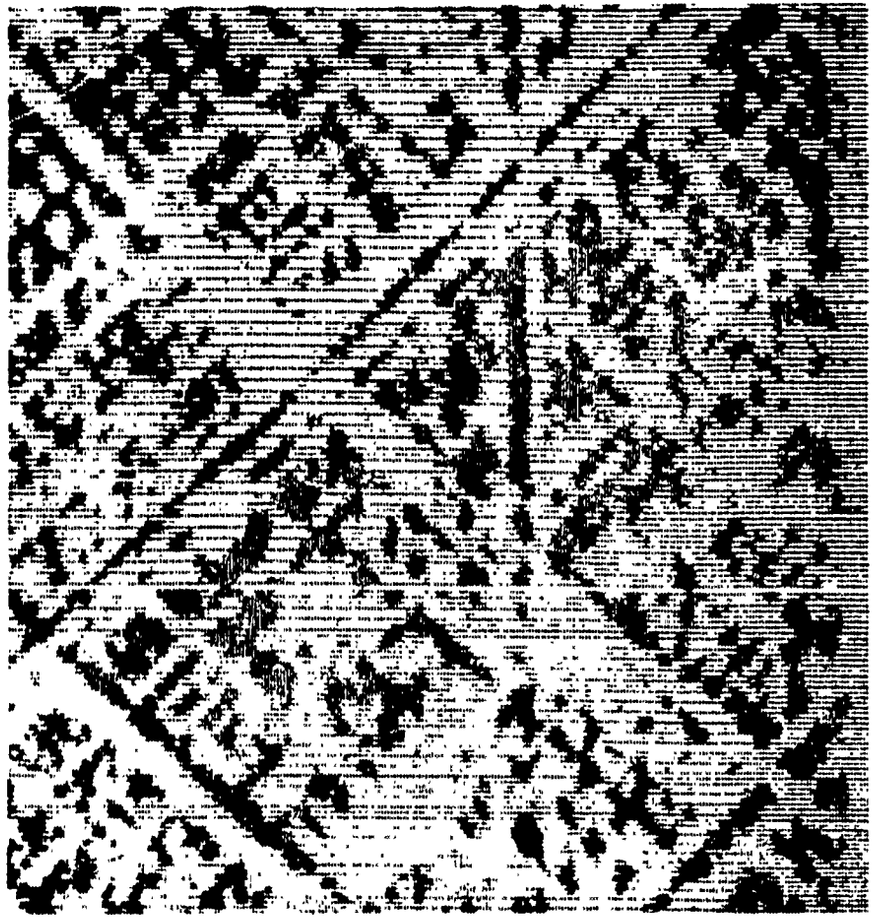
In addition to the materials testing programs, we have a very interesting program to nondestructively monitor full scale article testing. In the case of the Advanced Geometry Composite Rotor Blades, a complete nondestructive inspection was performed after fatigue and structural testing and after whirl tower testing. This gave us an opportunity to monitor and note the progression of defects in the blade. The locations of voids and other areas of interest, such as, areas of high ultrasonic attenuation, were marked directly on the blades after initial inspection and determination of growth or progression was relatively easy. Figure 48 shows an advanced geometry composite rotor blade nondestructive inspection "road map". This investigative nondestructive inspection monitoring will continue through the flight test program.

CONCLUSION

I would like to point out again that quality assurance of composite structures is a result of design quality, and the attendant inspectability; proper process control; and the in-sequence nondestructive evaluation of the hardware. None of the above elements can be neglected if we are to take maximum advantage of the several benefits offered by composite structures.



ULTRASONIC RECORDING OF 75% ATTENUATION LEVEL IN COMPOSITE MATERIAL



ULTRASONIC RECORDING OF 75% ATTENUATION LEVEL IN COMPOSITE MATERIAL

FIGURE 47

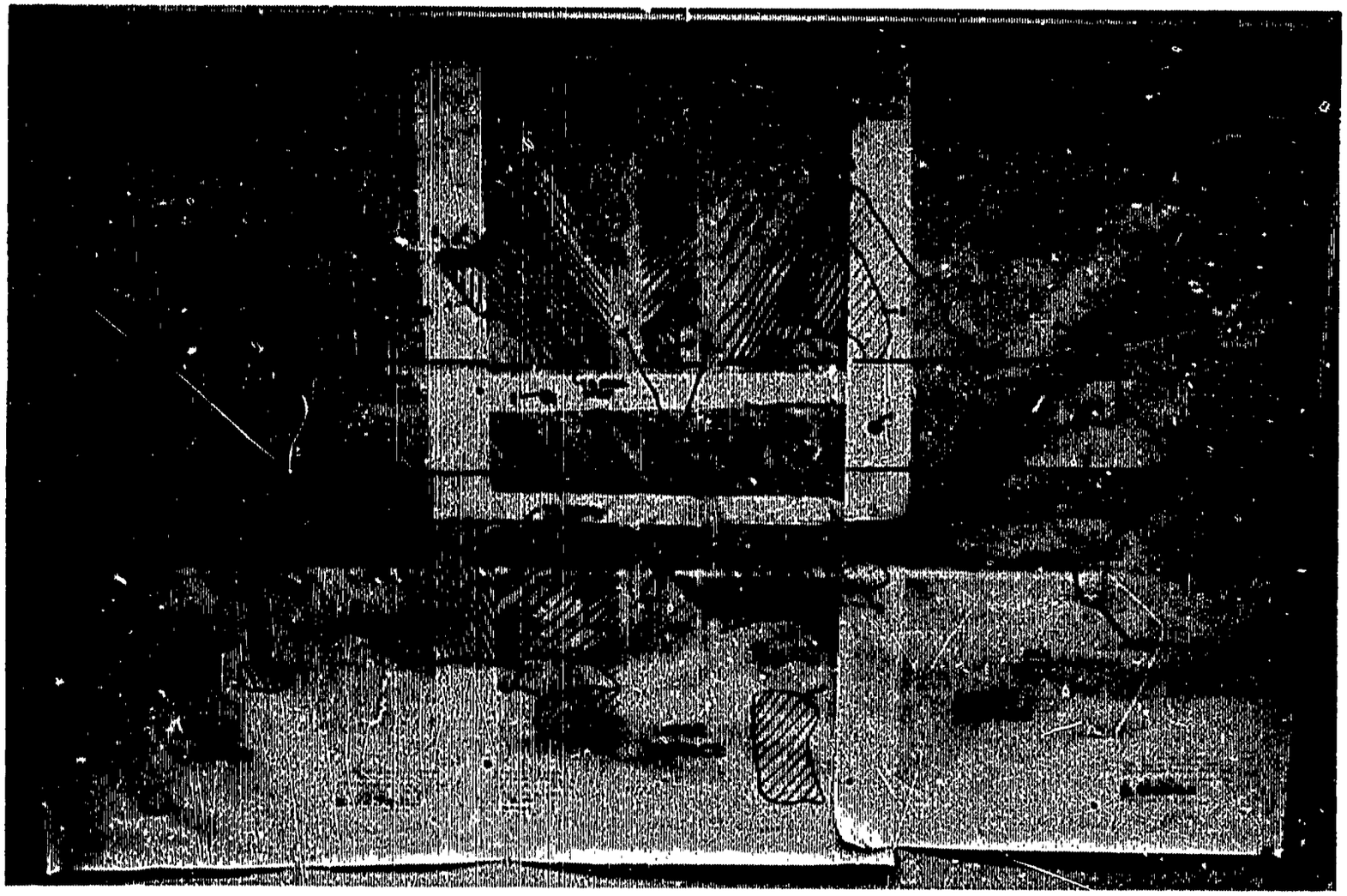


FIGURE 48

ULTRASONIC RECORDS FOR MONITORING OF
QUESTIONABLE AREAS DURING TEST

Nondestructive inspection technology development must continue, and must surpass the capability that we have for homogeneous materials. If we can master this goal, the design freedom and strength offered by composite structures can lead to a whole new realm of hardware fabrication concepts.

To optimize existing physical principle applications may not be enough. Certainly we can take advantage of certain benefits offered by composite structures with existing technology but consider what a very, very small portion of the total physical principle spectrum we utilize today for nondestructive inspection--we have hardly dented it.

The Boeing Company/Vertol Division intends to take full advantage of existing nondestructive inspection technology, as well as new technology, to assure product quality.

There are several new inspection concepts under study at The Boeing Company/Vertol Division, at the present time. It is expected that these systems will become a part of our total quality measurement capability just as the systems described in the preceding discussion.

QUALITY CONTROL METHODS APPLIED TO AN ADVANCED COMPOSITE F-111 HORIZONTAL TAIL

by

G. D. Darnell
Process Control

and

J. A. Riegert
Quality Assurance Research & Development
GENERAL DYNAMICS
Fort Worth Division

For Presentation at the
AFML/Aerospace/University of Dayton
Conference on NDT of Plastic/Composite Structures
Dayton, Ohio
March 18, 1969

ABSTRACT

New and more rigid methods of quality control have been used in the manufacture of boron composite structures. More exacting methods for inspecting raw materials and performing in-process inspection are being utilized. Conventional and new techniques are being investigated. Nondestructive test methods such as infrared, ultrasonics, Porta-Shear and x-rays are being used to inspect details prior to assembly, and to inspect the final bonded assembly.

I INTRODUCTION

Since the boron horizontal stabilizer program at General Dynamics/ Fort Worth was one of a research nature, any quality system used had to be congruent with that type program. Drawings, specifications, processes, etc. were constantly being changed for the sake of producibility. For this reason the quality control team had to ingest these changes while maintaining control of the quality in parts being manufactured.

Most of the actual labor involved was provided by factory personnel under the guidance of research and design engineers in facilities made available for the life of the program. For the most part, these people were not cognizant of factory quality control procedures or capabilities.

The first problem to be resolved by the quality control organization was to establish a quality system rigid enough to assure a quality part, yet flexible enough to be compatible with a research type program.

In this paper, systems and methods of control, from material acceptance to final "buy-off" of the completed assembly, are discussed.

II DESCRIPTION

To understand the processes and quality control of the assembly, a brief description of the stabilizer design is in order.

The boron stabilizer is composed of four "sandwich-type-construction" panels; (1) the main box section (2) the leading edge (3) the trailing edge and (4) the tip

The leading edge, trailing edge and tip sections are similar in construction. These are panels of simple design fabricated with boron, fiberglass and aluminum honeycomb core materials.

The box section is a more complex structure in that there is steel, titanium, boron, fiberglass and aluminum honeycomb core contained in the understructure.

All of the ribs, spars and closures are mechanically fastened to compose the framework of the box section. All other joints and ties are bonded.

The air flow skins of all four sections are entirely boron. These skins are bonded to aluminum honeycomb core and the structural members to complete the sandwich structure.

III QUALITY ASSURANCE OF RAW MATERIALS

To assure the highest composite structure quality, controls must start with the raw materials. For this purpose General Dynamics issued pro-

curement specifications for boron filaments, boron filament reinforced resins, and boron filament reinforced resins for machine lay-up. These specifications cover the physical and mechanical requirements for the boron raw materials. Additional specifications are used to cover standard materials, such as, fiberglass and metals used in boron assemblies.

Control of boron filament by the filament manufacturer included mechanical and physical tests such as tensile, modulus of elasticity, filament diameter and density.

Manufacture of the boron filament reinforced epoxy tape falls into categories of material control of resin and filaments, control of filament collimation, resin impregnation of the filaments, and finally the placement of the tape on the paper carrier. Resin impregnators run acceptance controls on the filaments to determine their conformance to the filament specification. Tests on the epoxy resin system are run by the impregnator only. Each resin batch is tested for physical and mechanical properties such as gel time and flexural modulus.

Specification requirements on the three-inch wide tape are most extensive since this is the final form used to manufacture parts. Mechanical and physical tests are performed on each batch of resin impregnated boron tape by both the manufacturer and General Dynamics as acceptance requirements.

Physical measurements, such as, resin solids and flow are important controls since our part fabrication process is based on a closely controlled resin content. Volitile content is another physical test used by General Dynamics for acceptance purposes.

Some very important inspection steps that can only be performed during tape manufacture are filament alignment and spacing and the precision placement of the tape on the perforated paper carrier. The boron tape location on the paper carrier is most important when using machine lay-up.

When General Dynamics receives boron tape a sample is removed from a randomly selected roll in each batch. Both physical and mechanical values are obtained from this sample. In addition to physical tests previously discussed, a test panel is fabricated with filaments in a zero degree orientation. From this panel, room temperature and 350° F. flexural tests are run at 0 and 90 degrees, as well, as interlaminar shear. A specimen from the laminate is polished at 90 degrees to filament orientation and photographed under magnification to check filament spacing.

A major problem in our present acceptance test procedure is that only the beginning of a roll can be tested since rolls of boron tape cannot be unrolled and rerolled without damage. Therefore, this makes it mandatory that each tape ply be inspected as it is laid to assure that filament alignment and spacing are correct. Continuing problems with tape quality are incompatible with a production operation.

IV IN-PROCESS INSPECTION

For adequate quality control of processes dealing with the many cure,

cleaning and secondary bond operations found in the stabilizer fabrication, in-process inspection is essential. For fabrication purposes, we utilized a planning sheet which becomes the historical quality record. This paperwork listed the fabricating operations sequentially. The fabrication operations were taken from detailed "Process Instructions" written by Advance Design, Manufacturing Research, and Processing Control personnel. Necessary inspection steps were inserted into the manufacturing sequence to insure thorough inspection at all stages of manufacture. During fabrication, completed operations and procedures had to be approved and recorded by inspection on the planning sheet before the next operation could begin.

The fabrication area was under surveillance of an inspector. It was his responsibility to see that the planning paper, process standards, engineering drawings and specifications were adhered to.

A. Boron Detail Fabrication

Fabrication of boron details required tedious visual inspection methods to insure quality. During individual ply lay-up, the fabricating personnel rework or remove all obvious defects in the material. One of the best quality control measures we had in the fabricating area is "defect awareness" on the part of the worker. Tape defects that are found during fabrication are (1) overlaps (2) gaps (3) eyebrows (4) waviness and (5) foreign objects. Four of thelarge, box section skins were partially laid by machine while the other boron details were hand laid. I shall discuss problems encountered with tape machine lay-up first.

The skins were fabricated by laying boron tape on individual ply mylar films which was then transferred to the curing tool one ply at a time. Individual ply inspection can be more readily performed when using this method of fabrication. By placing a light source behind the mylar film, defects are easily noticeable. Fabrication using mylar films allows thorough visual inspection.

Complete fabrication by machine has resulted in ply by ply inspection problems. When the plies are layed one on top of the other, there is less opportunity for thorough ply inspection. Gross defects can be detected but those of small dimension such as overlaps and foreign objects are almost impossible to detect. Laminate quality for this type of fabrication depends upon the tape quality which in turn relies on (1) tack (2) tape placement on the backing material, (3) filament collimation (4) individual filament tension and (5) absence of eyebrows, waviness, gaps and overlaps within the tape. For automated tape laying, laminate quality is no better than the material quality.

Since tape quality at the present time is inconsistant, a method for tape inspection before it is laid is needed. Since the boron cannot be unrolled before use, the only opportunity for thorough examination of an entire roll of material is during laying operation. Monitoring the tape as it comes off the reel enables the flagging of discrepancies contained in the tape prior to lay-up. Gross defects have to be repaired

before the next ply is begun. This results in machine downtime and increased cost. This emphasizes the need for improved and reliable tape quality. Investigation of inspection methods for machine laid tape has been initiated by our Research & Development Department.

B. Other Detail Fabrication

Detail fabrication of material other than boron presented few new quality problems. Normal production inspection and quality procedures were utilized for these detail fabrication controls.

C. Bonding of Major Assemblies

The four major assemblies discussed earlier had similar final bonds so I shall discuss the large "box" section only.

At this point the ribs, spars, closures and core have been assembled and are then numerically machined to mate with the fabricated boron skin. The core is inspected for crushed areas, contamination, and bond separations and is repaired as necessary. A good prefit of the skins to the understructure is essential for a void free bond. I might add that all tooling and parts dimension to the skin bond line to minimize tolerance build-up.

After prefit of the skin to the core assembly, an encapsulated adhesive check is made to confirm the prefit. This consists of adhesive covered on both surfaces with nylon film for release purposes. This adhesive-nylon sandwich is placed between the core surface and the boron skins. The assembly is then placed in the bonding tool, cured, and dismantled. The impressed adhesive is then examined for possible mismatches on both bonding surfaces of the box section. Rework in questionable areas is then accomplished and the assembly is prepared for final bond.

Prior to final bond, all fiberglass areas of the "box" are scuff sanded and blown with filtered air to remove surface contamination. The entire "box" section is then vapor degreased with stablized trichloroethylene and dryed at an elevated temperature to obtain complete removal of the solvent. The boron skins require only removal of the peel ply before bond.

When the "box" and both skins are ready for bond, the adhesive is applied, the skins installed onto the "box" section, all attachment bolts are inserted and torqued, and the assembly is placed into the bondform. Curing of the large assembly required close tolerance heat and pressure control.

All of the processes used in fabricating the tail assembly were monitored for conformance to process standards and engineering specifications by Quality Assurance Organizations Process Control personnel and by Inspection personnel. The high temperature presses were checked for heat uniformity, the curing and bonding presses for heat-up rates and for temperature uniformity.

V DESTRUCTIVE AND NONDESTRUCTIVE TESTING

A. Details

For all details in which an elevated temperature cure cycle is

necessary, representative test tabs accompany the details through all fabrication operations. For example, a boron skin would have a test tab fabricated from the same material and cured during the same cure cycle. When possible, test tabs were laid up and cured on the part tool. This practice not only assures material quality but also processing quality. Test specimens are prepared from the tab and tested by process control to the engineering material test specification. The data received must satisfy the acceptance values set forth in that specification. The specimen types are: (1) zero degree flexural (2) ninety degree flexural (3) horizontal or interlaminar shear. The specimens are tested at room temperature and at 350° F.

During testing of the tabs, the part is held by inspection pending test results. If the results are acceptable, inspection accepts the part and it continues to the next operation. When unacceptable test results are encountered, the specimens and test equipment are thoroughly evaluated to assure that test conditions were correct. In the past, when a test failure arose, the cause for failure was often found to be poor specimen preparation. It has been found that test data from the ninety degree flexural specimens is critical when the resin system is accepted for use at minimum test values.

For general purpose void or debond detection, commercial infrared systems reveal good bonds, partial bonds or complete debond areas. It is utilized to inspect the integrity of boron laminates less than .125 inch thick.

Infrared inspection equipment measures the heat or infrared radiation transfer of the material. The heat transfer of a laminate or bondline with voids or delaminations will not be uniform. To get maximum sensitivity on the test equipment, a flat black color is desired for maximum heat absorbtion and heat retention. The black color of the cured boron laminate allows it to be inspected by infrared methods without supplemental treatment.

At the present time, General Dynamics/Fort Worth has four production infrared test machines. To correlate test results, some experimental specimens with intentional variability have been used, though it is now apparent that carefully constructed reference standards are essential for the maximum utility of the infrared systems.

In some areas, ultrasonic inspection played an important roll in void detection. The ultrasonic inspection used to the greatest advantage was the through transmission method. This technique employs sound wave emission from a power transducer on the surface of the part. The sound waves pass through the part and are picked up on the opposite surface with a receiving transducer. Material that is solid will have little effect on the energy level, but a void or delamination will sharply reduce the energy level. This test method was used to inspect the bond between boron skin and the titanium scarf plate. A chart was made of recorded readings, evaluated and attached to the inspection history. All of the boron-titanium bonds in this area proved to be good.

X-ray inspection was valuable for confirming the internal geometry of the

structure, but did not prove capable of resolving bondline deficiencies or defects in laminates more than 8 plys thick.

The Porta-Shear is a General Dynamics/Fort Worth developed test equipment. It separates a precut, small diameter button at the bondline by applying a shear force. When the bondline fails, the load is recorded and translated into equivalent bondline strength. Porta-Shear qualification for typical boron composite joints is in progress. Selected areas of static and fatigue test horizontal stabilizers were tested with the Porta-Shear.

3. Assembly

Infrared inspection of the four major component skin bonds was run on both the static and fatigue test articles. Infrared recordings made after final assembly were correlated with photographs taken of the understructures before final skin bond. The infrared readings revealed questionable cold and hot areas. Upon review of the photographs, these areas were found to be core repairs or areas where a slightly thick glue line had developed. For thorough and complete evaluation of infrared recordings, the inspector must have a working knowledge of the understructure of the part being inspected.

The static tail was tested to failure and the remnants re-examined with infrared. This re-examination resulted in a high degree of confidence in the infrared inspection technique.

X-ray examination of the bonded assemblies was used when questions arose concerning internal geometry. Core splices, core node bond separations, and step mismatches can be seen with x-ray.

The bonded assemblies were checked ultrasonically to verify the infrared findings. The production ultrasonic bond tester is a mechanical impedance system; it proved useful in checking skin to spar and closure bonds.

Test specimens for the major assembly bonds were used to verify the adhesion and the process quality maintained during bonding.

Test specimens for the bond operations took two forms; one to test the shear strength in the boron to glass bond and the other to test the tensile strength in the boron to core bond areas. The specimens were made from the same adhesive batch with identical component materials. All details having been precured, the secondary adhesive joint completes the assembly during the last cure. After cure, test specimens were prepared. Because nondestructive test methods provide such limited knowledge of glue line strength, final assembly control specimens were cured on the bonding tool (or a secondary tool close by). These specimens provided process control with the data required for final acceptance of the tail assembly.

VI CONCLUSION

The quality control exercised during fabrication of the F-111 advanced composite horizontal stabilizer was adequate for the development nature of the program. The experience thus gained has resulted in increased awareness by management of quality areas that must be improved

prior to a production effort. Based on this experience, a Quality Assurance Plan is being developed for total control of quality from design review thru source control, material handling, fabrication, assembly, and test of the end article. Special emphasis is being given to improving inspection and test methods and to quality documentation retrievability and traceability.

In closing, I don't want to leave the impression that we have all of our quality problems resolved because we still have areas that can be improved on. We are planning ahead and attempting to benefit from our experience gained on the Research & Development Programs by recognizing the need to (1) obtain better control over initial tape quality (2) develop a means for automatically checking the lay-up quality of the tape as it is being laid, and (3) expand and refine our nondestructive testing techniques in addition to developing meaningful NDT acceptance criteria and reference standards.

J. A. Riegert

STUDIES OF COMPOSITE MATERIALS AND FAYING SURFACES UTILIZING THE SCANNING ELECTRON MICROSCOPE

By

Charles V. Cagle and Henry Lee
Research & Development Center
The Epoxylite Corporation
South El Monte, Calif.

A paper to be presented at the University of Dayton on March 20, 1969.

The strength of any adhesive bond depends to a major degree upon the nature of the substrate surface being joined, upon their physical and chemical composition, adherend cleanliness, and the ability of the resin to wet the surface of the substrates. This same theory can be applied to some degree to composite materials, i.e., resin wetting as applied to fibers, fillers and carriers and later when subjected to in-service conditions; the compatibility of these materials, plus the influence of degrading factors by environmental conditioning.

The Epoxylite Corporation has successfully applied the scanning electron microscope to these types of studies. This instrument has proven especially helpful in failure analysis, pertinent to studies of high temperature adhesives and reinforced composites. The ability to study faying surfaces and filiers under various conditions has proven invaluable in adhesive and composite testing, especially in the Epoxylite research programs in the field of dental and biomedical materials. For example, it is apparent that similar problems are encountered pertinent to adhesion in the human body that poses a constant struggle in the aerospace industry, i.e., adhesion and moisture or simply, interfacial problems.

The scanning electron microscope differs from the ordinary electron microscope in that instead of an electron beam being passed through the specimen, the electron beam is, in effect, bounced off the surface of the specimen at an angle. A primary beam of electrons from a heated tungsten filament is focused into a fine probe on the specimen and allowed to scan the surface in a raster pattern as in a TV set. Electrons liberated from the specimen by the probe are detected by a scintillator-photomultiplier system. The resulting signals are used to modulate the brightness of a cathode-ray tube screen that is scanned in synchronism with the electron probe scanning the specimen. The fine probe of electrons permits the instrument to examine the microtopography of the solid bulk specimens, whose surface roughness or other characteristics make it extremely difficult

or impossible to observe by conventional transmission electron microscopy (Fig. 1). The resolution is 250 Å and magnification is possible up to 100,000X and the depth of focus is 300 to 500 times greater than either conventional light or transmission electron microscopes. This great depth of field makes the instrument useful for close examination of surface irregularities. The time involved in sample preparation is nominal as compared for sample preparation pertinent to transmission microscopy.

In summary, this device offers the following advantages:

1. Direct and non-destructive observation of bulky specimens, as large as a 1 in. cube.
2. The resolving power is superior to that of an optical microscope.
3. The image mainly represents the surface topography of specimen and appears as one sees the specimen by the naked eye, except magnified; therefore the image is easily interpreted.
4. The image has great depth of focus, which makes it possible to measure large elevations of features on the specimen surface. One can obtain three dimensional clear images even if the surface of the sample is rough.

Fillers and Carriers

Figure 2 shows an aluminum oxide filler, approximately 30-40 microns in diameter and Fig. 3 is a microphoto of a fused quartz filler, 30-40 microns in size. This illustrates the close particle size examination that is possible utilizing this technique. Figure 4 shows sapphire whiskers approximately 1-3 microns in diameter. The study of the resin-filler composite after blending and curing is important to aid in optimization of filler content. Figure 5 is a microphoto of glass beads approximately 25 microns in diameter. Figure 6 is the same with a higher magnification. Note the dust and foreign matter in the beads in Fig. 6. In Fig. 7 a hollow glass sphere is shown and the extent of the cavity in the bead is abundantly clear. Figure 8 is ground Lucite and Fig. 9 is Rigidex. Figure 10 is a single strand of glass in resin. Note the poor wetting and air gap around the glass. Figure 11 is a polyurethane foam and Fig. 12 shows a syntactic foam. Figure 13 shows the surface of a high temperature epoxy resin after long term heat aging and destructive tests.

Surface Preparation

The SEM has proven helpful in surface preparation studies. Figure 14 is a microphoto of a sample of unmodified FEP Teflon and Fig. 15 is a piece from the same stock

that has been finely machined. Figure 16 is the same after annealing and Fig. 17 shows the surface after a sodium-THF-napthalene etch. Figure 18 shows the same material after etching and then annealing. Figure 19 shows the surface after annealing only. Figure 20 is an etched Teflon surface after annealing. Note the scales and cracks which are due to over-etching. Figure 21 is an unmodified 2024T3 aluminum surface and Fig. 22 is the same surface after sanding with 240 grit sandpaper. Figure 23 is a highly magnified shot of the same surface (40,000X). Note the oxides and foreign matter present on the surface. Figure 24 shows the aluminum surface after a sodium dichromate-sulfuric acid etch.

Failure Analysis

Figure 25 shows a high temperature epoxy adhesive on steel after destructive testing on a steel adherend. This appeared to be a clean adhesive failure, but the microphoto shows a considerable amount of adhesive remaining on the substrate, and evidence of cohesive degradation within the adhesive layer as well as the interface. However, in all probability the oxidation problems began at the interface.

Figure 26 is a microphoto of a polyimide system on 120 glass in laminate form. The glass strand spacings are evident through the outer layer of resin. Figure 27 and 28 are the identical panel after destructive tests. Note that the glass strands are not wetted, and adhesion is spotty. It is interesting to note that in Fig. 27 the resin did not break as would other supposedly rigid systems, which indicates more flexibility with the polyaromatic system than is sometimes assumed.

Figure 29 is a honeycomb prepreg face sheet after flatwise tensile tests in which the tensile strength was approximately 200 psi as compared to maximum expectation of 800 psi (controls). This appeared to be an adhesive failure for the aluminum core, but upon examination it is really adhesive from the glass. The real conclusion here is the effect of filleting. One would quickly note that the resin did not flow properly and produce a fillet around the cell walls of the core. Figure 30 is a closeup shot of higher magnifications and shows better the poor adhesion to the glass strands. Figure 31 is an epoxy filled with hollow glass spheres. This panel had gas entrapments as shown in Fig. 32, which is a minute section where the spheres are missing (10,000X). Figure 33 is a phenolic coated sample of wood. This particular sample picked up considerable moisture and a microphoto reveals the poor coverage of the wood.

In conclusion, the SEM can be used to great advantage in adhesive studies pertinent to NDT. Surely more and much better ways will be found in the future to utilize this equipment.

REFERENCES

1. Lee, Henry L., Cagle, C. V., "Adhesion of Epoxy and Polyurethane Resins to Dental Enamel", Gordon Conference, August, 1968.

2. Cagle, C. V., "Adhesive Bonding: Techniques and Applications", McGraw-Hill Book Company, 1968.

3. Lee, Henry L., Stoffey, Donald G., "Application of the New Stereoscanning Electron Microscope to Characterization of Polymer Surface Morphology", Journal of Applied Science, 1968.

4. Fenner, Otto H., "Evaluating Plastics and Resins", Chemical Engineering, November, 1968.

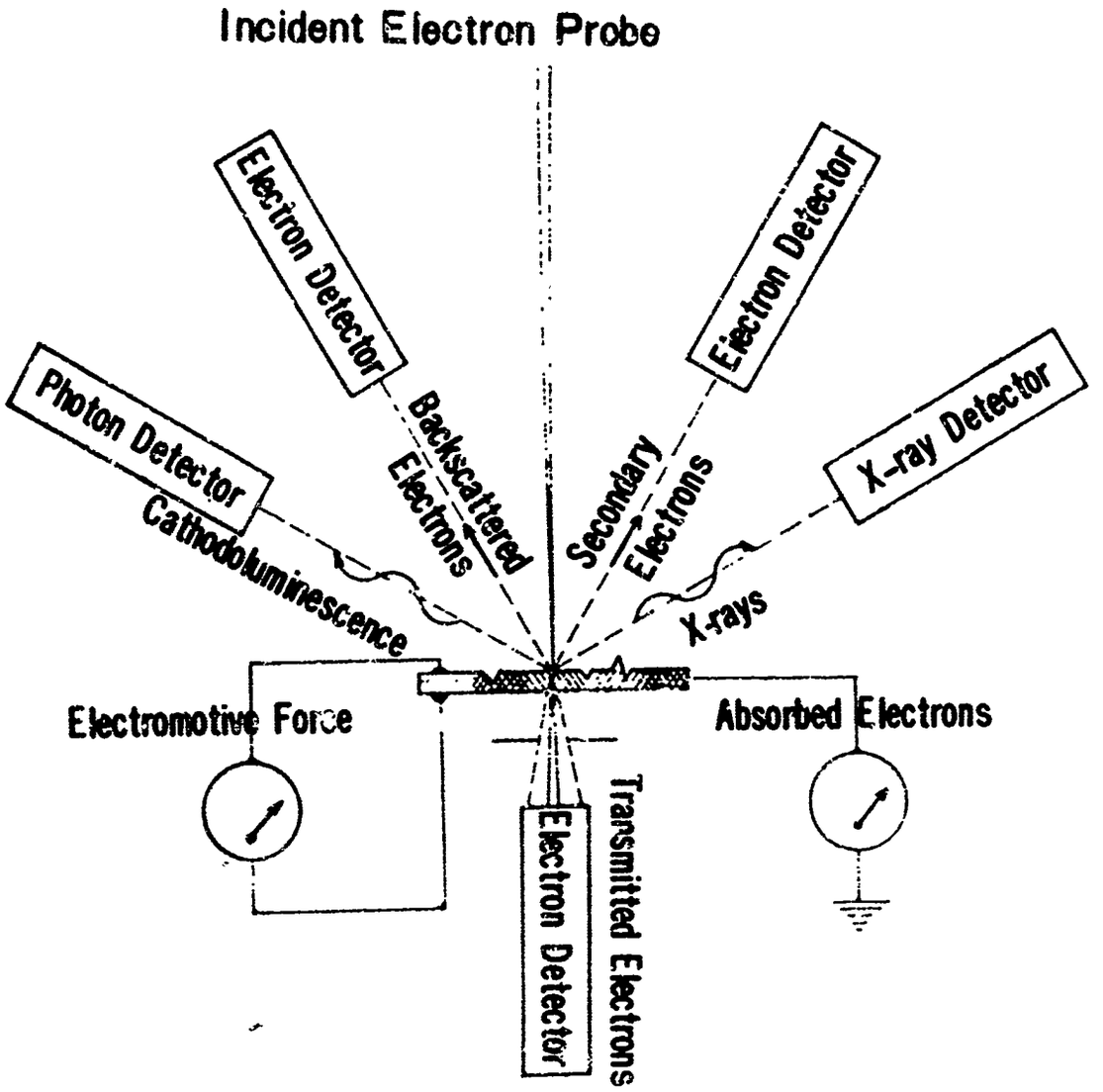
5. Kimoto, S., Suganuma, T., "Stereomicrography by Scanning Electron Microscope", Japan Electron Optics Laboratory, 1968.

6. Cagle, C. V. "Adhesive and Surface Studies Using the Scanning Electron Microscope", Adhesives Age, pending publication.

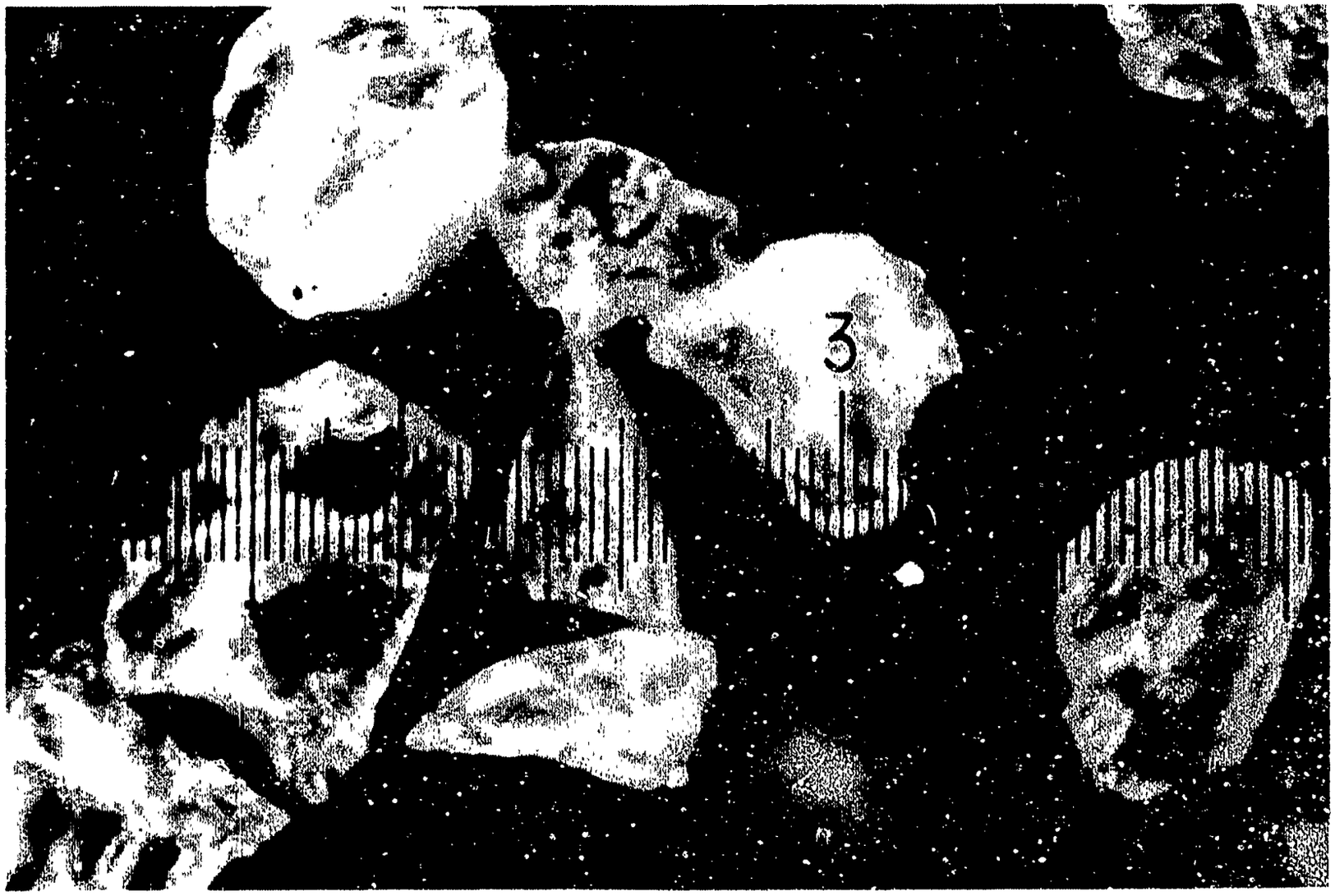
ILLUSTRATIONS

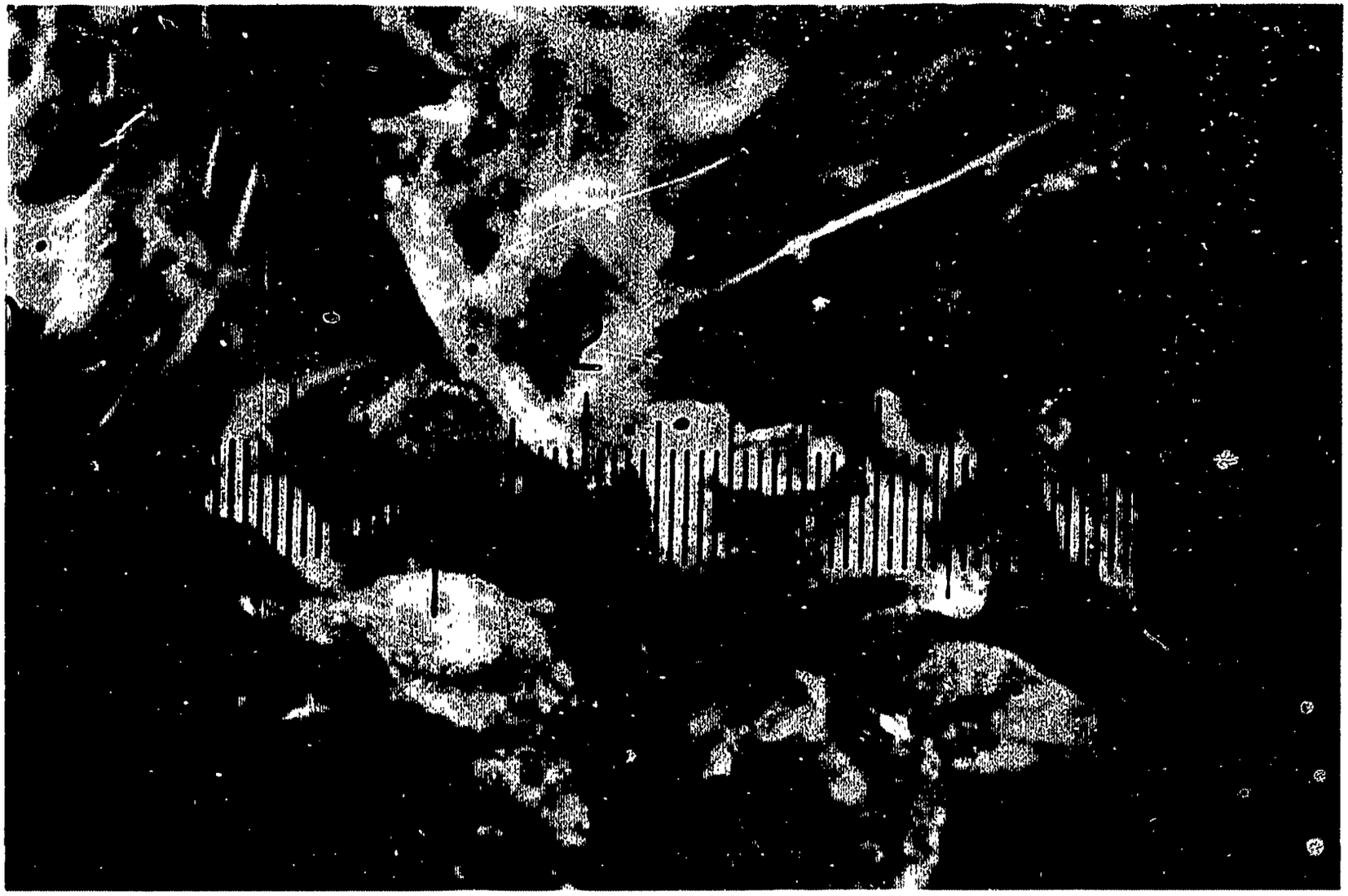
Figure

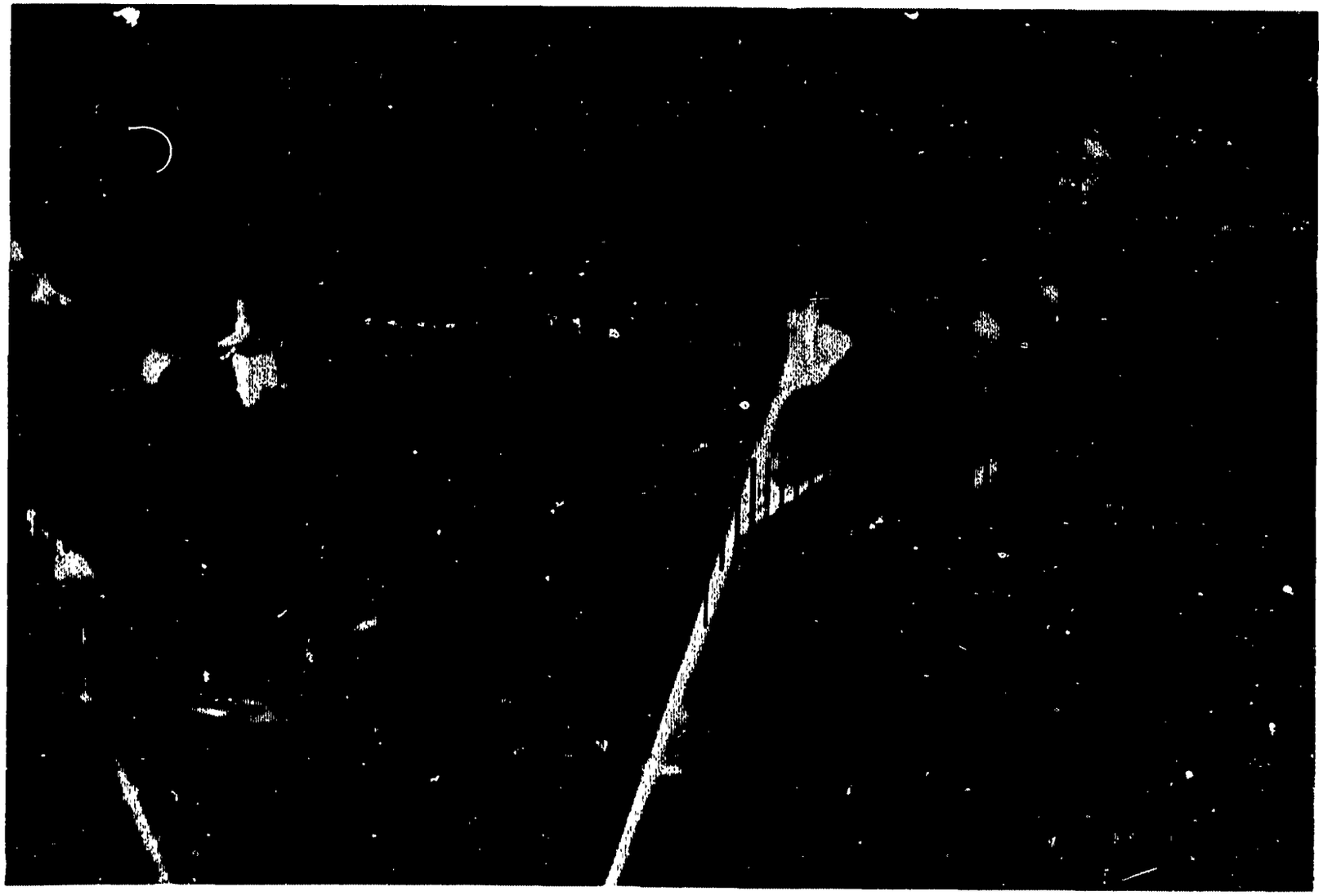
1. Simple Schematic of the Scanning Electron Microscope.
2. Fused Aluminum Used as a Filler for Adhesives.
3. Fused Quartz Filler.
4. Sapphire Whiskers, 1-3 Microns in Diameter.
5. Glass Beads, Approximately 25 Microns in Diameter.
6. Glass Beads, 25 Microns in Diameter (3000X).
7. Hollow Glass Spheres.
8. Rigidex at 10000X.
9. Ground Lucite.
10. A Single Glass Strand in Cured Resin.
11. A Polyurethane Foam.
12. A Syntactic Foam.
13. A High Temperature Epoxy After Long Term Heat Aging.
14. FEP Teflon, Unmodified Surface (1000X).
15. Machined FEP Teflon.
16. FEP Teflon, Annealed Only.
17. FEP Teflon, Sodium/Naphthalene/THF Etched.
18. FEP Teflon, Etched and Then Annealed.
19. FEP Teflon, Annealed.
20. FEP Teflon, Etched and Annealed.
21. Unmodified 2024T3 Aluminum.
22. 2024 Aluminum After Sanding with 240 Grit Sandpaper.
23. A Close Up, Highly Magnified Shot of 2024 Aluminum After Sanding.
24. 2024 Aluminum After Sodium Dichromate/Sulfuric Acid Etch.
25. Steel Surface After Failure at Elevated Temperatures, Bonded with Epoxy.
26. A Polyimide/Glass Laminate.
27. A Polyimide Laminate After Fracture (Mechanical Test).
28. A Polyimide/Glass Composite After Fracture.
29. Failure of Honeycomb Core from Facing.
30. An Epoxy After Fracture (Poor Adhesion).
31. A Low Density Potting Compound (Epoxy Filled with Hollow Glass Spheres).
32. A Close Up of Doubtful Area Shown in Fig. 31.
33. Wood Coated with a Phenolic Resin.

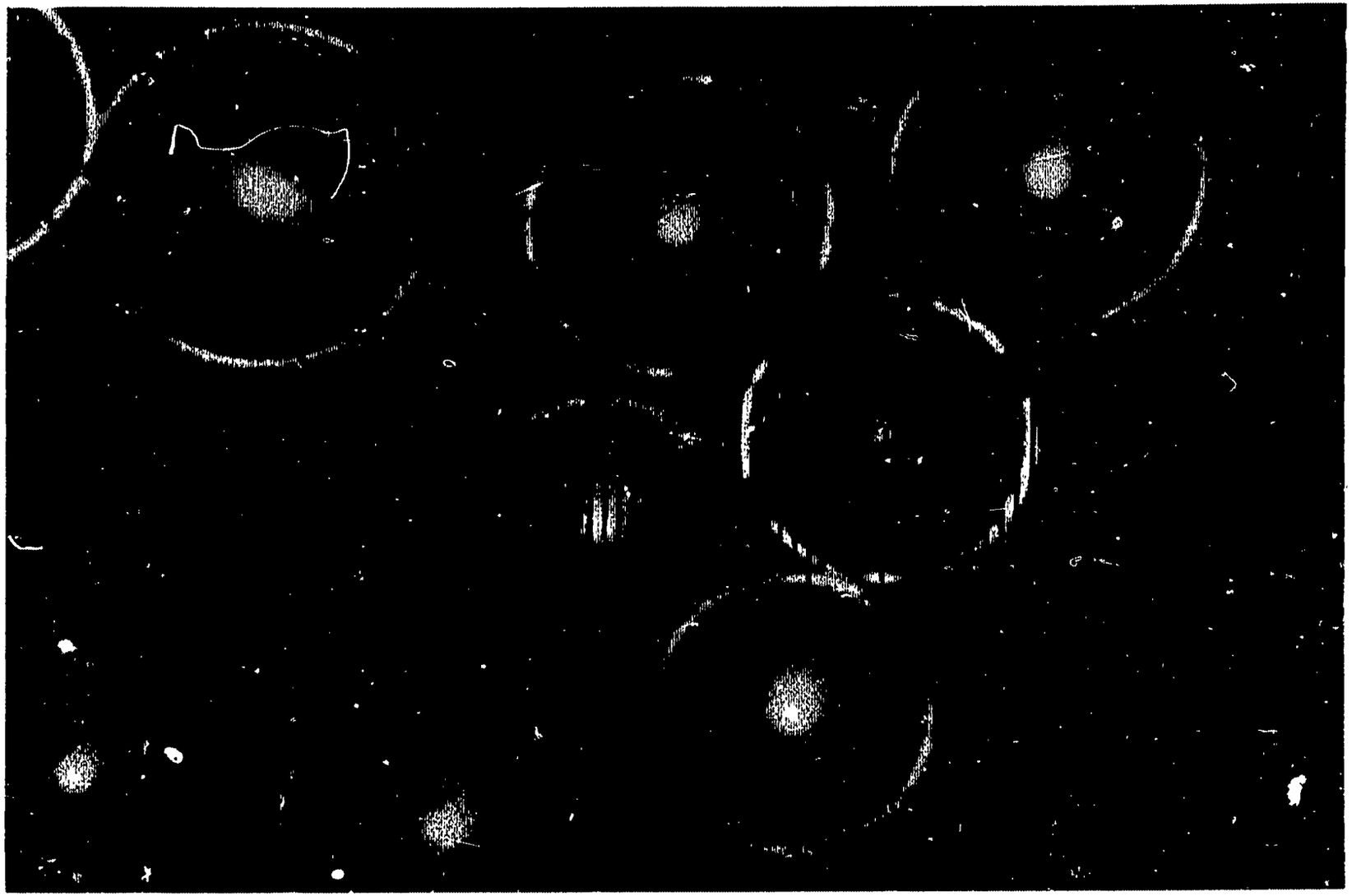


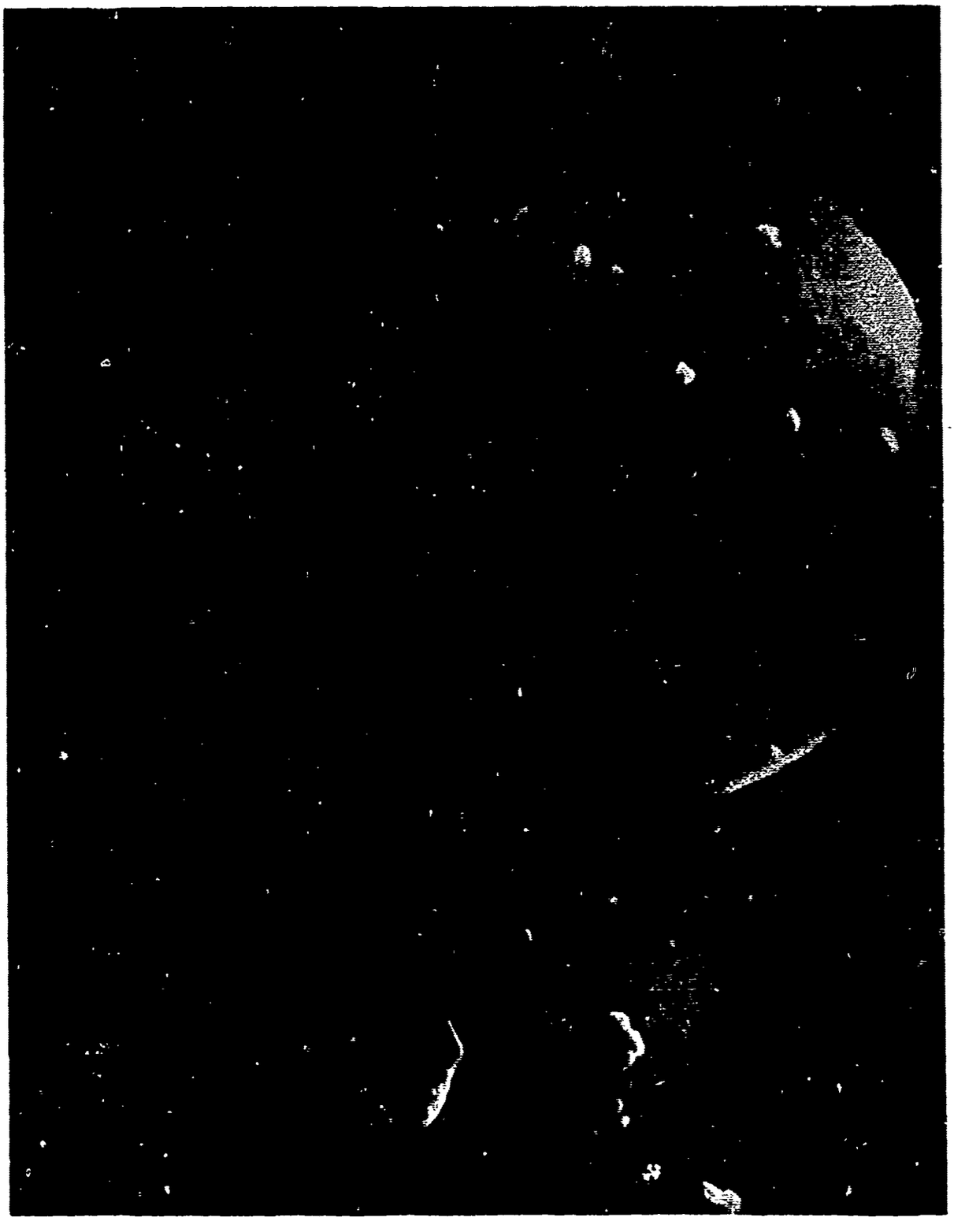
Information from Specimen by Bombardment of Incident Electron Probe

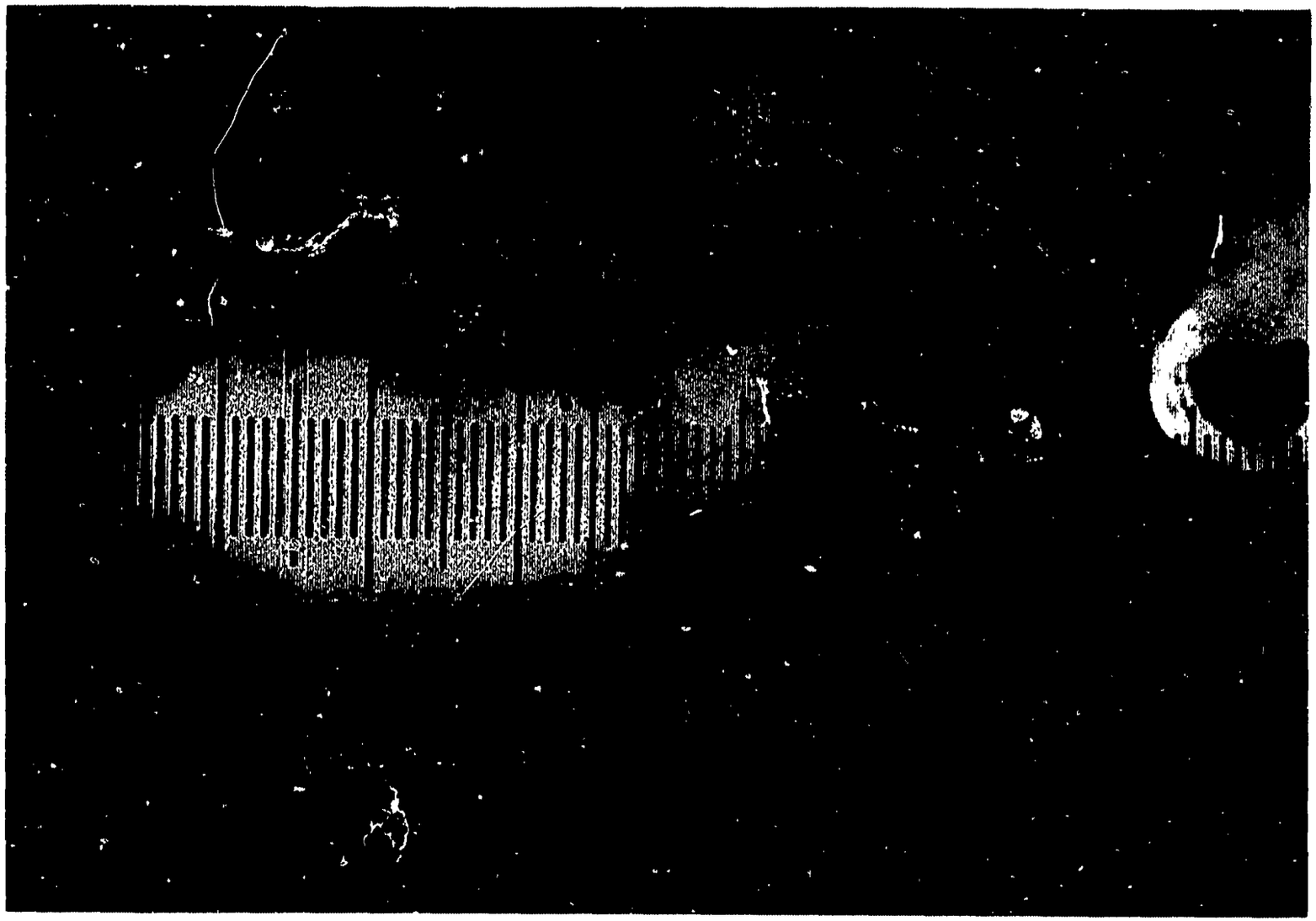

3

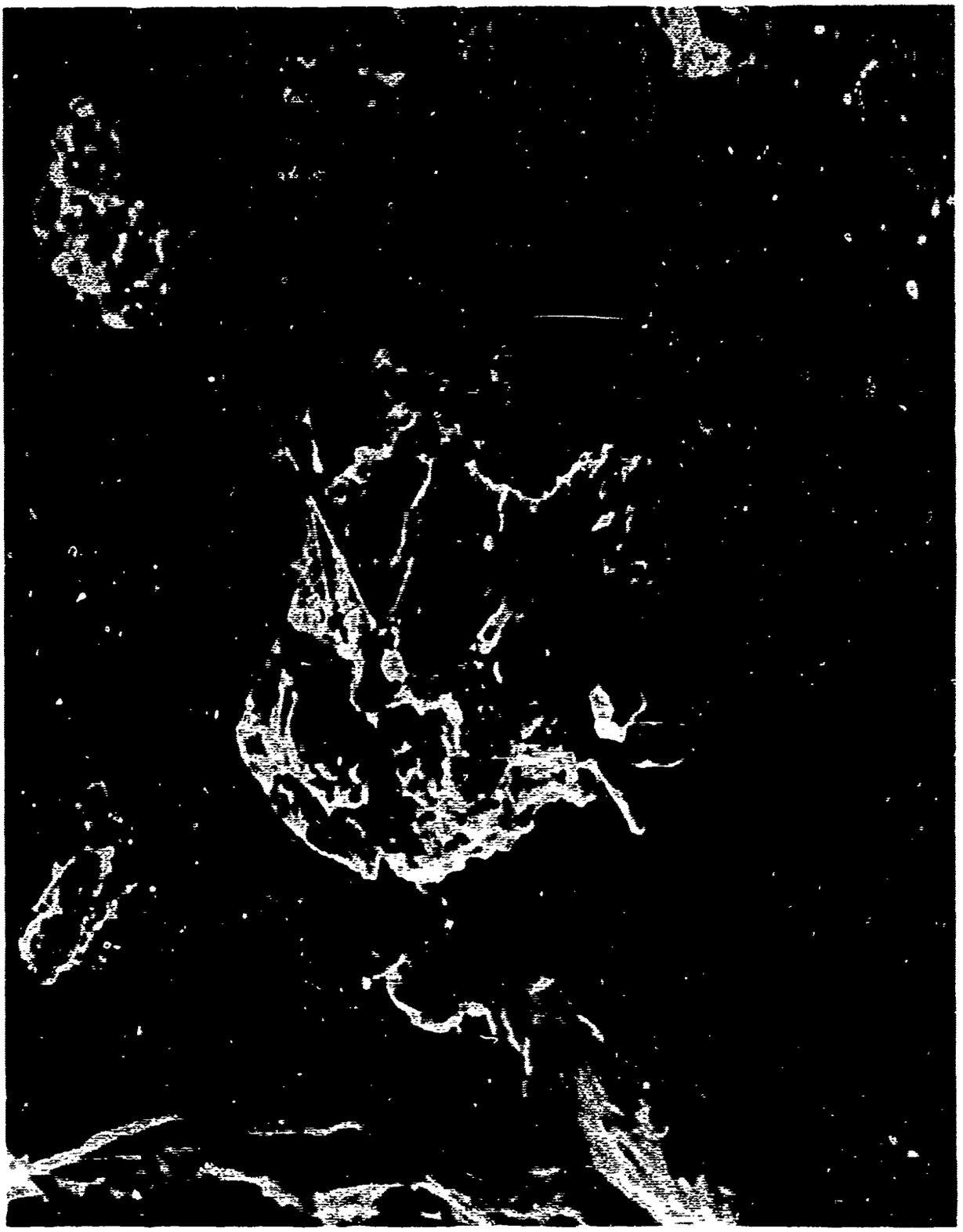


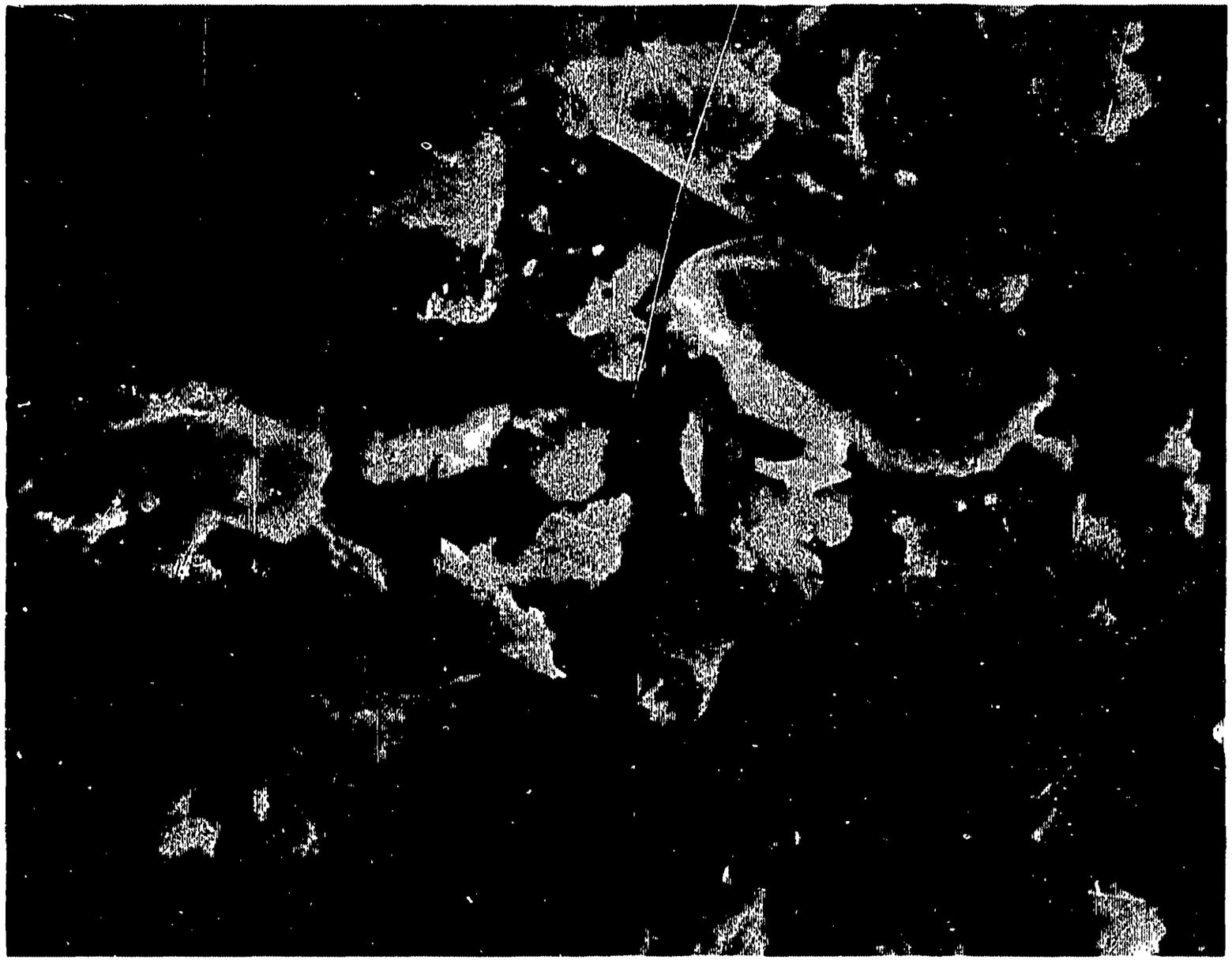




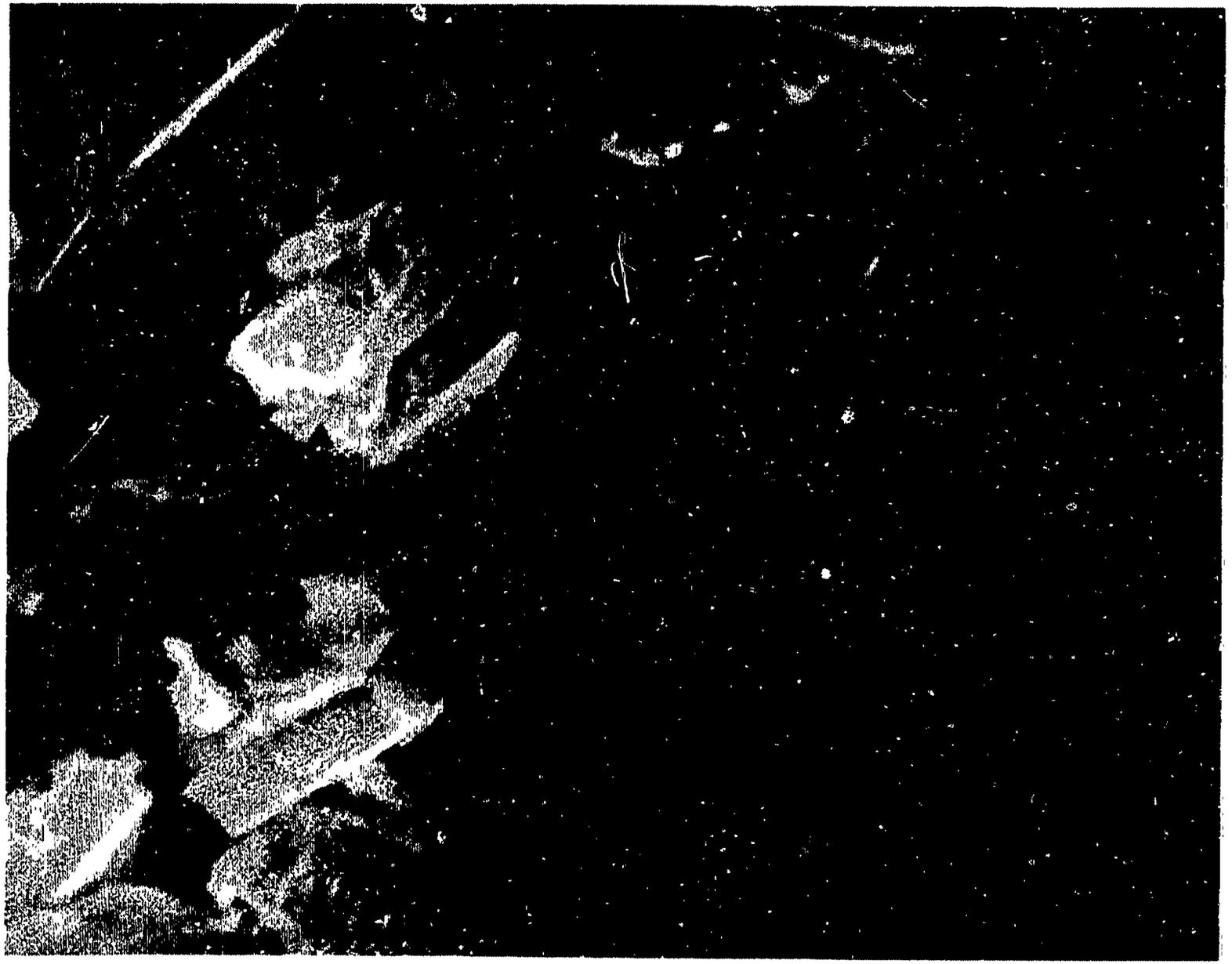


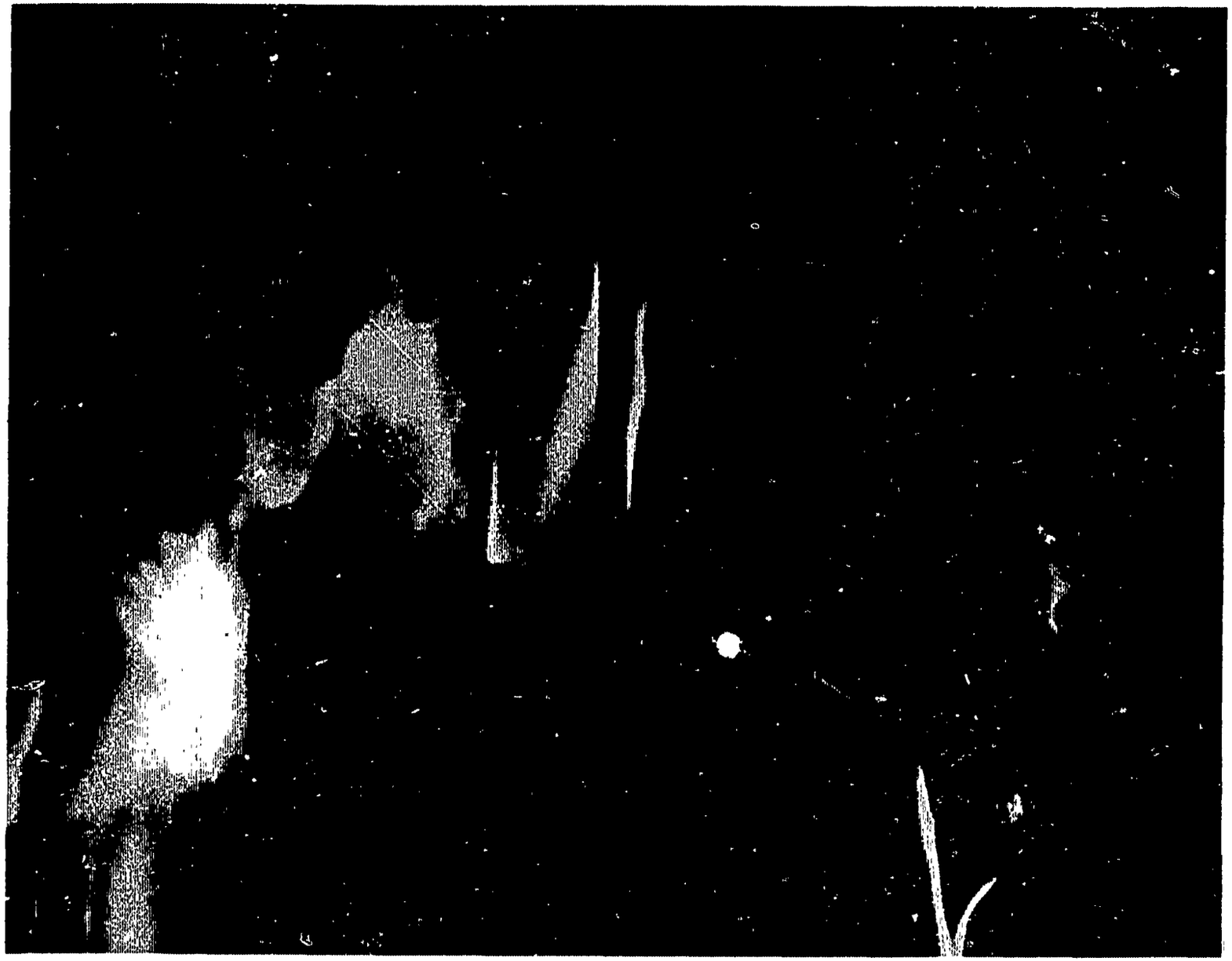










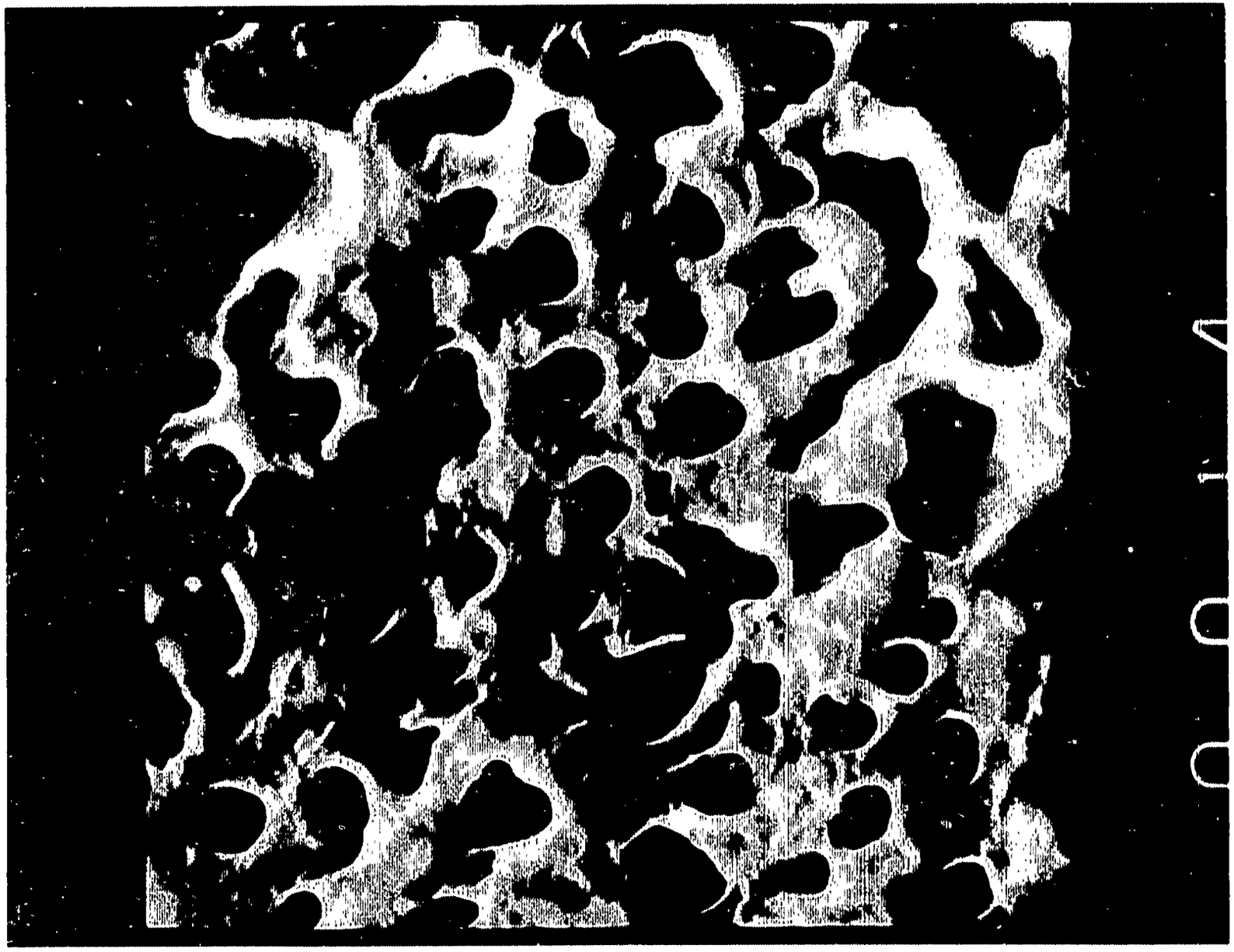


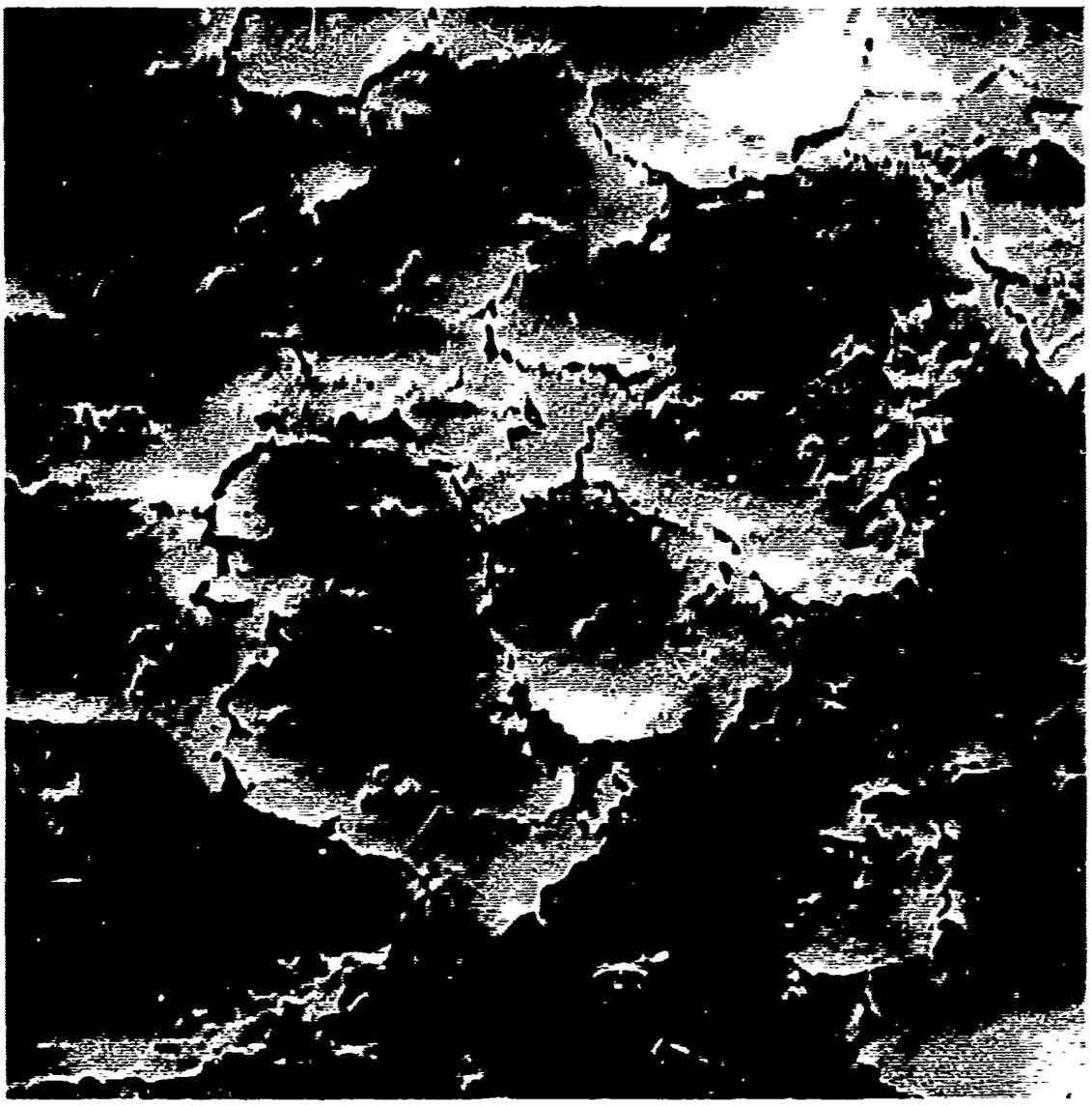


0017

MORE

0029

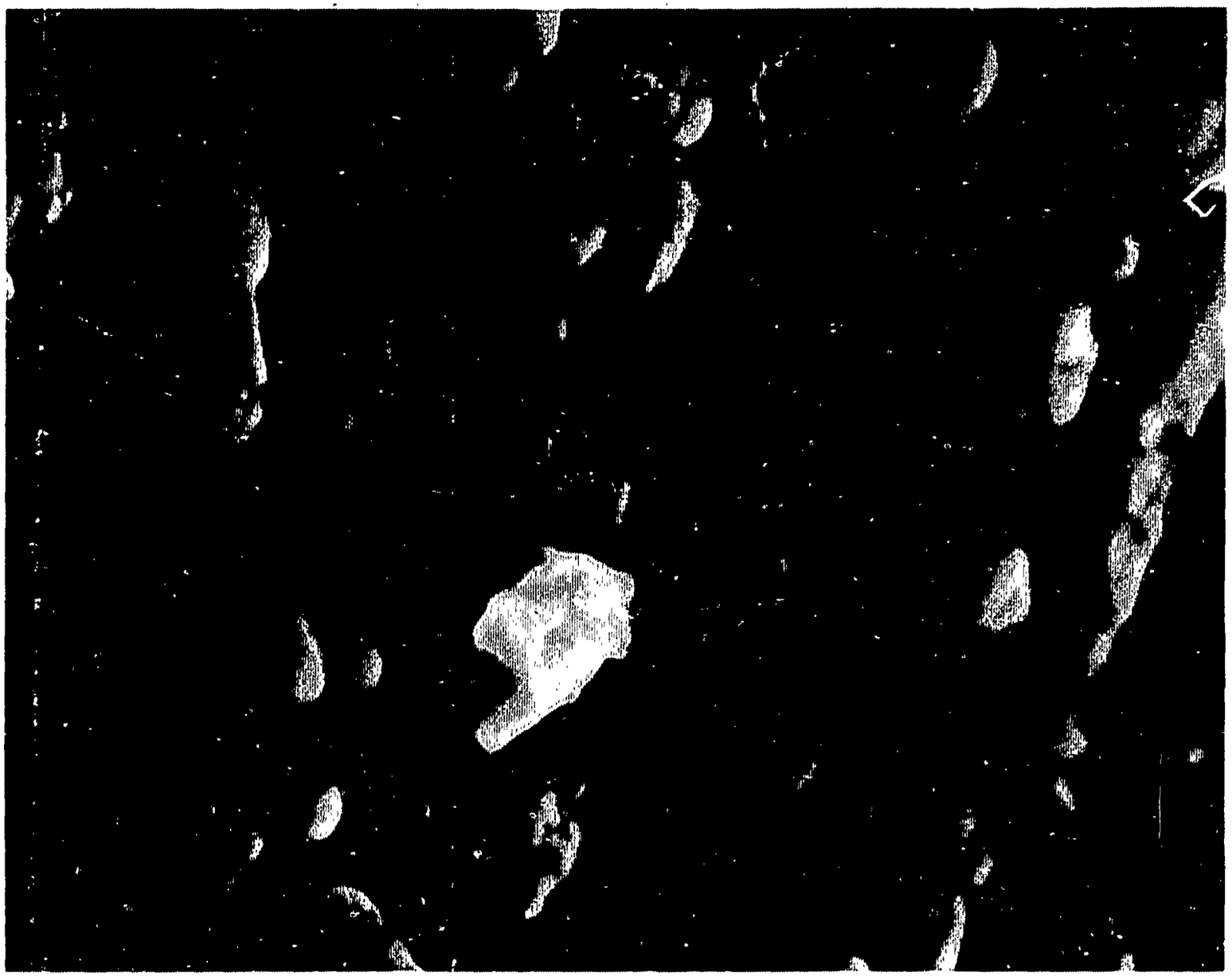




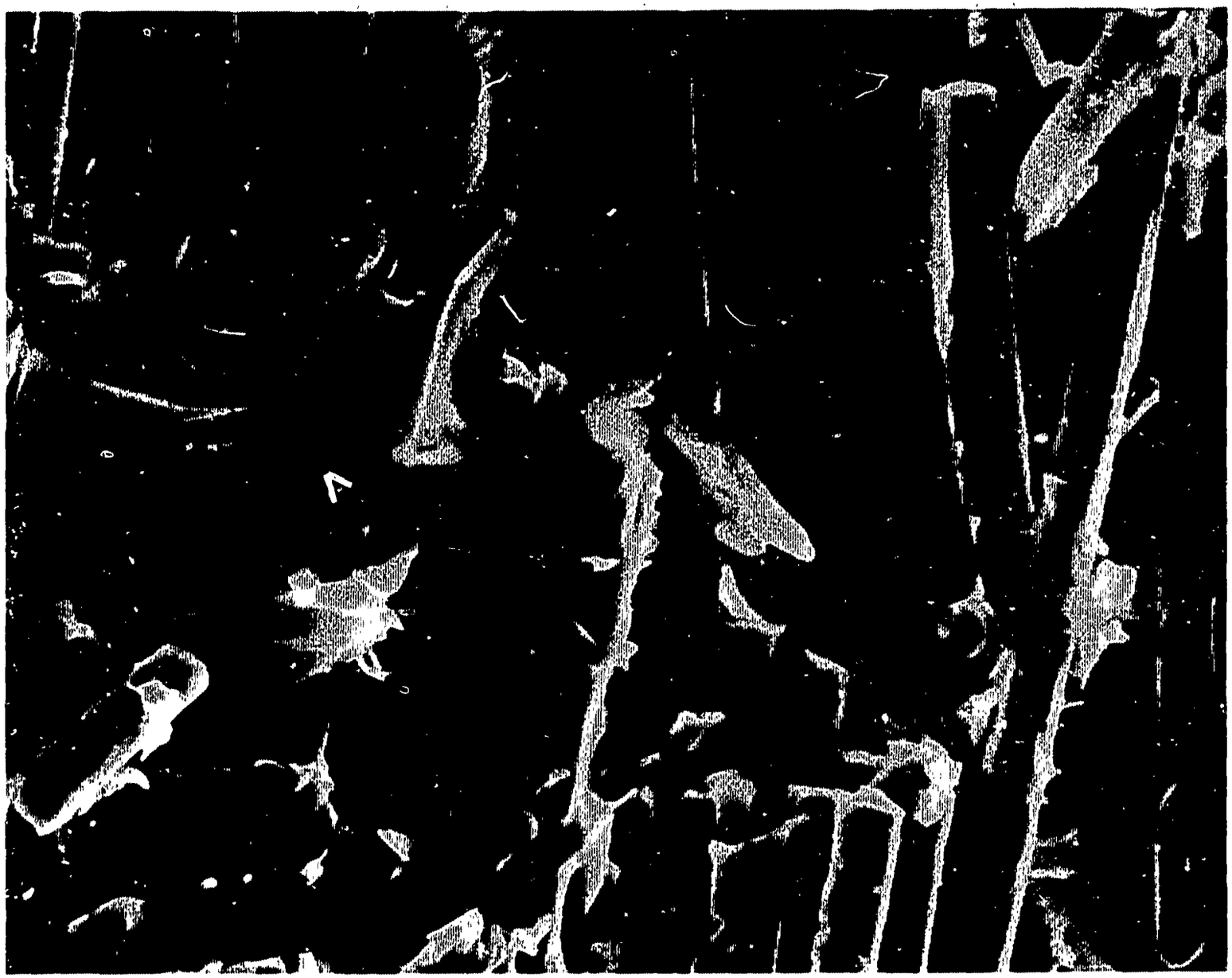


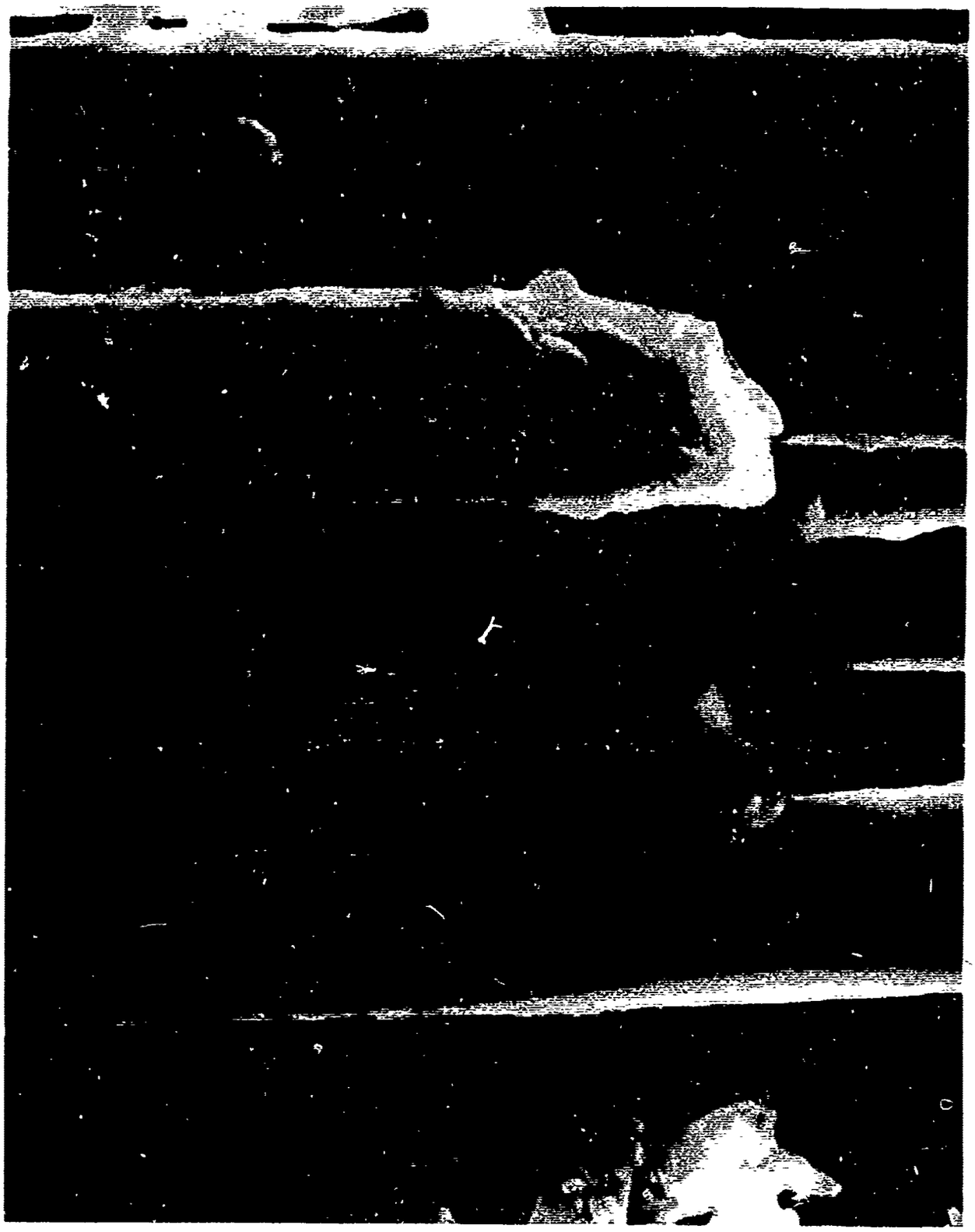




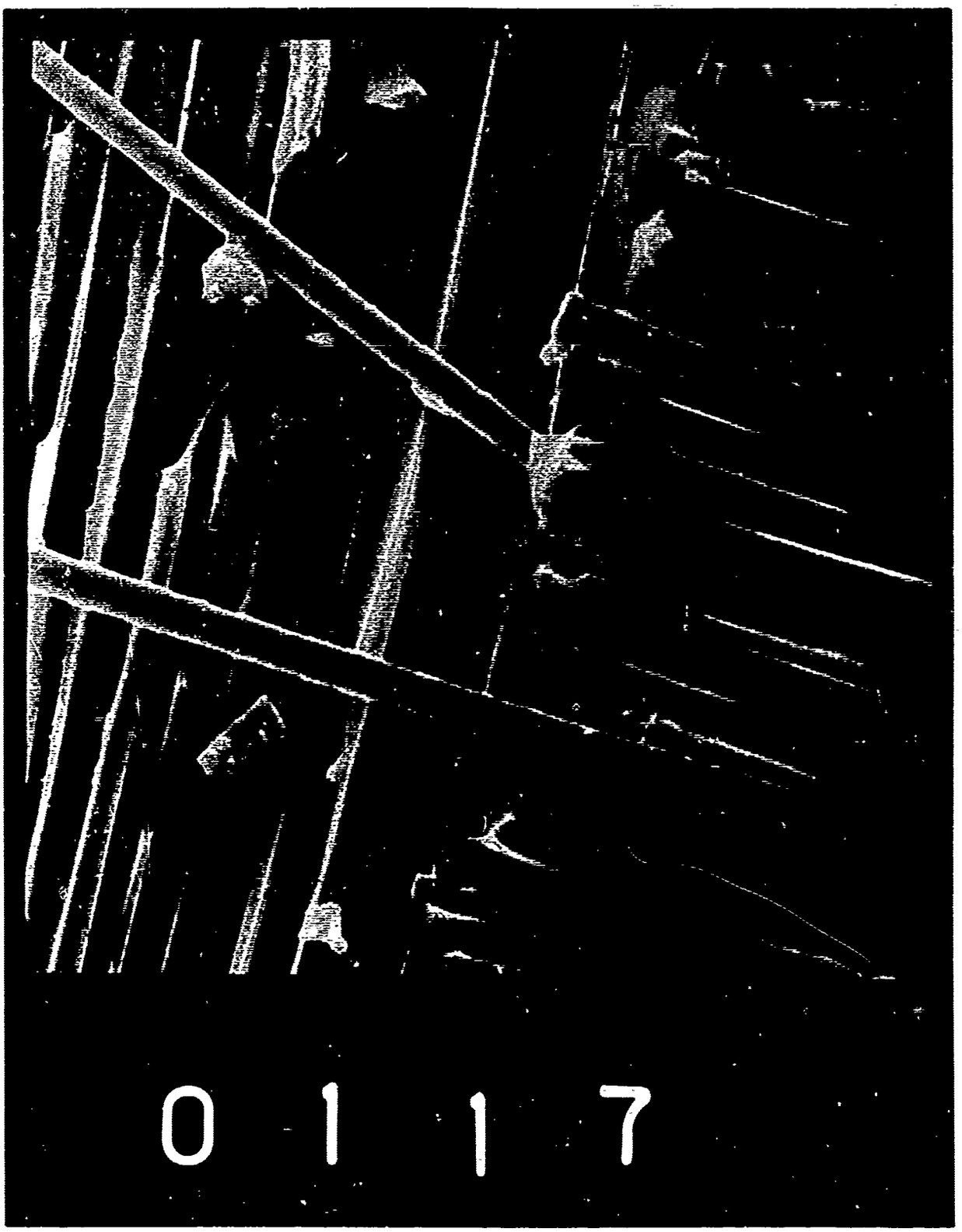


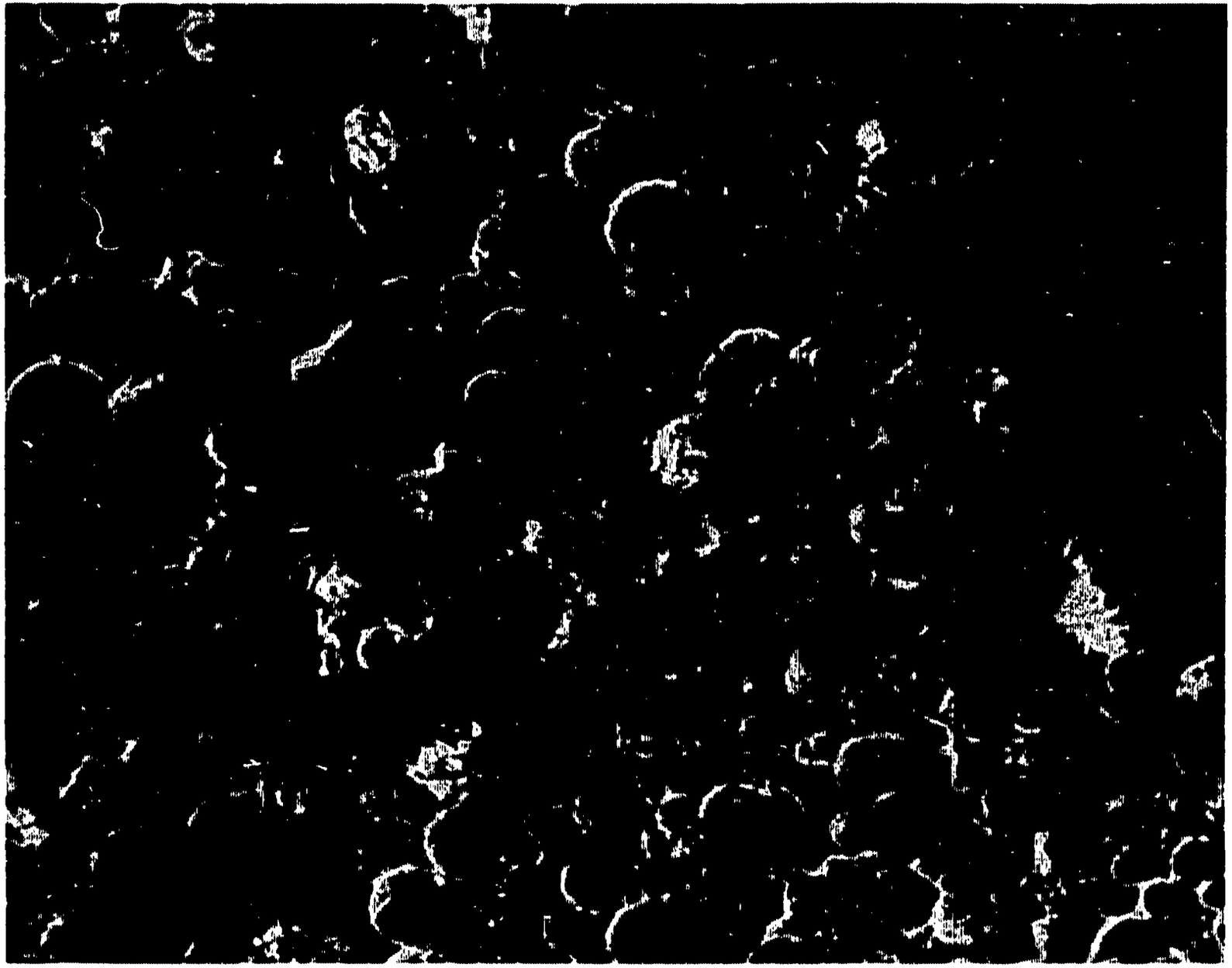




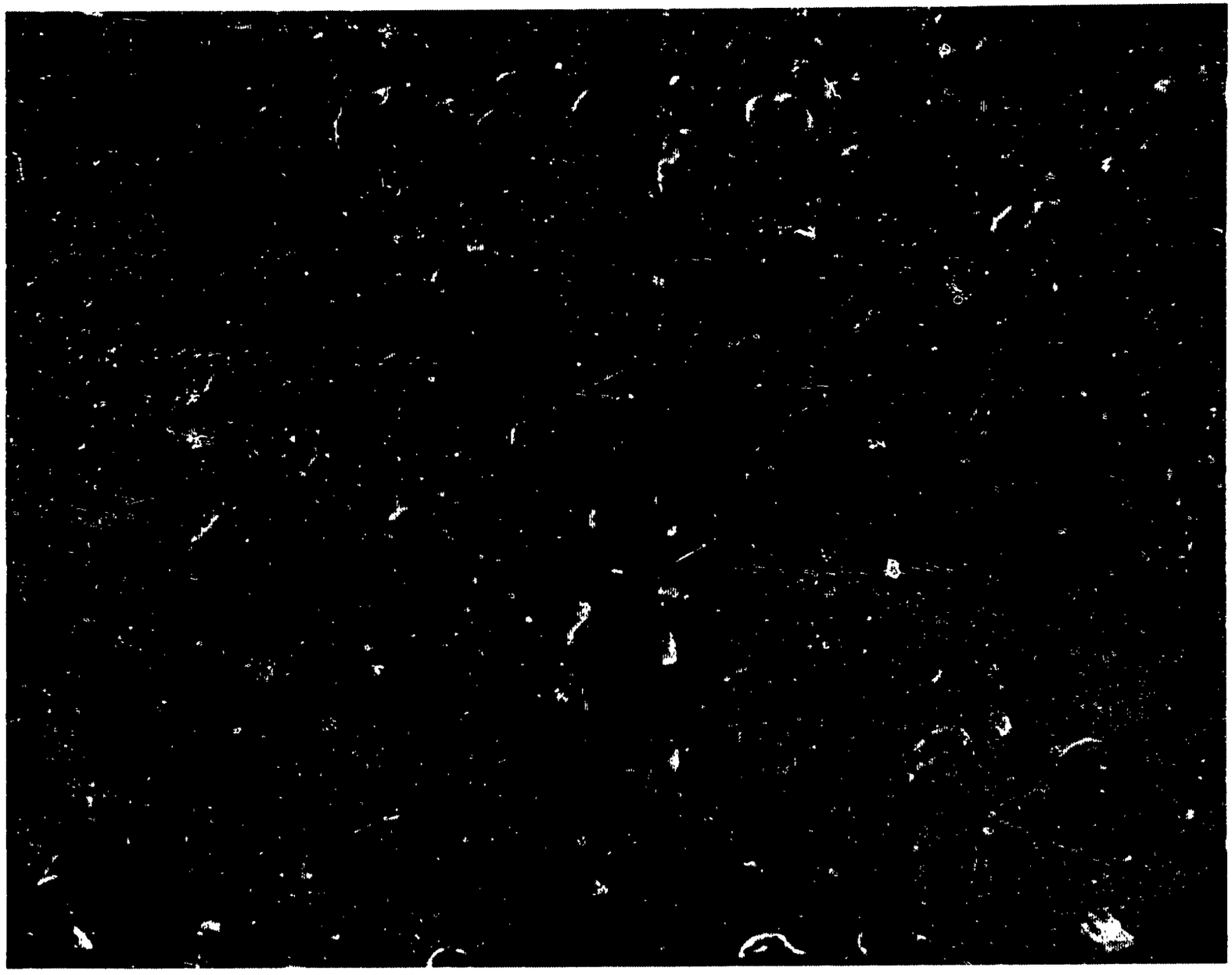





0117







ULTRASONIC INSPECTION TECHNIQUES

FOR

ADHESIVE BONDED COMPOSITES

by

William W. Mattson
Quality Control Department
Commercial Airplane Division
The Boeing Company
Seattle, Washington

For Presentation at the
Symposium on Nondestructive Testing
Dayton, Ohio
March 18-20, 1969

ABSTRACT

This paper discusses recently developed equipment and techniques for ultrasonically inspecting adhesive bonded structures in the Commercial Airplane Division of The Boeing Company. A unique scanning system presently being fabricated will be discussed including the solution to liquid coupling, recording, and parts handling problems. In addition, a new instrument will be described which performs ultrasonic through-transmission and contact inspection without liquid coupling. This paper will also briefly describe other research activities related to production adhesive bonded structures.

INTRODUCTION

The role of nondestructive testing in the Commercial Airplane Division of The Boeing Company for the inspection of adhesively bonded airplane components has become increasingly important in the past several years. There has been an enormous increase in the number and complexity of parts being fabricated as well as an increase in the reliability demanded of bonded structures. The growth of bonded structure usage on Boeing airplanes is shown in Table 1. This growth is well illustrated by comparing the 30,000 square feet being installed on the 747 with the 2,500 square feet used on the B-52, a 1200% increase. More than 1,000 assemblies are produced daily for the current production models, 747, 737, 727 and 707. Not only is this large quantity of major concern in the development of nondestructive testing methods, the variety of configuration poses additional problems. Materials include aluminum, titanium, fiberglas, and phenolic, both honeycomb and multiple laminates. Several adhesive systems are used. Sizes range from less than one square foot to over 100 square feet. Tapered trailing edge assemblies for control surfaces are common. The question then is how does one inspect this tremendous variety of parts and accomplish this inspection rapidly enough to assure an adequate sampling of the quantities produced? But even more basic than this, why consider nondestructive testing? For over ten years Boeing has produced bonded structures for their aircraft with few in-service problems. The answer to this question is cost. Present Boeing requirements call for periodic destructive tear-up of production assemblies to verify tooling. Replacing this practice with a nondestructive test would save thousands of dollars daily. An added advantage always associated with nondestructive testing is improved quality assurance which has justified a "shotgun" effort in which the most promising existing instruments were evaluated and new instruments and methods were developed. Thermal methods included infrared, liquid crystals, and heat-sensitive paper. Sonic instruments evaluated include: A Boeing developed tap-tester, Fokker Bond Tester, Sonic Resonator, Harmonic Bond Tester, Sondicator, and ultrasonic pulse-echo and through-transmission methods and equipment. Other investigations included evaluation of laser holography and the Porta-shear/Porta-pull devices. Effort is continuing in many of these areas and several new approaches are being actively researched.

The intent of this paper is to summarize the results of work accomplished to date and relate this to the inspection of nonmetallic fiberglas and phenolic adhesive bonded assemblies. Only those instruments and methods applicable to nonmetallic parts are discussed; to reiterate, these were evaluated as to their ability to:

1. Inspect a part quickly and economically.

2. Detect small defects regardless of location.

3. Accomodate many varieties and sizes of parts.

A brief summary of the applicable instruments and methods follows:

THERMAL METHODS

A Boeing engineer was the first to apply liquid crystals and heat sensitive paper for defect detection in certain adhesive bonded assemblies. These methods are reasonably sensitive to defects in certain structures, are highly adaptable to complex shapes, and provides rapid inspection capability for large structures. However, they are at times difficult to use and interpret and do not respond adequately to defects below the outer bondline. Evaluation of infrared equipment did not indicate any qualities noticeably better than these methods except for the elimination of part contact -- a definite advantage. However, the cost of equipment for high production capability was judged to be excessive and the method was not sufficiently adaptable to a variety of shapes and structures.

ULTRASONIC METHODS

Of the ultrasonic methods and instruments considered, the Sonic Resonator, the Sondicator, and the ultrasonic pulse-echo and through-transmission methods were judged worthy of further evaluation for nonmetallic structures. The following discussions summarize the respective evaluations.

Sonic Resonator

The Sonic Resonator, Figure 1, is a low frequency, continuous wave ultrasonic instrument developed by North American Rockwell. The piezoelectric probe is placed in contact with the part surface using a liquid couplant to provide adequate sound transmission. In most cases, the instrument is sensitive to defects throughout the depth of the parts by testing from one side. However, the advantage of one side inspection becomes a limitation when structural variations occur in the part. Tapered core, doublers and other structural changes cause up-scale readings on the instrument similar to void indications. The need to contact the part and use a couplant makes this method too slow and costly for production inspection. However, it has excellent capability for spot checking areas of bonded structure in the field.

Pulse-echo and Through-Transmission Ultrasonics

Ultrasonic pulse-echo is well known and has been used extensively for material inspection. Its advantages in adhesive bond inspection are found in its high sensitivity and its adaptability to rapid scanning and recording. The major disadvantage is the fact that its sensitivity is limited to defects just below the part surface, making it impractical for multilaminate structures.

Boeing has recognized the effectiveness of through-transmission ul-

trasonics for adhesive bond inspection for several years. It is the best method available for void detection through a multi-laminate assembly; it provides 100% automated coverage, and, with an automated scanning mechanism, it can provide a permanent recording. However, ultrasonic inspection by contact methods or automated scanning by immersing the parts or using wheel search units is not practical for production testing of odd shaped parts or assemblies too large or buoyant to submerge. Boeing's interest in through-transmission inspection increased when North American Rockwell successfully developed and applied water squirter housings and nozzles for inspecting the Apollo space capsule. These water squirters are capable of water path distances of 10 inches or more and have enough sensitivity to outline honeycomb cell structure on a C-scan recording. The development of quality water squirters has opened the way for practical production inspection of bonded airplane components. Accordingly, Boeing is procuring a through-transmission ultrasonic inspection system for research and production testing. This system, Figure 2, is designed for optimum versatility. Parts will hang from the center of the gantry or from an overhead rail system. The bridge can scan or index either horizontally or vertically and will inspect parts as wide as 14 feet with no limit on length. The system is self-contained and will travel along the floor using a guide rail to maintain alignment and recorder synchronization. A dry paper, facsimile recorder is used to provide a C-scan recording of each part. This system is expected to be in operation by May 1969.

Several aspects of this system are being investigated such as the effect of nozzle diameter and frequency on the transmitted signal, sensors to maintain a constant distance between the nozzles and test surface, multiple squirters to provide more rapid inspection capability and development of improved electronic and recording capability.

The most critical aspect of this inspection system is the transducers and water squirters used for sound transmission of which there is very little literature available describing their construction or performance. Therefore, an effort is in progress to optimize the water recirculation system, jet assembly configuration and the electronic and recording systems. Other accomplishments to date include:

1. The use of low frequency transmission (100-200Khz compared with the more commonly used 0.5 to 5 Mhz) has increased our ability to transmit sound through multilaminate and acoustically dampened materials.

2. The use of air jets above each water squirter to eliminate the momentary loss of signal caused by the water cascading onto the water column after impacting the surface of the test part.

3. Water jets have been designed that inject water into the squirter assembly parallel to the nozzle axis. This is accomplished by using an annular ring within the squirter with holes in the front and back to direct the incoming

water toward the nozzle tip and the transducer face. The water stream emerging from the nozzle appears to have less tendency to spiral over long paths when compared to the standard method of injecting the water normal to the axis of the probe body.

4. Inspection of assemblies with porous face sheets where water would normally penetrate into the cells can be ultrasonically inspected by either sealing the surface with a strippable coating or by placing the part in a vacuum bag.

5. Oil, grease and other contaminants in intimate contact with the test surface do not adversely affect the ultrasonic signal. It was originally thought that these contaminants would cause a loss of signal due to inadequate wetting of the surface of the part.

Upon delivery of this system, attempts will be made to adapt some of the other nondestructive testing methods such as the Harmonic Bond Tester, Sondicator and Sonic Resonator for use on this scanner. The implementation of automated inspection with through-transmission ultrasonics and other nondestructive testing methods will greatly enhance the quality control of adhesive bonded assemblies at Boeing.

Sondicator

The Boeing Company participated in the development of an air-coupled ultrasonic instrument with a local company -- Zetec, Inc. Our interest in this approach stemmed from the problems encountered in liquid coupling which would be eliminated by a device transmitting sound through the air. The developer was successful in producing such an instrument called the Sondicator, which has proven to have wider application and better sensitivity than was first anticipated. It operates in the low ultrasonic frequency ranges and employs transducers especially designed to reduce the impedance problems normally encountered when transmitting ultrasonic frequencies in air. It was designed for through-transmission inspection with the transducers up to several inches from the part surface. However, the developer also devised a contact probe for inspection from one side of a part. This probe consisted of two transducers, one transmitting and the other receiving, which detects unbonds when placed in contact with the surface. No liquid couplant is required.

In operation, the Sondicator, Figure 3, provides a pulsed sine wave signal to the piezoelectric transmitter, variable from 20 Khz to 40 Khz. Instrument controls allow for adjusting the repetition rate, pulse width, receiver amplifier gain and sample point. The received signal is amplified and displayed as a single dot polar display on the oscilloscope. This allows for simultaneous monitoring of phase and amplitude variations that occur at the sample point. Meters and flaw alarms were provided for monitoring the X and Y deflections on the scope.

The unique ability of this instrument to transmit ultrasound into a

part and detect it on the opposite side without contact or liquid couplant offers the first practical means for ultrasonic through-transmission inspection of bonded assemblies using an array of transducers to permit one-pass inspection. To demonstrate the feasibility of a monoscan inspection system, a prototype scanning bridge with a row of 18 pairs of transducers was successfully fabricated and tested. This apparatus was capable of detecting 1/2 inch defects over a 15 inch width in a single pass. A system capable of inspecting a 4 foot wide area of an assembly in one-pass is currently under development. This concept is shown in Figure 4.

Investigation to date has shown the Sondicator to be an extremely versatile instrument. It has successfully detected voids in metal-to-metal, metal-to-core, bonded fiberglas structures, silicone rubber bonded to aluminum, and other bonded materials.

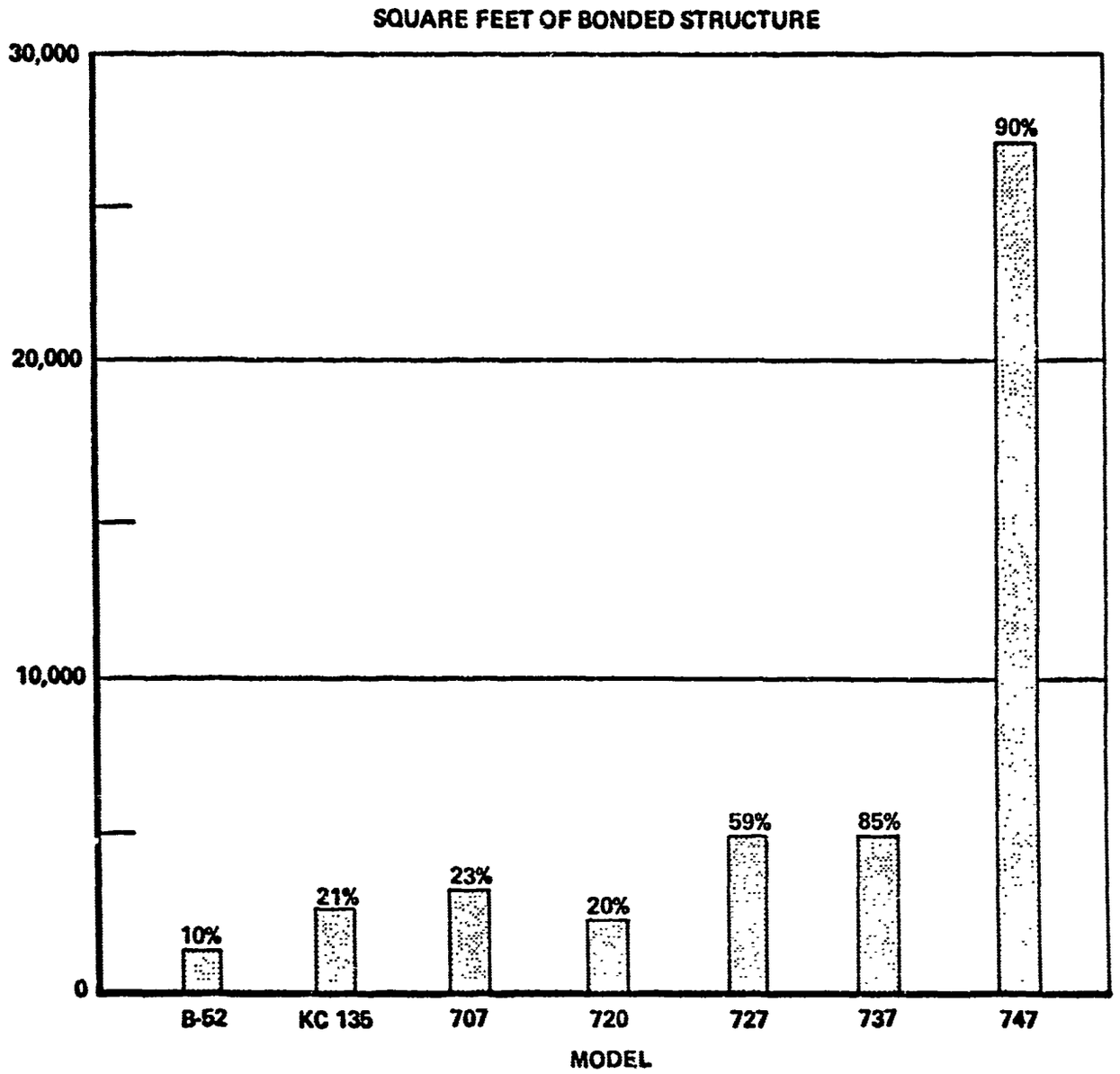
Most often no instrument readjustment was necessary during the testing of these various structures.

An extensive evaluation of the Sondicator is continuing on bonded production assemblies fabricated within Boeing. Work is also continuing on multiple probe arrangements, improved transducer designs to increase the capabilities of the instrument, and practical readout systems such as defect alarms, recorder adaptations, etc.

The eventual implementation of the Sondicator into production testing as a monoscan or wide-area scanning system potentially can reduce inspection time to the extent that a large part can be inspected in a matter of seconds. It has been shown that multiple probe scanning is feasible for many production parts.

CONCLUSIONS

Based on the Quality Control Research and Development studies at Boeing for nondestructive testing methods for adhesive bond inspection, it is felt that through-transmission ultrasonics using water squirters is the best and most sensitive inspection system available. Plans call for replacing much of the current destructive testing of production assemblies with this concept. Since scanning speeds with water squirters are too slow for routine production testing, the Sondicator with multiple probes for single pass inspection will be utilized for gross defect detection. Instruments such as the Sonic Resonator, Harmonic Bond Tester and Fokker Bond Tester show potential for in-service defect detection on the aircraft. Research is continuing toward more rapid automated inspection systems to support the increased production requirements for adhesive bond inspection.



GROWTH IN USE OF BONDED STRUCTURE

TABLE 1.

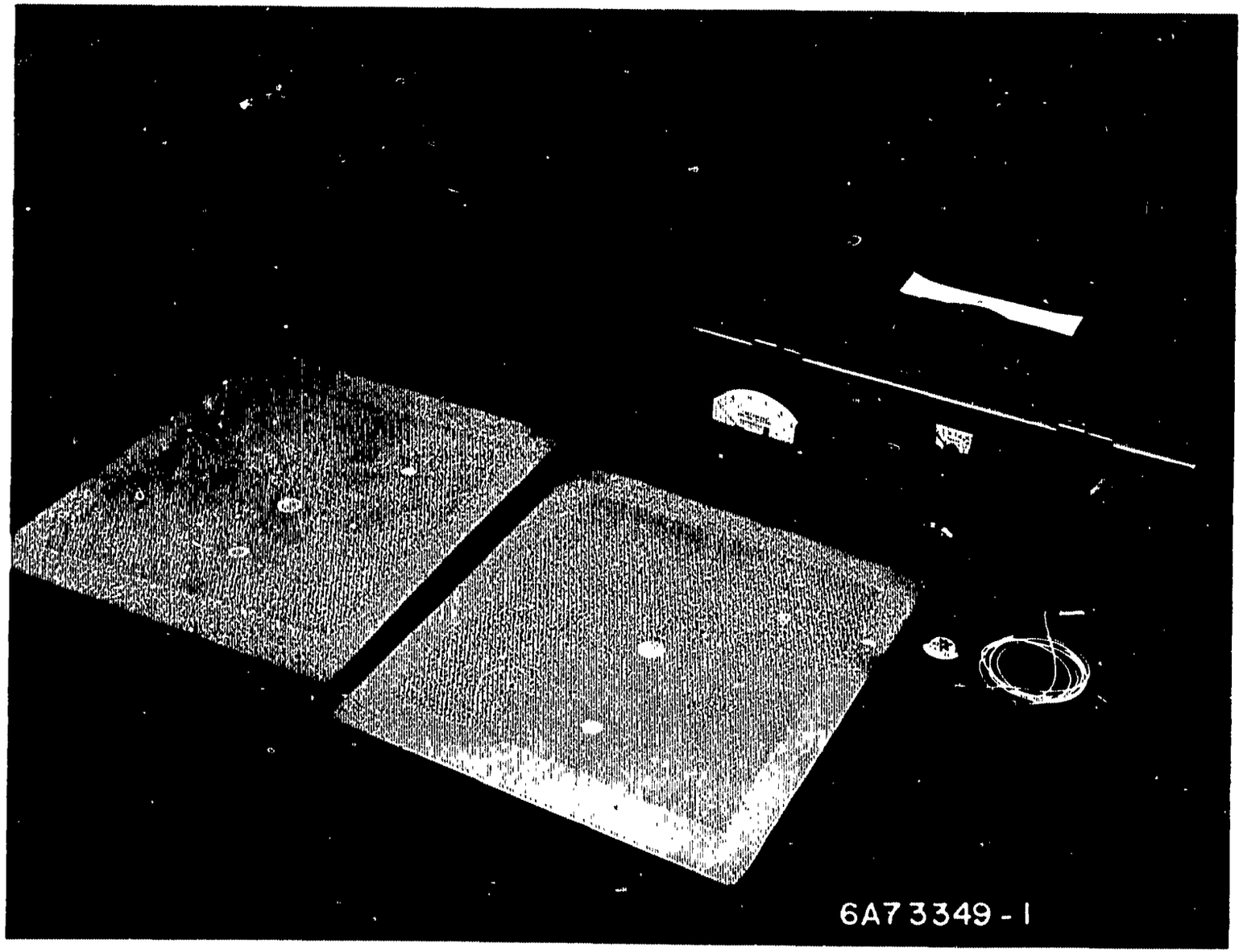


FIGURE 1. SONIC RESONATOR AND FIBERGLAS TEST PANELS

STRUCTURAL BONDING DEVELOPMENT
AUTOMATED ULTRASONIC THRU TRANSMISSION INSPECTION SYSTEM

CAPACITY-14' WIDTH;
UNLIMITED LENGTH

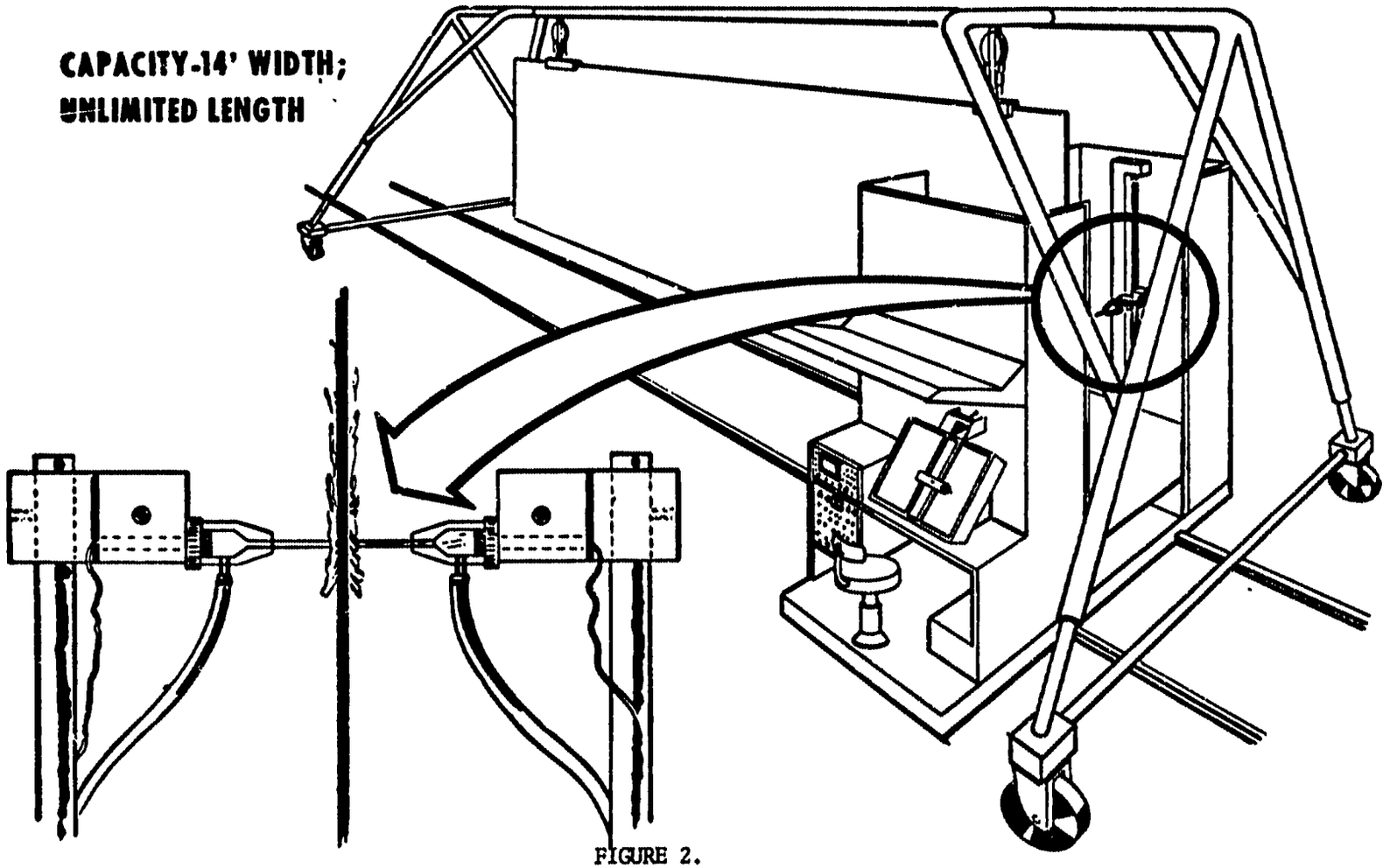


FIGURE 2.

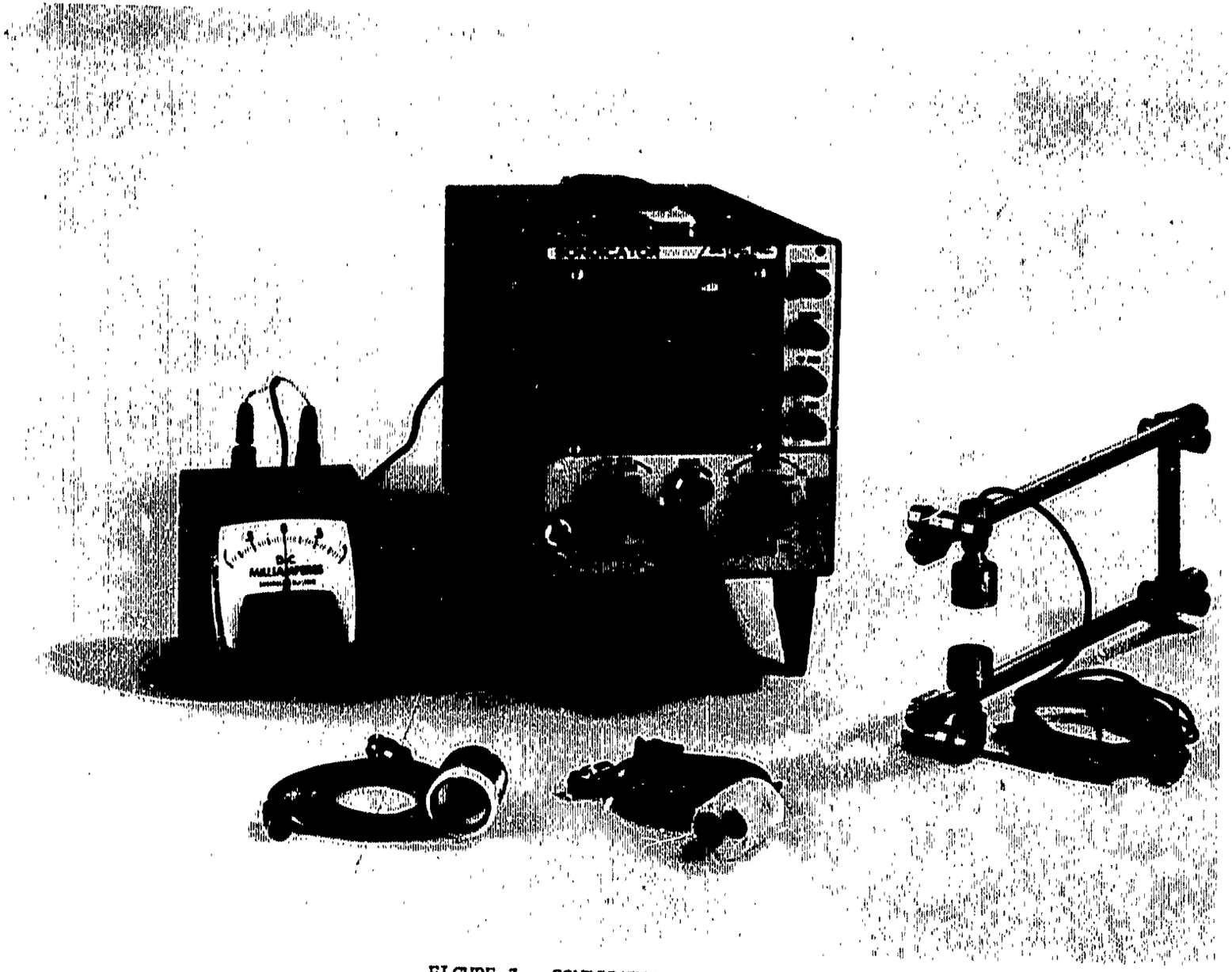


FIGURE 3. SONDICATOR AND PROBES

NONDESTRUCTIVE EVALUATION BY

SCHLIEREN METHOD OF ADHESIVELY BONDED STRUCTURES

Amos E. Holt
Test Engineer
Methods and Materials
Research Laboratory
Bell Helicopter Company
Fort Worth, Texas

A. S. Greer
Research Engineer
Automation Industries
Boulder, Colorado

March 18, 1969

NONDESTRUCTIVE EVALUATION BY

SCHLIEREN METHOD OF ADHESIVELY BONDED STRUCTURES

A Schlieren system is a precision optical and mechanical device for visually studying the effects of an acoustic wave propagating in a transparent media.

The concepts of the Schlieren visualization are not new, only the application of the system as an active tool in the field of Nondestructive Evaluation. One of the most valuable and irreplaceable aids to engineering is a visual representation of a system functioning under the actual conditions of usage. For some time Schlieren techniques have been employed in the observation of air-flow patterns established by test objects such as an airfoil section placed in a wind tunnel. More recently Schlieren techniques have proven useful in the study of ultrasonic wave propagation and sound beam behavior patterns. The Schlieren techniques were employed by Bell Helicopter Company to explain false ultrasonic indications in the inspection of main rotor blades. These indications were not found when the blades were destructively tested. The Schlieren system aided in the physical understanding of the phenomena which caused these indications. It is the application of Schlieren techniques in the field of ultrasonic Nondestructive Testing (N.D.T.) that will be discussed in this paper.

In the field of ultrasonic N.D.T., Schlieren techniques have proven to be of great value when used in the analytical study of acoustic wave behavior, ultrasonic inspection techniques, and as a training medium. The most obvious contribution of Schlieren techniques to each of these applications is the capability of visually observing the complete wave behavior pattern. The data obtained from this system provides an easier, quicker, and more accurate analysis of the problem as a whole. Other existing techniques require a series of data inputs which must eventually be pieced together to obtain the complete picture of the problem.

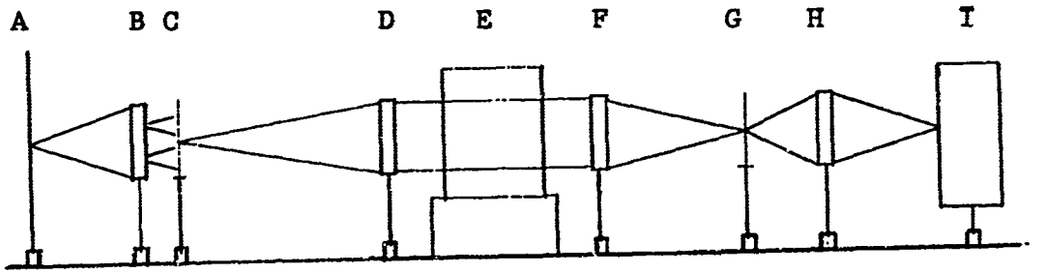
A general introduction to the concepts of ultrasonic Schlieren systems and its operation must precede the discussion of the application of Schlieren techniques.

Acoustical waves are stress waves and thus subject to reflection, refraction, diffraction, and interference. Although these phenomena are invisible, a beam of light passing through

a transparent medium will be influenced by the presence of an acoustical wave within the medium, which makes it visible. It is the influence of the acoustical wave that is viewed in a Schlieren image.

When free from external disturbances, water is a transparent medium having a uniform index of refraction. An acoustical wave propagating in water has regions of compression and rarefaction distributed along the axis of propagation. The water is compressed along the wave front such that the refractive index of the water is raised in the disturbed area. This causes regions of increased and decreased indices of refraction. The presence of an acoustical wave results in the diffraction of a collimated light beam passing through the water in the immediate regions of the differential pressures. This diffraction is called the Debye-Sears ultrasonic light diffraction phenomenon. A collimated light beam is passed through the water into a lens which focuses the light. This lens has a small diameter focal zone. A small opaque dot is placed in the focal zone to block the passage of the collimated light beam. This diffracted light travels in directions which are not parallel to the collimated light; therefore, it is focused at some point outside the primary focal zone on a view screen or photographic plate.

A Schlieren image may be displayed in two ways; as a dark field with the diffracted light visible by the use of a blocking dot, or, as a light field with the diffracted light absent by using an aperture. A diagram of an ultrasonic Schlieren system is illustrated in Figure I.



A - View Screen
B - Imaging Lens
C - Blocking Dot
D - Focusing Lens
E - Water Tank
F - Collimating Lens
G - Aperture
H - Condensing Lens
I - Light Source

FIGURE I

BLOCK DIAGRAM OF SCHLIEREN SYSTEM

It should be noted that the position of the lenses, aperture, and/or opaque blocking dot is critical. The relative placement of each is governed by the basic laws of optics.

The equipment, in addition to that shown in Figure I, required to produce a Schlieren image of an acoustical wave is a search unit, a pulse generator, which can adequately excite the search unit, and a suitable camera for obtaining permanent records. If the pulse mode of operation is required, a strobe light must be used as the light source and must be synchronized with the variable time delay circuit. The pulsed system affords the operator the capability of selecting a single pulse and observing this energy as it progresses with time.

Having thus discussed the general concepts of the operation of a Schlieren system, let us now consider some of the applications for which the Schlieren technique can be effectively utilized. We shall limit our discussion to the application of the Schlieren technique as (1) an educational tool, (2) an analytical tool, and (3) a tool for ultrasonic nondestructive testing. As an education tool, Schlieren techniques are used to demonstrate the basic fundamentals of wave propagation. This system provides a means of observing the real time propagation of an acoustical wave through a medium to an object, and the influence that that object has on the wave. The most interesting and far reaching application of the Schlieren system is its use as an analytical and developmental tool.

Let us consider the phenomena connected with the propagation of ultrasonic waves (reflection, refraction, diffraction, and interference), by placing in a transparent medium, specimens which are to be observed under the influence of ultrasonic energies. Energy absorption and velocity measurements can be made of these specimens. If opaque objects are utilized, the wave behavior pattern within the object cannot be observed, but from reflected and transmitted energies sufficient information can be obtained to determine characteristics of the media, i.e., the velocities of the different modes of wave propagation (longitudinal, shear, and surface). The relationship of the angle of incidence of a wave packet to the angles of reflection and refraction of the wave packet when incident on a media having different internal wave velocities is a statement of Snell's Law which we shall apply. By placing a section of a material in the tank of a Schlieren system and adjusting the ultrasonic search unit to the correct desired incident angle, the geometry of the entire wave pattern can be observed and measured. The angle of refraction of the wave within the material can be measured by noting the exit point

of the wave refracted through the test section. By Snell's Law and knowing the angle of incidence and the velocity of sound in water, one can easily calculate the velocity of sound within the material. With this information, perhaps even the material itself can be identified.

Physical methods of measuring absorption have not been consistent, and for this reason optical methods are employed. Knowing the necessary physical characteristic of the material (density, modulus, wave velocity, etc.), the energy absorption of the media can be determined. The amount of energy absorbed by the liquid must be known before another material can be immersed and tested. In ultrasonic inspection the complete absorption of energy in an area can be interpreted as a void or discrepant area in a bonded assembly. This interpretation is often invalid unless a complete understanding of the wave behavior in the media is known or can be predicted. In solids which are not transparent, the energy cannot be seen while in the part, but by basic mathematical expressions relating the incident, reflected, refracted, diffracted, and transmitted energies the necessary information is obtained to predict the behavior of the energy within the media. There are limitations to the visualization of energy in the Schlieren system with fluid media. There is an intensity at which the ultrasonic energy can no longer be seen by Schlieren methods. Thus, all the energy of a wave propagating in a media may not be observed. In changing the liquid media, the minimum intensity of energy in the media will change. The use of a pressure chamber and a gaseous media will allow the visualization of lower intensity energies. It will require less energy from the transducer or search unit to influence the media such that it can be observed.

The internal physical characteristics of materials such as steel and titanium may be observed by using ultrasonic Schlieren techniques. One of these characteristics is the accumulation of large, well-precipatated grain boundaries that are oriented in a preferred and pronounced direction. The boundary precipatated will appear as reflecting interfaces and, as such, will alter the path of the sound waves within the boundaries of the object. By impinging the sound wave on the object at a given incident angle in several different planes, and by obtaining a Schlieren image of the wave patterns resulting in each case, the angle of refraction of the sound wave within the object can be measured for each incident plane. Interpretation of these angles will indicate the presence of a preferred oriented grain boundary condition and simplify the approximation of the orientation direction.

Schlieren ultrasonics are presently being used by Bell Helicopter Company in the evaluation of bonded assemblies such as honeycomb panels and rotor blades.

Schlieren ultrasonics have been used to determine the paths through bonded assemblies to assist in the evaluation of new and better methods of ultrasonically testing the structures. In through transmission modes of ultrasonic testing the normality of the beam to the part becomes a problem especially when inspecting objects with complex configuration.

As previously mentioned, Schlieren techniques were used in the evaluation of false ultrasonic indications in rotor blades. These indications occured randomly and with no predictable sequence. It was determined this problem was due to an impedance resonance condition in the blade. The bondline thickness varies as a function of detail tolerances and fit. This changes the over-all impedance of the blade, thus, creating a one-fourth or one-half way phenomena in some blades. Although a solution for the problem has been determined, further evaluation of this problem is being continued in an effort to isolate this condition. The position of the indication with respect to the transmitter is critical for some indication. This has been determined a number of times in rotor blade ultrasonic inspection. It may be represented as shown by the work presently being conducted at Bell Helicopter Company on adhesive composites. The two photographs, Figure Nos. II-A and II-B, shows the incident energy on discrepant areas in the two laminates. The reflected and transmitted energies illustrates the discrepant areas of each laminate. In Figure No. II-A the reflected energy is interrupted and shows the defect more pronounced than in the transmitted energy. Except for different physical configurations, the indications in both photographs were of the same approximate size. As seen by the transmitter, the defect in Figure No. II-A was concave, and the defect in Figure No. II-B was convex.



FIGURE II-A

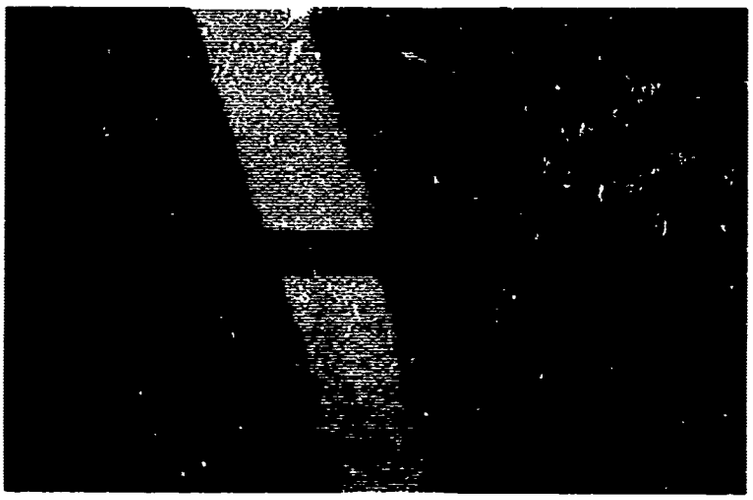


FIGURE II-B

This information supports the theory that in through transmission, specifically, ultrasonic inspection of bonded assemblies, a change in the location and position of the defect with respect to the transmitter can and does give different information to the receiver. The physical size of the rotor blade prevents the actual Schlieren image of this phenomena from being obtained with the present system. It may be necessary to scale down the object to obtain the information, or to section the part and observe a section at a time.

There are other fields of N.D.T. in which Schlieren techniques can be utilized. A simple example of this application would be when employed in the inspection of tubes. This is accomplished by observing the internal wave behavior patterns of a sound beam incident on a tube free of defects. The incident angle should be such that the sound energy is propagated along the periphery and internal section. This will result in a Schlieren image of the reflected and refracted sound energy as viewed inside the tube. The Schlieren image can be referenced as an acoustical signature of an acceptable tube.

When an unacceptable tube is placed within the Schlieren field, the internal defects of the tube will cause a behavior pattern that is different from the acoustical signature of the acceptable tube.

By comparing the acoustical signature of the standard with the wave behavior pattern observed from the tube being inspected, a decision as to acceptability of the tube can be made.

SUMMARY

This system is not a new N.D.T. system for production use, but the Schlieren system presents many possibilities to be used as a support system for training, for research, and for development.

One of the most valuable contributions of the Schlieren system, as previously mentioned, would be the physical observation of acoustic phenomena and wave behavior pattern. This allows the proper positioning of transmitter and receiver and affords the inspector a better means of understanding the results he obtains from a given system.

The application of ultrasonic Schlieren systems presents a means of better understanding the phenomena connected with the propagation of acoustical energy through a media.

NA-69-194

SERIAL NO.

NDT DEVELOPMENT FOR MEASURING ADHESIVE BOND STRENGTH IN HONEYCOMB COMPOSITES

J. F. Moore
Author

APPROVED BY

Geo. Martin
Program Manager

DATE 3.5.69
NO. OF PAGES

LOS ANGELES DIVISION OF NORTH AMERICAN ROCKWELL CORPORATION
INTERNATIONAL AIRPORT • LOS ANGELES, CALIFORNIA 90009 • TELEPHONE 213/670-9131

LOS ANGELES DIVISION
NORTH AMERICAN ROCKWELL CORPORATION

FOREWORD

This report presents a summary of development effort conducted under NASA Contract NAS8-20764 for the determination of bond strength in honeycomb composite materials. This report was presented at the Aerospace-AFML Conference on NDT of Plastic/Composite Structures sponsored by the Aerospace Corporation, Air Force Materials Laboratory and University of Dayton, March 18-20, 1969, at Dayton, Ohio.

ABSTRACT

This paper describes a program to develop NDT instrumentation for the determination of bond strength of adhesive in honeycomb materials suitable for large tankage such as the Saturn S-4B and SV vehicles by means of an analytical and experimental program relating the variation in viscoelastic properties of an adhesive to the cohesive bond strength of the adhesive. The adhesive damping data predicted that the composite vibrational response amplitude would decrease with elevated temperatures, and the relaxation character of the degraded adhesive would show a smaller activation energy. Vibration analysis measurements verified that the damping of the adhesive was related to the cohesive bond strength by determinations of the internal friction at the fundamental and harmonic frequencies of the relative vibration response peak amplitudes. The development of a nondestructive test system is described for measuring the damping in adhesive bonded honeycomb composites. Measurements on composite specimens at various temperatures showed a frequency-internal friction relationship which clearly distinguished differences in cohesive bond strength.

DESCRIPTIVE TERMS

Cohesive Bond Strength
Adhesive Joint
Honeycomb
Nondestructive Test
Vibration Analysis
DOT (Displacement Oriented Transducer) System

NDT DEVELOPMENT FOR MEASURING ADHESIVE BOND STRENGTH IN HONEYCOMB COMPOSITES

by

J. F. Moore
Materials and Producibility Laboratory
Los Angeles Division
North American Rockwell Corp.

For Presentation at the
AFML Conference on NDT of Advanced Plastic/Composite Structures
Dayton, Ohio
March 18, 1969

ABSTRACT

This paper describes a program to develop NDT instrumentation for the determination of bond strength of adhesive in honeycomb materials suitable for large tankage such as the Saturn S-4B and SV vehicle by means of an analytical and experimental program relating the variation in viscoelastic properties of an adhesive to the cohesive bond strength of the adhesive. The adhesive damping data predicted that the composite vibrational response amplitude would decrease with elevated temperatures, and the relaxation character of the degraded adhesive would show a smaller activation energy. Vibration analysis measurements verified that the damping of the adhesive was related to the cohesive bond strength by determinations of the internal friction at the fundamental and harmonic frequencies of the relative vibration response peak amplitudes. The development of a nondestructive test system is described for measuring the damping in adhesive bonded honeycomb composites. Measurements on composite specimens at various temperatures showed a frequency-internal friction relationship which clearly distinguished differences in cohesive bond strength.

INTRODUCTION

Previous deveopment programs have resulted in the development of reliable industrial instrumentation for the detection of bond/debond conditions in adhesive bonded honeycomb materials. These investigations have also shown the need for a method suitable for determining the actual or relative bond strength of such structures in cases where a bond exists. The primary objectives of this program were the development of a systematic approach to the measurement of adhesive bond strength, thorough investigation of a generalized conceptual model and the development of an industrial applicable NDT system.

TECHNICAL APPROACH

The failure of an adhesive bond generally occurs by a failure through the adhesive rather than at the interface between the adhesive and facing sheets or honeycomb core when proper manufacturing processes are employed. The failure through the adhesive was defined as cohesive failure, to distinguish it from adhesive failure, which is failure of the interface. The development problem was therefore to find a physical property of the adhesive related to cohesive strength. General tests on organic adhesives show that under stress they act as viscoelastic solids, and their response to an applied stress is time dependent. This effect is characterized by frequency (f) dependent peak of the internal friction tan δ according to the relation

$$\tan \delta = K f t/(1 + f^2 t^2)$$

where t is the relaxation time.

The internal friction is proportional to the energy dissipated per cycle of vibration; the maximum occurs when ft = 1. A curve plotting tan δ against ft will peak at this point, figure 1A. From the shape of this curve and the frequency dependency, it was considered that the underlying hypothesis of a Zener relaxation process was evident in a series of vibration tests on lap shear, figure 1B. With a greater internal friction, the adhesive absorbs more energy and is, therefore, a measure of its cohesive strength. It was, therefore, considered that honeycomb composite vibration tests should also show nondestructively a relationship between the adhesive bond strength of an adhesive and its internal friction.

A development plan was established for the following related and interdependent tasks:

a. Determination of the material properties of the honeycomb composite constituents and in particular the cohesive strength damping properties of the adhesive.

b. Mathematical analysis to define the interrelations of adhesive properties and their effect on the resonant frequency and damping of the composite including such parameters as the bond's viscoelastic properties, core stiffness, flexural stiffness of the face sheets, and thickness of the bond layer.

c. Preparation of representative composite specimens of varying cohesive strength to provide a test criteria for NDT system evaluation.

d. Vibration spectrum analysis to determine the elastic properties of the composite and deviations due to variations in cohesive strength with concurrent test method development.

MATHEMATICAL ANALYSIS

A comprehensive mathematical analysis of the vibrational response was conducted to: a) reliably determine the interrelationships of the elastic properties of the honeycomb composite, b) determine the viscoelastic properties of the adhesive, considered to be the primary damping contributor, and c) determine the composite vibrational response characteristics i.e. frequency, amplitude, etc. Experiments had shown that for composites having small honeycomb cells as compared with the transducer size, that the honeycomb core could be substituted by a continuum representing the core properties and the adhesive was assumed to act evenly over its surface. A mathematical model was developed and analyzed in terms of loading and effect. The adhesive which is viscoelastic in nature was expected to behave as a standard linear solid and was expressed as frequency-time dependent parameter. Relations were similarly developed for the core and facesheet materials and expressions were formulated relating applied stress to deflection and in turn to the vibration behavior of the honeycomb composite in terms of resonant frequencies, the shape of the frequency spectrum, and the maximum displacement of specific vibration modes. Briefly, the mathematical analysis showed that the resonant frequency was dependent on the geometrical configuration of the composite and the component metallurgical properties. The amplitude of deflection and half-band width was dependent on the damping of the composite components. The mathematical analysis was successful in defining the design criteria for a vibrational NDT method in terms of driving stress deflection magnitudes, and the resultant response frequency range. These parameters were initially verified in the preliminary development of the DOT Vibration Analysis Test System.

ADHESIVE PROPERTY MEASUREMENTS

Adhesive Rod Specimens for Damping Measurement

Adhesive specimens were prepared in rod form for damping determinations with an internal friction spectrometer. The specimens were prepared in block form by laying up 6-700 pieces of 2 by 2 inch HT-424 type III adhesive film and bonding in a restraining die, figure 2. The specimens were then machined to 1/4 inch diameter by 5 inch lengths. The essential feature of the spectrometer is the fact that it holds the specimen in oscillation at its resonant frequency and at a preset strain amplitude, regardless of the energy dissipated in the specimen, and measures the internal friction of the specimen through a measurement of the driving force necessary to maintain the preset amplitude. Consequently, the instrument permits continuous measurements of the specimen resonant frequency and hence Young's modulus.

Damping measurements on three adhesive specimens cured at a different temperature (200F, 250F, and normal bond of 350F) generally confirmed that the adhesive behaved as a "standard linear solid" for which the frequency resonance and elastic modulus vary with adhesive strength, figure 3A and 3B. Further, it was shown that the adhesive damping was directly related to test temperature, figure 3C, and in turn to bond strength.

Honeycomb Composite Specimens

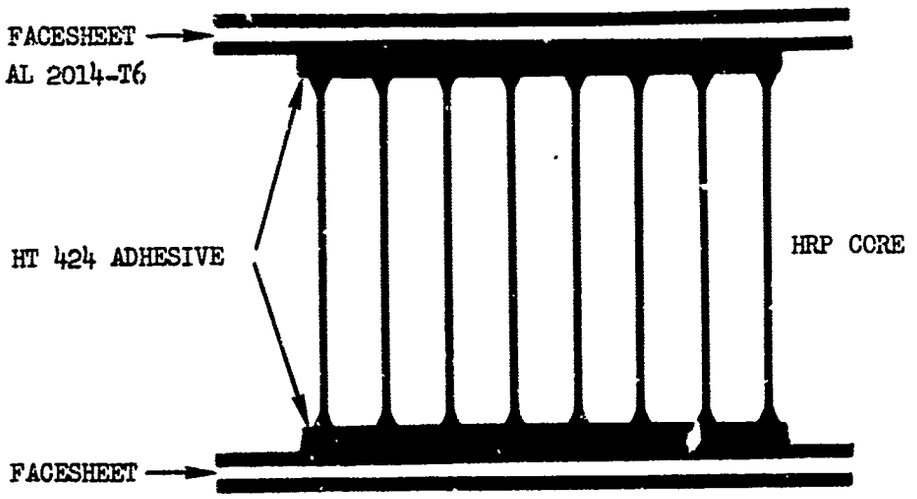
An empirical approach was followed for deliberate degradation of honeycomb composites of the type used in the Saturn common bulkhead. Various degrees of preaged adhesive film were used to simulate bond strength levels. Figure 4 shows that the bond degradation was successful and that a desired level of bond strength could be achieved with reasonable certainty. The fracture stress-time relationship was not linear and some degree of deviation was expected due to the chemical nature of the adhesive cure cycle. A significant variation in tensile strength values (from ± 50 to ± 100 psi) was noted for coupons cut from the same specimen. This variation was considered high but in accord with the manufacturer's test results.

Based on this degradation data, a series of honeycomb specimens were fabricated with varying bond strength values at either one or both of the honeycomb adhesive layers. To ensure reliable correlation, all specimens were prepared at one time using identical procedures and the same bulk material stock. A tabulation of the specimens fabricated to date is shown in table 1. The bond strength data are nominal design values as verified by destructive test data obtained from specimens cut from the same panel; however, due to the data spread in these types of tests, exact values were obtained for specific NDT areas.

Table 1

SPECIMEN DESIGNATION	FACESHEET THICKNESS	CORE THICKNESS	CELL SIZE	AVERAGE STRENGTH (PSI)
A	0.063	4.75	3/16	603
B	0.063	4.75	3/16	540
C	0.063	4.75	3/16	515
D	0.063	4.75	3/16	401
100	0.02	4.75	3/16	671
50	0.02	4.75	3/16	555
25	0.02	4.75	3/16	256

All dimensions in inches



NDT SYSTEM DEVELOPMENT

The mathematical analysis showed that a method of measuring the cohesive bond strength of an adhesive composite should determine either the resonance response amplitude or halfband-width and that measurement must be performed under controlled structure geometry conditions including boundaries, supports, transducer contact, etc., as well as controlled frequency, temperature and driving force parameters. Using the mathematical model, typical driving force levels were required in the order of 0.1 to 1 psi producing deflections of the order of one to 10 microinches for the Saturn type honeycomb composites. The frequency test range calculation was based on the boundary conditions established by the size of the honeycomb cells. The high frequency response was approximately 100 kHz for a 3/16 inch cell and 1 kHz for a 3/4 inch cell. The number of cells affected by the degrading adhesive determined the low frequency response. Therefore, the frequency range was defined for this investigation from several cycles to above 100 kHz. Further, since resonance and vibration analysis methods were used to determine the elastic properties, absolute measurements were complicated by the fact that contact type transducer measuring techniques could cause response deviations or change the nodal patterns within the structure causing the actual response to be obscured. Therefore, pseudo boundary conditions due to transducer fixturing and structure support required exacting analysis and control.

The DOT system employed a transducer with coaxially mounted electromagnetic driver and displacement sensor capable of differentiating between the vibrational responses of widely differing bond strength honeycomb composites. In general, the honeycomb composite frequency responses occurring below 0.8 kHz were affected by specimen supports. Response peaks at approximately 1.3, 1.9 and 2.5 kHz were characteristic of the composite damping properties exclusive of the effects from support geometry variations. However, the lower frequency peaks were considered equally representative of the composite damping properties as long as the geometry variables were carefully controlled.

The response vibration amplitude was expressed in terms of damping as

$$A = KF/\delta$$

where K is a proportionality constant, F is the excitation force and δ is the damping factor. For the electromagnetic type DOT transducer,

$$A = Ki_o^2/\delta$$

Therefore, the damping factor may be determined from vibration resonance measurements by either a direct measurement of the peak amplitude response by plotting A vs i_o^2 yielding the slope of the line (S) is equal to K/ or 1/S. Further, it was shown that

$$\frac{A_1}{A_2} = \frac{F_1}{\delta_1} \cdot \frac{\delta_2}{F_2} = \frac{\delta_2}{\delta_1}$$

since the drive force is maintained constant for comparative measurements. Other forms of excitation were considered a high energy, high frequency air pulse generation system was developed and evaluated. The air pulser utilized a Laval nozzle to produce supersonic airflow which was chopped at varying rates to produce a 0 to 20 kHz excitation source.

Displacement Oriented Transducer (DOT) System

The Displacement Oriented Transducer (DOT) System, figure 5 is basically a vibration analysis method capable of producing high level, automatically variable frequency excitation forces in a metallic structure and detecting microinch displacements and providing vibration response recordings. The simplified block diagram shown in figure 6 illustrates the major components including a swept frequency source and power amplifier driving an electromagnetic transducer. Excitation levels are available up to 15 amperes at 30 volts over the 10 Hz to 20 kHz frequency range. An operational amplifier is used to compare the input sine wave signal with a feedback signal proportional to the transducer current to correct for coil impedance changes and ensure constant current drive over the operating frequency range. The driver transducer can produce force levels of approximately 8 psi in the aluminum facesheet materials at the high excitation levels. The vibration response detection system uses a commercial fiber-optic displacement instrument with a displacement amplitude of 5 microinch/mv over a dc to 40 kHz frequency range. The fiber-optic probe, figure 7, was accurately positioned coaxially in the excitation transducer. The displacement instrument was modified to provide an amplified and demodulated ac output proportional to the measured dynamic displacement amplitude. The displacement signals were monitored directly on a cathode ray type spectrum analyzer and/or plotted on an X-Y recorder as a function of the excitation frequency. This system provided an automatic recording of the dynamic frequency response of the structure. Other system components included an auxiliary heater-controller system, temperature recorders and indicators, and a digital frequency counter.

Operation of the DOT system is based on the comparative vibration response measurements on composite materials of known strength properties and system calibration of the strength deviation from the norm in terms of either a resonance response amplitude, frequency or half band-width measurement. The DOT transducer is operated either noncontact or supported

on the composite with varying sized rings or three point contacts. The composite is swept frequency driven at selected excitation levels until a significant response is indicated. Particular frequency resonances related to the geometry effects of the test system are ascertained and only these resonances associated with the damping of the composite are measured.

Vibrational response measurements using the DOT system were carried out at elevated temperatures using two approaches a) the entire specimen and DOT transducer assembly were thermally cycled in an oven and b) the specimen was maintained at ambient with the local surface area heated by the DOT transducer exciter coil by eddy current heating supplemented by an auxiliary resistance type heater.

Oven Tests

The low frequency response data for fourteen tests are shown in figure 10 and in figure 11. It was noted during the test that particular frequency peaks shifted with temperature and the data were plotted by comparing the amplitude of the same frequency peak in each specimen response. It is evident that the low frequency response peak amplitude in the 150 to 160 Hz range increased significantly with increasing temperature tests. It was further evident that an optimum test temperature could be selected in the 130 to 160°F range giving an amplitude test range of 200 to 250 milivolts.

Increasing the excitation current from 5 to 10 amperes increased the amplitude range to approximately 0.1 to 1.0 volts. A comparison of the expected temperature relationship shown in figure 8 with the general trend in figure 9 shows the predicted spread in bond strength data for the different specimens. The predicted adhesive damping-temperature relationship was confirmed.

The high frequency response data for the same specimen test series is summarized in figure 10. The data were plotted using response frequency peaks at approximately 1300 Hz. The same bond strength data relationship was evident with a lower response amplitude. The frequency changes for the four specimens are shown in figure 11 and represent another means of differentiating between good and degraded composites.

The elevated temperature tests performed in the oven showed conclusively that the DOT vibration response and analysis method of determining bond strength was a practical means. This method alone would suffice for testing composite materials of suitable size or configuration where either the entire structure or selected areas could be environmentally heated to test temperatures, however, the applicability of this method for complex structures such as a Saturn vehicle was considered limited. Therefore, the DOT system was evaluated for one sided self-heating capability.

Self-Heating Tests

This evaluation was conducted under laboratory environmental conditions with the DOT transducer driver employed to heat a local area of the composite by eddy current effect and supplemented by a guard-type resistance heater integrally mounted around the DOT periphery. The heated area was approximately 6 inches in diameter, and tests were conducted at intervals of 10 to 15 minutes allowing temperature stabilization of ±2°C.

In considering the transition from the oven tests, a preliminary evaluation showed that clamping was not necessary for damping measurements above 0.8 kHz. Further, the application of heat from only one side of the composite reduced the response peak amplitudes by approximately 25 percent, which still permitted a reasonable signal-to-noise level.

The same specimen series tested in the oven evaluation were retested. The measurement method included a frequency scan to determine response frequencies related to the composite properties and unaffected by the specimen geometry or support. Vibration response measurements were made at four or five temperatures after thermal stabilization. The response peak amplitudes were recorded as a function of frequency at 5, 7, 10, 12.5, and 15 ampere driving coil current.

The peak response amplitude data at 15-ampere drive were plotted as a function of bond strength as shown in figure 12. The amplitude-strength relationship is in accord with the previous oven test data and shows a proportionately increasing response amplitude with increasing strength. Figure 13 also shows the response frequency dependence with strength as predicted and as observed in the oven test data. It was therefore concluded that the transition from the oven tests to laboratory self-heating conditions was successful.

It is worthwhile to examine the test results of oven and laboratory DOT in terms of the damping characteristics determined for the adhesive rods. According to the adhesive damping characteristics, it was expected that the vibration amplitude of high cohesive strength composite at resonance would be larger than that of a low-strength composite under the same conditions of stress drive since the amplitude of vibration at resonance is proportional to the driving force and inversely proportional to the damping. Therefore, since the adhesive damping was considered to be the dominant contribution to the total composite damping, the vibration amplitude was expected to decrease with increasing temperature; at any one temperature, the amplitude of vibration was expected to increase with increasing bond strength since the damping characteristics are displaced to higher temperatures with increasing bond strength.

This amplitude increase is based on the fact that the relaxation time for adhesive deformation increases as the adhesive cure proceeds to completion. The adhesive damping at lower temperatures is smaller, thereby minimizing the differences between the vibration amplitudes in the high- and low-strength composites. In addition, the slope of the resonant frequency versus temperature plots for the composites was expected to also show the influence of cohesive bond strength since the adhesive rod-damping characteristics shown were apparently the low-temperature slope of the relaxation maximum. At the damping, the modulus of the material goes from an unrelaxed state and is commonly known as the modulus defect typical in all mechanical relaxation mechanisms. This "defect" always corresponds to a lowering of the modulus and is superimposed upon the normal temperature dependence of the resonant frequency. Thus, at a given measurement frequency, this effect occurs at lower temperatures for the lower strength specimens, and the average slope of the resonance frequency versus temperature curves should be larger for the low-strength bonds than for the high-strength bonds. The DOT development was premised on the fact that the measurement frequency and temperature scale were selected so that the maxima in the damping curves occurred at the higher temperature condition. The test results for the oven and laboratory DOT tests agree with the above analysis and conditions. It was concluded that the measured response amplitudes of the composites were controlled primarily by the adhesive, and that a good correlation of nondestructive test and cohesive bond strength was established for both the damping and resonant frequency properties. It was a little surprising that the effects show up in the resonant frequencies since the adhesive contribution to the modulus was expected to be small; however, the modulus defect of the adhesive is apparently large enough to contribute significantly to the measurements.

CONCLUSIONS

The DOT vibration analysis has shown that semiquantitative cohesive bond strength measurements are practical under elevated temperature conditions. The mathematical model accurately predicted the need for control of geometry, driving force and temperature. The DOT System verified the conditions by direct measurement of each parameter and its effect on the determined values or cohesive bond strength.

The DOT measurement method included two forms of vibration response amplitude determination and a vibration response band-width determination. The data from all three methods show excellent agreement, although the amplitude-force measurement method is considered potentially the more

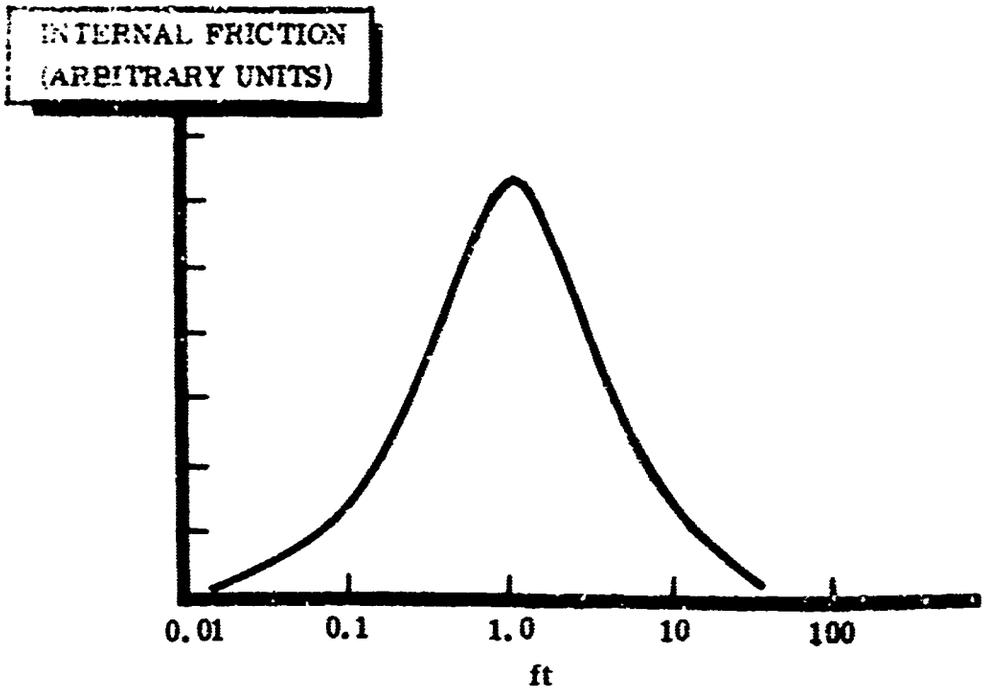
promising since the technique permits direct normalization of the damping data between measurements on a single specimen or between similar specimens designed to have comparable or even dissimilar materials as long as the measurements are made at resonance. Further, materials with varying geometry such as the tapered Saturn bulkhead can be tested by absolute comparison of the amplitude response data from either thin or thick sections.

It is therefore concluded that the DOT System is fundamentally established as a practical method for determining cohesive bond strength. In its present state of development it is a useful laboratory model for semiquantitative measurements. The final system development for production type applications must depend on further material characterization and system optimization for particular test conditions.

ACKNOWLEDGEMENTS

The effort described in this paper was conducted by North American Rockwell Corporation, Los Angeles Division, under Contract NAS8-20764 for the George Marshall Space Flight Center, NASA. The work was administered under the direction of Mr. Wayman N. Clotfelter, Propulsion and Vehicle Engineering Laboratory, Materials Division, George Marshall Space Flight Center. The author expresses his appreciation to Mr. Clotfelter for encouragement and permission to disseminate this information, and to Dr. George Martin, Program Manager, whose guidance and personal research were combined to make the program successful, and Dr. D. Thompson for the damping analysis and adhesive testing.

A. FREQUENCY DEPENDENCE OF INTERNAL FRICTION



B. INTERNAL FRICTION RELATIONSHIP TO BOND STRENGTH

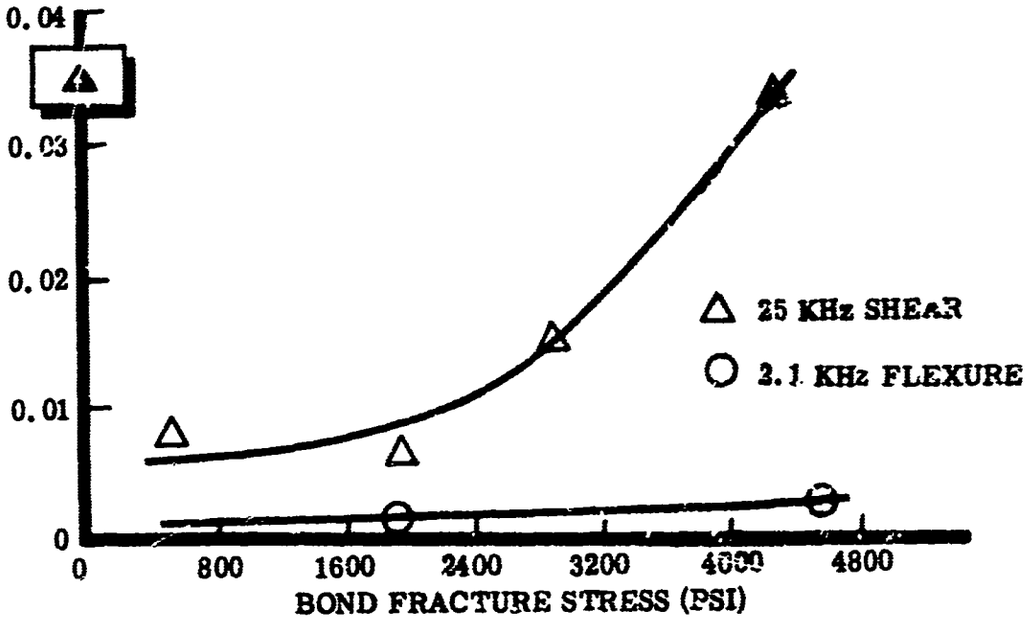


Figure 1. Internal Friction Relationships

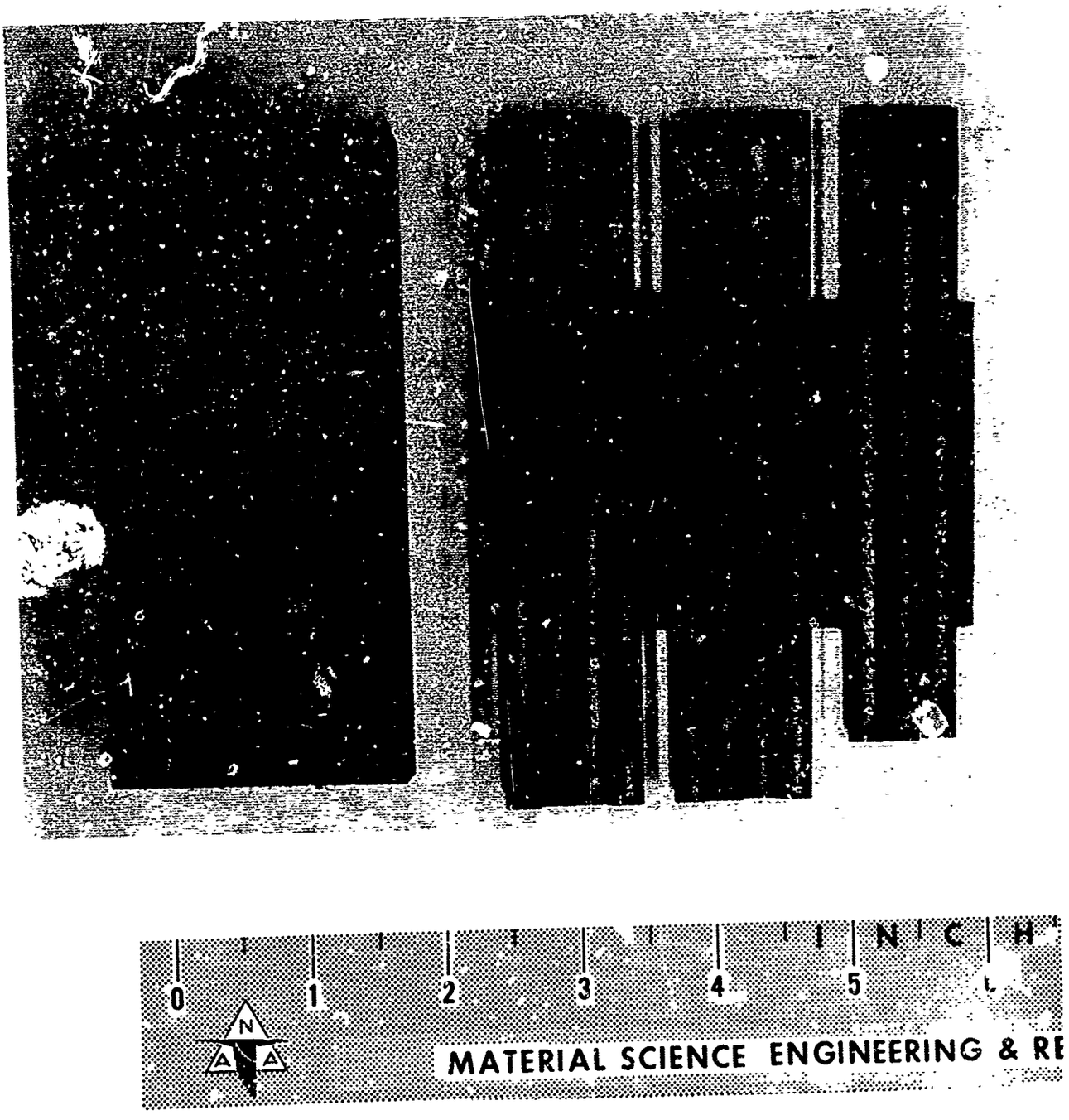


Figure 2. HT-424 Type Adhesive Specimens for Damping and Tensile Testing

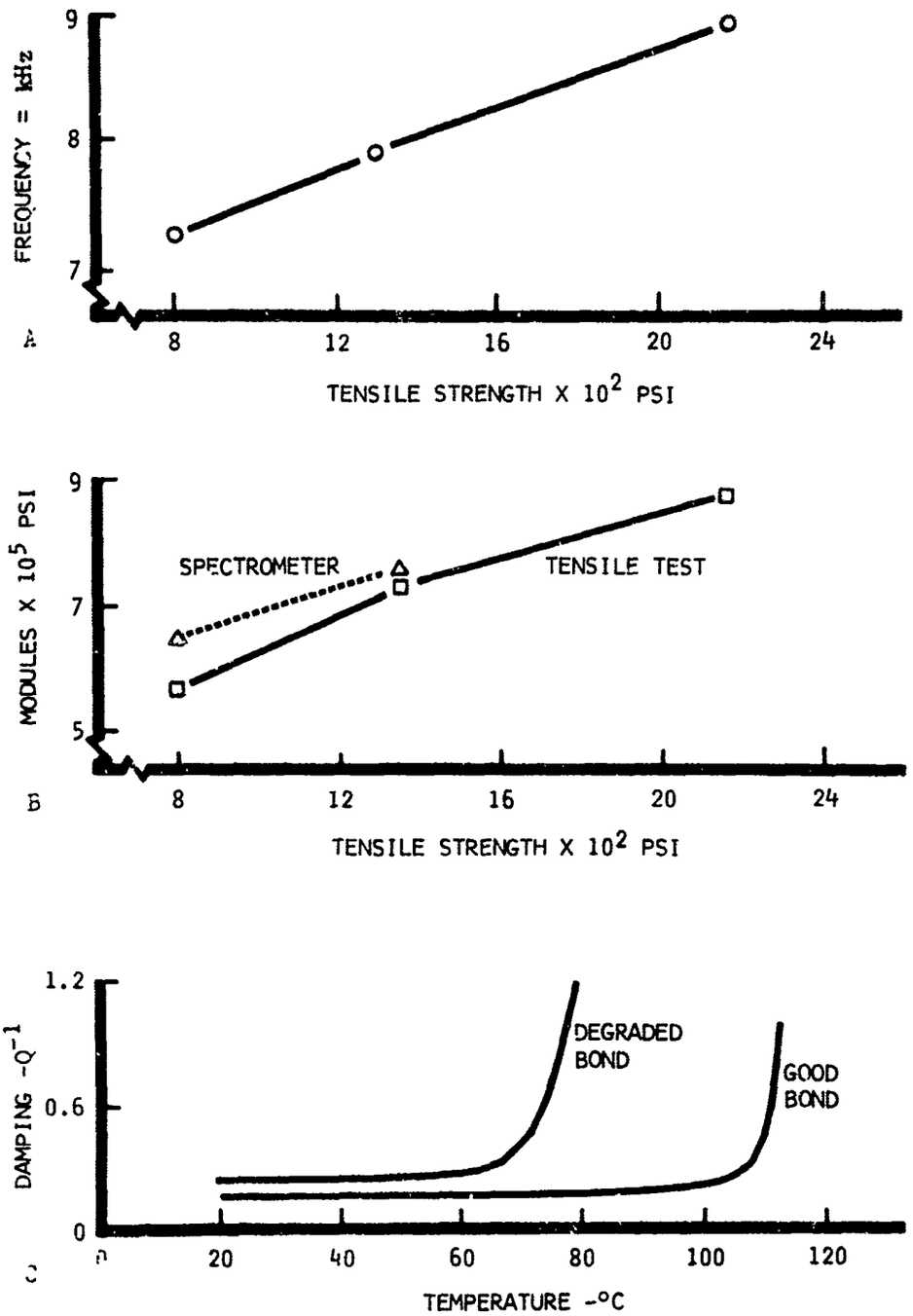


Figure 3. Internal Friction Spectrometer Data for Bloomingdale HT-424 Adhesive

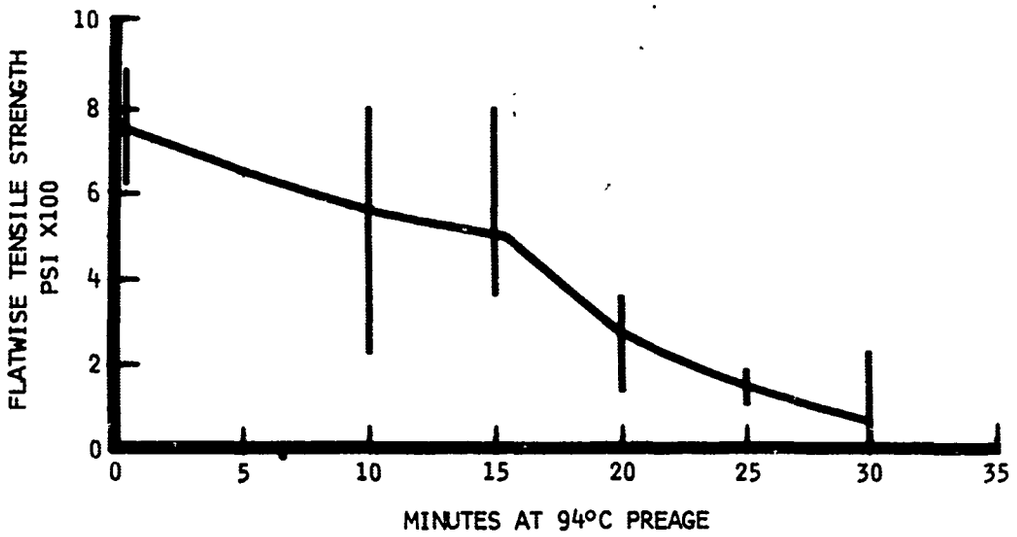


Figure 4. Tensile Stress-Time Relationship for Varying Preaging Conditions

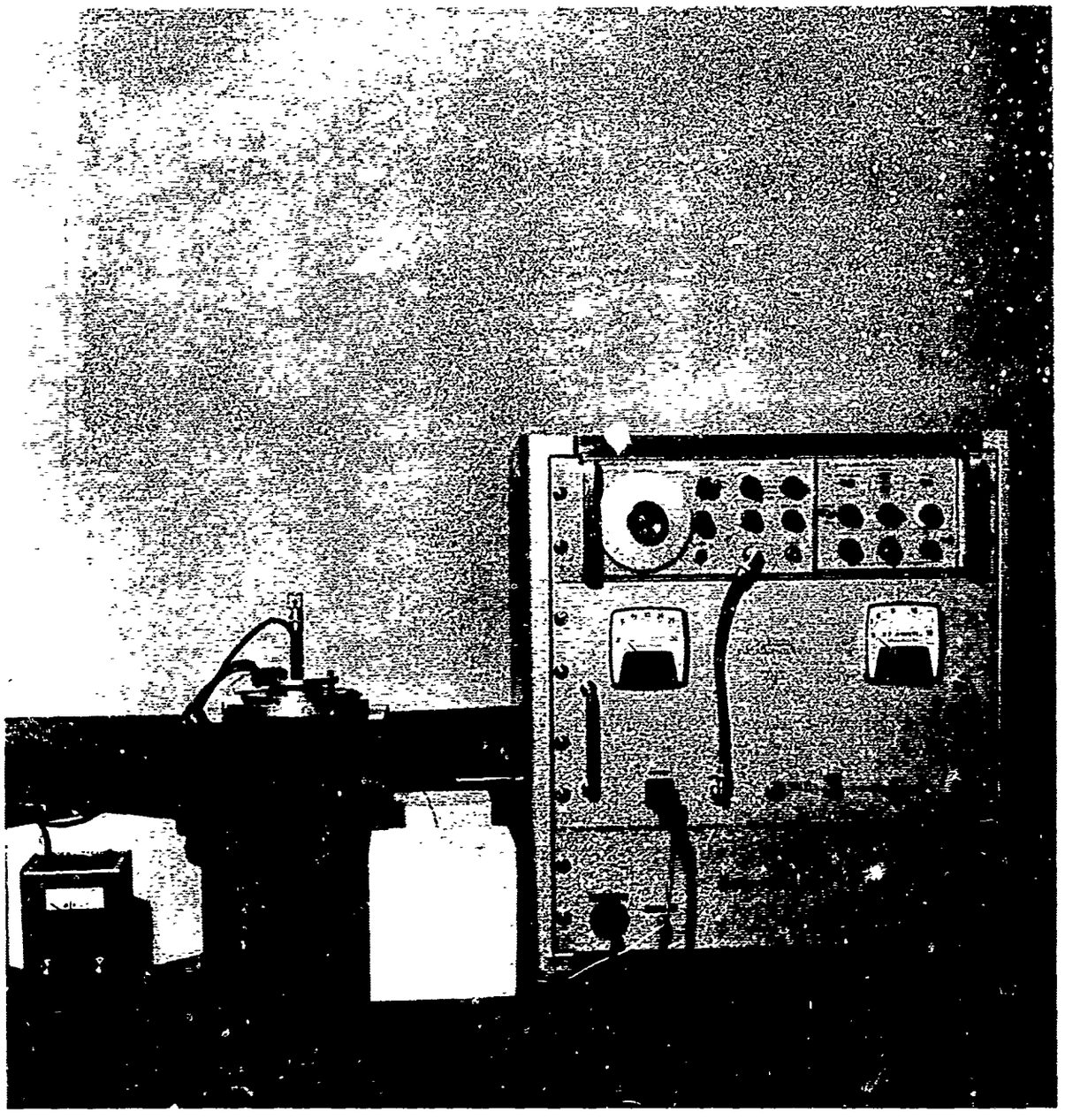


Figure 5 . Photograph of the NR DOT Bond Strength Tester

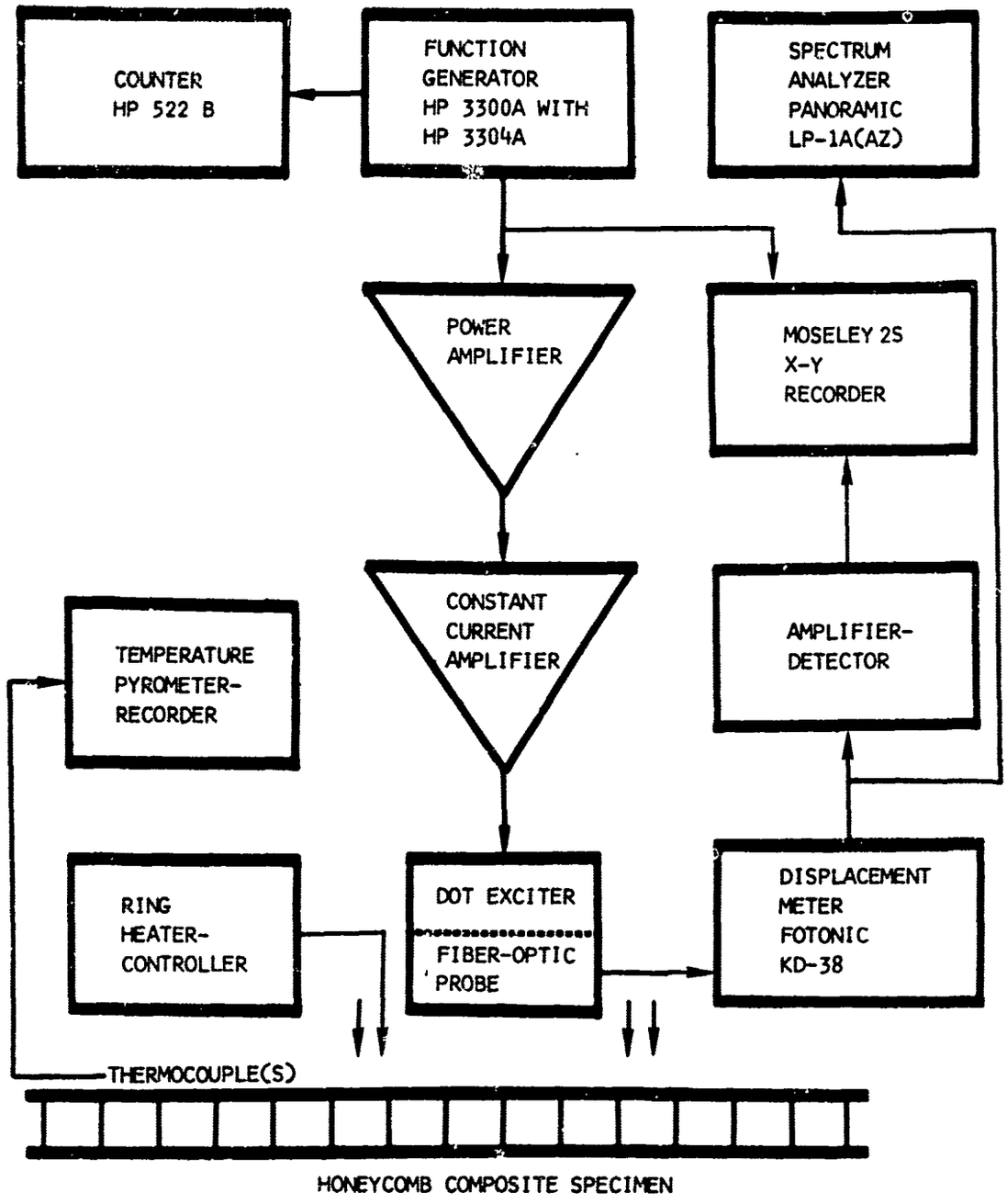


Figure 6. Block Diagram of the DOT Vibration Analyzing System

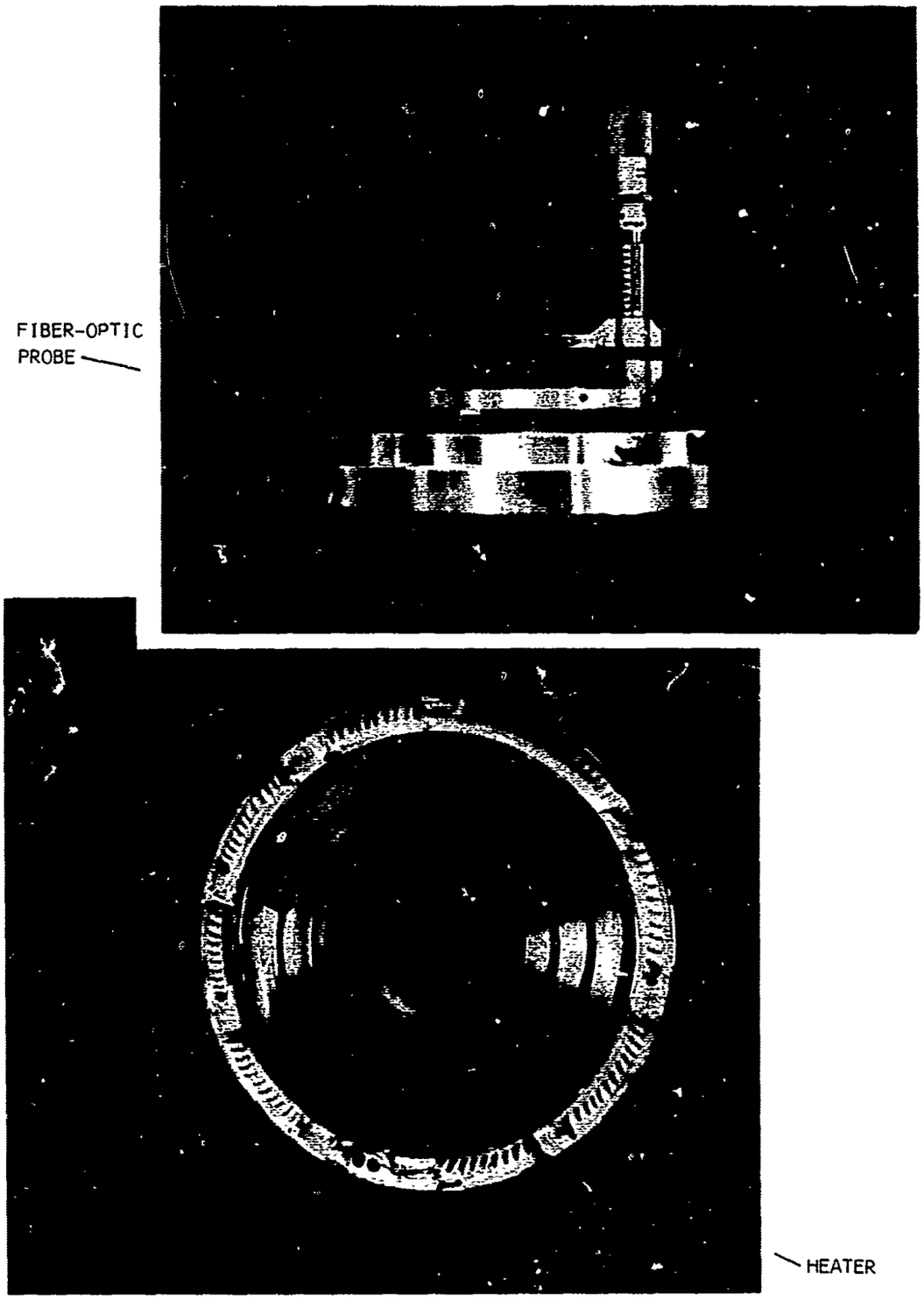


Figure 7. ROI Transducer Holder Showing Fiber-Optic Probe and Heater

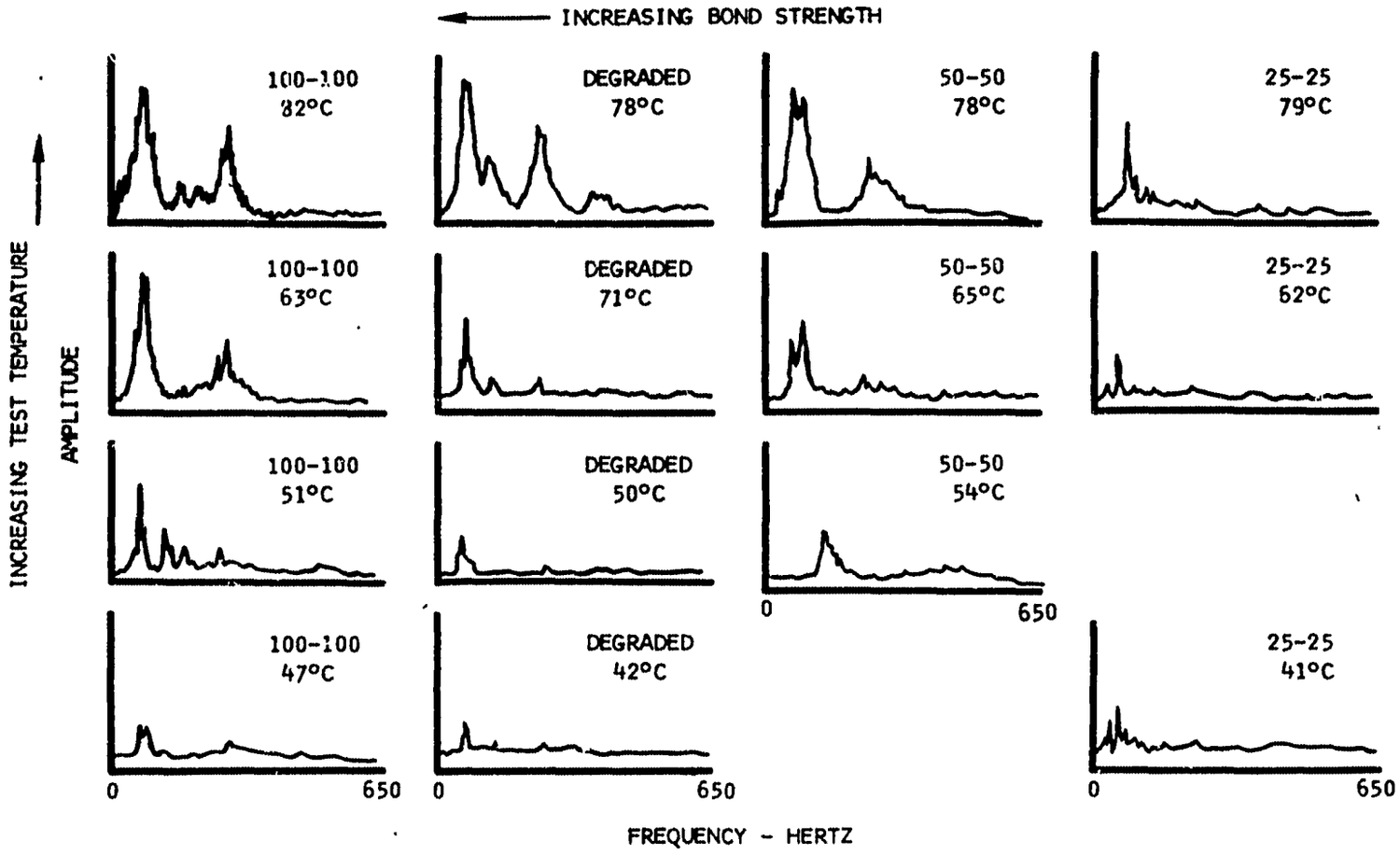


Figure 8. Low-Frequency Response Waveforms for Varying Bond Strength Specimens and Test Temperature (0.02-Inch Facing Sheets)

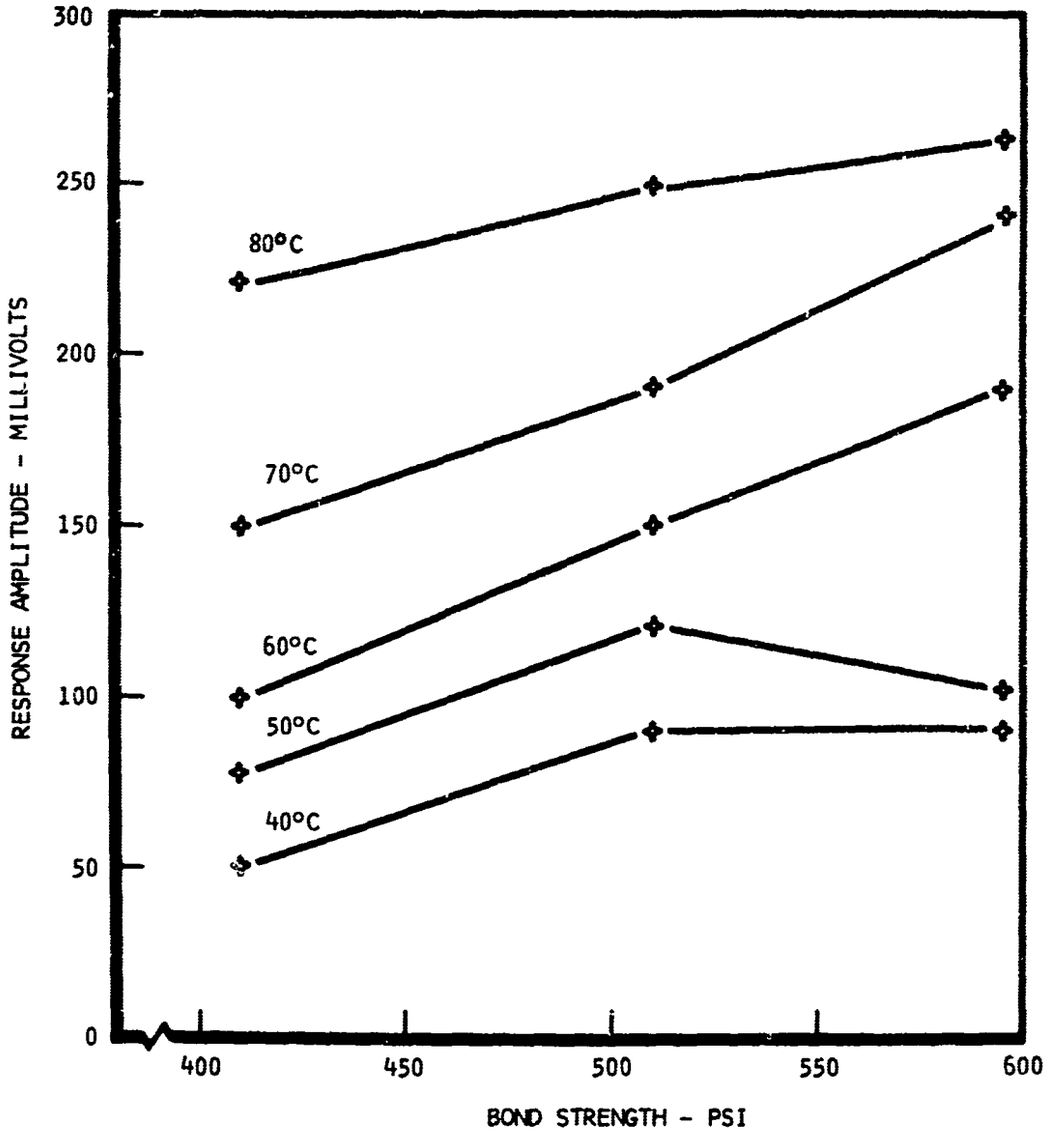


Figure 9 . Low-Frequency Relationship Between Bond Strength and DOT Response Amplitude (0.02-Inch Facing Sheets)

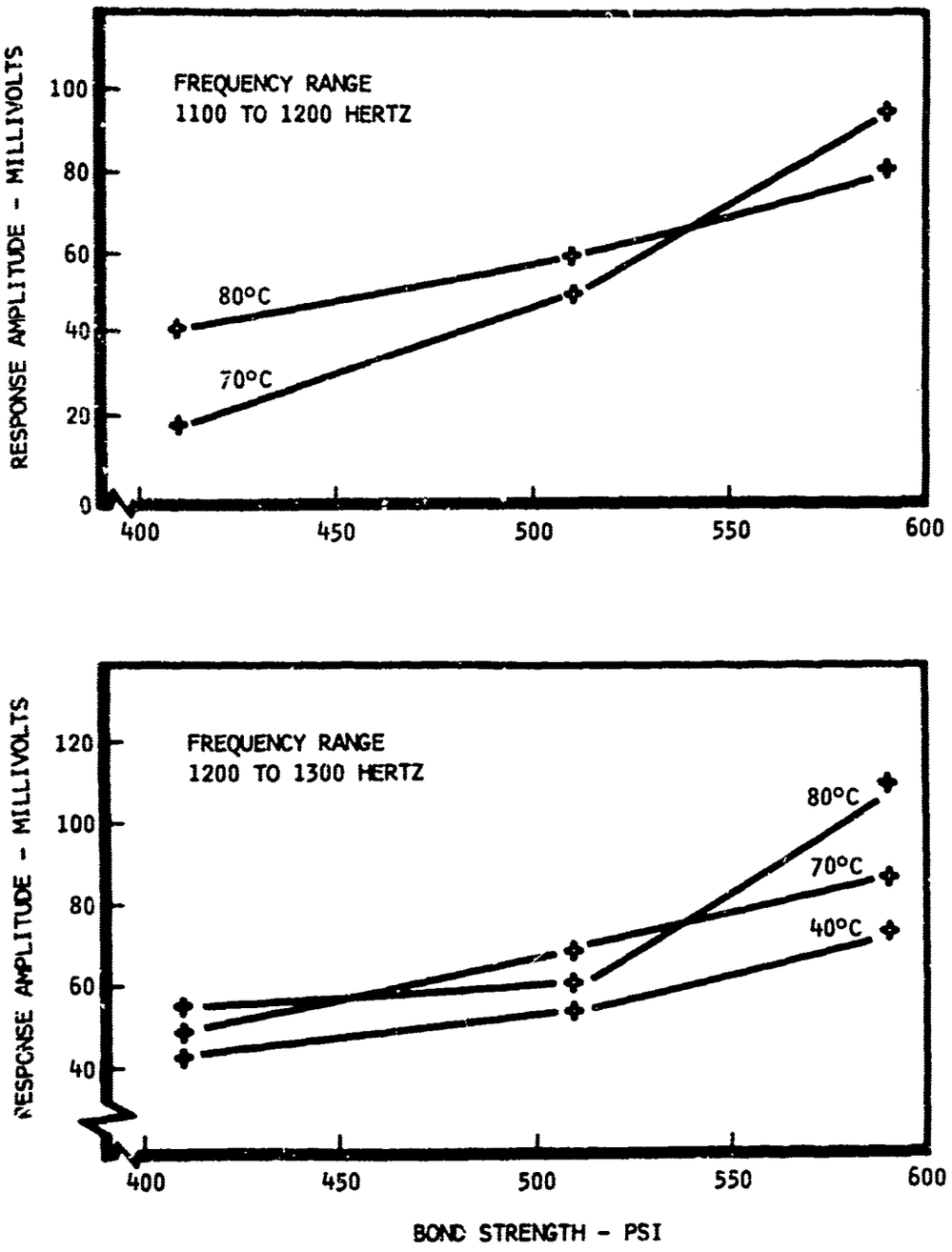


Figure 10. High-Frequency Relationship Between Bond Strength and DOT Response Amplitude (0.02-Inch Facing Sheets)

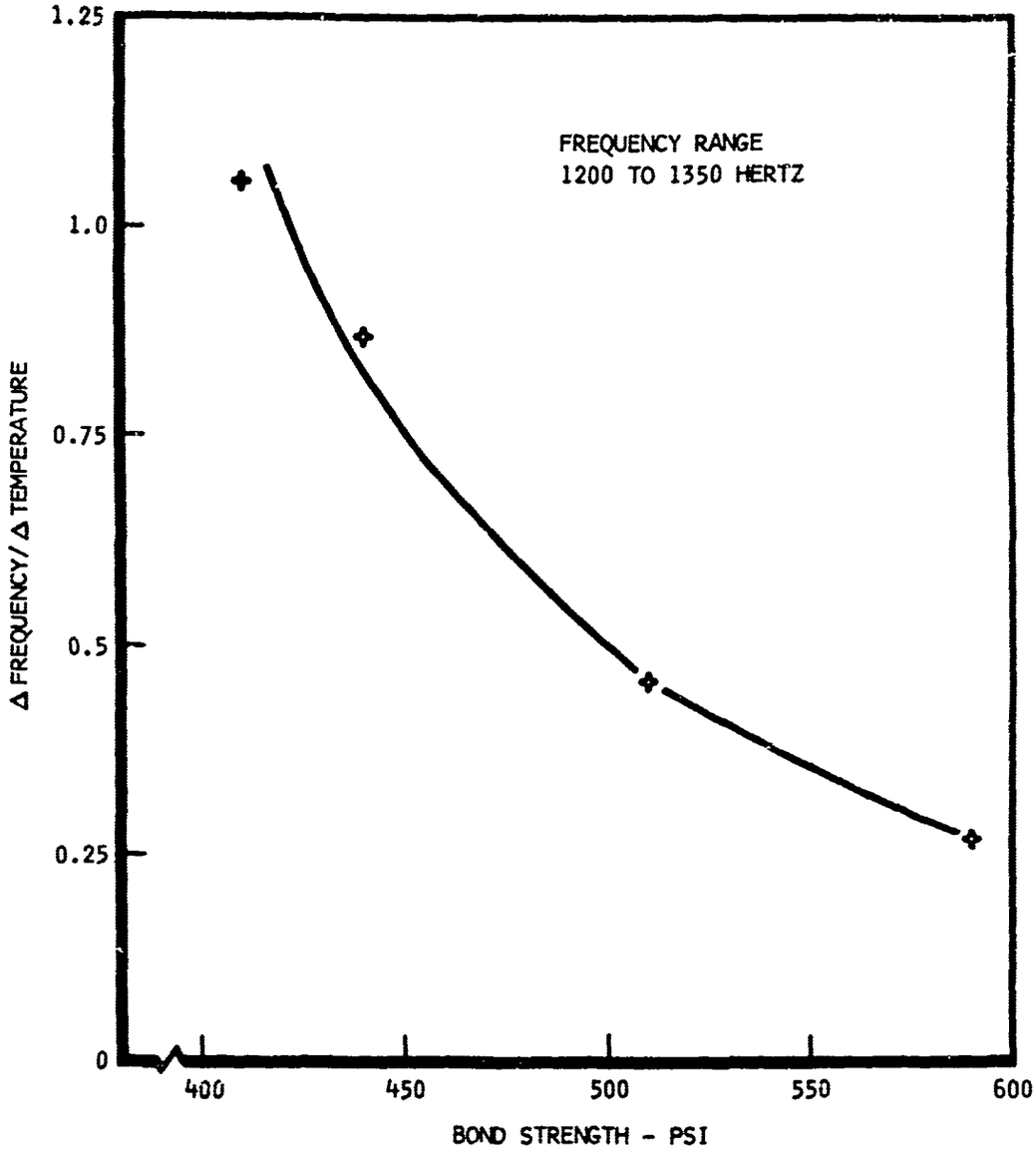


Figure 11. Change of High-Frequency Resonance as a Function of Test Temperature and Bond Strength (0.02-Inch Facing Sheets)

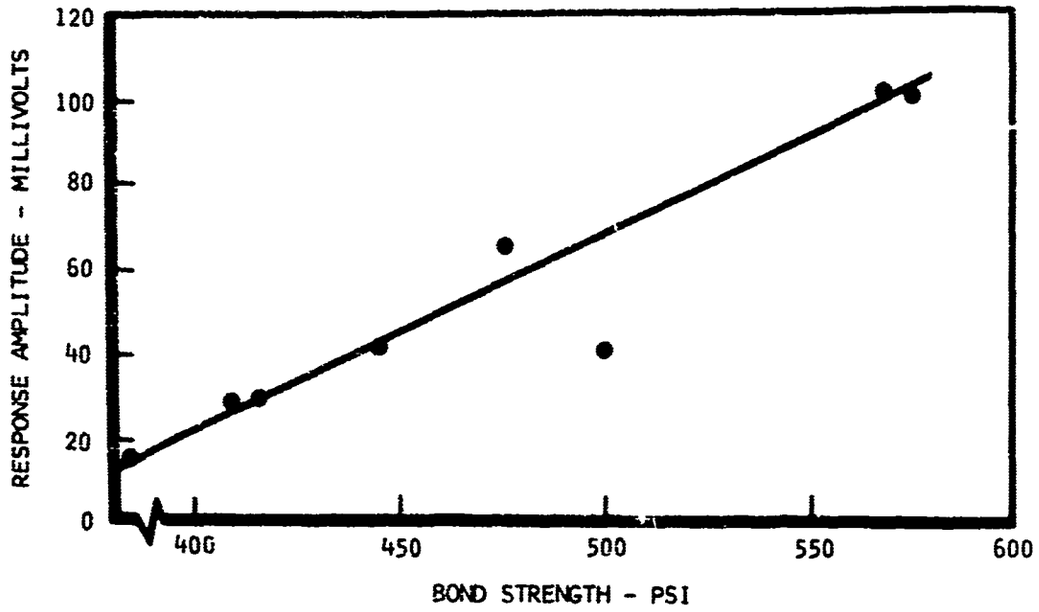


Figure 12. DOT Vibration Response Data Using Self-Heating for Unclamped Honeycomb Composites With 0.063-Inch Facing Sheets

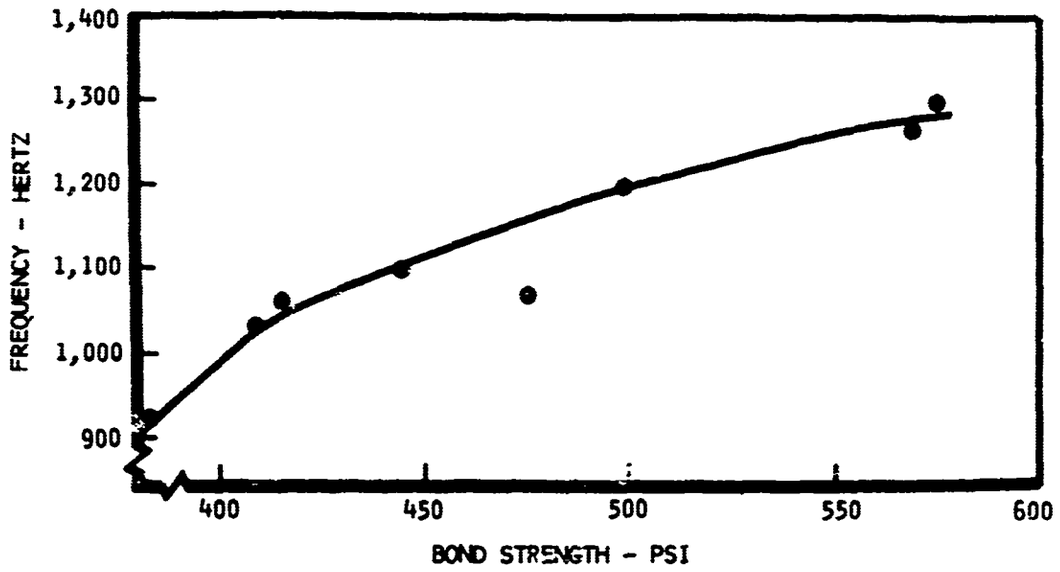


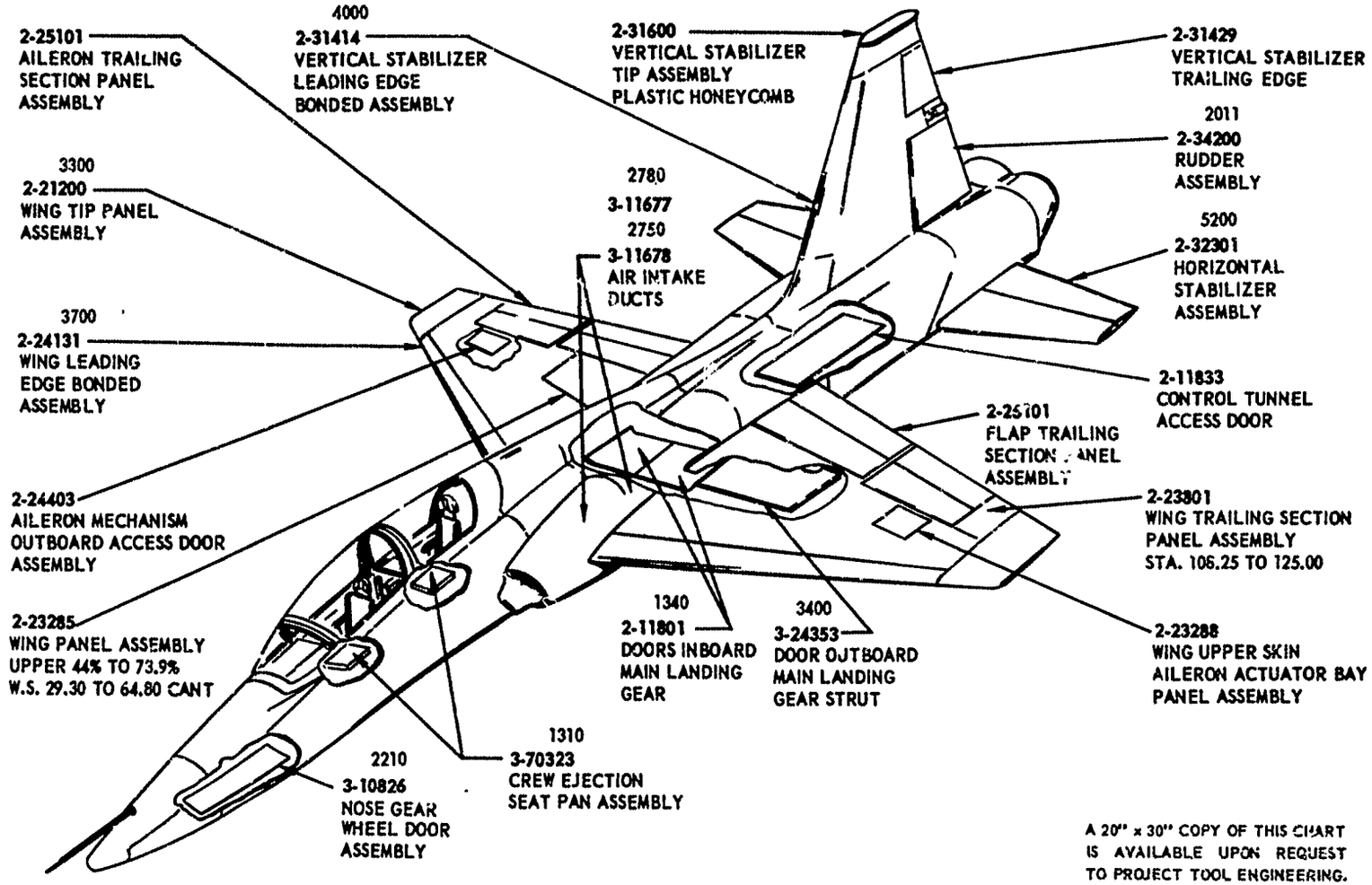
Figure 13. DOT Vibration Response Frequency Versus Bond Strength (0.063-Inch Facing Sheets)

APPLICATION OF NONDESTRUCTIVE TESTING OF ADHESIVE BONDED STRUCTURES FOR NORTHROP NORAIR's F-5 & T-38 AIRCRAFT

by

Robert E. Clemens
Quality Engineering
Northrop Norair
Hawthorne, California

For Presentation at the
Conference on NDT of Plastic/Composite Structures
Dayton, Ohio
March 1969



A 20" x 30" COPY OF THIS CHART IS AVAILABLE UPON REQUEST TO PROJECT TOOL ENGINEERING.

HONEYCOMB ASSEMBLIES

T-38

ABSTRACT

This paper discusses the fabrication of qualitative and quantitative test standard panels, the development of nondestructive test procedures and the implementation of methods into production.

In it are described qualitative procedures for detection of internal honeycomb core damage, unbonded areas in multiple metal to metal laminates and quantitative procedures based on correlation of ultrasonic response with bond strength of both honeycomb sandwich and metal to metal adhesive bonded structures.

Problems encountered with the new low cure temperature adhesives, as they influence nondestructive testing parameters of specific honeycomb type structures, are presented and some methods of problem resolutions are described.

The Fokker Bond Tester, an ultrasonic resonance type instrument is used for all quantitative nondestructive testing of bonded structures at Northrop Norair.

INTRODUCTION

Adhesive bonded structures are normally classified into two general configurations. Metal to metal, consisting in its simplest form, of two pieces of sheet metal bonded together, and honeycomb sandwich structures, which is more or less self-explanatory in that a piece of honeycomb core is bonded between two pieces of sheet metal. There are many variations of these basic configurations, and depending upon the applications, the structures can be very complex.

The design engineer who selects a certain adhesive system, makes his choice based on mechanical properties which have been established by the manufacturer or the laboratory of his own company.

With bolted joints, it is sufficient to test a number of bolts in order to be able to calculate with reasonable accuracy, the strength of the joint. However, this is not the case with adhesives.

Preparation of test specimens in the laboratory, using the same adhesive as in the actual production operation, give results that will not tell much about the quality of the bonded production structures.

The mechanical properties of the cured adhesive material are the results of the process itself, consequently there can be many reasons why the laboratory specimens will yield different strength values from the production joints, which have been made with the same adhesive.

The strength figures given in adhesive data sheets have been established by testing standardized specimens. Since the stress distribution in the bonded joints of the specimens may be completely different than those in the production structures under load, the quality of every important bonded joint should be compared in some way with the desired quality level.

These facts make quality control of adhesive bonded structures very difficult. The normal quality control procedures for bonded structures, requires periodic acceptance tests of adhesive material, and rigid controls over the processes used in the bonding operation. These controls are used in conjunction with destructive tests of coupons which are processed with the assemblies. The bond strength of the part is assumed to be that of the test specimens.

We at Northrop Norair do not feel this to be true. These procedures do not evaluate the strength of a particular joint, but only define the quality of bonding on a statistical basis. Testing of completed joints was limited to methods such as visual inspection, simple mallet or coin tapping techniques, proof loading or cutting out of small test buttons. Therefore, it was evident that a nondestructive method for determining the bond strength of a joint was necessary to assess the quality of an adhesive bond. The questions with which we were concerned was not only do we have unbonded or void areas, but how strong is the bond? To determine this, it was necessary we come up with instrumentation and procedures which would give us a quantitative evaluation of bonded joints.

After an evaluation of several ultrasonic instruments, the Fokker Bond Tester was selected. Since we were to determine the strength of the bonded joint, it was necessary that we base our curves on destructive tests that could be correlated to instrument response.

TEST SPECIMEN PREPARATION

The importance of test specimen cannot be over emphasized since the major problem in preparing correlation curves is fabricating test specimens with quantiative variations in bond strength. Specimens prepared in accordance with conventional methods were found inadequate to control the quantitative variations in bond line thickness.

Specimens of intermediate strength are particularly difficult to prepare due to the many variables affecting bond strength, the response sensitivity of the Fokker Bond Tester to these variables, and the necessary relationship between discrepancies in the test panels to those causing weak bond strength in production assemblies.

Test specimens were prepared using the same metal thickness combinations, [illegible] surface preparation, bonding processes and adhesive materials as the [illegible] assemblies.

Our whole concept of quantitative evaluation of bonded structures was based on the mismatch of detail components and bonding tool wear which allows gaps between adherends to exceed bond line tolerances.

Various methods of producing satisfactory test specimens were tried. The final and most accurate methods are shown in Figure 1 which is a picture of the type panel for lap shear specimens, and Figure 2 which shows the configuration for honeycomb flatwise tensile.

It will be noted that the shims support the bond area on all sides. This type of shimming reduces the problem of having a concave center which would not be a reliable specimen for testing. During cure a heavy caul or pressure plate is positioned on top of the panel with a piece of rubber on top. It has been found that the pressure plate is necessary to prevent adverse pressure distribution which results in the above mentioned concave condition.

Prior to fabricating test panels for quantitative evaluations it is necessary to conduct tests to determine the limits of gaps which can be tolerated. Once this has been established test panels can be prepared using shims up to the top limits as determined by the preliminary data.

Our normal procedure is to fabricate test panels using no control of bond line thickness, and panels with .010" .012" .015" or other shims as deemed necessary.

As an example, when test panels were prepared for plotting correlation curves with a vinyl-phenolic adhesive the shim sizes ranged from .008 inch to .025 inch. With this range we were able to plot very good correlation curves; however with a nitrile epoxy adhesive the shims ranged from .006 inch to .016 inch.

To clarify our concept of shimming to induce a low pressure bond area, we do not care if the gap between the test panel adherends is exactly the size of the shim. All we are concerned with is that there is a difference in Bond Tester reading and physical strength.

Normal procedure is to prepare sufficient test panel to be able to use at least 100 specimens for data evaluation and plotting the correlation curves.

All lap shear panels are prepared with a 0.5 inch overlap. All honeycomb flatwise tensile specimens are prepared 2" x 2" x core thickness.

To prevent peeling of lap shear specimen made from thin metal, the specimens are ultrasonically inspected and then thicker metal back plates are bonded on each side. This reduces the error which would result from peeling action and metal failure.

All specimens are cured using the same cure cycle as for the production assemblies.

DATA EVALUATION

Figure 3 is an actual laboratory work sheet which tabulates correlation data of frequency shift quality units versus destructive lap shear strength.

The correlation curves are established by plotting the points and drawing the best fitting curve. Honeycomb flatwise tensile are evaluated in the same manner; however when testing the flatwise tensile specimens ultrasonically a total of nine readings are taken on each side of the sandwich (depending on probe diameter). These readings are then averaged and depending on which side, top or bottom, fails in tension the average ultrasonic reading is noted for the tensile value obtained.

It is possible to have what is called a substandard reading and still have an acceptable test. The failing stress is really an average of the area being tested, therefore the above type condition is acceptable.

The failure mode of all specimens, both lap shear and flatwise tensile is noted. To obtain reliable correlation, specimen failure must be caused by exceeding the cohesive strength of the adhesive layer. Failures caused by exceeding the strength of the adherend, or the strength of adhesion at the adhesive - adherend interface do not correlate with cohesive bond strength or with Fokker Bond Tester readings.

Figure 4 is the lap shear correlation curve obtained from the work sheet in Figure 3.

A typical honeycomb flatwise tensile laboratory work sheet is indicated in Figure 5 and correlation curve is shown in Figure 6.

It is necessary to use another type of correlation curve for lap shear called the quality diagram, to correlate the nondestructive and destructive shear strength of a bonded joint. This is due to the non-linear relationship between bond strength and bond area, or thickness of adherends. This condition is caused by deformation of the adherend under load, which causes stress concentration in the joint.

Details on how to prepare this type curve will be found in the ASTM "Proposed Method for Inspection of Adhesive Bonded Structures Utilizing the Fokker Bond Tester".

DATA VERIFICATION

Once the laboratory work has been completed and correlation curves and acceptance limits established, the methods and procedures are introduced into normal production inspection. It might be felt that this is a dangerous procedure, since all the data available has been obtained from laboratory specimens; however, all adhesive bonded structures follow a so-called dissection schedule which requires that a completed assembly be dissected, examined and tested periodically. Table 1 indicates this schedule.

Prior to dissection, each qualification assembly is ultrasonically inspected in accordance with the specified procedures. All instrument readings are recorded, the assembly is cut into lap shear and honeycomb flatwise tensile specimens and destructively tested.

From the ultrasonic readings, the physical strength of the specimen is estimated from the applicable correlation curve. This value plus the actual value are plotted to show statistical correlation between nondestructive and destructive test values. Figure 7-8 and Table 3.

These data are accumulated until the degree of reliability is such that it is feasible to open up the dissection schedule to that shown in Table 2.

This procedure is used for each adhesive bonded structure on the F-5 and T-38 aircraft.

One item which I feel everyone is very interested in is cost savings. Adhesive bonded structures are expensive and each time one is rejected money goes down the drain; however before the recent change of adhesive systems at Northrop Norair the dissection of bonded structures was

reduced from one out of every 30th unit to one out of every 100th unit. This was not only a cost saving item, but also with the verifiable data a greater degree of quality assurance was obtained.

TABLE 1

DISSECTION SCHEDULE (Each Bonding Tool)

Accumulated Assemblies	Dissect
1 through 10	1
11 through 25	1
26 through 50	1
Each 30 thereafter	1

TABLE 2

(After Verifiable Ultrasonic Data)

DISSECTION SCHEDULE

Accumulated Assemblies	Dissect
1 through 8	1
9 through 15	1
16 through 50	1
Every 50 thereafter	1

METAL TO METAL MULTIPLE LAMINATES

The quantitative evaluation of multiple bond lines is very difficult. The problem encountered is the effect of each bond line upon the other from the standpoint of instrument response.

A great deal of study has been made by Norair of this condition and the final analysis has been to evaluate multiple bond lines qualitatively since the results of the quantitative study indicated that the scatter was too great for good correlation. The procedures established utilize so called step panels Figure 9 for ultrasonic comparison. Testing multiple bond lines for voids is based on the principle that the zero quality (void) and ideal bond quality can be determined by a standard having a void in the top sheet. Adjusting for zero on the top sheet permits testing the first bond line. Adjusting zero on a well bonded laminate equal to the thickness of sheet 1 and 2 can be used for checking the second bond. This method will detect voids or unbonded area in laminates containing 4 bond lines and location of the void can be determined.

BUCKLED AND CRUSHED HONEYCOMB CORE

Certain honeycomb structures for the F-5/T-38 aircraft are crushed edge assemblies. The exterior surface is flat; however, the inner skin surface is a pan type configuration with a transition area at the edges forming the crushed edge.

The honeycomb and skins are assembled and then crushed under hydraulic pressure. If the inner pan section is under tolerance it is possible that the field core will be buckled during the crushing operation.

To detect this possibility a procedure was developed for nondestructive inspection of these assemblies.

It was possible to establish limits based on degree of buckle. Figure 10 and Figure 11 show the difference in scale readings between a good section and a crushed section.

Low frequency transducers in the range of 50-70 KHz are utilized for this type inspection. The method has been used for field service and found to be very accurate.

RUPTURED HONEYCOMB CORE

The possibility of honeycomb core adhesive bonded structuring sustaining core rupture or discontinuity is not common, however it does occur due to some type damage and a method of nondestructive inspection is necessary to detect this condition. Norair utilizes through transmission for this type of nondestructive inspection.

To properly inspect by this method it is necessary to provide test samples of known quality to establish a relationship between the ultrasonic equipment and the parts to be tested.

The reference standards should be fabricated using the same adhesive system and processing cycles including the finishing paint system if applicable. The reason for including the paint system on the standards is due to field service where it is not advisable to attempt to remove the paint.

The reference standards are marked off in areas indicating percent of rupture covered by the receiving transducer crystal (i.e. 50% area indicates that 50% of the receiving transducer crystal area is located over ruptured core). Figure 12 and Figure 13 show how the reference standards are prepared and utilized. Figure 14 is a curve indicating approximate rupture size versus relative signal amplitude. Figures 15, 16, 17 & 18 indicates wave form amplitude corresponding to rupture size.

In order to conduct through transmission inspection accurately it is mandatory that the transmitter and receiver be in exact opposition. Figure 19 & 20 show the type templates which are used for this inspection.

NEW ADHESIVE SYSTEMS

The original correlation curves for production nondestructive inspection, were based on assemblies bonded with a vinyl phenolic adhesive system. Due to the "gap filling" properties of this adhesive, the problems of producing good correlation curves was minimal. It could be stated that the instrument reading and strength reductions were almost proportional to the gap size between adherends.

However, with the introduction of the modified epoxy low cure temperature adhesive systems, problems were encountered with tapered or wedge type honeycomb sandwich structure.

It appears that these type adhesives which do not have gap filling properties, that affect the density of the material, requires a lower frequency for nondestructive inspection. This is where the problems occur, because using low frequency of the resonance type not only measures the cohesive properties of the adhesive, but also the core thickness.

Full scale needle deflection occurs during test from the thick section of the sandwich structure to the thin trailing edge. No degree of correlation could be established between instrument readings and physical strength using the normal transducers.

Considerable time was expended testing various type transducers and crystals in an attempt to establish the correct frequency and vibration mode.

Special crystals were manufactured to our requirements and some success has been achieved, since procedures and correlation curves have been established for all but two of these type F-5 and T-38 honeycomb structures, and it is anticipated that additional studies will result in complete resolution of this problem.

The established procedures are very sensitive and has necessitated retraining of N.D.T. operators and calibration of all equipment to establish frequencies at specific instrument settings.

NONDESTRUCTIVE TESTING IN PRODUCTION

The introduction of a nondestructive test method into the normal production inspection procedures is the culmination of all the previous laboratory work.

Northrop Norair's procedure is spelled out in the Process Specifications which give the part configuration, metal thickness combinations, Fokker Bond

Tester probe size, applicable instrument settings, acceptance limits and percent of assembly area to be inspected. This ranges from 100% to 10% depending on the critical loading of the assembly. No templates are used for testing, thereby a random type sampling is obtained. Sketches of all honeycomb assemblies are available for inspection personnel to record sub-standard readings and locations.

I do not want to give the impression that the introduction of nondestructive methods of testing adhesive bonded structures was accomplished without some differences of opinion. I am sure that most nondestructive test engineers have encountered the problem of inspecting a production assembly, finding discrepancies, and rejecting the part.

Production personnel are a hard breed of people to convince that a little black box can determine the quality of their assemblies. In our case it was necessary to dissect several production assemblies to convince the skeptics that the results of the nondestructive tests were valid. After several of these cases, we made "believers" of them, and at the present time the results of nondestructive inspection are not questioned.

CONCLUSIONS

The work with the Fokker Bond Tester over the past eight years has resulted in the application of this type of nondestructive testing for quality control of various adhesive systems involving a number of bonded structures.

Basically, the method is capable of determining cohesive strength of metal-to-metal and skin-to-core type bonds. It is necessary to prepare suitable correlation curves to correlate nondestructive test parameter with bond strength. The primary limitations of the Fokker Bond Tester method is its inability to evaluate the strength of adhesion at the interface unless either voids or sufficient porosity are present to affect ultrasonic response.

Rigid process control is still required since the instrument is relatively insensitive to degradation of bond strength due to improper compounding, contamination or incomplete cure of the adhesive material. These type conditions cannot be accurately determined by the Fokker Bond Tester or by any other existing nondestructive test method.

The implementation of nondestructive testing, utilizing the Fokker Bond Tester, at Northrop Norair has resulted in the following:

1. Increased quality assurance resulting from verifiable data as to bond strength.
2. Increased quality assurance resulting from verifiable data as to internal conditions of honeycomb core.
3. Increased production due to the ability to determine quality of assemblies during normal nondestructive inspection.

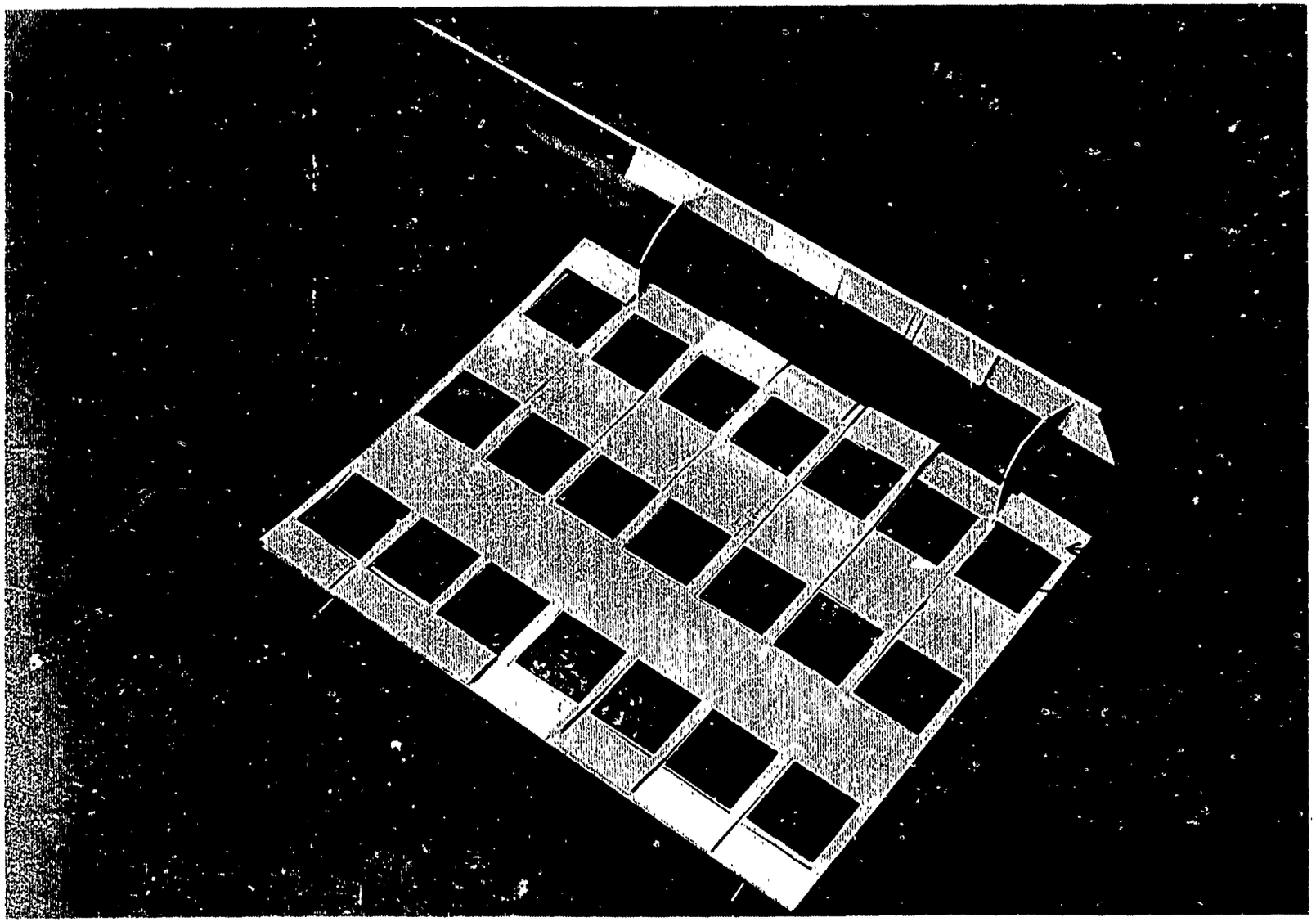


FIG. 1

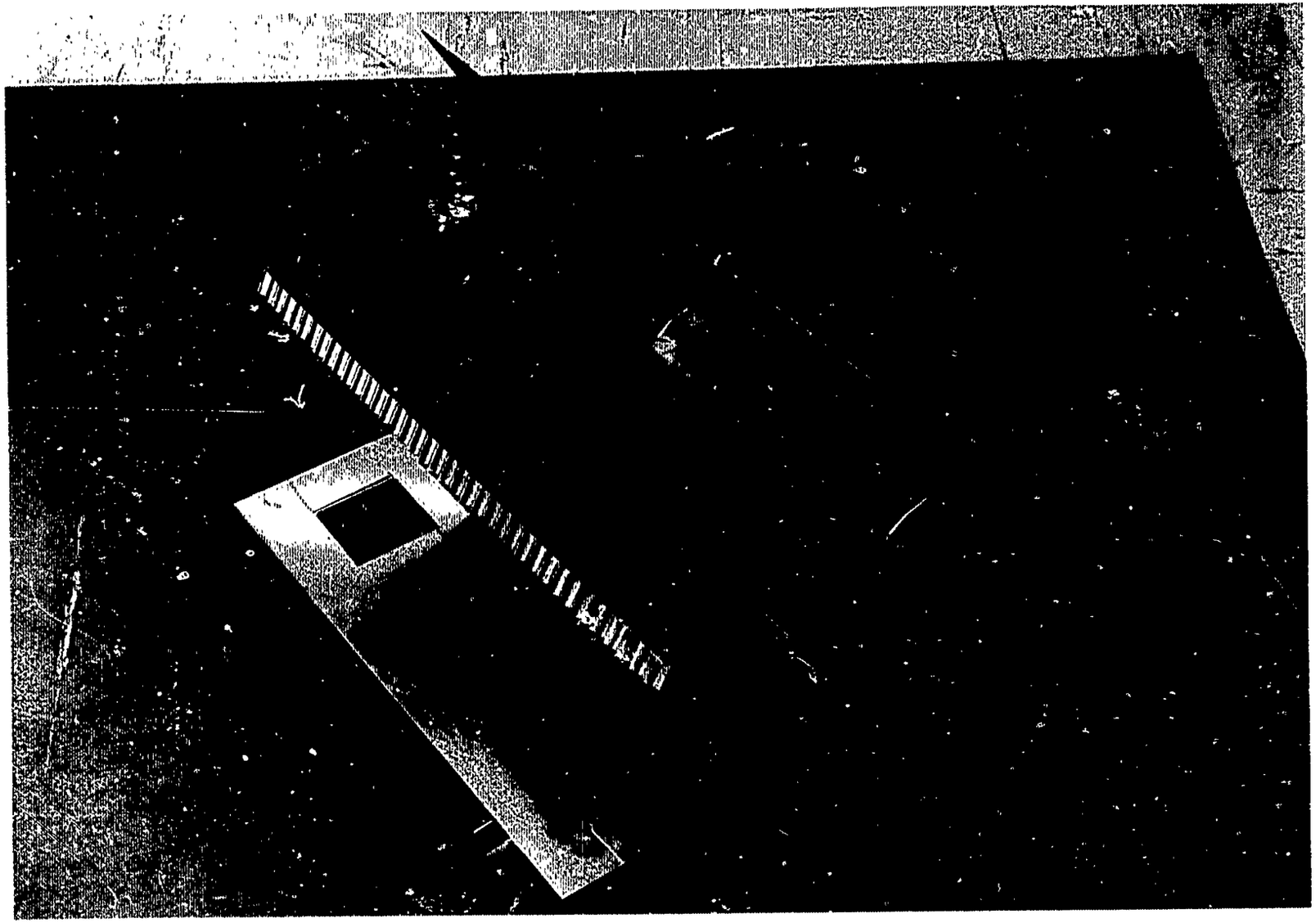


FIG. 2

ADHESIVE FM 123 - .015"

LAP SHEAR
CORRELATION DATA
WORK SHEET

.032"-.032" Skin Thickness

Fokker Readings:

18R	19R	20R	21R	22R	23R	24R	25R	26R	27R	29R	30R
5197	5084	4929	4804	4657	4455	4450	4014	3873	3538	3238	3106
5131	5047	5000	4856	4417	4495	4319	3981			3162	3166
5151	5098	4892	4864	4751	4400	4255	4050			6400	3064
5139	5142	4886	4773	4625	4444	4190	12045				3200
5144	5000	4955	4775	4667	4505	17214					12536
25762	5034	24662	24072	4591	4450						
	5026			27708	4421						
	5068				31170						
	5102										
	5077										
	5078										
	5091										
	5041										
	65888										
Avg.	5152 psi	5068 psi	4932 psi	4814 psi	4618 psi	4453 psi	4305 psi	5015 psi	3873 psi	3538 psi	3200 psi	3134 psi

Fokker Readings:

30L	25L	23L	20L	18L	17L	16L	15L	10L	8L	7L	6L
3021	2625	2380	2024	1870	1773	1688	1558	1010	863	719	624
3039	2575		1936	1870	1799			1002		720	626
6060	5200		2110	3740	1740			2012		1439	623
			2010		1789						1873
			2183		7101						
			10263								
Avg.	3030 psi	2600 psi	2380 psi	2053 psi	1870 psi	1775 psi	1688 psi	1558 psi	1006 psi	863 psi	719 psi	624 psi

Fokker Readings:

5L	4L	3L	2L	1L	0
558	417	339	220	118	80
500	488	388	205	170	49
539	428	727	237	288	74
515	472		260		37
2112	1805		922		100
					340
Avg.	528psi	451psi	364 psi	231 psi	144 psi	68 psi

Fig. 3

FORM 66-11A
(R. 9-68)

ENGINEER	NORTHROP CORPORATION NORAIR DIVISION	PAGE
CHECKED		REPORT NO.
DATE		MODEL

Fig. 4

ADHESIVE FM 123 - .015"

FLATWISE TENSILE
CORRELATION DATA
WORK SHEET

Tapered
Skin Thickness .025" - Core - .025"

Fokker Readings:

35	40	43	45	47	50	52	54	55	56	57	59
763 cr	693 cr	507 cr	594 cr	687 cr	705 cr	753 cr	752 cr	735 cr	650 cr	781 cr	750 cr
688 cr	649 cr	660 cr	705 cr	709 cr	700 cr	750	741 cr	722 cr	734 cr	714 cr	744 cr
723 cr	1346	1167	1300	1396	664 cr	756	1493	731 cr	1386	730 cr	1494
710 cr					690 cr	2259		724 cr		720 cr	
525 cr					641 cr			769 cr		723 cr	
3409					3400			3682		700 cr	
										4368	
Avg. 682 psi	673 psi	584 psi	650 psi	698 psi	680 psi	753 psi	747 psi	736 psi	693 psi	728 psi	747 psi

Fokker Readings:

60	63	64	65	66	69	70	73	75	76	80	83	95
749 cr	755 cr	640 cr	742 cr	714 cr	611	575	431	436	439	384	327	125
724 cr	724 cr	745 cr	738 cr	711 cr	608	580	472	467	430	380	179	128
753 cr	738 cr	1385	741 cr	1428	614	580	904	458	435	389	506	126
2226	2217		714 cr		610	560		486	434	1153		120
			738 cr		612	575		488	1738			499
			714 cr		3055	585		2335				
			711 cr			3455						
			5099									

Avg. 742 psi | 739 psi | 693 psi | 728 psi | 714 psi | 611 psi | 575 psi | 452 psi | 467 psi | 434 psi | 384 psi | 253 psi | 125 psi

cr = Core Rupture

Fig. 5

FORM 58-11A
(R. 7-58)

ENGINEER	NORTHROP CORPORATION NORAIR DIVISION	PAGE
CHECKED		REPORT NO.
DATE		MODEL

PLASTICS TENSILE

Fig. 6

ESTIMATED STRENGTH FROM FOKKER READINGS VS DESTRUCTIVE TEST STRENGTH

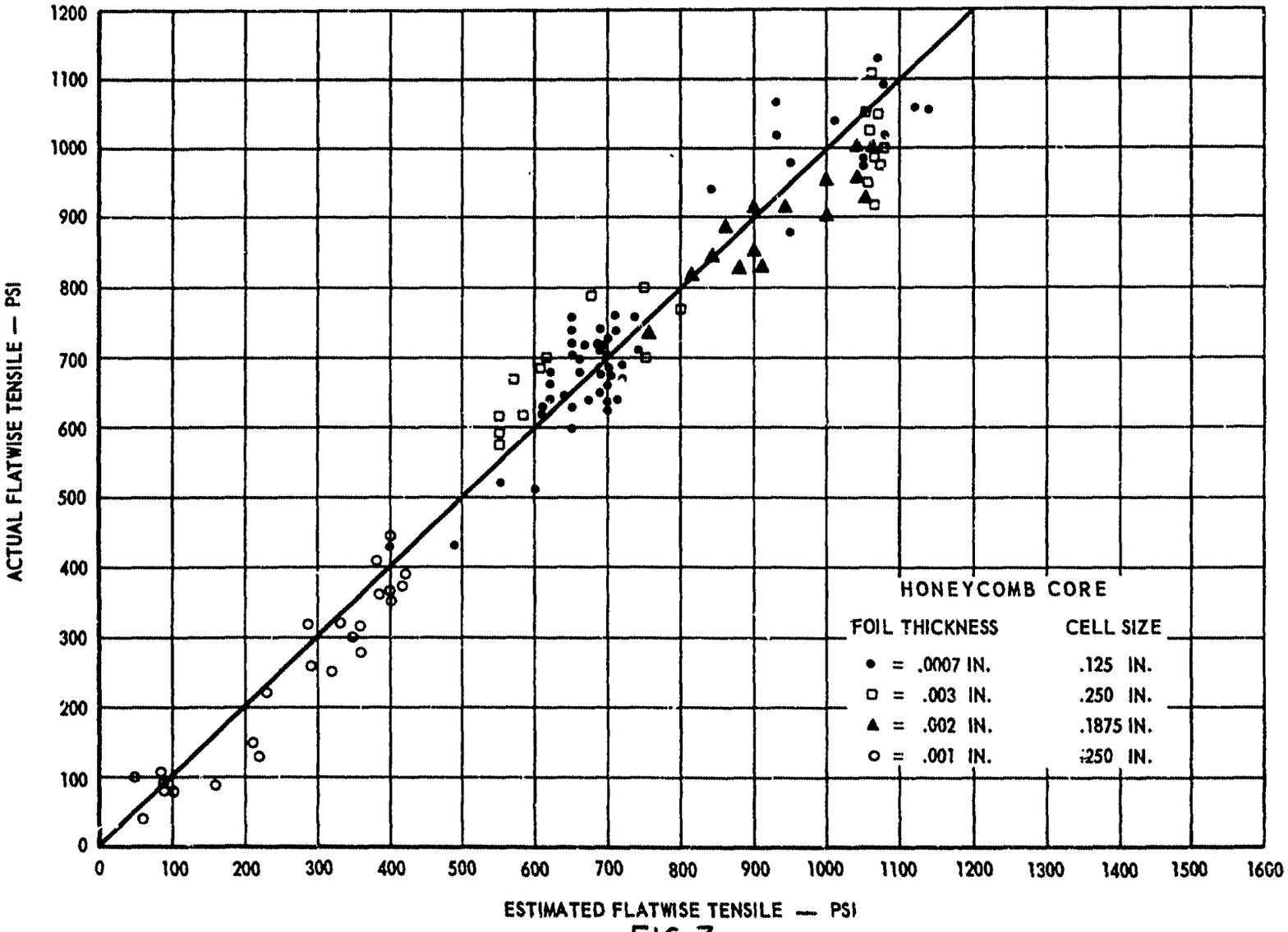


FIG. 7

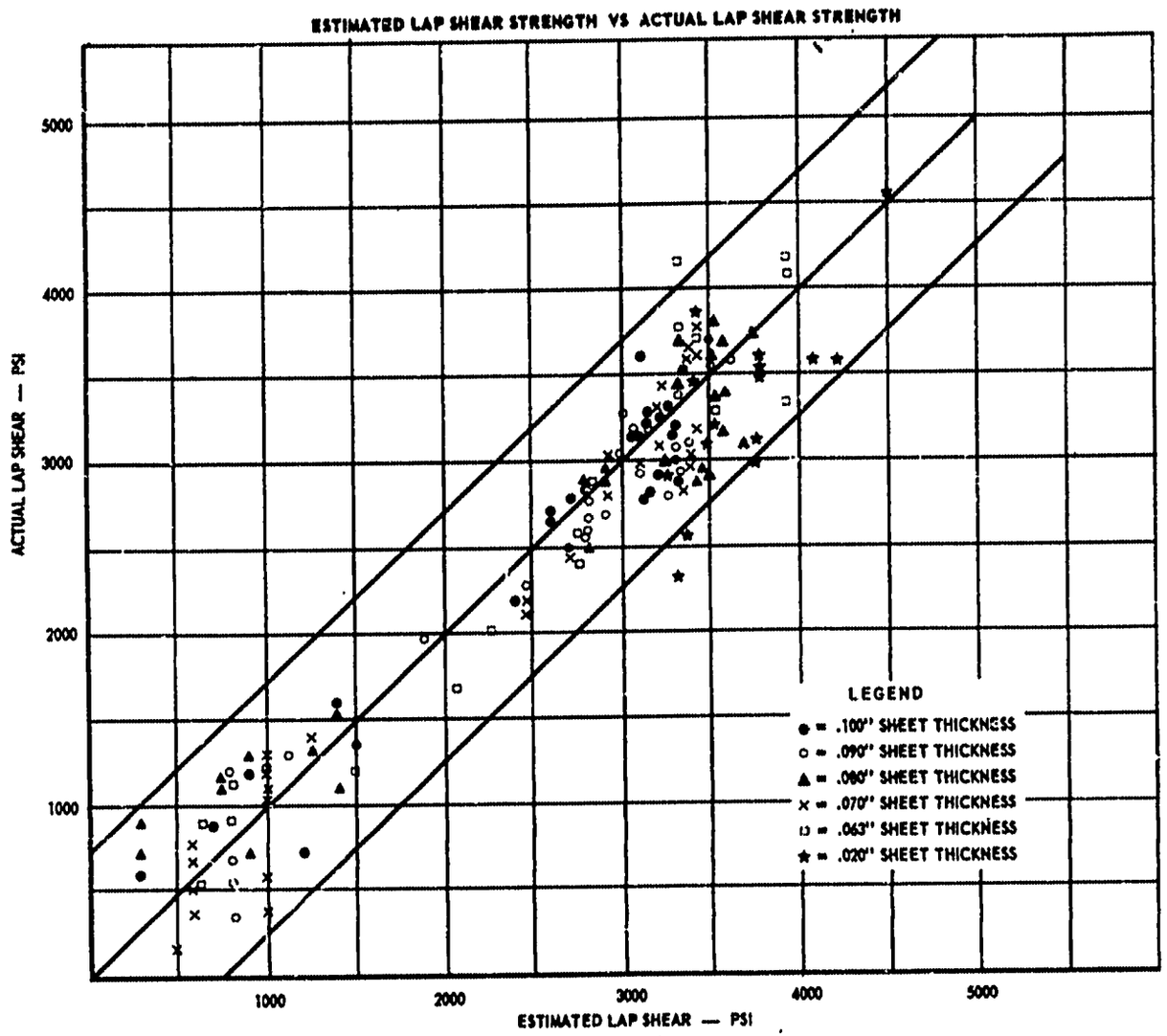
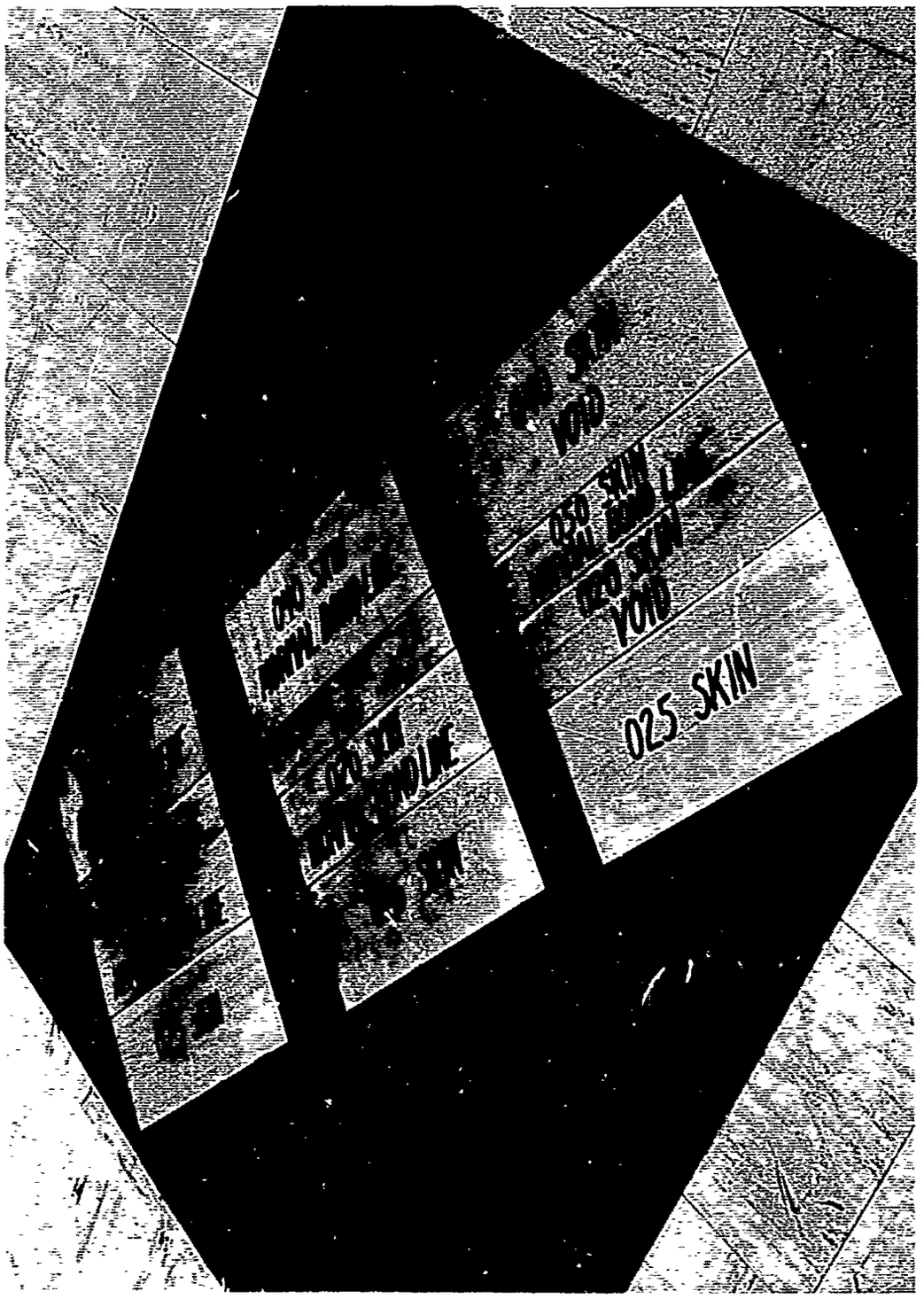
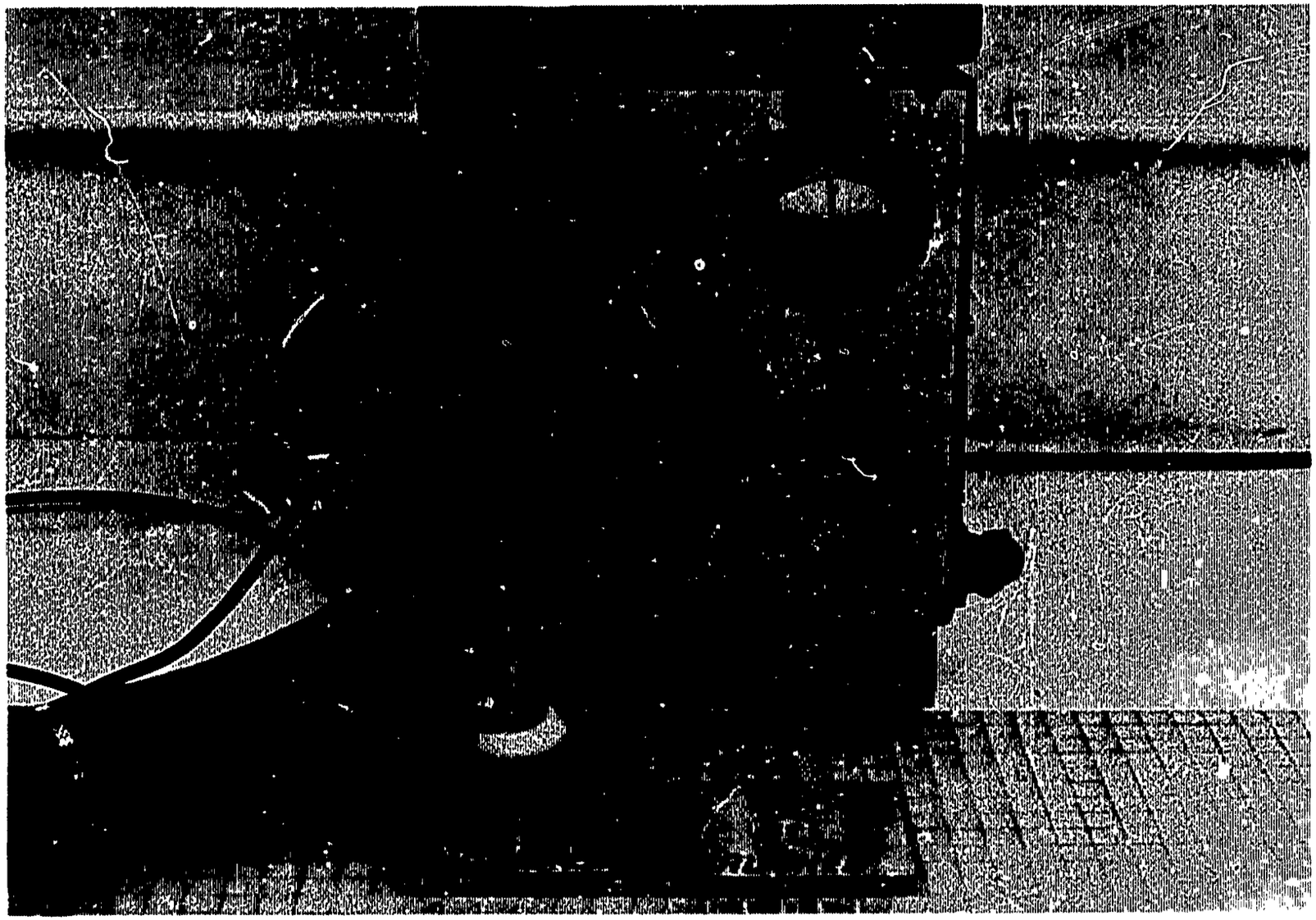

ESTIMATED LAP SHEAR STRENGTH VS ACTUAL LAP SHEAR STRENGTH
ACTUAL LAP SHEAR — PSI
ESTIMATED LAP SHEAR — PSI
1000
2000
3000
4000
5000
LEGEND
● = .100" SHEET THICKNESS
○ = .090" SHEET THICKNESS
▲ = .080" SHEET THICKNESS
× = .070" SHEET THICKNESS
□ = .063" SHEET THICKNESS
★ = .020" SHEET THICKNESS

FIG. 8



STEP PANELS

FIG. 9



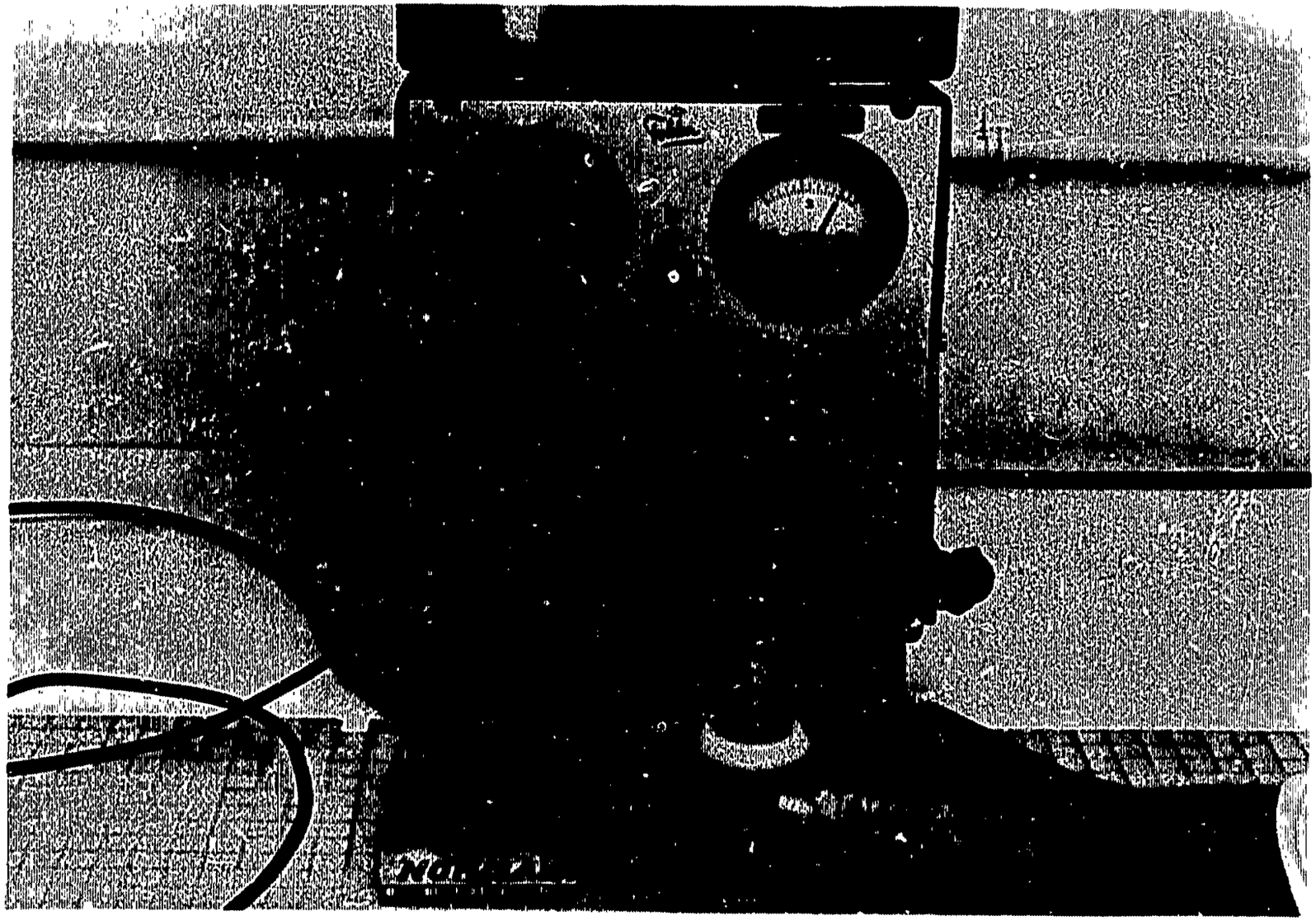


FIG. 11

RUPTURED HONEYCOMB CORE REFERENCE STANDARD

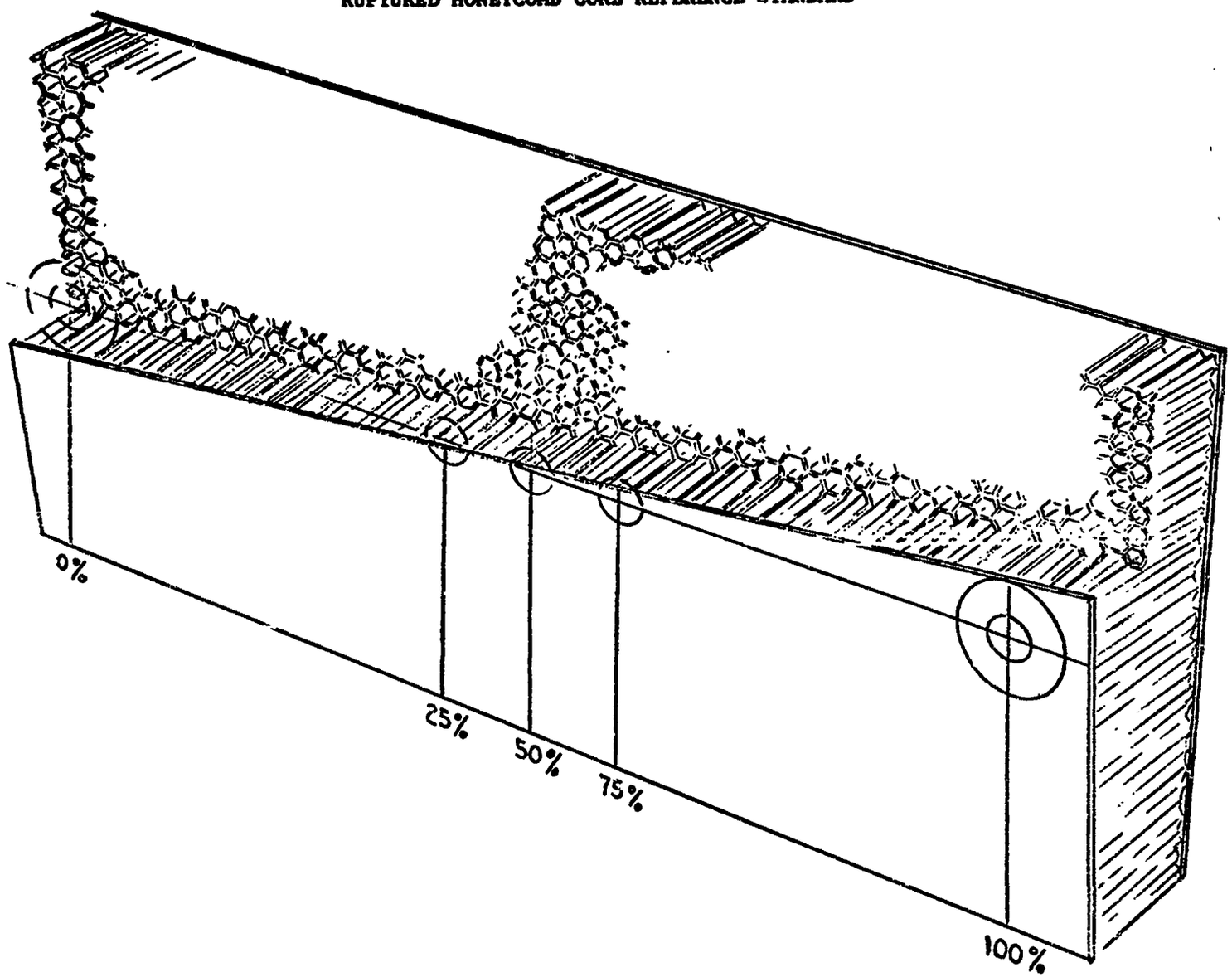


FIG. 12

REFERENCE STANDARD AND HOLDER

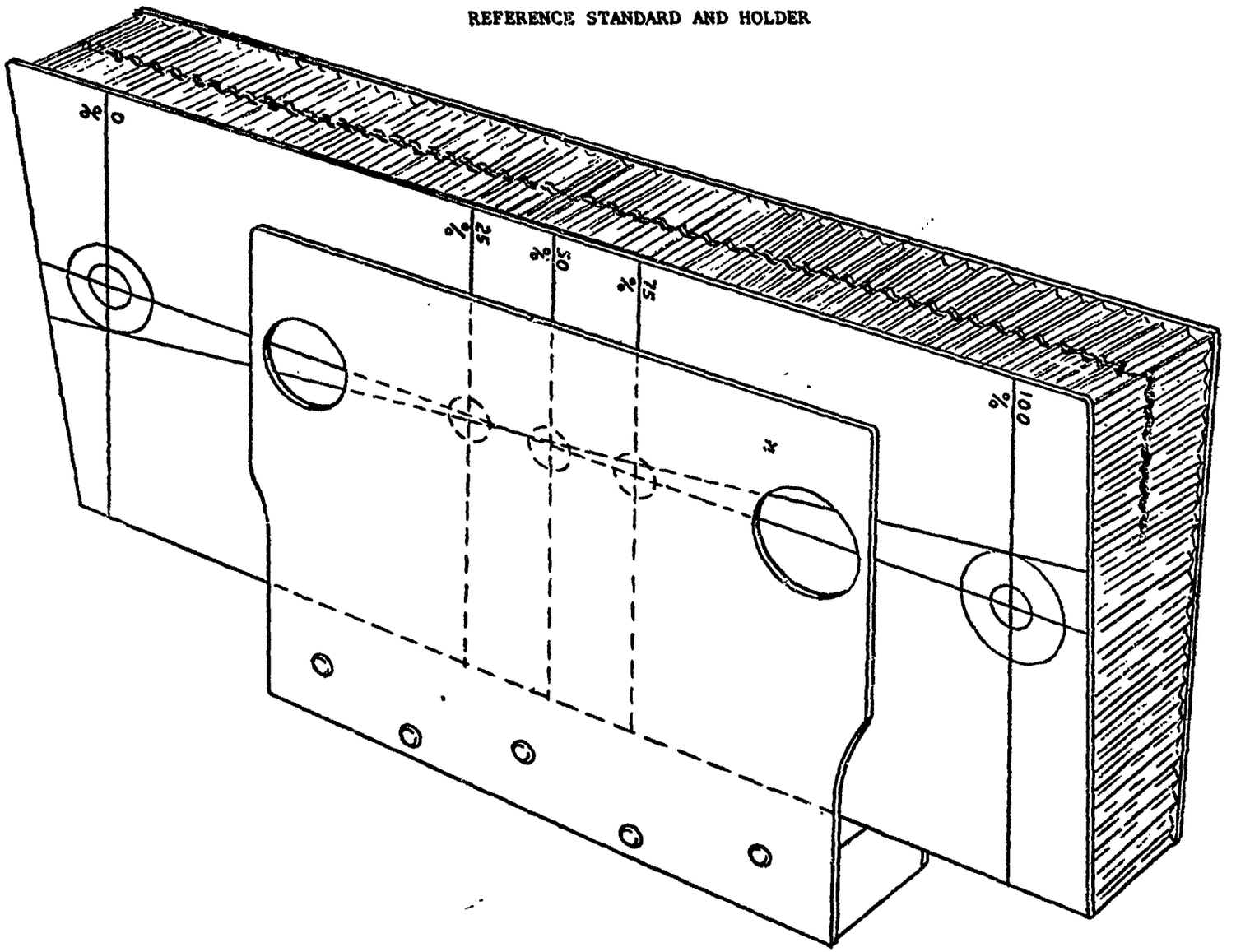


FIG. 13

ULTRASONIC RESPONSE TO RUPTURED CORE DEFECTS
THROUGH-TRANSMISSION

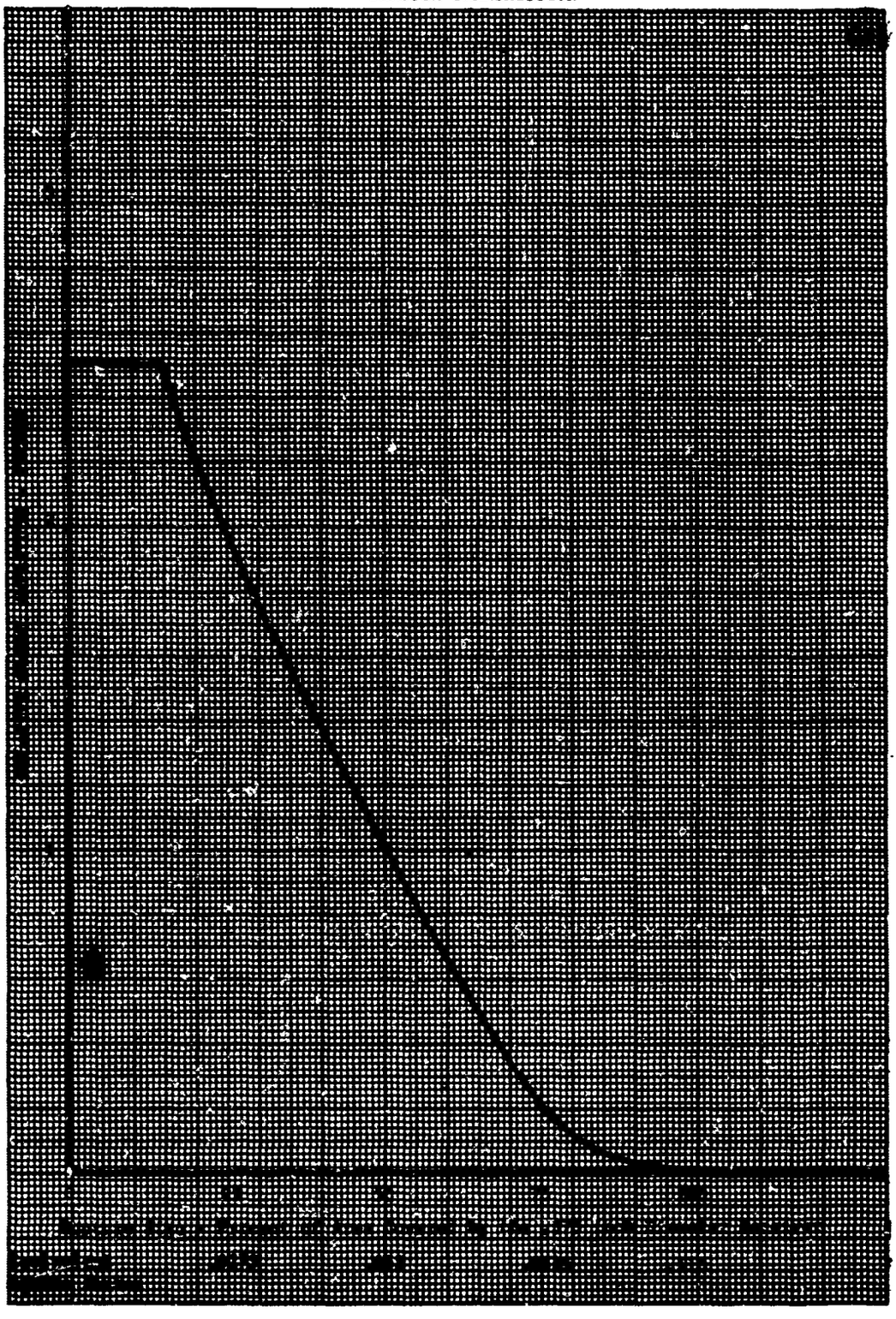


Fig. 14

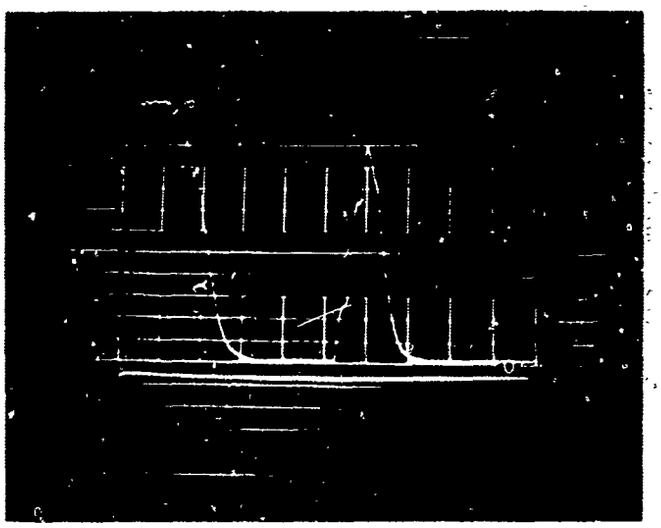


FIG. 15

Ruptured Size - 25% of the area covered by the .312 inch diameter Receiver

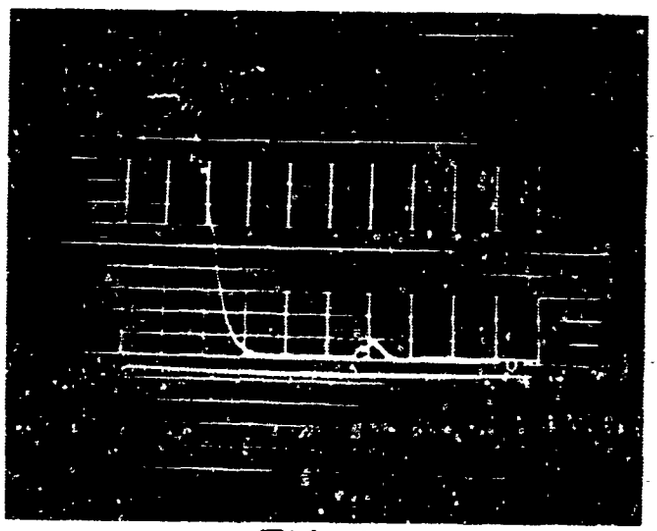


FIG. 16

Rupture Size - 75% of the area covered by the .312 inch diameter Receiver

Note - 100% rupture of area covered by the Receiver will indicate no "pip" on the base line.

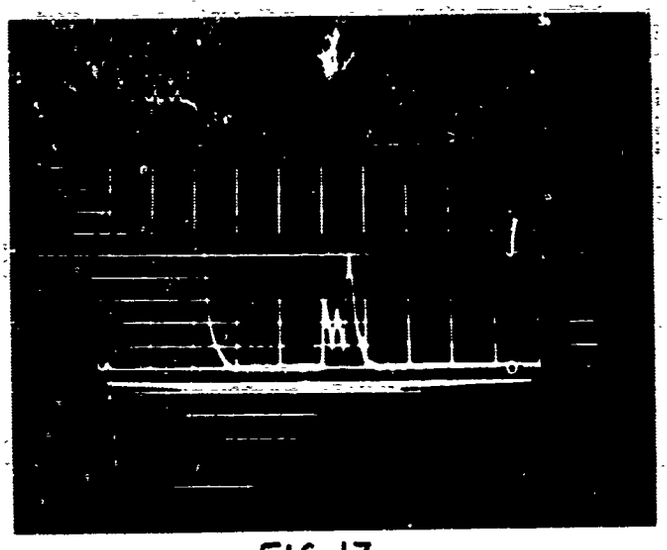


FIG. 17

Rupture Size - 50% of the area covered by the .375 inch diameter Receiver

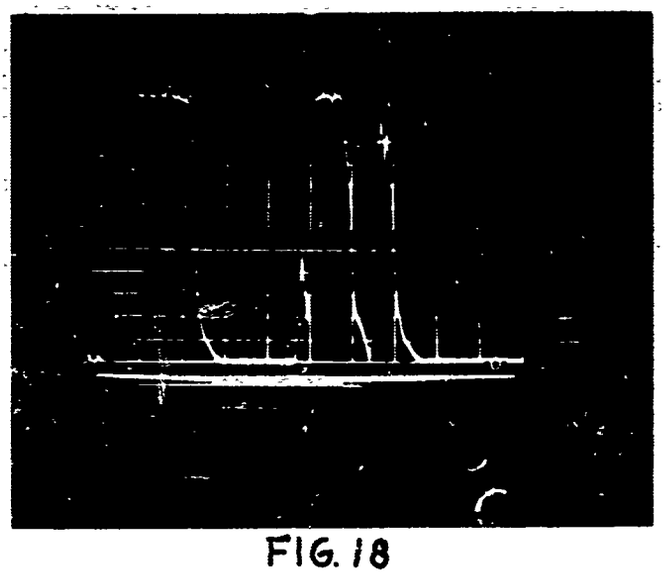


FIG. 18

No Rupture - 100% of the area covered by the .375 inch diameter Receiver

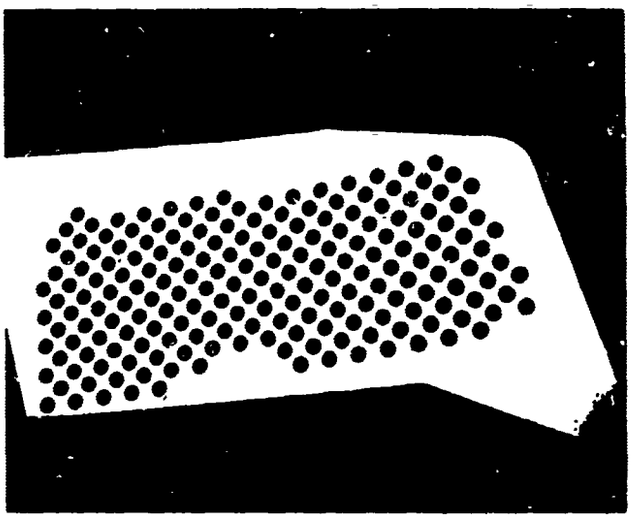


FIG. 19

Alignment Template Exterior Surface
Wing Panel Assembly Upper

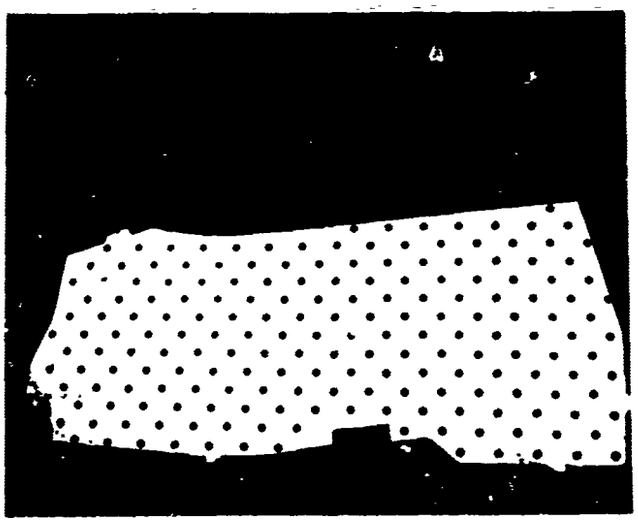


FIG. 20

Alignment Template Interior Surface
Wing Panel Assembly Upper

ESTIMATED STRENGTH FROM CORRELATION CURVES VS. ACTUAL PHYSICAL STRENGTH
F-5 & T-38 QUALIFICATION ASSEMBLIES

NITRILE EPOXY ADHESIVE

Estimated Lap Shear psi	Actual Lap Shear psi	Estimated Flatwise Tensile psi	Actual Flatwise Tensile psi
5000	5161	1090	1314
5000	5374	1060	1296
4450	4832	1110	1390
4750	4917	1110	1144
3000	3224	1260	1383
2200	2342	1240	1378
5000	5151	1210	1482
5000	5335	1160	1191
5000	5050	1360	1234
4750	4620	1280	1471
4750	5094	1300	1331
4000	4280	1240	1356
2800	3220	1340	1240
4750	4931	1260	1464
4750	4864	1280	1444
2800	3020	1280	1455
2800	3084	1200	1281
3850	4003	1460	1560
3150	3330	1400	1440
2800	2985	1400	1530
3850	3973	1380	1305
5000	5228	1550	1543
5000	5074	1340	1200
5000	4902	1400	1470
5000	5080	1400	1510

TABLE 3

"Thermal Inspection of Adhesive Bonded Structures"

E. J. Barton, Research Engineer
Automation Industries, Inc., Boulder, Colorado

INTRODUCTION

Infrared nondestructive inspection is a term rather generally applied to types of testing where the amount of heat in a part or the heat flow through a part is measured to evaluate its quality. This term is somewhat misleading since the true probing energy is actually the heat. Infrared is simply one means of temperature readout, specifically that portion of the spectrum to which radiometers (remote temperature measuring instruments) are sensitive. Thermal NDT would be a more suitable term since the temperature readout could be accomplished by several methods such as thermometers, thermocouples, and heat sensitive materials including paints and liquid crystals.

Thermal NDT as we shall now refer to this type of inspection, naturally breaks down into two categories: passive testing and active testing. Passive testing involves the monitoring of the natural temperature variations of a part. An example would be testing an operating circuit board for hot spots indicating defective components or improper design. Another example of passive testing would be measurement of human body temperatures to detect variations indicating disease or poor blood flow. Measurement of furnace walls for hot spots indicating thin areas would also be a passive test.

Active testing includes tests where the investigator applies or removes heat from the part and measures temperature variations to determine the internal characteristics. Most of the work discussed in this paper was directed at evaluating materials and structures and therefore used the active testing techniques.

BASIC THEORY

The basic test configuration is shown in Figure 1. Heat energy in the form of visible radiation is applied to the test surface. The heat diffuses into the part at a rate dependent on the internal characteristics. Surface temperature, an indication of the diffusion rate, is measured by a radiometer viewing the infrared radiation emitted from the surface. It should be noted that the heat could be applied by such means as hot air or flame heating. The surface temperature could also be measured by means other than a radiometer. The important factor in the test is initiation of heat flow through the part.

Notice that the heating radiation and the temperature readout are unrelated in origin. The heat originates in the heat source; the infrared originates at the test surface. The test is not a measure of reflected energy since natural isolation occurs between the heater and sensor due to their difference in wavelength. Also notice that neither heater nor sensor physically contacts the test part, a characteristic which is often desirable in practice.

The method by which the surface temperature indicates subsurface defects can best be described by referring to Figure 2. If heat is applied evenly over the test surface it diffuses uniformly into the part. If, however, a defect is present, as in this case the unbond between the two laminates, the uniform heat flow will be obstructued. After a short time a heat buildup will occur over the defect due to the obstruction. This hot spot can then be detected on the surface and indicate the subsurface defect. This explanation would apply equally well to solid materials with voids, facing sheets bonded to honeycomb structures, or foreign materials in a parent material.

The time required for the hot spot to appear on a test surface is important. Referred to as the time delay between heating and temperature measurement, this parameter controls the penetration depth of the test. Long delays allow the applied heat to penetrate deeply into the part before the surface temperature is measured. This would be required for slow conducting materials such as nonmetallics or for defects deep in a part. Short delays allow only shallow penetration as would be required for near surface defects or for materials that rapidly conduct heat such as most metals.

TEST METHODS AND RESULTS

In practice there are a wide range of test configurations and equipment available to perform infrared or thermal NDT. As mentioned, the techniques discussed here will be most applicable to material evaluation since active testing is used.

Figure 3 shows a simple technique for a single line scan across a part. This method involves using a stationary heat source and radiometer and a moving sample. The radiometer views a single point on the sample and the relative motion of the test part generates the line scan. The heat spot, typically in the form of focused heat lamp filaments is imaged on the test part and swept from left to right in this figure. The radiometer's view is aimed a short distance behind the leading edge of this moving heat spot. This short delay allows the applied heat to diffuse into the test part and form hot spots over the subsurface defects. The delay time depends

on the scan speed and the delay distance. Typically, delays of less than one second are used for most metallic samples while nonmetallics might require several seconds delay. Typical scan speeds for tests of this type would be in the range of 1 inch/second. Notice that longer delays do not necessarily mean slower scan speeds but rather an increased distance between the leading edge of the heat spot and the radiometer's view.

The graph shown in this figure is an actual recording of an aluminum honeycomb structure. The radiometer signal, proportional to sample surface temperature, is presented on the vertical scale. The horizontal scale represents distance along the sample. This particular sample consisted of 1/32 inch aluminum facing sheets adhesively bonded to a 1/4 inch thick aluminum honeycomb structure with 3/16 inch diameter cells. An unbond had been simulated by removal of a portion of the sheet adhesive on one facing sheet.

The line scan starts on the left side at room temperature, increases sharply as it moves onto the sample, increases again over the defect, and returns to room temperature off the right side of the sample. The vertical scale is approximately 10°C per division indicating the sample is heated 12 to 15°C above ambient while the defect is 15°C hotter than the normal sample temperature. This temperature increase over the defect is caused by the obstruction of the heat flow from the facing sheet into the honeycomb core. A similar passive test could have been performed if the part had already been warm. No additional heat would have been required and the defects would have appeared as cool spots instead of hot spots.

The actual system used for this test is shown in Figure 4. This is essentially the same configuration as presented in the line drawing of Figure 3. The test sample is carried on a moving platform past the heat source and tripod mounted radiometer. The heat source consists of a pair of tungsten filament bulbs focused by reflecting optics onto the material surface. If significant area coverage is required over larger parts and speed is of primary importance, a method termed area scan testing is much more appropriate. The configuration of such a test is illustrated in Figure 5. The basic heat penetration principle is used but a "paint brush" heat pattern is substituted for the previous spot heater. The surface temperature is then monitored by an oscillating radiometer. The data is presented on a facsimile recorder so that true area scan results are obtained.

Figure 6 is a schematic representation of such an area scan system. The "paint brush" heat source moves across the sample. A short time delay allows the applied heat to penetrate into the part. An oscillating radiometer then measures the surface temperature. This oscillating motion is synchronized with the X-axis drive on the facsimile recorder.

The sample speed is matched to the Y-axis (paper feedout) of the recorder. Temperature information from the radiometer is then used to intensity modulate the Z-axis of the recorder so that hot spots on the surface appear as dark spots on the facsimile recording. The paper width is matched to the test path width on the sample so that a full-scale permanent thermal area presentation of the test part is obtained.

Figure 7 shows a photograph of such a system. The radiometer is enclosed in the equipment cover and focused onto the target immediately following the heat source, by means of deflecting mirrors. As the sample passes the heat source and radiometer's view, an area recording is directly produced on the recorder.

Figure 8 shows typical test results on a honeycomb structure. This part consisted of a thin fiberglass facing sheet adhesively bonded to an aluminum core. The honeycomb core had been separated from the facing sheet to simulate an unbond condition. This unbond is indicated by the dark or hot spot in the recording. Notice also that the individual cells can be detected. The cell walls appear cool since they rapidly conduct the applied heat away from the facing sheet while the cell centers are hot because they present a thermal barrier to the applied heat.

The inspection speed for such a test is quite fast. The rapidly oscillating radiometer scans a 7 inch wide path on the sample; the linear scan speed along the part is typically 1 inch/second. These combined motions result in an inspection speed of approximately 3 square feet/minute depending on the material tested.

Other typical applications include inspection of laminate structures. Figure 9 shows test results on a carbon-fiberglass laminate. This part was used as a calibration standard to determine test capabilities. Seven flat bottom holes of various sizes from 1/2" dia., to 1/8" dia. were put in the fiberglass side of this part. These holes extended through the fiberglass to the bond line to simulate unbond conditions. Four 1/2" dia. holes of varying depths were also put in the fiberglass. These holes simulated defects at various material depths from 1/16" to 3/16". The thermal NDT was performed from the carbon side opposite the calibration holes As the test results indicate, all of the varying sized holes were easily detected. Two of the varying depth holes were detected. Detection of the two deeper defects would have required longer delays associated with deeper penetration into the part.

The system of Figure 7 was intended for laboratory or limited inspection of parts up to about 2 feet wide. If larger parts, such as production aircraft parts, are to be inspected, different part handling fixtures are required.

Figure 10 shows a large production inspection system. The parts, too large to easily move, are placed on the test table. The test system is then moved over the stationary part producing a similar facsimile recording.

These systems which provide area coverage could be used to inspect various types of parts including laminates and honeycombs fabricated of metallics, nonmetallics, or composites of both materials. An optimum test surface is any relatively flat surface. Successful tests have been performed on aircraft parts such as wing sections and helicopter blades. Shapes such as cylinders and spheres have also been tested but more care is required so that the heat source and radiometer remain focused at the test surface.

CONCLUSIONS

Two thermal NDT methods have been presented. Typical equipment as well as actual results on various samples have been shown. Two areas which have not been discussed in regard to thermal testing are surface emissivities and defect resolution. Generally emissivity, an indication of the surface reflectivity is not a major problem in testing. For example, highly reflective surfaces like bare aluminum are difficult to test because they reflect the applied heat and do not emit sufficient infrared energy. This is overcome by applying an easily removable coating such as a water soluble paint or a strippable coating. Any coatings applied in the manufacturing process are generally acceptable test surfaces. Even white paint provides sufficient uniformity for accurate testing. Uniform test surfaces such as many steels and etched surfaces as well as most nonmetallic surfaces do not require any treatment for thermal testing. Plastics and nonmetallic composite structures usually have a uniformly dark surface in the infrared, and in this respect are especially well suited for thermal NDT.

Since the probing energy is heat, the thermal method is best suited for near surface defects. The defect resolution does decrease as defects extend deeper into the part simply because the excessive material over the defect diffuses the developed hot spot. Typically, defects must have a lateral diameter approximately 2 or 3 times their depth for easy detection. For example, a defect 1/16 inch deep in a part must have a lateral diameter of about 1/8 inch to be easily detected by thermal techniques. The normal dimension can be quite small since heat flow will be interrupted by a very thin discontinuity. These types of defects normally appear in bonded structures such as laminates and honeycombs. The test method need not, however, be limited to only these structures, but can be applied to any sample which contains defects that would affect heat flow through the part.

The advantages of thermal NDT such as rapid inspection, noncontact with part, and insensitivity to minor alignment variations easily offset the limitations. As more people become familiar with techniques and as more equipment becomes available, thermal NDT will fill a significant position in quality assurance, materials evaluation, and maintenance operations.

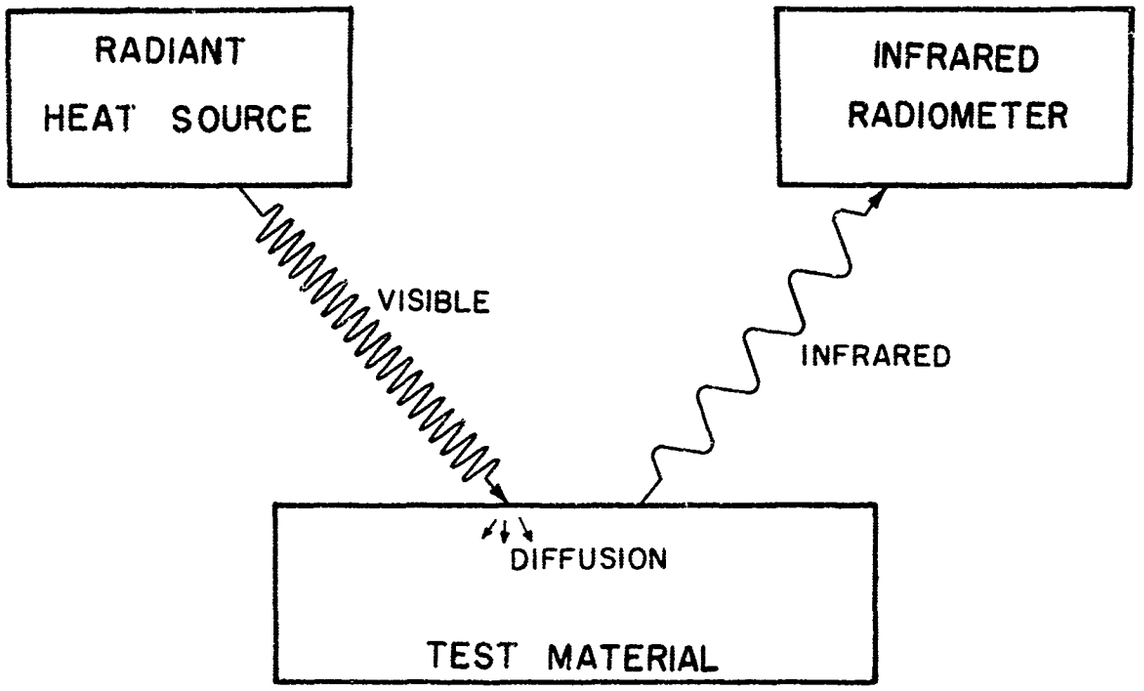


Figure 1. Basic Test Configuration

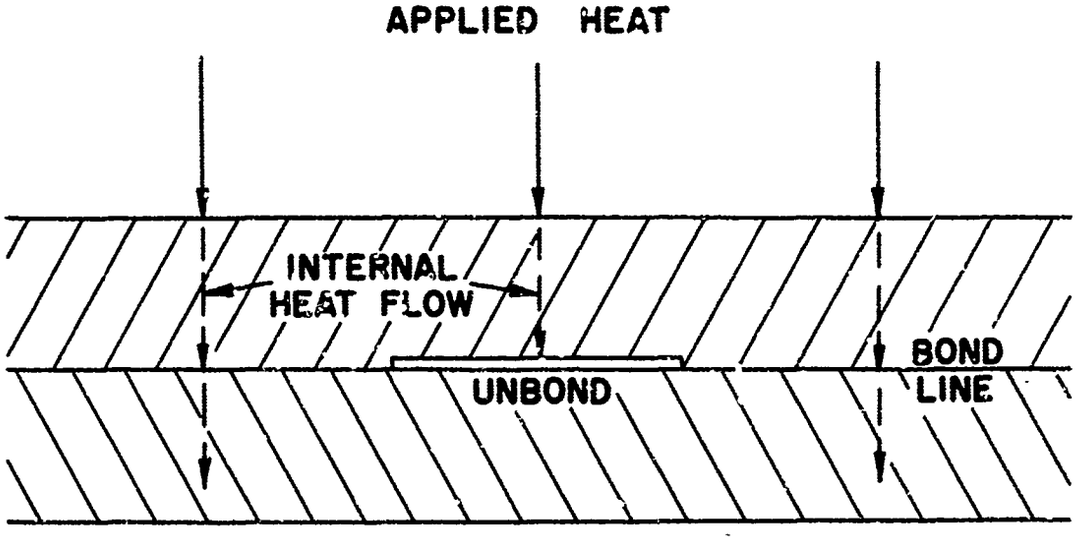


Figure 2. Heat Flow in a Laminate

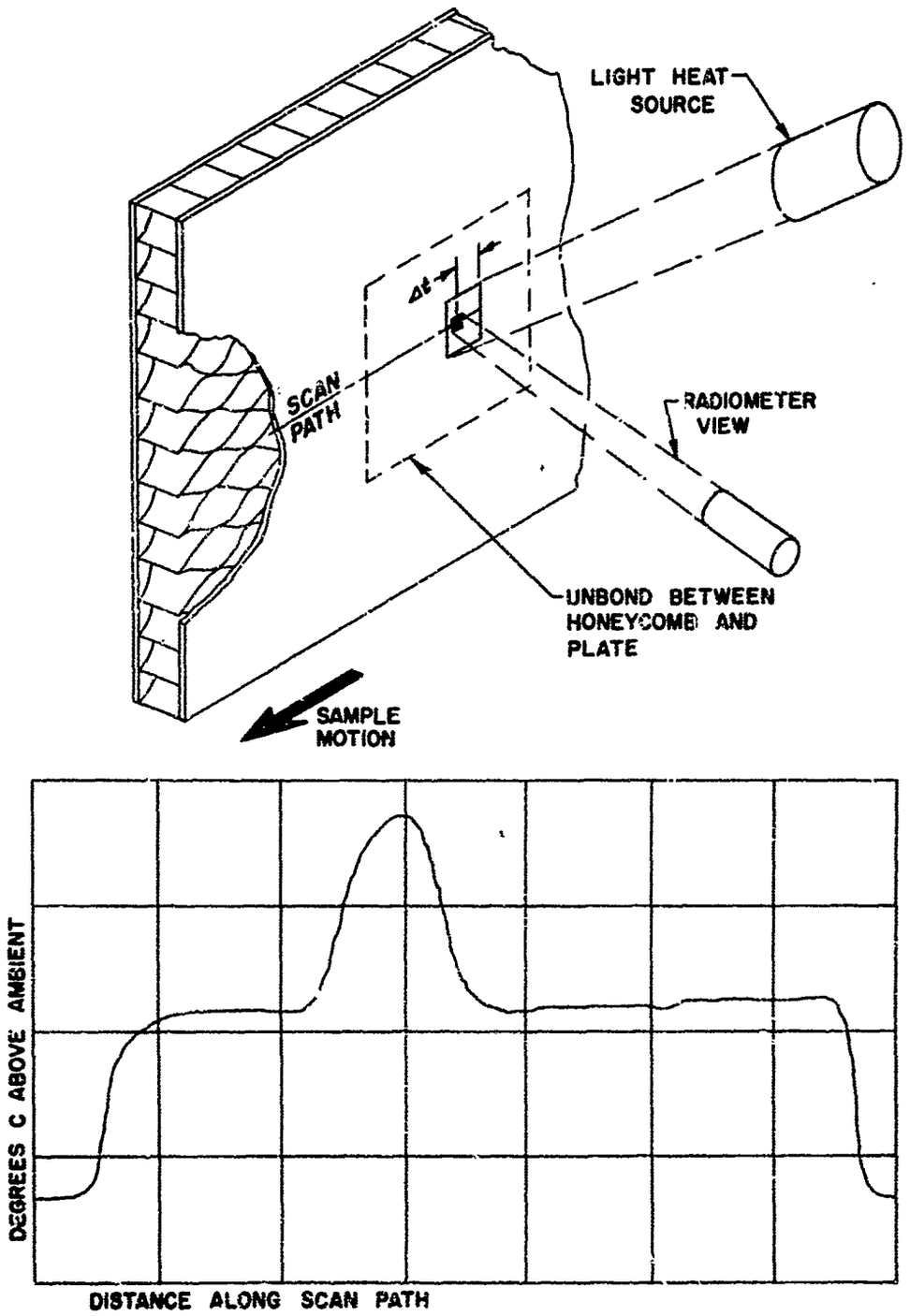


Figure 3. Line Scan Test

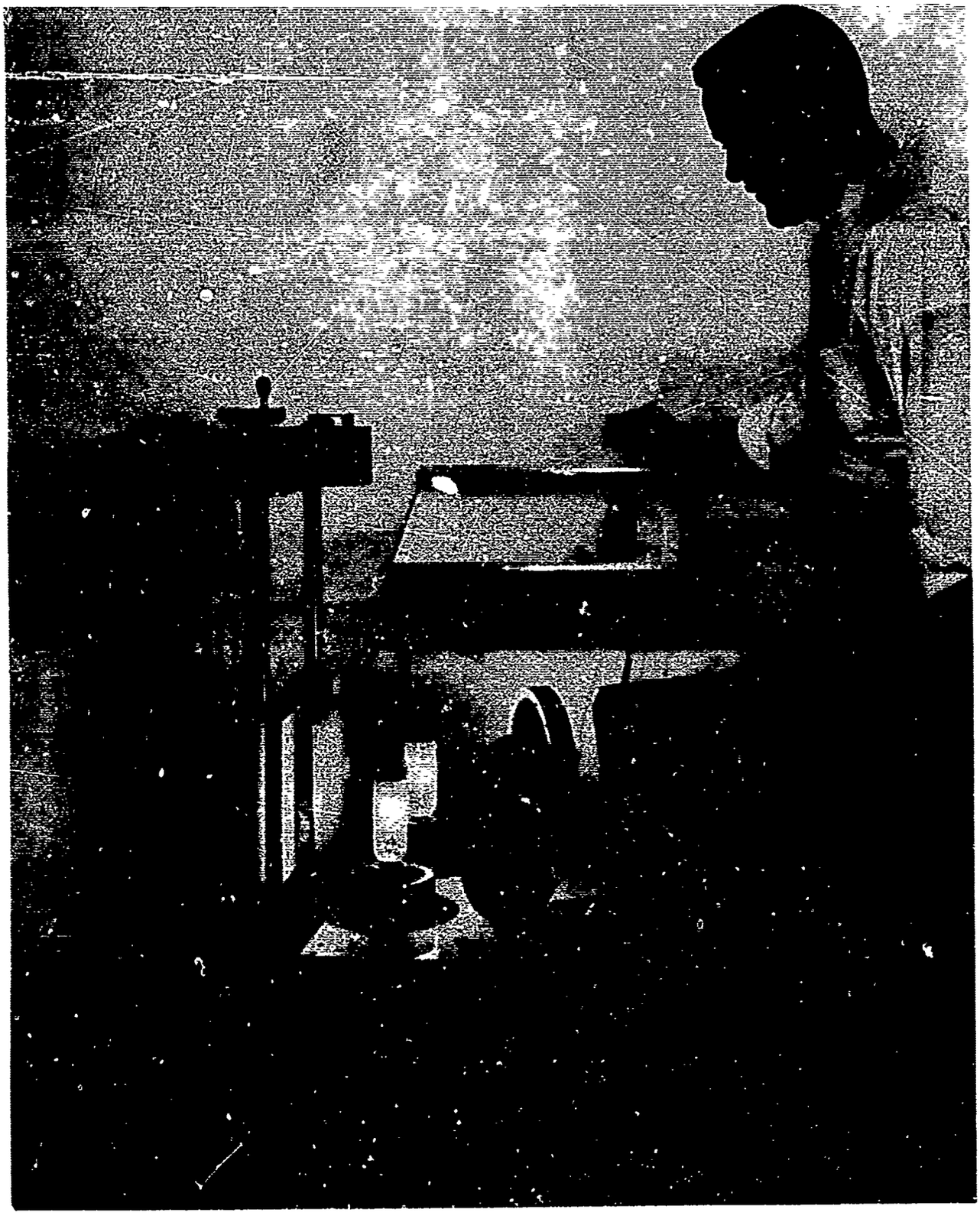


Figure 4. Line Scan System

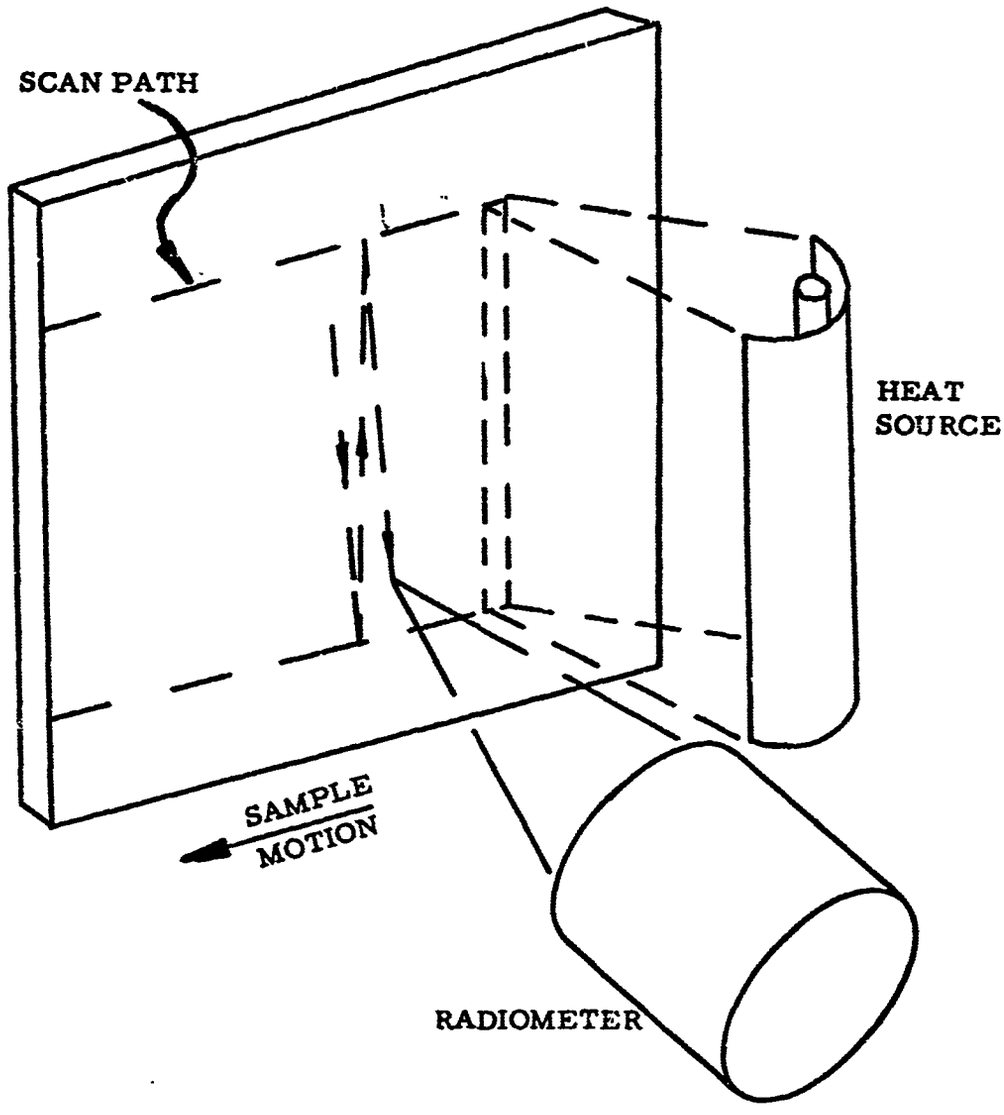


Figure 5. Area Scan Test

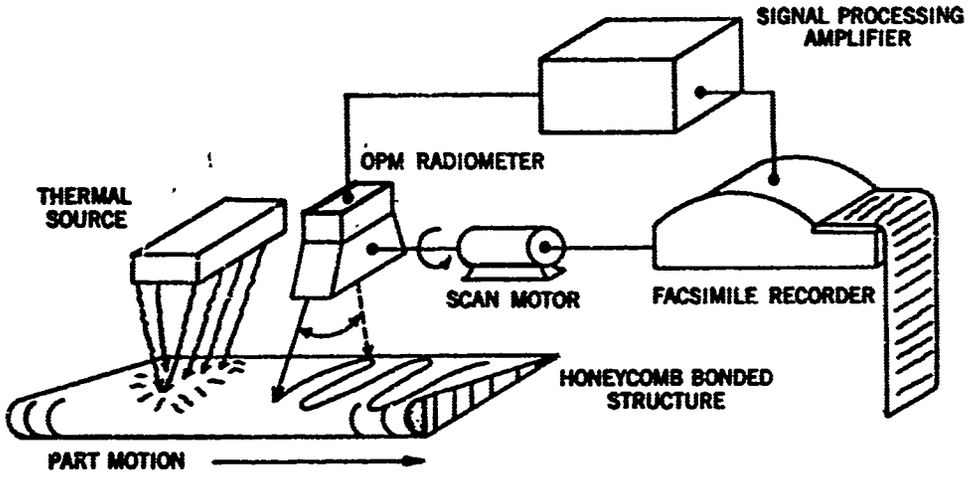


Figure 6. Area Scan Schematic



Figure 7. Area Scan System

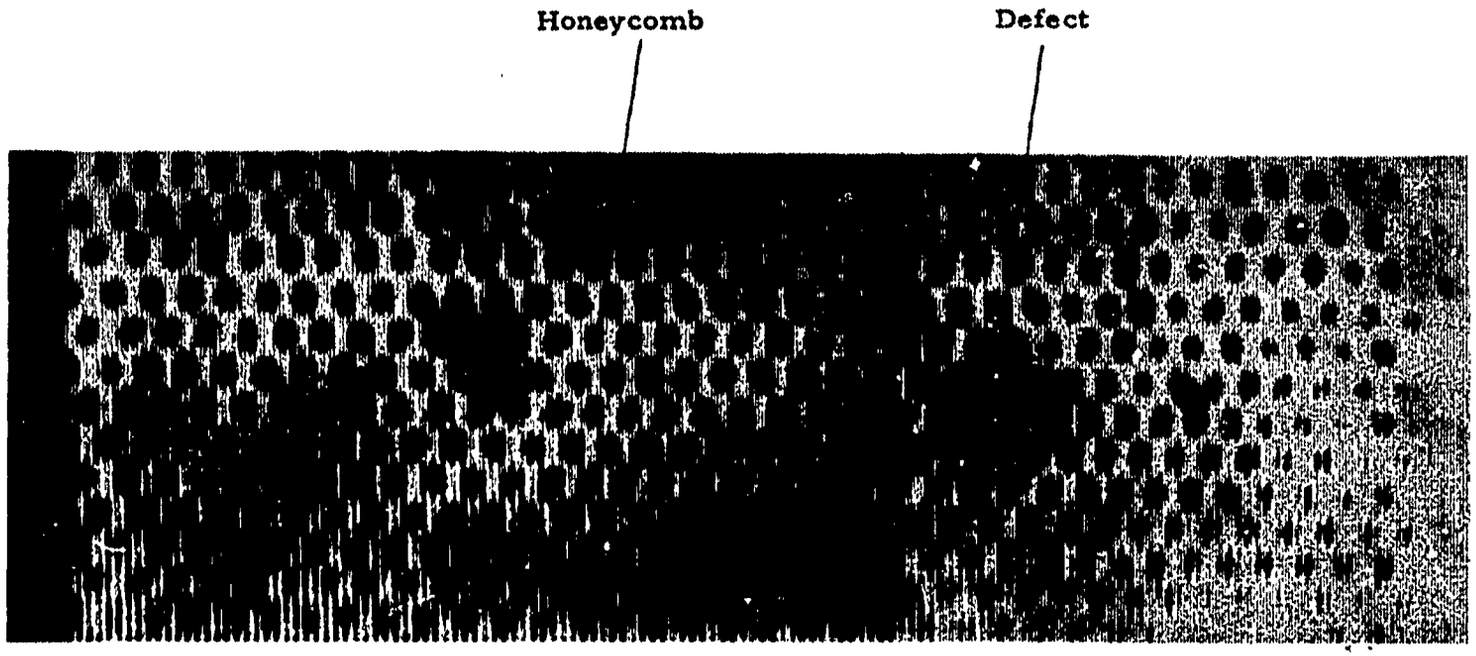
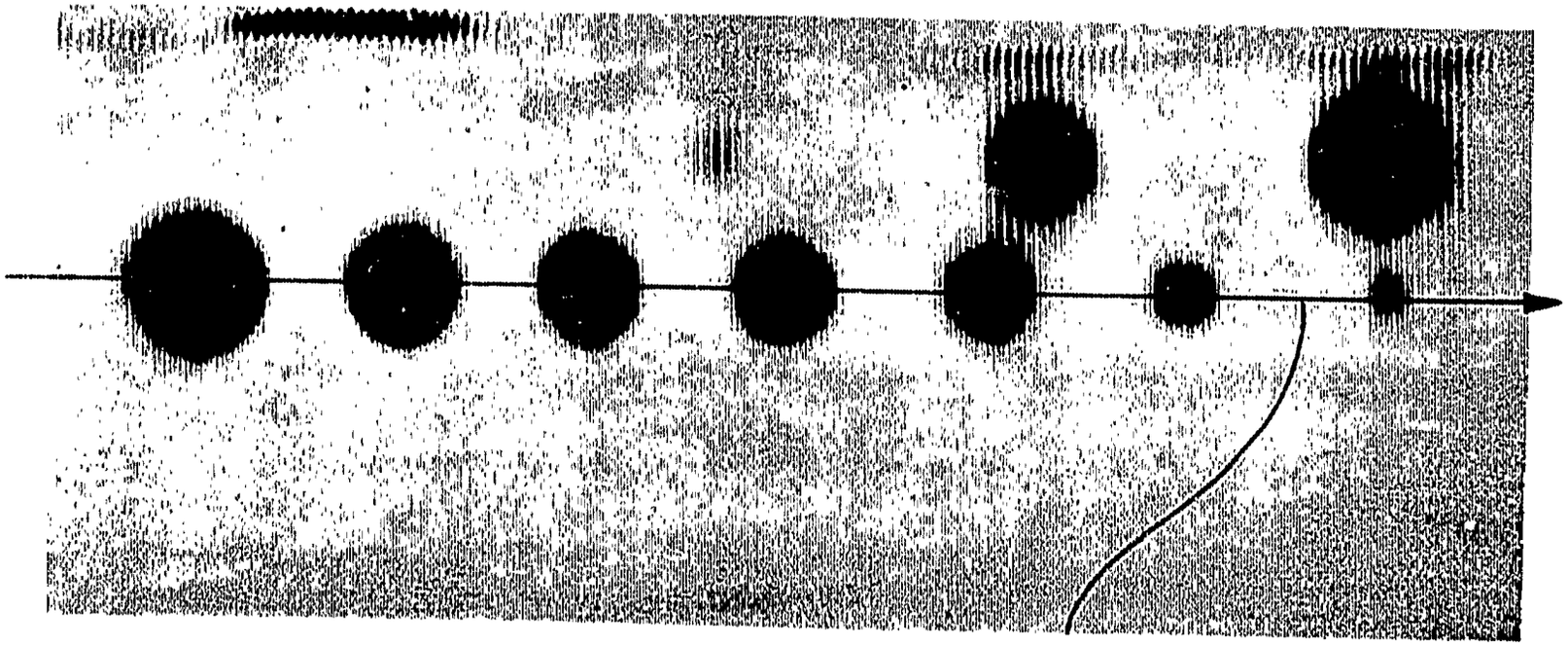


Figure 8. Fiberglass-Aluminum Honeycomb Test Results

VARYING DEPTH DEFECTS



VARYING SIZE DEFECTS

Figure 9. Carbon - Fiberglass Laminate

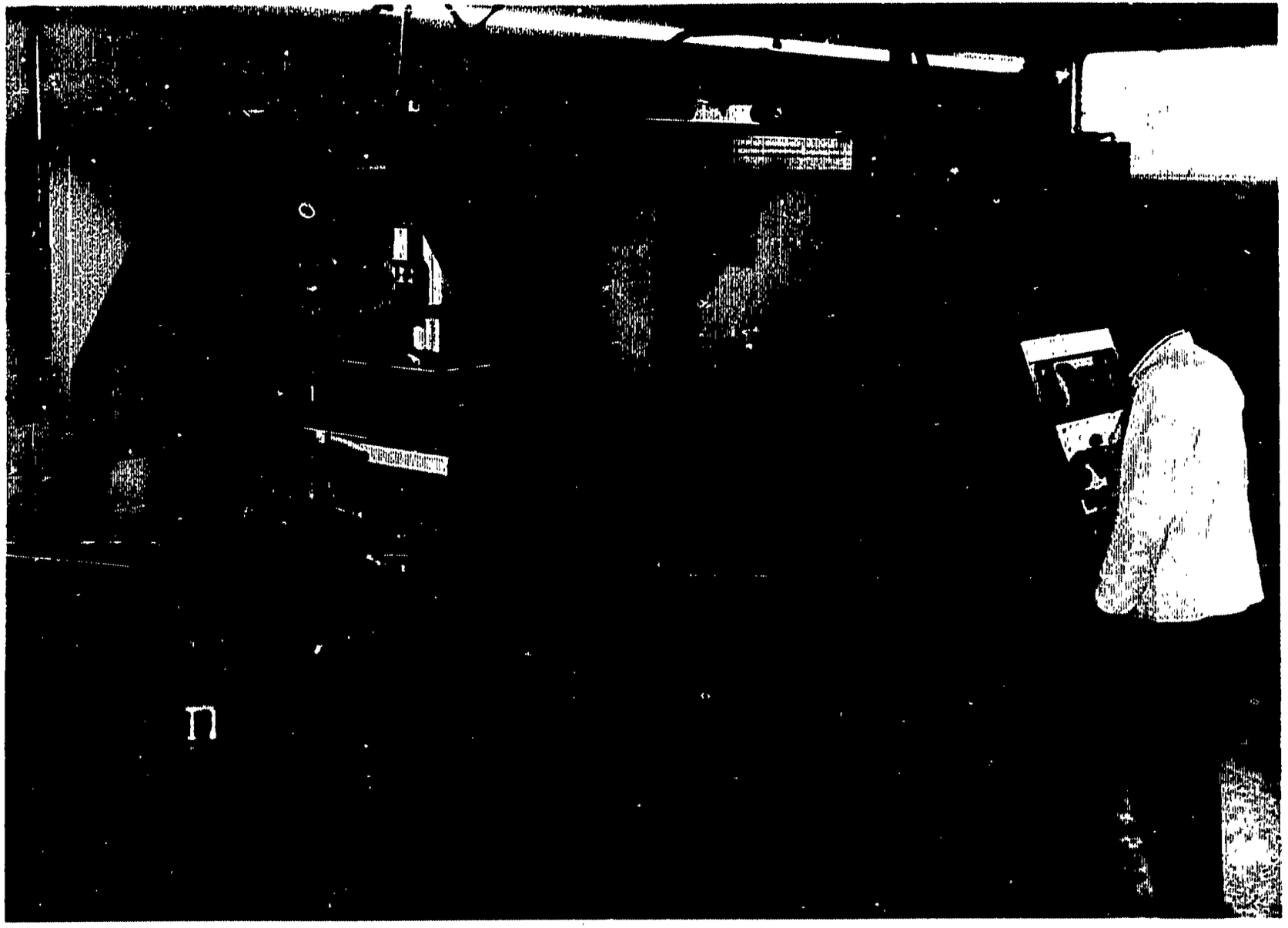


Figure 10. Production Inspection System

PRELIMINARY NONDESTRUCTIVE EVALUATION OF RESIN MATRIX COMPOSITES SUBJECTED TO IMPULSIVE LOADING

by

J. L. Cook
J. S. Evangelides
D. F. Moon
J. E. Zimmer

Materials and Methods - Research and Engineering
McDonnell Douglas Astronautics Company -
Western Division
Santa Monica, California

For Presentation at the
Aerospace-AFML Conference on NDT
of Plastic/Composite Structures
Dayton, Ohio
March 18-20, 1969

ABSTRACT

The study of the mechanical behavior of materials at high loading or strain rates is limited by equipment capabilities. Moving crosshead machines are currently limited to rates below 30,000 inches per minute. To simulate higher loading rates, high velocity impacting flyer techniques are employed, such as gas gun and exploding foil impact tests. Measurement and definition of material response and structural changes resulting from exploding foil impact (plate slap) tests have not been standardized and vary widely depending upon individual visual interpretation. Nondestructive examination before and after such tests can indicate changes that have occurred which are not detectable by visual examination.

To assess the extent of change within resin matrix composites after impulsive loading, pre- and post-test nondestructive examinations were performed on two-directional and multidirectional reinforced quartz-phenolic composite specimens. Film radiography, acoustic velocity measurements, and attenuation C-scan mapping were employed to characterize material changes. Comparison of the pre- and post-test X-ray radiographs showed little indication of change. Analysis of the velocity and attenuation data showed that the acoustic velocity of the composite materials decreased and the attenuation increased due to plate slap testing. It is shown that this decrease in velocity and increase in attenuation can be related to an increase in impulsive loading for both the two- and multidirectionally reinforced composites.

INTRODUCTION

One of the major applications of resin matrix composites is for re-entry vehicle heat shields. These heat shields may be subject to in-flight impulsive loading which can produce unfavorable material changes - a reduction in mechanical strength and a decrease in ablation resistance. The effect of these material changes on the vehicle performance is of importance to the design engineer. Therefore, a need exists to know how impulsive loading will affect the resin matrix composite heat shield materials and what material changes have occurred which would affect the vehicle performance.

To simulate in-flight impulsive loading, high strain rate tests can be performed on the heat shield materials. Such tests include tension and compression tests with moving crosshead machines. These moving crosshead machines are currently limited to rates below 30,000 inches per minute. To obtain higher loading rates, impact testing has been used. Included in this type of testing are Hopkinson's bar testing and high loading rate impact testing employing gas gun or exploding foil techniques. One such technique is plate slap testing. This technique involves impacting a plate of one material, the flyer plate, against a target of another material at a high velocity, producing a short duration stress wave in the impacted material, (Figure 1).

Each of these tests can cause changes in the properties and the structure of the tested material. A method for measuring these material changes is necessary. Mechanical testing of material that has been preshocked by Hopkinson's bar testing has been used to assess these material changes[1]. Another method of assessing the changes in impact tested material is by visual examination. This visual examination allows only a qualitative assessment of changes in material properties and as a result, there is a need to quantitively and more accurately assess these changes for plate slap testing. Other possible methods for such an evaluation includes nondestructive analysis, physical property tests, such as ablation and heat transfer, and impact testing of preshocked material.

This paper describes the preliminary work on the assessment of material changes in resin matrix composites due to plate slap testing using several nondestructive techniques. This paper covers the initial aspects of an intensive study currently in progress at McDonnell Douglas Astronautics Company - Western Division (MDAC-WD) to relate nondestructive analysis and mechanical testing to material changes and plate slap test parameters.

TECHNICAL APPROACH

The materials evaluated in this program were a two-directionally reinforced laminate and a multidirectional full-angle interlock (designated DACLOCK 120) quartz-phenolic composite. The two directional laminate was fabricated at MDAC-WD such that the fiber direction in each layer was 90° from the direction of the layers immediately adjacent (Figure 2). These alternating layers are perpendicular to the thickness direction. This fabric was impregnated with Monsanto SC1008 resin and cured. This two-directional composite is currently being used on re-entry vehicle systems.

The multidirectional full-angle interlock quartz phenolic composite was woven at Monsanto in Durham, North Carolina and then impregnated with SC1008 and cured at MDAC-WD. The multidirectional construction of this fabric consists of fibers at 90° to each other in layers with additional fibers at a 30° angle to the layers (Figures 3 and 4). This multidirectional composite has recently received considerable attention for re-entry vehicle heat shields due to its superior properties (interlaminar shear strength) in the thickness direction, which provides resistance to stress wave propagation damage and increased ablation and spallation resistance over other woven composites.

The two-directional laminated composite subjected to an impulsive loading test was expected to delaminate since the direction of stress wave propagation was perpendicular to the layers. Such delamination is visually apparent after severe impulse loading tests (Figure 5) and is reflected in spallation and complete delamination of the specimen. After less severe tests, some delamination may be seen at the specimen edges and sectioning can reveal delaminations within the specimen.

The multidirectional composite with the full-angled construction will not delaminate in the same sense as the two-directional laminated composite. Rather, internal changes such as micro-cracking or crazing of the resin matrix might be expected.

The assessment of material changes due to impulse loading has at present been accomplished primarily by visual examination. However, this technique has not been capable of completely assessing and quantitizing the changes within the material. Visual examination of the surface or microstructure is a subjective assessment dependent on the individual performing the examination and it is not always clear if all material changes can be detected by visual examination.

Nondestructive analysis may be applied to the evaluation of plate slap specimens to provide a means of detecting and quantitizing material changes. The changes occurring due to plate slap testing in the two- and multidirectional composite specimens are

expected to effect ultrasonic wave propagation. Small cracks, crazed resin, and delaminations cause the material to be a discontinuous medium which will inhibit the transmittance of ultrasonic waves. Therefore, the longitudinal wave velocity is expected to decrease and the acoustic attenuation to increase in a tested plate slap specimen.

Changes in fiber orientation or weaving geometry due to impulse testing might be revealed by X-ray radiography. This technique has been successfully used at MDAC-WD to study weaving irregularities in woven composites. Therefore, to aid in the quantitization of these changes, three nondestructive techniques, acoustic velocity, attenuation C-scan mapping and X-ray radiography, were applied before and after impact testing.

A pulse-echo technique which operates on the principal of reflecting ultrasonic waves from a discrete discontinuity within a material was used in the pre-test evaluation of the two-directional composites specimens to detect delaminations and other discrete defects[2,3]. The equipment used (Figure 6) utilized an Alden hot wire recorder to provide C-scan maps of the specimens. This technique could not be applied to the post test evaluation due to the high attenuation of the two directional laminate and multidirectional composite specimens after impact testing. A highly attenuating material will significantly reduce the strength of the reflected signal to the point of reducing the effectiveness of the pulse echo technique.

The acoustic attenuation or loss of signal strength through a material was measured by a through transmission technique Figure 7)[2,4]. Attenuation (expressed in units of decibels) is defined as the logarithm of the ratio of input to output power where power can be expressed as impedance times voltage squared[6]. Thus, the attenuation A_s of a specimen is given by

$$A_s = -10 \log \frac{z_1 V_1^2}{z_2 V_{2s}^2}$$

and the attenuation of the specimen-free water path is given by

$$A_w = -10 \log \frac{z_1 V_1^2}{z_2 V_{2w}^2}$$

where

z_1, z_2 are the impedances of the input and output networks, respectively.

V_1, V_2 are the input and output voltages of the transmitting and receiving transducers, respectively.

This through transmission technique measures the difference in these two attenuations:

$$A_s - A_w = -20 \log \frac{V_{2w}}{V_{2s}}$$

This equation shows that attenuation measured by this technique is independent of the type of apparatus used and of the impedances of the transmitting and receiving circuits. The impedances of the receiving network components must be matched, since reflections occur, due to impedance mismatch which cause nonlinear attenuation losses[7]. The measured attenuation, using the calibrated attenuator, is the attenuation of the specimen since the attenuation of the water is negligible (.002 db/cm).

The through transmission technique was used for attenuation measurements because the materials under study possess a high attenuation level after plate slap tests prohibiting the use of pulse-echo techniques. The equipment used to measure and record the acoustic attenuation is shown in Figure 7. An increase or decrease in the attenuation of the energy passing through the specimen was indicated by the changing amplitude of the displayed signal. Using the decibel attenuator, specific levels of attenuation were recorded with the writing current for the Alden hot wire C-scan recorder being switched on or off by the signal height. The sensitivity of this on-off writing is less than 1 db. Specific decibel losses were measured through each specimen at frequencies ranging from 0.5 MHz to 2.5 MHz to determine the frequency dependence of attenuation for the resin matrix composites[8].

During the course of the program it was found necessary to study several factors affecting the accuracy and repeatibility of the C-scan maps of the specimens. An initial study was undertaken to determine the effects of flat and focused transducers on the through transmission technique. This was accomplished by making separate C-scan maps on one specimen with a flat and then focused transmitter. Also studied were edge effects, identified by making C-scan maps at different attenuation levels on the same specimen.

The longitudinal wave velocity was measured by a through transmission technique employing two transducers in direct contact with the specimens, using glycerin as the couplant (Figure 8)[2,5,9]. The pulse traveling through the specimen was detected by the receiving transducer and compared to an undelayed pulse which triggered the scope. The difference in these two times, as measured at the initial frequency cycle of the pulse, was the time required for the wavefront to traverse the specimen. Due to the high attenuation of the specimen and the frequency dependence of attenuation, velocity measurements were made at one relatively low frequency, 0.5 MHz.

All X-ray radiographs were taken with a Penetrex 50 kv constant potential beryllium window unit. While exposures varied slightly between the laminated and multidirectional composites, the most common parameters were 50 kv at 10 ma for two minutes with a film-to-source distance of 24 inches. All film (Kokak M Redipak) was processed under the same conditions through automatic equipment (Kodak Industrial X-Omat).

RESULTS AND DISCUSSION

Ultrasonic velocity measurements conducted on pre- and post-test plate slap specimens of two directional and multidirectional quartz-phenolic composites are given in Tables 1 and 2. Evident is a significant decrease in acoustic velocity as a result of plate slap testing. Also in Table 2 is the pre- and post-test attenuation of the multidirectional composite, which shows a large increase in the attenuation of the composite due to plate slap testing.

The X-ray radiographs of selected multidirectional plate slap specimens (Figure 9) show little change in the pre- and post-test specimens. Weave irregularities present in the untested material seem to be unchanged in the tested material and in general, the regular weave pattern does not seem to be altered.

Through transmission attenuation C-scan maps (Figure 10) were made for the untested and tested two directional composite. The dark areas correspond to regions of the specimens which are more attenuating. The attenuation reccrding level is greater for the tested material, again showing the large increase in attenuation due to plate slap testing. The C-scan maps are excellent for outlining the areas of greater material change in the tested specimens. The location of material change as a result of the plate slap test can indicate how the material was affected and how uniformly the material responded to impulsive loading.

The attenuation of the multidirectional quartz phenolic composite was found to be frequency dependent. For the untested material, the attenuation increased from 15 db to 36 db for an increase in frequency from 0.5 MHz to 2.25 MHz. All C-scan maps shown in this paper were made using a frequency of 1.0 MHz.

The outlining of the untested specimen on the attenuation C-scan maps in Figure 10 is due to edge effects. At low attenuation levels, scattering of the ultrasonic wave by the edges decreases the intensity of the received signal and the apparatus records this loss in signal strength as an increase in attenuation (dark area on C-scan map). At higher attenuation levels, this scattering does not significantly affect the strength of the received signal and outlining does not occur.

Figure 11 shows an example of pre- and post-test C-scan maps for the multidirectional composite. The attenuation level is greater for the tested material and the area of greater material change is outlined as for the two-directional composite. C-scan maps were made at different attenuation levels (Figure 12) for the tested multidirectional composite. This figure shows that the attenuation varies among the specimens and that the material change is greater in the center region of the specimen.

The above C-scan maps were all made using a 3/4-inch diameter flat transmitting transducer and a 3/8-inch diameter flat receiver. The use of a focused transmitting transducer was investigated and found to provide excellent C-scan maps. A 1 inch diameter focused transducer with a 3-inch focal length was focused on the back surface of the specimen. The effect of this focused transducer versus a flat transducer on attenuation C-scan mapping is shown in Figure 13. The outlining of the higher attenuating areas is more distinct and exact with the focused transducer.

The limitation of visual examination as a method for the assessment of material change is illustrated in Figure 14. The photographs of the impacted side of the three plate slap specimens indicate a large difference between the specimens where as the corresponding attenuation and velocity measurements do not indicate that there is a difference among the specimens. The relative material change, as measured by the attenuation and velocity techniques, is approximately the same for each specimen. The attenuation and velocity measurements show that there is internal material change due to plate slap testing which is not apparent and can not be quantitized by visual examination.

Nondestructive analysis may provide a quantitive assessment of material change as a result of plate slap testing. The relationships between acoustic velocity and a plate slap test parameter for the two-directional and multidirectional composites are given in Figures 15 and 16, respectively. These graphs show that for an increase in impulsive loading, the change in pre- and post-test velocity decreases. This decrease in velocity indicates a greater degree of material change associated with increasing impulsive loading.

Similar relationships exist between attenuation and the plate slap test parameter for both the composites (Figures 17 and 18). These graphs show that for an increase in impulsive loading, the attenuation of the tested material increases, indicating a change in the properties of the material.

CONCLUSIONS AND RECOMMENDATIONS

Nondestructive analysis can be used to assess material changes resulting from plate slap testing of resin matrix composites. The acoustic velocity decreased and the attenuation increased between untested and tested material. For increasing levels of impact, the acoustic velocity of the tested material decreased and the attenuation increased. X-ray radiography did not indicate any material changes.

Further work is required on the application and development of nondestructive techniques for the assessment of material change. The use of focused transducers as both transmitter and receiver and the use of smaller diameter flat receivers for attenuation C-scan mapping must be investigated. Mechanical testing and microstructural examination of material subjected to impact testing and nondestructive analysis needs to be completed. To accurately define the effect of material change on attenuation and velocity, a study is required to relate these measurements to tensile and compressive percent strain-to-failure. Also, by selected material removal, attenuation measurements need be made on an impact tested specimen to determine the through-thickness gradient of material change.

This work is planned or currently in progress at MDAC-WD as part of a continuing program to relate nondestructive analysis and mechanical testing to material change and plate slap test parameters.

ACKNOWLEDGEMENTS

The fabrication and the impact testing of the two-directional composite was accomplished under an Air Force Materials Laboratory contract (No. F33615-68-C-1414, Project No. PR 8M 308c4), A Critical Evaluation of Plate-Slap Technology. The multidirectional composite fabrication and impact testing was accomplished under a SAMSO contract (No. AF04 (694) - 953, Task 3), Re-entry Systems Environmental Protection. The nondestructive analysis was performed under McDonnell Douglas Astronautics Company - Western Division Independent Research and Development Program.

REFERENCES

1. S. J. Green, S. G. Babcock and R. D. Perkins, Fundamental Behavior Study, Final Report, Vol 1: Response of Several Reentry Vehicle Materials to Impulsive Loads, BSD-TR-67-23, February, 1967.

2. R. C. McMaster, Nondestructive Testing Handbook, Volume II, Ronald Press Company, 1959.

3. C. J. Adams, N. H. Radtke, and J. D. Klein, Ultrasonic Techniques and Standards for Testing Filament Wound Structures, ML-TDR-64-117, May 1964.

4. R. W. B. Stephens and A. E. Bate, Acoustics and Vibrational Physics, Edward Arnold Publishers Ltd., 1966.

5. G. E. Lockyer, A. W. Shultz, S. Serabian, and S. W. Carter, Investigation of Nondestructive Methods for the Evaluation of Graphite Materials, AFML-TR-67-128, April 1968.

6. B. Banks, G. E. Oldfield, H. Rawding, Ultrasonic Flaw Detection in Metals, Prentice Hall Inc., 1962.

7. J. Millman and H. Taub, Pulse, Digital and Switching Waveforms, McGraw Hill Book Co., 1965.

8. S. Serabian, Influence of Attenuation, Upon the Frequency Content of a Stress Wave, Pocket in Graphite, Journal of Acoustical Society of America, Vol. 42, No. 5, Nov. 1967.

9. J. R. Zurbrick, Development of Nondestructive Methods for the Quantitative Evaluation of Glass Reinforced Plastics, Technical Report AFML-TR-66-269, March 1967.

ULTRASONIC VELOCITY DATA FOR TWO DIRECTIONALLY REINFORCED COMPOSITE PLATE SLAP SPECIMENS

VELOCITY AT 0.5 MEGAHERTZ

SPECIMEN	PRE-TEST	POST-TEST
1	3057 M/SEC	2120 M/SEC
2	3069	1660
3	3117	1990
4	3061	1820
5	3072	1910
6	3194	2620

TABLE 1.

ATTENUATION AND VELOCITY DATA FOR MULTIDIRECTIONAL PLATE SLAP SPECIMENS

SPECIMEN NUMBER	ATTENUATION AT 1.0 MEGAHERTZ		VELOCITY AT 0.5 MEGAHERTZ	
	PRE-TEST	POST-TEST	PRE-TEST	POST-TEST
15	25 db	> 44 db	2303 M/SEC	1429 M/SEC
24	24	46	2267	834
19	31	45	2295	976
2	24	> 44	2307	1705
3	24	> 44	2307	1372
1	24	> 24, < 34	2307	2246
7	24	> 44	2366	1764
12	24	45	2303	2483
4	25	> 44	2307	1350
9	25	> 44	2366	1314
10	25	> 44	2366	1161
26	24	> 34, < 44	2251	1326
21	25	38	2267	2021
16	24	> 44	2295	1187
38	24	> 24, < 34	2181	1911
17	24	> 44	2295	1400
11	26	> 34, < 44	2303	1247

TABLE 2.

PLATE SLAP TEST
SINGLE PLATE EXPLODING FOIL ASSEMBLY

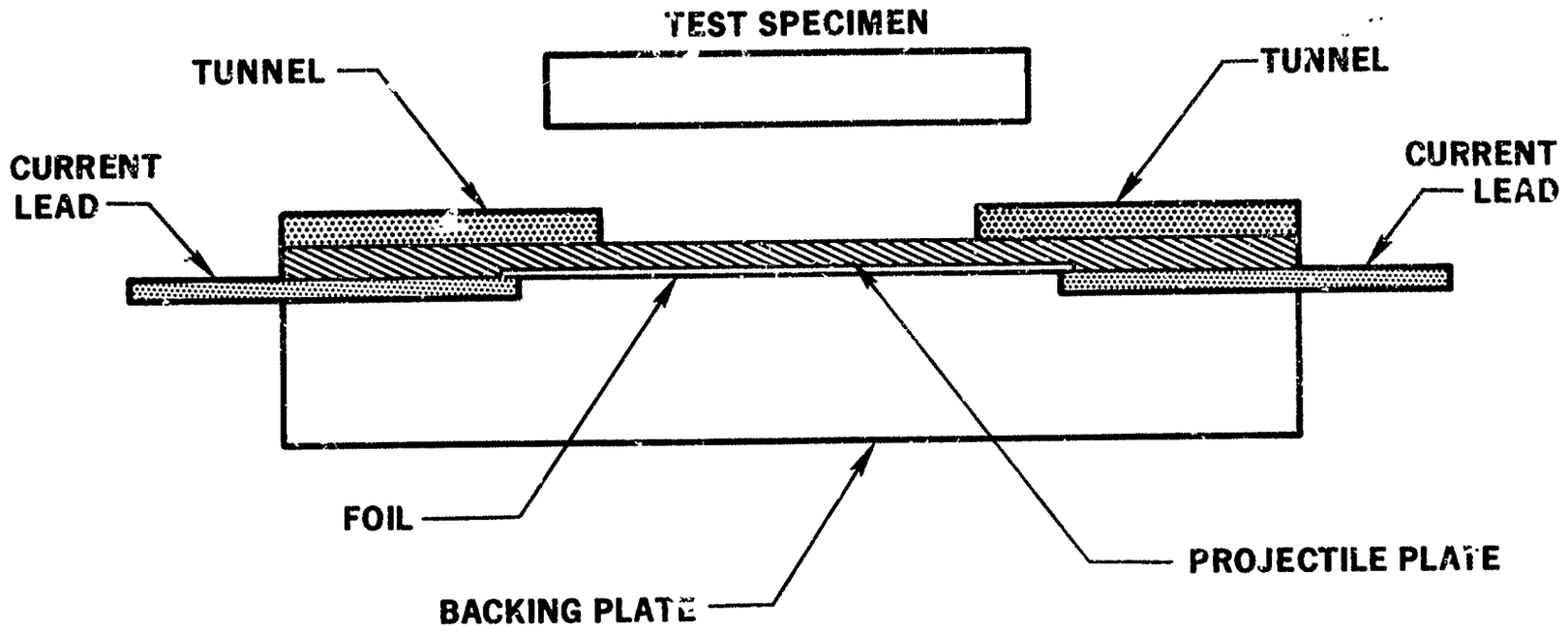


FIGURE 1

PHOTOMICROGRAPH OF TWO DIRECTIONAL LAMINATE TAKEN PARALLEL TO DIRECTION OF REINFORCEMENT - 25 X

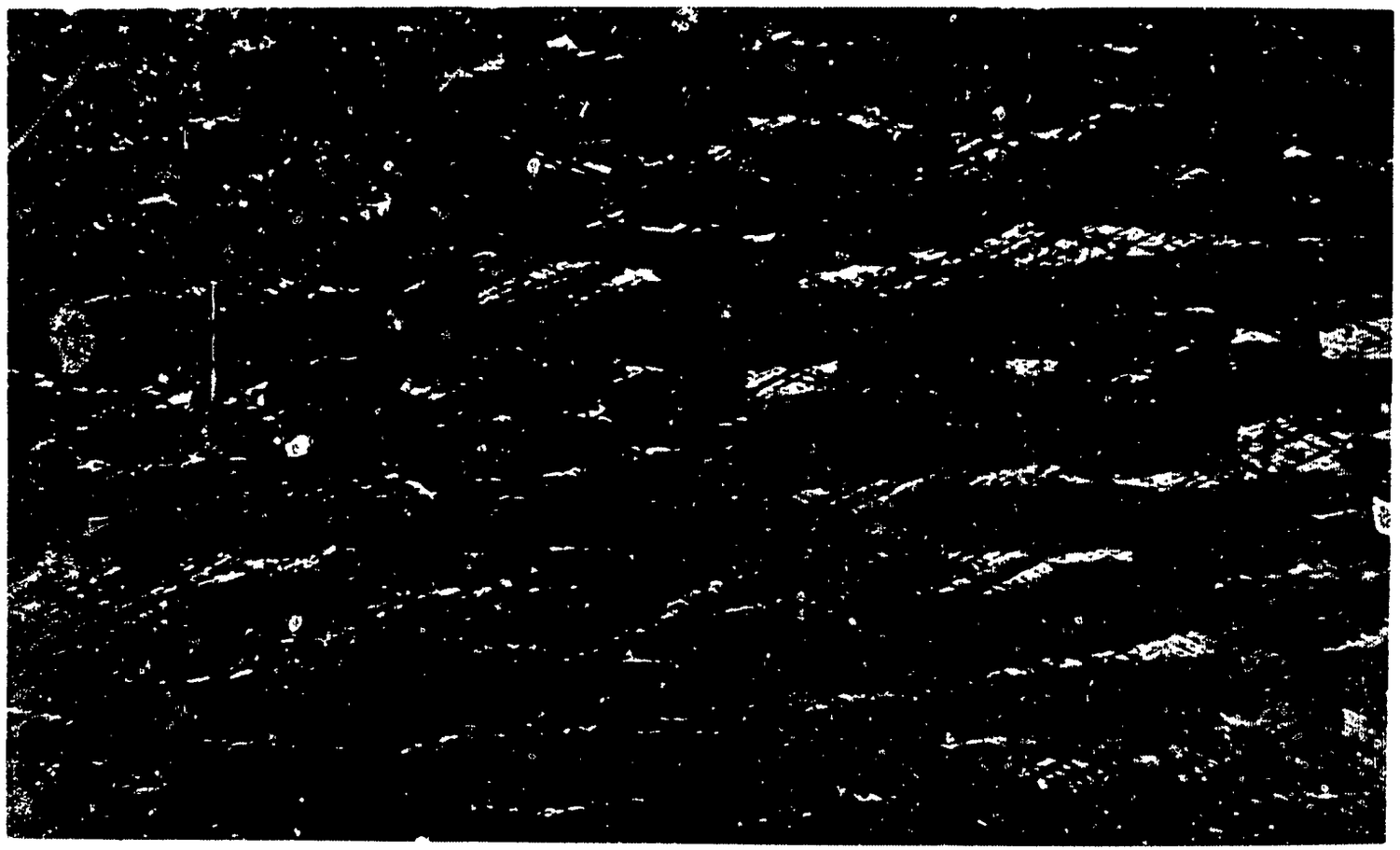


FIGURE 2

DACLOCK 120 WEAVE PATTERN

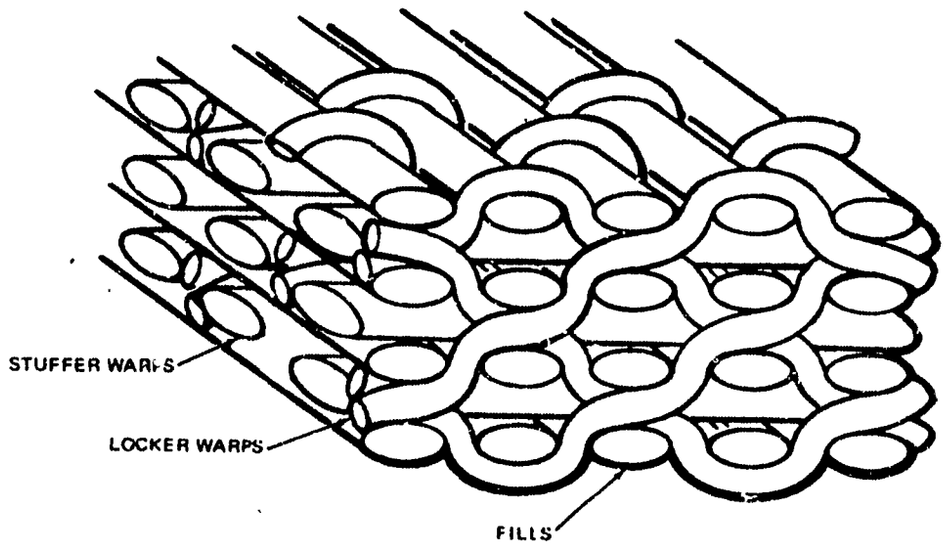
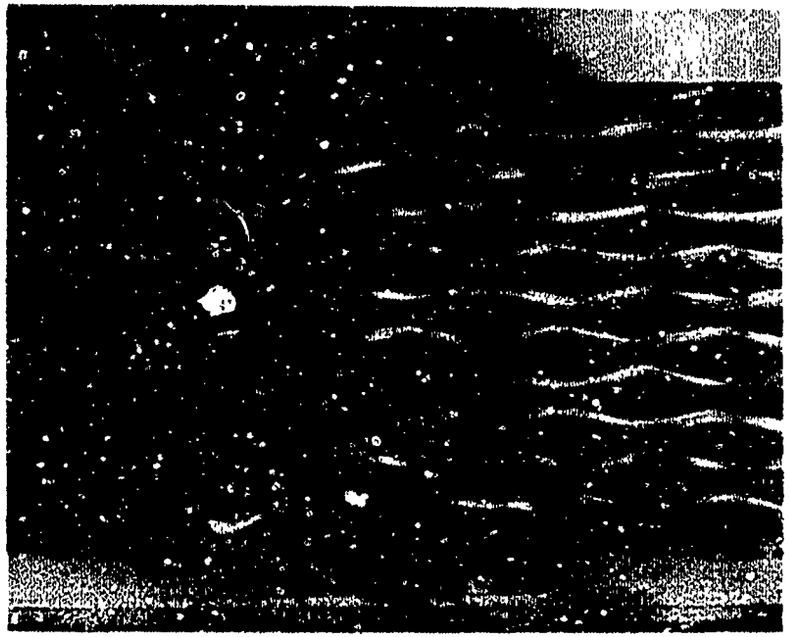


FIGURE 3

PHOTOMICROGRAPHS OF DACLOCK 120
WEAVE PATTERN - 10 X



a) END WARP



b) END FILL

FIGURE 4

PHOTOMACROGRAPH SHOWING DELAMINATION IN TWO DIRECTIONAL LAMINATE AFTER IMPULSE TESTING - 25 X

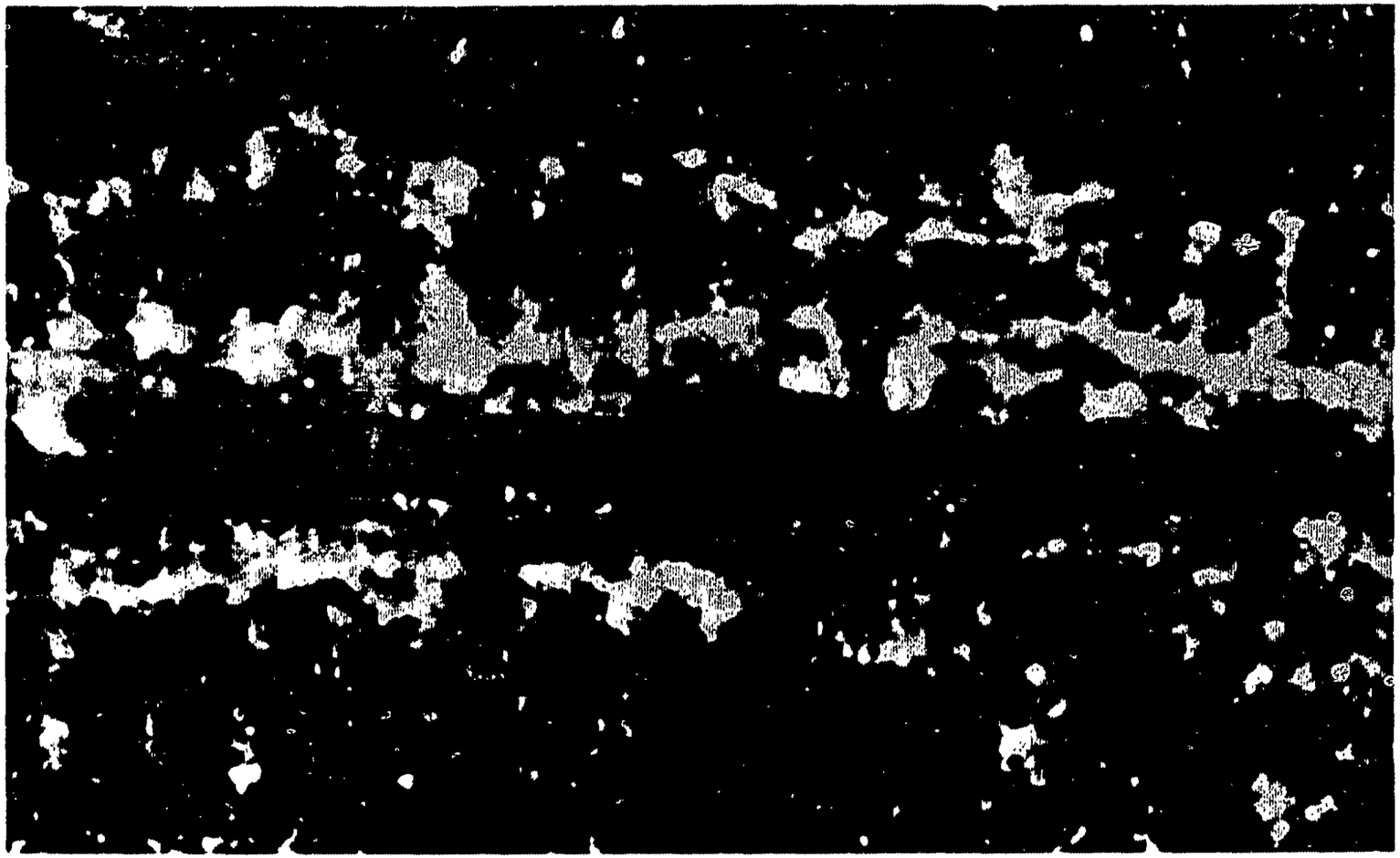


FIGURE 5

PULSE ECHO EQUIPMENT ARRANGEMENT

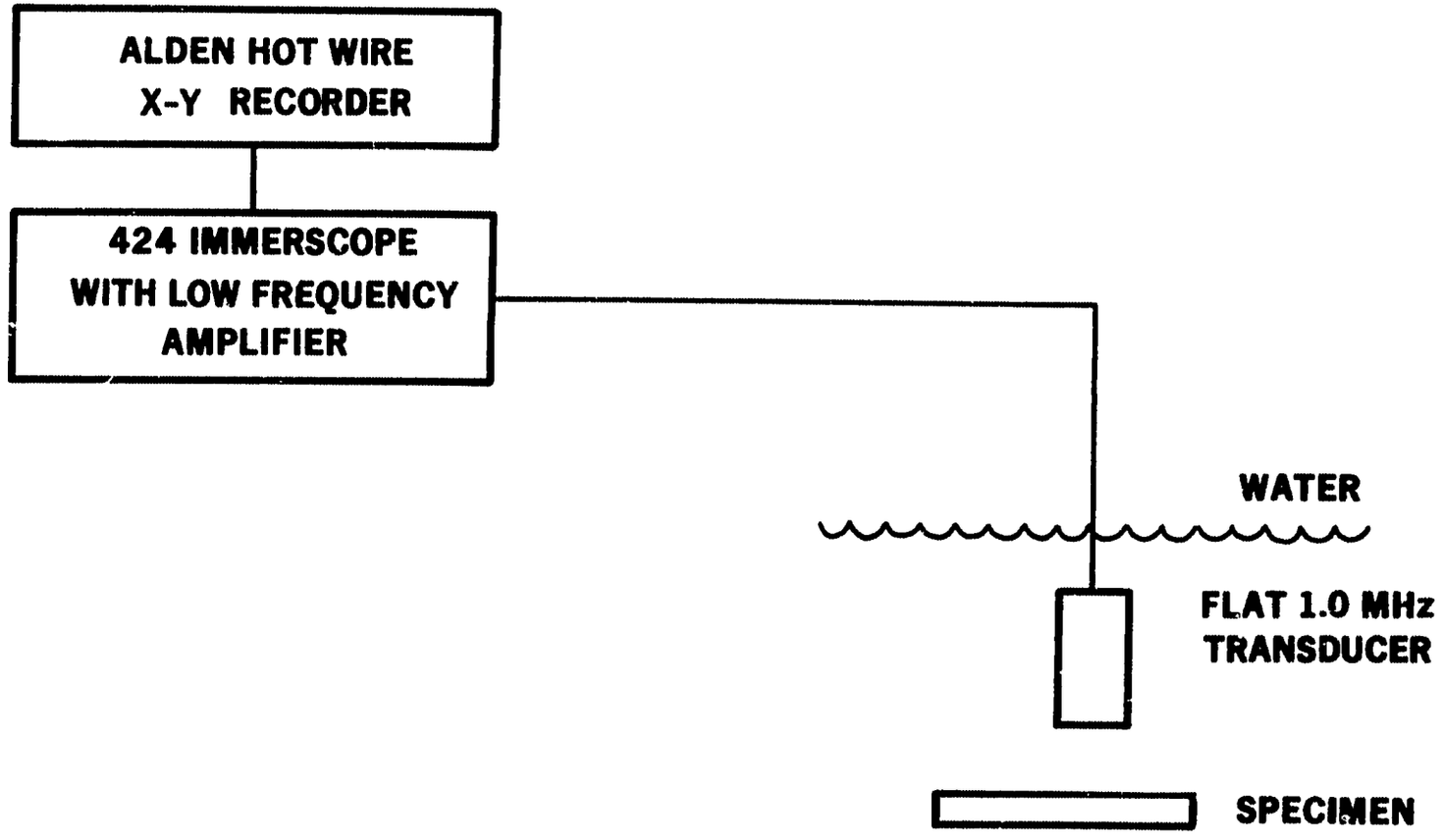


FIGURE 6

APPARATUS FOR THROUGH TRANSMISSION ATTENUATION MEASUREMENT

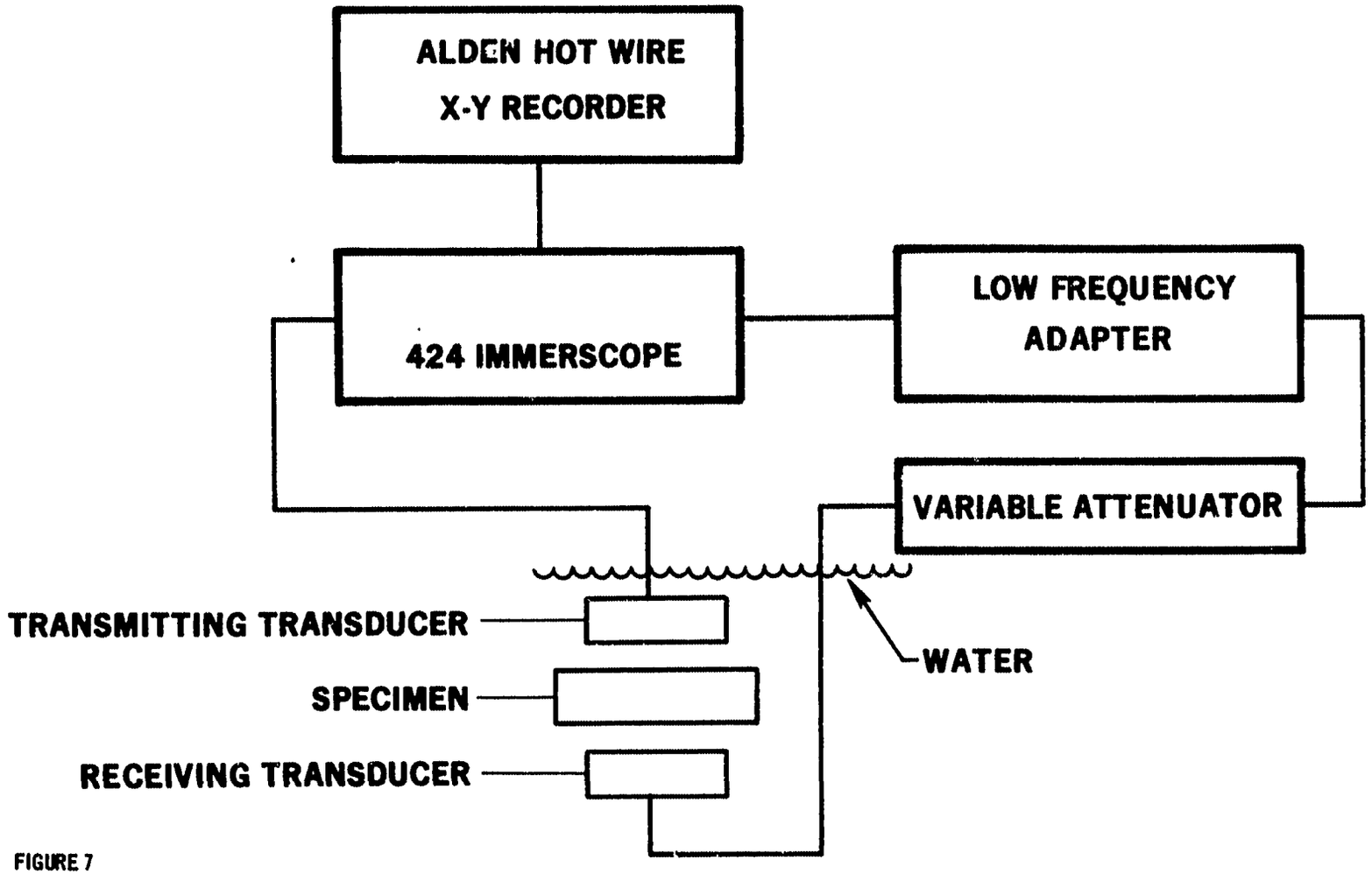


FIGURE 7

APPARATUS FOR ULTRASONIC PULSED THROUGH TRANSMISSION VELOCITY MEASUREMENT

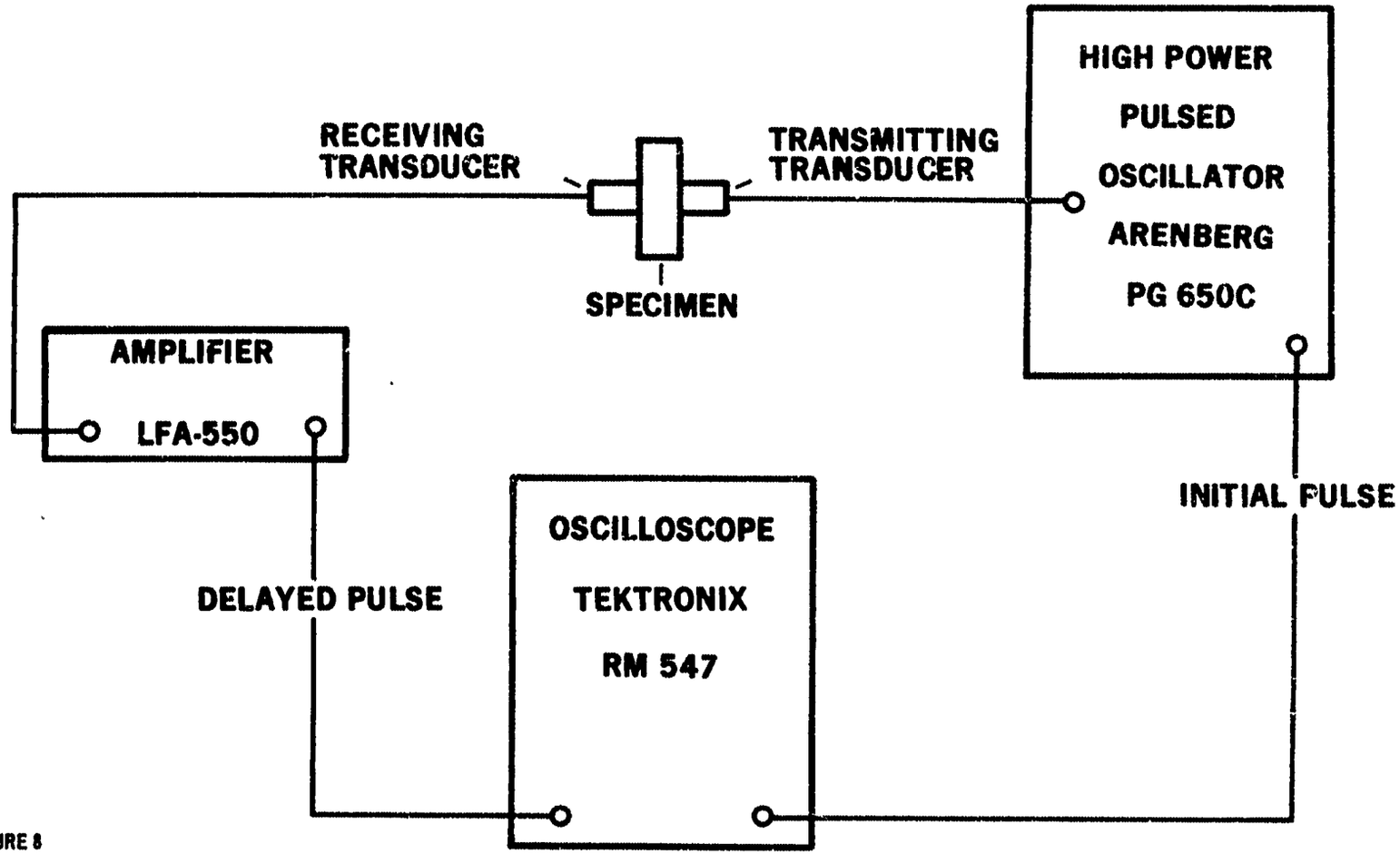


FIGURE 8

X-RAY RADIOGRAPHS OF MULTIDIRECTIONAL PLATE SLAP SPECIMENS

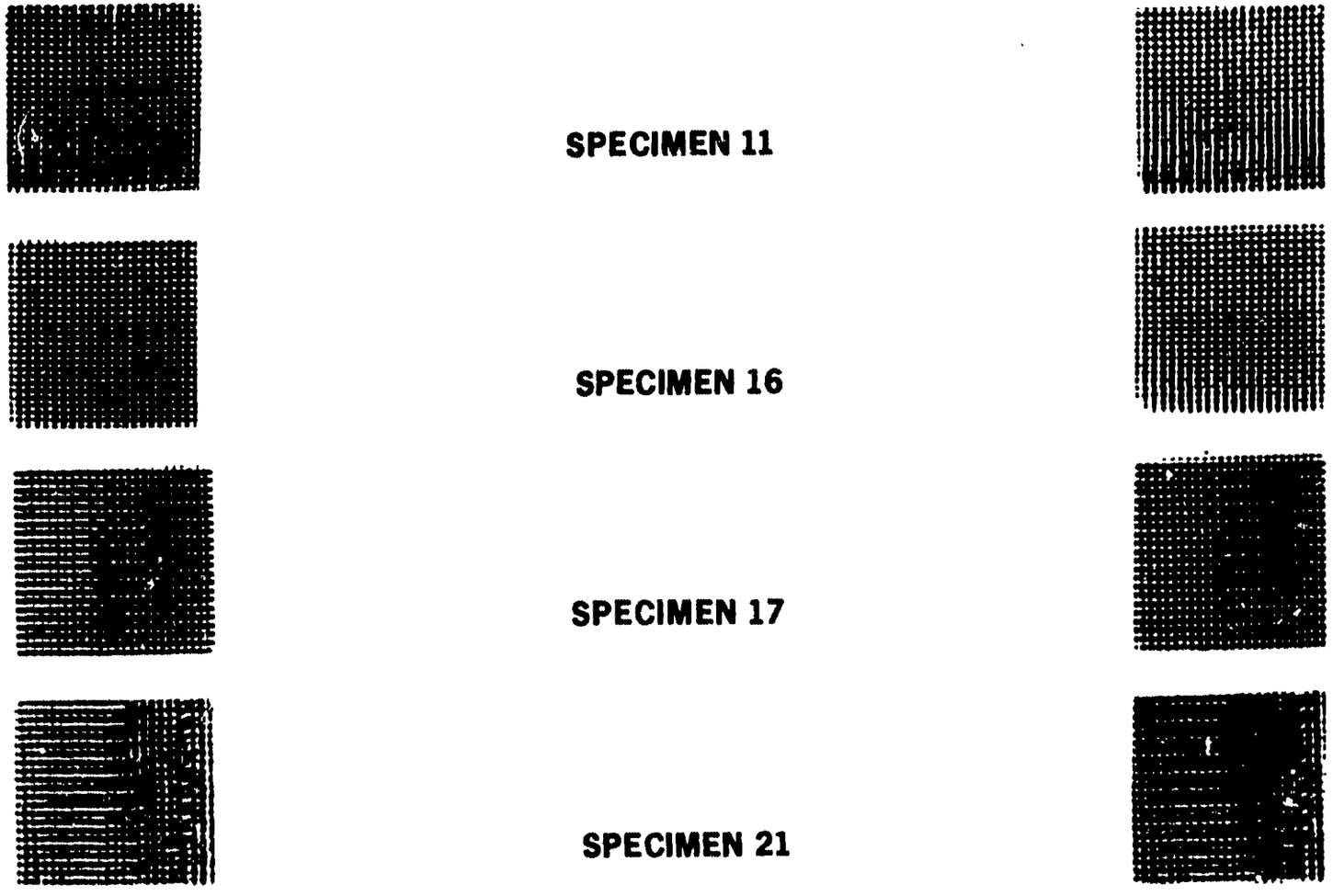
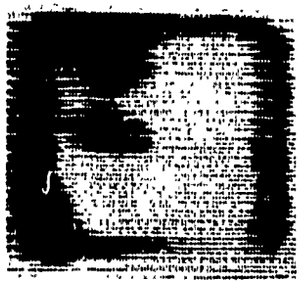


FIGURE 9

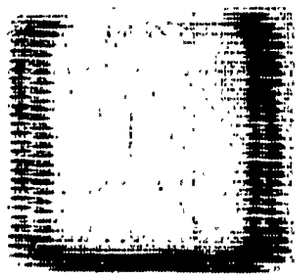
ATTENUATION C-SCAN MAPS OF TWO DIRECTIONAL COMPOSITE PLATE SLAP SPECIMENS

PRE-TEST

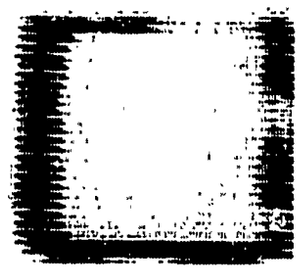
RECORDED AT 8 db



SPECIMEN 1



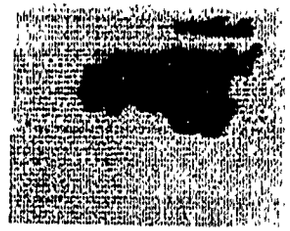
SPECIMEN 2

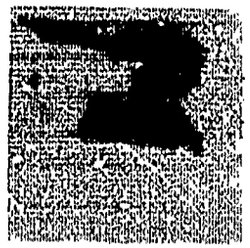


SPECIMEN 3

POST-TEST

RECORDED AT 30 db





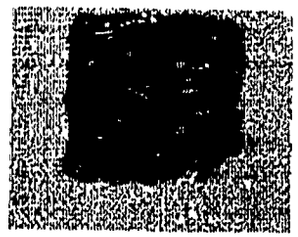
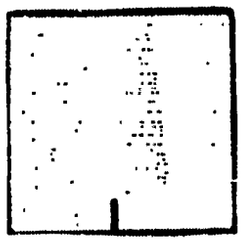


FIGURE 10

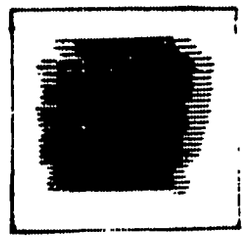
C-SCAN MAPS OF MULTIDIRECTIONAL PLATE SLAP SPECIMEN



SPECIMEN 1

PRE-TEST C-SCAN MAP

RECORDED AT 24 db



SPECIMEN 1

POST-TEST C-SCAN MAP

RECORDED AT 24 db

FIGURE 11

M68267

POST-TEST ATTENUATION C-SCAN MAPS OF MULTIDIRECTIONAL PLATE SLAP SPECIMENS

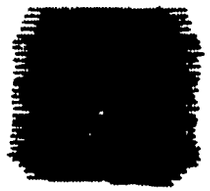
ATTENUATION LEVEL \ SPECIMEN NUMBER	1	11	10
24 dB			
34 dB			
44 dB			

FIGURE 12

EFFECT OF FOCUSED TRANSDUCER ON C-SCAN MAP OF TESTED PLATE SLAP SPECIMEN



SPECIMEN 5



3/4" DIA. FLAT TRANSDUCER

1" DIA. FOCUSED TRANSDUCER
3" FOCAL LENGTH

FIGURE 13

COMPARISON OF MULTIDIRECTIONAL COMPOSITE SPECIMENS AFTER IMPULSE TESTING



295

#10 MINIMUM VISUAL DAMAGE



334

#16 MODERATE VISUAL DAMAGE



277

#3 SEVERE VISUAL DAMAGE

ATTENUATION		VELOCITY (M/SEC)	
PRE-TEST	POST-TEST	PRE-TEST	POST-TEST
25 db	> 44 db	2366	1161
< 24	> 44	2295	1187
< 24	> 44	2307	1372

FIGURE 14

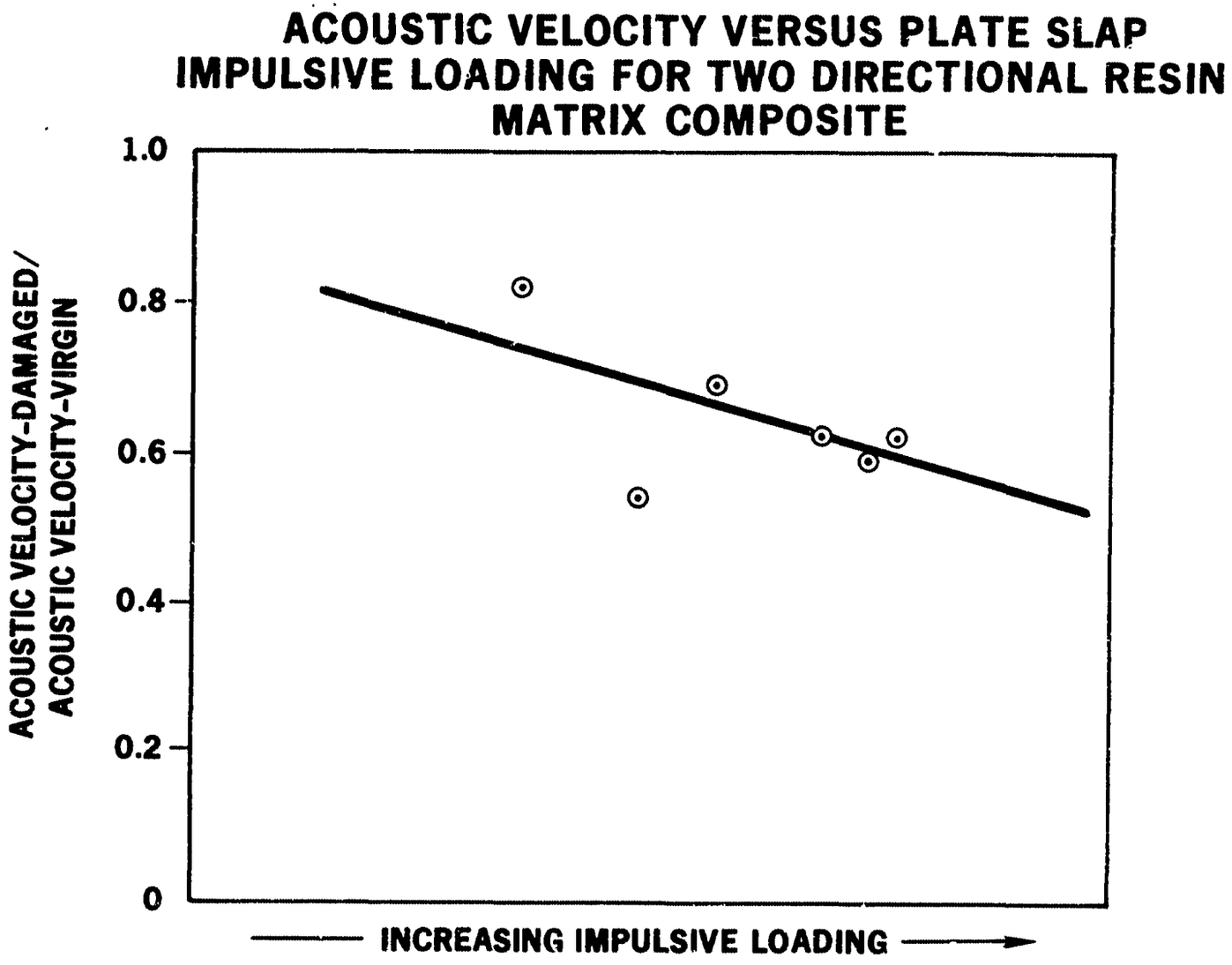

ACOUSTIC VELOCITY VERSUS PLATE SLAP IMPULSIVE LOADING FOR TWO DIRECTIONAL RESIN MATRIX COMPOSITE
ACOUSTIC VELOCITY-DAMAGED/ ACOUSTIC VELOCITY-VIRGIN
1.0
0.8
0.6
0.4
0.2
0
INCREASING IMPULSIVE LOADING

FIGURE 15

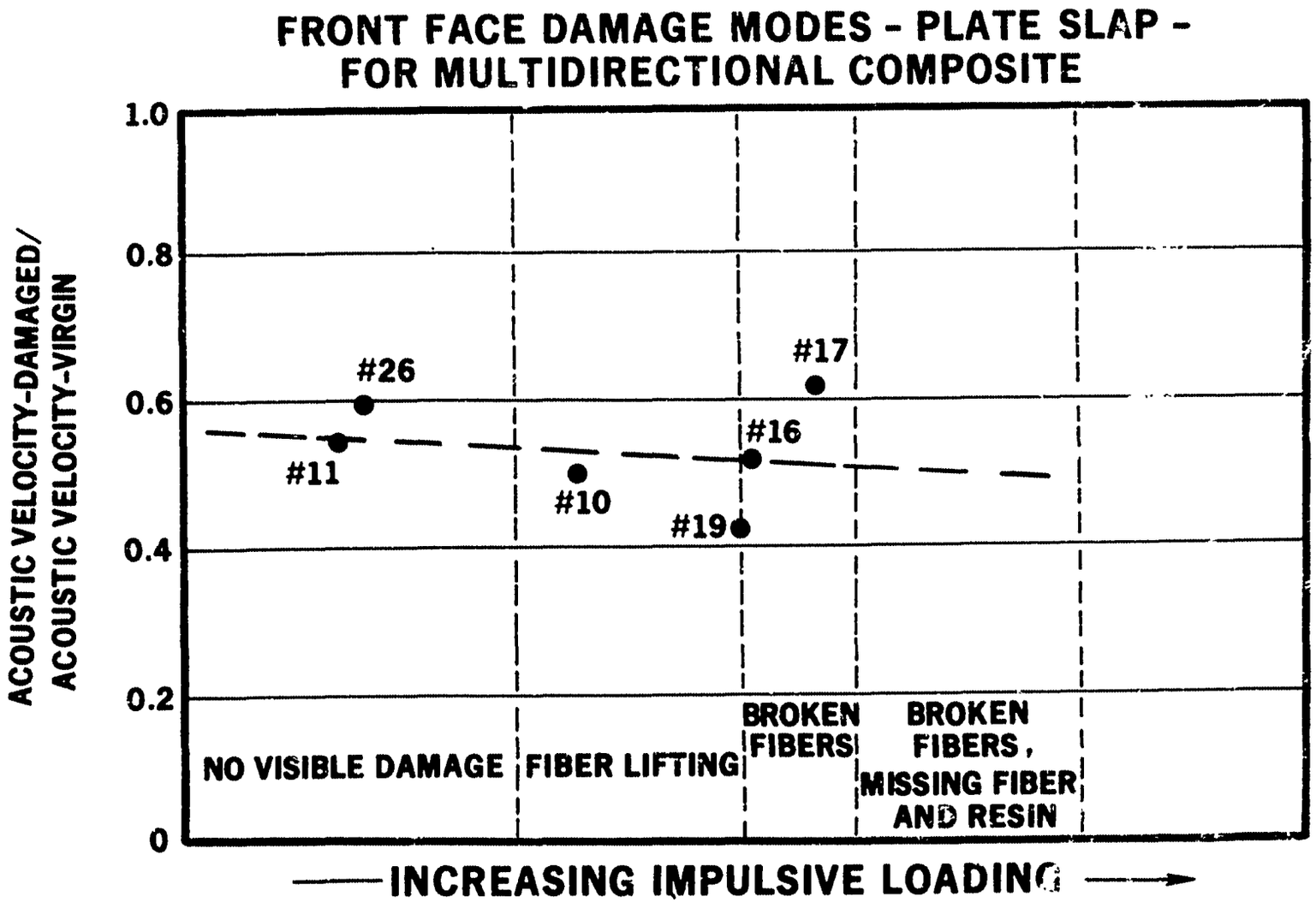

FRONT FACE DAMAGE MODES - PLATE SLAP -
FOR MULTIDIRECTIONAL COMPOSITE
ACOUSTIC VELOCITY-DAMAGED/
ACOUSTIC VELOCITY-VIRGIN
1.0
0.8
0.6
0.4
0.2
0
#26
#11
#10
#19
#16
#17
NO VISIBLE DAMAGE
FIBER LIFTING
BROKEN FIBERS
BROKEN FIBERS, MISSING FIBER AND RESIN
INCREASING IMPULSIVE LOADING

FIGURE 16

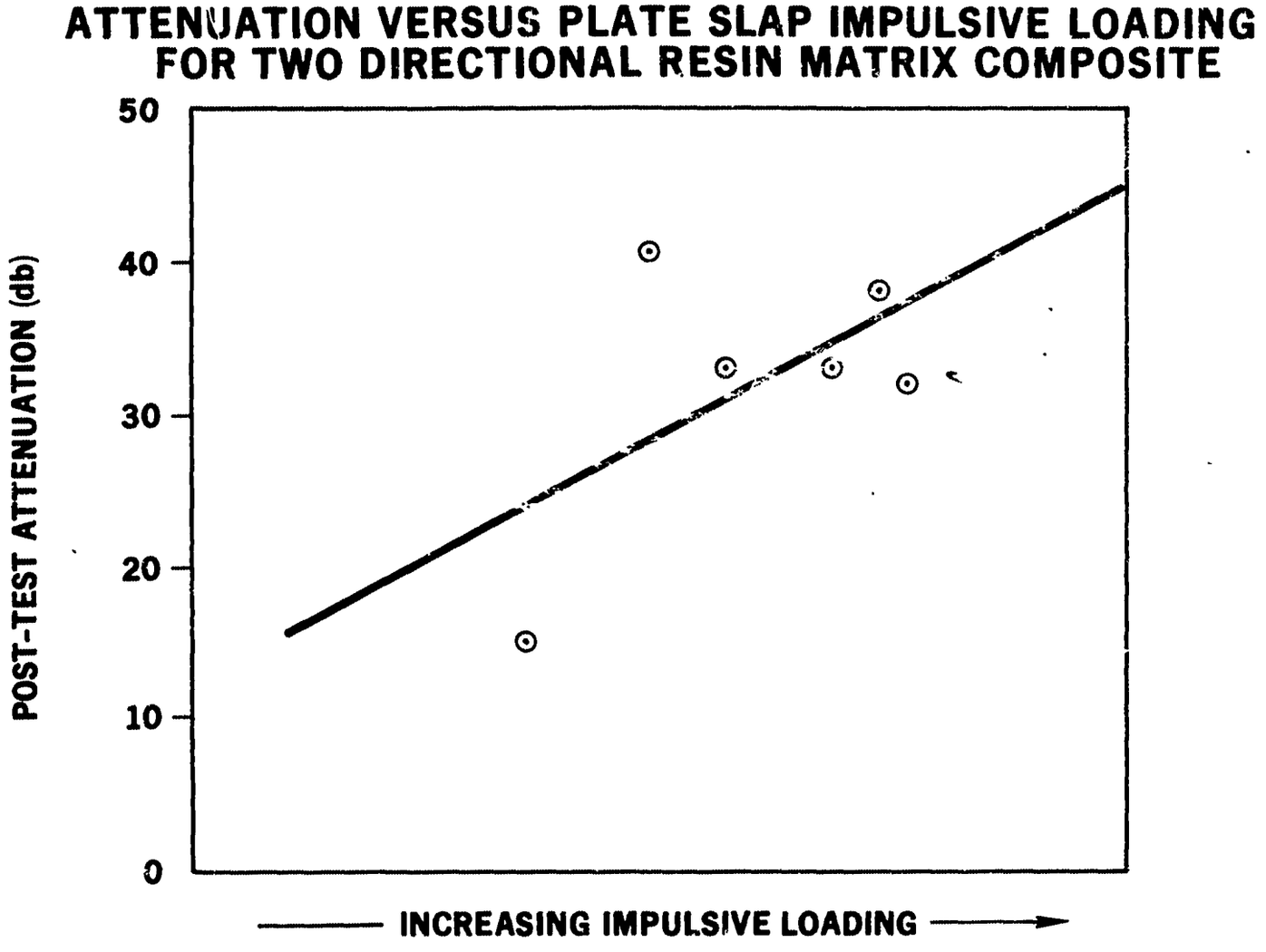

ATTENUATION VERSUS PLATE SLAP IMPULSIVE LOADING
FOR TWO DIRECTIONAL RESIN MATRIX COMPOSITE
POST-TEST ATTENUATION (db)
50
40
30
20
10
0
INCREASING IMPULSIVE LOADING

FIGURE 17

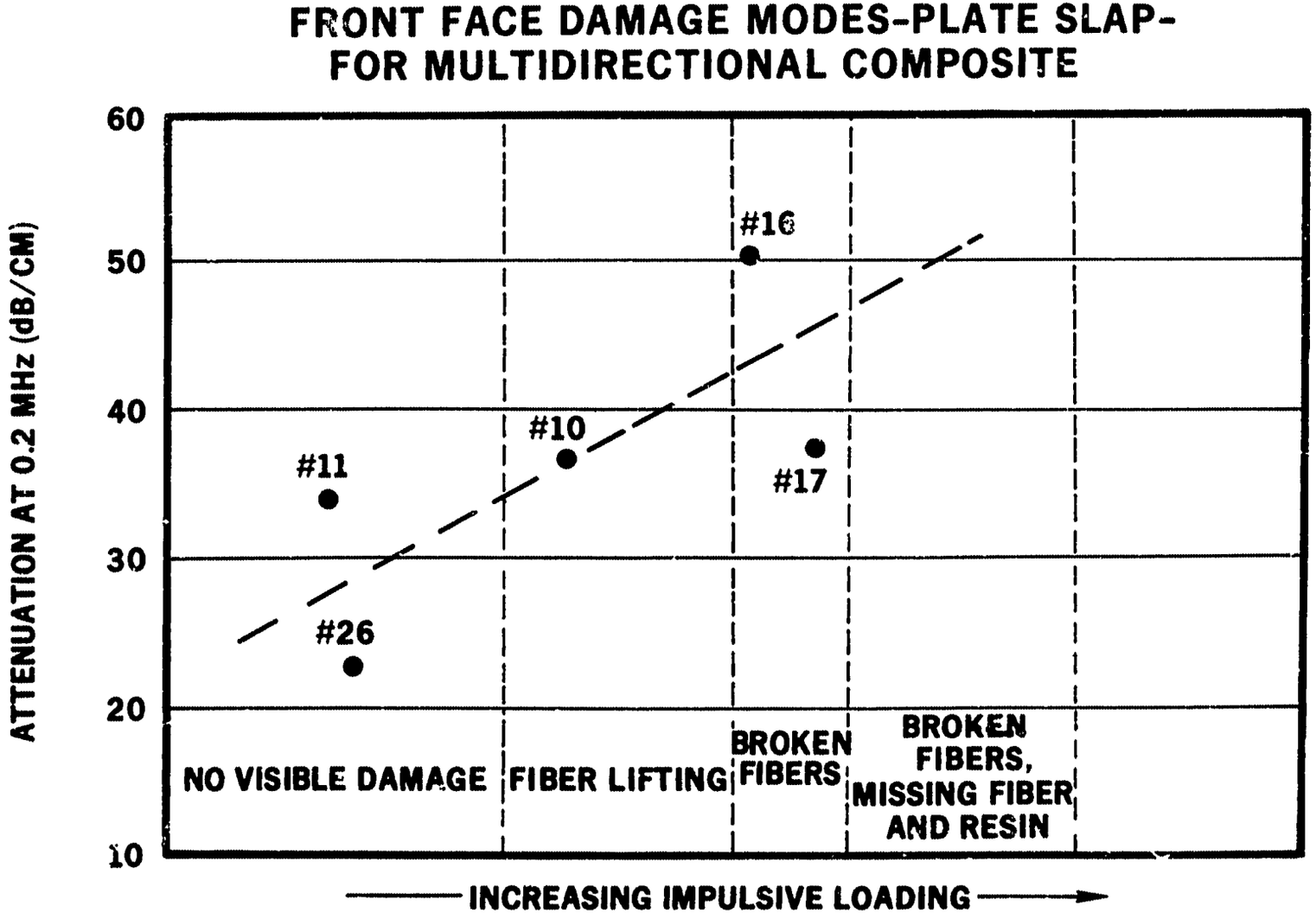

FRONT FACE DAMAGE MODES-PLATE SLAP-
FOR MULTIDIRECTIONAL COMPOSITE
ATTENUATION AT 0.2 MHz (dB/CM)
60
50
40
30
20
10
#16
#10
#11
#17
#26
NO VISIBLE DAMAGE
FIBER LIFTING
BROKEN FIBERS
BROKEN FIBERS, MISSING FIBER AND RESIN
INCREASING IMPULSIVE LOADING

FIGURE 18

VARIANT PROPERTIES

OF

COMPOSITE MATERIALS

by

John R. Zurbrick
Nondestructive Test Evaluation Section
Avco Space Systems Division
Lowell, Massachusetts

AVSSD-0022-69-CR

For Presentation at the
Conference on NDT of Plastic/Composite Structures
University of Dayton
Dayton, Ohio
March, 1969

ABSTRACT

VARIANT PROPERTIES OF COMPOSITE MATERIALS

by J. R. Zurbrick*

We have found that the $V_L^2\rho$ versus polar angle (θ) relationship provides the true value for isotropic modulus ($\bar{E}$) for the particular laminate being evaluated, and this value, in turn, is the key to linking micromechanics theory to practical, real reinforced plastics materials. The rapidly-obtained quantitative NDT response values from ultrasonic velocity (V_L) and gamma radiometric density (ρ) measurements provide the necessary information for calculating 16 pieces of information which provide a practically complete elastic property characterization of the laminate. This has been accomplished by solving the existing micromechanics equations together, and simplifying them to obtain an equation for predicting the theorstical modulus (E_θ) versus polar angle (θ) relationship. Sixty relationships have been developed, and 25 of them have been reported covering six completely different resin systems, (epoxy, phenolic, polybenzimidazole, polyimide, polyester, and silicone) and three reinforcements, 181-style E-glass fabric, Thornel 40 fiber, and boron filament. One particularly exciting outcome of this data correlation and analysis has been the ability to calculate the reinforcing fiber effective elastic modulus as it exists in the finished laminate. The calculated isotropic shear modulus value, $\bar{G}$, and across-fiber single ply stiffness, E_{22}, appear to reflect the influences of porosity content and location, and interfacial bonding. More study is currently underway to confirm this.

INTRODUCTION

Whatever the scientific discipline, technological specialty, or business viewpoint, those concerned today with composite materials know the sting of a seemingly irreducible problem: testing of practical, real composite materials for meaningful design properties.

Out from a rather remote and little-understood, perhaps misunderstood, corner of technology has come the long-sought-after solution. That technology is nondestructive testing, and the solution it offers is the subject of this paper.

We began four years ago to apply the probing energy forms used in nondestructive testing for the purposes of quantitatively measuring inherent variability within and between reinforced plastic laminates. The work was sponsored by the Air Force Materials Laboratory, Metals and Ceramics Division, who had the desire and foresight to fund such an approach. As the work progressed, ultrasonic velocity (V_L) measurements and gamma radiation absorption measurements began to show trends and correlations with elastic properties, sometimes with ultimate properties, and with component volume fractions and density (ρ). From the overview there appeared a "thread of continuity" among all fiber reinforced composites but the puzzle was never quite complete for any one composite system or family.

From among the analytical approaches the viewpoint of micromechanics appeared to hold the most promise, although no provision for porosity effects or other abnormalities were accounted for in the modeling. Porosity, its location and orientation were identified as the primary degradant of the properties supplied by fiber and matrix. It became apparent that the problem must be solved as a unit; that solving one small portion at a time only deepens the confusion.

The joining of recent revelations in micromechanics theory with quantitative nondestructive test results brought forth the total solution, at least for elastic properties.

Modulus as a Function of Polar Angle

The elastic properties — modulus of elasticity in tension and compression (E), shear modulus (G), and Poisson's ratio (σ) — of advanced plastic composites are important in the design of structural, load-bearing components produced from these materials. The beneficial anisotropic character of fiber reinforced plastics requires, however, a new set of constituitive equations, other than those used to describe the elastic properties of isotropic materials.

The micromechanics discipline has developed the theory, through tensor analysis, for identifying elastic properties in terms of some fiber orientation, usually that of a surface fiber (0-degree orientation).

Theories and relationships developed through micromechanics provide a general understanding of the polar angle versus tensile/compressive elastic moduli, shear modulus, and Poisson's ratio. A case in point is shown in Figures 1, 2 and 3 for fiber and matrix properties approximating those of a boron/epoxy laminate containing a boron volume fraction of 0.65 (References 1 and 2). The three plots cover crossply ratio (m) of m = 0 (90 degrees unidirectional), m = 1 (balanced orthogonal), and m = 3 (unbalanced orthogonal where 75 percent of the filaments are aligned in the 0-degree direction). Other relationships cover the case of off-axis (non 0- to 90-degree orientations) at some angle α to the 0-degree axis.

One of the major barriers to applying these micromechanics theories to real laminates fabricated by people using various processing techniques and conditions has been a great lack of experimental isotropic modulus values, which fulfill the needs of micromechanics theoretical equations and allow the necessary calculations. The theoretical calculations can be made using assumed values, but the supporting real laminate values rarely agree with them, due to the problem of producing an "ideal" laminate in fact. The expense of developing a reasonably complete set of supporting test data for even one case is enormous.

These questions, then, have been widely heard: "Are the micromechanics theories and equations unrealistically ideal? Are the laminate producers capable of fabricating truly designable reinforced plastics composite materials?" The following discussion proposes to answer firmly these questions by showing that the link between micromechanics theory and actual laminate practice lies in the realm of nondestructive testing, and that the proper application of ultrasonic and gamma radiometric techniques allow the calculation of a real laminate's theoretical and actual elastic properties, for comparison and understanding. It will be shown that the micromechanics theories and equations are not unrealistically ideal and that reinforced plastics are truly designable materials.

THEORETICAL BASIS

Efforts over the past few years to bring micromechanical theories and relationships into practical focus have been aimed toward seeking realistic values for the isotropic stiffness ($\bar{E}$) and shear rigidity ($\bar{G}$) values for a composite system of interest. These values are the axes around which the cosine and sine functions oscillate in the micromechanical predictive equations of modulus versus polar angle. The isotropic modulus value "pegs" the polar function, and if not properly chosen, there occurs a large disagreement between the thoery and practical destructively-obtained modulus values for a real laminate. The isotropic modulus can be computed from moduli obtained with a number of specimens cut at equal intervals of angle, by taking the simple average. Because of the sinusoidal nature of the relationship, this operation requires at least 18, (10-degree intervals) and preferentially 36 (5-degree intervals) specimens from a single panel. George Lubin and W. C. Tappe of Grumman have performed this tedious, expensive, and time-consuming operation for a few glass fabric laminates (Reference 3). Unfortunately, the panels were consumed in the process, and there is no assurance that those values would apply to the next laminate.

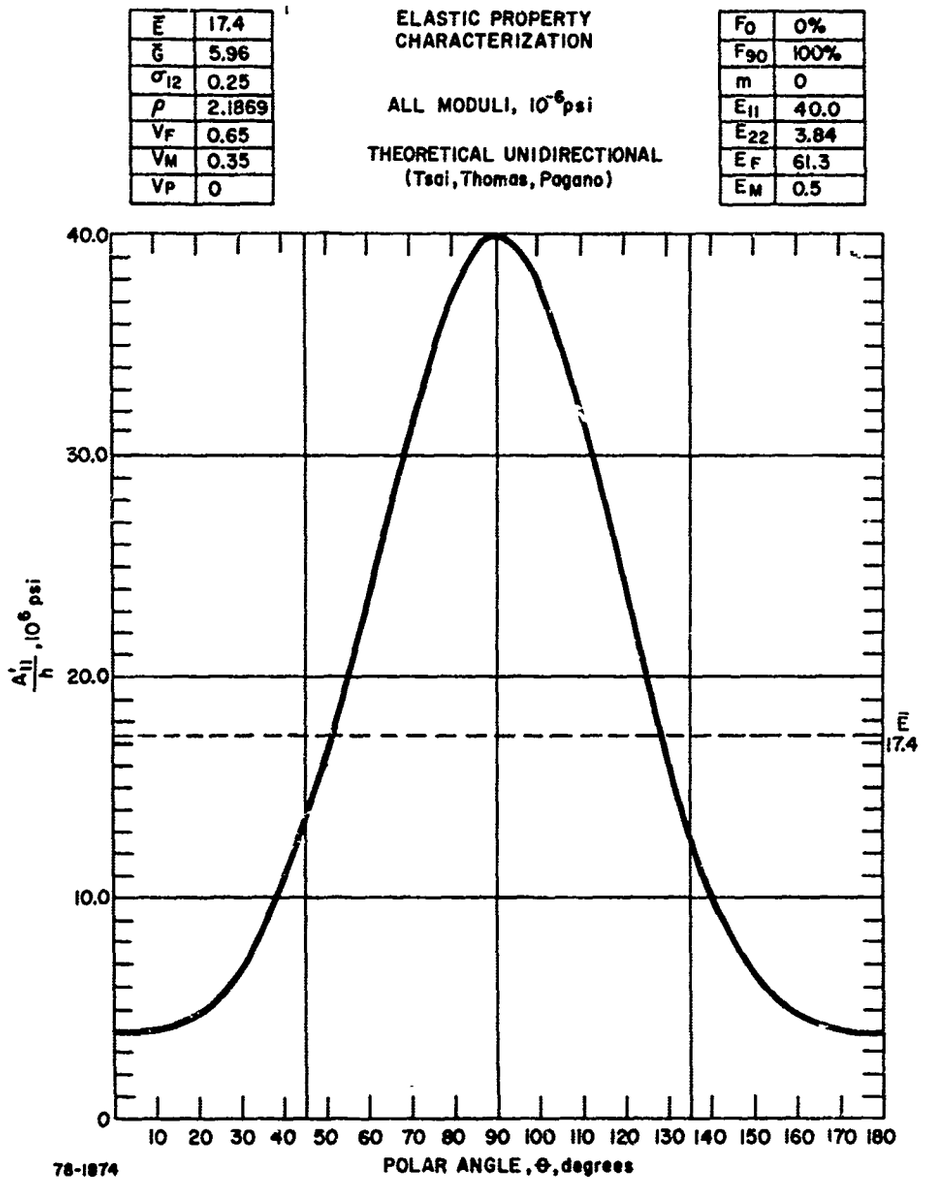


Figure 1 THEORETICAL CURVE FOR MODULUS AS A FUNCTION OF POLAR ANGLE IN A UNIDIRECTIONAL LAMINATE

$\bar{E}$	17.4
$\bar{G}$	5.96
σ_{12}	0.25
ρ	2.1869
V_F	0.65
V_M	0.35
V_P	0

ELASTIC PROPERTY CHARACTERIZATION

ALL MODULI, 10^6 psi

THEORETICAL BALANCED
(Tsai, Thomas, Pagano)

F_0	50%
F_{90}	50%
m	1
E_{11}	40.0
E_{22}	3.84
E_F	61.30
E_M	0.5

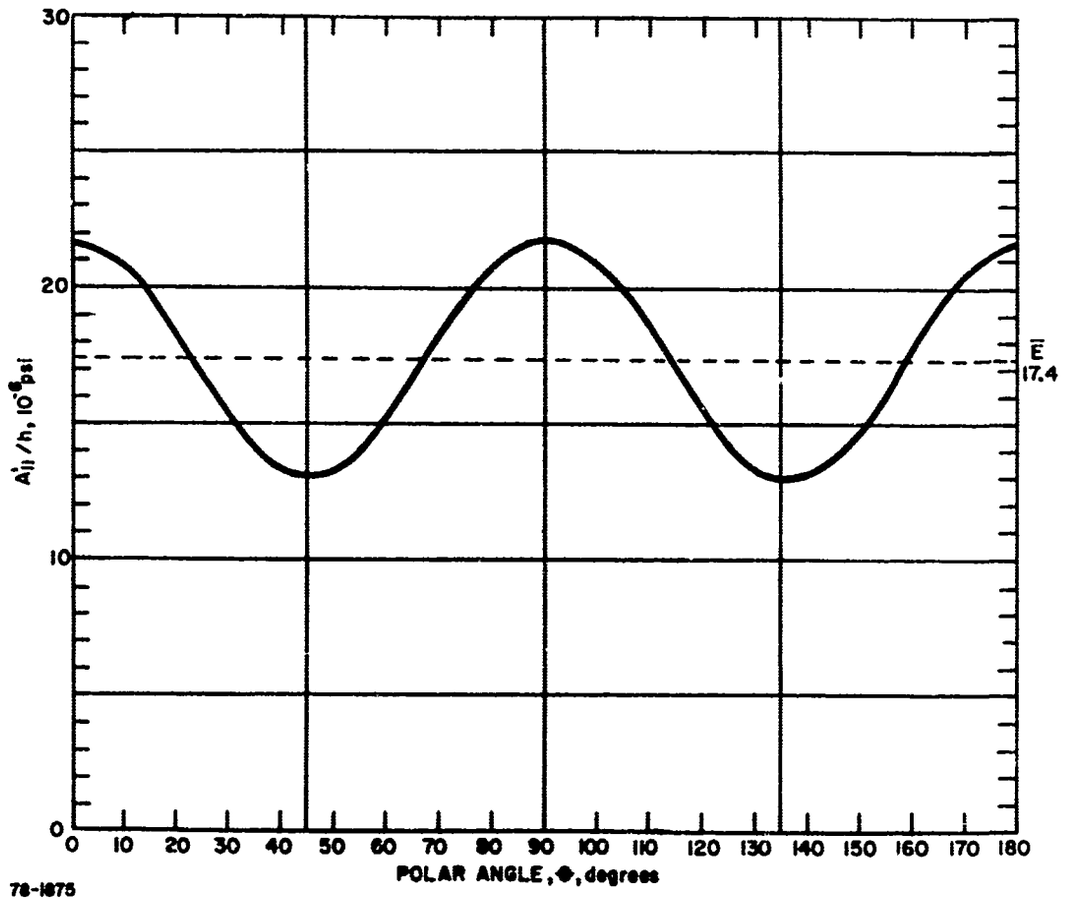


Figure 2 THEORETICAL CURVE FOR MODULUS AS A FUNCTION OF POLAR ANGLE IN A BALANCED 0°-90° LAMINATE

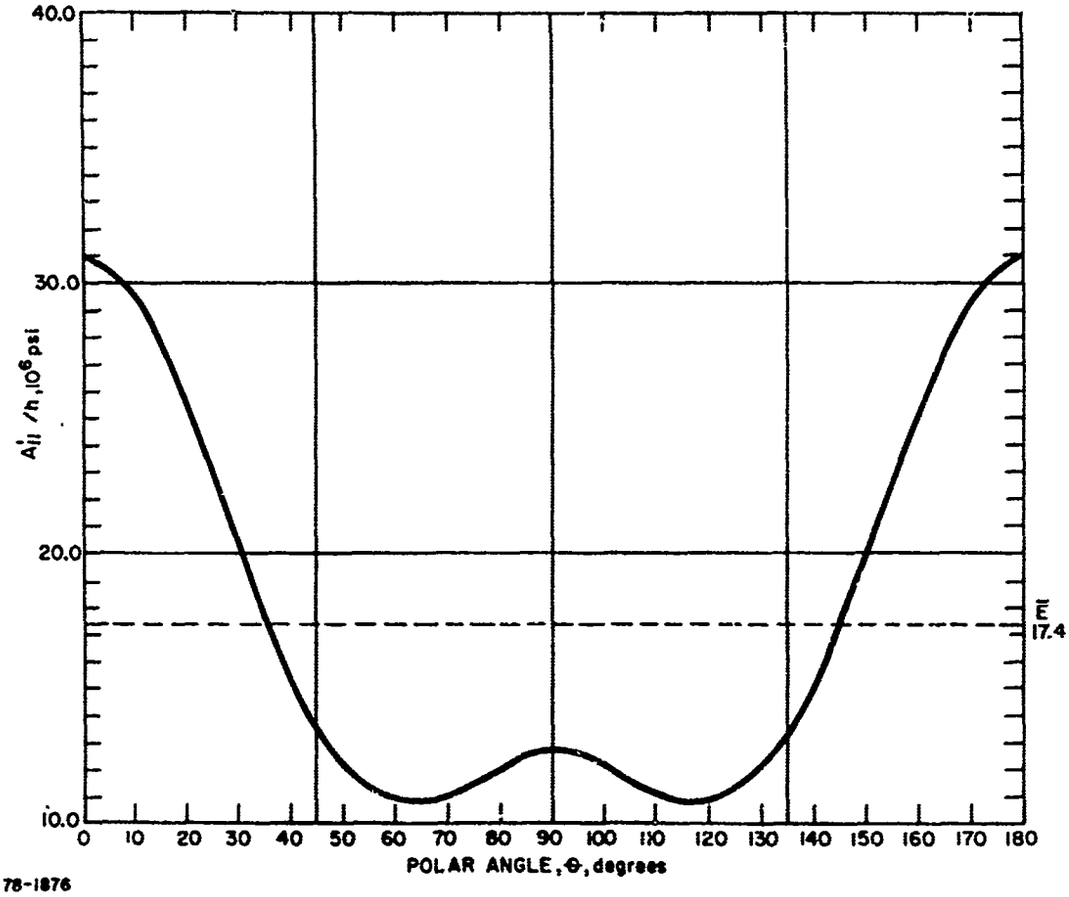
$\bar{E}$	17.40
$\bar{G}$	5.96
σ_{12}	0.25
ρ	2.1869
V_F	0.65
V_M	0.35
V_P	0

ELASTIC PROPERTY CHARACTERIZATION

ALL MODULI, 10^6 psi

THEORETICAL UNBALANCED
(Tsai, Thomas, Pagano)

F_0	75%
F_{90}	25%
m	3
E_{11}	40.00
E_{22}	3.84
E_F	61.30
E_M	0.50



78-1876

Figure 3 THEORETICAL CURVE FOR MODULUS AS A FUNCTION OF POLAR ANGLE IN AN UNBALANCED 0 - 90· LAMINATE

In lieu of the destructive test approach, Tsai and Thomas (Reference 1) have proposed the following approximations:

$$\bar{E} = \frac{3}{8} E_{11} + \frac{5}{8} E_{22} \quad (1)$$

$$\bar{G} = \frac{1}{8} E_{11} + \frac{1}{4} E_{22} \quad (2)$$

where

E_{11} is the single-ply stiffness in the fiber axis direction, and

E_{22} is the single-ply stiffness in the direction across the fiber axis.

The E_{11} value may be calculated from the law of mixtures:

$$E_{11} = V_F E_F + V_M E_M \quad (3)$$

where

V_F = volume fraction fiber (glass or graphite, for example)

V_M = volume fraction resin (epoxy, polyimide, etc.)

E_F = modulus of elasticity of the fiber

E_M = modulus of elasticity of the cured resin.

The calculation of E_{22} is more difficult, especially for a value matched to a specific laminate, and this becomes a barrier point. Assumed values result in undesirable errors.

Reported experience at Avco/SSD has shown that the term $V_L^2\rho$ for ultrasonic velocity values taken in the ply-plane direction is related, through Poisson's ratio, to modulus of elasticity. Therefore, $V_L^2\rho$ values taken at 5-degree intervals around a disc cut from a real laminate could be averaged to obtain the desired isotropic modulus value:

$$\bar{E} = \frac{\rho \sum (V_L)^2}{n(0.0124)} \quad (4)$$

where

ρ = the density of the disc

V_L = ply-plane longitudinal wave velocity at 1 MHz

n = the number of V_L values summed (36 for 5-degree intervals)

Up to this point we are assuming that, in any polar direction, E_θ and $(V_L)^2_\theta$ are values linked to the same materials entities, and are therefore linked by a constant ($C\, f(\sigma) = 0.0124$) to each other.

For ply-plane V_L measurements we have reported

$$V_L^2\rho = 0.0124E \tag{5}$$

from which

$$C\, f(\sigma) = 0.0124 \tag{6}$$

where:

C = the units conversion from $(\text{in.}/\mu\text{sec})^2$ (gm/cm^3) to 10^6 psi, 0.010687

and

$$f(\sigma) = \frac{(1+\sigma)(1-2\sigma)}{(1-\sigma)}$$

allowing the calculation for Poisson's ratio function:

$$f(\sigma) = \frac{0.0124}{0.010687} = 1.16 \tag{7}$$

and computation of Poisson's ratio:

$$\sigma_{12} = 0.230 \tag{8}$$

Armed with a real laminate value for $\bar{E}$ obtained from nondestructive tests, we were then in a position to reexamine the micromechanics predictive equations for a method of calculating the theoretical E'_θ versus θ relationship for any given real fabricated laminate.

The recent AFML report and book chapter on "Invariant Properties of Composite Materials" by Tsai and Pagano served as the guide for the following derivations (Reference 2). The curves shown in Figures 1, 2 and 3 had been obtained by Tsai, Thomas, and Pagano using:

$$A'_{11}/h = Q'_{11} = U_1 + U_2 \cos 2\theta + U_3 \cos 4\theta \tag{9}$$

where:

U_1 = constant in Q_{ij} transformation equation

U_2 = coefficient of cos 2θ term in Q_{ij} transformation equation

U_3 = coefficient of cos 4θ term in Q_{ij} transformation equation

Q'_{11} = reduced stiffness for bodies under plane stress; the prime connotes at a polar angle

A'_{11} = elastic constant of laminated composite; the prime connotes at a polar angle

h = thickness of laminated composite

as simplified according to the following:

$$U_1 \cong \bar{E} \tag{10}$$

$$U_2 = \frac{Q_{11} - Q_{22}}{2} \cong \frac{E_{11} - E_{22}}{2} \tag{11}$$

$$\frac{U_3 = Q_{11} + Q_{22} - 2Q_{12} - 4Q_{66}}{8} \tag{12}$$

but, for a coupling function of constituent stiffness ratio and fiber volume fraction (β) equal to 1 and for a Poisson's ratio (σ_{12}) of 0.25 (value produced in NDT is 0.23), we can substitute:

$$Q_{66} = G_{12} = 3/8\beta E_{22} \tag{13}$$

$$U_3 \cong \frac{E_{11} + E_{22} - 2\sigma_{12}E_{22} - 4(3/8\beta E_{22})}{8} \tag{14}$$

and reduce to

$$U_3 \cong \frac{E_{11} + E_{22}\,(1 - 2\sigma_{12} - 3/2)}{8} \tag{15}$$

$$U_3 \cong \frac{E_{11} - E_{22}\left[1/2 + 2\,(0.25)\right]}{8} \tag{16}$$

$$U_3 \cong \frac{E_{11} - E_{22}}{8} \tag{17}$$

Finally by taking

$$E_\theta = \frac{A_{11}}{h} \tag{18}$$

and substituting, we obtain the useful form of the predictive equation:

$$E_\theta = \bar{E} + \left(\frac{E_{11} - E_{22}}{2}\right)\cos 2\theta + \left(\frac{E_{11} - E_{22}}{8}\right)\cos 4\theta \tag{19}$$

It can be further simplified by remembering the approximation:

$$\bar{E} = 3/8E_{11} + 5/8\,E_{22} \tag{20}$$

$$E_{22} = \frac{8}{5}\,\bar{E} - \frac{3}{5}\,E_{11} \qquad (21)$$

giving us

$$E_\theta = \bar{E} + 0.8\,(E_{11} - \bar{E})\cos 2\theta + 0.2(E_{11} - \bar{E})\cos 4\theta \qquad (22)$$

This equation requires only two experimentally determined values for its solution, E_{11} and $\bar{E}$. The rule of mixtures produces E_{11}, from component volume fraction values that can be determined nondestructively through gamma radiometry or by means of a gravimetric resin burn-out procedure.

The nondestructive ultrasonic through-transmission technique for longitudinal wave velocity produces the $\bar{E}$ value. The cosine functions may be found in trigonometric tables.

Equation 22 is actually not complete for the general laminate case, as it was derived for only the case of a unidirectional laminate where 100 percent of the fibers lie in the 0-degree orientation direction.

The crossply ratio term:

$$m = \frac{\text{Thickness of Layers in 0-degree Direction}}{\text{Thickness of Layers in 90-degree Direction}} \qquad (23)$$

has been used in micromechanics to identify the cases of balanced (0 -90) degree laminates and unbalanced laminates.

No mention, however, is made of its influence as a modifier of Equation 22. The derivation of a modifier term as a function of crossply ratio was necessary to perform the desired predictive calculations of E_θ from the nondestructive test data generated under the subject program. That term $(\mathfrak{s}) = f(m)$ was derived and has been named "orthogonal unbalance factor." Noting that the cos 2θ term of Equation 22 controls the undirectional case and the cos 4θ term controls the perfectly balanced case, we arrive at the most general form of the micromechanics theoretical equation:

$$E_\theta = \bar{E} + 0.8\,\mathfrak{s}(E_{11} - \bar{E})\cos 2\theta + 0.2(E_{11} - \bar{E})\cos 4\theta \qquad (24)$$

This equation is applicable to any and all 2-D orthogonally-oriented fiber reinforced composite materials.

The practical use of Equation 24, the rule of mixtures, nondestructively predicted values of ρ, V_F, V_M, and $(V_L)_\theta$, and handbook values for E_M and E_F, will allow, today, the complete elastic characterization of any real laminate as follows:

1. Isotropic Modulus of Elasticity, $\bar{E}$
2. Modulus versus θ, Theoretical, E'_θ
3. Modulus versus θ, Actual, E_θ
4. Isotropic Shear Modulus, $\bar{G}$
5. Poisson's Ratio, σ_{12}
6. Density, ρ
7. Volume Fraction Fiber, V_F

8. Volume Fraction Resin, V_M
9. Volume Fraction Porosity, V_P
10. Percent Fibers in 0^o Orientation, Effective, F_0
11. Percent Fibers in 90^o Orientation, Effective, F_{90}
12. Cross-Ply Ratio, m
13. Single Ply Stiffness in Fiber Axis Direction, E_{11}
14. Single Ply Stiffness in Direction Across Fibers, E_{22}
15. Elastic Modulus of Fiber, E_F
16. Elastic Modulus of Matrix, E_M

EXPERIMENTAL VERIFICATION

The approach toward experimental verification was one of simply determining the $(V_L)_\theta$ values at 5- or 10-degree intervals on discs cut from the laminate panels produced and tested under the subject program. Sixty such discs, 1-1/4 inch in diameter, were cut from the 181 style, E-glass/polyimide and Thornel 40/epoxy panels. Similar discs had been retained from the previously reported programs; and these 181 style, E-glass fabric laminates containing epoxy, phenolic, polyester, polybenzimidazole, and silicone resin systems, were also evaluated for the polar angle relationship. This comprised a reasonably broad cross section of reinforced plastics technology existing today.

These same discs were used for gamma radiometric calibrations and gravimetric resin-burn-out determinations.

The center portion of polar graph paper was bonded to each disc, the 0-degree line aligned with the fabric warp direction, or the surface fiber direction in the case of Thornel 40. This provided the angle reference during ply-plane ultrasonic velocity measurements at a center frequency of 1.0 MHz. A total of 4300 units of data were generated, producing over 1200 $(V_L)^2_\theta \rho$ values. Computerized data reduction greatly aided this study.

Utilizing this information, plots of theoretical E'_θ versus θ and NDT experimental values of $(V_L)^2_\theta \rho$ versus θ would reveal

a. the validity of Equation (5),

b. the validity of the "rule of mixtures",

c. the validity of the orthogonal unbalance factor, Z,

d. the accuracy of between-ply coupling functions assumed in the tensor analysis, and

e. the over-all practicality of using the generalized micromechanics theoretical equation in the characterization and design of fiber reinforced plastic laminates.

A disc cut 2 years ago from a minimum-porosity polyester/181, E-glass laminate, 3/8-inch thick, provided the answer, Figure 4. This laminate had come closest to approximating the ideal, and in doing so positively proved that the nondestructive test approach to characterizing elastic properties was correct.

$\bar{E}$	4.48
$\bar{G}$	1.28
σ_{12}	0.23
ρ	2.048
V_F	0.559
V_M	0.441
V_P	0

ELASTIC PROPERTY CHARACTERIZATION

$V_L^2 \rho = 0.0124E$

ALL MODULI, 10^6 psi

181, E-GLASS/POLYESTER
0900-20 R-13

F_0	50%
F_{90}	50%
m	1.00
E_{11}	6.18
E_{22}	2.03
E_F	10.50
E_M	0.70

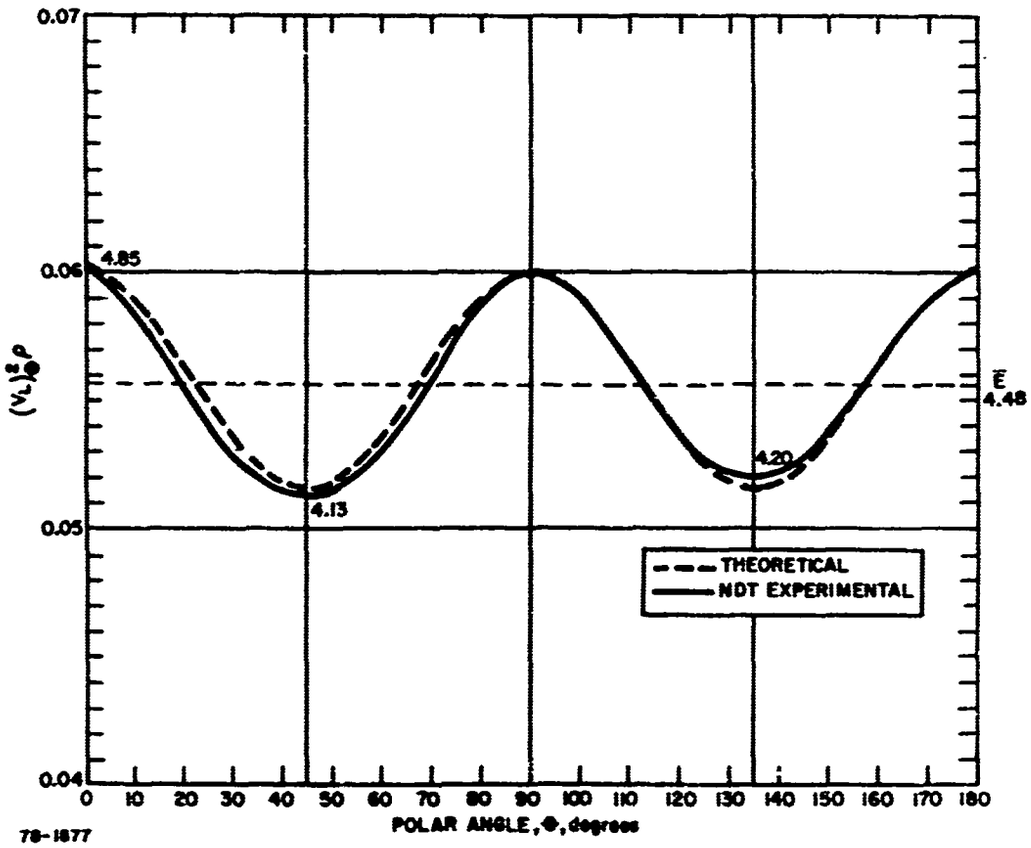


Figure 4 MODULUS VERSUS POLAR ANGLE FOR A MINIMUM POROSITY, 181, E-GLASS FABRIC/POLYESTER LAMINATE

But one amazingly perfect correlation was not considered to have described the situation with "non-ideal" laminates, those which

a. contain porosity, micro or macro,

b. were improperly laid up:

   1. fabric placed warp to fill
   2. improper fabric nesting
   3. twisted or distorted fabric
   4. resin rich interlayers.

c. were over-"B"-staged,

d. were improperly cured,

e. contained a sizeable degree of orthogonal unbalance, and

f. contained gross defects.

Nor does the polyester case relate directly to destructively-determined mechanical test values.

Lubin and Tappe (Reference 3) provided the link to destructive test values, which serve as the referee in the comparison.

The E_θ versus θ plot from 36 angle-cut tensile specimens is shown, with the theoretical prediction, in Figure 5, for a 181 style, E-glass/epoxy laminate. The ultimate properties are shown also in Figure 6, to exhibit the similarity in the UTS_θ versus θ relationship. Compare Figure 5, then, with E_θ versus θ predictions based on nondestructive test data for a minimum porosity, 181 style, E-glass fabric/epoxy laminate prepared at Avco/SSD, Figure 7. The destructively-determined modulus values from tensile and flexure bars, cut close to the R-16 disc, provided high values of E_{0^o} and E_{90^o} as predicted in this figure.

To relate to the current program, plots for the 181, E-glass/Quantad 159, Figure 8, 181, E-glass/PI-2501 system, Figure 9, and for the Thornel 40/epoxy system, Figure 10, were prepared. In Figures 9 and 10, significant values of orthogonal unbalance factor were indicated. Note that each graph contains all 16 of the elastic characterization values.

Other polyimide resin systems, porosity situations, and layup error responses are presented with brief commentary in 18 additional graphs. Besides these we have developed 40 more such plots which exhibited very similar correlations. These have not been published in the interest of brevity.

ELASTIC PROPERTY CHARACTERIZATIONS

Elastic property characterizations for representative discs cut from 18 different laminates are presented. Five types of resin, eight resin systems, and two reinforcements were covered in this work. The brief commentary for each figure discusses the salient materials influences exhibited in the $(V_L)^2_\theta P$ versus θ relationships.

$\bar{E}$	2.27
$\bar{G}$	0.727
σ_{12}	0.23
ρ	2.11
V_F	0.669
V_M	0.331
V_P	0

ELASTIC PROPERTY CHARACTERIZATION

$V_L^2 \rho = 0.0124E$

ALL MODULI, 10^6 psi

181, E-GLASS/EPOXY

F_0	50%
F_{90}	50%
n	1.0
E_{11}	7.19
E_{22}	0.686
E_F	10.50
E_M	0.5

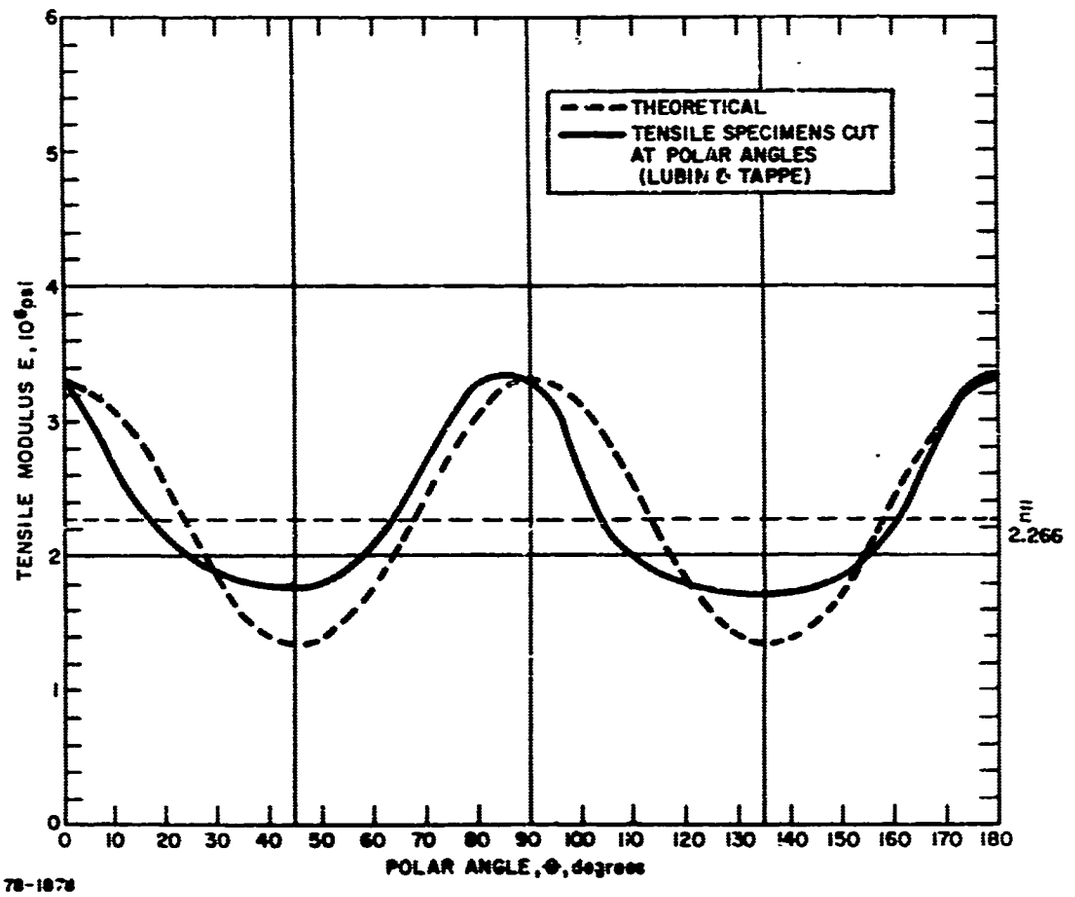


Figure 5 MODULUS VERSUS POLAR ANGLE FOR A 181, E-GLASS FABRIC/EPOXY LAMINATE

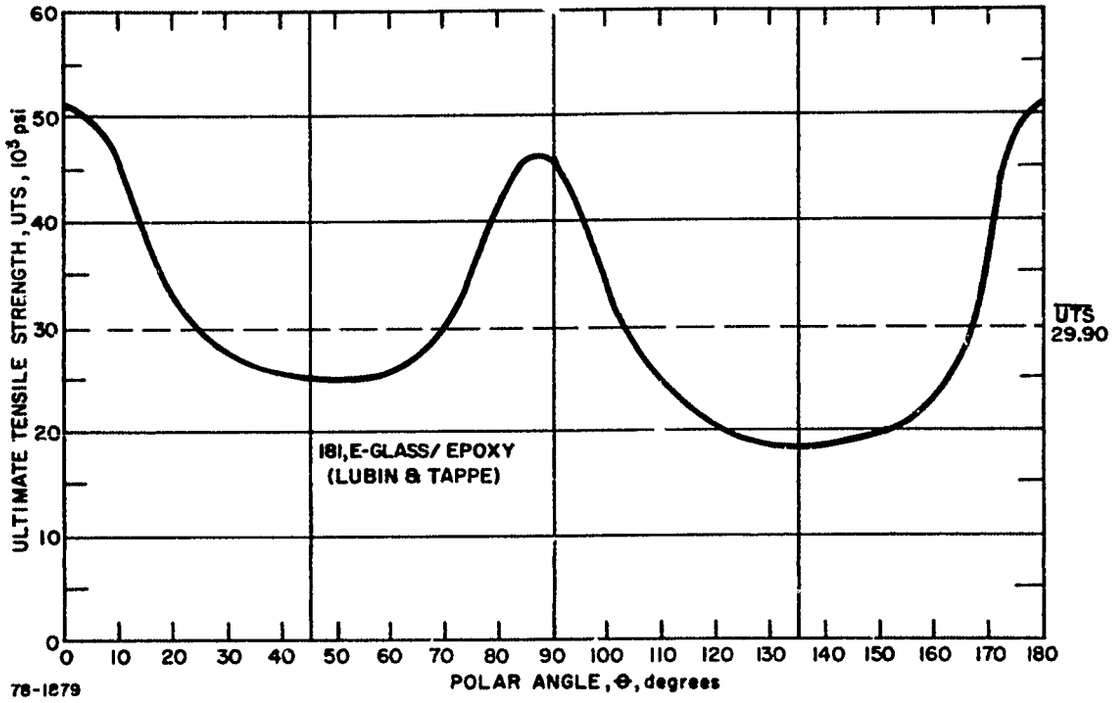


Figure 6 ULTIMATE TENSILE STRENGTH VERSUS POLAR ANGLE FOR A 181, E-GLASS FABRIC EPOXY LAMINATE

$\bar{E}$	4.49
$\bar{G}$	1.64
σ_{12}	.23
ρ	1.997
V_F	.562
V_M	.418
V_P	.020

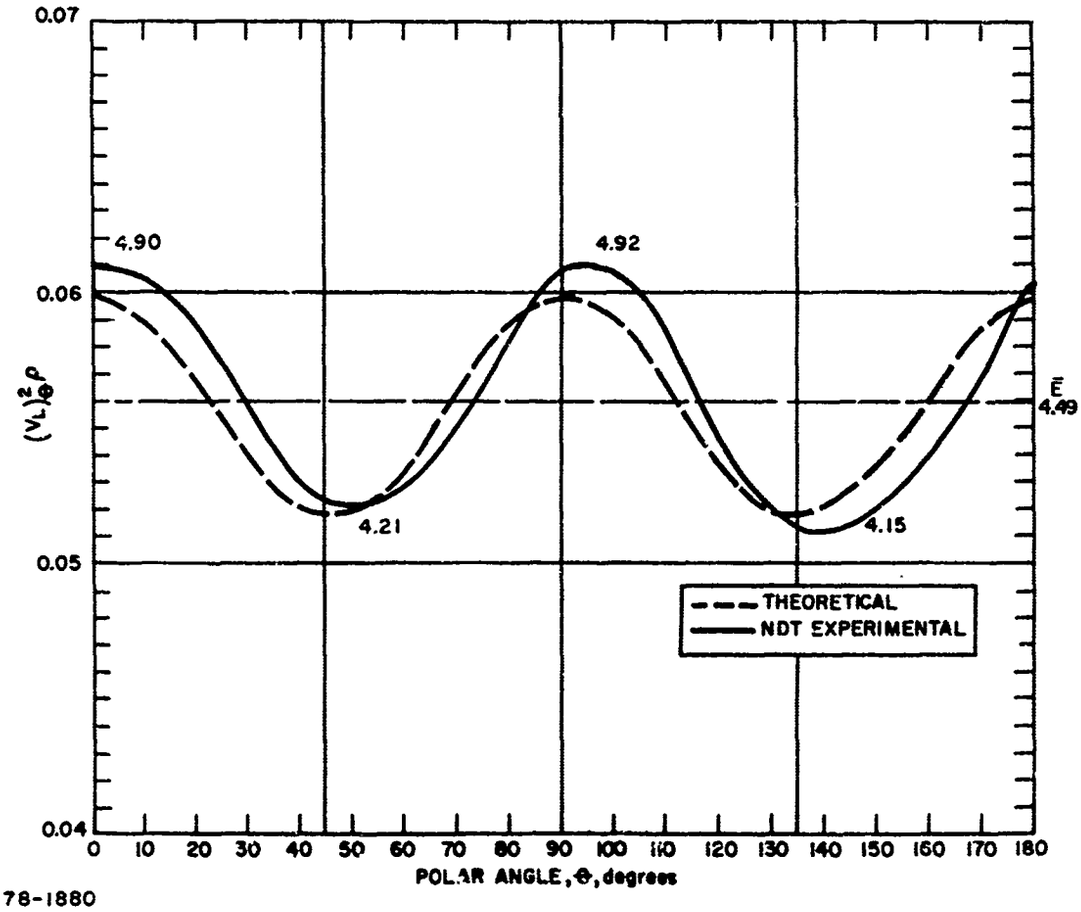
ELASTIC PROPERTY CHARACTERIZATION

$V_L^2 \rho = 0.0124E$

ALL MODULI, 10^3 psi

181, E-GLASS / EPOXY
D900-8 R-16

F_0	50%
F_{90}	50%
m	1.0
E_{11}	6.11
E_{22}	3.52
E_F	10.5
E_M	0.5



78-1880

Figure 7 MODULUS VERSUS POLAR ANGLE FOR AN AVCO-PRODUCED, 181, E-GLASS FABRIC EPOXY LAMINATE

$\bar{E}$	3.46
$\bar{G}$	1.26
σ_{12}	0.23
ρ	1.8497
V_F	0.429
V_M	0.582
V_P	0

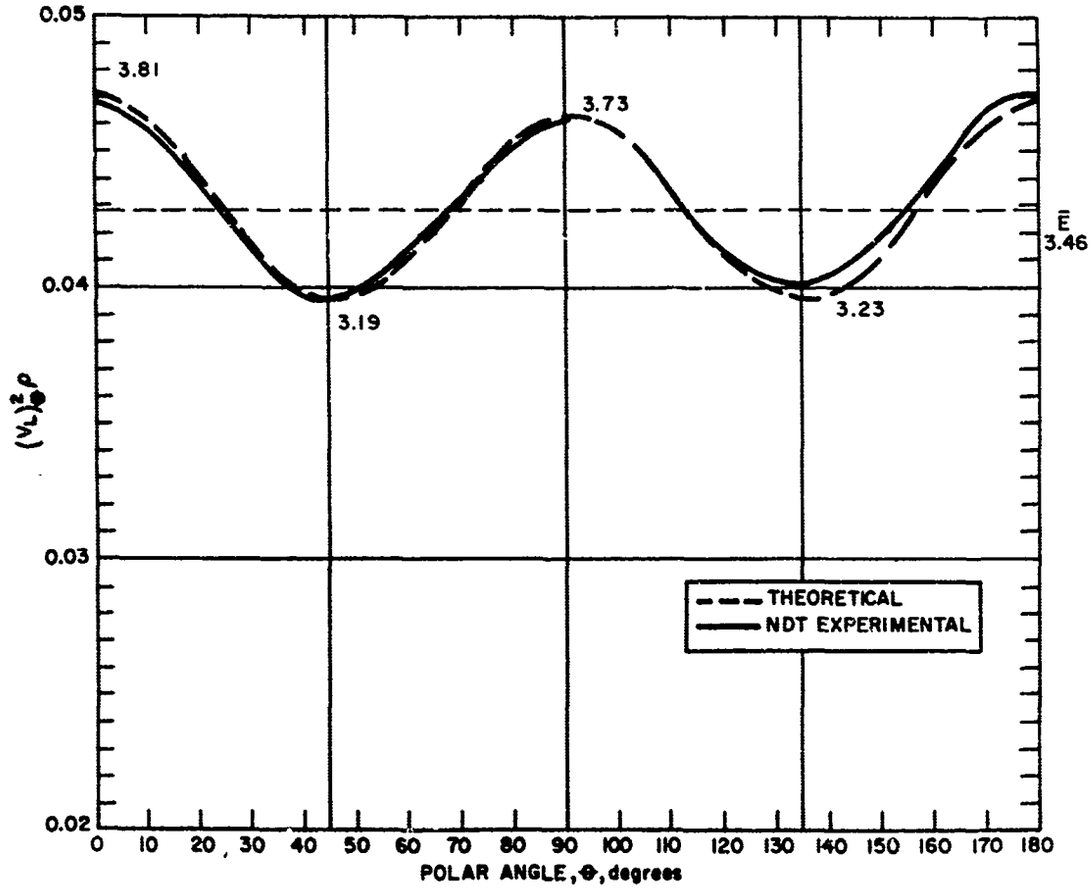
ELASTIC PROPERTY CHARACTERIZATION

$V_L^2 \rho = 0.0124E$

ALL MODULI, 10^6 psi

181, E-GLASS / POLYIMIDE
CH132A R-1

F_0	51.0%
F_{90}	49.0%
m	1.04
E_{11}	4.91
E_{22}	2.59
E_F	10.50
E_M	0.70



78-1891

Figure 8 MODULUS VERSUS POLAR ANGLE FOR A 181, E-GLASS FABRIC/QUANTAD 159 POLYIMIDE LAMINATE

$\bar{E}$	3.75
$\bar{G}$	1.34
σ_{12}	0.23
ρ	1.8736
V_F	0.582
V_M	0.281
V_P	0.137

ELASTIC PROPERTY CHARACTERIZATION

$V_L^2 \rho = 0.0124E$

ALL MODULI, 10^6 psi

181, E-GLASS/ POLYIMIDE
CH116 R-1

F_0	56.3 %
F_{90}	43.7 %
m	1.29
E_{11}	6.31
E_{22}	2.22
E_F	10.50
E_M	0.70

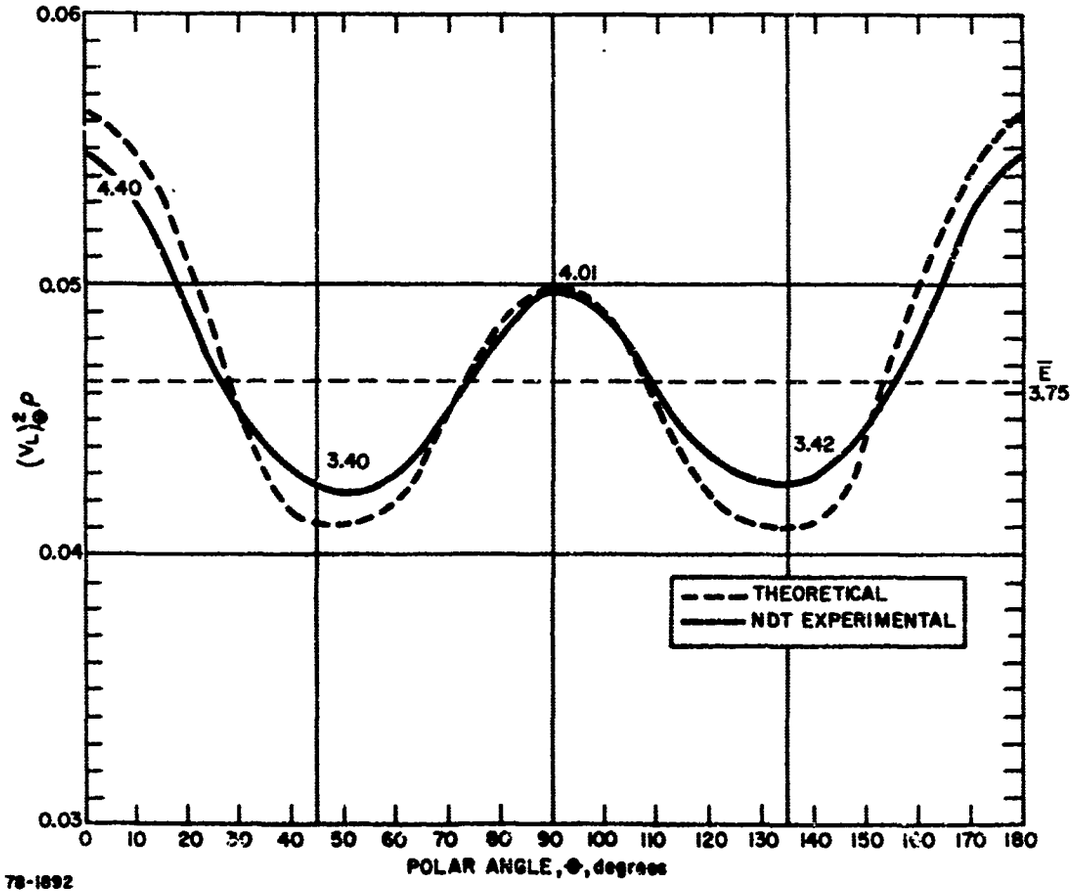


Figure 9 MODULUS VERSUS POLAR ANGLE FOR A 181, E-GLASS FABRIC/PI-2501 POLYIMIDE LAMINATE

$\bar{E}$	9.2
$\bar{G}$	3.09
σ_{12}	.23
ρ	1.4580
V_F	.659
V_M	.310
V_P	.031

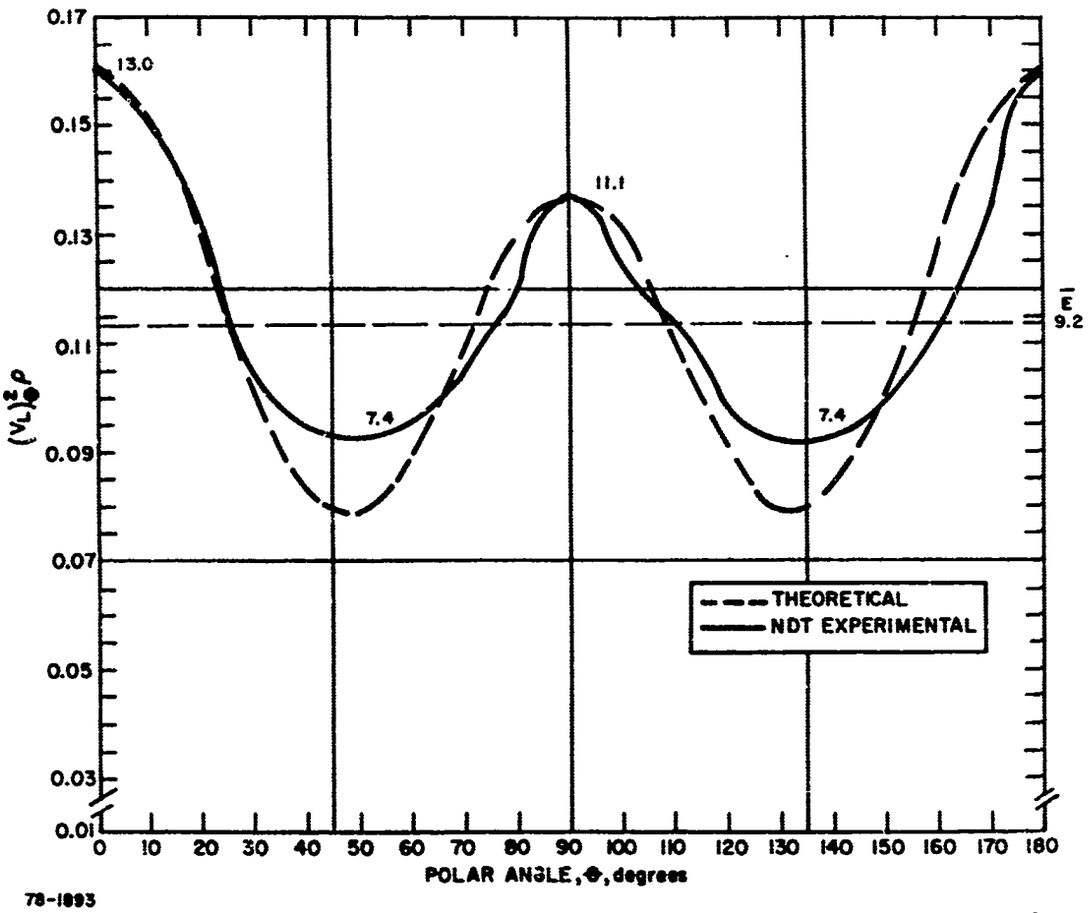
ELASTIC PROPERTY CHARACTERIZATION

$V_L^2 \rho = 0.0124E$

ALL MODULI, 10^6 psi

THORNEL 40 / EPOXY
486-75 R-1

F_0	54.0%
F_{90}	46.0%
m	1.17
E_{11}	23.22
E_{22}	0.75
E_F	35.0
E_M	0.5



78-1893

Figure 10 MODULUS VERSUS POLAR ANGLE FOR A THORNEL 40/EPOXY LAMINATE

1. Figure 11 — 181, E-glass/epoxy (Z849-41 R-13)

A close correlation between NDT experimental values and the micromechanical prediction is shown. The off-axis maximum and minimum values of 5 to 7 degrees experienced were a direct result of between-ply macroporosity as it interacted with the epoxy resin matrix.

2. Figure 12 — 181, E-glass/epoxy (D900-5 R-17)

Both the off-axis shift and deviation in the second-quadrant minimum from theoretical were shown. Slight between-ply macroporosity caused the 5- to 10-degree shift, while a slight within-strand microporosity contributed the deviation (Reference 4). The one-lobe appearance suggests that the "fill" strands contained the needle-like porosity.

3. Figure 13 — 181, E-glass/phenolic (D900-11C R-14)

An extremely close fit between theory and experience was shown. This was particularly interesting because it involved a crossply ratio considerably less than 1.0. Porosity in this phenolic laminate was entirely within-strand microporosity.

4. Figure 14 — 181, E-glass/polybenzimidazole (N-3 R-12)

In spite of severe between-ply macroporosity and slight within-strand microporosity, a close correlation was obtained. The between-strand load transfer capabilities of the PBI system where porosity exists has been remarkably high.

5. Figure 15 — 181, E-glass/silicone (D900-32 R-12)

All off-axis shifts, minimum-value deviations, greater-than-one crossply ratio, and general lack of correlation were exhibited with the silicone resin system. All of these were attributed to lack of fiber-matrix bond and ply-to-ply cracking in the resin matrix. Note the magnitude of E_{22} as compared to E_{11}, relative to the previous figures.

6. Figure 16 — Thornel 40/epoxy (486-74 R-2)

Significant orthogonal unbalance, as exhibited by the crossply ratio (m) values, was typical of these materials, even for the so-called "balanced" 12-ply and 4-ply layup systems. Orthogonal unbalance has been attributed more to fiber-count-per-ply rather than simply plies-per-direction count.

It is then conceivable that a perfectly balanced (m = 1) laminate can be fabricated which contains an odd number of plies, for optimum neutral-axis shear strength considerations. The deviation in the second-lobe minimum from theory has been attributed to 0-degree oriented within-strand microporosity.

$\bar{E}$	3.78
$\bar{G}$	1.37
σ_{12}	0.23
ρ	1.9035
V_F	0.514
V_M	0.456
V_P	0.030

ELASTIC PROPERTY CHARACTERIZATION

$V_L^2 \rho = 0.0124E$

ALL MODULI, 10^6 psi

181, E-GLASS/EPOXY
Z849-41 R-13

F_0	50%
F_{90}	50%
m	1.00
E_{11}	5.62
E_{22}	2.68
E_F	10.50
E_M	0.50

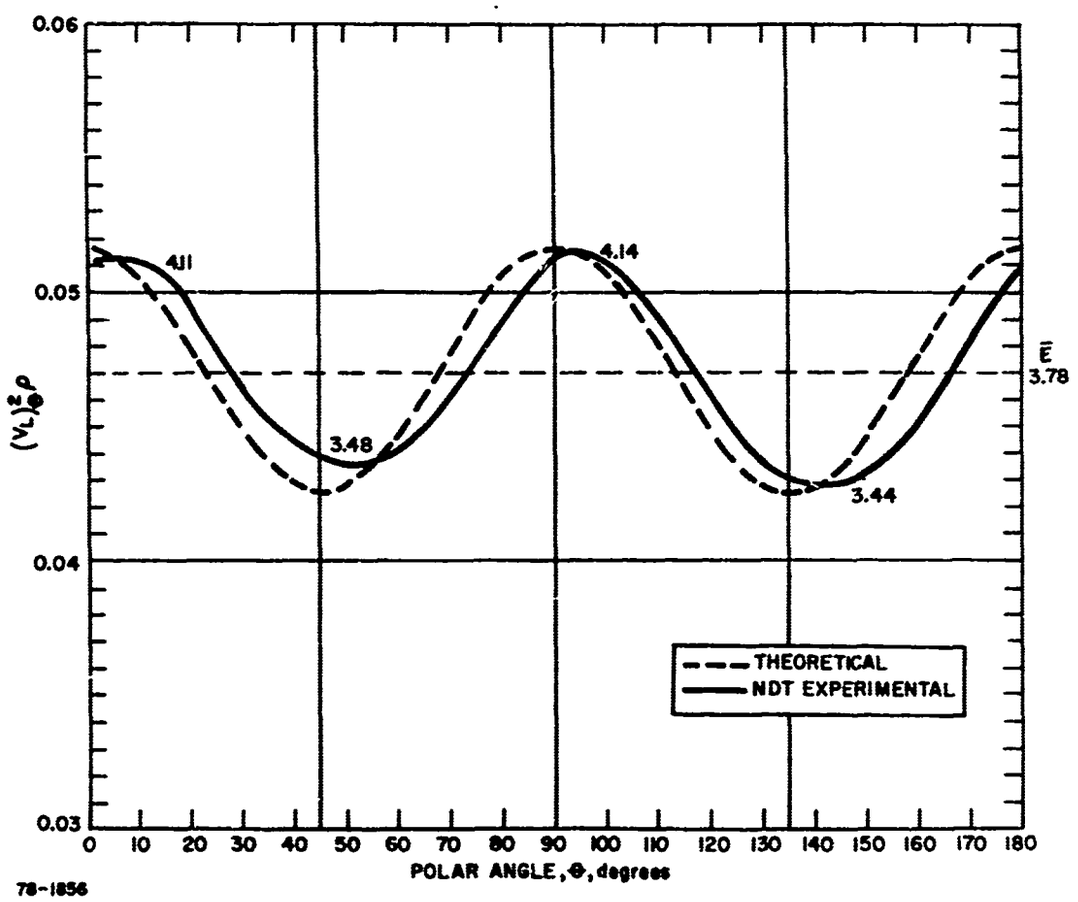


Figure 11 ELASTIC PROPERTY CHARACTERIZATION OF A 181, E-GLASS FABRIC/EPOXY LAMINATE

$\bar{E}$	3.47
$\bar{G}$	1.26
σ_{12}	.23
ρ	1.8630
V_F	.468
V_M	.517
V_P	.015

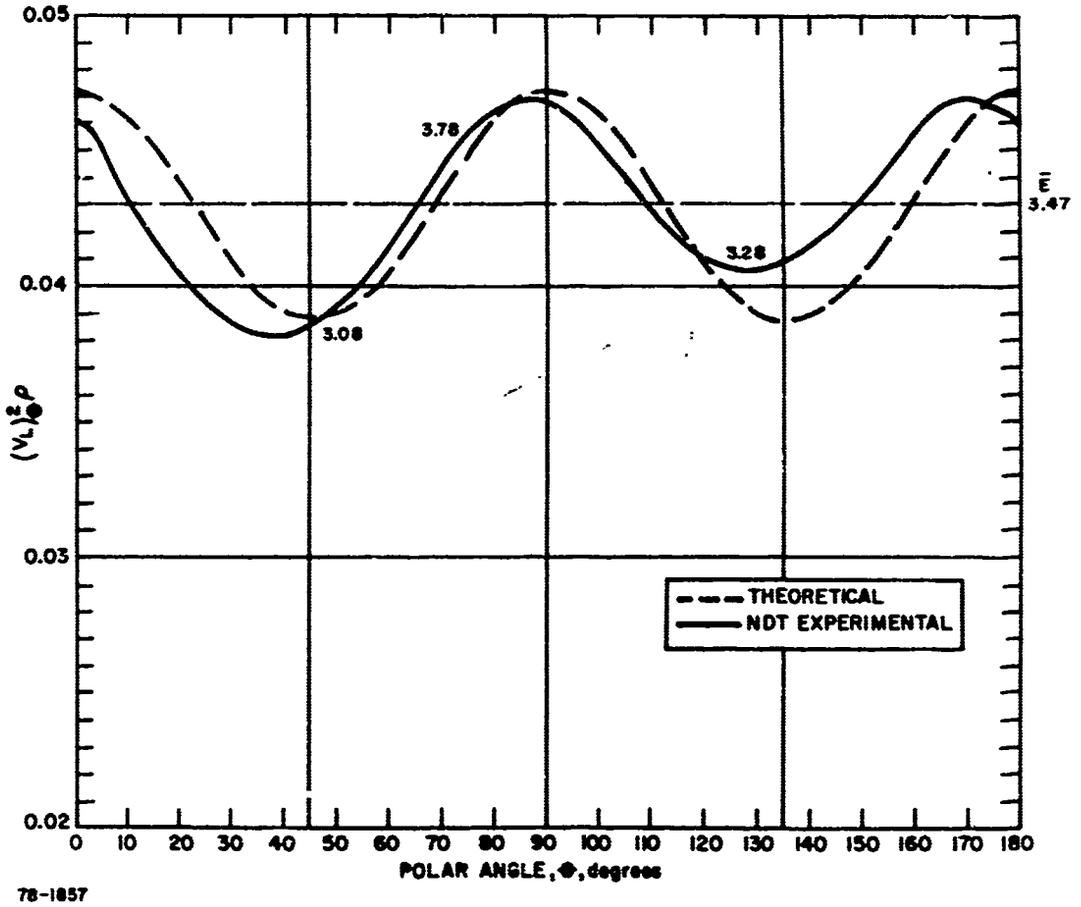
ELASTIC PROPERTY CHARACTERIZATION

$V_L^2 \rho = 0.0124E$

ALL MODULI, 10^6 psi

181, E-GLASS / EPOXY
D900-5 R-17

F_0	50%
F_{90}	50%
m	1.0
E_{11}	5.17
E_{22}	2.45
E_F	10.5
E_M	0.5



78-1857

Figure 12 ELASTIC PROPERTY CHARACTERIZATION OF A 181, E-GLASS FABRIC/EPOXY LAMINATE

$\bar{E}$	4.69
$\bar{G}$	1.71
σ_{12}	0.23
ρ	2.0553
V_F	0.594
V_M	0.354
V_P	0.052

ELASTIC PROPERTY CHARACTERIZATION

$V_L^2 \rho = 0.0124E$

ALL MODULI, 10^6 psi

181, E-GLASS / PHENOLIC
D900-11C R-14

F_0	46.2%
F_{90}	53.8%
m	0.858
E_{11}	6.49
E_{22}	3.60
E_F	10.50
E_M	0.70

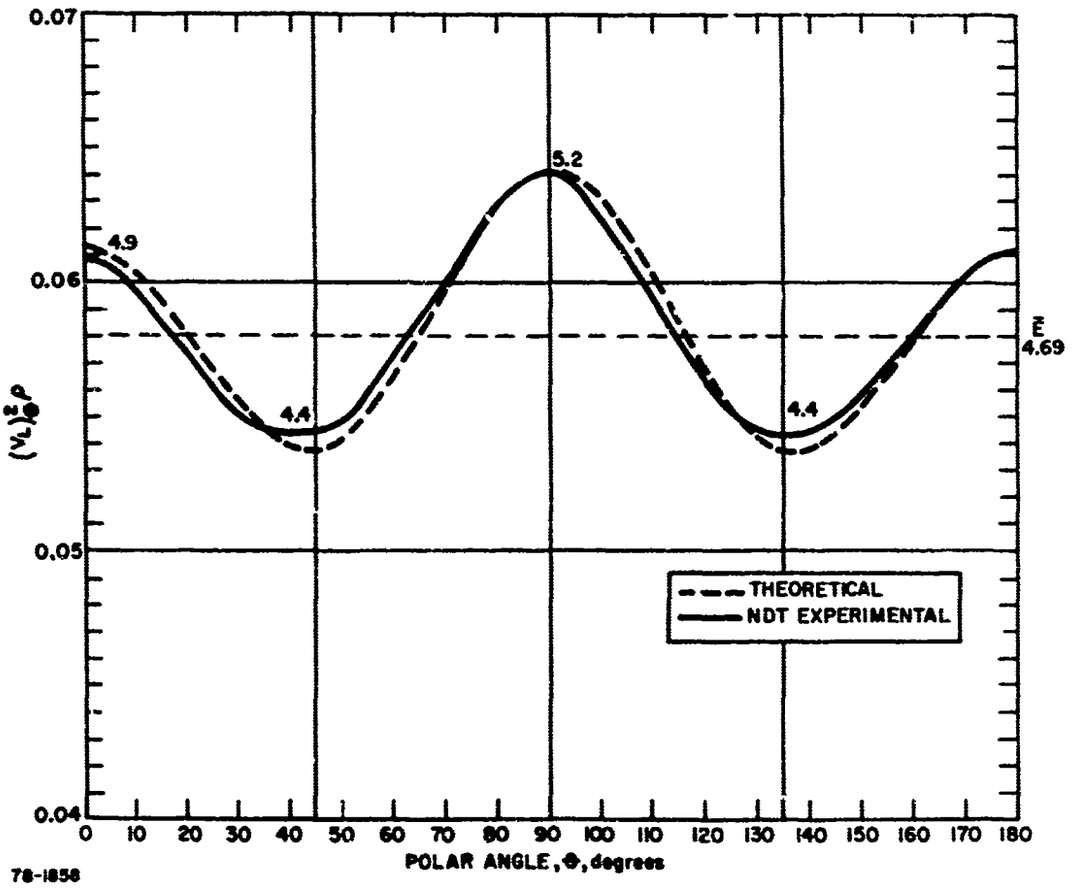


Figure 13 ELASTIC PROPERTY CHARACTERIZATION OF A 181, E-GLASS FABRIC/PHENOLIC LAMINATE

$\bar{E}$	2.82
$\bar{G}$	1.02
σ_{12}	0.23
ρ	1.4520
V_F	0.376
V_M	0.342
V_P	0.282

ELASTIC PROPERTY CHARACTERIZATION

$V_L^2 \rho = 0.0124E$

ALL MODULI, 10^6 psi

181, E-GLASS / POLYBENZIMIDAZOLE
N-3 R-12

F_0	52.5%
F_{90}	47.5%
m	1.11
E_{11}	4.19
E_{22}	2.00
E_F	10.50
E_M	0.70

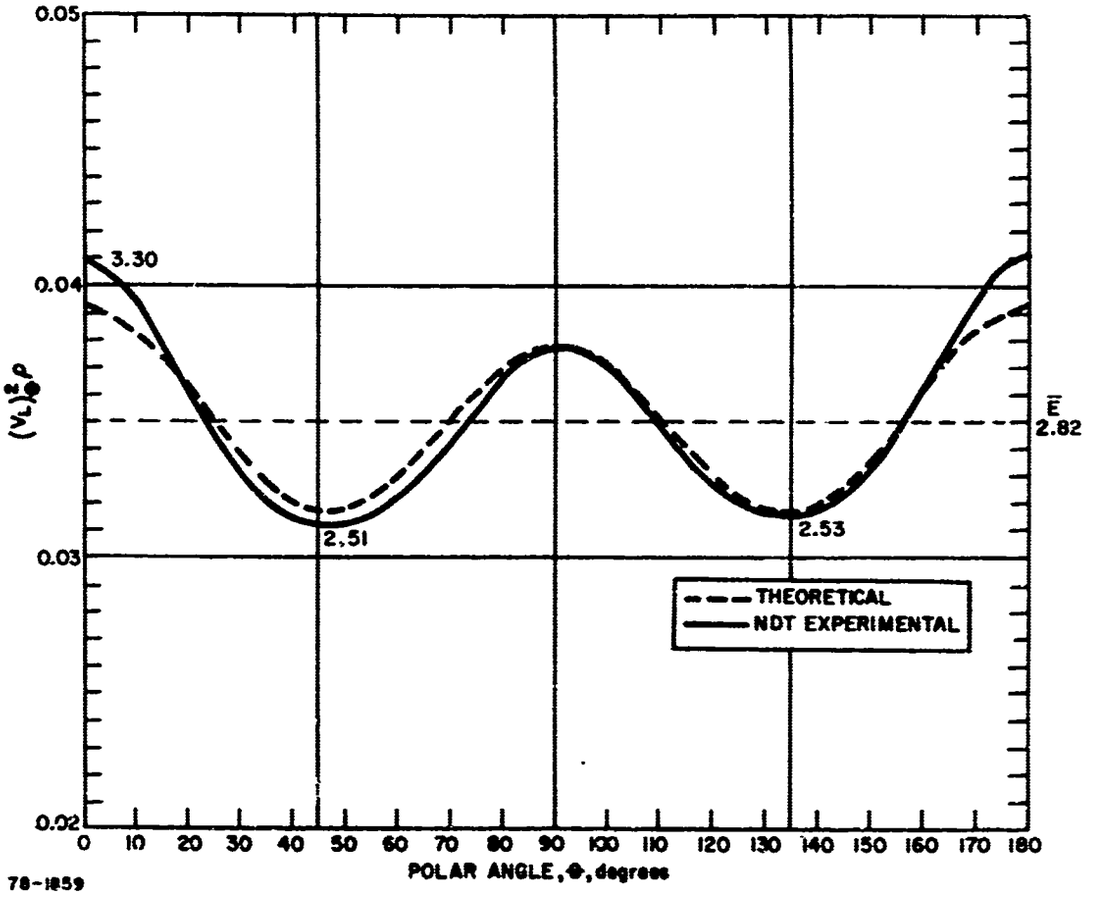


Figure 14 ELASTIC PROPERTY CHARACTERIZATION OF A 181, E-GLASS FABRIC/POLYBENZIMIDAZOLE LAMINATE

$\bar{E}$	2.03
$\bar{G}$	0.69
σ_{12}	0.23
ρ	1.8776
V_F	0.423
V_M	0.492
V_P	0.085

ELASTIC PROPERTY CHARACTERIZATION

$V_L^2 \rho = 0.0124E$

ALL MODULI, 10^6 psi

181, E-GLASS/SILICONE
D900-32 R-12

$\bar{r}_0$	55.6%
F_{90}	44.4%
m	1.25
E_{11}	4.68
E_{22}	0.44
E_F	10.50
E_M	0.50

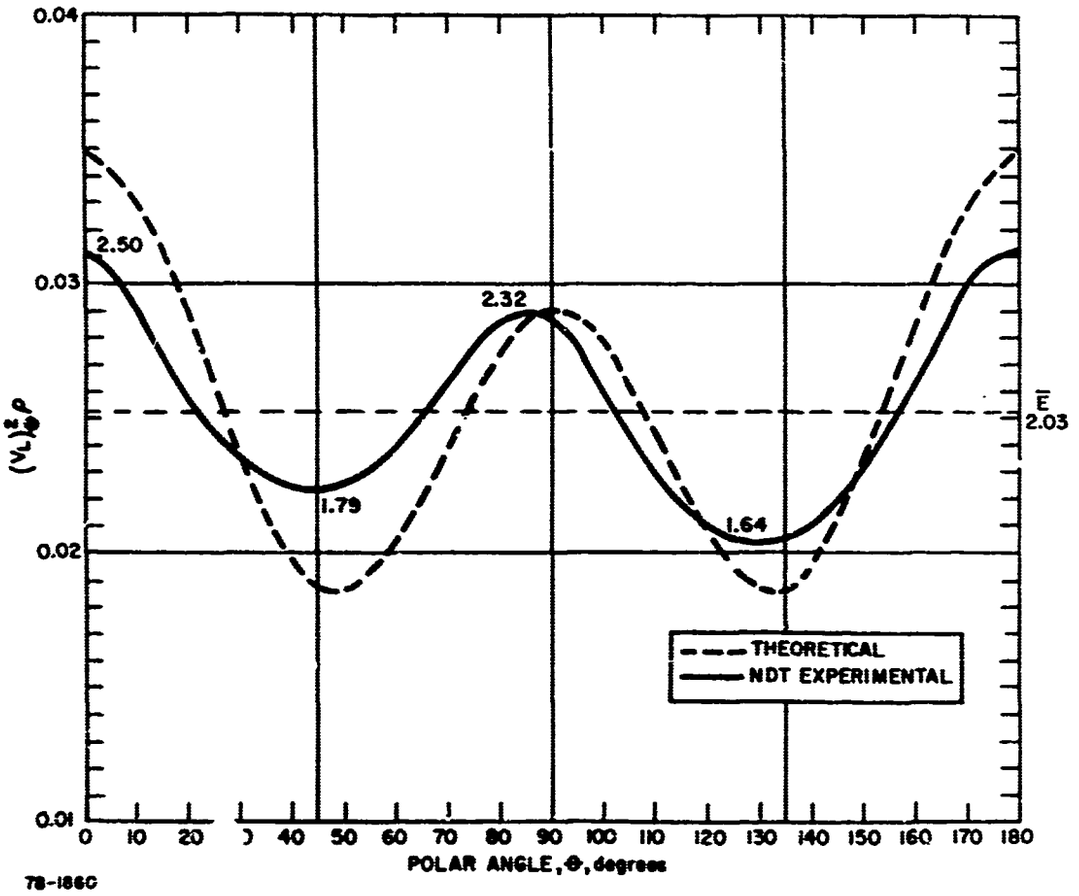


Figure 15 ELASTIC PROPERTY CHARACTERIZATION OF A 181, E-GLASS FABRIC/SILICONE LAMINATE

$\bar{E}$	8.00
$\bar{G}$	2.68
σ_{12}	0.23
ρ	1.4161
V_F	0.511
V_M	0.471
V_P	0.018

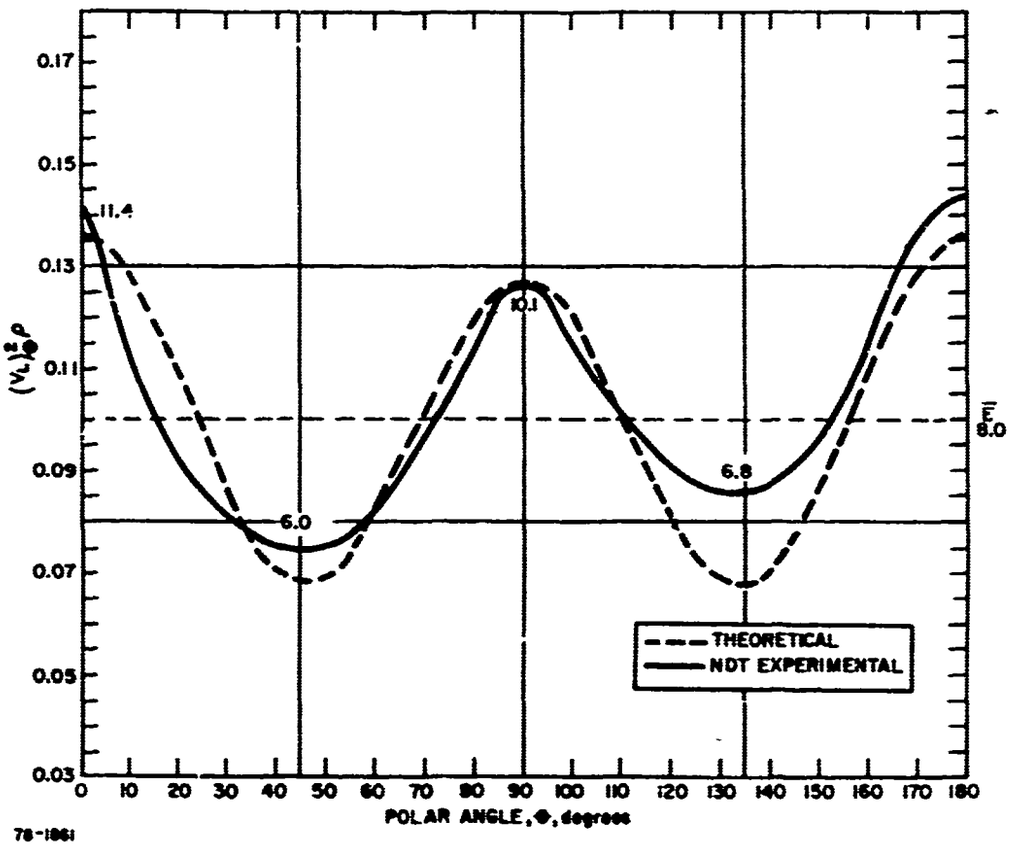
ELASTIC PROPERTY CHARACTERIZATION

$V_L^2 \rho = 0.0124E$

ALL MODULI, 10^6 psi

THORNEL 40/EPOXY
486-74 R-2

F_0	52.0%
F_{90}	48.0%
m	1.09
E_{11}	20.68
E_{22}	0.395
E_F	40.00
E_M	0.50



78-1861

Figure 16 ELASTIC PROPERTY CHARACTERIZATION OF A 13-PLY THORNEL 40/EPOXY LAMINATE

7. Figure 17 -- Thornel 40/epoxy (486-76 R-1)

The shape of the NDT experimental curve was as expected from ply-layup considerations. The theoretical curve provided a very close correlation.

8. Figure 18 -- Thornel 40/epoxy (486-81 R-1)

Note that by odd-ply count a crossply ratio less than one should have occurred with laminate. The fiber count per direction dominated to produce the experimental curve.

9. Figure 19 -- Thornel 40/epoxy (ARPA No. 1 X-3)

This "balanced" panel of 12 plies was considerably unbalanced. The unbalance has been attributed to the shear coupling weakness of the 90^{o} - 90^{o} pair of neutral axis plies.

10. Figure 20 -- Thornel 40/epoxy (ARPA No. 2 X-2)

A first attempt at correlation for this panel, using a Thornel 40 modulus of elasticity (E_F) of 40 x 10^6 psi, was rather poor. By using the NDT experimental data and back-calculating for E_F, a value of 48 x 10^6 psi was obtained. This strongly suggested that the fiber used in fabrication of this panel was actually Thornel 50, and not Thornel 40 as intended.

11. Figure 21 -- Thornel 40/epoxy (ARPA No. 3 X-2)

This panel also provided a poor correlation using E_F = 40 x 10^6 psi. Back calculation provided a value of 50.6 x 10^6 psi, again suggesting the use of Thornel 50 in its fabrication. The balance in this panel is as expected, indicating that both ply-count balance and proper fiber-count-per-ply were obtained.

12. Figure 22 -- 181, E-glass/polyimide (CH-132A R-2)

Elastic modulus values for the 181, E-glass/polyimide system fell below anticipated values. This typical situation was evident here and in the following three figures, and it has been attributed to the within-strand microporosity as it interacts with the brittle resin system. The disastrous effect on shear modulus ($\bar{G}$) and transverse-ply stiffness (E_{22}) is evident in the tabular characterization. The crossply ratio is remarkably greater than m = 1 for the 181 style fabric in this figure.

13. Figure 23 -- 181, E-glass/polyimide (CH-132B R-1)

This low-porosity, high resin content laminate provided a fairly close correlation with theory. All porosity was of the within-strand microporosity type.

14. Figure 24 -- 181, E-glass/polyimide (CH-132C R-2)

A theoretical fit which accounted for the observed orthogonal unbalance did not improve the general fit situation.

$\bar{E}$	7.09
$\bar{G}$	2.54
σ_{12}	.23
ρ	1.3809
V_F	.490
V_M	.469
V_P	.041

ELASTIC PROPERTY CHARACTERIZATION

$V_L^2 \rho = 0.0124E$

ALL MODULI, 10^6 psi

THORNEL 40 / EPOXY
486-76 R-1

F_0	53.6%
F_{90}	46.4%
m	1.15
E_{11}	19.83
E_{22}	.559
E_F	40.0
E_M	0.5

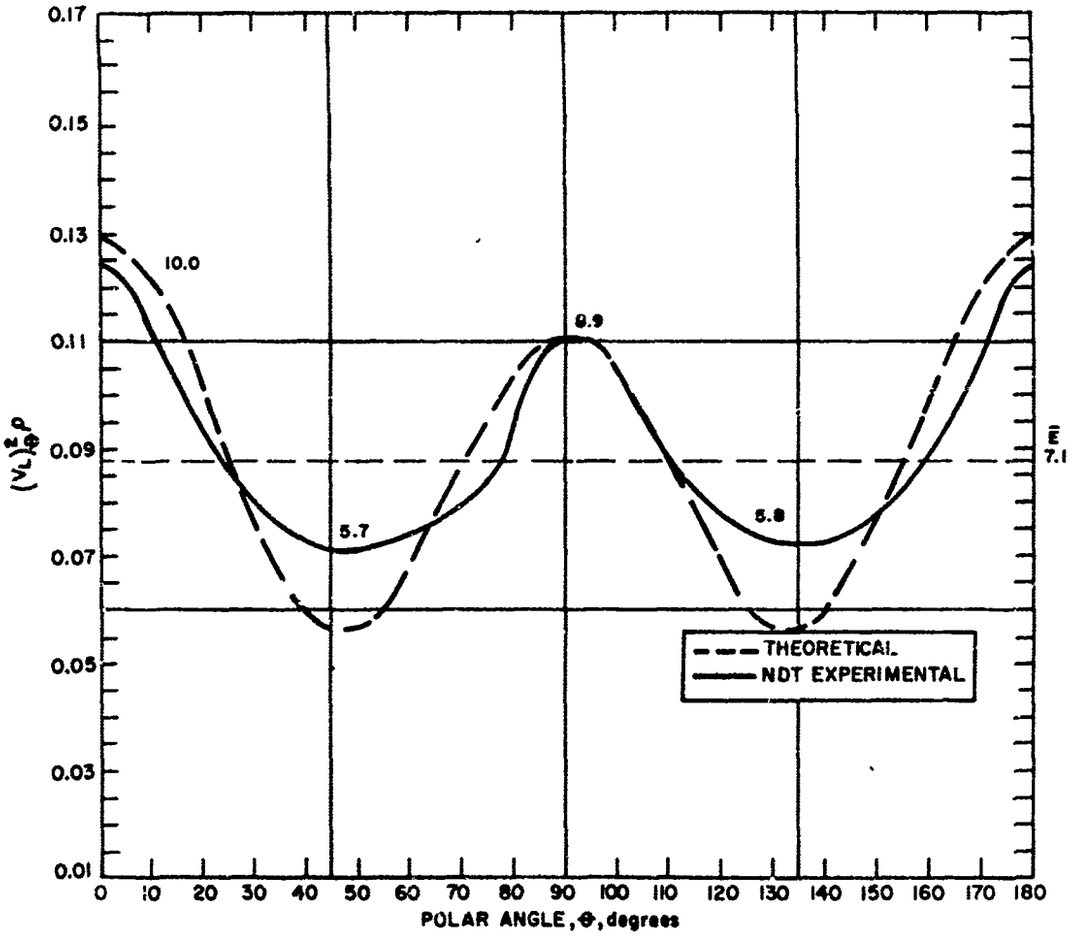


Figure 17 ELASTIC PROPERTY CHARACTERIZATION OF A 13-PLY THORNEL 40/EPOXY LAMINATE

$\bar{E}$	6.06
$\bar{G}$	2.01
σ_{12}	0.23
ρ	1.3427
V_F	0.410
V_M	0.545
V_P	0.046

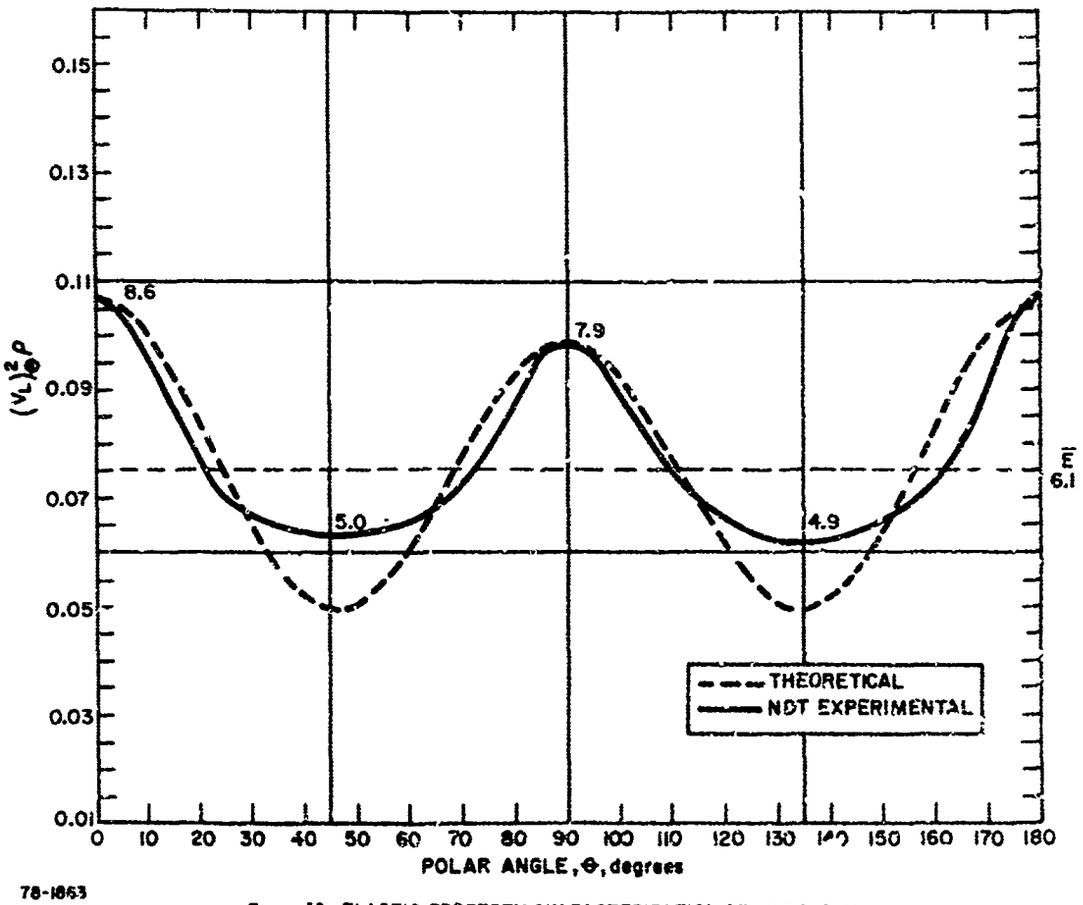
ELASTIC PROPERTY CHARACTERIZATION

$V_L^2 \rho = 0.0124E$

ALL MODULI, 10^6 psi

THORNEL 40/EPOXY
486-81 R-1

F_0	51.9%
F_{90}	48.1%
ν_{12}	1.08
E_{11}	16.67
E_{22}	-0.287
E_F	40.00
E_M	0.50



78-1863

Figure 18 ELASTIC PROPERTY CHARACTERIZATION OF AN 11-PLY THORNEL 40/EPOXY LAMINATE

$\bar{E}$	6.84
$\bar{G}$	2.27
σ_{12}	0.23
ρ	1.3564
V_F	0.462
V_M	0.488
V_P	0.050

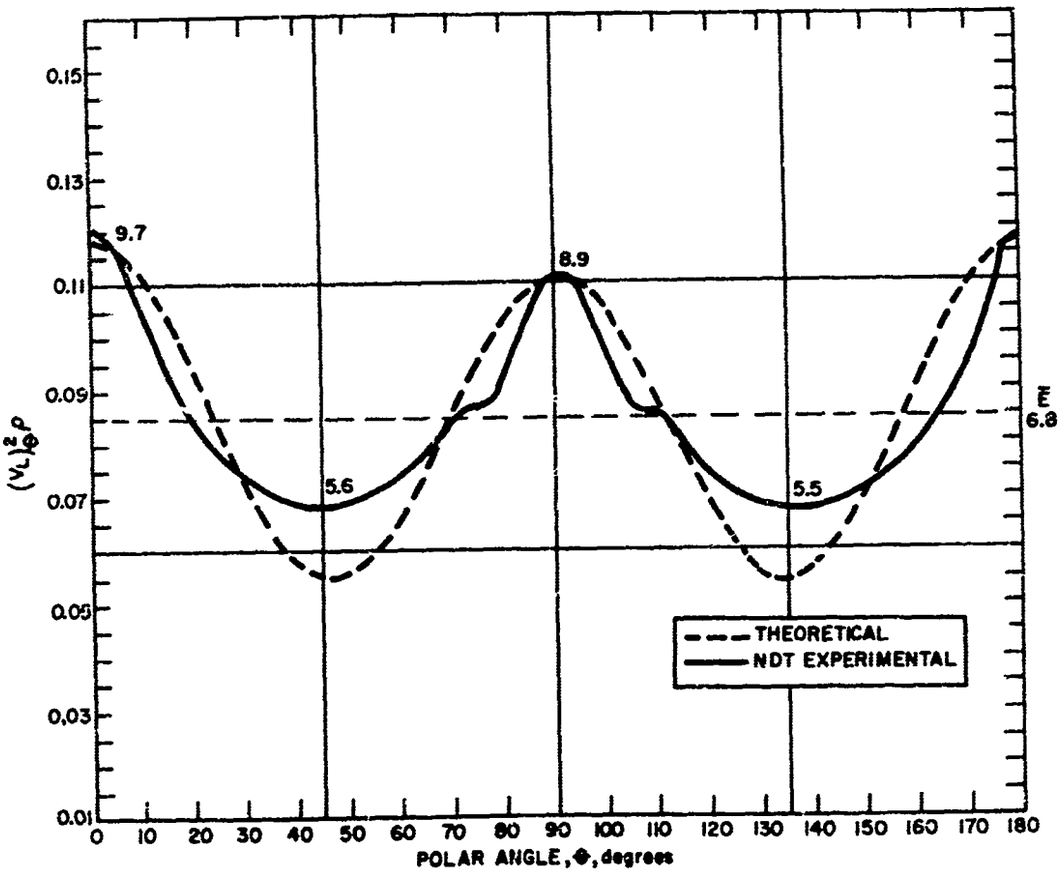
ELASTIC PROPERTY CHARACTERIZATION

$V_L^2 \rho = 0.0124E$

ALL MODULI, 10^6 psi

THORNEL 40/EPOXY
ARPA NO.1 X-3

F_0	51.6%
F_{90}	48.4%
m	1.07
E_{11}	18.72
E_{22}	-0.292
E_F	40.00
E_M	0.50



78-1864

Figure 19 ELASTIC PROPERTY CHARACTERIZATION OF A 12-PLY ARPA THORNEL 40/EPOXY LAMINATE

$\bar{E}$	9.12
$\bar{G}$	2.96
σ_{12}	0.23
ρ	1.418
V_F	0.536
V_M	0.439
V_P	0.026

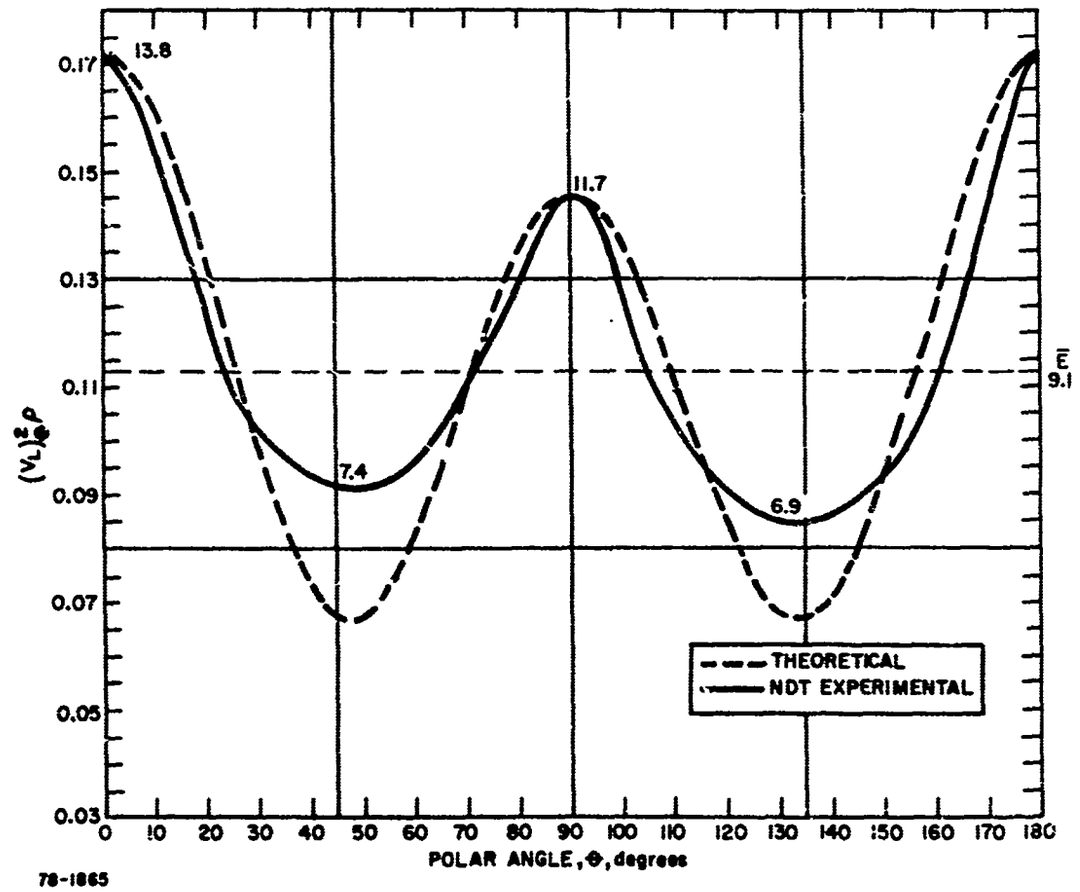
ELASTIC PROPERTY CHARACTERIZATION

$V_L^2 \rho = 0.0124E$

ALL MODULI, 10^6 psi

THORNEL 40/ EPOXY
ARPA NO.2 X-2

F_0	53.7%
F_{90}	46.3%
m	1.16
E_{11}	27.359
E_{22}	-1.835
E_F	50.63
E_M	0.50



78-1865

Figure 20 ELASTIC PROPERTY CHARACTERIZATION OF A 12-PLY ARPA THORNEL 50/EPOXY LAMINATE

$\bar{E}$	9.12
$\bar{G}$	2.94
σ_{12}	0.23
ρ	1.437
V_F	0.586
V_M	0.389
V_P	0.025

ELASTIC PROPERTY CHARACTERIZATION

$V_L^2 \rho = 0.0124E$

ALL MODULI, 10^6 psi

THORNEL 40/ EPOXY
ARPA NO.3 X-2

F_0	50%
F_{90}	50%
m	1.00
E_{11}	28.32
E_{22}	-2.413
E_F	48.00
E_M	0.50

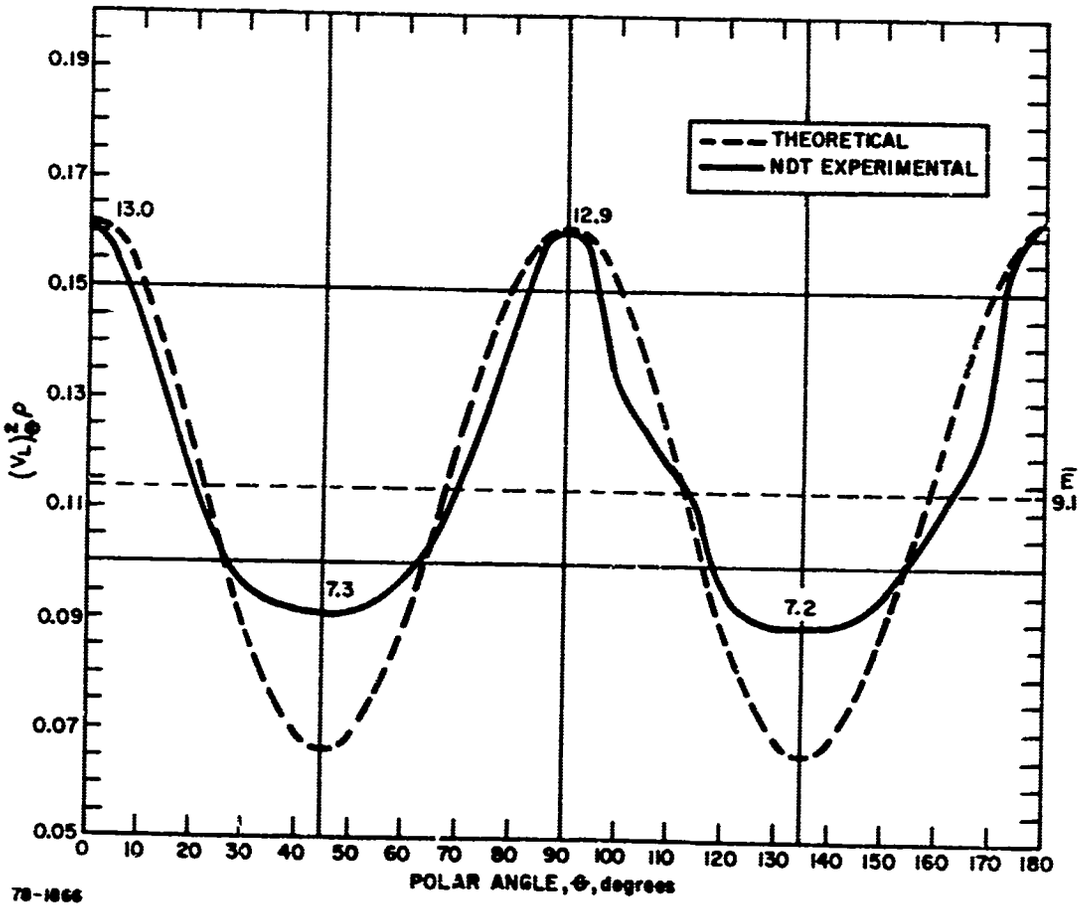


Figure 21 ELASTIC PROPERTY CHARACTERIZATION OF A 4-PLY ARPA THORNEL 50/EPOXY LAMINATE

$\bar{E}$	2.40
$\bar{G}$	0.838
σ_{12}	0.23
ρ	1.7970
V_F	0.435
V_M	0.523
V_P	0.042

ELASTIC PROPERTY CHARACTERIZATION

$V_L^2 \rho = 0.0124E$

ALL MODULI, 10^6 psi

181, E-GLASS/POLYIMIDE
CH132A R2

F_0	54.9%
F_{90}	45.1%
m	1.22
E_{11}	4.93
E_{22}	0.885
E_F	10.50
E_M	0.70

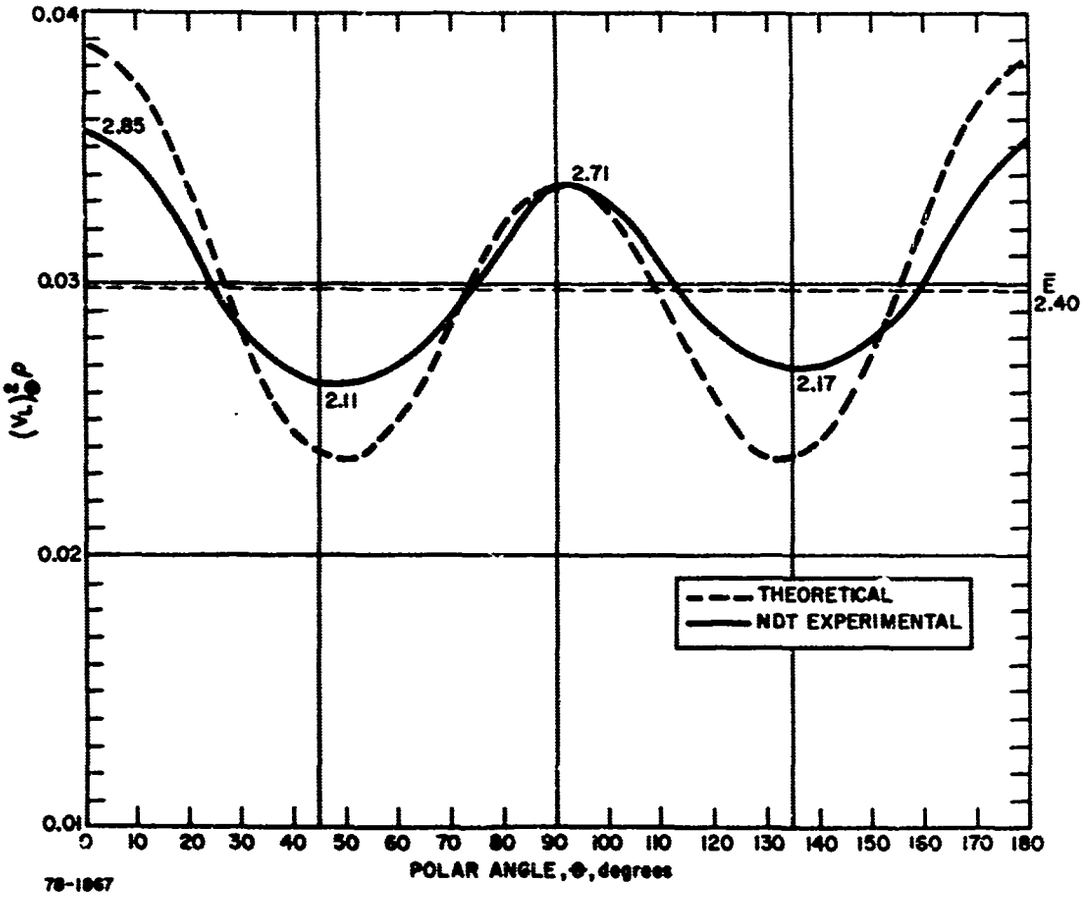


Figure 22 ELASTIC PROPERTY CHARACTERIZATION OF A 181, E-GLASS FABRIC/QUANTAD 159 POLYIMIDE LAMINATE

$\bar{E}$	2.88
$\bar{G}$	1.02
σ_{12}	0.23
ρ	1.8582
V_F	0.447
V_M	0.537
V_P	0.016

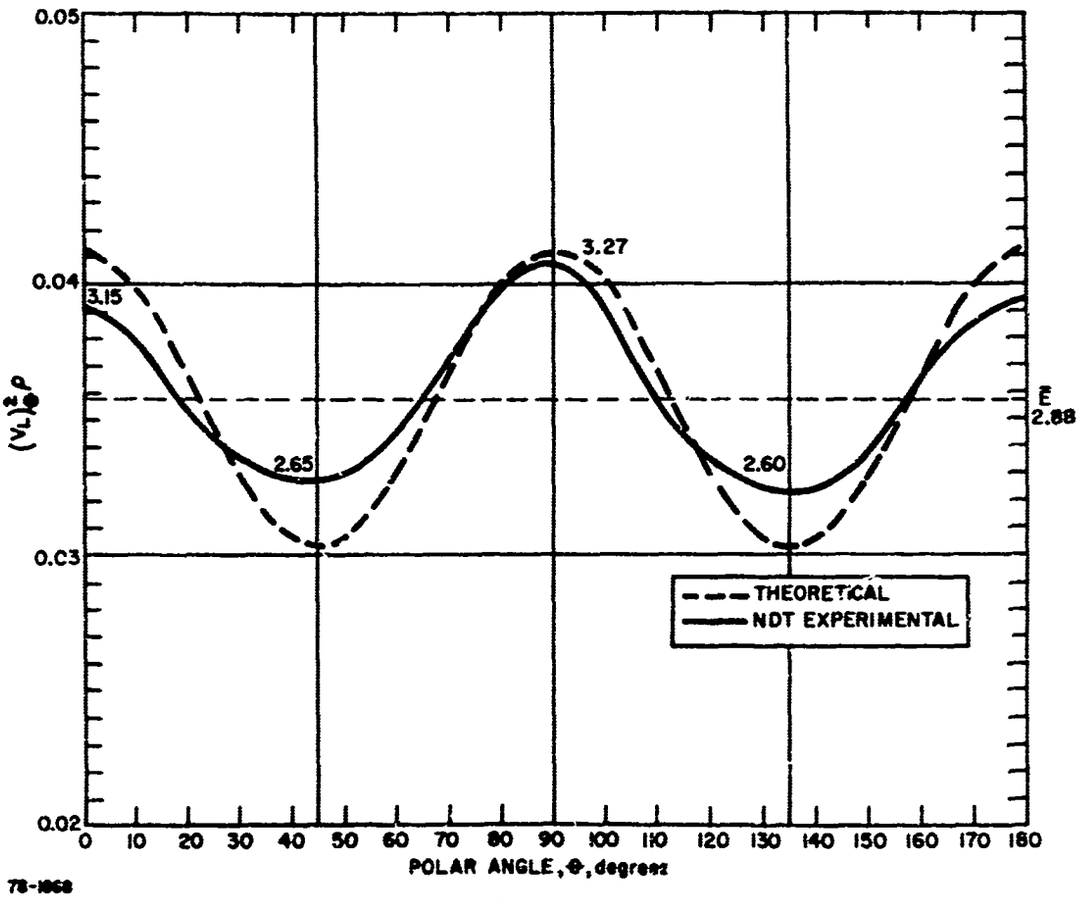
ELASTIC PROPERTY CHARACTERIZATION

$V_L^2 \rho = 0.0124E$

ALL MODULI, 10^6 psi

181, E-GLASS/POLYIMIDE
CH1328 R-1

F_0	50%
F_{90}	50%
m	1.00
E_{11}	5.07
E_{22}	1.56
E_F	10.50
E_M	0.70



78-1868

Figure 23 ELASTIC PROPERTY CHARACTERIZATION OF A 181, E-GLASS FABRIC/QUANTAD 159 POLYIMIDE LAMINATE

$\bar{E}$	2.34
$\bar{G}$	0.815
σ_{12}	0.23
ρ	1.7874
V_F	0.424
V_M	0.536
V_P	0.040

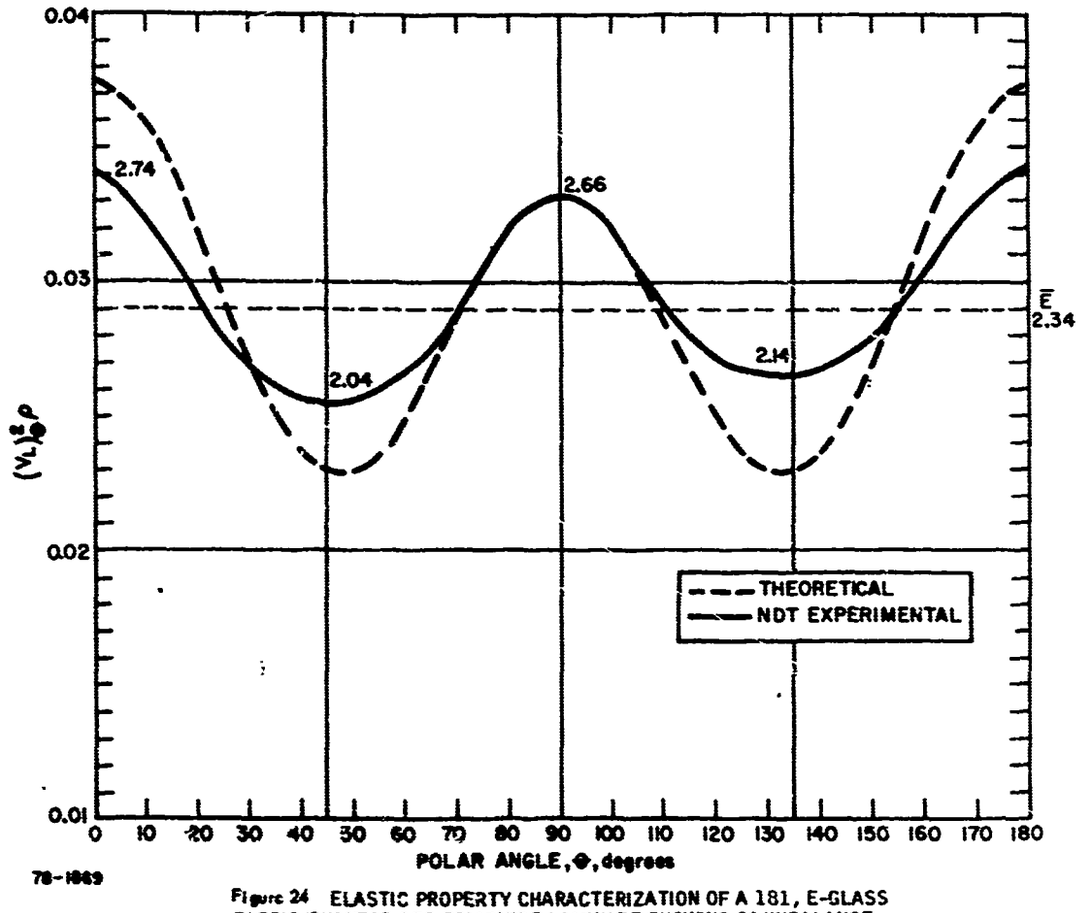
ELASTIC PROPERTY CHARACTERIZATION

$V_L^2 \rho = 0.0124E$

ALL MODULI, 10^6 psi

181, E-GLASS/POLYIMIDE
CH132C R-2

F_0	54.4%
F_{90}	45.6%
m	1.19
E_{11}	4.83
E_{22}	0.546
E_F	10.50
E_M	0.70



78-1869

Figure 24 ELASTIC PROPERTY CHARACTERIZATION OF A 181, E-GLASS FABRIC/QUANTAD 159 POLYIMIDE LAMINATE SHOWING 0° UNBALANCE

15. Figure 25 — 181, E-glass/polyimide (CH-132E R-3)

As in the previous figure, the low glass content resulted in a reduction of all elastic moduli.

16. Figure 26 — 181, E-glass/polyimide (CH-140 R-2)

Cure conditions were such in this laminate that the resin appeared crazed when observed under the microscope. Obviously this crazing, or a 0-degree ("fill") orientation to within-strand microporosity, or both, produced the severe second-lobe deviation. All three specimens cut from the laminate exhibited this same experimental curve shape.

17. Figure 27 — 181, E-glass/polyimide (CH-138E R-1)

What happens when the fabric plies are distorted during batch prepregging? This is shown well for the Skybond 704 thermoplastic polyimide resin system. The cosine relationship has disappeared, although a theoretical fit, using a crossply ratio of m = 3.1, provided a fair approximation.

18. Figure 28 — 181, E-glass/polyimide (CH-138E R-2)

In this example, fabric ply distortion was extremely severe. The distortion could be easily observed in radiographs of the original panel. Any attempt at using the cosine relationship for a theoretical fit was rather useless. A cosine fit where some angle-ply (α) relationship is factored in may have provided a close fit. The angle-ply theory from micromechanics will be investigated in the near future. This figure demonstrates, from the positive side, the versatile designability of reinforced plastic composite materials, and the capability of nondestructive testing to record it.

SUMMARY

We have found that the $V_L^2\rho$ versus polar angle (θ) relationship provides the true value for isotropic modulus ($\bar{E}$) for the particular laminate being evaluated, and this value, in turn, is the key to linking micromechanics theory to practical, real reinforced plastics materials.

The rapidly-obtained quantitative NDT response values from ultrasonic and gamma radiometric measurements provide the necessary information for calculating 16 pieces of information which provide a practically complete elastic property characterization of the laminate.

This has been accomplished by solving the existing micromechanics equations together, and simplifying them to obtain an equation for predicting the theoretical modulus (E'_θ) versus polar angle (θ) relationship, which then may be used to analyze the NDT-predicted polar modulus values.

Sixty relationships have been developed, and 25 of them have been reported, covering six completely different resin systems, (epoxy, phenolic, polybenzimidazole, polyimide, polyester, and silicone) and three reinforcements, 181-style E-glass fabric, Thornel 40 fiber, and boron filament.

$\bar{E}$	2.24
$\bar{\zeta}$	0.773
σ_{12}	0.23
ρ	1.7734
V_F	0.437
V_M	0.500
V_F	0.063

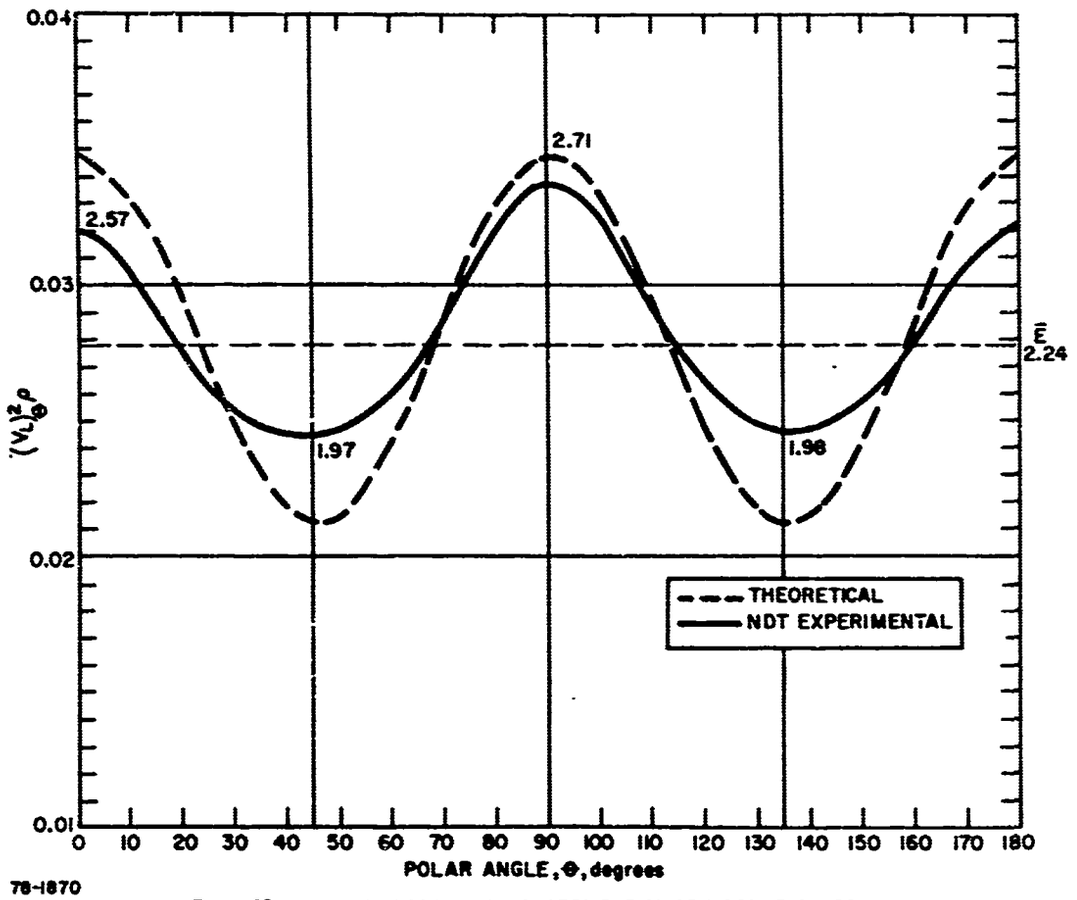
ELASTIC PROPERTY CHARACTERIZATION

$V_L^2 \rho = 0.0124E$

ALL MODULI, 10^6 psi

181, E-GLASS / POLYIMIDE
CH132E R-3

F_0	50%
F_{90}	50%
m	1.00
E_{11}	4.94
E_{22}	0.624
E_F	10.50
E_M	0.70



78-1870

Figure 25 ELASTIC PROPERTY CHARACTERIZATION OF A 181, E-GLASS FABRIC/QUANTAD 159 POLYIMIDE LAMINATE SHOWING 90° UNBALANCE

$\bar{E}$	1.66
$\bar{G}$	0.566
σ_{12}	0.23
ρ	1.5273
V_F	0.337
V_M	0.482
V_P	0.181

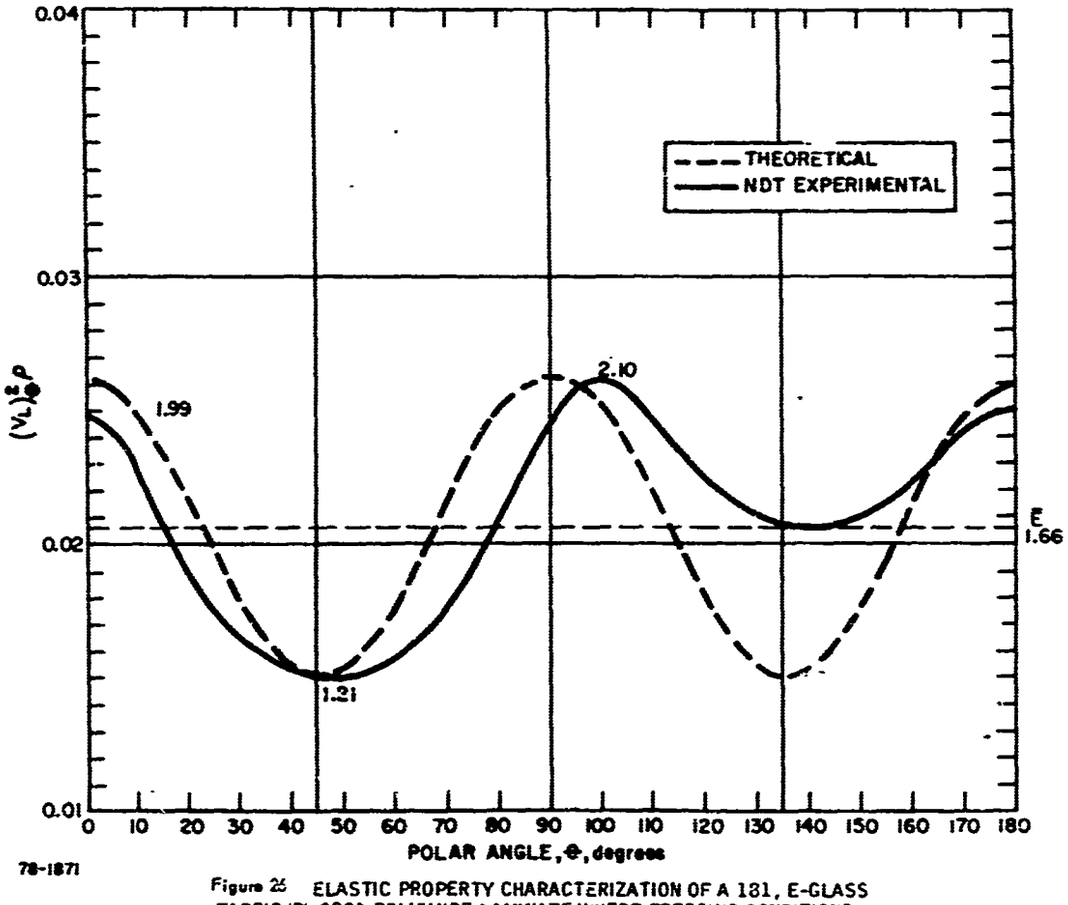
ELASTIC PROPERTY CHARACTERIZATION

$V_L^2 \rho = 0.0124E$

ALL MODULI, 10^6 psi

181,E-GLASS / POLYIMIDE
CH140 R-2

F_0	49.9%
F_{90}	50.1%
m	0.995
E_{11}	3.88
E_{22}	0.326
E_F	10.50
E_M	0.70



78-1871

Figure 25 ELASTIC PROPERTY CHARACTERIZATION OF A 181, E-GLASS FABRIC/PI-3301 POLYIMIDE LAMINATE WHERE PRESSING CONDITIONS PRODUCED RESIN CRAZING

$\bar{E}$	2.79
$\bar{G}$	1.01
σ_{12}	0.23
ρ	1.7065
V_F	0.350
V_M	0.603
V_P	0.047

ELASTIC PROPERTY CHARACTERIZATION

$V_L^2 \rho = 0.0124E$

ALL MODULI, 10^6 psi

181, E-GLASS/POLYIMIDE
CH138E R-1

F_0	75.6%
F_{90}	24.4%
m	3.10
E_{11}	4.10
E_{22}	2.01
E_F	10.50
E_M	0.50

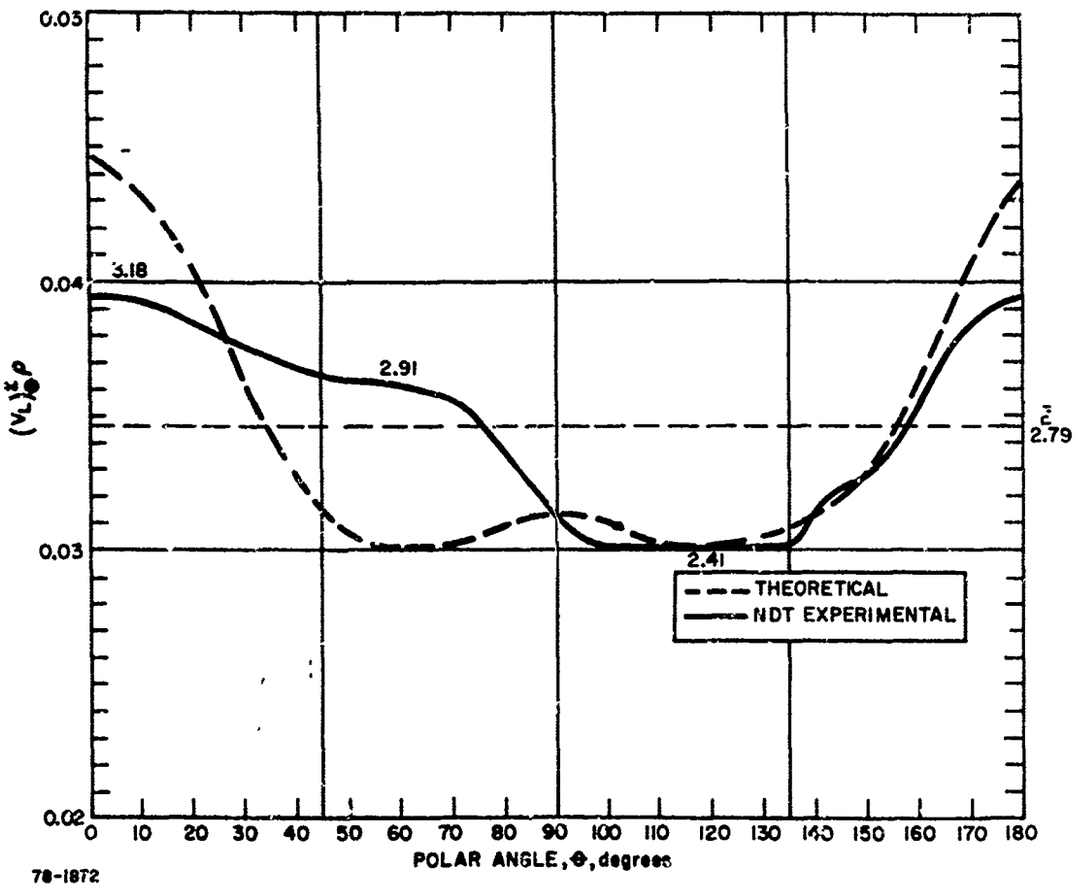


Figure 27 ELASTIC PROPERTY CHARACTERIZATION OF A 181, E-GLASS FABRIC/SKYBOND 704 POLYIMIDE LAMINATE SHOWING MODERATE FABRIC DISTORTION EFFECTS

$\bar{E}$	2.44
$\bar{G}$	0.879
σ_{12}	0.23
ρ	1.6884
V_F	0.333
V_M	0.604
V_P	0.063

ELASTIC PROPERTY CHARACTERIZATION

$V_L^2 \rho = 0.0124E$

ALL MODULI, 10^6 psi

181, E-GLASS / POLYIMIDE
CH138E R-2

F_0	74.1%
F_{90}	25.9%
m	2.86
E_{11}	3.92
E_{22}	1.56
E_F	10.50
E_M	0.50

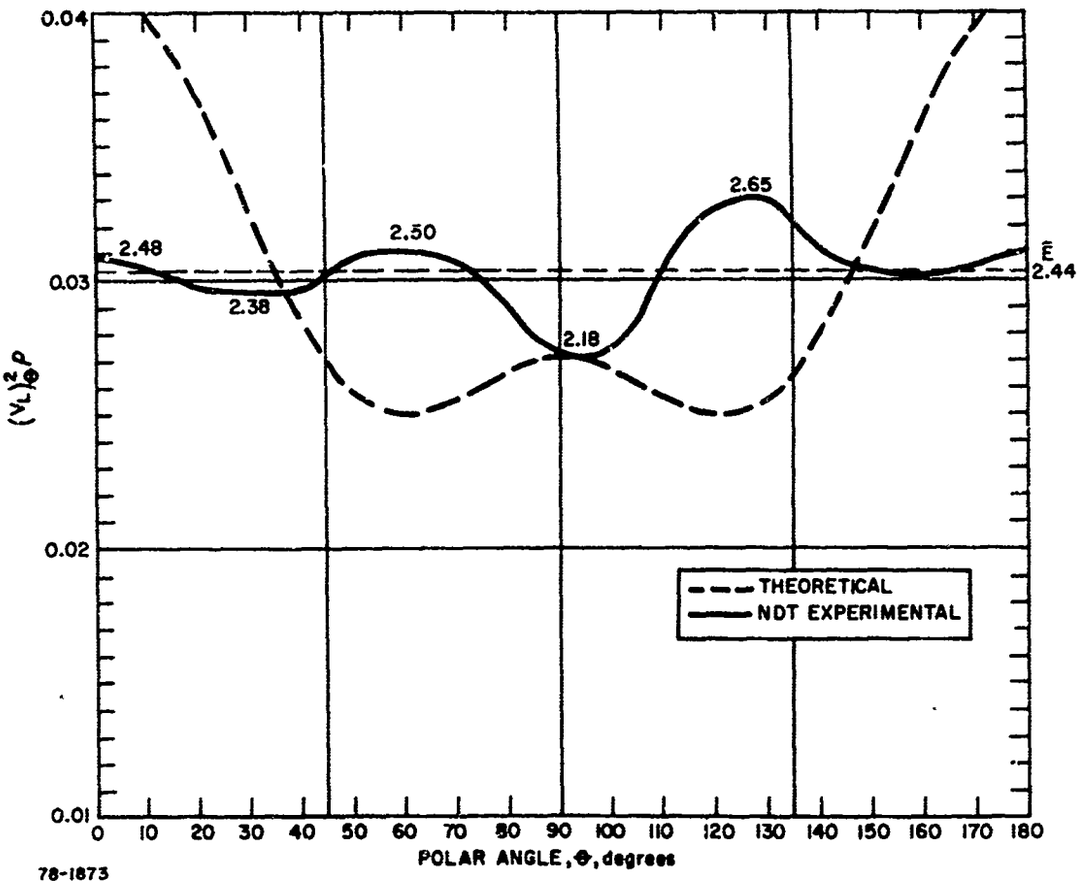


Figure 28 ELASTIC PROPERTY CHARACTERIZATION OF A 181, E-GLASS FABRIC/SKYBOND 704 POLYIMIDE LAMINATE SHOWING SEVERE FABRIC DISTORTION EFFECTS

One particularly exciting outcome of this data correlation and analysis has been the ability to calculate the reinforcing fiber effective elastic modulus as it exists in the finished laminate. The calculated isotropic shear modulus value, $\bar{G}$, and across-fiber single ply stiffness, E_{22}, appear to reflect the influences of porosity content and location, and interfacial bonding. More study is currently underway to confirm this.

SPONSORSHIP ACKNOWLEDGEMENT

This work was performed under U. S. Air Force Contracts AF33(615)-1705 and F33615-67-C-1285, initiated by the Air Force Materials Laboratory, AFSC, Wright Patterson Air Force Base, Ohio. Mr. H. W. Kamm and Lt. Lee Gulley, respectively, served as Air Force Project Monitors for the Processing and NDT Branch, Metals and Ceramics Division.

REFERENCES

1. Tsai, S. W. and R. L. Thomas, "A Critical Design Comparison of Composite Stiffness," Proceedings of SPE Baltimore-Washington Section RETEC, Stability of Plastics, Section G, Washington, D. C. (September 1967).

2. Tsai, S. W. and N. J. Pagano, Variant Properties of Composite Materials, Technical Report AFML-TR-67-349, Air Force Materials Laboratory, Wright-Patterson AFB, Ohio, (March 1968), 23 pages.

3. Lubin, G. and W. C. Toppe, "Factors Causing Scatter and Unreliable Design Data for Fiberglass Fabric Laminates for Aerospace Applications," Proceedings of the SPI, 22nd Annual Meeting of the Reinforced Plastics Division, Washington, D. C. (February 1967) Section 14-D.

4. Zurbrick, J. R., Development of Nondestructive Tests for Predicting Elastic Properties and Component Volume Fractions in Reinforced Plastic Composite Materials, Technical Report AFML-TR-68-233, Air Force Materials Laboratory, Wright-Patterson AFB, Ohio (September 1968) Figure 15, pg. 40.

APPLICATION OF NONDESTRUCTIVE TESTING FOR ADVANCED COMPOSITES

Robert T. Anderson
Thomas J. DeLacy

Convair Division of General Dynamics
San Diego, California

For Presentation at the
March 1969 AFML/Aerospace/University of Dayton Conference
on NDT of Plastic/Composite Structures

ABSTRACT

Application of Nondestructive Testing for Advanced Composites

Robert T. Anderson
Thomas J. DeLacy

Convair Division of General Dynamics

The special radiographic and ultrasonic techniques necessary for testing metal matrix composites are described. Approaches to display and analysis of ultrasonic and radiographic data are presented. Real-time filtered video, analog and digital computer methods provide means for enhancing and displaying these data.

Other nondestructive testing methods which have been investigated include: thermal gradient methods (infrared radiometry and cholestric liquid crystal detectors), eddy current and neutron radiography. The applications and limitations of these methods are discussed.

Methods of nondestructively testing graphite filament reinforced resin matrix materials are also presented. Microwave and vacuum microradiography methods have been explored and results are presented.

FOREWORD

This paper was prepared for presentation at the March 1969 AFML/Aerospace/ University of Dayton conference on NDT of Plastic/Composite Structures and represents a summary of portions of the following Convair division of General Dynamics programs:

RD-1-111-1031-911 - Nondestructive Testing of Plastic Laminates, Adhesive Bonded Honeycomb, and Diffusion Bonded Metals

RD-1-111-1248-911 - Nondestructive Testing of Advanced Aerospace Materials

RD-1-111-6807-170 - Nondestructive Testing of Metal Matrix Composite Materials

RD-1-111-6807-172 - Nondestructive Testing of Aerospace Materials and Components

RD-1-111-6906-156 - Nondestructive Test Development.

INTRODUCTION

We paraphrase a quote of Carlton Hastings[1] who defines a material as a collection of defects. Acceptable material is an accidental or organized collection of defects. Scrap material is an unfortunate collection of defects. He further defines a defect as an imperfection, sometimes significant, sometimes irrelevant.

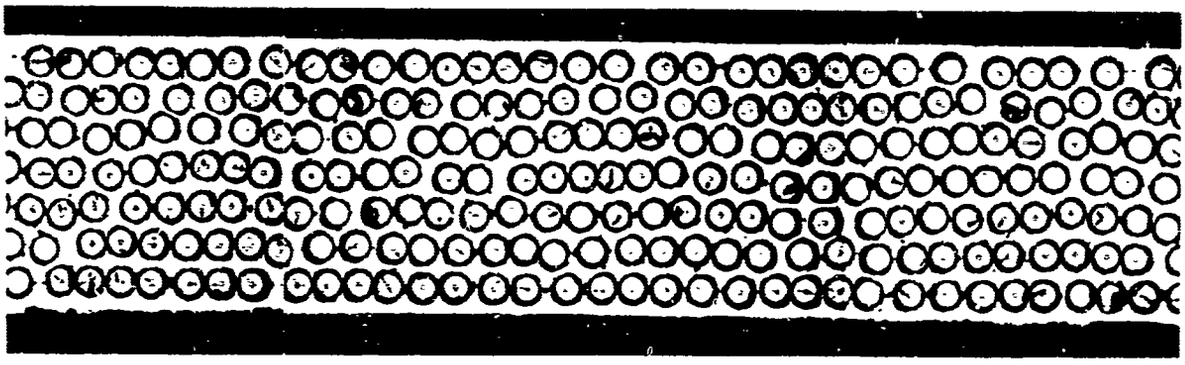


Figure 1. Cross section of 50% boron filament reinforced aluminum matrix composite 0.037 inch thick.

These thoughts are particularly appropriate if one considers the material in Figure 1. This unique material can possess some highly desirable properties. For example, consider the following comparisons:

	Typical Aluminum Alloy	Typical Alloy Steel	6061 Aluminum-50% Boron Composite
Ultimate tensile strength	45 ksi	180 ksi	180 ksi
Yield strength (σ_y)	40 ksi	160 ksi	180 ksi
Young's modulus (E)	10×10^3 ksi	30×10^3 ksi	32×10^3 ksi
Specific gravity	2.70	7.75	2.70
Specific strength*	410	570	1,840
Specific stiffness**	102	107	327

*Specific strength $= \sigma_y / \rho$ ρ = density (lb./in.^{3})

**Specific stiffness $= E/\rho$

The last two entries tell the story. Pound for pound, the aluminum-boron composite has more than four times the strength of aluminum, three times the strength of steel, and is more than three times as stiff as both steel and aluminum. It is logical to ask, "Why aren't many structures made from this material?" To answer this, some limitations must be pointed out. Foremost, is the extremely high cost. Cost effective applications are few, mainly limited to weight- and stiffness-critical designs like upper-stage missile components or aircraft structures. Secondly, the composite specified in the table has unidirectional filament orientation; transverse or cross-tension strength is 12 to 15 ksi. Wide variability in mechanical properties often results from difficulties in producing uniform quality.

Looking again at Figure 1, one should ask, "at what scale should one think when considering the applications of nondestructively testing this material?" For a nondestructive test to be useful, it must, at least, detect discontinuities. But imagine looking for discontinuities in the filaments. One square foot of the material shown in Figure 1 contains 16,800 feet of filaments, just over three miles. One linear inch transverse to the filament direction intercepts seven layers of 200 filaments each. This yields 1,400 inherent discontinuities per linear inch; and that piece is less than 0.040-inch thick, about three-quarters the thickness of a dime!

The question of scale is one of philosophy. Certainly there is some "weakest link" in the material at which point it would fail if sufficiently loaded. But is it necessary to consider all discontinuities, even the natural, inherent ones, in order to find only the critical ones? Or can all the irrelevant detail be "filtered out" by some means? If so, at what point should the filtering be done? Shall the NDT probing media be "detuned" so that the many individual small inherent discontinuities will not interact? Or shall the highest possible sensitivity between the probing media and test object be utilized, and the resulting data filtered? In early stages of both material and test method development, the latter approach seems better. If all possible data are obtained initially, the data which turns out to be irrelevant can simply be ignored. This approach does not preclude the existence of oversights in data analysis; however, once obtained, the data can be subjected to as many forms of analysis as the experimenter's imagination and finances permit.

At this early stage of composite materials development, many other basic questions remain unanswered. However, improvements in processing, testing and data analysis have reduced the variability and increased the overall quality and properties of these materials. Benefits accruing from concurrent NDT and materials development are several: (1) the materials engineer has feedback from which he can minimize his destructive testing; (2) the material producer can better control and improve his process; (3) the designer has more confidence in the developed design allowables, and (4) most of the quality control inspection problems have been exposed prior to production runs.

Some analyses have been made which attempt to attribute the significance of defects. One study[2] lists defects which are likely to be important to metal-matrix composites (in decreasing order to relative importance):

1. Volume ratio variations
2. Filament degradation
3. Changes in matrix modulus
4. Matrix degradation (disbonds, voids, diffusion zones, etc.)
5. Filament misalignment
6. Filament breakage
7. Filament-matrix disbonds

The analysis leading to this listing requires a volume fraction greater than a certain critical value. However, this critical value is exceeded in materials of practical interest. Experience in working with this material indicates that except for the order of importance which is a highly dependent variable, this list is probably correct both for metal and non-metal matrix composites. If so, the nondestructive methods employed so far are useful in detection, and to some extent, characterization of all the defects except filament degradation (number 2) and changes in matrix modulus (number 3). These are the most difficult problems for NDT and require further attention.

ULTRASONIC TESTING

Although most of the work reported herein was performed on metal matrix composites, some resin matrix materials were also tested. Generally, the information given here on metal matrix materials applies equally to any filament-reinforced composite.

Of major significance in any NDT application to composites is the problem of separating relevant signals from noise. Aside from any other factors involved, this signal-noise problem could lead one to conclude that ultrasonic methods might not be applicable (consider the cross-section in Figure 1 again). The small area between filaments in Figure 1 is the zone of matrix diffusion bonding. Note that these areas average only about 1/4 of the projected area of the adjacent filament-matrix contact surfaces. Considering incident acoustic energy as plane waves, 3/4 of the incident plane area intercepts reflecting, scattering, and diffracting interfaces at the very first ply of boron. The energy which gets by the first ply is subjected to the reflecting, scattering, and diffracting interfaces of the next ply, and so on. Thus, even in material with sound matrix bonds, the natural internal scattering is tremendous. And yet, the aluminum-boron composites do transmit substantial amounts of energy.

There is fair transmission from the aluminum matrix through the mechanical and chemical bond to the filament. In fact, even with complete matrix disbond, as long as the matrix and filaments are in contact, a sizable amount of energy is transmitted. Calculation of the transmission coefficient shows that about 90% of the normal incident energy is transmitted through the aluminum-boron interface. Furthermore, the critical angle is about 30 degrees for longitudinal waves incident on boron from aluminum. Thus, these waves are transmitted into the filament within plus and minus 0.001 inch from the centerline, and the filament is only 0.004-inch diameter. As a result, reflection losses are not as great as one might suspect; however, diffraction and scattering loses are quite significant. Matrix disbonds, even though very small areas, have a fairly large effect on both reflected and transmitted energy. Unlike the fractional, scattered reflections from filaments, matrix disbonds cause virtually total reflection and mostly in the 180-degree backward direction. Thus, a small disbond removes a substantial amount of energy from the transmitted beam.

One of the more useful techniques of testing thin materials for defects aligned parallel to the principal surfaces is the through-transmission method. A variation of this method is a single-transducer, reflector plate technique shown in Figure 2. Ultrasonic energy transmitted through the specimen is returned to the transducer from a smooth reflector. If disbonds are present, reflection of sound at the interfaces results in less transmitted energy. The resultant is readily detected as a decrease in the strength (amplitude) of the reflected signal. Figure 3 shows the signal presentation on the cathode-ray tube (CRT) of the ultrasonic test instrument. The gated signal, input to a recording amplifier, provides an output voltage of the proper level to the recorder. The gating circuits can provide a go/no-go output or a variable output. With the go/no-go selection, only gated signals above a preselected amplitude cause an output to the recorder. In the variable mode, the signal output to the recorder is proportional to the gated signal amplitude.

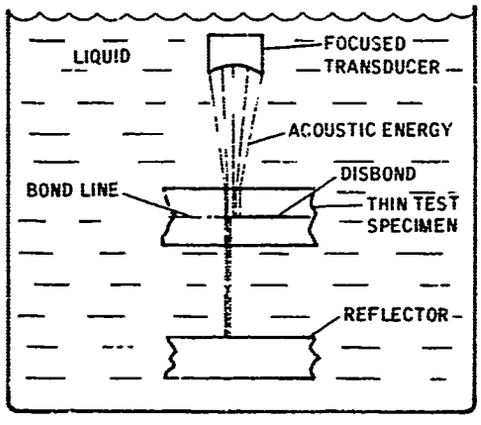


Figure 2. Single transducer, through-transmission reflector plate ultrasonic test method.

The C-scan recorder of Figure 4 is mechanically linked to scan and index motions of the transducer and electrically connected to the recorder amplifier. With a signal in the gate, the recorder receives the amplified signal and "writes" during that time. A series of line scans synchronized with the movement of the test transducer (or test specimen) provides a full-scale plan view of the test object and shows defects in either black and white or variable shades.

Since the fall of 1967, nearly 30,000 square inches of aluminum-boron composite have been tested by these methods. Procedures have been developed whereby a 6-step gray-scale is

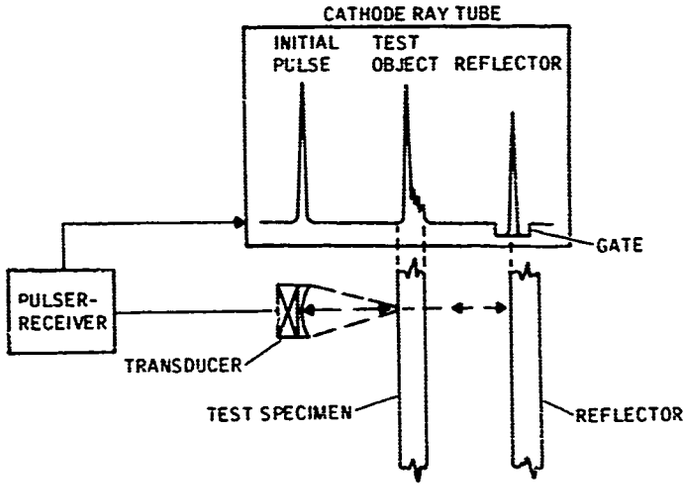


Figure 3. Signal presentation of the reflector plate ultrasonic technique.

reproduced corresponding to known attenuation steps. Figure 5 shows the arrangement of the ultrasonic instrumentation. The scanning bridge, bridge controls, transducer, tank and recorder are on the right. The ultrasonic instruments are at left center and strip chart recorder at the extreme left. Figure 6 is a close view of the ultrasonic instrument and recorder showing the attenuators which are used to provide reproducibility between different setups or different configurations.

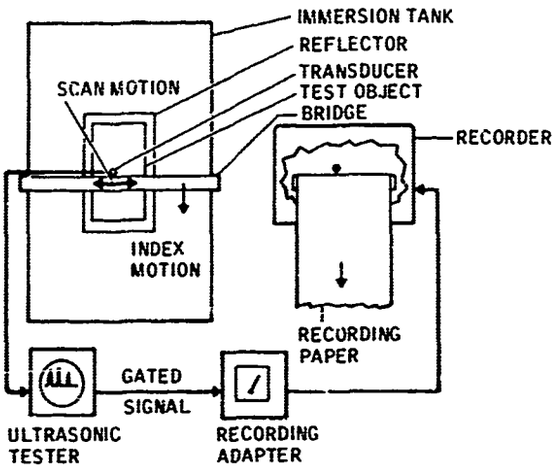


Figure 4. Ultrasonic testing system arrangement used to produce permanent C-scan recordings.

Throughout the course of this work, numerous specimens have been sectioned for comparison with ultrasonic response. Figure 7 illustrates a typical comparison between the C-scan recording, a strip chart recording, and metallurgical sectioning.

The 6-step gray scale represents the most steps which we were able to resolve by this method of recording. While the strip chart recording shows a wider variance in a single scan, the facsimile-type recorder does not provide discrimination between signals much beyond 6 shades of gray. Because of this, a completely different method of recording is highly desirable.

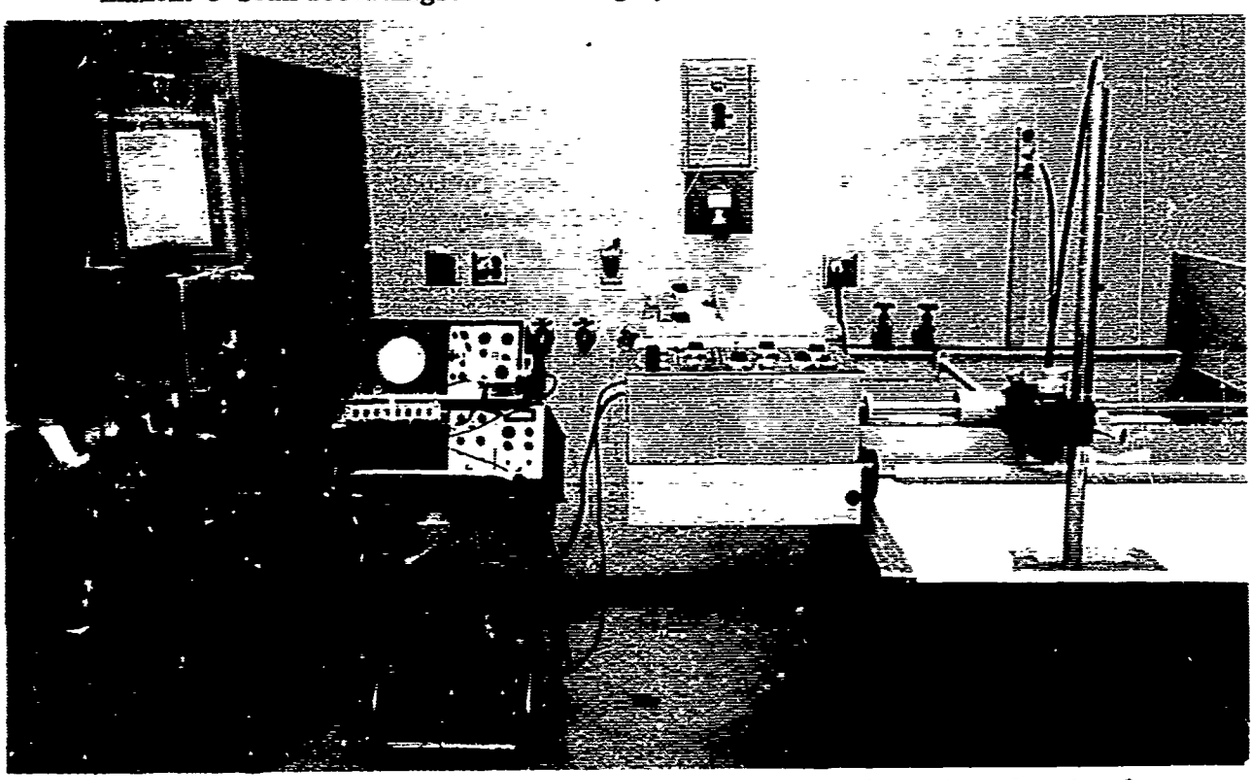


Figure 5. Laboratory arrangement of ultrasonic testing equipment used to develop test techniques for composite materials.

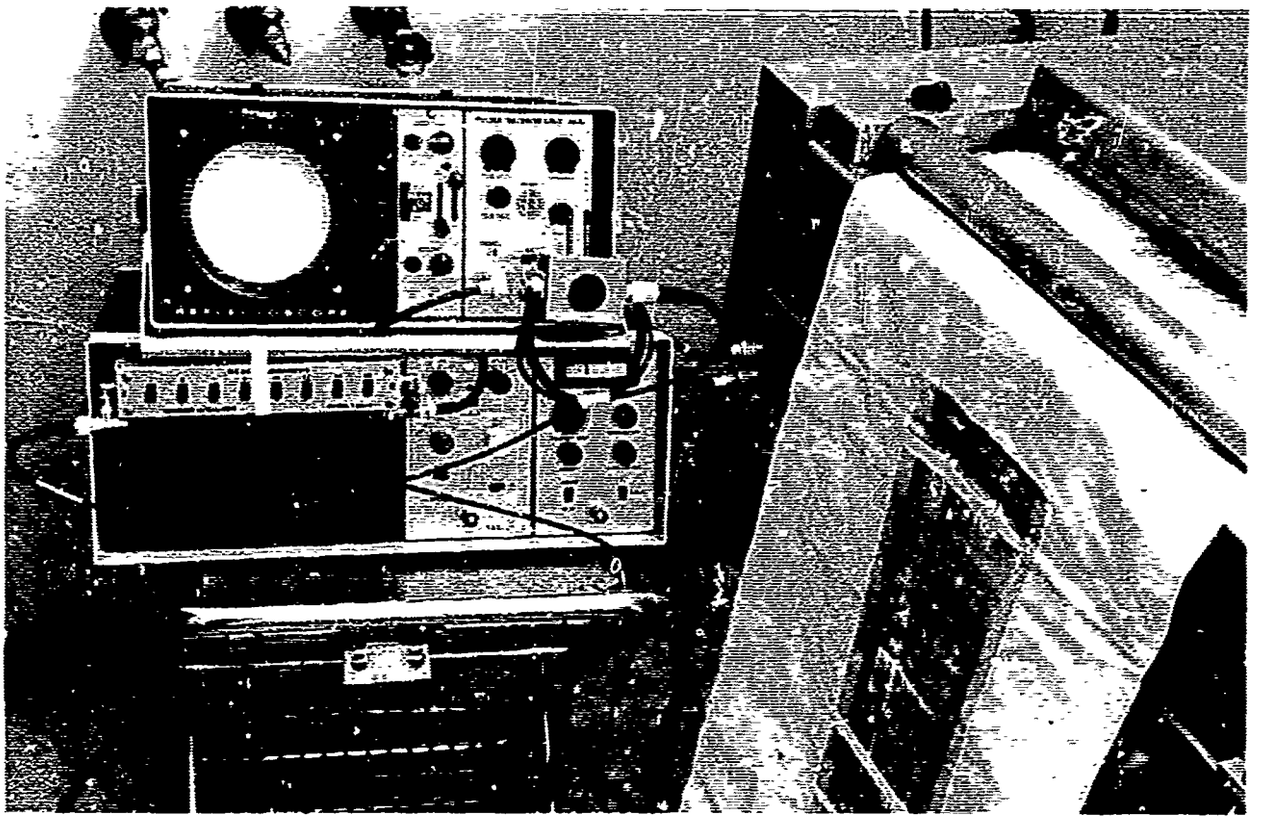


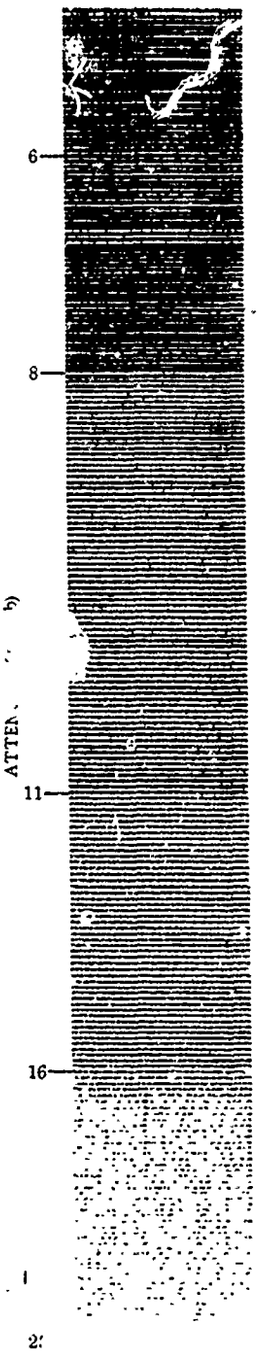
Figure 6. Ultrasonic equipment showing typical A-scan and C-scan displays and attenuators used in setup.

One of the continual frustrations in working with NDT methods for composites is the inability to adequately cope with the data generated. This inability is a combined failure of current instrumentation and human sensory capacity. More advanced methods of data presentation and analysis are required than those presently available.

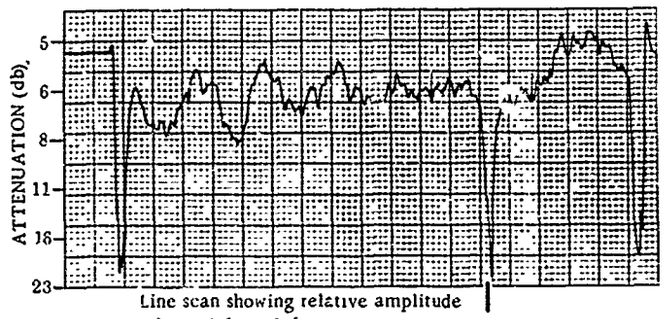
RADIOGRAPHIC TESTING

Aluminum-Boron Composites

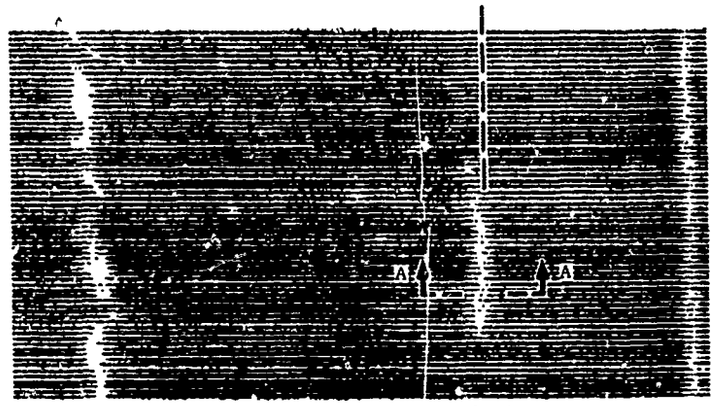
The X-ray absorption difference between tungsten (atomic number 74) and aluminum (13) makes radiography feasible for detecting variation in boron-reinforced aluminum matrix composites. The individual half-mil diameter tungsten cores upon which the boron is deposited are distinguishable on the radiographs even in multilayer material. Alignment, spacing, and integrity of the tungsten cores conveys information about the boron which may or may not be visible on the radiograph. While maximum contrast between aluminum and tungsten is obtained at bout 70 KeV (effective energy), the signal contrast is high between the tungsten core and matrix at energy levels both above and below this value (see Figure 8). Where filament images are not overly superimposed, as in very thin materials, the use of low energy allows more control over the exposure. Alignment and filament breakage may be determined without penetrating the tungsten cores.



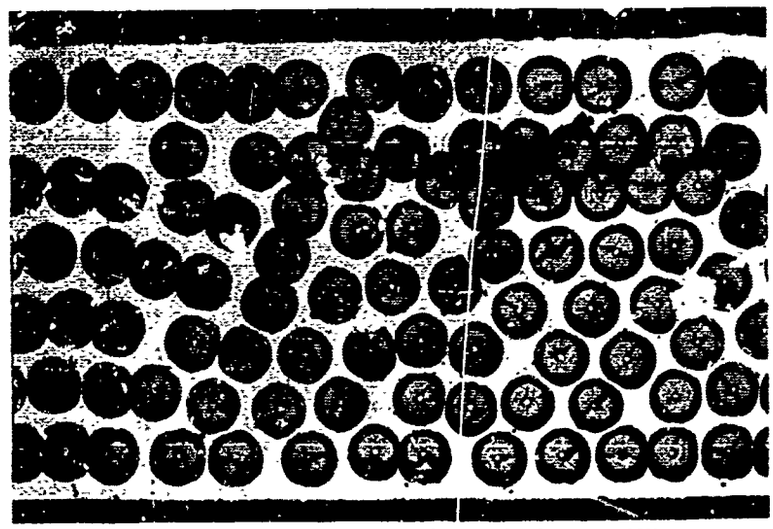
Calibration strip (gray scale) showing attenuation value (db) corresponding to the gated signal amplitude.



Line scan showing relative amplitude of signal from defect.



C-scan recording showing location of defect.



Section A-A. Microstructure through area of defect (mag 65X).

Figure 7. Correlation between ultrasonic test results and metallurgical examination.

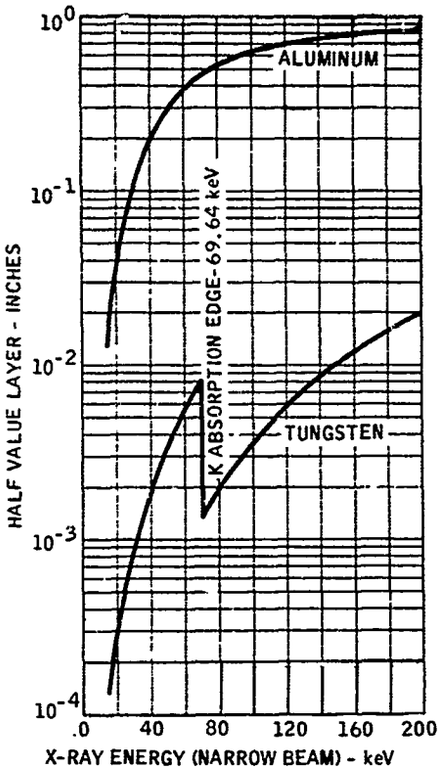


Figure 8. Half-valve layer versus energy.

For thick material and increased volume loading, higher energy is needed. While 40 KeV is sufficient energy to penetrate a single tungsten core, considerably higher energy is required to produce an effective energy which will penetrate both superimposed filaments and matrix and produce a readable image. The most significant factor is scatter buildup whch increases with energy, reducing both contrast and sharpness of the image. For thick composites or where relatively high energy x-rays are employed (100 KeV), it was found advantageous to place a thin lead foil between the specimen and film.

Routine considerations must be given to geometric factors which affect detail or definition sensitivity. Of these factors film selection is perhaps the most important. The thickness of double emulsion films, 0.007 to 0.009 inch, is sufficient to cause unsharpness due to parallax of the tungsten core images. These losses are apparent at 7X magnification within about a two-inch radius from the central axis of the exposure (based on a source to film distance of 36 inches). To eliminate error due to this image parallax, radiography was performed using single-emulsion fine grain x-ray film. Magnification of the image up to approximately 40X is possible with these emulsions.

The radiography described is used to detect relaxed, misaligned, broken and missing filaments in aluminum-boron composites. While the approach to radiography is conventional, high radiographic quality is necessary. The perception of small detail is often difficult because of the high noise level inherent in "busy" material. Techniques to reduce this noise and enhance the images of subtle variations in the material will be discussed in a later section.

Alignment between filaments is determined from the image of the tungsten cores. The maximum allowable misalignment is about one degree. Where the image of crossed filaments can be separated from the background, i.e., in low volume fraction or thin material, tungsten core images crossover and form a Moiré-like geometric pattern on the radiograph. While the distance between fringes is a measure of filament alignment, making numerous measurements over a large area is much too tedious to be practical. However, since the fringe distance increases as the inter-ruling angle between filaments decreases, this pattern can serve to qualify the material on the basis of maximum possible misalignment. Uniformity of the layup may also be observed from these patterns. Figure 9 shows a radiograph of a 0-90° crossply Al/B composite in which an abrupt change in layup occurred in the 0° direction. Misalignment is most severe in the case of

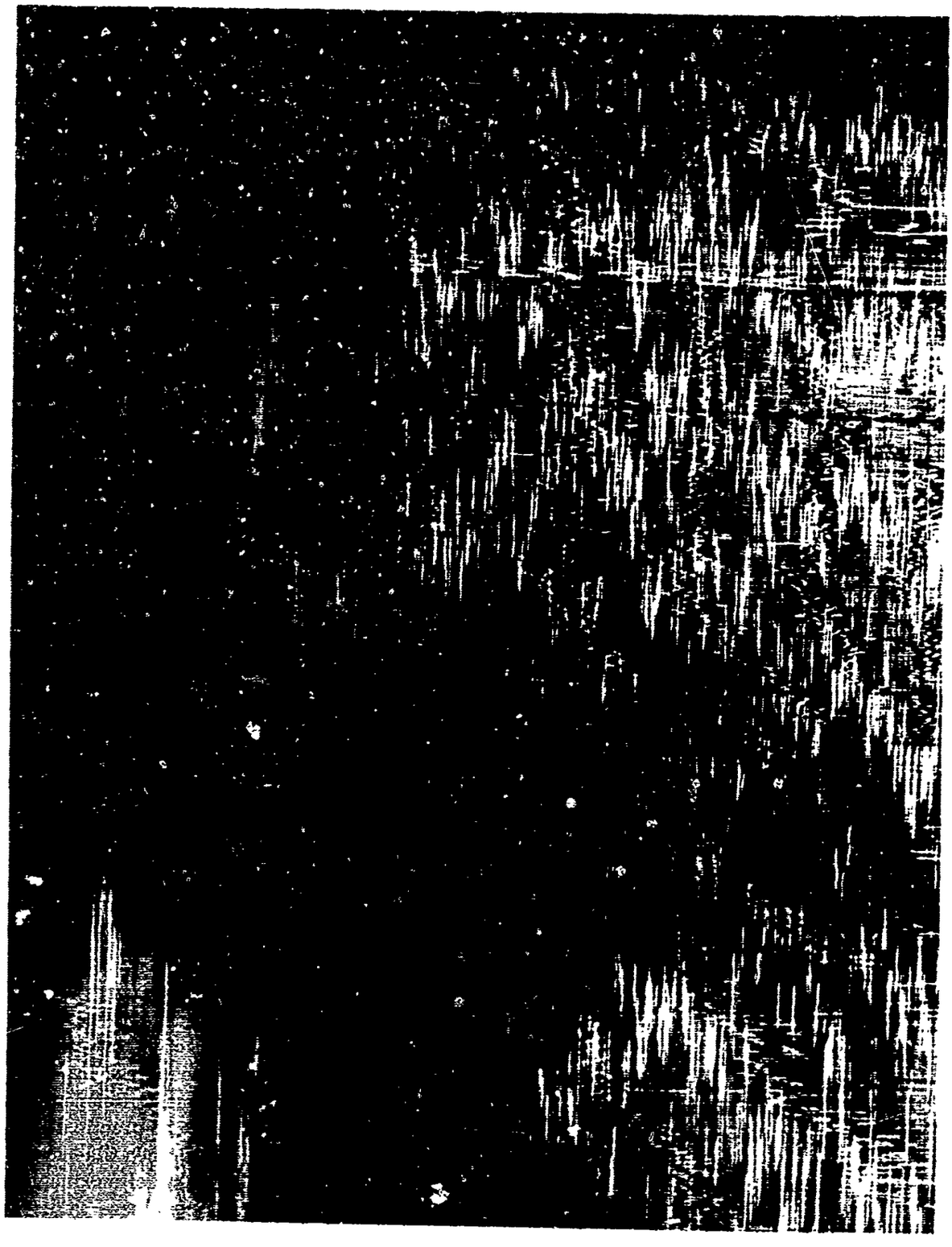


Figure 9. Moiré-like patterns resulting from projected crossover of misaligned filaments.

the more closely spaced pattern. The change is attributed to either a break or end in the filament spool during layup of the composite.

Broken filaments are detectible as a distinct separation of the tungsten core, Figure 10. The separation gaps range from about 0.001 to more than 0.005 inch. Magnification is required to detect breaks which are less than about 0.005 inch, particularly where other filament images are superposed.

Resin Matrix Composite

For resin matrix composites such as glass-reinforced epoxy and epoxy-graphite, contrast sensitivity is the most limiting factor. Since x-ray absorption in these materials approaches that in air, very low-energy x-rays must be employed to detect subtle variations within the composite. Exposures must be made within vacuum to prevent the absorption of low-energy photons by the air within ordinary exposure chambers. Single-emulsion fine-grain x-ray film is used for routine radiography. Energy levels ranging from about 2 to 25 KeV are employed; the energy being determined by thickness and density of the test specimen, and to a lesser extent by required detail. Bare film techniques prevent absorption of the x-rays by cassette material covering the emulsion.

The x-ray device used by Convair to perform radiography on these materials is shown in Figure 11. The x-ray unit has an extremely thin (0.010-inch) beryllium window and is capable of generating x-rays up to 110 KeV. The unit may be used without external shielding for protection to personnel during the exposure. The vacuum chamber inside the cabinet can be removed from the x-ray machine. The chamber is made of



Figure 10. Radiograph showing broken filaments in aluminum-boron composite.

3/16-inch aluminum and is lined inside with lead to provide a high photoelectric cross-section for minimum scatter.

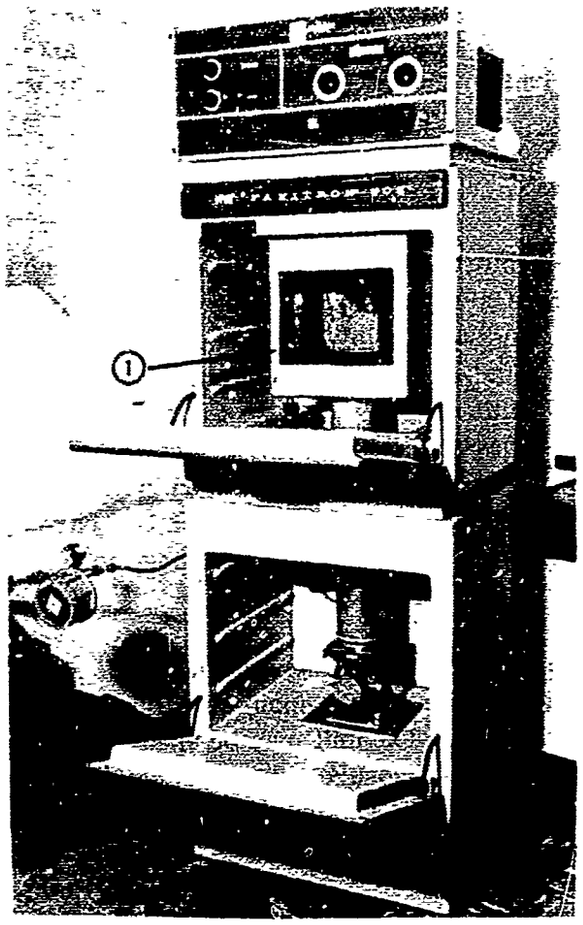


Figure 11. X-ray unit and vacuum chamber, (1), used for microradiography of epoxy-graphite.

Microradiography was used to study detail beyond the resolution of commercial x-ray emulsion. High resolution photographic plate (2,000 lines/mm) is used in lieu of x-ray film (approximately 100 lines/mm). Following development of the image, the plate is viewed through a microscope. Magnification up to 500X may be employed to study various detail in the specimen.

Figure 12 shows radiographs of various hybrid unidirectional and cross-ply epoxy-graphites. The radiographs, produced in vacuum on high resolution plate, required up to 72 hours of exposure.

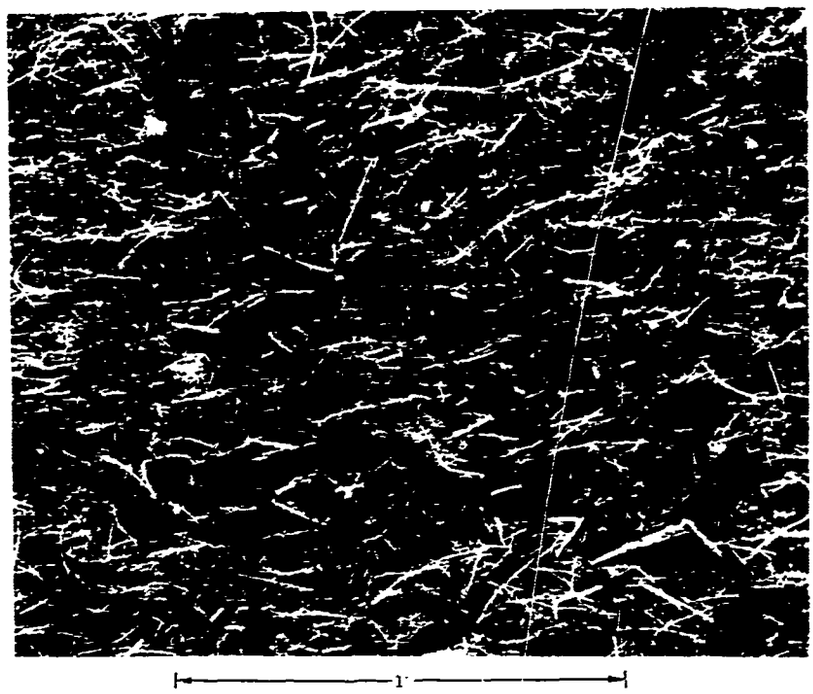
Neutron Radiography

Neutron radiography has been suggested for Al/B composites. However, as mentioned earlier, x-ray techniques are successful in defining filament alignment and integrity because the 0.0005-inch tungsten core provides a highly contrasting subject image as compared with the aluminum matrix. In the neutron radiograph, the high-contrast subject is boron which is 0.004-inch diameter. Hence, in a multilayered composite, absorption in the first layer of boron masks the image of underlying filaments (see Figure 13). During the course of our studies, several neutron radiographs have been made of aluminum/boron composites. The results show that neutron radiography provides no advantages over x-radiography for inspecting this material.

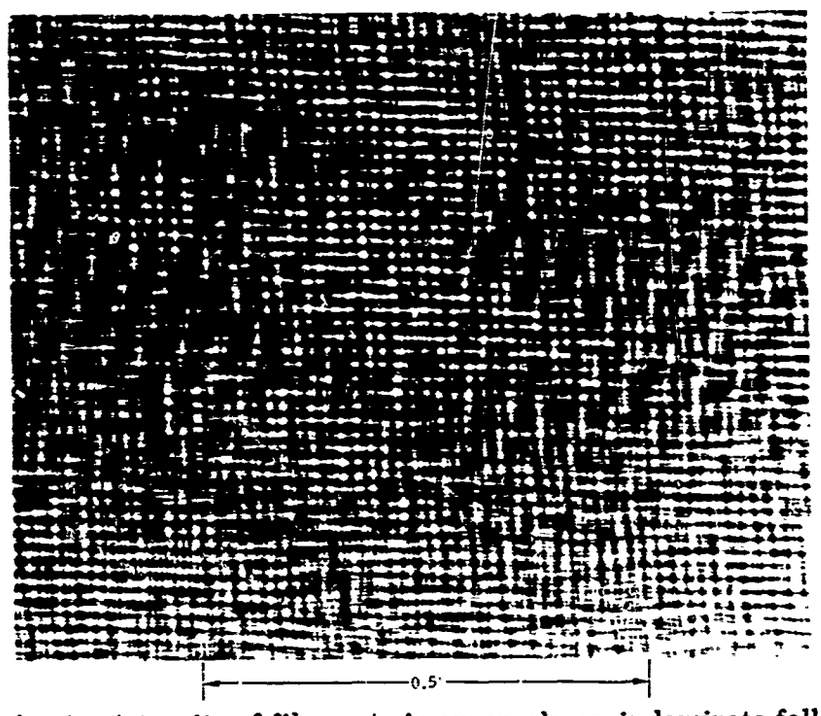
THERMAL TECHNIQUES

Cholesteric Liquid Crystal Detector

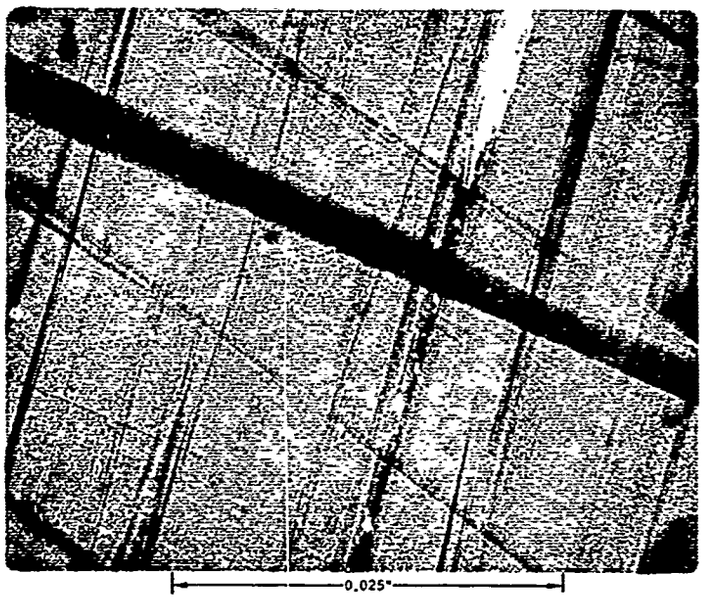
Aluminum/boron test panels containing from 25 to 50 per cent boron were evaluated at Convair using liquid crystals. The panels, ranging from 0.020 to 0.080 inch thick, contained known matrix disbonds. The panels were coated with a 0.003-inch thick



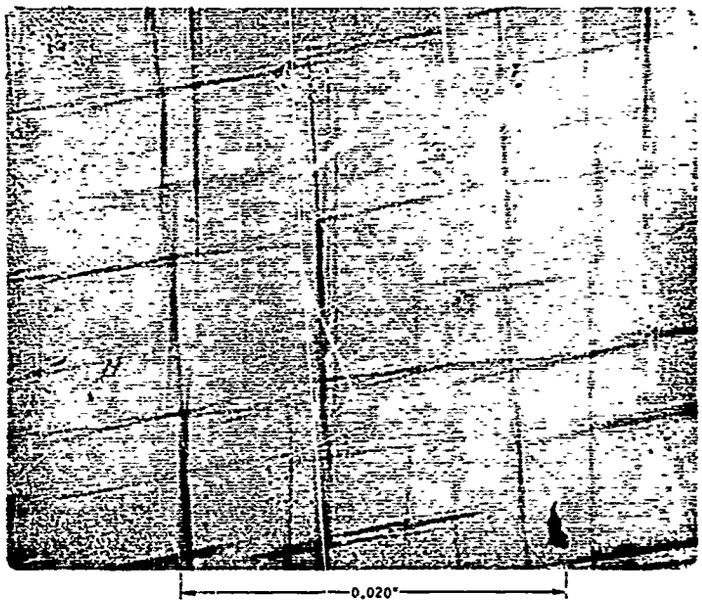
Radiograph of asbestos reinforced epoxy-graphite showing condition of filament layup hidden by asbestos. Exposure: 5 KVP, 2 ma, SFD, 24 in., 60 hr. (vacuum).



Radiograph showing integrity of filaments in cross-ply resin laminate following interlaminar failure. Exposure: 18 KVP, 2 ma, SFD, 24 in., 70 hr. (vacuum).



Microradiograph of hybrid epoxy-graphite showing separation between filaments, entrapped foreign material, resin rich area, etc. Exposure: 5 KVP, 2 ma, SFC 24 in., 72 hr. (vacuum).



Microradiograph of epoxy-graphite showing 0.0003 in. dia., glass filaments entrapped during layup. Exposure: 5 KVP, 2 ma, SFD 24 in., 72 hr. (vacuum).

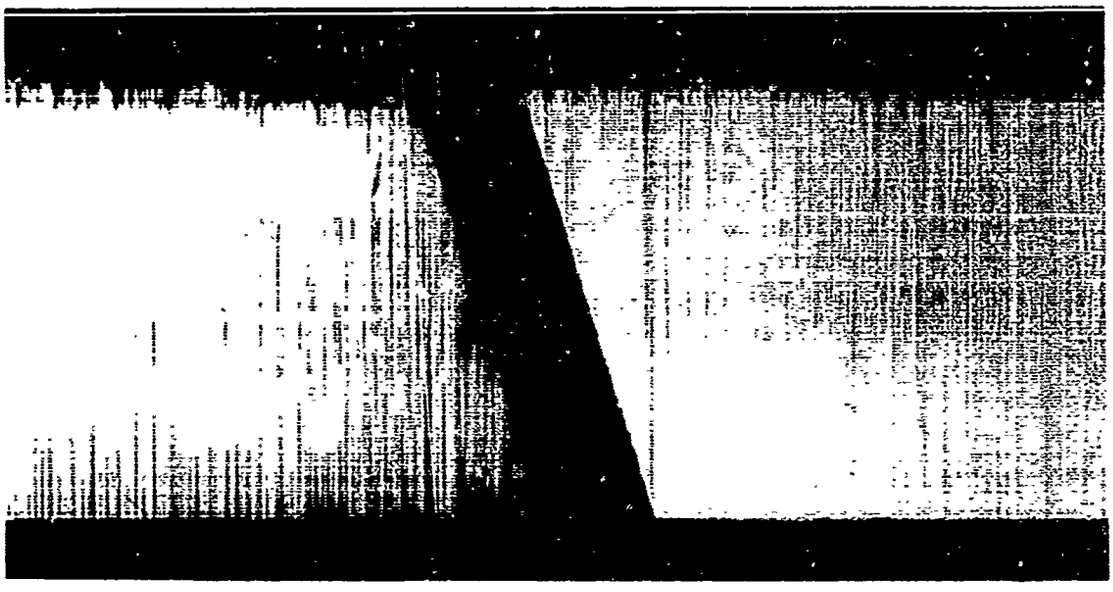


Figure 13. Neutron (left) versus x-ray radiograph (right) of Al/B composite.

pressure-sensitive vinyl to provide a background for observing color changes in the crystal. Various water soluble paints were also used but were found less satisfactory than the vinyl coating.

Liquid crystals were applied to the panels by spraying. Transient conditions were established through regulation of the back side heat input and front side cooling. Six distinct colors were observed — brown, red, yellow, green, violet and blue. The change through the color spectrum, i.e., clear to clear required about 3° C. With careful manipulation of the heat input and cooling, a steady state was maintained; however, with the exception of the edges, only a single color was observed over the surfaces of the disbonded panels.

Known disbonds contained in the parels were not detected (or at least not recognized) by the above technique. However, in the Al -B panels used, heat conduction is only slightly affected by the presence of boron. In aluminum alloys, a direct relationship exists between factors affecting thermal and electrical conductivity. It is not known whether 50 per cent boron displacement of aluminum reduces the thermal conductivity by 50 per cent as it does the electrical conductivity. Even if that were the case, the composite would still be an effective conductor of thermal energy. It is probable that a fast transient condition best establishes a detectible thermal gradient. However, since the complete color spectrum requires 3° C, each color represents about 0.5° C. While theoretically it is possible to establish a ΔT of 0.5° C in 0 050-inch thick aluminum over an air-filled laminar separation (0.001-inch thick) located in the middle of a panel, the transient period would undoubtably be too fast to be observed visually. Color-sensitive, photometric scanners would probably be required to detect such changes.

Various LC detectors and thicknesses were applied to the panels. In no instances were satisfactory conditions established whereby the LC material repeatedly revealed the presence of known defects (delaminations) in the material.

Infrared Testing

Additional thermal tests were conducted using infrared-sensitive radiometric scanning equipment. The panels were scanned using the arrangement illustrated in Figure 14. Five parallel scans were made along each panel as shown in Figure 15. Figure 16 shows the recorded thermograph for one of the panels; the high temperature change to the left is apparently edge effect. As with the LC material, identification of known disbonds was not possible using the method. While illustrating the capability for detection of gross discontinuities, these results indicate that infrared testing is less sensitive and probably less reliable than ultrasonic testing for examining aluminum matrix material.

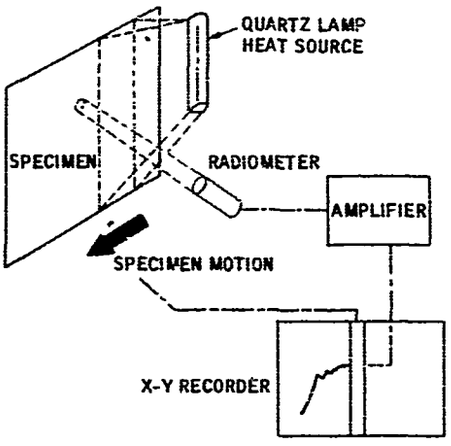


Figure 14. Infrared scanning arrangement for thermal testing.

Boron filament reinforced epoxy matrix composites have been successfully tested with thermal methods developed by the Fort Worth division of General Dynamics. The thermal properties of the resin matrix materials are much different from the metals. Interlaminar bond defects and faulty resin ratios are detectable.

EDDY CURRENT TESTS

Eddy current testing of Al-B composite materials has also been evaluated. With reference standards, most of the commercial eddy current testing instrumentation is suitable for direct determination of electrical conductivity. At ordinary temperatures aluminum is about 12 orders of magnitude more conductive than boron. Since the conductivity of boron is negligible, the conductivity of a 50 per cent boron composite is about equal to that of 50 per cent dense aluminum, except for a small correction due to the half mil tungsten core.

A variable frequency (50 KHz-300KHz) instrument was used to study the behavior of eddy currents in Al/B. A test frequency of about 200 KHz was found to provide adequate sensitivity with minimal effects from liftoff. Various discontinuities were detectible; however, because of the exponentially decreasing field penetration, near-surface defects produced much greater response than did deeper-lying defects. The necessity for scanning large areas of the test object as well as the problem of recording data is a major disadvantage of the method.

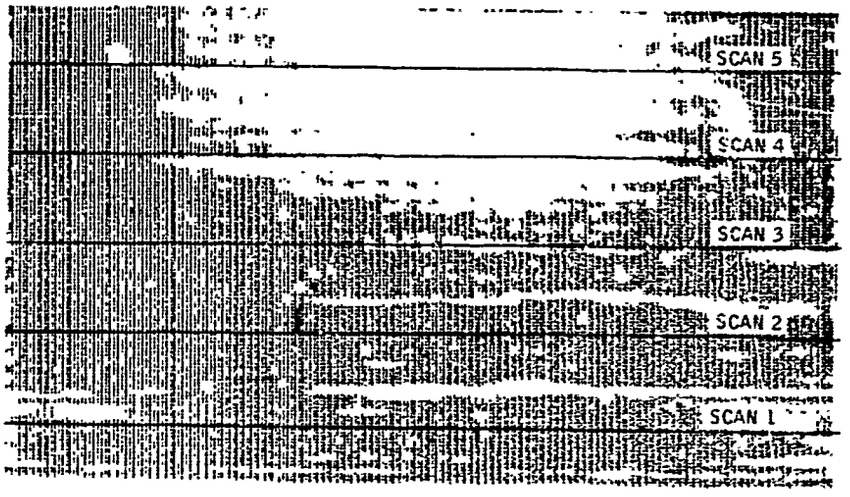


Figure 15. Position of thermal scans shown on ultrasonic C-scan of panel containing known disbond.

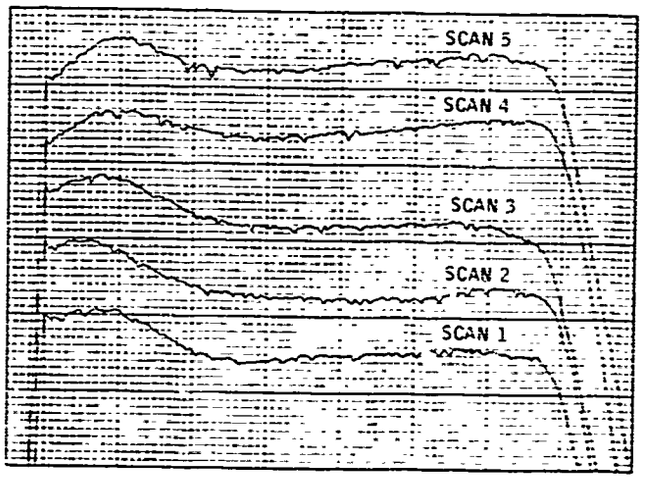


Figure 16. Thermal scans - Panel Al-50% B.

The most useful application of eddy current testing is in volume fraction determination. Figure 17 shows the relationship between volume fraction and conductivity for 6061 and 2219 aluminum alloy matrix materials. Two factors are important in the application of this method for volume fraction determination.

1. Measurements should be made in areas where no radiographic or ultrasonic indications are apparent, and
2. Eddy current test frequency should be carefully selected to preclude penetration through the thickness of the test specimen.

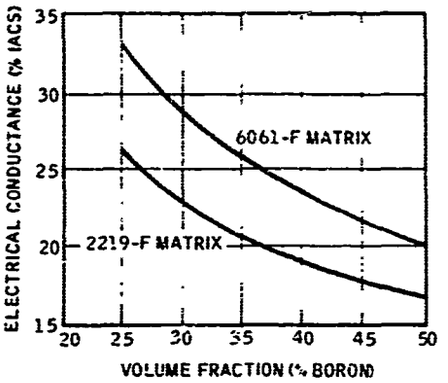


Figure 17. Volume fraction versus electrical conductance as determined by eddy current methods.

MICROWAVE TESTING

A limited study was conducted to evaluate microwave methods for NDT of glass-filament reinforced phenolic honeycomb structures.[3] Honeycomb test panels, 20 by 20 inches, were constructed. Artificial defects, including simulated disbonding at the various interfaces, were introduced into the panels. Several glass-phenolic laminate panels up to 0.25-inch thick and containing artificial defects were also prepared.

Microwave reflectometry was performed at a test frequency of 9.4 GHz. Figure 18 is a simplified block diagram of the test setup. The reflectometer was manually scanned over the surfaces of the test panels. Data output from the instrumentation indicated the amplitude of the standing wave at the reflectometer. Variations in the specimens resulted in variations in the reflected microwave signal and, hence, produced variations in the resultant standing wave.

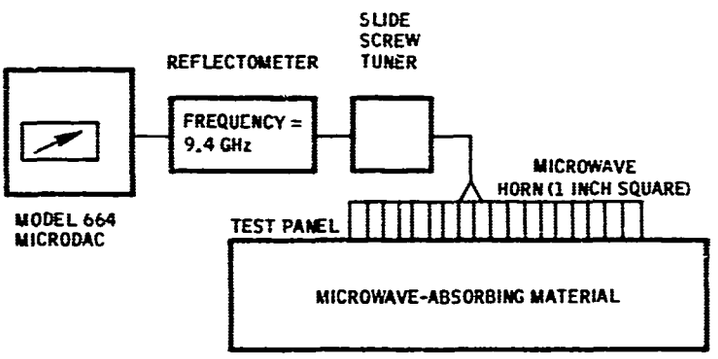


Figure 18. Simplified block diagram of microwave nondestructive testing setup.

Nearly all artificial defects were found by this test method. Some could be detected from either side of the panel, with greater sensitivity always occurring when the anomaly was on the same side of the panel as the reflectometer. Laminar discontinuities were detectible where a physical separation was present, but very tight disbonds were not detected. With appropriate tooling, this nondestructive test method would be an effective method for testing non-metallic honeycombs and laminates. A major advantage is that no intermediate coupling agents are required. The microwave method, although less sensitive than ultrasonics for detecting delamination, is superior for detecting deep-lying defects.

NDT DATA ANALYSIS

The data resulting from NDT of composites are voluminous. Sensitive radiographs show an extremely busy, noisy background. Images of interest are scattered throughout the background and are, generally, only a minute fraction of the total information available. Ultrasonic C-scans are similarly encumbered. Eddy current and thermal tests and, in fact, any NDT in which penetrating energy reacts with the filaments, exhibits noise if the test method is sufficiently sensitive to be useful.

It became apparent from the very first radiograph of aluminum/boron that interpretation of the data would be extremely tedious. At least 6X magnification is needed for a trained observer to identify most of the filament breakage, aligned stray boron and crossover. However, the field of view becomes more and more restricted as magnification is increased. Adding to the difficulty are the effects of motion which become exaggerated with magnification. Pencil and paper recording of the data is a two-man job.

A search for a more convenient, less demanding system led to consideration of special-purpose video devices. Not only can magnification be readily handled, but more importantly, video signals can be processed in a variety of ways and in real time. In addition, wide flexibility is available in recording capabilities. Interfacing the video signals with computers is relatively simple, although it is not yet completely clear whether computer processing will provide any advantage over video processing alone.

The video system developed at Convair is shown in Figure 19. Basic system elements are:

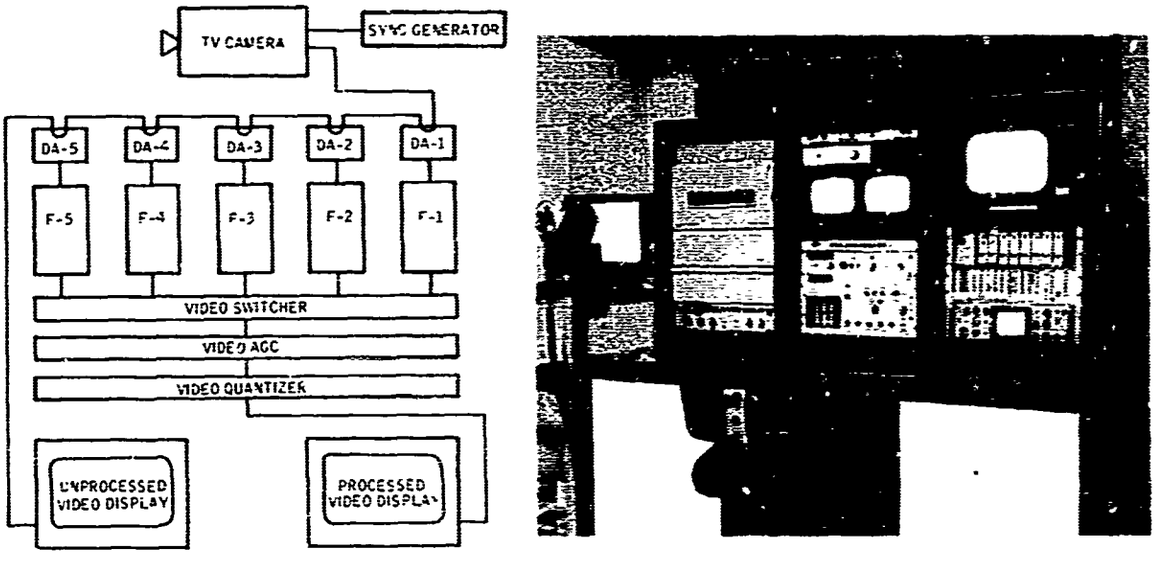


Figure 19. Experimental video system used in image enhancement tests.

Camera

A vidicon camera is used with a resolution capability of at least 800 lines. It has a separate-mesh one-inch vidicon with electromagnetic focus and deflection. Extension tubes behind the lens allows good focus at close working distances. Magnifications of greater than 40X at an 11-inch wide television monitor are easily achieved.

Distribution Amplifiers

Video from the camera control unit is fed to a series of distribution amplifiers to provide isolation and additional gain as required by the various video filters.

Video Filters

Various filters — high pass, low pass, and several selected bandpass — are used in processing the video to eliminate various background elements and accentuate desired images.

AGC Amplifier

Automatic gain control is used to keep video level constant at the input of the video quantizer. Synchronizing and blanking pulses are also reformed and added to the signal in this device.

Video Quantizer

The quantizer operates on the real-time video signal and provides a thresholded output at any desired level. Thresholding is on the basis of brightness values. The quantizer also provides a slow scan output at a very much reduced bandwidth for transmission of the video information to computers or other devices which cannot operate in real time due to limited bandwidth and storage capability.

Displays

Any standard television monitor can be used to display both processed and unprocessed outputs of the system. All necessary synchronizing pulses are present in these outputs. Screen size is determined by viewing distances and amount of detail needed.

The video signals corresponding to what the camera "sees" can be electronically processed in various ways to provide image enhancement. This enhancement is considerably more than just contrast enhancement and is accomplished by processing the video signal with an optimum receiver. Optimum receiver design is a well-developed branch of communication engineering and is general enough to cover the many different cases of background and image brightness distributions likely to be encountered in radiographs. Under many conditions the object of interest will be only a faint line

image or a series of dots, but this signal will be the only thing left in the picture if all of the background clutter can be eliminated. In this way a slightly distorted but enhanced image is the only thing presented on the monitor or to the alarm logic of an automatic flaw detection device. The enhanced image can also be superimposed over a normal presentation of the radiograph.

Currently, radiographs are placed in front of the television camera and the resulting video is processed by a combination of digital and analog means. Convair is also investigating the use of flying-spot scanner devices as a possible replacement for the television camera. These scanners offer increased reliability and more stable performance and may be more cost effective than conventional vidicon camera systems particularly for the applications discussed here.

Typical Examples

Convair's approach to image enhancement is to process the video coming directly from the camera with analog filters and a digital threshold device. In the photograph shown on the right in Figure 19 the unprocessed video is displayed on the left monitor and the processed video to the immediate right. The large monitor on the extreme right displays either processed or unprocessed pictures or a combination of the two.

In Figure 20 are three representations of a stray boron filament 0.25-inch long in an aluminum-50% boron composite 0.021-inch thick, unidirectional layup. The stray filament's presence in the composite during pressure diffusion bonding caused aligned filaments to break. Figure 20(A) shows the normal, unprocessed video presentation on an 11-inch wide monitor; Figure 20(B) shows the filtered video presentation of the same radiograph. Note that much of the background has been eliminated and only the main defect is distinct. Another alternative display is shown in Figure 20(C). Here the video has been filtered and then thresholded in the video quantizer. Brightness level discrimination by the quantizer provides a go/no-go signal. Obviously, this is an extreme form of contrast enhancement, and when coupled with the advantages of background elimination can be preset to show only images beyond a selected brightness level. In addition, the final image may be shown in either a positive or negative mode.

Figure 21 shows a condition of stray boron also in a unidirectional layup. In this case there was no accompanying filament breakage. Figure 22 shows the condition in a 0°-90° cross ply. For the cross ply material shown in the figure, only the horizontal filament images have been suppressed by filtering the video. Ideally, cross-ply material should be scanned from the directions of both layups.

Figures 23 and 24 are examples of crossed-over filaments in unidirectional and cross-ply materials, respectively. Crossover results in two undesirable situations: local off-axis alignment and volume fraction variations.

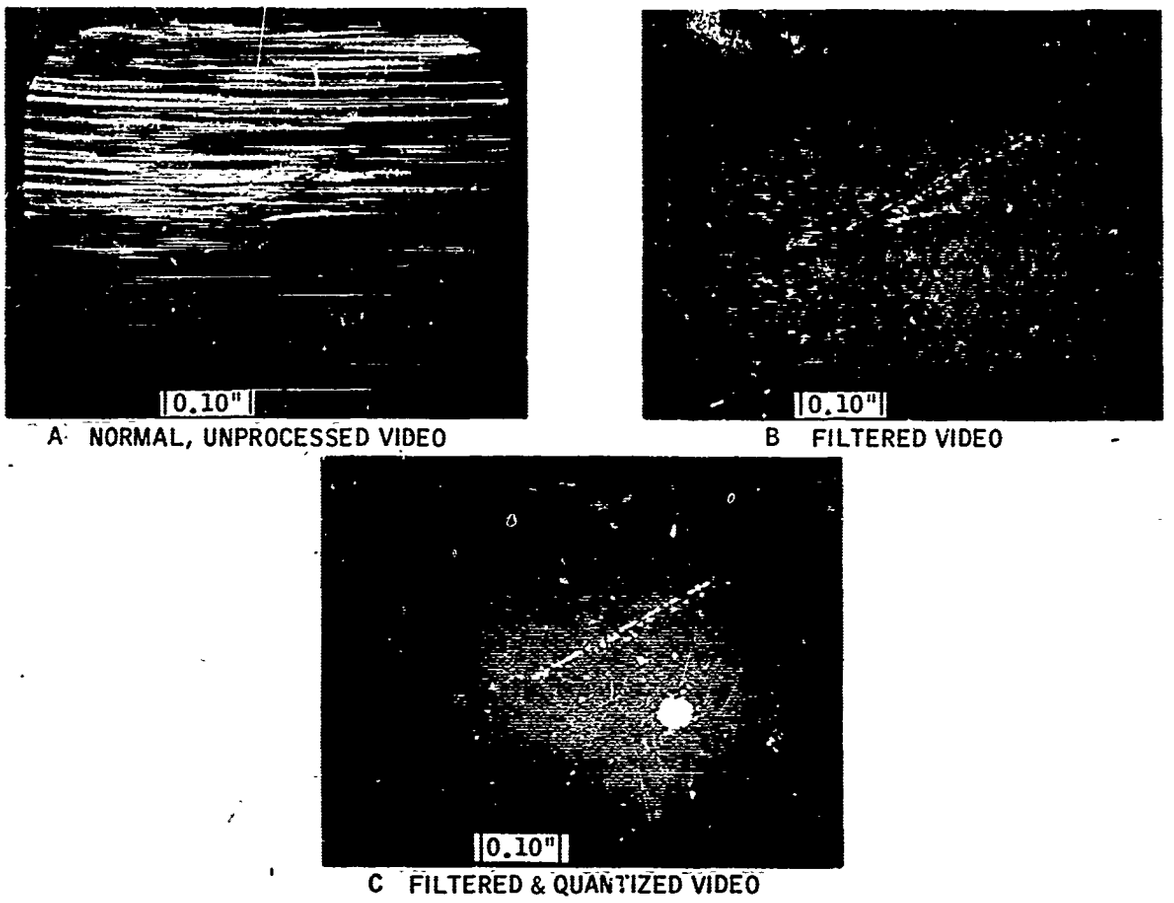


Figure 20. Stray boron filament in unidirectional aluminum-boron composite.

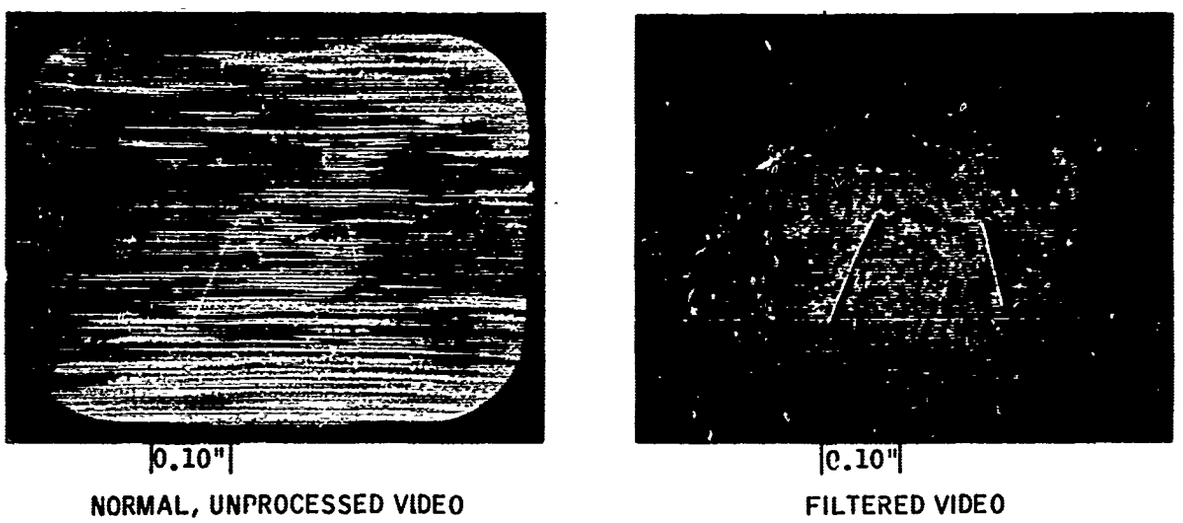


Figure 21. Stray boron filaments in unidirectional aluminum-boron composite.

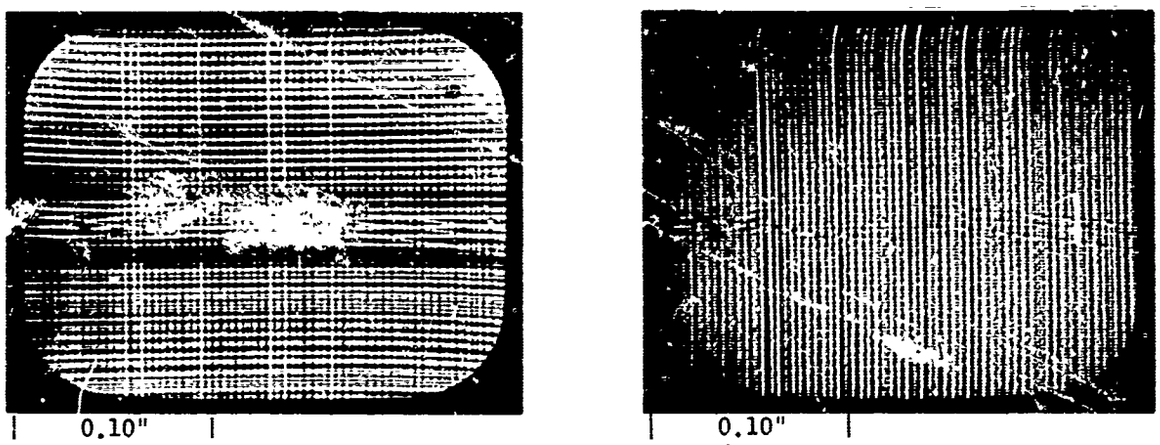


Figure 22. Crossed-over filaments in 0-90° cross-ply aluminum-boron composite.

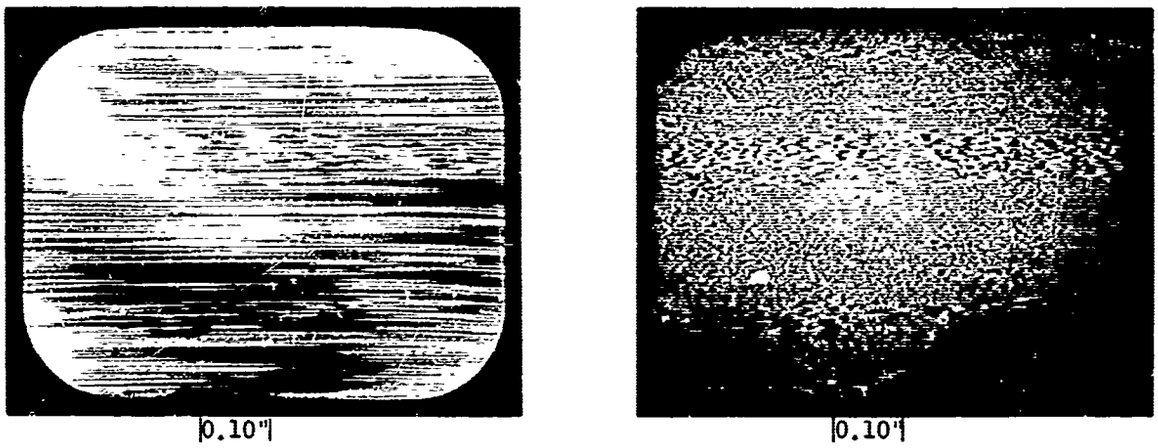


Figure 23. Crossed-over filaments in unidirectional aluminum-boron composites.

The slow-scan feature of the quantizer provides a vertical "gate" by which any of the possible display modes — normal, filtered, quantized or combinations — can be scanned. The output from the slow scan is a brightness analog from the particular video mode selected. For example, at the upper left of Figure 25 is the picture on the monitor of a weld radiograph showing porosity and inclusions. The slow-scan output from the unprocessed video is shown on the accompanying oscillogram (below). The quantized video is shown on the right with its corresponding slow-scan output below.

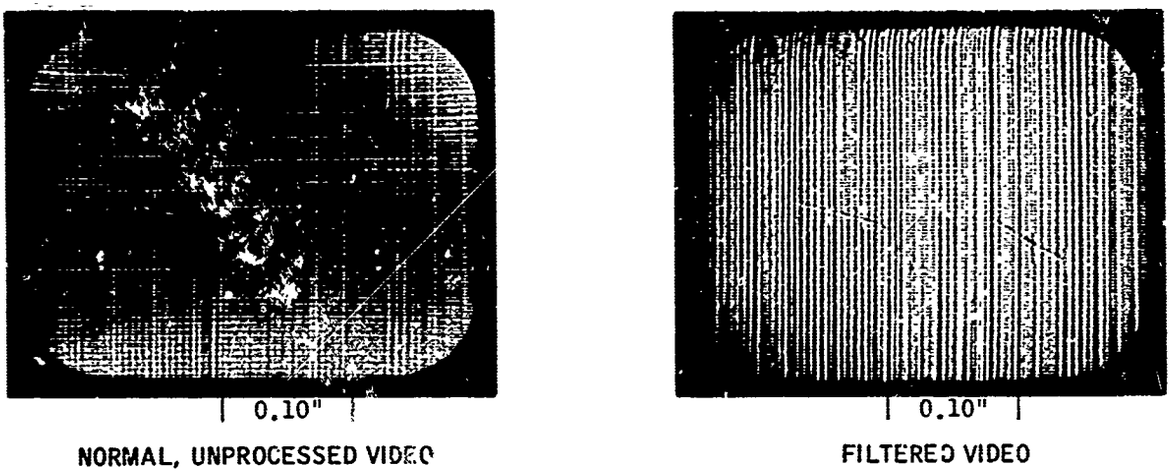


Figure 24. Stray boron filaments in 0-90° cross-ply aluminum-boron composite.

This system is highly flexible and can be adapted to fully automatic interpretation. It is evident that various gating schemes are applicable. It is easy to visualize a fully integrated system into which preset specification limits could be set. The system could be simplified, miniaturized, and tailored for specific applications.

Although not yet thoroughly investigated, many other possibilities for NDT data analysis exist. For example, ultrasonic and electromagnetic data could be generated in X, Y, and Z analogs, just like conventional ultrasonic C-scan recordings. Instead of being immediately displayed, the data could be magnetically recorded on a disc, or recorded on tape then transcribed to a disc. Magnetic disc recording is the feature by which the now familiar "instant replays," slow motion and stop action are reproduced by television broadcasters. This form of recording would permit input to video systems of data taken at very slow speeds as compared with television speeds, for example, from ultrasonic systems. Also feasible is direct integration with existing x-ray sensitive vidicon closed-circuit TV systems, now in fairly wide use throughout industry. Fluoroscopic systems, widely used in medicine and industry, are also adaptable to this concept.

OTHER NDT METHODS APPLICABLE TO COMPOSITES

Some recent nondestructive methods which hold promise for evaluating composites include optical and acoustic holographic techniques and stress wave acoustic emission analysis. While these methods have not been applied to composites, techniques have been developed successfully for a variety of other materials.

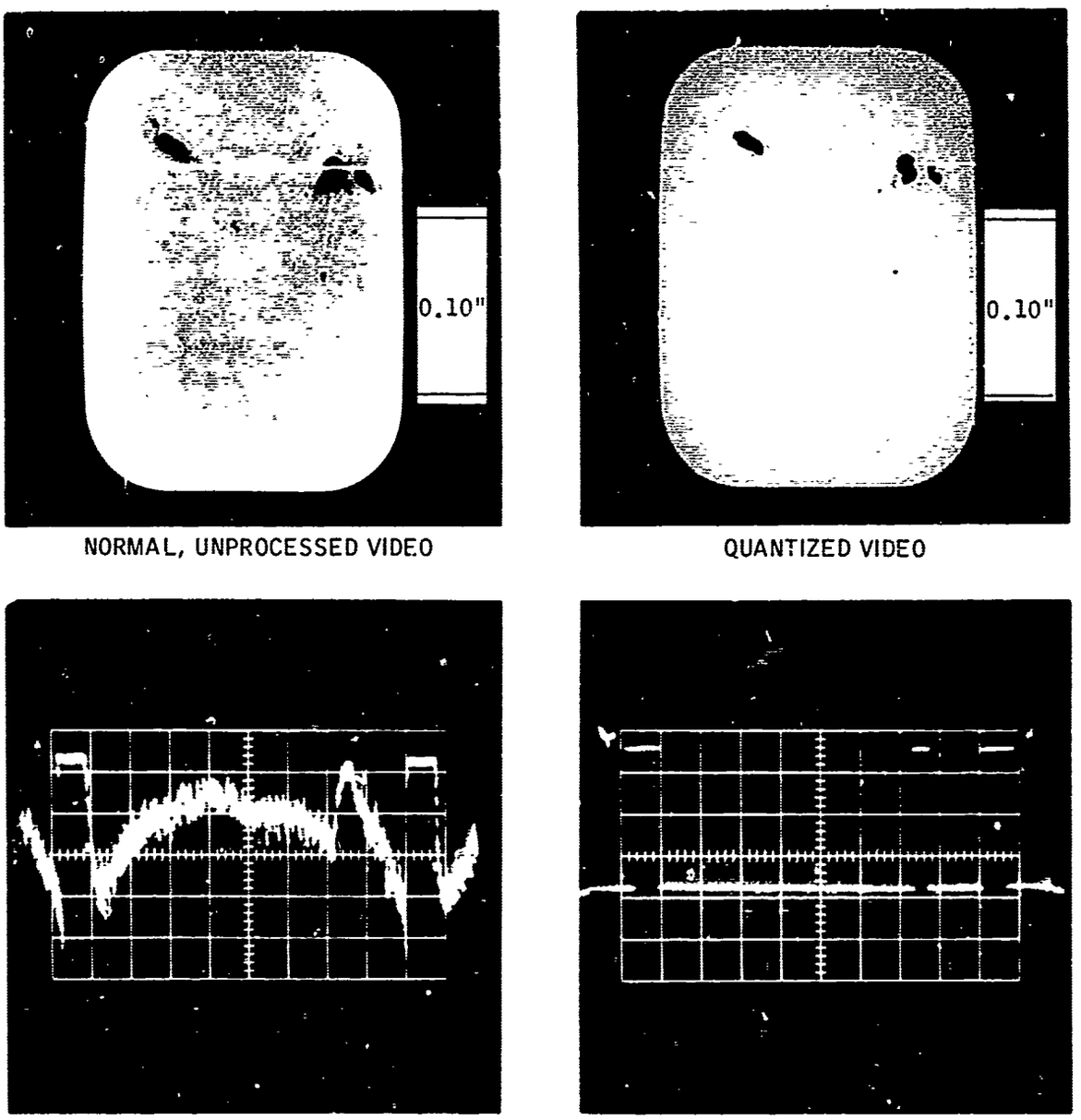


Figure 25. Porosity and inclusions in a thin aluminum weld.

Holography

Holography is a method of recording the amplitude and phase of the optical wavefronts reflected from an object and when reconstructed, these wavefronts have the relative amplitude and phase of the original wavefronts. Three-dimensional properties are contained in the image of the reconstructed wavefronts. Acoustic holography is a means by which scattered (or reflected) sound waves are converted into optical wavefronts to obtain the same properties. The lightwaves do not suffer the reflection and mode conversion problems associated with acoustic energy.

In theory, the vibrational "signature" of sound material differs from the signature of defective material; holograms provide a means for comparing the signatures of relatively large areas of materials or structures against known acceptable standards. The use of optical holography for locating leakage in aluminum-skin honeycomb has been reported by the Boeing Company.[4] Techniques have been developed for shell thicknesses up to about 0.070 inch.

Ultrasonic holography[5] has been applied to detect various interactions of sound waves within a material in the form of attenuation and/or interference. Techniques for performing coherent mapping of the data are based on a holographic recording of coherently pulsed ultrasonic wavefronts over a line, along a plane, or throughout a volume. While the method promises improved sensitivity and resolution over conventional ultrasonic imaging, considerable development is required to make the method practical.

Acoustic Emission

Stress wave acoustic emission analysis has been successfully applied to measure certain mechanical properties of metals and glass filament reinforced structures. Materials emit sound as they are strained. Some of the low-intensity, inaudible sounds are precursors or incipient indicators of failure. Microphones or accelerometers can be used to detect these signals. Both the frequency of emission and amplitude of the sound can be analyzed in real time or recorded.

Acoustic emission analysis may be highly applicable both to measuring bond integrity and to predicting ultimate strength in some composites. In-service, nondestructive monitoring may be another application.

CONCLUSIONS

Of the various NDT applied to composites, radiographic and ultrasonic tests have proven most beneficial so far. However, the sensitivity of tests must be relatively high, approaching current state-of-art thresholds. At these very high sensitivities, the complicated sub-structures of composite material stands out as noise. Methods of noise suppression and image enhancement are highly desirable, perhaps essential.

High-contrast radiography has proven most useful for routine testing of metal and resin matrix composites. Microradiography has been used during materials development phases, particularly with the resin matrix materials.

The transmission reflection method of ultrasonic testing is extremely sensitive to interlaminar matrix disbonding. The method is only effective, however, for fairly thin sections of uniform cross section. For more complex shapes, other techniques will be necessary.

Thermal methods have most application on the resin-matrix composites. Interlaminar defects and faulty resin ratios can be detected. It is concluded that the thermal methods are not as reliable as ultrasonic methods for testing the metal matrix.

Eddy current methods are most effective for volume fraction measurement on the metal matrix material; there is limited application for defect detection. Microwave methods have not been adequately investigated to determine their ultimate potential on the resin matrix materials.

Methods which should be investigated in the future include holography and stress wave acoustic emission. Vibrational methods, particularly those which can be confined to small areas, may also prove useful.

Whatever the methods of NDT which prove most effective, data analysis and data display techniques need immediate attention. Computer and other mechanical/electronic devices should be integrated with NDT test and inspection equipment. In general, more systems-oriented approaches to NDT will be required for the advanced composites.

REFERENCES

1. From a presentation of Mr. Hastings at AFML-Aerospace Corporation Seminar on NDT Methods for Plastic Materials and Structures, El Segundo, California, 13 April 1967.

2. G. Martin, and J. F. Moore., "Research and Development of Nondestructive Testing Techniques for Composites," Technical Report AFML-TR-66-270, U.S. Air Force Contract No. AF33(615)-2865, February 1967, page 9.

3. "Microwave Nondestructive Testing of Fiberglass Reinforced Honeycomb Panels, Report on Study Performed under Convair Division of General Dynamics Contract No. 46-06242 by Microwave Instruments Co.

4. Private communication with C. R. Pond, The Boeing Company, Seattle, Washington.

5. J. L. Kreuzer, "Ultrasonic Holography for Nondestructive Testing," Proceedings: 1968 Symposium on the NDT of Welds and Materials Joining, Los Angeles, Calif. 11-13 March 1968.

ACKNOWLEDGEMENT

The authors credit the efforts of F. F. Jorrey and S. Naber who prepared the metallurgical sections, C. N. DeMund who assisted in the video analysis, and R. Botsco of Microwave Instruments Company who performed the microwave analysis.